Danmarks Miljøundersøgelser
Afd. for Flora- og Faunaøkologi
Kalø, Grenåvej 12, 8410 Rønde

Ministry of
the Environment

National Environmental
Research Institute

Proceedings of the 5th
International Symposium on

Arctic Air Chemistry

Copenhagen, Denmark,
September 8-10, 1992

NERI Technical Report No. 70

Niels Z. Heidam (ed.)
Department of Emissions and Air Pollution

Ministry of the Environment
National Environmental Research Institute
March 1993

Data sheet

Title:	Proceedings of the 5th International Symposium on Arctic Air Chemistry, Copenhagen, Denmark, September 8-10, 1992
Editor:	Niels Z. Heidam
Department:	Department of Emissions and Air Pollution
Serial title and no.:	NERI Technical Report No. 70
Publisher:	Ministry of the Environment. National Environmental Research Institute ©
Year of Publication:	March 1993
Typist:	Lene Thorsted
Please quote:	Heidam, N.Z. (ed.) (1993): Proceedings of the 5th International Symposium on Arctic Air Chemistry, Copenhagen, Denmark, September 8-10, 1992.National Environmental Research Institute. - NERI Technical Report No. 70.
	Reproduction permitted only when quoting is evident.
ISBN: ISSN:	87-7772-094-6 0905-815X
Printed by: Circulation: Price :	Grønager's Bogtryk & Offset 100 DKr 425,00 (incl. 25% VAT excl. freight)
For sale at:	National Environmental Research Institute Department of Emissions and Air Pollution P.O. Box 358 Frederiksborgvej 399, DK-4000 Roskilde Denmark Tlf. + 45 46 30 12 00 Fax. + 45 46 30 11 14

Contents

Introduction

NATIONAL ENVIRONMENTAL RESEARCH INSTITUTE
Division of Emissions and Air Pollution
Roskilde, DENMARK

January 1993

Fifth International Symposium on Arctic Air Chemistry

Editor's Foreword

Niels Z. Heidam

The 5th International Symposium on Arctic Air Chemistry, held in Copenhagen, Denmark in September 1992, was - as implied by the name - the most recent in a series of successful and inspiring meetings on this fascinating subject.

The first of these meetings took place in Norway in 1977 and was in reality more of a workshop. It was actually the first international meeting between scientists interested in arctic air pollution and it marked the beginning of international cooperation in the field. As a result Arctic Air Symposia were convened in the following years in Rhode Island, USA in 1980, in Ontario, Canada in 1984, and again in Norway in 1987.

In my view the 5th Symposium proved a worthy successor where the contributions in terms of scientific interest and merit in every respect measured up to the standards set at the previous meetings. The 5th Symposium did however differ from it's predecessors by a larger proportion of deposition studies, in particular studies of deep ice core deposits. The spectrum of topics have thus been expanded in a way that can put the present arctic air quality into perspective.

The contributions from the 32 participants in the Symposium amounted to 24 oral presentations and 8 posters. The present Proceedings contain the full texts for more than three quarters of these contributuions. In the few remaining cases the abstracts received have been inserted.

The Proceedings from the three preceding symposia were published as special issues of *Atmospheric Environment* (2, 3, 4) that proved indispensable for the continued work - once they were available. By reverting to the original form of the Proceedings as an institution report (1) the conveners and the editor for this 5th Symposium attempt to recapture an essential aspect of the intended purpose - that of fast dispersion of scientific information. The price to be paid is the limited circulation but since the number of active scientists in arctic atmospheric pollution is in fact quite small this may be a minor disadvantage only. Another drawback is that no proper peer-review has taken place.

In consequence the Editor encourages the contributors of these Proceedings to try their luck in the open litterature. There is every prospect for success.

References

1. Symposium on Arctic Air Chemistry 1977: Proceedings.
Sources and Significance of Natural and Man-made Aerosols in the Arctic. NILU Report 1977. Norway.

2. Symposium on Arctic Air Chemistry 1980: Proceedings.
*Atmospheric Environment 1981 **15** No. 8.* Special Issue.

3. Symposium on Arctic Air Chemistry 1984: Proceedings.
*Atmospheric Environment 1985 **19** No. 12.* Special Issue.

4. Symposium on Arctic Air Chemistry 1987: Proceedings.
*Atmospheric Environment 1989 **23** No. 11.* Special Issue.

5th Symposium on Arctic Air Chemistry
September 8 to 10, 1992, Copenhagen, Denmark

Welcome Address

C. Lohse
National Environmental Research Institute
Department of Emissions and Air Pollution

Mankind is currently carrying out an experiment with the global climate. Not intentionally, but an experiment nevertheless.

Each year billions of tons of different gasses, mainly carbon dioxide, methan, nitrous oxide and chlorofluorocarbon are being released into the atmosphere as a result of human activities. As a consequence the atmospheric concentrations of these gases have been increasing with large implications for the worlds climate.

A common name for these gasses are greenhouse gasses. On one side they can be considered as very useful compounds as the world in their absence would be somewhat 35° colder and covered by a sheet of ice. On the other side, we all have a fear that the increasing greenhouse effect would be followed by a rapid heating of the planet so mankind, animal life and the ecosystem as a hole could not adapt in time. In addition there is a risk, that the halogenated compounds already released into the atmosphere would deplete the stratospheric ozone layer and lead to enhanced AV-radiation.

The study of these processes goes on all over the world. However, the arctic region (and the antarctic) offers by far the best possibilities for these studies. The reason is obvious. A remote place, a pristine area, is not influenced by local human activities followed by local pollution. What we study on the arctic is a result of long range transport and the chemical compounds on the aerosols cauth on and inside the arctic ice sheet is a measurement of the changes on the Northern Hemisphere as a hole.

These studies are by far an easy task. The arctic environment is hostile, energy suppliers are absent as well as all other facilities present on a university campus. In addition, the amount of substance available for the studies is very scarce so the normal analytical technique cannot be used.

These facts could be considered as difficulties. I am, however, happy to see that you, the scientific community consider these facts not as difficulties but as a scientific challenge. Large

amount of work have been invested in the invention of the new techniques applied in the arctic studies and the result so far presented are successful and impressive.

The general public are very interested in the result of these studies and popular magazines and newspaper have a very fast follow up of new scientific achievements in arctic research.

This is unusual and certainly flattering and demonstrates that your studies can write, on one side applied science. this joint venture is also important as scientists in most countries, and certainly in Denmark have a great need for public support as they are constantly under pressure to demonstrate the production of socalled strategic results.

I, my self, is a chemist. I started my carrier at the age of 11 mainly with gunpowder and other explosives. Time have changed since and young people to day are much more interested in environmental subjects. I can think of no better field to enter than the studies on Arctic (not just air) as you on one side can travel the history of the earth thousands of years back in time and on the other side closely follow the change in the state of the environment year by year.

The research in these areas are a research in the global change. The papers which are going to be presented at this conference are all bricks in a large global change study.

There can be no doubt that these studies are of utmost importance for mankind and the society as a hole, and the results when added together should be used by our decision makers in the governmental bodies to make wise decision looking forward a bit further beyond the next election period.

However, this hope might be to ambitious. What we can do is to exchange scientific results and present scientific work of high quality.

I wish you welcome to Denmark and I declare this 5th International Symposium on Arctic Air Chemistry for opened.

5th Symposium on Arctic Air Chemistry
September 8 to 10, 1992, Copenhagen, Denmark

Symposium Overview

Dr. H.C. Martin
Atmospheric Environment Services
Ontario, Canada

The Fifth International Symposium on Arctic Air Chemistry was held in Copenhagen, Denmark, September 8 to 12, 1992. Just over thirty scientists presented twentyfive oral papers and eight poster papers.

My purpose in presenting this overview is to give my reaction to the overall scientific program discussed at the meeting rather than to make scientific comments on individual areas of study.

Arctic science is a term often used. In a way, it is peculiar since it does not refer to a discipline, but the region where the work occurs. There is a suggestion that these interdisciplinary meetings on Arctic Air Science shall not occur again, since in the future the aerosol people will meet with all their counterparts at the common disciplinary conferences as will the stratospheric,climate change and toxics, scientists. There is a great danger to the advancement of arctic air chemistry if we fall into this tradition of meeting along strict disciplinary lines. Three considerations come to mind.

First, the number of scientists working in the Arctic is small, while the region is immense. The transfer of information between researchers, across somewhat artificial lines must occur and must be efficient. Working in disciplinary isolation will impair progress in this last frontier of atmospheric research. Second, the cost of field research in the Arctic is practically unacceptable. Logistics for field work can be daunting. Our interdisciplinary campaigns, with shared infrastructure (transport, lodging, site facilities etc) and shared collection or measurement tasks, offer one way of reducing these costs and maximizing progress. Meetings such as this one offer important occasions for developing and maintaining cost-sharing strategies. Third, in their own right, these meetings counter a debilitating trend in science towards greater specialisation and isolation. In my view the reversal of this trend is healthy and energizing, accepting that it sometimes requires patience.

Over the past decades, it seems environmental research has changed from an examination of how nature works to one which examines how man has changed the way nature works. This change is very evident in atmospheric studies. There is a great public concern for the consequence of anthropogenic perturbations on the natural system and, in turn, there are resources provided for

us to examine the perturbations. However, in our reports, including those given at this meeting, the public issue or the relevance of our studies to a public issue, is not always identified. This oversight can be financially risky to the maintenance of our work. If the urgent problems in the arctic atmosphere are to be explained and corrected, the goal I trust, then we must identify ourselves in this process. The relevance of working in this cold, dark, remote place, should be obvious to the people holding the resources.

There is no point sketching here the salient results in the papers that follow. I will, therefore, express a few personal notes.

While the mix of topics is excellent, the absence of several circumpolar countries was regrettable.

I was delighted to be introduced to the discipline which I will call archaeo-air chemistry, the study in glaciers of wet and dry deposition which occurred tens of thousands of years ago. The relevance of this work to the current debate on climatic change is enormous.

The speculation concerning methane gasses producing a massive plume downwind of Bennett Island has been silenced. This story should teach us all prudence and temper our exotic imaginations when simple science, in this case meteorology, will suffice.

We will struggle with the question "Is it snowing?" for some time. The idea of shutting the snow collector when the wind is above a certain speed is not scientifically elegant, though it does remove some confusion between falling snow and/or blowing snow entering the collector.

The long-range transport of anthropogenic compounds is an underlying theme in many papers. Our work on acid rain (a topic not discussed) over the past two decades will continue to serve us well here. The Pinatubo eruption has added a fascinating twist to this discussion.

Our ability to maintain our momentum in the understanding of arctic air chemistry will depend greatly on our ability to overcome measurement problems in the field. Selfcontained, robust, automated instruments are desperately needed in order to reduce costs of placing scientists in the field.

Russia has the largest piece of the arctic region. Dramatic political change has opened this region to vigourous international collaboration. The work will have to be done. With care and clever uses of our pooled financial resources we can, as a group, move quickly towards a truly circumpolar program using the enormous intellectual resources of our Russian colleagues.

In parallel with the examinations of the polar atmosphere, there are programs in several laboratories to develop atmospheric models. This work is very timely and welcome and is providing guidance to both field interpretation and to domestic and international measures to correct pollution problems. One major handicap in the modelling effort is the lack of appropriate emission inventories. Even simple inventories on the required scale, are very expensive. This situation should be corrected through close international cooperation.

Session 1

Overviews

Chairman:
C. Lohse

A DECADE OF ARCTIC TROPOSPHERIC AIR CHEMISTRY STUDIES IN CANADA.

L.A. Barrie
Atmospheric Environment Service, 4905 Dufferin St. Downsview, Ontario, M3H 5T4, Canada.

In the decade of the 1980's, a variety of air chemistry studies have been undertaken in Canada to elucidate the natural and anthropogenic influences that affect the Arctic. These include routine observations of the trace gas and aerosol composition of the troposphere related to arctic haze, intensive studies of chemical reactions occurring at polar sunrise, modelling studies of the pathways of pollutants into the Arctic, glacial ice chemistry observations and assessments of the climatic impact of aerosols.

Chemistry studies have been undertaken at several locations in the Canadian Arctic. Initially, they were focussed on defining the origin, nature, occurrence and impact of particulate pollution commonly known as Arctic haze. After ten years new light has been shed not only on air pollution but also on natural cycles of dust and marine aerosols and on chemical reactions at polar sunrise involving aerosols.

Analysis of aerosols collected at Alert, NWT over the decade of the 1980s has been undertaken for major ions by ion chromatography and for trace elements by instrumental neutron activation analysis and inductively coupled plasma emission spectroscopy. In addition, lead and sulphur isotope measurements have been made on selected years of observations. In the late 1980s, black carbon measurements were made routinely.

The picture that has emerged in the Canadian high Arctic is one of distinctly different seasonal variations for four aerosol components: anthropogenic, sea salt, soil and photochemical products generated at polar sunrise. In addition, there are marked trends in some constitutents such as lead that are consistent with changes in northern hemispheric emissions and glacial ice ccre records.

The polar sunrise component of the aerosol seems to be strongly linked to photochemical reactions at polar sunrise. From a climatic point of view the conversion of SO_2 to $SO_4^=$ is an important reaction at this time of year. In addition lower tropospheric ozone is destroyed over the Arctic ocean after polar sunrise in a reaction that is accompanied by changes in the concentrations of marine halogens and light hydrocarbons.

Abstract to the 5th International Symposium On Arctic Air Chemistry
8-10 September 1992 Copenhagen Denmark

Abstract to : 5th International Symposium on arctic air chemistry, September 8-10, 1992, Roskilde, Denmark.

SIX YEARS OF OBSERVATIONS OF PAN AT ALERT, N.W.T., CANADA

Jan W. Bottenheim, Atmospheric Environment Service, 4905 Dufferin St, Downsview, Ontario, Canada.

It has become clear in recent years that PAN (peroxy acetyl nitrate) is a major component of the total abundance of nitrogen oxides in remote atmospheres. As such it plays an important role in the global nitrogen budget, and may influence tropospheric ozone levels. Measurements of this important species are rather limited for remote locations. We started making routine observations of PAN at the remote arctic station Alert (82.5° N, 62.5° W) in 1986, after earlier short-time campaigns in 1985 and 1986 in conjunction with major Arctic Haze studies showed the feasibility of such measurements, and will report here on the first six years of data.
A clear seasonal pattern is observed with very low levels of PAN during the summer (generally below the detection limit of 20 pptv), and a continuing increasing mixing ratio starting in early September, rising to a spring maximum of 300-500 pptv. This pattern is similar but not necessarily identical to that reported for SO_x (the sum of SO_2 + $SO_4^=$). The data will be discussed in light of concurrently observed nitrate data, showing the preponderance of PAN over the inorganic nitrates. A comparison with ozone observations will also be reported. Finally, the potential impact on midlatitude tropospheric chemistry will be addressed.

Study of ammonium to nss sulphate molar ratio in air and snow at high latitudes.

Eric SILVENTE and Michel LEGRAND.

LGGE FRANCE.

Abstract : Aerosol sampling and snow pit studies have been conducted at ATM, the solar-powered camp near Summit, Greenland (72°20'N, 38°45'W, 3190 m elevation). in the summer s 1990 and 1991. To avoid contamination, the aerosol filters as the snow samples, were stored in ultra clean airtight glass bottles. We study, here, the NH_4^+/SO_4^{2-} molar ratio in the aerosol phase and in a 5 meters snow pit. The mean value in the aerosol phase was 1.01 and in snow samples, 0.216. This ratio exhibits strong seasonal variations. NH_3 has a very weak anthropogenic source. Its maxima is in summer due to decay of dead marine organisms and biomass burning (Talbot et al, in press). SO_4^{2-} has a maximum in spring due to Arctic Haze phenomenon. The mean value Ca^{2+}/SO_4^{2-} molar ratio (0..21) is closed to the mean NH_4^+/SO_4^{2-} molar ratio. NH_3 and $CaCO_3$ has the same impact on the neutralisation of the background acidity in high latitudes.

Ammonia is one of the main base of the atmosphere together with carbonates. It can therefore interact with a lot of atmospheric chemical cycles, including partial neutralisation of nitric acid and sulphuric acid. Unfortunately, there are only a few available data for high latitudes remote regions (Legrand, 1985 ; Gras, 1983 ; Savoie et al, 1992). In the Antarctica atmosphere, the particulate NH_4^+ to nss SO_4^{2-} molar ratio has been found to be between one and two (Gras, 1983 ; Savoie et al, 1992). So, it indicates that NH_4^+ nearly fully neutralises acidic sulphate. NH_4^+ to $nssSO_4^{2-}$ molar ratio in ice core and snow pit is very different. NH_4^+ can be neglected in the ionic balance of the Antarctic snow during the Holocene period

(Legrand, 1985). With this work, we want to know if same discrepancy can be seen between snow and aerosol data in Greenland.

Experimental procedure : During each of the ATM90 and ATM91 season, we collected nearly 30 aerosol samples, using Gelman Zefluor (1 mm pore size,90 mm diameter). After collection, all the filters were stored in clean, airtight glass bottles except for 15 samples during the 1990 campaign that have been stored in accuvettes. Glass bottles were washed in an ultrasonic bath filled with ultra clean deionized water for one hour. The filters were not cut nor ultrasonically extracted because of possible contamination by ammonia even in clean flow bentch. We tried to minimise as much as much as possible contact between the filters and the air in our laboratory. re-extraction of filters showed that in most cases, 95 % of the filter was washed at the first extraction (without ultrasonic procedure).
We also sampled a 6-meter snowpit during ATM90 and more than ten fresh snow samples during ATM91. Air and snow samples were analysed with ion chromatography (Dionex 4000 and 4500) with an Omnipak 500 (anions) and CS 10 columns (cations).

Results : In this paper, we present only data from 1991 summer season. The aerosol composition is dominated by acidic sulphate particles (Table 1). The concentrations of Na^+ is very low indicating on the average ≥99 % of sulphate was of non-sea-salt origin. NH_4^+ is the main cation measured (Table 2). Anion to cation ratio is close to 2, indicating that the aerosol is indeed acidic. Average NH_4^+-to-nssSO_4^{2-} ratio is close to 0.9. There is only a partial neutralisation of acidic sulphate by ammonium in the aerosol over Summit (Figure 1).

The NH_4^+ concentrations measured in the snowpit show strong seasonal variations (Figure 2). Looking at dO_{18} and SO_4^{2-} data (Grootes and Mayewski, unpublished data), we can identify a spring peak and a summer peak. The spring peak could be associated with anthropogenic sulphate or could be due to a rapid transport from the

mid latitudes. Possible sources of summer peak include biomass burning or rotting sea ice (Talbot et al, in press).

The NH_4^+ to nss SO_4^{2-} molar ratio also exhibits clear seasonal variations too (Figure 2). This ratio reaches its maximum during summertime due to the fact that sulphate reaches its minima during summertime.

Ca^{2+} concentrations (Mayewski, unpublished data) are maximum in early spring, we can see a shift in the dominant base. During winter and early spring, calcium carbonate is the dominant base. During the end of spring and in summer, NH_4^+ is the dominant base (Figure 3).

Table 3 shows some of the fresh snow data. Scavenging ratio of ammonia and sulphate are not very different, with NH_4^+-to-nssSO_4^{2-} molar ratio close to one in all of our fresh snow samples. Overall, these results do not indicate strong deviations.

Conclusion : Aerosol, snowpit and fresh snow NH_4^+-to-nssSO_4^{2-} molar ratio are very similar during summertime. We think that Antarctica aerosol data should have been contaminated. So, we think that ammonia is not a dominant base in a global scale. NH_4^+ data also show that anthropogenic contribution for ammonia is weak : our measurements in fresh snow are close to 0,4 meq l^{-1}, while Legrand et al (1992) found background values for ancient ice of the GRIP core close to 0,3 meq l^{-1}.

References

Gras J.L., Ammonia and ammonium concentrations in the Antarctic atmosphere, Atmos. Environ., 17, 815-818, 1983.

Legrand M. , chimie des neiges et glaces antarctiques : un reflet de l'environnement, thèse de doctorat d'état de l'université Grenoble I, Publication n°478 du LGGE, 439 pp, 1985.

Legrand, M., M. de Angelis, T. Staffelbach, A. Neftel and B. Stauffer, Large perturbations of ammonium and organic acids content in the Summit-Grennland Ice core, Fingerprint from forest fires?, Geophys. Res. Lett. 19, 473-475, 1992.

Savoie D.L., J.M. Prospero, R.J. Larsen and E.S. Saltzman, Nitrogen and sulfur species in aerosols at Mawson, Antarctica, and their relationship to natural radionucleides, J.Atmos. Chem., 14, 181-204, 1992.

Talbot, R.W., A.S. Vijgen, and R.C. Harriss, J. geophys. Res., in press. (special issue on GTE ABLE 3A).

	F^-	CH_3COO^-	glyc.	$HCOO^-$	MSA	Cl^-	NO_3^-	SO_4^{2-}	$C_2O_4^{2-}$
neq m^{-3}	0.0017	0.033	0.027	0.152	0.056	0.058	0.011	2.458	0.052
s	0.0035	0.032	0.018	0.179	0.044	0.134	0.013	1.261	0.044

Table 1 : anion concentration in aerosol during 1991 summer campaign.

	Na^+	NH_4^+	K^+	Mg^{2+}	Ca^{2+}
neq m^{-3}	0.157	1.093	0.097	0.026	0.098
s	0.264	0.547	0.062	0.019	0.079

Table 2 : cation concentration in aerosol during 1991 summer campaign.

	Scavenging	Ratio	
Fresh snow events	SO_4^{2-}	NH_4^+	molar ratio NH_4^+/SO_4^{2-}
7.7.91	1100	720	0,7
7.15.91	400	540	1
8.6.91	300	230	0,8
8.24.91	1550	1390	1,4

Table 3 : scavenging ratio in four fresh snow events.

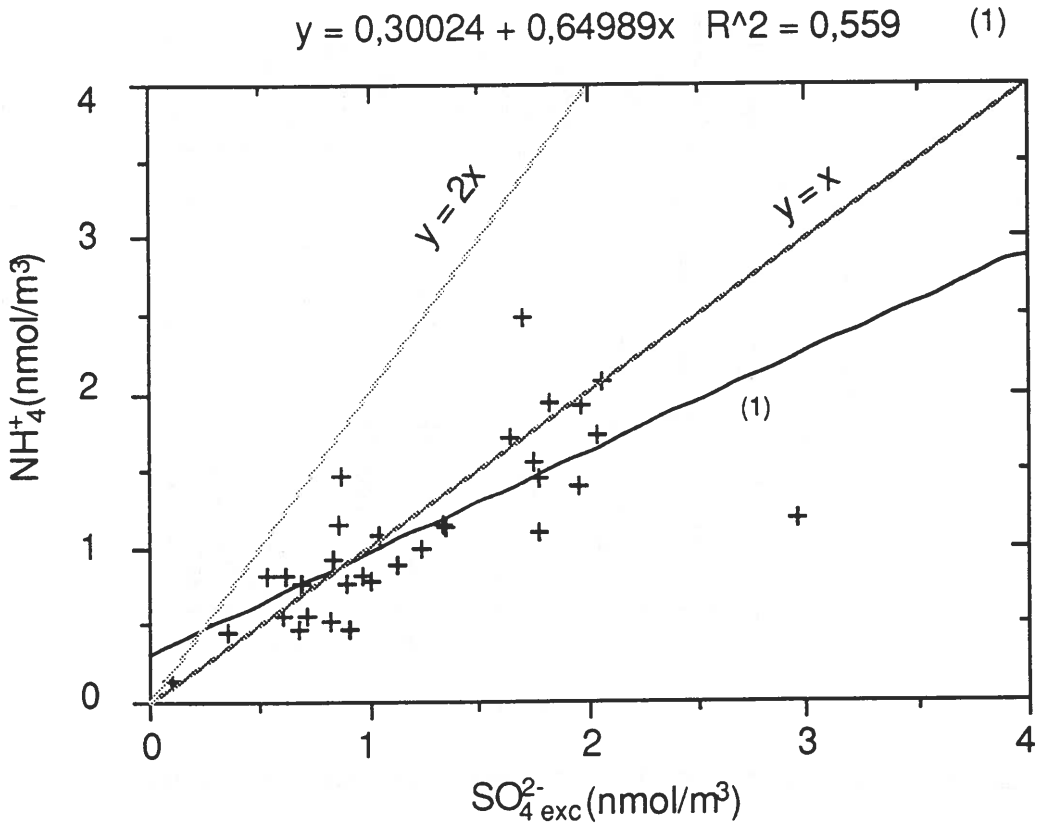

figure 1 : neutralisation of sulphate by ammonium.
y=x : fully neutralisation.
y=2x : half neutralisation

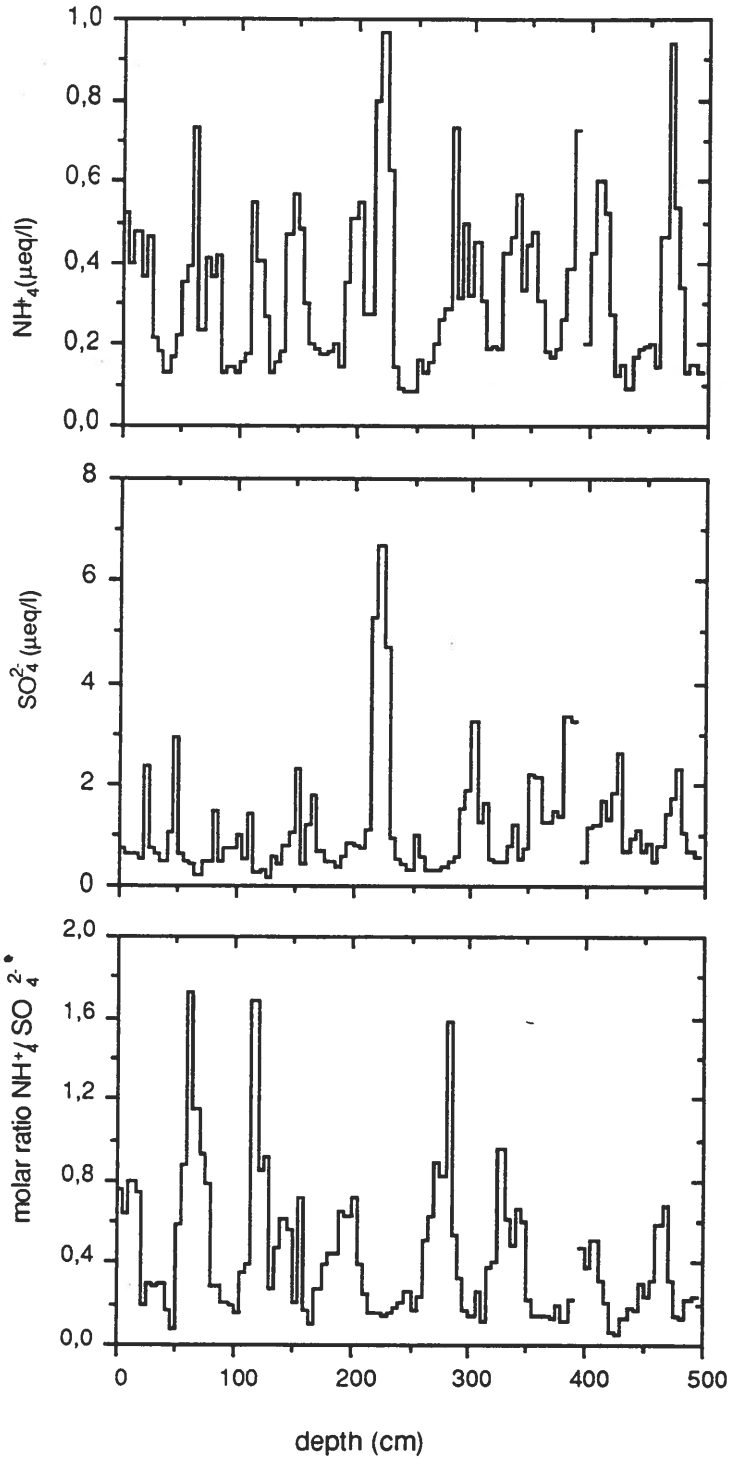

Figure 2 : seasonal variations of ammonium, sulphate and ammonium to sulphate ratio

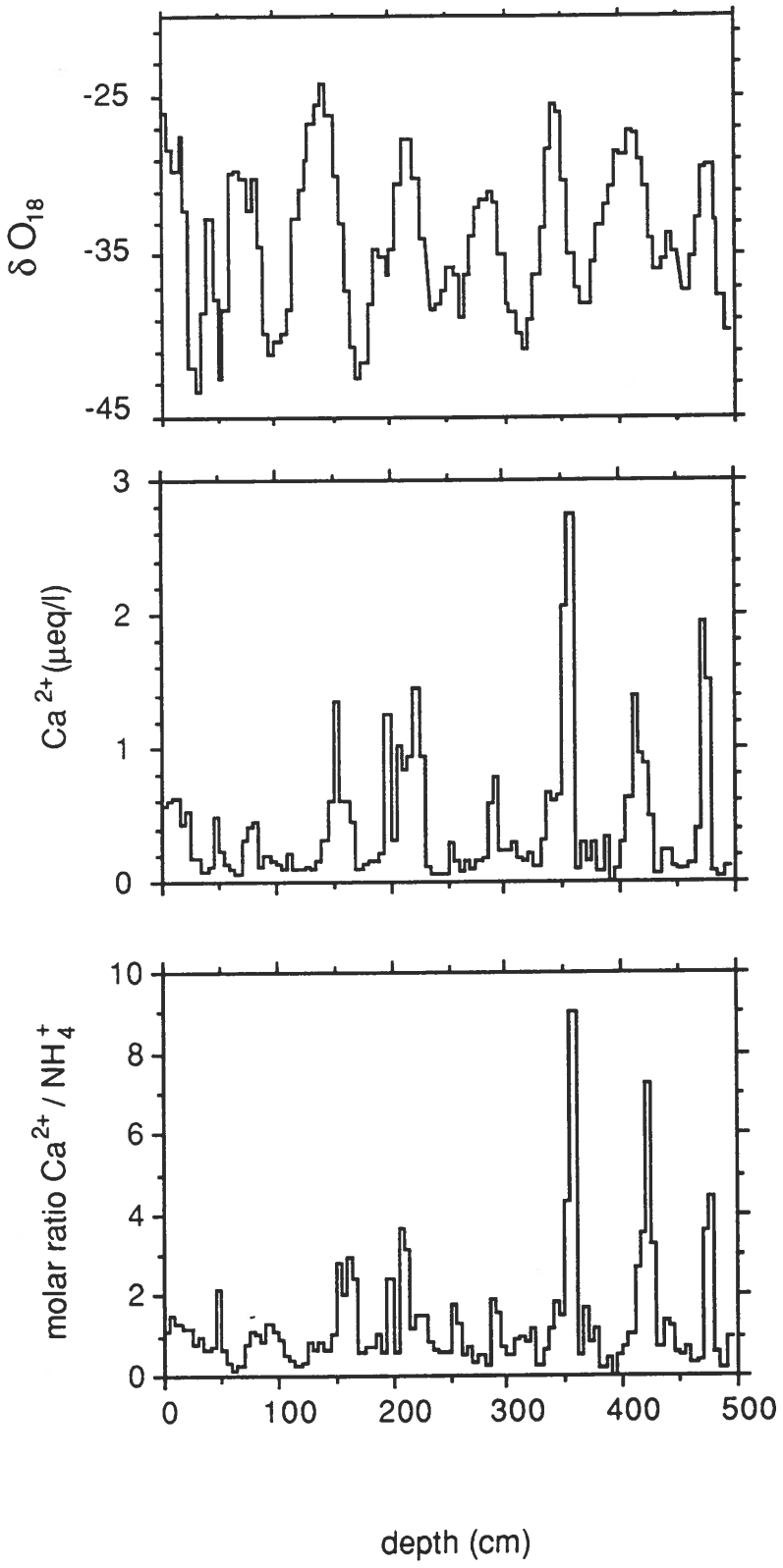

Figure 3 : seasonal variations of dO_{18}, calcium and calcium to ammonium ratio

Session 2

Gas- and Aerosol Measurements

Chairman:
J.W. Bottenheim

HYDROCARBONS IN THE ARCTIC : OBSERVATIONS ON THE ZEPPELIN MOUNTAIN IN NY-ÅLESUND.

Frode Stordal, Sverre Solberg and Norbert Schmidbauer
Norwegian Institute for Air Research, Lillestrøm, Norway

Øystein Hov
Department of Geophysics, University of Bergen, Norway

Abstract

Regular observations of a number of nonmethane hydrocarbons at Ny-Ålesund, Svalbard (79°N, 12°E) from September 1989 to the end of 1991 are presented. The concentrations of the individual NMHCs peaked in January and February with a maximum sum of 43 ppbC and were very low during summer, with a minimum sum of 1.5 ppbC. In January and February the 30 days running average of the sum of the NMHCs was close to, and even exceeded, the sum of the NMHCs observed at the European background station Birkenes, at the south coast of Norway.

Transport analysis based on trajectory calculations have been performed. The highest average concentrations of the individual NMHCs in winter occurred when the transport was from southeast, and the lowest from southwest.

We found several indications of nearby sources of ethene and propene : The summer to winter average was smaller than expected from European anthropogenic emissions, and the fraction of the sum of these components increased in summer. Also the trajectory calculations suggest that there are local or nearby sources.

1 INTRODUCTION

Nonmethane hydrocarbons (NMHC) contribute to the formation of photochemical oxidants (notably ozone, O_3, hydrogen peroxide (H_2O_2) and peroxyacetyl nitrate, PAN), and they are precursors of carbon monoxide (CO) and carbon dioxide (CO_2). Both directly and indirectly (through CO), the nonmethane hydrocarbons influence the atmospheric hydroxyl radical (OH) concentration. NMHCs are therefore linked to a range of atmospheric environmental issues: acid deposition through OH, H_2O_2 and O_3, photooxidant formation which takes place when nitrogen oxides (NO_x=NO+NO_2) and NMHCs react under the presence of sunlight and global tropospheric change through the influence on the OH radical concentration, CO and CO_2.

The quantitative role of the NMHCs in photooxidant formation or global change is not settled, for many reasons. The sources of anthropogenic and natural hydrocarbons are complex and variable in time and space and the knowledge of the atmospheric concentration distribution of the individual nonmethane hydrocarbons can at best be characterized as fragmentary.

The role of NMHC in photooxidant formation is considered sufficiently settled to justify international negotiations to reduce the emissions. At present within UN Economic Commission for Europe (ECE) the negotiations are aiming at an international NMHC (or VOC=volatile organic compounds) protocol where the signatories commit themselves to an agreed emission reduction.

In the EUREKA project Eurotrac, the sub project Tropospheric Ozone Research (TOR) was established in 1986 with the purpose to identify and quantify the processes which determine the ozone change over Europe and adjacent areas both in the short and long term (trend). As a part of the TOR project, a ground based rural station network in Europe with high quality instrumentation

was set up, among them two sites in Norway: Birkenes (58°N, 8°E, 119 m a.s.l.) close to the south coast of Norway and Ny-Ålesund (79°N, 12°E, 474 m a.s.l.) on the west coast of Svalbard (Fig. 1). In this paper, the relationship between the sources of individual hydrocarbons in Europe, and the measured concentrations at Ny-Ålesund, is investigated.

Individual NMHCs have been measured on the Zeppelin Mountain since October 1989. Manual samples are taken in stainless steel bottles (SS 304) of 0.8 l volume with a metal-bellow pump every second day, although there have been irregular intervals due to practical difficulties. The subsequent analysis is made in the laboratory at NILU using gas chromatography equipped with a flame ionization detector. A detailed description of the sampling technique and analytical method is given in Schmidbauer and Oehme (1986) and Hov et al. (1989 and 1990) and in Hov and Schmidbauer (1992).

Surface ozone has been measured continuously at Ny-Ålesund, Spitzbergen, since mid October 1988. Measurements are taken each hour throughout the whole year, by use of UV-absorption. In mid September 1989 the monitor was moved from a station close to the coast and up to the nearby Zeppelin Mountain, 474 m above sea level.

Daily average concentrations of NO_2, SO_2, sulphate aerosol, sum of nitric acid and nitrate aerosol and sum of ammonia and ammonium aerosol are also measured on the Zeppelin Mountain since many years. In 1991 an Ecophysics high sensitivity NO, NO_2 and NO_y chemiluminescense analyzer with a photolytic and gold converter was installed on the Zeppelin Mountain, and since the summer of 1989 an automatic PAN analyzer based on GC-EC has been in operation in periods. In 1992 a CO and H_2 continuous analyzer was installed. The analysis programme for NMHCs has been extended to cover more compounds. Methane is also analysed, as are selected chlorofluorocarbons based on GC-EC and the pressurized air samples taken three times per week. These measurements will be reported at a later stage.

2 SECTOR ANALYSIS METHOD

The measuring site at the Zeppelin Mountain is remote from anthropogenic emission areas, and at 79° N the local photochemical activity is low or non-existent most of the year. It is therefore crucial for the understanding of the observed concentrations of NMHCs to investigate the influence of long range transport from different geographical areas.

To look at different transport patterns in different seasons, we calculated trajectories arriving at the Zeppelin Mountain for three complete years (1989-1991). We believe this gives a better indication of the origin of the air mass, than using the observed wind direction at the Zeppelin Mountain directly.

The trajectories calculated were 4 day back trajectories each 6 hour on the pressure surface 925 hPa. We used meteorological data from the Norwegian Meteorological Institute for the three years 1989 - 1991, and calculated the trajectories on the EMEP grid as described by Hov et al. (1991). The Zeppelin station normally is situated somewhat below the pressure level 925 hPa (approx. 700 m), introducing some uncertainty in the trajectory calculations.

More questionable is the use of pressure (or sigma-) coordinates. It is well known (Iversen, 1989b) that poleward air flow into the Arctic in the absence of significant diabatic processes, follows isentropic surfaces. These surfaces are steepening towards high latitudes, causing a lifting of air masses when approaching the Arctic. As an example, an air parcel originating at 1000 hPa at 60°N and moving on an isentropic surface to 80°N could typically be lifted to 875 hPa (Iversen, 1989 b). In reality diabatic processes alter this, e.g the radiative cooling of the air causing a slow subsidence. But we claim that the trajectory calculations can be used to distinguish transport from different larger areas, not that the trajectories are very accurate representations of the air mass flow pattern.

When assigning transport sectors to the trajectories, we used two methods, one for analyses of the transport direction itself and one for analyses of the gas concentrations from different directions.

The distribution of the transport sectors in different seasons (Fig. 2) was calculated using four equally wide sectors (N, E, S, and W), and using only the part of the trajectory between 150 and 880 km (the distance to the nearest grid boundary) from the Zeppelin Mountain, to avoid any bias due to different sector areas.

We see that in the winter season the transport was predominantly from N and E, and to a smaller extent from S. At this time of the year the site is usually north of the polar front for extended periodes of time, with the prevailing wind from E. In the same season efficient mixing with air from lower latitudes occurs in episodes with approaching cyclonic systems, and also in situations with a cold anticyclone situated over the Eurasian continent producing a blocking event. This has been confirmed by several authors and has been proposed as an explanation for the elevated levels of anthropogenic trace gases in late winter in the Arctic (Iversen 1989a, Isaksen et al.,1985).

Calculations by Iversen (1989a) indicate that winter and spring are the seasons with the most efficient meridional transport from mid latitudes into the Arctic. Isaksen et al. (1985) estimated a transport time of one week between 60° and 80° N in winter, and four weeks in summer. The calculated transport time between 40° and 80° N, on the other hand, was much longer.

The spring season in the period 1989 - 1991 at Ny-Ålesund was dominated by transport from N, as seen on Fig. 2. Approximately 35 % of all 6h-trajectories were calculated to come from the north. During spring the polar cap of cold, stable air breaks up, and frequent episodes of Arctic air reaching lower latitudes, occur. In addition the large scale cyclonic systems usually travel further north in spring than in winter, and frequent episodes of transport from the southerly directions are expected. The figure shows that the relative number of trajectories from S was almost the same in spring as in the winter (18 %). Iversen's climatological statistics (1989a) indicate that in spring time the frequency of poleward transport is of the same order as in winter.

Summer has, according to Iversen, the least frequency of meridional mixing between lower latitudes and the Arctic. In Figure 2 it is seen that in the summer months (1989 - 1991) trajectories from W and S are most common. During this time of year Ny-Ålesund is characterized by gentle winds and weak cyclonic activity favouring the slow meridional exchange (Isaksen et al. 1985).

The distribution of the trajectories in the fall resembles the spring, as seen in Fig. 2. Iversen's meridional index for this season is larger than in summer, but smaller than in winter and in spring.

For the study of NMHC concentrations from different regions, we divided the 360° circle into 5 sectors as pictured in Fig. 3, with the two sectors towards north beeing twice as wide as the rest to account for trajectories meeting the grid boundary and uncertainties in the meteorological data. A transport sector for the NMHCs was then allocated for each day the NMHCs were sampled (usually 3 times/week) by using the coordinates of the four 6h trajectories for that day if more than 50 % of the coordinate points were inside one sector (Hov et al. 1991).

3 SEASONAL VARIATION OF INDIVIDUAL HYDROCARBONS

A number of light nonmethane hydrocarbons have been analysed in pressurized air samples from the Zeppelin Mountain station since October 1989 (Hov et al. 1989, Hov et al. 1991). The analytical technique has recently been intercalibrated with European standards (De Sayer and Tsani-Bazaca, 1992).

In Fig. 4 is shown the sum of the nonmethane hydrocarbons (on ppbC basis) from 1989 to the end of 1991. In Figures 5 and 6 are shown the 30 d average values in an annual cycle (based on data from the same three years) for the individual components together with the standard deviation. The standard deviation was calculated using all the individual measurements in the 30 d periode in the years 1989 - 1991 (as explained in the figure caption). In Fig. 7 is shown the sum of the hydrocarbons for Ny-Ålesund compared with the sum at the Birkenes station (1987-1991).

Except for propene, all components show a distinct seasonal cycle on the Zeppelin Mountain, with maximum values in January/February, and a minimum in the summer.

The peak value for the sum of the nonmethane hydrocarbons occurs in late January 1990 with a value of 43 ppbC. The minimum is reached by midsummer 1991 with 1.5 ppbC. The 30 d average maximum is also in late January (28 ppbC).

Compared to Birkenes we see that the seasonal cycle is more pronounced on the Zeppelin Mountain. In the period January to March the 30 d average sum of the nonmethane hydrocarbons is close to, or higher, than at Birkenes. Towards summer the amount of NMHC on the Zeppelin station decreases more rapidly than at Birkenes, and the average summer values are lower.

The high amount of NMHC at Ny-Ålesund in winter reflects the combined effect of low chemical activity, and thereby longer lifetime, and the efficient meridional exchange (Hov et al. 1989, Isaksen et al., 1985). In winter the characteristic transport time from 60° to 80° N of one week, estimated by Isaksen et al (1985), is shorter or of the same magnitude as the chemical lifetimes, while in summer the opposit is the case. However, this characteristic exchange time of one week in winter is calculated from climatological circulation data. The real exchange time in a given time interval can differ significantly from this number.

Table 1 shows the average concentrations of the individual hydrocarbons and their sum for winter and summer, together with the ratio. Also given is an estimate of their chemical lifetimes determined from the OH reaction alone, and of their transport time from 60°N in the two seasons. The chemical lifetime was calculated from the rate constants of Atkinson (1990), assuming $[OH] = 6.5*10^5$ molecules/cm^3 and a temperature of 283 K in summer, and $1*10^5$ molecules/cm^3 and 273 K in winter. The transport time, T, from 60°N was calulated from the equation $X = X_0\, e^{-T/\tau}$, where X and X_0 are the seasonal averages on the Zeppelin Mountain and at Birkenes, respectively, and τ is the chemical lifetime. The seasonal averages were calculated with data from 1989 - 1991 on the Zeppelin Mountain, and from 1987 - 1991 at Birkenes.

The missing values in the table are due to missing coefficients for the reaction rate of iso-pentane with OH (Atkinson, 1990), and due to the fact that the average winter concentration of propane is higher on the Zeppelin Mountain than at Birkenes.

Table 1 shows that the W/S concentration ratio is much lower for the alkenes than what would be expected from the OH - reaction alone. The reaction with O_3 tend to reduce this ratio because the ozone concentration is similar in the two seasons, as opposed to OH. But this is not sufficient to explain the small ratio, the lifetimes with O_3 is approx. 15 days for ethene and 2 days for propene (Atkinson, 1990). This supports the idea of local, probably oceanic, sources of the alkenes (Hov et al., 1989a, Rudolph et al., 1989).

For the other components we see that ethane has the smallest winter to summer ratio, and iso-butane and iso-pentane the largest. This is reasonable in a qualitative sense when looking at their lifetimes, varying from about 600 days (ethane) to 5 days (n-pentane).

	C_2H_6	C_2H_4	C_2H_2	C_3H_8	C_3H_6	n-C_4H_{10}	i-C_4H_{10}	n-C_5H_{12}	i-C_5H_{12}	SUM
Winter	4.6	0.87	1.4	4.1	0.15	2.5	1.3	1.2	1.3	17.5
Summer	1.5	0.17	0.14	0.21	0.14	0.08	0.04	0.05	0.04	2.4
W/S	3	5	10	20	1	28	30	26	34	7
$\tau^{1)}$ winter	594	12	160	122	4	51	54	33	-	
$\tau^{1)}$ summer	87	2	24	19	0.7	8	9	5	-	
$T^{2)}$ winter	48	7	15	-	5	12	8	12	-	
$T^{2)}$ summer	41	3	24	29	0.8	23	25	13	-	

Table 1: Average concentrations of hydrocarbons on the Zeppelin Mountain 1989-1991. All values are in ppbC.

1) τ is chemical lifetime in days from the OH reaction (Atkinson,1990).

2) T is calculated transport time in days from 60°N, as explained in the text..

The estimated transport times in winter are similar for acetylene and the alkanes n-butane and n-pentane (12 - 15 days), but different from the value calculated for ethane. In summer the calculated transport times are longer, with values of 23 - 41 days for the components ethane, acetylene, propane, n-butane, and i-butane. But the average concentration of n-pentane is higher than expected, and the calculated transport time for this component in summer is shorter than the other alkanes .

The table shows that the calculated transport time is much shorter for the alkenes than for the other comnponents in the summer. This indicates that there must be other processes controlling the alkene concentrations on the Zeppelin Mountain than anthropogenic emissions and OH chemistry. Since the reactions with ozone is not a sufficient explanation, this suggests the existence of local sources of the alkenes.

Fig 8 shows the seasonal cycle of the relative distribution of the individual nonmethane hydrocarbons as per cent of the total (on a ppbC basis). In winter the distribution is uniform throughout the season, with around 26 % ethane, 23 % propane, and 15 % n-butane as the most abundant components, the remaining components are below 10 % each. These numbers agrees fairy well with Hov et al. (1989). During spring the relative amount of ethane rises rapidly to above 70 % in summer. At the same time the rest of the alkanes fall off. This reflects the chemical age of the air mass at Ny-Ålesund during the year. In summer the air masses have lost most of the more volatile components, with long lived ethane as the dominating one (Hov et al., 1989). The uniformity of winter air indicates that this composition of hydrocarbons is representative of free tropospheric background air in winter.

The diagrams show that the relative amounts of ethene and propene increase in late spring and early summer, and reach a maximum in August (few data in July). These have the shortest lifetimes of all the components, so this is a further indication of nearby oceanic sources in the spring and summer season.

Light hydrocarbons have been measured on occasions at other Arctic stations. Rasmussen et al. (1983) showed that the concentrations at Pt. Barrow followed the amount of Arctic haze, with a maximum in spring and a minimum in summer. Their values of 2872 pptv of ethane, 686 pptv acetylene, and 1260 pptv of propane for early spring, are similar to our values. Their level

of 75 pptv ethene, however, is far below the concentration of 250-400 pptv observed on the Zeppelin Mountain in early spring

The measurements of Bottenheim et al. (1990) from Alert agree fairly well with the concentration levels on the Zeppelin Mountain. The acetylene concentration at Alert varied from approx. 1.6 ppbC to 0.8 ppbC, and ethene from 0.6 ppbC to 0.2 ppbC in the period from the beginning of March to end of April 1988.

4 SECTOR ANALYSIS OF HYDROCARBONS

Sector analysis of the NMHCs have been performed for the three years 1989 - 1991 according to the method expained in section 2.

Fig. 9 shows the average concentration for each sector for the period 15. November to 15. March during these years for ethane, ethene, n-pentane and the sum of all the hydrocarbons. The patterns are quite similar, with the highest concentrations coming from SE, followed by somewhat lower values from N, and even lower from S. The smallest concentrations follow transport from the Atlantic Ocean sector, SW.

From sector SE the average sum of the hydrocarbons in this periode was calculated to be 25 ppbC, and from SW 16 ppbC. This is in agreement with the findings of Iversen (1989b), that the surface air pollution observed at Ny-Ålesund during winter is most influenced by the closest source areas to the SE with similar surface air temperature as in Ny-Ålesund. This is due to the nearly isentropic air flow, causing emissions from warmer regions to be lifted into the troposphere where they can be found as pollution layers in the stable wintertime Arctic troposphere.

The level of 16 - 19 ppbC from the north, and from SW, is not far from the average NMHC sum of 19 - 22 ppbC observed at Birkenes in the same time periode (Fig. 7), which indicates a mixing of the above mentioned hydrocarbons through large portions of the northern hemisphere in the winter and early spring.

The similar shape of the concentration roses in this period, except for ethene, shows that the relative amount of the individual NMHCs is relatively constant in all directions, indicating low chemical activity. The difference between ethene and the other components is consistent with the fact that ethene is destroyed by ozone, which varies considerably less over the year than OH.

Fig. 10 shows the average sector values of the fraction of four of the hydrocarbons relative to the total sum of all the nine components (in %) during the period 15. May to 15. September (1989 - 1991). This is the periode with the elevated relative amount of the alkenes (Fig. 8).

The relative amount of ethene and propene is highest from S (6 and 7 %, respectively), but compared to n-butane we see that the distributions from the different sectors are much more even. If the elevated fraction of the alkenes were caused by anthropogenic emissions (as n-butane), we would expect very low concentrations from the SW, NW and NE sectors in summer, due to the very short lifetime. The fact that the average sector concentrations are more even, points to a local source in the ocean.

Fig. 10 shows that the ethane fraction of the sum of the hydrocarbons is the least from S (40 %), reflecting the fact that the more short lived species are relatively more abundant, indicating that transport from this direction is associated with the most recent emissions.

5 SUMMARY

From September 1989 a number of nonmethane hydrocarbons have been measured regularly at Ny-Ålesund, Svalbard (79°N, 12°E)

The hydrocarbons peaked in late January, with a maximum value of 43 ppbC as the sum of the nine NMHCs analysed. In January and February the 30days average of this sum was close to, or exceeded, the sum observed at the European background station Birkenes, at the south coast of Norway. In the winter the average concentration was the highest when the transport was from southeast and the lowest from southwest.

The seasonal cycle in the NMHCs was more pronounced than at Birkenes, with lower values in summer and fall at Ny-Ålesund, and a winter to summer ratio of 7 in the sum of the nine components.

We found several indications of nearby sources of ethene and propene : The summer to winter average was smaller than expected from European anthropogenic emissions, and the fraction of the sum of these components increased in summer. Also the trajectory calculations suggest that there must be local or nearby sources.

In winter the composition of the individual NMHCs was uniform with approx. 26, 23, and 15 % of ethane, propane, and n-butane respectively on a ppbC basis, in summer the ethane fraction increased to about 70 %.

Acknowledgements

This contribution to the TOR subproject EUROTRAC is sponsered by the Norwegian Reseach Council for Science and the humanities (NAVF). The sector analyses have been based on meteorological data provided by the EMEP/MSCW at the Norwegian Meteorological Institute.

References.

Atkinson, R. (1990) Gas-phase tropospheric chemistry of organic compounds : A review. Atm. Env. 24A, pp 1-41.

De Sayer, E., and E. Tsani-Bazaca (1992) EC intercomparison of VOC measurments. Draft report. Joint Research Centre, Enviroment Institute, Ispra, Italy.

Hov, Ø. and N. Schmidbauer (1992) Atmospheric concentrations of nonmethane hydrocarbons at a North European coastal site. J.Atmospheric Chemistry, 14, 515-526.

Hov, Ø., N.Schmidbauer and M.Oehme (1989) Light hydrocarbons in the Norwegian Arctic. Atmospheric Environment, 23, 2471-2482.

Hov,Ø., N.Schmidbauer and M.Oehme (1990) C2-C5 hydrocarbons in rural south Norway. Atmospheric Environment, 24A, 2889-2890.

Schmidbauer, N. and M.Oehme (1986) Improvement of a cryogenic preconcentration unit for C2-C5 hydrocarbons in ambient air at ppt levels. J. High Res. Chromatogr. & Chromatogr. Commun., 9, 502-505.

Hov, Ø., T. Krognes, and F. Stordal (1992) Measurments of ozone and precursors at Ny-Ålesund on Svalbard and Birkenes on the south coast of Norway, ozone profiles at Bjørnøya, and interpretation of measured concentrations, 1991. EUROTRAC Annual Report 1991, Part 9 TOR,International Scientific Secretariat, Garmisch Partenkirchen, in press.

Isaksen, I. S. A., Ø. Hov, S.A. Penkett, and A. Semb (1985) Model analysis of the measured concentration of organic gases in the Norwegian Arctic. J. of Atmos. Chem., 3, 3-27.

Iversen, T. (1989a) Some statistical properties of ground level air pollution at Norwegian Arctic stations and their relation to large scale atmospheric flow systems. Atm. Env., Vol. 23, No. 11, pp 2451-2462.

Iversen, T. (1989b) Numerical modelling of the longe range atmospheric transport of sulphur dioxide and particulate sulphate to the Arctic. Atm. Env., Vol. 23, No. 11, pp 2571-2596.

Rasmussen, R. A., M.A.K. Khalil, and R.J. Fox (1983) Altitudinal and temporal variation of hydrocarbons and other gaseous tracers of Arctic haze. Geophys. Res. Lett., 10, 144-147.

Rudolph, J., R. Koppmann, F.-J. Johnen, and J. Khedim (1989) The distribution of light nonmethane hydrocarbons in the troposphere and their potential impact on photochemical ozone formation. Ozone in the atmosphere, Proceedings of the quadrennial ozone symposium 1988 and tropospheric ozone workshop (ed. Bojkov, R. D., and P. Fabian), A. Deepak publishing, pp 561-564.

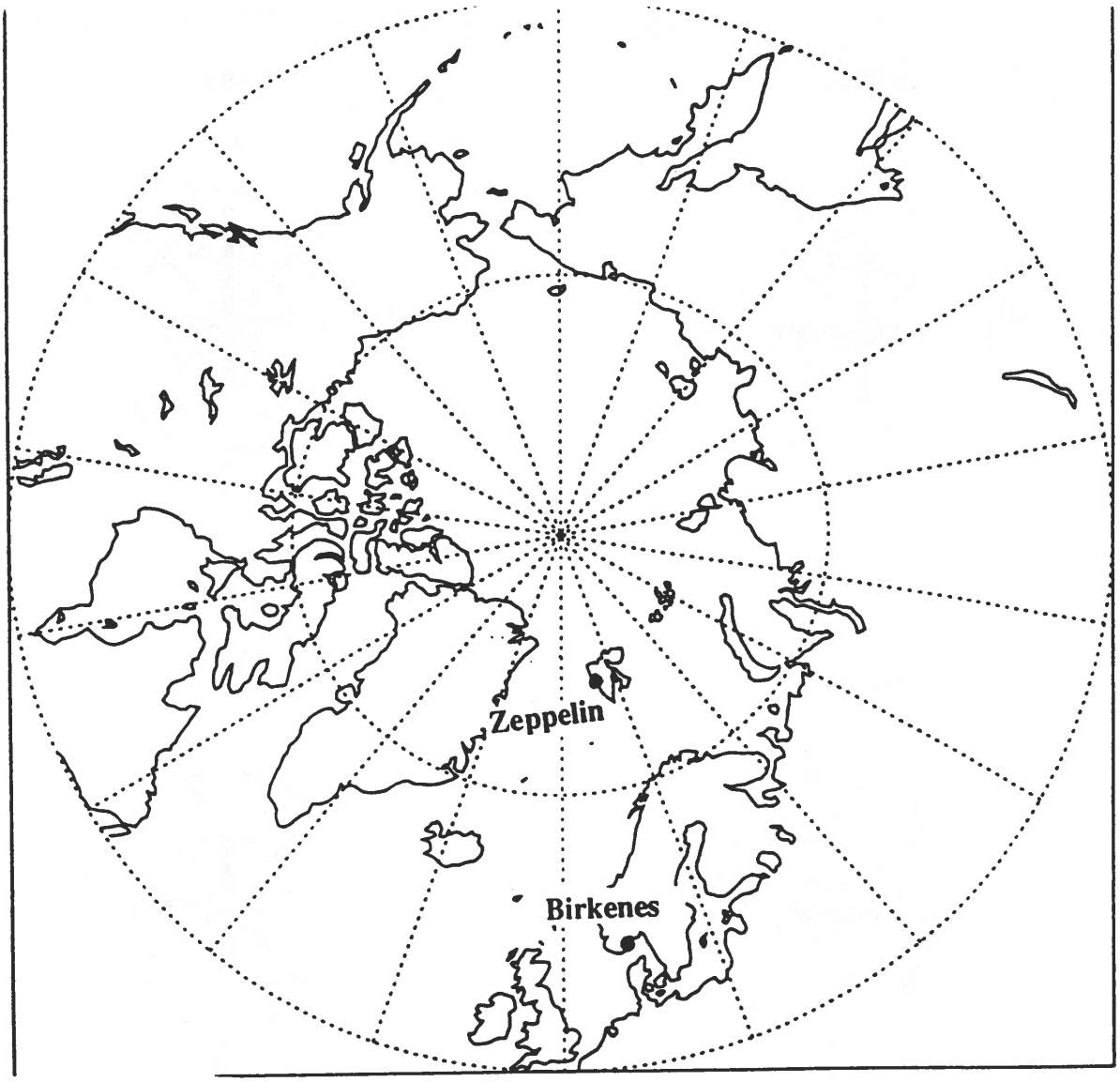

Fig. 1. Map showing the locations of the TOR stations Zeppelin Mountain and Birkenes.

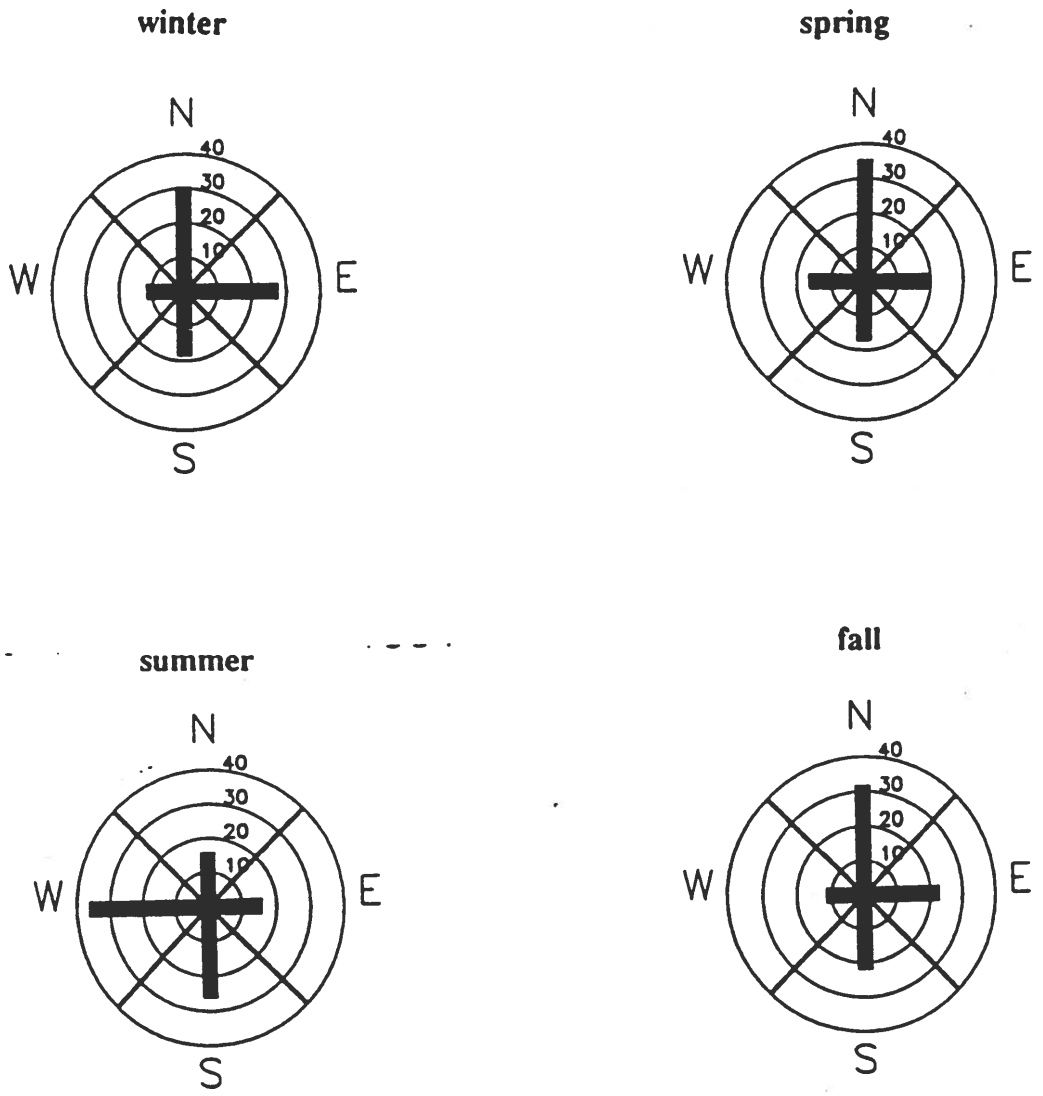

Fig. 2. Spatial distribution of trajectories arriving on the Zeppelin Mountain as per cent of the total number of trajectories for the winter (Dec-Feb), spring (Mar-May), summer (Jun-Aug), and the fall (Sep-Nov).

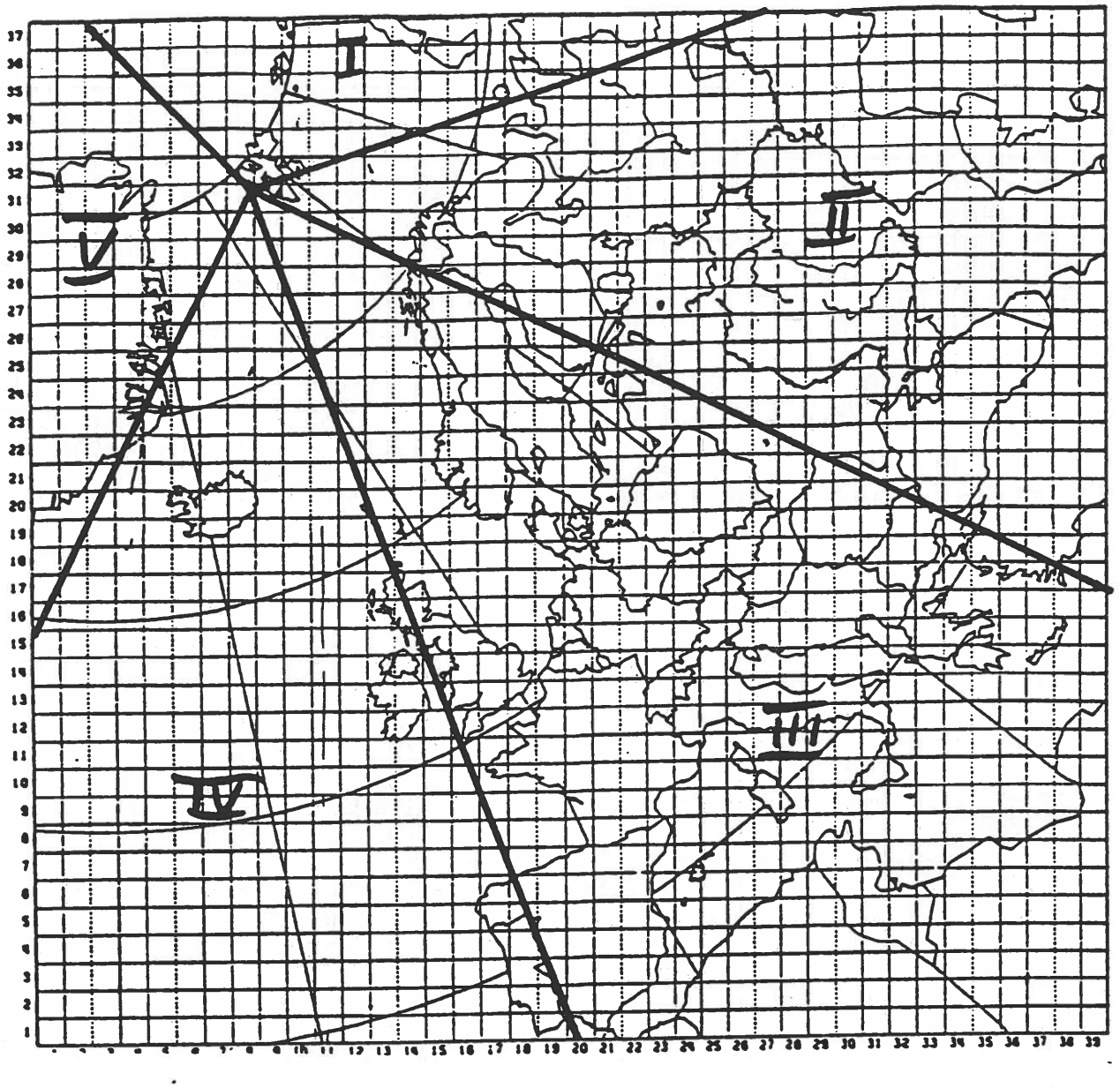

Fig. 3. Map showing the sector borders and the EMEP grid used in the transport calculations for the Zeppelin Mountain.

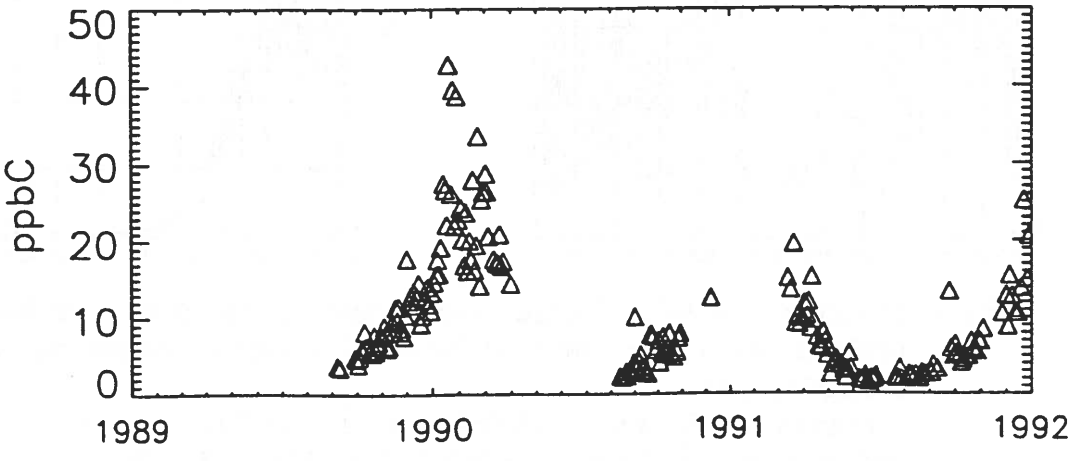

Fig. 4. The sum of the measured hydrocarbons on the Zeppelin Mountain in ppbC from the start in 1989 to the end of 1991.

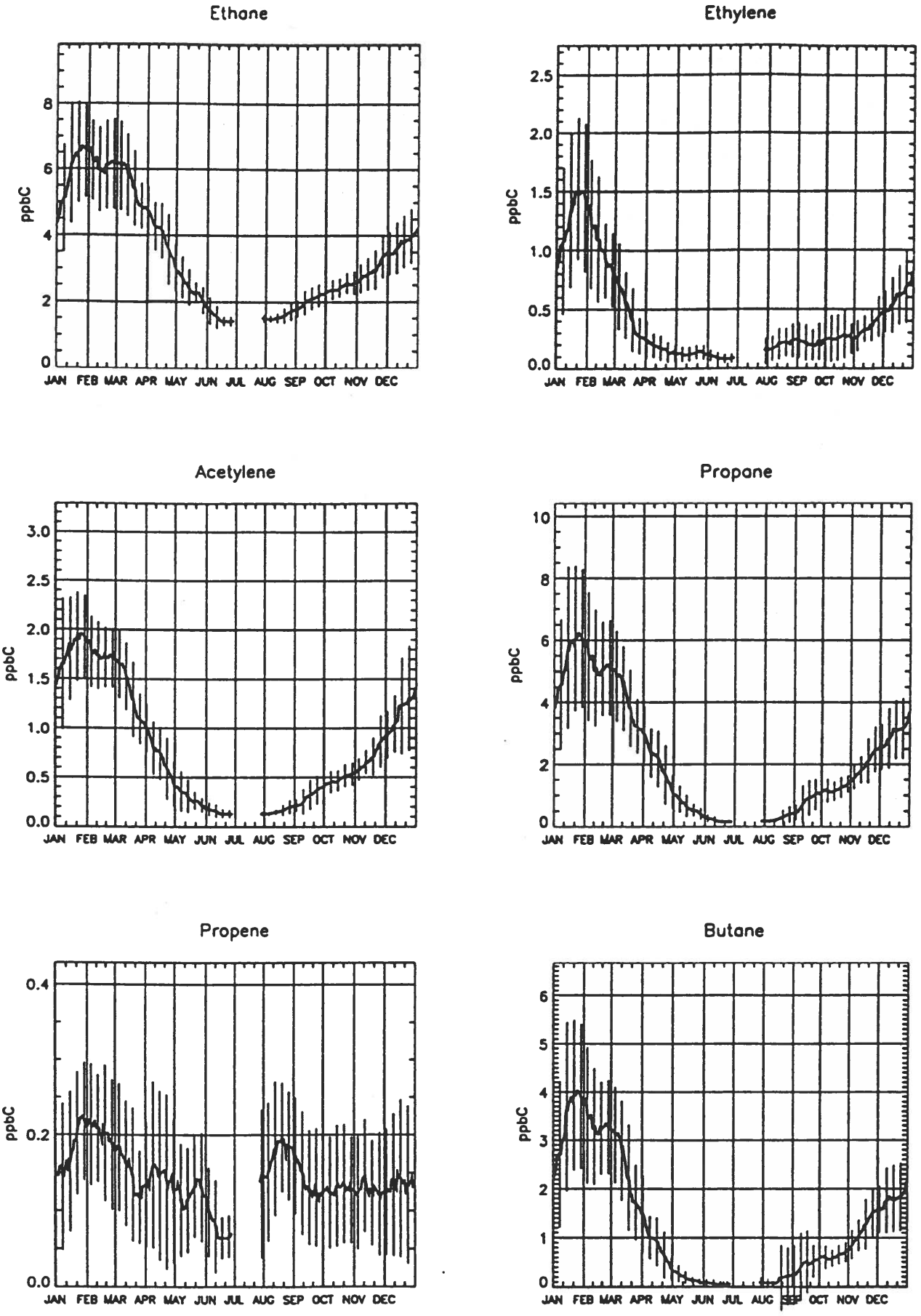

Fig. 5. The 30 days running average concentration and standard deviation for all data (1989 - 1991) in an annual cycle for individual hydrocarbons (ppbC) on the Zeppelin Mountain.

The average ($\overline{X}$) was calculated from : $\overline{X} = 1/N \Sigma x_i$, i=1, ..., N
and the st. dev. (σ) from : $\sigma^2 = 1/(N-1) \Sigma (x_i - \overline{X})^2$, i = 1, ..., N
where x_i are all the N observed values (1989 - 1991) in the +/-15 days period each date.

(The st. dev. bars are only plotted each week for clarity.)

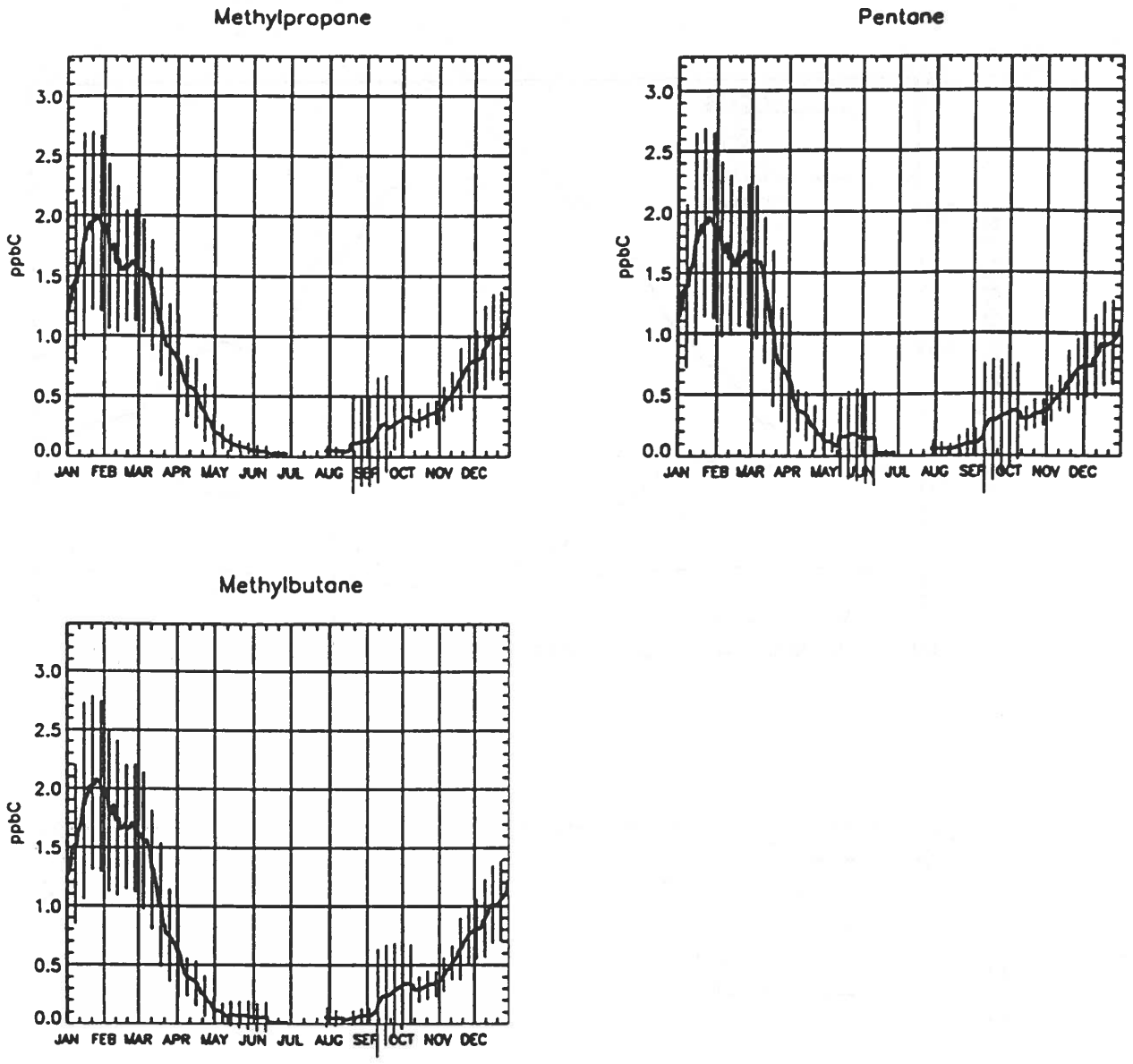

Fig. 6. Same as Fig. 5.

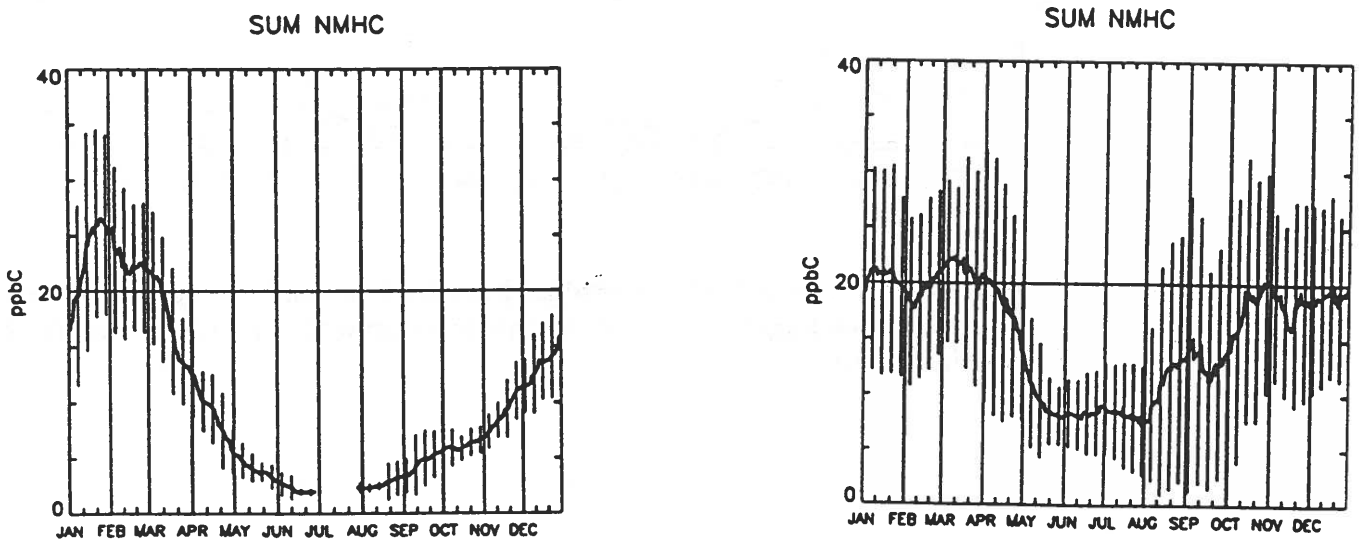

Fig. 7. The 30 days running average and standard deviation of the sum of the hydrocarbons in an annual cycle on the Zeppelin Mountain (left) and at Birkenes (right). The average and st. dev. were calculated as explained in Fig.5 with data from 1989 - 1991 at the Zeppelin Mountain and from 1987 - 1991 at Birkenes.

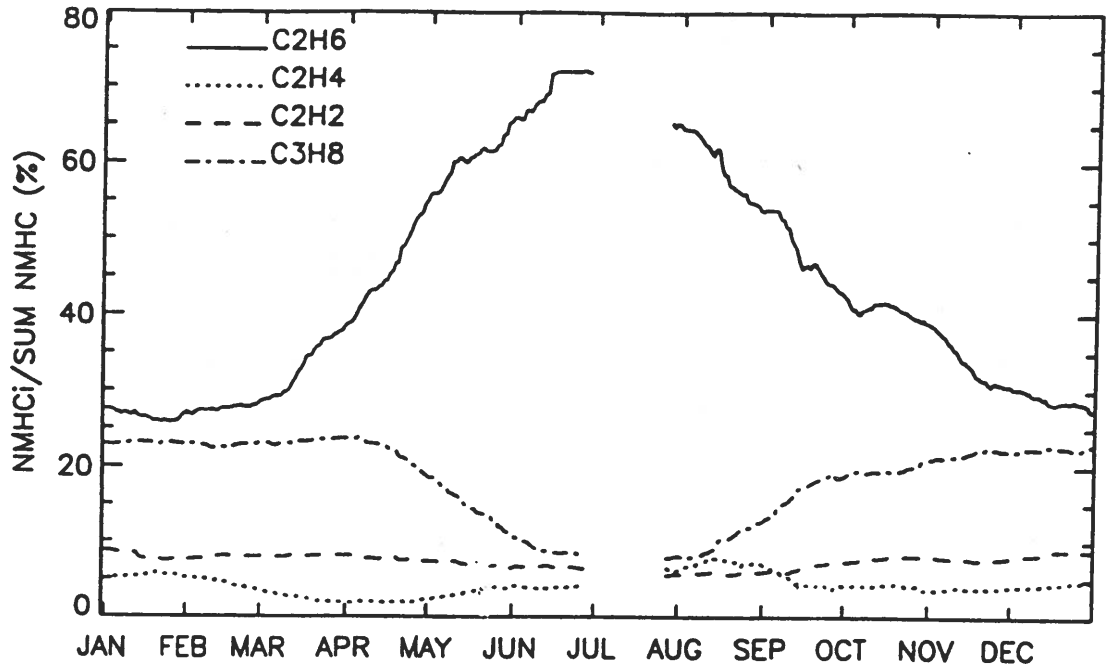

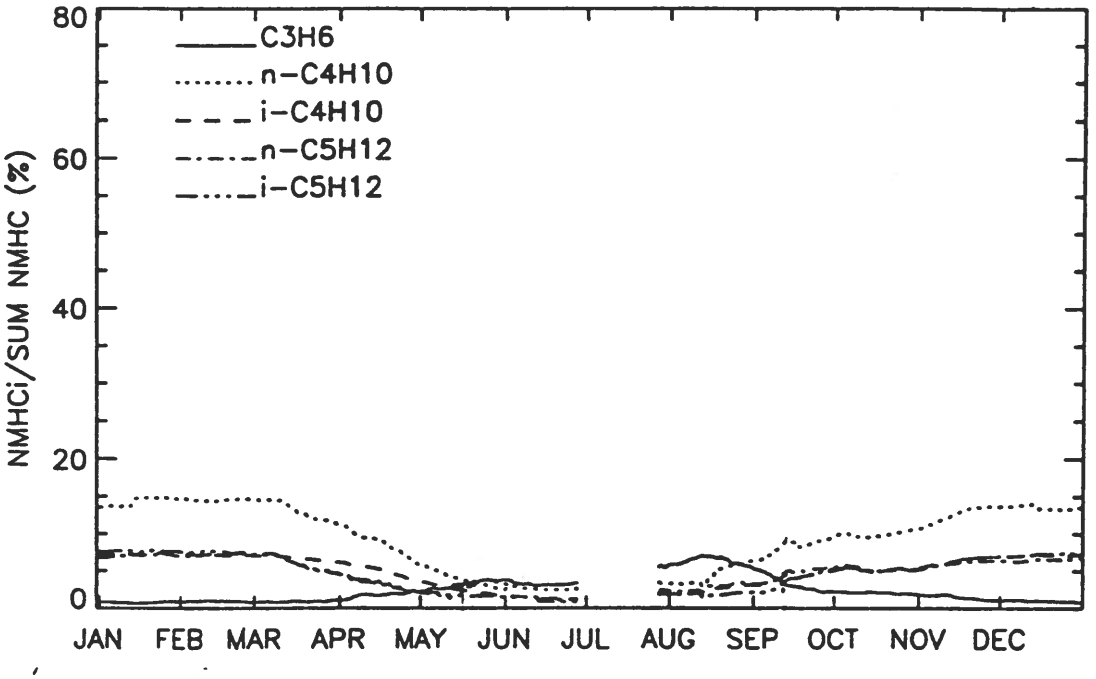

Fig. 8. The relative distribution of the individual hydrocarbons on the Zeppelin Mountain as per cent (on a ppbC basis) of the sum in an annual cycle (data from 1989 - 1991 are included).

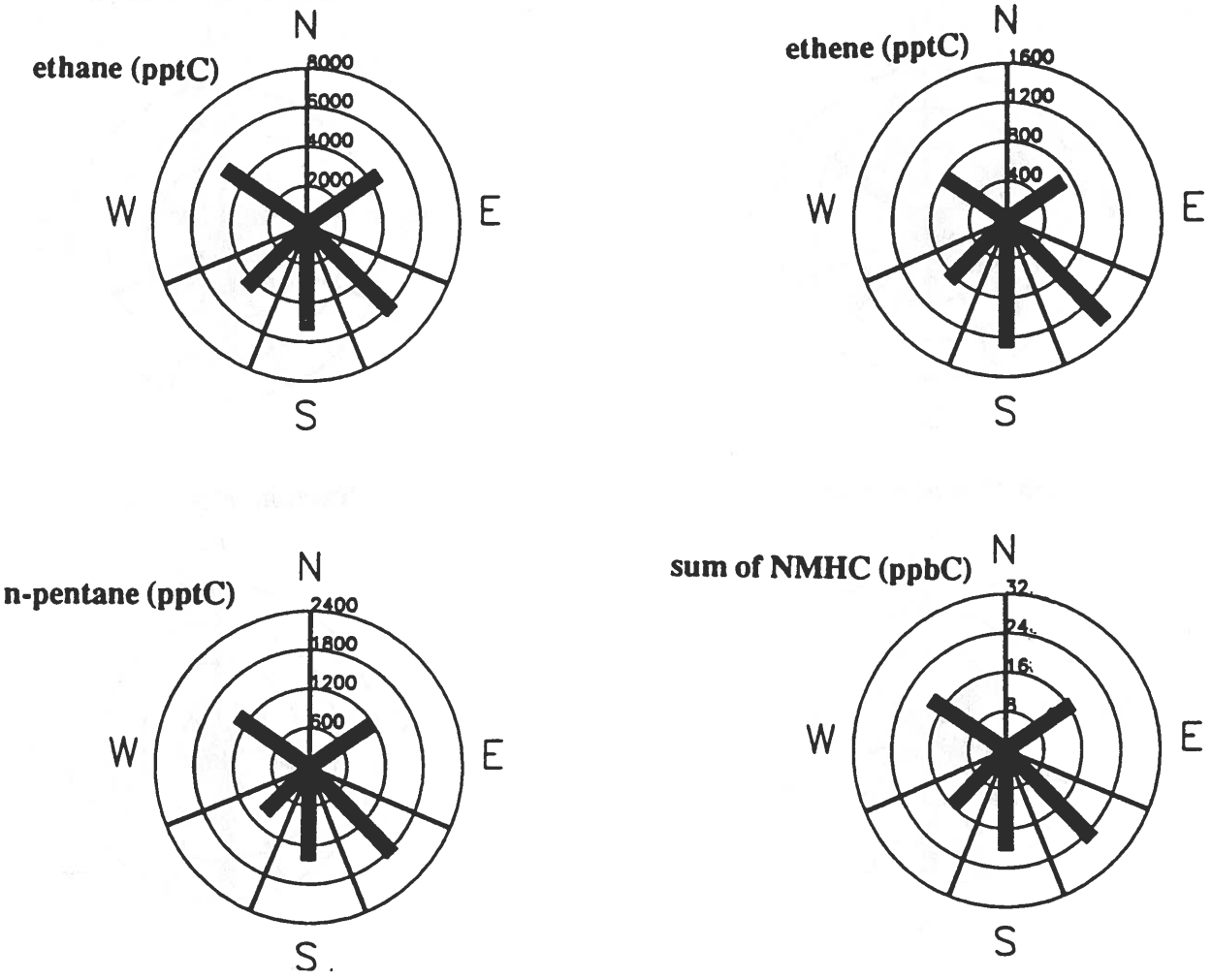

Fig. 9. The average sector concentrations in the time period from 15. November to 15. March during the years 1989 - 1991 on the Zeppelin Mountain for ethane (pptC), ethene (pptC), n-pentane (pptC), and the sum of all the inividual hydrocarbons (ppbC).

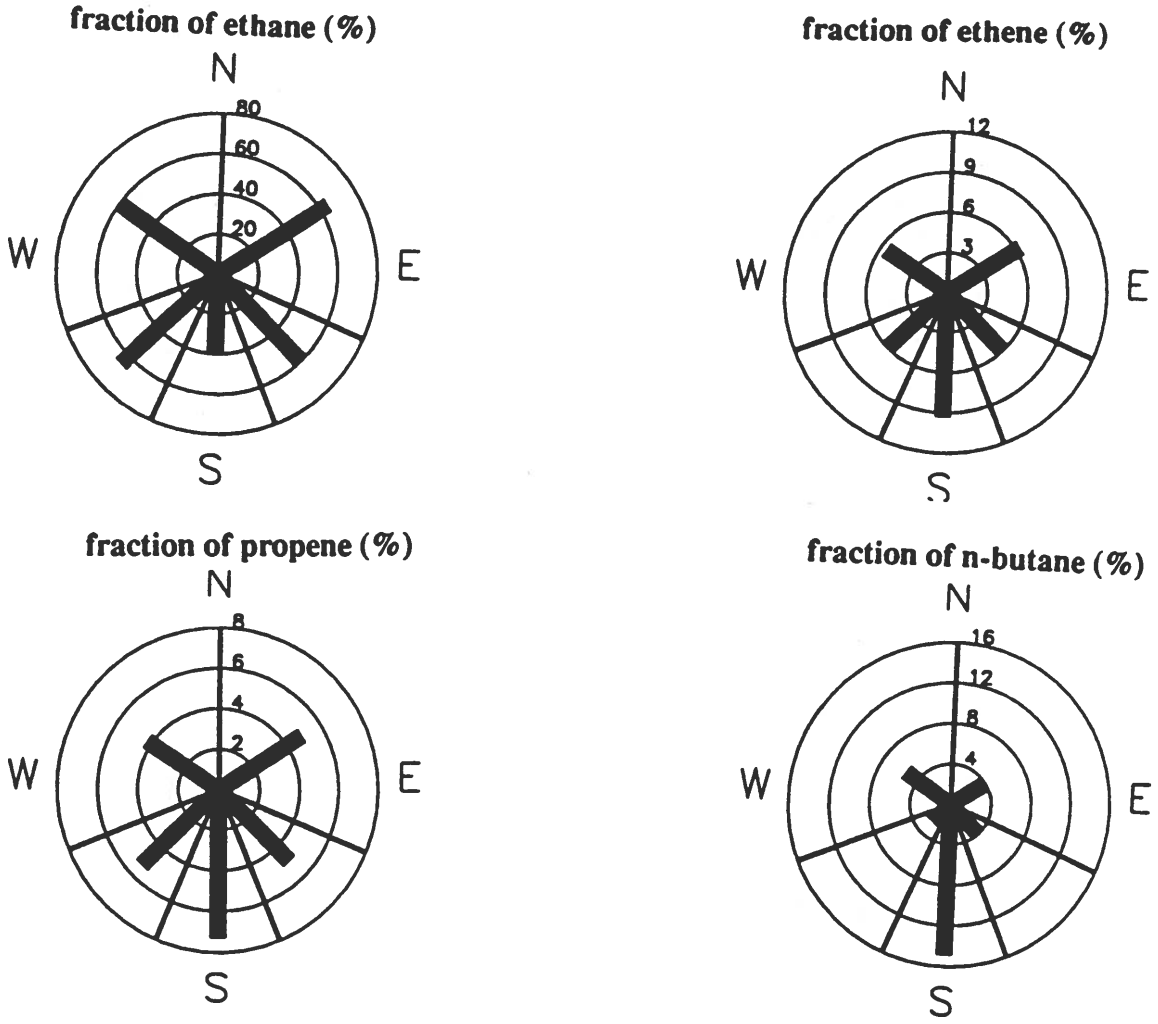

Fig. 10. The average fraction of individual NMHCs relative to the sum of all nine components in each sector (in %) for the time period 15. May to 15. September during the years 1989 - 1991, on the Zeppelin Mountain for ethane, ethene, propene and n-butane.

Abstract for the Fifth Symposium on Arctic Air Chemistry
Copenhagen, September 8-10, 1992

Measurements of Carbon Dioxide, Methane, and Carbon Monoxide in the Alaskan Arctic, March - April, 1992

T.J. Conway and P.M. Lang
NOAA Climate Monitoring and Diagnostics Laboratory,
325 Broadway, Boulder, CO 80303

E. J. Dlugokencky and P. C. Novelli
Cooperative Institute for Research in Environmental Sciences,
University of Colorado, Boulder, CO 80309

As part of the LEADEX/AGASP IV project conducted during March-April 1992, samples of dry air were collected in 0.5 L glass flasks on 7 flights of the NOAA WP-3D Orion aircraft. The flights enabled sampling in the boundary layer, the free troposphere, and the lower stratosphere in the Alaskan Arctic. The samples were returned to the NOAA/CMDL laboratories in Boulder, CO where mixing ratios of CO_2, CH_4, and CO were measured. The methods and relative analytical uncertainties for CO_2, CH_4, and CO are: nondispersive infrared, 0.1%; gas chromatography with flame ionization detection, 0.2%; and gas chromatography with HgO reduction/resonance absorption detection, 1%.

Samples collected in vertical profiles show that the mixing ratios of all three gases generally decreased with increasing altitude. However, on several occasions elevated mixing ratios were found aloft, usually in layers containing elevated aerosol concentrations. The previous three AGASP missions have shown that the elevated aerosol concentrations are due to long range transport of anthropogenic emissions from lower latitudes. The variations in the mixing ratios of CO_2, CH_4, and CO show significant correlation. A linear regression of CH_4 vs. CO_2 for all samples gives a slope of 13.6 ppb CH_4 / ppm CO_2 ($n = 212$, $\sigma = 0.2$, $r^2 = 0.85$). For CO vs. CO_2 the linear regression slope is 12.0 ppb CO / ppm CO_2 ($n = 212$, $\sigma = 0.3$, $r^2 = 0.74$). These results are consistent with those from AGASP II and AGASP III, in situ surface measurements at Barrow, and flask measurements at Arctic sites.

AEROSOL MEASUREMENTS OVER THE EAST SIBERIAN SEA

A.D.A. Hansen [1], A.V. Polissar [2] and R.C. Schnell [3]

(1) Lawrence Berkeley Laboratory, University of California
(2) Institute of Atmospheric Physics, Russian Academy of Sciences
(3) Mauna Loa Observatory, NOAA/CMDL

Abstract

In April 1992 we performed measurements of aerosol species aboard an aircraft flying over the East Siberian Sea from Cherskiy (69°N, 161°E) to Bennett Island (76.5°N, 149°E). Eight round-trip flights were made over this 1000 kilometer path, with each flight incorporating several profiling descents from approximately 4.2 km altitude to the surface. On a 10-second timebase we recorded measurements of aerosol black carbon, condensation nuclei, air temperature and absolute barometric pressure, from which the altitude was deduced. Some profiles showed considerable vertical structure with numerous temperature inversions and stratified aerosol layers. Peak concentrations exceeded 1000 ng m^{-3} of aerosol black carbon and 1000 cm^{-3} of condensation nuclei. Occasionally, extremely clean air was found in some layers. Other descents showed almost constant temperature profiles, with aerosol black carbon and condensation nuclei well-mixed throughout the lower 4 km of the atmosphere. In most cases, the surface temperature-inversion layer showed high concentrations of aerosol species. We conclude that the atmosphere in this remote area is strongly affected by anthropogenic emissions from distant source regions, and that the meteorological and aerosol concentration profile structures were similar to those regularly observed in the western sectors of the Arctic in springtime.

1. INTRODUCTION

The phenomenon of Arctic Haze has been extensively studied in the Western sectors of the Arctic (e.g. Rahn and McCaffrey, 1980; Schnell, 1984; Albritton, 1989). In the late winter and spring months, anthropogenic emissions are transported into the north polar airmass and accumulate, reaching concentrations that are comparable to those measured in U.S. cities. Aircraft studies showed that the concentrations of these species are highly stratified in layers, whose air temperatures may show numerous transitions, in addition to the usual surface temperature inversion. The concentrations of pollutants may be an order of magnitude greater in a layer at an altitude of a few hundred meters than in the surface atmosphere. Thus, aircraft studies are essential to determine the overall atmospheric burden of these species, in addition to providing geographic coverage. Surface measurements are routinely made at the NOAA/CMDL observatory at Barrow, Alaska; at Alert, Canada; at Ny Alesund, Spitzbergen; and at other locations at lower latitudes. Starting in 1988, aerosol samples have been collected at the Ushakovskoye Polar Station on Wrangel Island, Russia (71°N, 178°W) (Hansen et al., 1991): however, relatively few other results have been reported from ground stations in the Eastern sector of the Arctic, and no work has been reported from aircraft studies in this area.

In April 1992, an aircraft mission was organized to collect gas and aerosol samples from the vicinity of Bennett Island (76.5°N, 149°E) in the New Siberian Islands group. Unexplained plumes of unknown origin and composition arising from the vicinity of Bennett Island have been observed on satellite photographs for a number of years (Kienle et al., 1983; Matson, 1986). One explanation hypothesized that these plumes were due to the release of methane from hydrate deposits in the shallow ocean floor. The results of the analysis of these samples, and further discussion of the plume phenomenon, are reported in another article (Schnell et al., 1992). The aircraft used in this work was based at Cherskiy, on the north coast of Russia, and the necessary 1000 km transit flight provided the opportunity to perform aerosol studies in the same program. These measurements paralleled similar studies in the fourth Arctic Gas and Aerosol Sampling Program (AGASP-IV), based in Anchorage, Alaska and working in an area north of Barrow, Alaska.

2. EXPERIMENTAL DETAILS

The measurements were performed from a Russian "Antonov-26". This is a twin-turboprop aircraft with an airspeed of from 350 to 440 km/h (approximately 100 to 120 m/s), an operational ceiling of approximately 6 km altitude, and a load capacity of 4 to 5 tons. The particular aircraft that we used was modified for long-range work by the addition of extra fuel tanks, allowing for flights of 8 to 10 hours' duration with adequate reserves. This aircraft is routinely used for air supply and reconnaissance in the Arctic. It does not require heated hangaring, and is normally operated from a cold soak at the prevailing ambient temperature (down to -30°C in the period of this program). Thus, scientific equipment installed on the aircraft must either be able to withstand these temperatures, or must be removed at the end of each flight. It was not possible to interface the aircraft navigational systems to the data acquisition system in the instrument package, and so the latitude and longitude were recorded manually and subsequently transcribed. Altitude aboard the aircraft was deduced from a barometric pressure sensor. The equipment package included a similar sensor whose output was continuously recorded, and the altitude recording was constructed by intercomparison.

The air inlet to the aerosol measurement package was constructed from a length of stainless steel tubing of inside diameter 0.75" (1.9 cm), bent in a smooth S-curve and passing through a plate inserted in the window opening of the forward passenger door. The centerline of the inlet probe was approximately 15 cm from the aircraft fuselage. This was the maximum extension possible that also allowed the door to open. Inboard, the steel probe tube was connected to the aerosol instrument package by a length of 0.875" ID polypropylene tubing. The instrument rack was located in the forward cabin as close to the door as was practical. Aerosol sampling was therefore sub-isokinetic, leading to a possible artifact over-sampling of particles of large aerodynamic diameter. However, in this remote region, we did not anticipate large concentrations of large particles. At the side of the inlet probe tip, a thermistor sensor was attached to measure the ambient air temperature. An additional inlet of 0.375" diameter stainless steel tubing was connected to the trace-gas system that compressed the samples into glass and stainless steel flasks for subsequent analysis.

The aerosol equipment package consisted of an Aethalometer to measure the concentration of aerosol black carbon, a nephelometer to measure optical scattering, and a condensation nucleus counter (CN). The thermistor sensor was connected to a linearizing circuit to give an output voltage proportional to the external ambient temperature. The Aethalometer and the condensation nucleus counter both used positive-displacement pumps to draw sample air: the Aethalometer flowrate varied from approximately 30

SLPM at high altitudes to 65 SLPM at low altitudes, and was continuously measured with a mass flow meter. The nephelometer was connected directly to the air sample tube, and was aspirated at its outlet by a fan. Thus, the entire system had to operate at (or close to) ambient pressure, limiting our measurements to an operational maximum altitude of approximately 5 km.

During measurements, the aircraft pressurization system was set to zero pressure boost, and a vent (designed for emergency depressurization) was opened to the outside atmosphere. At constant airspeed, the cabin pressure maintained a fixed differential with respect to the true external pressure due to the forward velocity of the aircraft. The fact that the aerosol inlet probe was sub-isokinetic insured that ram pressure would provide sufficient pressure boost to cause a slight positive pressure and hence a large airflow through the very small flow resistance of the nephelometer and aspirating fan. The fan exhaust was vented through a port on the side of the equipment rack, and it was easy to check at all times that a large positive airflow was maintained through the system. The Aethalometer and condensation nuclei counter inputs were connected to the inlet tube by shallow-angle catheter probes. These were thermostatically heated to insure that those instruments would not be affected by large changes in ambient air temperature, and also so that the sample streams would be warmer than the -30°C ambient temperatures. A barometric pressure sensor was mounted in the equipment rack to measure cabin pressure. The airspeed-induced cabin pressure offset was determined by comparing its output with the aircraft's external barometric pressure sensor. We observed that the aerosol system's pressure sensor was able to accurately reproduce the true barometric pressure, enabling us to use its output as an altitude indicator.

Data from the instruments was recorded by a portable computer equipped with a 16-bit analog-digital converter. The computer controlled the cyclic functioning of the Aethalometer, and a multiplexer allowed for the acquisition of signals from the nephelometer, condensation nucleus counter, temperature and pressure sensors. Data was acquired continuously, and averaged over a 10-second timebase. The data was recorded on magnetic disk, and also printed out as a backup. The entire package operated from the 27-volt DC power available on the aircraft, with low-voltage pumps, DC-DC converters and DC-AC inverters to power the equipment. Total current consumption was approximately 30 amperes, well within the limit available from an auxiliary power circuit on the aircraft. The equipment package was mounted in a single steel rack cabinet. By request, hot air was blown onto the cabinet for an hour or two prior to each flight to raise the temperature of the pumps and equipment from the overnight cold soak at -10°C to -30°C before applying power. Nevertheless, it was our experience that the equipment required up to an hour of power-on time before stabilizing and working satisfactorily.

3. FLIGHT PROFILES

Figure 1 shows a map of the project area: the flight track indicates the usual locations of aerosol measurement regions. The research flights typically departed Cherskiy at 11 am local time, i.e. 2300 Z of the previous standard calendar day. The flight plan was a straight vector to the north-west in the direction of Bennett Island. This path passed over no significant habitation in the short distance to the coast, and there were very few local aerosol sources other than the town of Cherskiy. The first portion of the flight was a climb to 4-5 km altitude followed by the start of the first slow outbound descent profile, at which point aerosol measurements were started. We do not believe that any of the data were affected by local emissions. Each profile was maintained at a constant airspeed of 360 km/h with a 1 m/s rate of descent. When the lowest altitude of 100 m was reached, the aircraft flew level for 5 minutes before climbing back to the top for the second descent. By the end of the second straight descent profile, we were approaching Bennett Island. The aircraft then climbed to an altitude specified for observation of Bennett, and performed a slow spiral descent around the island at the same airspeed and vertical velocity as before. When a low altitude was reached, it was usual to spend some considerable time collecting gas samples over the ice pack, over the island, and over any open water. The aerosol system collected data at 100 m altitude for this period, and this was combined with the data from the spiral descent. When we had completed the gas sample collection, the aircraft climbed again rapidly to the top of the first inbound descent profile. Two such profiles could be made on the inbound transit before reaching the coast and the approach to Cherskiy. Each flight therefore usually yielded five profiles: one over and around Bennett Island, and two pairs along the flight track at comparable geographic locations, although separated in time by several hours. On some flights this plan was changed, but we were able to collect data over 33 profiles in this region between the surface and a maximum altitude of 4 to 5 km in the program period of 16 days.

4. RESULTS

We report on data from the air temperature sensor (T), the condensation nucleus counter (CN), and the Aethalometer measuring aerosol black carbon (BC). These three quantities are studied as a function of barometric pressure (P, from which altitude may be deduced) and geographic location along the flight tracks. Unfortunately, a technical malfunction that could not be repaired in the field prevented the nephelometer from operating satisfactorily, and very little valid data was obtained.

4.1 Temperature Profiles:

The temperature profiles usually fell into four categories:

(1), a surface inversion of delta-T approximately 5°C at pressure levels of 950 to 1000 mb;
(2), one or more strong inversions (delta-T from 7°C to 12°C) at higher levels up to 800 mb pressure;
(3), a mixed temperature profile showing very little decrease from 950 to 750 mb; and
(4), a complex vertical structure showing many smaller inversions at a number of altitudes.

Examples of these four categories are shown in Figures 2(a)-(d).

4.2 Aerosol Profiles:

The aerosol profiles showed a wide degree of variability, but displayed high concentrations of CN and BC. Layers of 'clean' air were sometimes detected, in which these levels were low. However, in the vast majority of profiles the Arctic air was distinctly polluted throughout the column from ground level to the 5-km operational ceiling. Examples of different categories of vertical profiles of T, CN and BC are shown in Figures 3 through 6.

4.2.1 Well Mixed Column. Figure 3 shows an example of a situation in which the vertical column is almost uniformly polluted from ground level to 5 km altitude. The CN count varied only a little, from approximately 250 to 400 cm^{-3}. The BC concentration showed lower concentrations near the surface, with values down to 150 ng m^{-3} in the surface temperature inversion layer that was capped at the 960 mb level. BC values then ranged from 300 to 600 ng m^{-3} from this level up to the top of the profile. The temperature profile shows an inversion at 840 mb, which was reflected in a change in BC concentration but not at all in the CN record. The BC data may be interpreted as showing the presence of as many as eight superimposed polluted layers, from 1000 to 720 mb pressure. The many small (but distinct) peaks in the CN record may indicate even finer vertical structure. Note that the values of the BC and CN data were not unusually high, but that their constancy throughout the vertical column implies a large total atmospheric burden.

4.2.2 Polluted Layer Aloft. Figure 4 shows two profiles through an airmass that displayed relatively clean air at lower altitudes, but substantially polluted air aloft. Figures 4(a), 4(b) and 4(c) show the T, CN and BC profiles for the second vertical sounding on the outbound transit on 15 April 1992. Figures 4(d), 4(e) and 4(f) show the corresponding data for the first profile of the return trip (i.e. in the same general geographic area), taken 200 minutes later. The aerosol data show relatively low concentrations below the 840 mb level, with a substantial increase above that level up to the top of the profile. Aerosol BC increases from 100-200 ng m^{-3} below, to 800-1000 ng m^{-3} above 850 mb. The CN count varies by a factor of two to three between these two regimes. The situation is one in which a thick layer of heavily polluted air overlies a deep surface layer of relatively clean air. Note in Figure 4(d) that a small temperature inversion is displayed at the 930 mb level, and is reflected in Figure 4(f) in a small peak in the BC data at that altitude. This may suggest that an intrusion of a low-level layer of polluted air had occurred by the time of sampling on the return journey. The peak BC concentrations observed at some 10,000 feet altitude - almost 1 microgram per cubic meter - exceeds the annual mean BC concentration for the city of Berkeley in the San Francisco, California metropolitan area.

4.2.3 Well Defined Layers. Figure 5 shows a situation in which there appear to be three or four distinct layers of different aerosol characteristics within the profile. The temperature profile, shown in Figure 5(a), shows two strong inversions separating the column into three portions: below the 970 mb level, from 970 to 900 mb, and above 900 mb. Closer examination shows a small inversion at 790 mb that is reflected in BC, but not in CN. Between the 900 and 790 mb levels BC concentrations are relatively high (from 300 to 400 ng m^{-3}), and the CN counts range from about 80 to 180 cm^{-3}. Above this altitude, BC concentrations are quite low, while the CN data show variations but no obvious general trend. From 900 to 970 mb, the CN counts are very low, as are the BC concentrations. From 970 mb to the surface, the CN counts are below detection while the BC data show a recovery to approximately 150-200 ng m^{-3}. This suggests that these overlaying air masses may have had distinctly different histories, as discussed below.

The lowest layer may be well-aged polluted air in which the remnants of soot remain, while the nuclei have coagulated and been greatly reduced. The second layer, from 970 to 900 mb, is cleaner with a few CN and little BC. The layer from 900 to 790 mb is a deep layer of moderately polluted air, typically 100 CN cm^{-3} and 350 ng m^{-3} BC. The uppermost layer, above 790 mb to the 5 km ceiling, shows similar levels of CN but very low values of BC. This layer might be, for example, a layer of clean marine air rapidly advected from lower latitudes. The temperature data show that the lower air masses are definitely not in equilibrium with a

'standard' mixed scenario, while the uppermost layer (above the 790 mb level) conforms more closely to the adiabatic lapse rate.

4.2.4 Polluted Layer Near Surface. Figure 6 shows an observation of polluted air at the very surface, over the ice, 1000 km from the nearest significant habitation. This data represents about 100 minutes of observation starting with a descent from 5 km altitude near Zhanetta Island (approximately 200 km to the east of Bennett Island), followed by low-altitude flight to Genrietta Island and thence to Bennett. All three of these islands are completely uninhabited. The descent profile shows a fairly constant concentration of aerosol species, with small peaks in the BC data at the 880 and 790 mb levels, possibly mirrored in the CN data. The CN counts are moderate, at around 300 cm^{-3}, and the BC is generally low, at around 150 ng m^{-3}. The temperature profile shows a conventional adiabatic lapse with a surface inversion below about 1000 mb. The aerosol data do not show any correlation with the onset of the inversion, but they do show a large range of values at the lowest altitudes, represented by points almost on the x-axes of the plots. In this lowest surface layer, the air temperature showed a range of values from -21°C to-25°C, probably representing the variations due to flight over fast pack ice (colder air) or broken ice with leads (warmer air over open water). The CN count ranged from the upper-level median value of around 300 cm^{-3} to a maximum of more than 700 cm^{-3}: the BC concentrations ranged from 150 ng m^{-3} to almost 400 ng m^{-3}. Although these maximum values are not as great as those shown earlier for stronger haze layers (Figure 4, for example), the data show an example of a very shallow polluted layer right at the surface on the Arctic ice pack. The aircraft was flying at an altitude of approximately 100 m at this time, and we can estimate that this surface layer was probably no more than one to two hundred meters thick.

5. DISCUSSION

The results presented above illustrate the various categories of temperature and aerosol profiles that we observed on this project. In general, the Arctic atmosphere was distinctly polluted. Given the experience of the 'AGASP' programs and other programs in the Arctic, this fact is no longer surprising. However, we note that 'AGASP-IV', operating over the west Beaufort Sea at the same time as this work, encountered relatively little haze. The meteorological situation prevailing in the AGASP-IV study area frequently included an intrusion of marine air in a low-pressure system moving up from the Aleutian Islands through the Bering Strait, effectively displacing the 'haze front' to the north and east of the Alaskan Arctic. Thus, during this study

period, the atmosphere north of Siberia was representative of the Arctic Basin more frequently than the atmosphere north-east of the Brooks Range.

Cherskiy is close to the Arctic Ocean, and is rarely affected by Pacific marine air masses. This combination of geographical and meteorological attributes makes Cherskiy an attractive base from which to conduct studies of the Arctic atmosphere. Its northerly location (69°N, 700 km further north than Anchorage) means that an aircraft can be over the ocean ice pack in less than twenty minutes from take-off. This contrasts with the ferry flights of two hours in each direction required for an aircraft based at Anchorage. The management, crew and ground staff at the Cherskiy Air Base were extremely cooperative in supporting the goals of our mission, and have many years of experience of flying in the Arctic for air supply of polar stations and drifting ice stations. It is possible to telephone directly from Anchorage to Cherskiy, via dedicated lines across the Bering Strait connecting Alaska with Chukotka and Yakutia. In this way, a scheduled daily call informed us of conditions as seen by satellite over the Bennett Island area, and allowed for the coordination of sampling between the two aircraft programs.

A value of 300 ng m^{-3} of aerosol BC for the tropospheric column from sea level to 5 km altitude is representative of the data gathered during this project. This yields a total column burden of 1.5 mg m^{-2}. If deposited on the ice, the BC optical absorption cross-section of approximately 10 m^2 g^{-1} would lead to an optical absorption of 0.015 per deposition cycle. Aerosols in the Arctic are believed to have a lifetime on the order of two to four weeks, implying that this deposition cycle is repeated several times during the winter and spring 'Arctic Haze' season. The deposition of black carbon ("soot") to the ice surface may therefore lead to an accumulated absorption coefficient as high as 0.1 over the season. This is large enough to substantially perturb the surface albedo, and lead to an accelerated absorption of solar radiation when the sun rises in springtime. More accurate modeling is needed to determine whether this deposition of black aerosol onto the formerly-white snow and ice cover across the entire Arctic (one-sixth of the area of the planet) may lead to a forcing term for global climate change.

6. ACKNOWLEDGMENTS

We would like to thank all the members of the Cherskiy Aviation Authority, Yakutia-Sakha SSR, Russia, for their cooperation in this project. We particularly thank V.P. Ozernoi, Commander of Cherskiy Avia, and Captain V.A. Bogdan and the crew of aircraft 26030. We acknowledge the rapid and efficient work of the Cherskiy Aviation Technical Bureau in fabricating the aerosol inlet and installing the equipment on board the aircraft in less than two days. We thank all members of Cherskiy ground operations for making our stay pleasant and effective.

We thank the NOAA Working Group 8 coordinators, Mr. R. Etkins and Ms. R. Tatusko, for considerable assistance with planning, international arrangements and visas. We thank the pilots and staff of Bering Air, especially Ms. T. Horvath, for extra efforts in transporting us and the equipment between Nome, Alaska and Provideniya, Russia.

We thank the staff of the NOAA/NWS center in Anchorage, Alaska, for allowing us continuous access to the satellite images of the Bennett Island area, especially Robert Moore for developing custom programming that greatly facilitated the displays.

This work was supported by the NOAA, DOE, EPA, ONR, USGS, and NSF agencies of the U.S. Government, and also by Magee Scientific Company. One of the authors (ADAH) thanks the Lawrence Berkeley Laboratory for leave of absence to participate in this project.

7. REFERENCES

Albritton, D.L., 1989, "Arctic Haze Combined Issue", *J. Atmos. Chem.* **9**, 1, 2 & 3.

Hansen, A.D.A., V.N. Kapustin and A.V. Polissar, (1991) "Measurements of carbonaceous aerosols in the Eastern Arctic", *Izvestiya Akad. Nauk SSSR, Fizika Atmosfery i Okeana* **27**, 614-620. (in Russian)

Kienle, J., J.G. Roederer and G.E. Shaw, 1983, "Volcanic event in Soviet Arctic?", *EOS* **64** (20), 377.

Matson, M., 1986, "Large plume events in the Soviet Arctic", *EOS* **27** (48), 1372-1373.

Rahn. K.A., and McCaffrey, R.J., 1980, "On the origin and transport of the winter Arctic aerosol", *Ann. N.Y. Acad. Sci.* **338**, 486-503.

Schnell, R.C., 1984, "Arctic haze and the Arctic Gas and Aerosol Sampling Program (AGASP)", *Geophys. Res. Lett.* **11** (entire issue).

Schnell, R.C., A.D.A. Hansen, E. Dlugokency, T.J. Conway, A.V. Polissar and G.S. Golitsyn, 1992, "Airborne investigation of the Bennett Island Plume", *proc.* 5th Symposium on Arctic Air Chemistry Copenhagen, Denmark, Sept. 8-10, 1992.

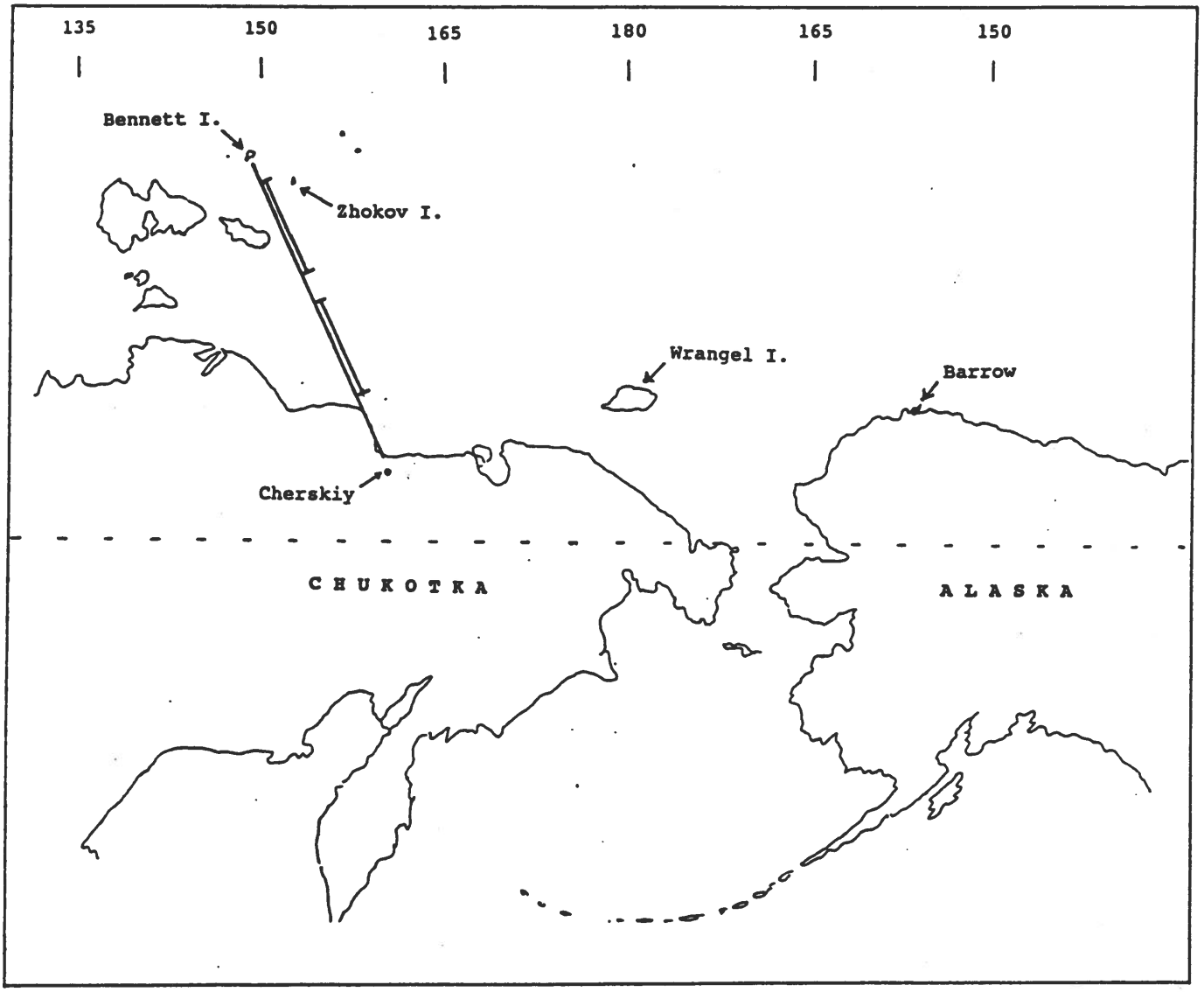

Figure 1:

Outline map showing the study area. The approximate locations of the aerosol sampling profiles are indicated along the flight paths.

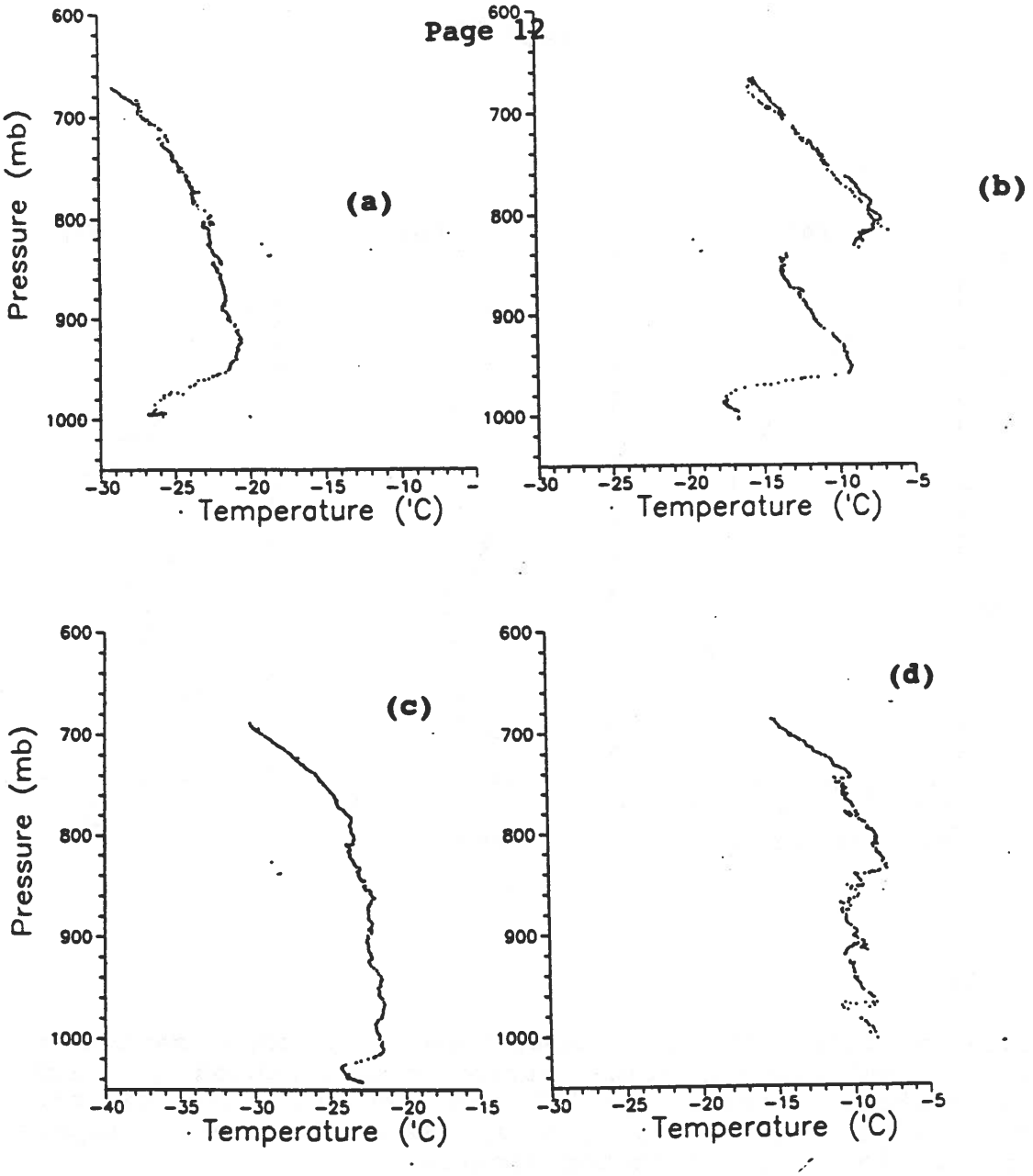

Figure 2:

Examples of air temperature profiles observed over the East Siberian Sea.

(a): surface temperature inversion, stable lapsing profile above. Flight 7, 16 April 1992, first outbound descent profile.

(b): two strong temperature inversions: one near the surface (960-980 mb level), the other at a higher altitude (810-830 mb level). Flight 5, 11/12 April 1992, first outbound descent profile.

(c): mixed-layer temperature profile showing a weak inversion close to the surface, and very little temperature change between the 1010 and 780 mb levels. Flight 3, 8 April 1992, first inbound descent profile.

(d): complex vertical structure showing a number of minor inversions superimposed on a generally unstable, mixed profile: Flight 5, 12 April 1992, second inbound descent profile. Up to eight small inversions may be counted.

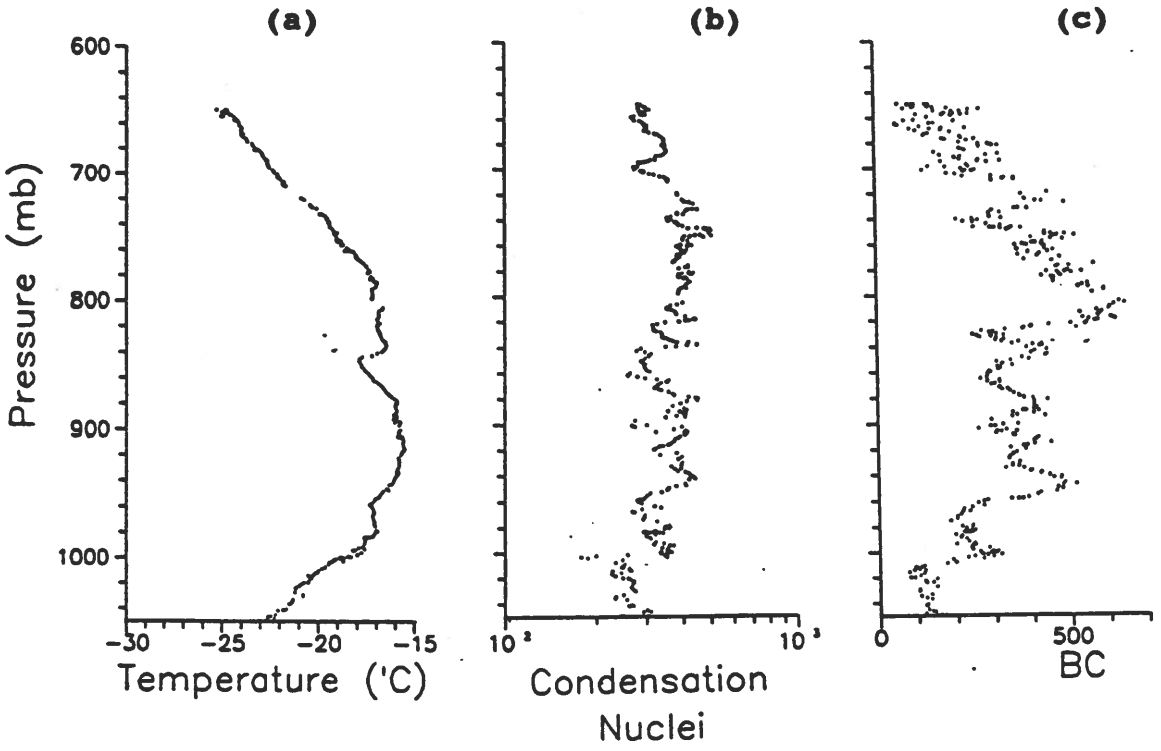

Figure 3:

Vertical profiles of air temperature (a), condensation nuclei count (b) and aerosol black carbon concentration (c) for the second outbound descent profile in the vicinity of the New Siberian Islands, flight 4, 10 April 1992. Up to eight layers may be apparent in the black carbon profile.

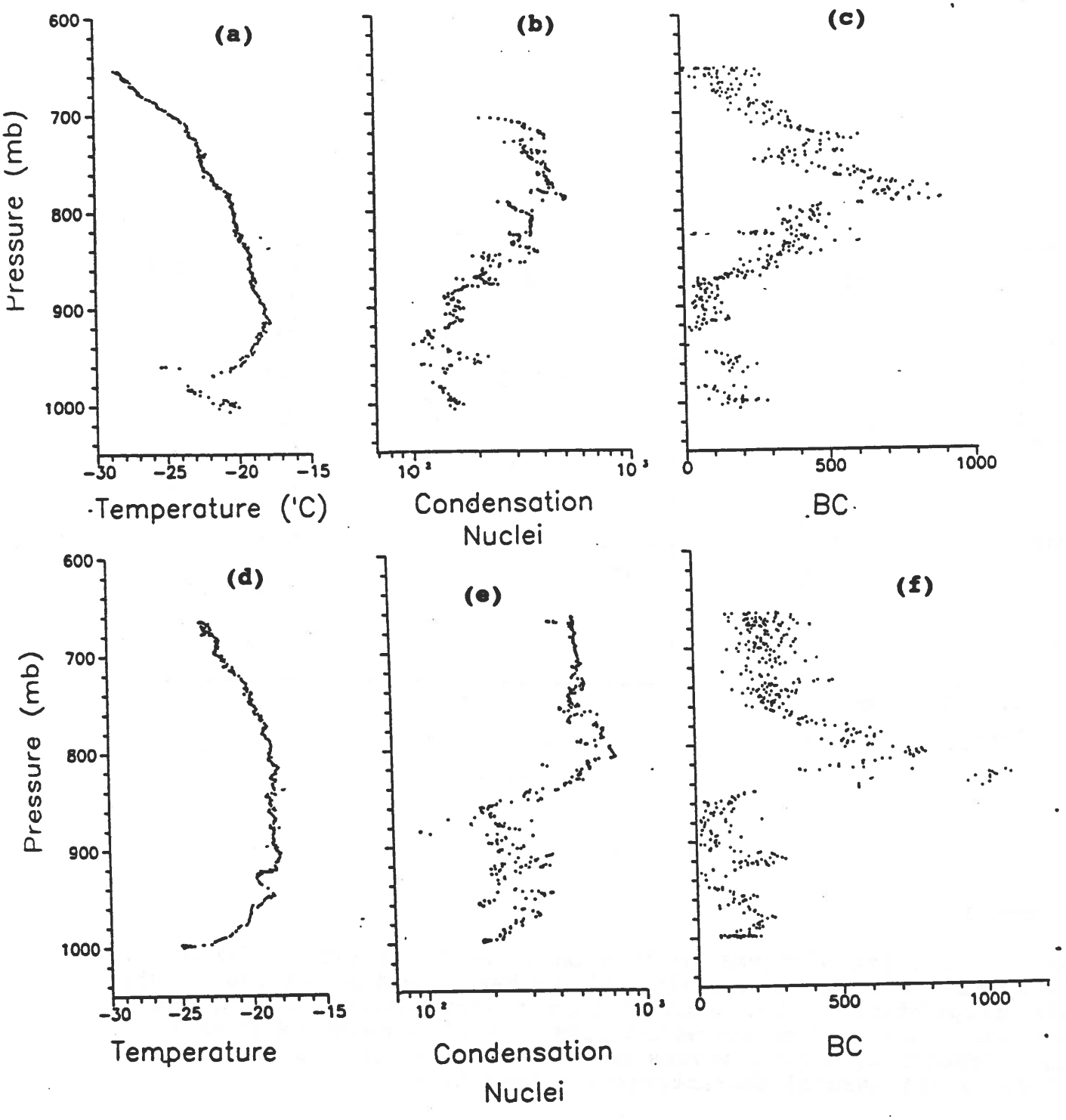

Figure 4:

Two profiles through an air mass exhibiting substantial pollution aloft, taken in the same region (appx. 74°N, 152°E) but separated in time by about 3 hours.

The first three panels (a, b, c) are data from the second outbound vertical profile of flight 6 starting at 01:25 Z on 15 April 1992,

The second three panels (d, e, f) are data from the first vertical profile of the inbound transit starting at 04:43 Z on the same day.

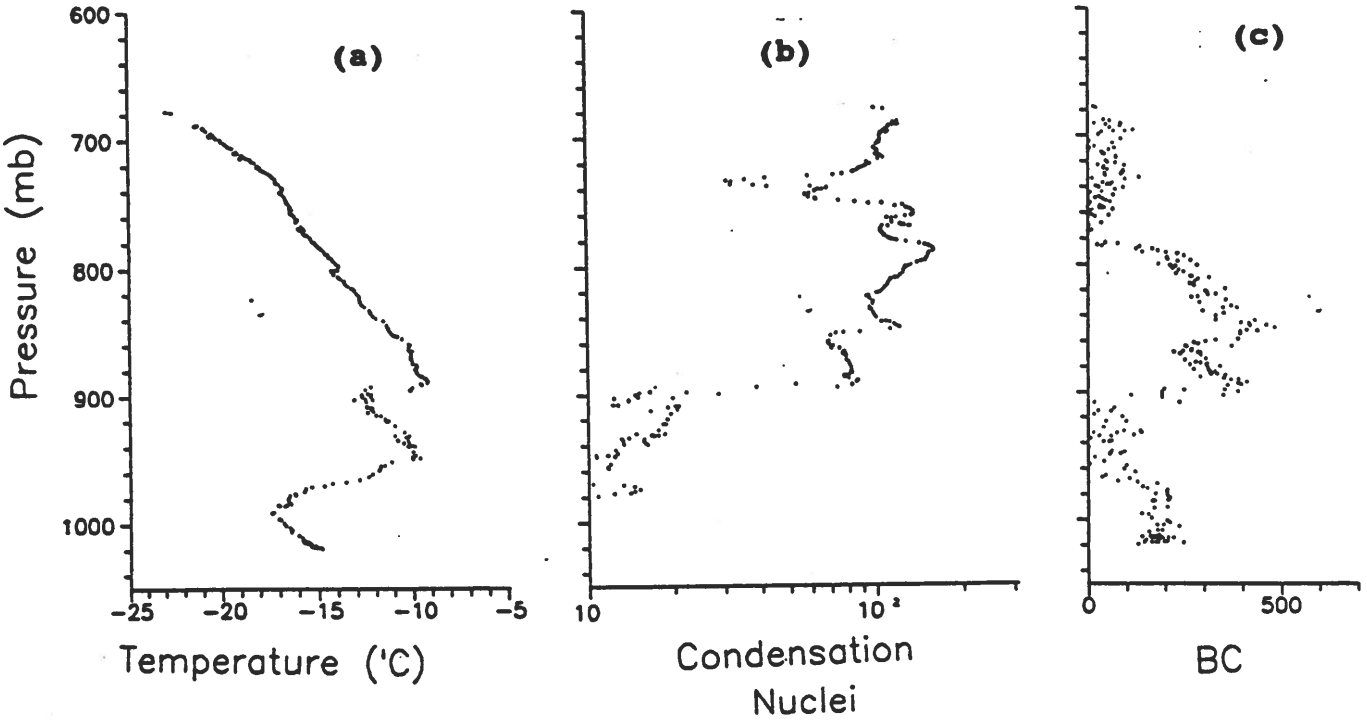

Figure 5:

Data from first vertical profile on inbound transit on flight 5, 12 April 1992, in the vicinity of the New Siberian Islands. (a), air temperature; 5(b), condensation nuclei concentrations; (c), aerosol black carbon concentrations. The temperature data show the presence of strong inversions which appear to separate layers of different aerosol characteristics (see text).

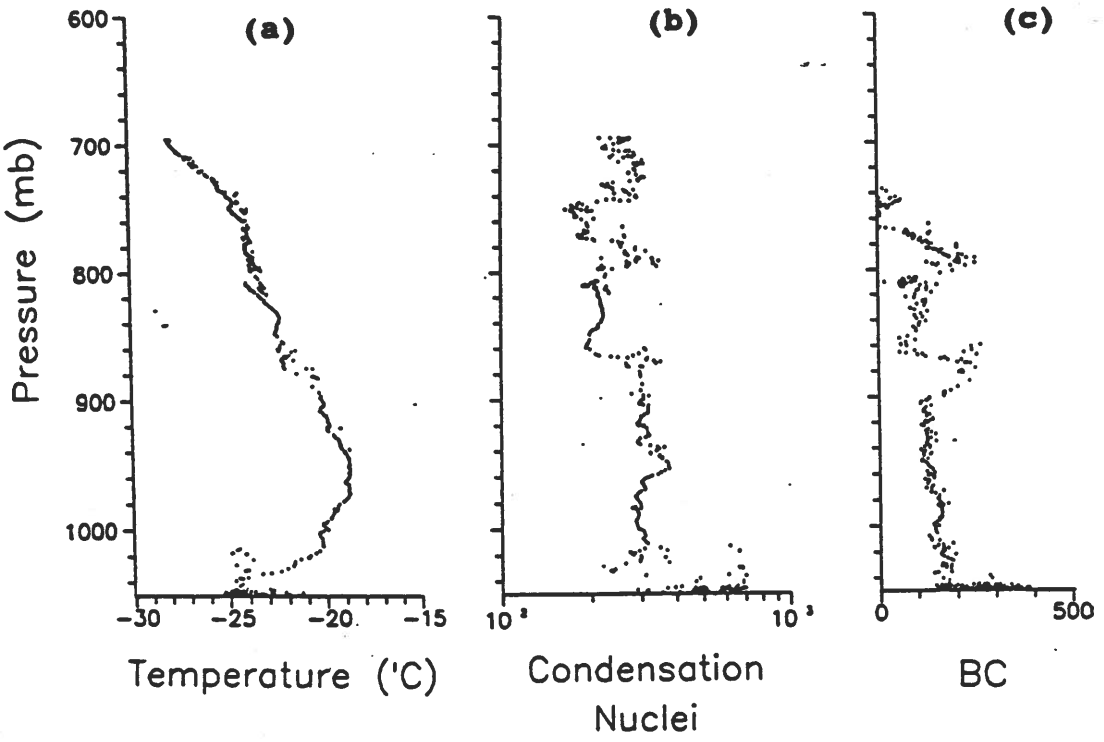

Figure 6:

Illustration of a shallow layer of polluted air right at the surface. (a), air temperature; (b), condensation nuclei concentrations; (c), aerosol black carbon concentrations. The data were taken during flight 3, 8 April 1992, combining a descent profile over Zhannetta Island (about 200 km east of Bennett Island), followed by low-altitude flying from Zhannetta Island, past Genrietta Island, to Bennett Island. The lowest-altitude data accounts for about one-half of the data points in this set. While the higher altitudes are moderately polluted with some slight vertical structure, the surface data show concentrations of CN and BC that are two to three times larger. The closest significant habitation to this region is approximately 1000 km distant.

Session 3

Airborne Measurements

Chairman:
W.J. Megaw

AEROSOL CHEMISTRY MEASUREMENTS OVER THE BEAUFORT SEA DURING AGASP-IV/LEADEX, APRIL 1992

by

Patrick Sheridan

Cooperative Institute for Research in Environmental Sciences, University of Colorado, Boulder

Russell Schnell

NOAA/Climate Monitoring and Diagnostics Laboratory, Mauna Loa Observatory, Hilo, Hawaii

Thomas Conway

NOAA/Climate Monitoring and Diagnostics Laboratory, Boulder, Colorado

Ronald Ferek

Department of Atmospheric Sciences, University of Washington, Seattle

INTRODUCTION

The Fourth Arctic Gas and Aerosol Sampling Program (AGASP-IV), a component of the Arctic Leads Dynamics Experiment (LEADEX), was conducted over the Beaufort Sea during late March and April 1992. The NOAA WP-3D (P-3) Orion research aircraft was the primary measurement platform for AGASP-IV, and was one of several airborne laboratories used for atmospheric measurements in LEADEX. The NOAA P-3 was instrumented to measure atmospheric gas and aerosol species, radiation parameters at multiple wavelengths, and meteorological state variables. The purpose of these airborne measurements in LEADEX was to complement and compare with concurrent baseline station, ice camp, ice buoy and submarine measurement programs.

The NOAA P-3 flew a total of 9 research missions in the Beaufort Sea area (~90 research hours), and operated at altitudes between ~10 and 10,500 m above the ice. The major objectives of AGASP-IV were to 1) measure the concentration and composition of gaseous and particulate constituents of springtime Arctic haze in the Alaskan Arctic; 2) determine components of the atmospheric (especially the marine) S cycle, through measurements of DMS, MSA, SO_2, OCS, and $SO_4^=$ in the inversion layer over lead-filled pack ice; and 3) determine whether significant amounts of Mt. Pinatubo volcanic aerosols were present in the lower stratosphere and upper troposphere over Alaska and the Beaufort Sea.

This paper presents preliminary results from the AGASP-IV experiment, with an emphasis on lower tropospheric and boundary layer gas and aerosol measurements. Data collected onboard the NOAA P-3 are compared with similar measurements taken on the University of Washington C-131 research aircraft. High altitude flight data, which show elevated aerosol concentrations and significant numbers of large (supermicrometer) particles in the lower stratosphere and upper troposphere, suggest the presence of volcanic debris. These aerosol layers of probable Mt. Pinatubo origin are not discussed here but will be addressed in a future paper.

METHODS

Atmospheric samples were collected when the aircraft was flying at low altitude over lead fields in the pack ice and over coastal polynyas, or in lower to middle tropospheric aerosol layers within a few hundred kilometers of Barrow, Alaska. Of all the scientific measurements made on the P-3, relatively few aerosol and trace gas observations are reported here. This exemplifies the preliminary nature of these data, which at this writing are but a few months old. Many of the supporting aircraft measurements (e.g., winds, temperature, other chemical species) from the April 1992 flights have not yet been analyzed. Only brief descriptions of sample collection and analytical procedures are presented in this section. References which detail identical or similar methods from other experiments have been provided.

High volume (500-700 SLPM flow rate, depending on altitude) aerosol samples were collected on 11.0 cm filters in teflon-coated filter packs. Sampling duration was typically 1-2 hours; this long period was necessary to overcome filter blank values. The first stage in each stack was a 1.0 μm pore size Fluoropore Teflon mesh filter. The high filter face velocity insured quantitative capture of particles as small as 0.1 μm in diameter. Gas phase acidic species which passed the particulate filter were quantitatively captured on two rayon filters treated with K_2CO_3. These filter deposits were then analyzed using ion chromatography (IC) for the presence of major anions and cations and MSA. A Dionex Model 4506i ion chromatograph equipped with Dionex AS4A and CS-10 columns was used for the analyses. Details concerning sampling strategies, extraction procedures and detection limits for various species have been published elsewhere [Sievering *et al.*, 1992].

Other relevant chemistry measurements are listed below. Sulfur dioxide was determined continuously through the use of a TECO Model 43S UV fluorescence SO_2 monitor modified for thermal stability [Sievering *et al.*, 1992]. This provided an independent measure of the ambient SO_2 concentration in addition to the treated filter/IC method. Atmospheric particulate deposits collected on pre-fired quartz filters were continuously analyzed for aerosol black carbon (ABC) concentrations using an aethalometer modified for high-flow aircraft use [Rosen *et al.*, 1992]. Ambient air samples were collected in glass flasks for the subsequent determination of the carbon cycle gases CO_2, CO, CH_4 and OCS [Komhyr *et al.*, 1983; Novelli *et al.*, 1991; Steele *et al.*, 1987]. The sample collection period for each flask was ~2 minutes, providing for excellent time (i.e., altitude) resolution in vertical profiles. The OCS analyses have not been completed and will not be discussed further. Dimethylsulfide (DMS) was collected by adsorption onto fine gold wire inside quartz sampling tubes. Sampling for DMS generally required a 15 minute sample collection period, and was performed at the lowest altitudes over open and partially refrozen lead fields. A thermal desorption step and gas chromatography using flame photometric detection were used for analysis [Ferek *et al.*, 1992].

RESULTS AND DISCUSSION

The most obvious preliminary result from the AGASP-IV experiment was the lack of significant amounts of Arctic haze in the Alaskan Arctic during April. The scarcity of haze was determined both visually and instrumentally during the flights, and was supported by meteorological analyses in the field and afterward.

One of the best indicators of the anthropogenic (i.e., pollution) component of Arctic haze is ABC. Table 1 shows a comparison of our overall AGASP-IV measurements of ABC from the Alaskan Arctic with April 1992 measurements taken in the Siberian Arctic [Hansen *et al.*, 1992] and with previous AGASP ABC data [Hansen and Rosen, 1985]. The relatively high concentrations of ABC in the Siberian Arctic agree well with previously-measured (1983) springtime values from the Alaskan Arctic, where ABC maxima of ~1.5 μg m^{-3} were

observed between the upwind and downwind samples, although the downwind samples showed an average concentration 0.06 nmol m^{-3} (~1.4 pptv) higher than the upwind samples. The difference between upwind and downwind DMS concentration is probably lessened because sampling was performed not just along one lead, but in a lead-filled area of pack ice. Thus, even "upwind" samples were collected downwind of other proximal leads. The total range of DMS values from this study was 2.3-8.1 pptv, which agrees well with similar measurements (DMS levels 1-8 pptv) taken during the same period aboard the University of Washington aircraft [Ron Ferek, personal communication]. These DMS levels are also in the range reported by Bates *et al.* [1992] for remote, high southern latitude Pacific air.

Our MSA measurements showed that we had more difficulty detecting MSA above field blank levels in our above-ice inversion layer samples than in our free troposphere and North Slope samples. This is probably because sampling periods were longer in these latter samples, with significantly larger sampled volumes of air. Only one sample of the five inversion layer samples was above blank for MSA, at 0.34 nmol m^{-3}. This is in the range we would expect if our DMS values are accurate and if the MSA to SO_2 branching ratio is large. Since MSA production from OH-initiated photochemical oxidation of DMS is favored over SO_2 production at colder temperatures [Hynes *et al.*, 1986; Yin *et al.*, 1990], we believe that these are both reasonable assumptions. The lower average MSA concentrations in the other samples probably are indicative of the increased distance these samples were collected (geographically or vertically in the atmosphere) from the oceanic source, and the associated transport/mixing time.

The reasons for the somewhat atypical springtime trace gas and aerosol values we measured may lie in the winter/spring 1992 temperature trend in the Alaskan Arctic and the associated meteorology. Figure 2 shows the departure from the climatological average monthly temperatures at Barrow for a seven month period around the AGASP-IV field experiment [NOAA, 1992]. While the early winter months at Barrow were colder than normal, a warming trend began in late February which kept temperatures higher than normal until the early summer. March was one of the warmest at Barrow in recent decades. The warm temperatures at Barrow suggest that we were not sampling Arctic air masses over the south Beaufort sea during much of AGASP-IV.

Rawinsonde data from several Alaskan stations and aircraft dropwindsonde observations over the North Slope of Alaska support this likelihood. Winds often showed a southerly component and free troposphere relative humidities were higher than expected. Cirrus and cirrostratus clouds were commonly documented over the ice and over much of Alaska [Herbert *et al.*, 1992]. These meteorological features of the atmosphere over Alaska are consistent with the notion of advection of northern Pacific marine air masses into the Arctic Basin.

Recent atmospheric trajectory analysis further endorses this concept. Figure 3 shows isobaric 5-day backward air mass trajectories [Harris, 1982] for six flights which arrive at the P-3 during an aerosol sampling cycle and which span nearly the entire AGASP-IV field program. Figures 3a, 3e and 3f show trajectories calculated for the beginning and near the end of the AGASP-IV program that originate in the northern Pacific region. These trajectories are consistent with observations of relatively warm, moist air over the Beaufort Sea during much of the experiment. Figures 3b and 3c show trajectories originating within the Canadian Archipelago, another region without significant pollution sources. Figure 3d shows a trajectory from the one period in which long range transport from the Russian Arctic may have occurred during AGASP-IV. This trajectory is from the 18 April flight, during which the carbon cycle gas profile in Figure 1a was collected. This brief episode of what appears to be organized transport from the Russian Arctic lasted only ~2 days, and by the next flight on 21 April (trajectories in Figure 3e) had completely disappeared. The well mixed vertical profile of carbon cycle gases in Figure 1b is representative of this clean, remote Pacific air mass.

SUMMARY

The NOAA P-3 flew a total of 9 research flights over the Beaufort Sea and Alaskan North Slope during AGASP-IV. Due to an aircraft problem, eight of these flights occurred late in the program, between 10 and 23 April. Meteorological observations, climatological data and air mass trajectory analyses all indicate that the Alaskan North Slope and southern Beaufort Sea were under the influence of northern Pacific air for much of the AGASP-IV field experiment. At other times, air passing over northern Canada entered the research area. In both of these cases, which accounted for a large majority of the research period, the air mass histories suggest no significant pollution component to the April 1992 Alaskan Arctic aerosol. This was confirmed by chemical analysis of AGASP-IV trace gas and particulate samples. Aerosol black carbon, carbon cycle gases, non-sea-salt sulfate and sulfur dioxide concentrations were all significantly lower than expected based on past springtime Arctic haze research. The sulfur cycle species DMS, MSA, SO_2 and non-sea-salt sulfate concentrations were, however, similar to those recently determined for high southern latitude Pacific air masses. Assuming concentrations of these species are similar over the remote northern Pacific Ocean, then this would explain the observed values over the Beaufort Sea in April 1992.

Air mass trajectories and Barrow rawinsonde observations suggest that a brief, coherent long range transport event occurred during 17-18 April. While S-containing species were not significantly elevated during this period, the carbon cycle gases and aerosol black carbon displayed modest increases in atmospheric aerosol layers. These increases were small when compared with past measurements of Arctic haze layers conducted by our group.

We have just begun to analyze the voluminous AGASP-IV/LEADEX atmospheric data set. Further detailed study is necessary before we can be certain of sources and transport mechanisms affecting Arctic aerosol chemistry in the spring of 1992. At this time, indications are that a relatively unpolluted Alaskan Arctic atmosphere in April 1992 was the result of persistent intrusions of clean northern Pacific and Canadian air masses into the Beaufort Sea region.

REFERENCES

Barrie, L.A., G. den Hartog, J.W. Bottenheim and S. Landsberger (1989) Anthropogenic aerosols and gases in the lower troposphere at Alert Canada in April 1986.

Bates, T.S., J.A. Calhoun and P.K. Quinn (1992) Variations in the methanesulfonate to sulfate molar ratio in submicrometer marine aerosol particles over the south Pacific Ocean. *J. Geophys. Res.* **97**, #D9, 9859-9865.

Brock, C.A., L.F. Radke, J.H. Lyons and P.V. Hobbs (1989) Arctic hazes in summer over Greenland and the North American Arctic. I: Incidence and origins. *J. Atmos. Chem.* **9**, 129-148.

Conway, T.J., L.P. Steele and P.C. Novelli (1992) Correlations among atmospheric CO_2, CH_4, and CO in the Arctic, March 1989. Accepted for publication in *Atmospheric Environment*, 1992.

Ferek, R.J., and D.A. Hegg (1992) Measurements of dimetylsulfide and SO_2 during GTE/CITE-3. Submitted to *Journal of Geophysical Research*, 1992.

Hansen, A.D.A., and H. Rosen (1985) Horizontal inhomogeneities in the particulate carbon component of the Arctic haze. *Atmos. Environ.* **19**, 2175-2180.

Hansen, A.D.A., T.J. Conway, L.P. Steele, B.A. Bodhaine, K.W. Thoning, P. Tans and T. Novakov (1989) Correlations among combustion effluent species at Barrow, Alaska: Aerosol black carbon, carbon dioxide, and methane. *J. Atmos. Chem.* **9**, 283-299.

Hansen, A.D.A., R.C. Schnell and A.V. Polissar (1992) Aerosol measurements over the East Siberian Sea. Published in these Proceedings.

Harris, J.M. (1982) The GMCC atmospheric trajectory program. NOAA Tech. Memo. ERL ARL-116, NOAA Environmental Research Laboratories, Boulder, CO, 30 pp.

Herbert, G.A., P.J. Sheridan, R.C. Schnell and M.Z. Bieniulis (1992) The analysis of meteorological conditions during AGASP-IV: 30 March-23 April 1992. NOAA Tech. Memo., NOAA Environmental Research Laboratories, Boulder, CO, in press.

Hynes, A.J., P.H. Wine and D.H. Semmes (1986) Kinetics and mechanisms of OH reactions with organic sulfides. *J. Phys. Chem.* **90**, 4148-4156.

Komhyr, W.D., L.S. Waterman and W.R. Taylor (1983) Semiautomatic nondispersive infrared analyzer apparatus for CO_2 air sample analyses. *J. Geophys. Res.* **88**, 1315-1322.

NOAA Local Climatological Data for Barrow, AK, Monthly Summaries, National Climatic Data Center, Asheville, NC, Dec. 1991-Jun. 1992.

Novelli, P.C., J.W. Elkins and L.P. Steele (1991) The development and evaluation of a gravimetric reference scale for measurements of atmospheric carbon monoxide. *J. Geophys. Res.* **96**, 13109-13121.

Rosen, J.M., B.A. Bodhaine, J.F. Boatman, J.J. DeLuisi, Y. Kim, M.J. Post, R.C. Schnell, P.J. Sheridan and D.M. Garvey (1992) Measured and calculated optical property profiles in the mixed layer and free troposphere. *J. Geophys. Res.* **97**, #D12, 12837-12850.

Sievering, H., J. Boatman, Y. Kim and D. Wellman (1992) SO_2 heterogeneous conversion to the sulfate observed over Lake Michigan. Submitted to Atmospheric Environment.

Steele, L.P., P.J. Fraser, R.A. Rasmussen, M.A.K. Khalil, T.J. Conway, A.J. Crawford, R.H. Gammon, K.A. Masarie and K.W. Thoning (1987) The global distribution of methane in the troposphere. *J. Atmos. Chem.* **5**, 125-171.

Thornton, D.C., A.R. Bandy and A.R. Driedger III (1989) Sulfur dioxide in the North American Arctic. *J. Atmos. Chem.* **9**, 331-346.

Yin, F., D. Grosjean and J.H. Seinfeld (1990) Photooxidation of dimethyl sulfide and dimethyl disulfide, I, Mechanism development. *J. Atmos. Chem.* **11**, 309-364.

FIGURE CAPTIONS

Figure 1. (a) Descent profile of carbon cycle gas concentrations collected during AGASP flight 406 on 18 April 1992. An Arctic haze layer at ~2500 m above the ice surface showed modest enhancements of CH_4, CO_2 and CO. (b) Descent profile collected during AGASP flight 407 on 21 April 1992. The atmosphere over the Beaufort Sea on this day was well mixed up to the tropopause at ~7000 m above the ice.

Figure 2. Seven month record of the departure from normal climatological monthly average temperatures at Barrow, Alaska.

Figure 3. Five-day isobaric backward air mass trajectories arriving at the aircraft position during AGASP-IV flights. Alternating letters and numbers along each trajectory are separated in time by 12 hours. (a) 30 March 1992 - AGASP flight 401; (b) 13 April 1992 - AGASP flight 403; (c) 16 April 1992 - AGASP flight 405; (d) 18 April 1992 - AGASP flight 406; (e) 21 April 1992 - AGASP flight 407; (f) 22 April 1992 - AGASP flight 408.

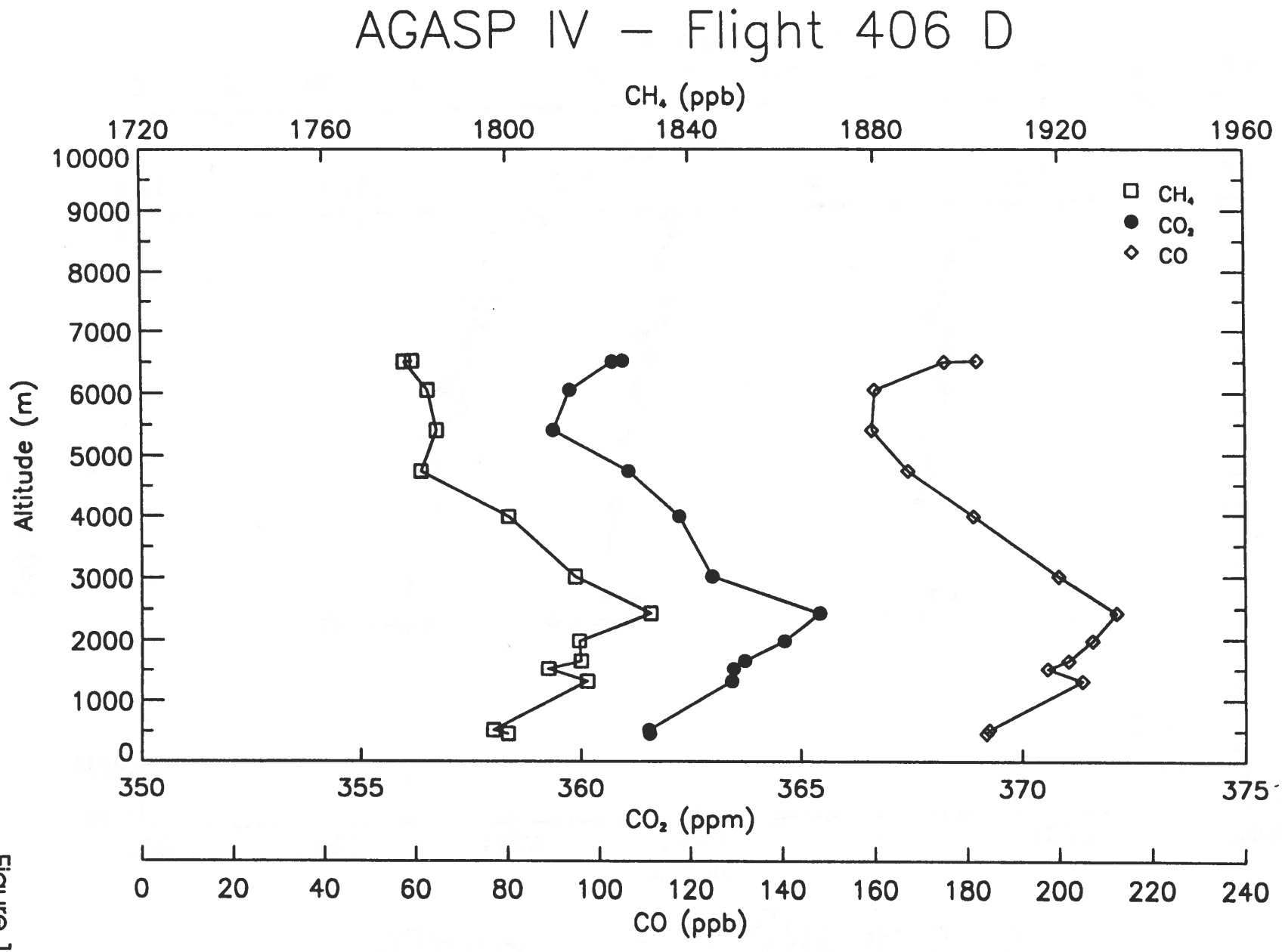
AGASP IV – Flight 406 D
CH₄ (ppb)
1720
1760
1800
1840
1880
1920
1960
Altitude (m)
10000
9000
8000
7000
6000
5000
4000
3000
2000
1000
0
CH₄
CO₂
CO
350
355
360
365
370
375
CO₂ (ppm)
0
20
40
60
80
100
120
140
160
180
200
220
240
CO (ppb)

Figure 1a

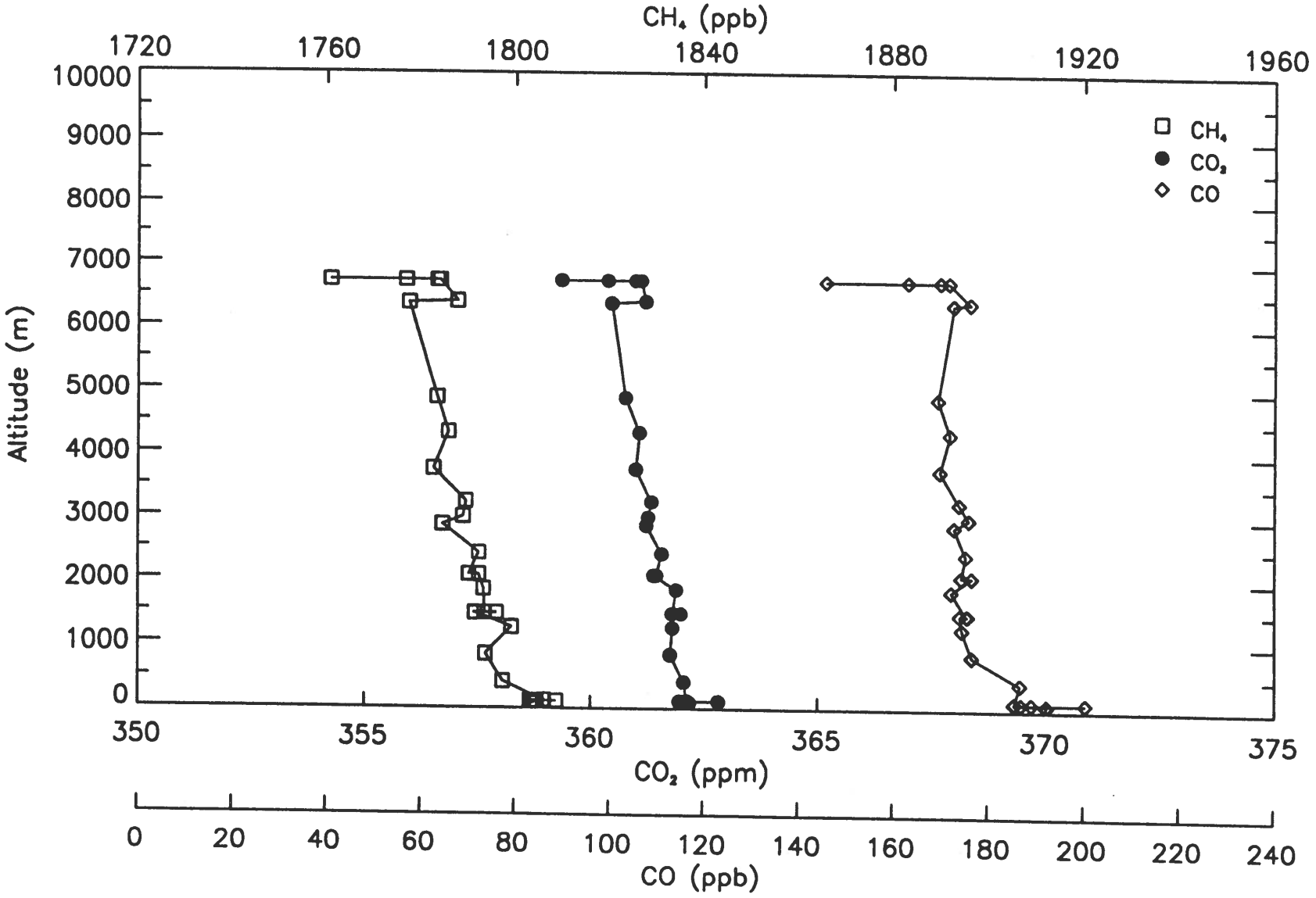
AGASP IV – Flight 407 D
CH₄ (ppb)
1720
1760
1800
1840
1880
1920
1960
10000
9000
8000
7000
6000
5000
4000
3000
2000
1000
0
Altitude (m)
CH₄
CO₂
CO
350
355
360
365
370
375
CO₂ (ppm)
0
20
40
60
80
100
120
140
160
180
200
220
240
CO (ppb)

Figure 1b

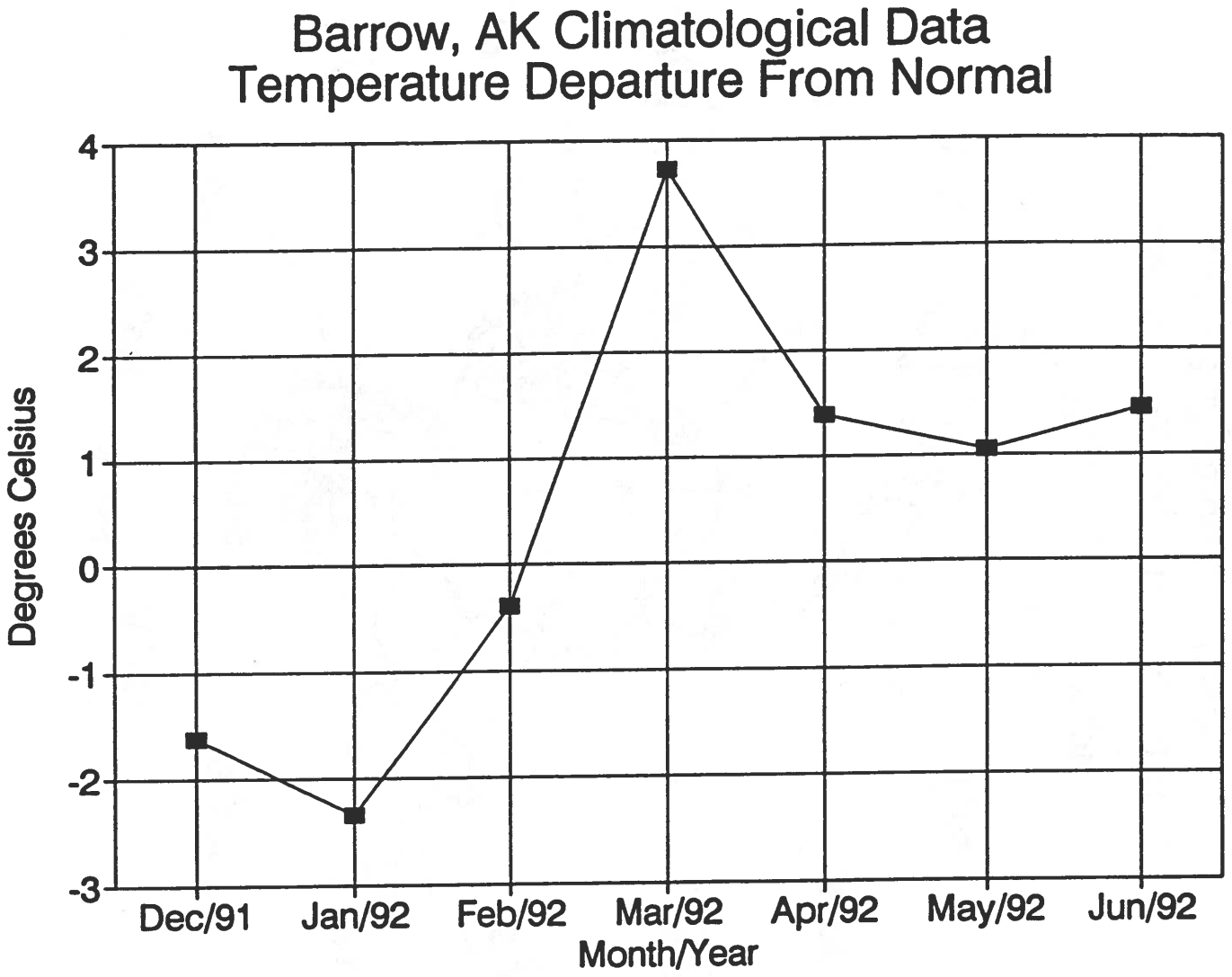
Barrow, AK Climatological Data
Temperature Departure From Normal
Degrees Celsius
4
3
2
1
0
-1
-2
-3
Dec/91
Jan/92
Feb/92
Mar/92
Apr/92
May/92
Jun/92
Month/Year

Figure 2

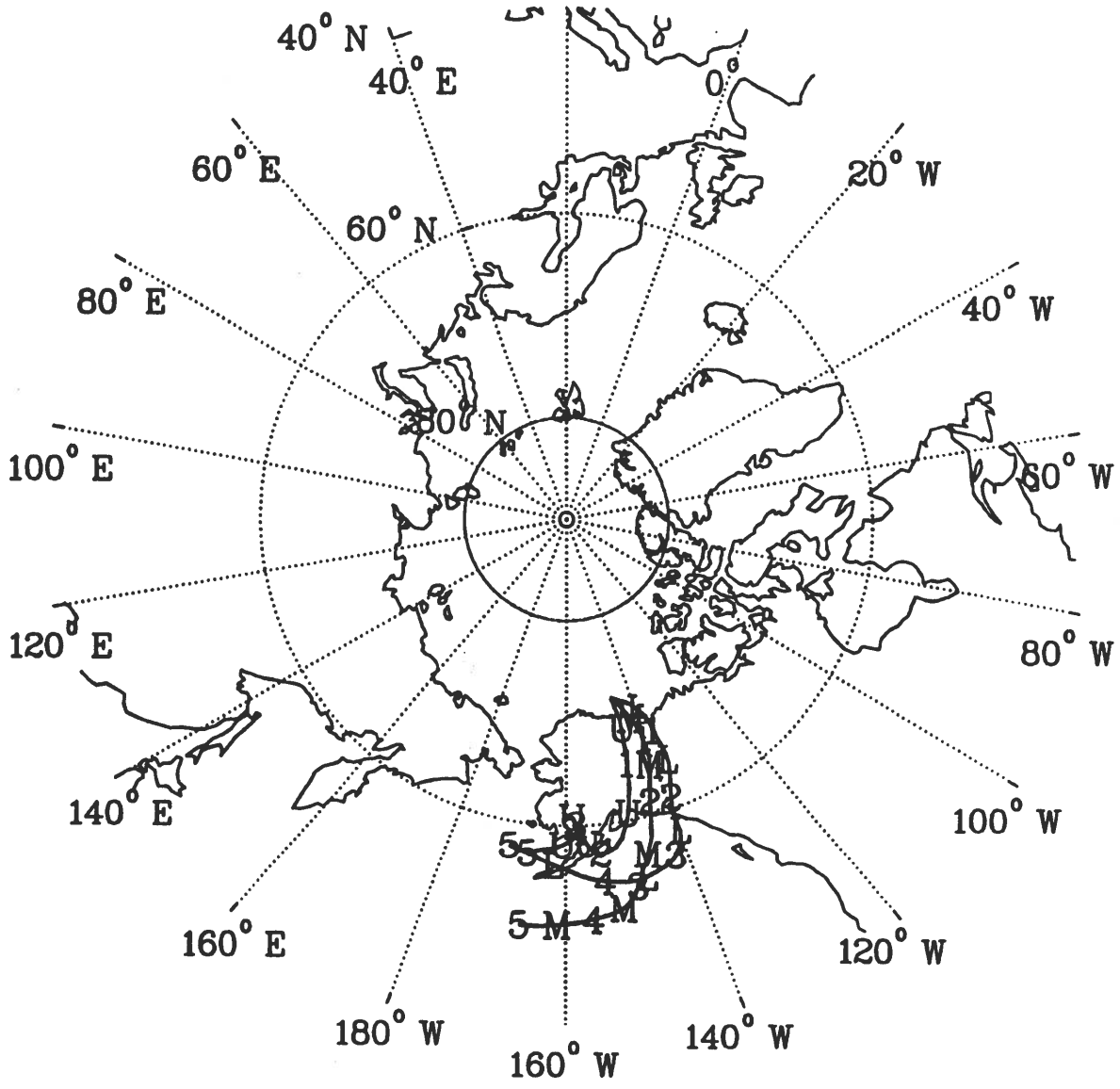
TRAJECTORIES TO S01 (72.00N,146.00W)
92090 – 3/30/92 AT 2100 UT
L: 850 hPa M: 700 hPa U: 500 hPa
40° N
40° E
0°
60° E
20° W
60° N
80° E
40° W
80° N
100° E
60° W
120° E
80° W
140° E
100° W
160° E
120° W
180° W
140° W
160° W

Figure 3a

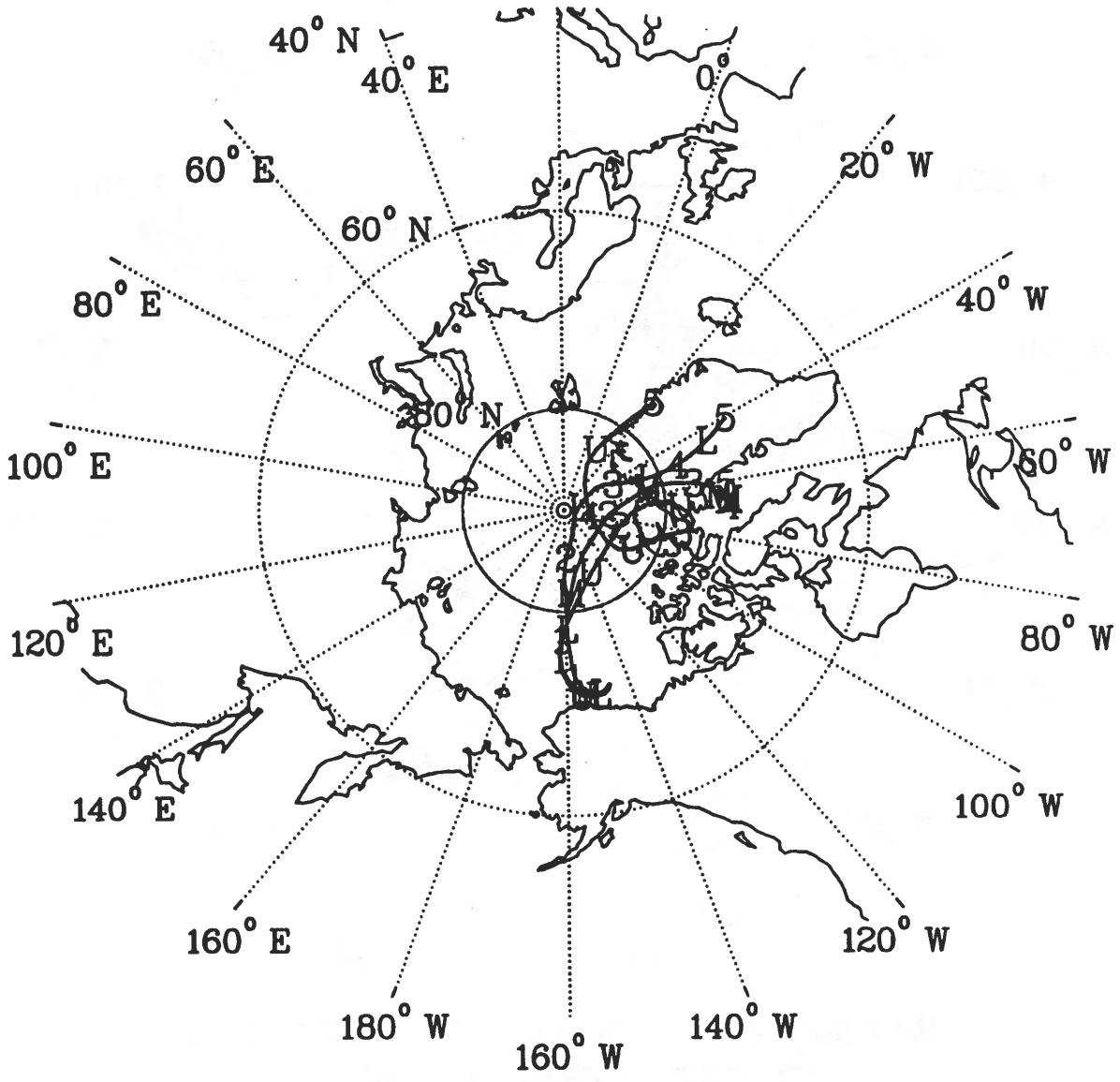
TRAJECTORIES TO S03 (72.50N,146.00W)
92104 – 4/13/92 AT 2000 UT
L: 850 hPa M: 700 hPa U: 500 hPa
40° N
40° E
0°
60° E
20° W
60° N
80° E
40° W
80° N
100° E
60° W
120° E
80° W
140° E
100° W
160° E
120° W
180° W
140° W
160° W

Figure 3b

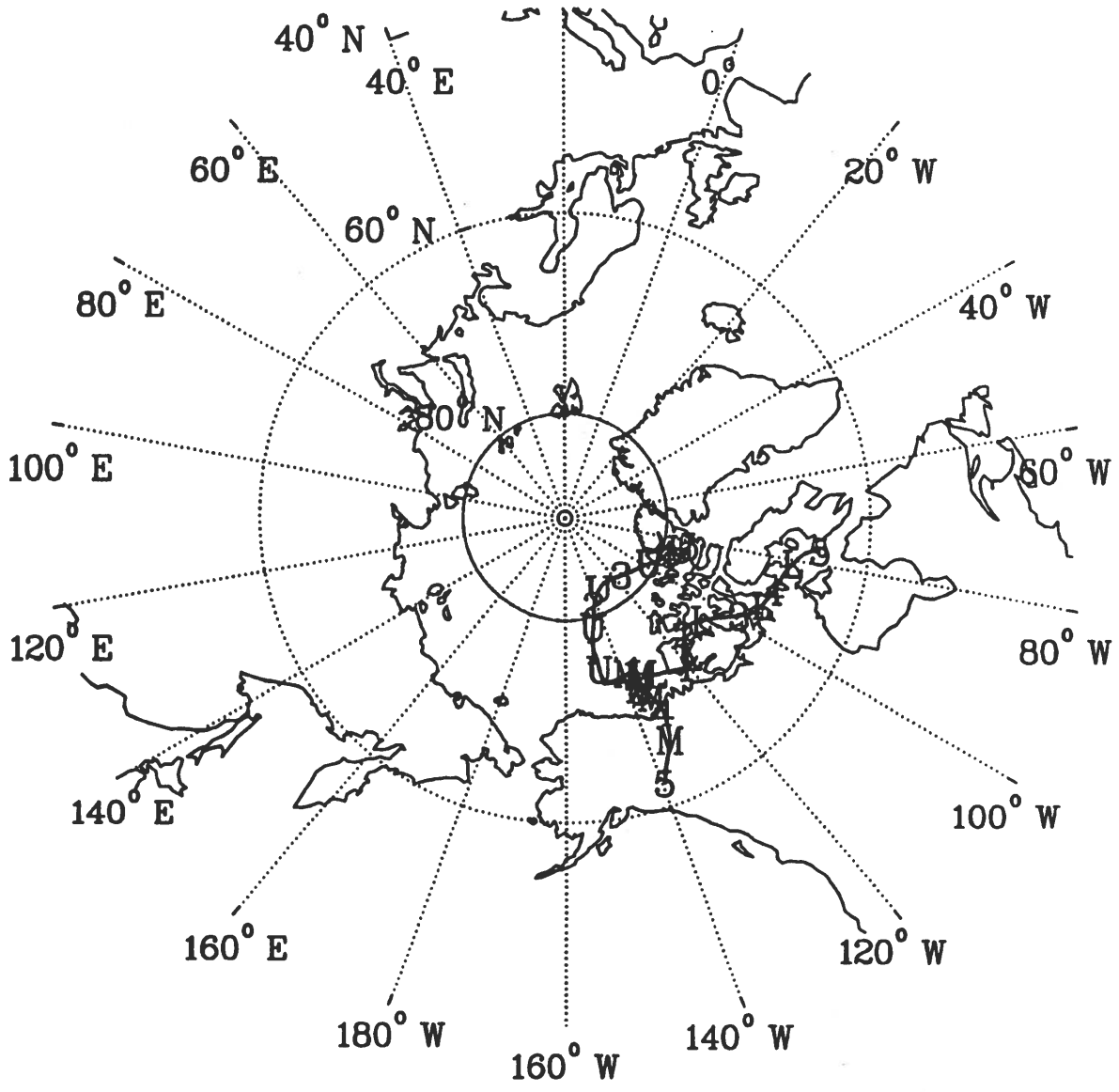
TRAJECTORIES TO S06 (73.50N,147.00W)
92107 – 4/16/92 AT 2300 UT
L: 850 hPa M: 700 hPa U: 500 hPa
40° N
40° E
0
60° E
20° W
60° N
80° E
40° W
80° N
100° E
60° W
120° E
80° W
140° E
100° W
160° E
120° W
180° W
140° W
160° W

Figure 3c

TRAJECTORIES TO S07 (73.50N,141.00W)
92109 – 4/18/92 AT 2000 UT
L: 850 hPa M: 700 hPa U: 500 hPa

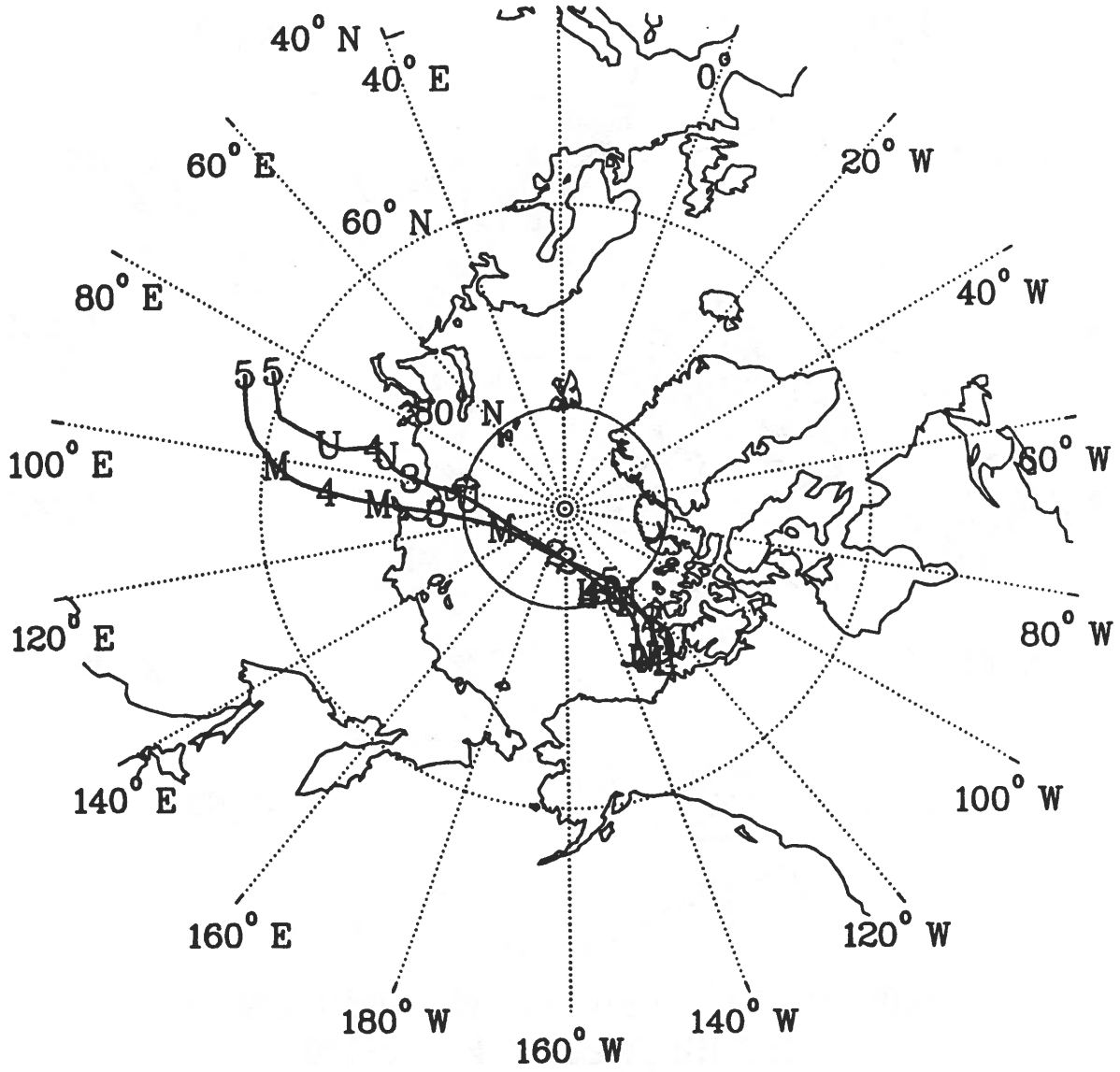

Figure 3d

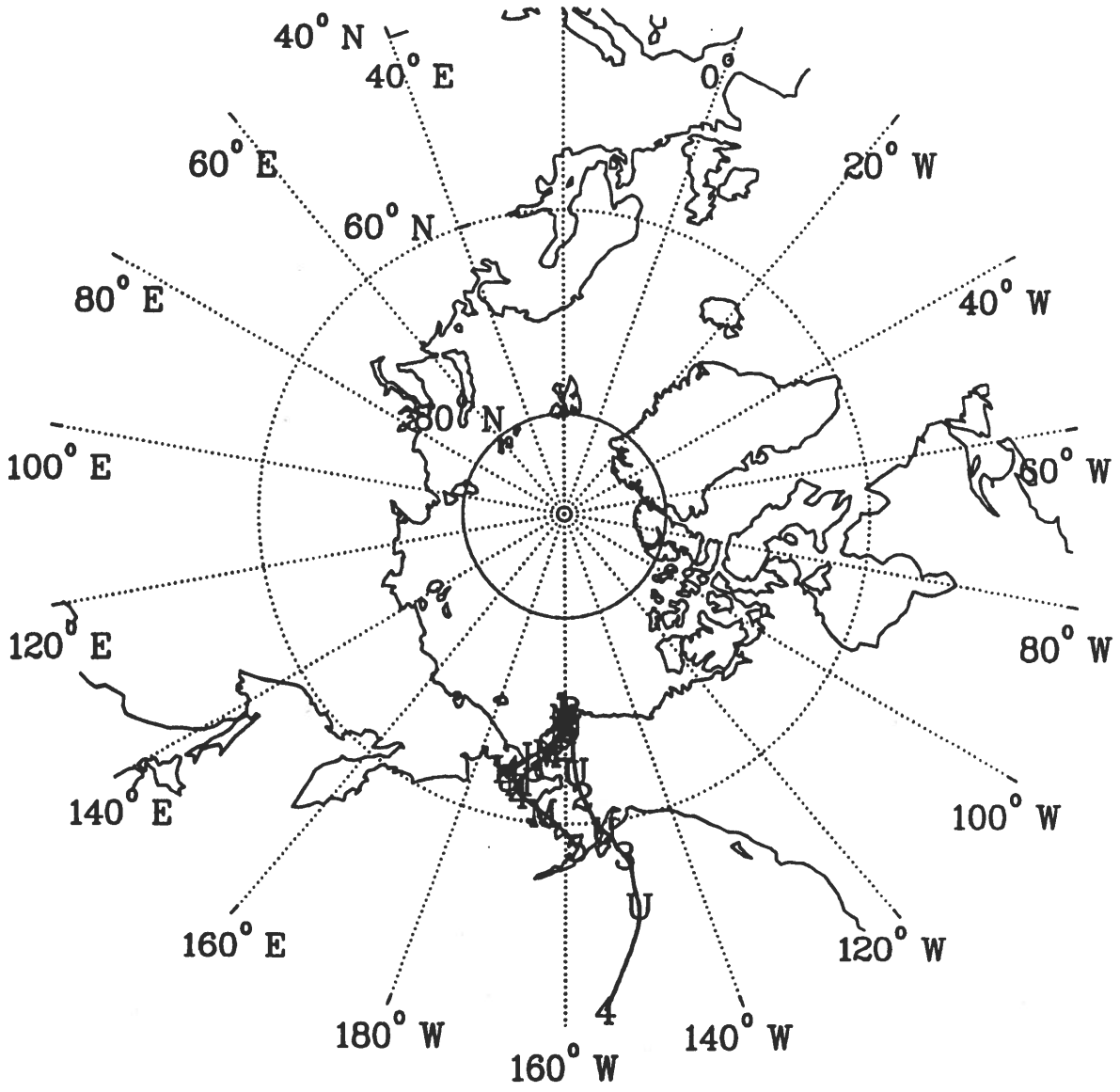
TRAJECTORIES TO S09 (71.50N,159.00W)
92112 – 4/21/92 AT 2100 UT
L: 850 hPa M: 700 hPa U: 500 hPa
40° N
40° E
0°
60° E
20° W
60° N
80° E
40° W
80° N
100° E
60° W
120° E
80° W
140° E
100° W
160° E
120° W
180° W
140° W
160° W

Figure 3e

TRAJECTORIES TO S10 (71.00N,147.00W)
92113 – 4/22/92 AT 2300 UT
L: 850 hPa M: 700 hPa U: 500 hPa

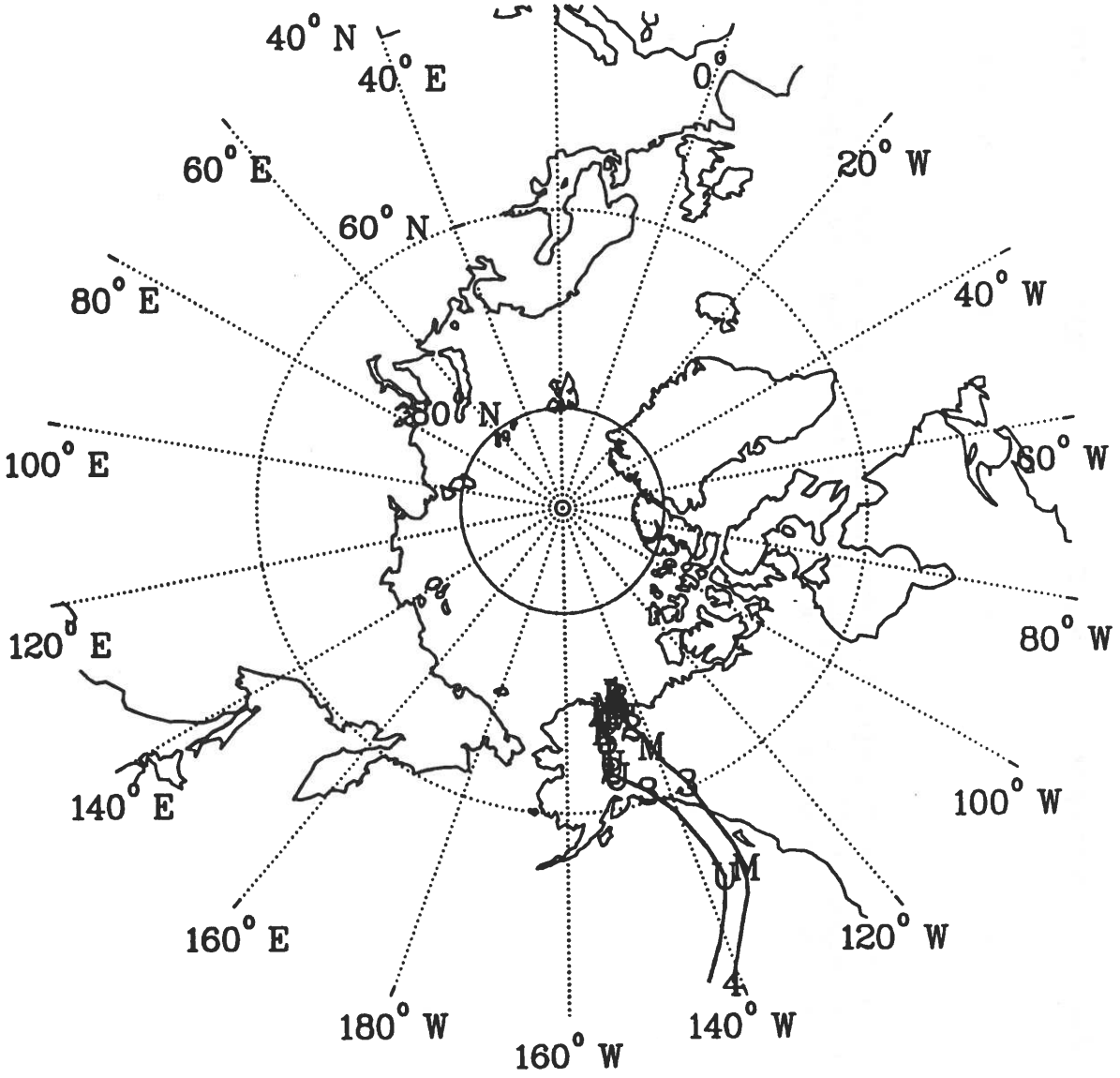

Figure 3f

Table 1. Concentrations (in ng m^{-3}) of aerosol black carbon determined from April 1992 measurements in the Siberian and Alaskan Arctic.

	Aerosol Black Carbon		
	1992 Siberian Arctic	1992 Alaskan Arctic	1983 Alaskan Arctic
Maximum Concentration	>1000	<200	~1500
Column Average	~300	50-100	Not Reported[1]

[1]From Hansen and Rosen (1985). Although column averages were not discussed in this paper, inspection of the published data indicates column averages of several hundred ng m^{-3} were observed for the reported flights.

Table 2. AGASP-IV airborne measurements of S-cycle species in various sampling scenarios. Values listed are the sample mean + sample standard deviation (in nmol m^{-3}). For ease of comparison, other units (e.g., ng m^{-3}, pptv, etc.) are given in the text. Number of samples on which the values are based is given in parentheses.

Filter Pack Measurements

	Below Inversion (5 samples)	Free Troposphere (5 samples)	Prudhoe Bay (2 samples)
SO_2	0.9±0.5	Blank	2.0±0.2
Total $SO_4^=$	2.8±1.8	1.5±0.6	2.3±0.1
nss-$SO_4^=$	2.0±1.3	1.4±0.8	2.2±0.2
nss/tot $SO_4^=$	0.72	0.91	0.94
MSA (# of samples above blank)	0.34 (1)	0.15±0.07 (4)	0.12±0.02 (2)

DMS Measurements

(5 upwind samples, 5 downwind samples)

DMS (downwind side of large leads)	0.25±0.11	NA	NA
DMS (upwind side of large leads)	0.19±0.08	NA	NA

Proceedings, 5th International Symposium on Arctic Air Chemistry, Copenhagen, Denmark, Sept. 8-11, 1992

AIRBORNE INVESTIGATION OF THE BENNETT ISLAND PLUME

R. C. Schnell
Mauna Loa Observatory, NOAA/CMDL, Hilo, Hawaii 96721-0275

A.D.A. Hansen
Lawrence Berkeley Laboratory, University of California, Berkeley

E. Dlugokencky
CIRES, University of Colorado, Boulder, Colorado

T.J. Conway
Carbon Cycle Group, NOAA/CMDL, Boulder, Colorado

A. V. Polissar and G. S. Golitsyn
Institute of Atmospheric Physics
Russian Academy of Sciences, Moscow

Abstract. In April 1992, eight aircraft missions were flown to Bennett Island (76.5°N, 149°E) with an instrumented Russian AN-26 aircraft to investigate the atmospheric plume phenomena regularly observed in satellite images and known as the Bennett Island Plumes. These plumes, often up to 250 km long, appear to arise from the vicinity of the island once or twice per month in the winter and spring. Various explanations had been put forward for their origin, with one of the most interesting being that the plumes were caused by the 'geyser-like' release of CH_4 from clathrate deposits beneath the shallow ocean floor. If true, this finding with its implication for CH_4 sources in the high Arctic would be an important input to models of the budget of radiatively-important trace gases.

We collected 48 flask samples of the ambient atmosphere in the vicinity of Bennett Island over the space of 3 weeks at altitudes from sea level to 5 km: over the island, over the upwind fast ice, and over the downwind open water. Missions were flown at times just before satellite observations of a plume, just after one, during the time interval between plumes, and within one plume. Laboratory analyses indicate that the CH_4 mixing ratios and CH_4/CO2 ratios in the air samples were representative of background Arctic air giving no evidence for the CH_4-release hypothesis. Present evidence suggests that the plume is initiated by orographic flow over Bennett Island (426m) even though the base of the plume may be 3 km or higher above the surface.

1. INTRODUCTION AND BACKGROUND.

For almost 20 years, large plumes of unknown origin have been observed on satellite photographs, emanating from a specific point in the New Siberian Islands, Russian Arctic. One of the first published views of a Bennett Island plume is presented in Figure 1 as it appeared on the cover of EOS (Kienle et al., 1983). These plumes are generally observed every couple of weeks in the winter and spring, often are up to 250 km long, and yet are only a few tens of km wide. Their origin point was definitely identified as Bennett Island (76.5°N, 149°E), a small island of unremarkable topography: approximately 30 km long by 10 km broad, rimmed by low cliffs rising to a central ice dome of 426m ASL. The plume events may last from 1/2 day to 1 day (Kienle et al., 1983; Clark et al., 1986; Matson, 1986; Weisburd, 1987). There are other islands in the general area, suggesting that some special attribute of Bennett Island was responsible for the remarkable plumes. There is no habitation on Bennett Island, nor frequent periodic visits.

The area of the New Siberian Island is devoid of volcanic, geothermal or tectonic activity: consequently, volcanic or geyser eruptions were ruled out as being an explanation for the plumes. In any case, these mechanisms could not reasonably explain the regularity of the observed phenomenon. One of the more intriguing explanations was that the plumes were caused by the periodic release of CH_4 from gradually-decomposing clathrate deposits trapped beneath the shallow ocean floor (Clarke et al., 1986; 1991).

The entire Siberian shelf area is underlain by permafrost, which has been flooded in recent geologic times by the gradual depression of the north-eastern Siberian coastal plain (Barkan and Vornonov, 1982). It was hypothesized that the decay of organic materials in and beneath the sub-ocean permafrost would result in the gradual accumulation of CH_4 clathrate, a physically-bonded structure that is stable at low temperatures and high pressures. If subsequently warmed, the clathrate would decompose releasing CH_4. Once venting began, the reduction in pressure would lead to an explosive release of all of the CH_4 in the local area of the release point. This CH_4 would surge up through the ocean and the pack ice, bringing with it copious quantities of entrained water. The CH_4 gas would be at a low temperature due to rapid expansion. This eruption would then loft a huge cloud of cold gas and water into the atmosphere, resulting in the observed plume with a 'cold' infrared signature as seen from the satellite images (Clarke et al., 1986; 1991).

It has been estimated that the total amount of CH_4 bound in subsurface clathrates exceeds the amount of carbon in all other fossil fuel deposits by a large factor. Climate change models predict that global warming will be amplified in polar regions. Potential warming of the Arctic could thus produce an additional

CH_4 positive-feedback scenario. Global annual atmospheric CH_4 concentrations are greatest in the Arctic, peaking at 1790 ppb at the latitude of Bennett Island compared to 1640 ppb at the equator and throughout the southern hemisphere (1989 data, CMDL/NOAA 18, 1990).

2. THE BENNETT ISLAND FIELD PROJECT, APRIL 1992.

The above background led us to organize an aircraft-based research program to collect gas and aerosol samples in the vicinity of Bennett Island in April of 1992. With substantial assistance from the civil and military authorities of Russia, we contracted the use of an aircraft based at Cherskiy (69oN, 161oW, on the north coast of Yakutia). Gas flask sampling and aerosol measuring equipment was pre-packaged in Berkeley and flown to Provideniya, Russia by a U.S. carrier. At Provideniya the equipment, sampling flasks, and assorted support items were loaded on a Russian AN-26 and flown to the Arctic. Pre-built probes were mounted into the AN-26 at Cherskiy. Only three days elapsed between arrival in Russia and the first flight. See Hansen et al., 1992 for a description of the equipment and its operation.

Flight operations were coordinated with NOAA-11 and -12 satellite observations of the plume phenomenon received directly at the Anchorage, Alaska, National Weather Service office. Plume event observations were telephoned to Dr. Hansen in Cherskiy within minutes of their detection. Direct calls to his hotel or the Cherskiy airport were generally completed in a minute or two using the telephone circuits crossing the Bering Sea from Alaska to far eastern Russia.

The aircraft transit from Cherskiy to Bennett Island (approximately 1000 km) allowed for an extensive program of sampling the 'Arctic Haze' pollution aerosol in addition to gas-flask sample collection in the target region. Eight flights of about 8 hours duration each were flown, with sampling following a plume observation, several days afterwards, just beforehand, and one in the latter stages of a plume event. On each flight, between three and twelve flask and pressurized canister samples of the ambient atmosphere were collected.

These samples were returned to NOAA/CMDL, Boulder, Colorado, and were analyzed within one week after the conclusion of the mission. The gas chromatographic analytical techniques used to analyze the samples have high precision and are routinely used for the global gas sampling network operated by the NOAA/CMDL Carbon Cycle Group. During the same time period as this mission to Russia, the NOAA WP-3D aircraft-based component of AGASP-IV was collecting similar gas flask samples over the Alaskan sector of the Arctic Ocean. An intercomparison flight between the NOAA WP-3D and Russian AN-26 was conducted over the north Bering Strait at 166°W,

72°N on April 22, 1992, Simultaneous gas flask sample were collected during the intercomparison. Continuous CH_4 measurements and discrete flask samples were also taken with an in situ GC at the NOAA/CMDL Barrow Baseline Station, Alaska over the duration of the project. Thus, we can directly compare the Bennett Island samples with samples from nearby locations at the same time period and analyzed on the same system.

Most of the gas samples were collected both upwind and downwind of Bennett Island near the surface over fast ice and over open water. Some samples were collected at altitudes up to the aircraft's operation ceiling of 6 km in order to determine a vertical profile of gas species concentrations. On no occasion was anything unusual seen visually in the region of Bennett such as bubbles on/in the water or visible venting from land or sea. The pilots and crew, who had many years experience flying in the Arctic, did not perceive any special qualities in the appearance of the environs of Bennett Island on any of the flights including the plume penetration flight.

3. RESULTS.

Figure 2 shows the CH_4 concentrations measured around Bennett Island (open boxes) compared to the continuous CH_4 record at Barrow (solid trace). From this figure we observe that the CH_4 concentrations in the Bennett Island samples are similar to the Barrow surface CH_4 concentrations except for the April 11-12 Bennett Island samples which are lower in CH_4 concentration. These latter samples were taken in a profile (above the island) up to the aircraft ceiling and exhibit the normal decrease of CH_4 concentration with altitude observed in the Arctic (Conway and Steele, 1989).

A satellite view of the plume of interest was first observed on the NOAA 12, 18 April 92, 0522Z pass. The plume stretched west north-west from Bennett Island for a distance of 150 km. Satellite derived cloud top irradiance temperatures of the plume top ranged from -27oC to -30oC. The plume was still visible in the 2255Z pass (17 hours later) but appeared to be getting thinner and more diffuse than earlier in the day. The AN-26 took off at 2300Z and intercepted the plume over Bennett Island at 0200Z, April 19. The plume was not observed on the next available satellite image read out at 0500Z, April 19.

Approaching Bennett Island at 6 km altitude on April 19, nothing unusual was seen at that altitude or on the ocean surface, while a street of clouds at an intermediate altitude was observed departing the island and streaming downwind. Descending, the AN-26 flew through this cloud stream centered in the altitude range of 3.3 to 3.0 km. Condensation nuclei (CN) concentrations were 500 nuclei cm-3 in the plume, dropping to 200 cm-3 beneath the cloud

and remaining at 200 cm-3 to the surface. Aerosol black carbon (BC) concentrations were 200-300 ng m-3 in the plume with concentrations of 100 ng m-3 above and below the plume. Temperatures were -23oC at the top of the plume and -19oC at the base. Thus, both the plume and the highest CN and BC concentrations observed in the profile were essentially coincident. Descending to lower altitudes, the aircrew were able to determine that the ocean surface appeared perfectly normal. Looking upward, they could clearly see the train of clouds forming at a higher altitude and streaming downwind in the lee of Bennett Island.

Figure 3 shows the correlation between CH_4 and CO_2 concentration for all the Bennett Island gas samples. The slope of the regression, representing a correspondence of 0.015 moles of incremental CH_4 per mole of incremental CO_2, is in close agreement with earlier studies of the CH_4/CO_2 ratios in arctic haze (Conway and Steele, 1989) and is undistinguishable from the CH_4/CO_2 ratios measured in the April 1992 flasks from the NOAA WP-3D AGASP-IV samples and the Barrow samples. These two gases appear to have a correlated source in the springtime Arctic.

Neither the Figure 2 nor Figure 3 data show any evidence whatsoever for the presence of any additional or unusual CH_4: and certainly not in the massive concentrations that would be expected for a release sufficiently large to produce a plume of the observed magnitude. Also, although small, the solubility of CH_4 in water is such that traces of additional CH_4 would be expected to linger long after a sub-surface CH_4 release and thus be detected by the extremely precise analytical techniques used in this research. None of the samples collected during periods bracketing plume events exhibit any anomalous CH_4/CO_2 ratios.

4. DISCUSSION.

Given that there is no excess CH_4 in the Bennett Island plume and that the plume originates 3 km above a topographical feature, and not from the surface, we are left with the question: What is the composition of the plume and how does it form?

Without invoking any new phenomenon, we suggest that the plume is a mountain wave cloud. Evidence to support this suggestion is presented below. But, first, it behooves us to study prior knowledge of arctic mountain wave clouds to put the Bennett measurements in perspective.

Earlier research by Durran (1986) has shown that mountain waves can initiate clouds well above the elevation of the wave inducing terrain. In situations where there is pronounced lower atmospheric stability (i.e. arctic winter) and the topography has a gentle windward slope and a steeper lee slope (as is the case for Bennett Island with southerly air flow), a vertically propagating

wave may form with a single wave crest. Typically, such a wave crest will extend many km above a relatively small topographic feature. Such a wave can explain the uplift required to initiate a cloud street above Bennett Island.

Plumes are often observed flowing downwind of Novaya Zemlya, a large island in the western Soviet Arctic. Some of the plumes appear to have a point source similar to the Bennett Island plumes. Parmenter-Holt (1987) presents a strong argument, now generally accepted, that these plumes are natural hydrometeor clouds initiated by island topographic features. The plumes form when moist cool air, associated with a frontal disturbance, flows over the island. The plumes stream out in the jet shear associated with the front and may extent 100's of km in otherwise cloud-free air.

A paper published after we completed the Bennett Island flights (Fett, 1992) discusses the formation of Arctic cloud plumes. Fett shows that cloud plumes are regularly formed in the lee of arctic islands within the arctic frontal zone. Of particular interest to the current study, he presents illustrations of plumes events originating over Kvitoya Island east of Svalbard. Kvitoya Island is slightly larger than Bennett Island but is similar in elevation (Bennett = 426m; Kvitoya = 432m) and topography. The cloud plumes extend 100's of km and may have cloud top temperature as cold as -37°C and rise to > 5 km altitude. A neighboring island, with higher topography, did not produce a plume under the same conditions.

Fett (ibid) presents a strong case for using the presence of arctic island plumes to indicate the location arctic fronts because the fronts themselves are so often weakly or not at all defined by other cloud forms. Further, the direction of plumes may be used to indicate the direction of the low level jet stream associated with the fronts.

Finally, during the period of the Bennett Island Project, a 200 km long plume was observed streaming from Gerald Island which is east of Wrangel Island. Gerald Island is similar in size and topography to Bennett Island; the highest elevation on Gerald Island is 366m compared to 426m on Bennett. The Gerald Island plume event lasted for at least 15 hours and was essentially identical in appearance to a typical Bennett Island plume. The Gerald Island plume was associated with an arctic frontal passage.

The Bennett Island plume of April 18-19, 1992, was also associated with an arctic front. Enroute to Bennett Island, the AN-26 flew through the frontal zone and broke clear of the upper level cirrus deck 100 km south-east of the island. The plume was observed to flow in stable air above a strong inversion located at 850mb. No moisture measurements were taken on the flight, and radiosonde station 21432 at 76°N, 138.9°E ≈ 300 km west of Bennett Island was unable to release a radiosonde during the period of the

plume event due to the high local winds associated with the front. We do, though, have radiosonde profiles from 21432 for April 4 and 5 when a previous arctic front associated with a Bennett Island plume was observed. These soundings shows that the air was essentially saturated from 950 to 550-600mb above which ($\simeq$ -35oC) the humidity sensor became unreliable. For the present, we assume that the soundings for April 18-19 would also exhibit a saturated region in the vicinity of the altitude of the plume (3-3.5 km). The AN-26 missed the April 5 plume event by about 2 hours.

The study of the Bennett Island plume was designed to test the CH_4 plume hypothesis and thus concentrated on collecting air samples for later laboratory analyses. Had we expected the plume to be a mountain wave cloud feature, we would have instrumented the aircraft for cloud physics and air motion studies. As such, further meteorological analyses (now underway) of the April 18-19 Bennett Island plume is being conducted with the available data collected by radiosondes, surface stations, and satellites. Each of these data sources, though, are relatively meager in the region of Bennett Island.

5. CONCLUSIONS.

We conclude that the Bennett Island plumes are mountain lee wave clouds produced within arctic frontal zones. The plumes stream out in the low level jets associated with the fronts and persist until the moisture surge associated with the front moves out of the region. The unique topography of Bennett Island (gentle slope on the upwind side and sharp drop on the lee side) is probably a critical factor in producing the type of standing lee wave (Durran, 1986) that can sustain a long streaming cloud with a base in the region of 3+ km above the wave initiating terrain. There is no evidence whatsoever to support the idea that CH_4 releases in the region of Bennett Island could be a cause of, or associated with, the Bennett Island plume.

A final argument for stating that the Bennett Island plumes are frontal associated orographic clouds is that two plume events were successfully predicted in April and May, 1992, based upon a study of weather map analyses and numerical model projections. The predicted plume event of May 7, 1992 has clear evidence of the associated frontal system clouds as viewed in satellite imagery.

Acknowledgements. This research was supported by the National Oceanic and Atmospheric Administration, National Science Foundation, United States Geological Survey, United States Environmental Protection Agency, United States Department of Energy, and Magee Scientific. The program was organized under the auspices of US-USSR Working Group VIII.

REFERENCES

Barkan, Y.S. and A.N. Voronov, 1982, Zones of possible hydrate formation in the USSR, Int. Geogl. Rev., 11, 37-41.

Clarke, J. W., P. St. Amand and M. Matson, 1986, Possible cause of plumes from Bennett Island, Soviet Far Arctic (abs.): American Association of Petroleum Geologists Bulletin, 70, 5, 574.

Clarke, J.W., P. St. Amand, and M. Matson, 1991, Possible cause of plumes in vicinity of Bennett Island, East Siberian Sea, Soviet Far Arctic, full manuscript to be submitted.

CMDL/NOAA, Summary Report No. 18, 1989, W. Komhyr and R. Rosson (Eds.), NOAA/ERL, Boulder, CO, pp 141.

Conway, T.J. and L.P. Steele, 1989, Carbon dioxide and methane in the Arctic atmosphere, J. Atmos. Chem., 9, 81-99.

Durran, D.R., 1986, Mountain waves, Mesoscale Meteorology and Forecasting, P.S. Ray, Ed., Amer. Meteor. Soc., 472-492.

Fett, R.W. 1992, Major cloud plume in the Arctic and their relation to fronts and ice movements, Mon. Wx. Review, 120, 925-945.

Hansen, A.D.A., T.J. Conway, L.P. Steele, B.A. Bodhaine, K.W. Thoning, P. Tans, and T. Novakov, 1989, Correlations among combustion effluent species at Barrow, Alaska: Aerosol black carbon, carbon dioxide, and methane, J. Atmos. Chem., 9, 283-299.

Hansen, A.D.A., A.V. Polissar, and R.C. Schnell, 1992, Aerosol measurements over the East Siberian Sea, Proc. 5th Symposium on Arctic Air Chemistry, Copenhagen, Sept. 8-10, 1992.

Kienle, J., J.G. Roederer, and G.E. Shaw, 1983, Volcanic event in Soviet Arctic?: EOS, 64, 20, 377.

Matson, M. 1986, Large plume events in the Soviet Arctic: EOS, 27, 48, 1372-73.

Parmenter-Holt, F., 1987, The large plumes of Novaya Zemlya, EOS 68, 1129-1142.

St. Amand, P., J. Clark, and M. Matson, 1986, Curious plumes from Bennett Island, in Proceedings of the Arctic Oceanographic Conference and Workshop, June 11-14, 1985, Naval Ocean Research and Development Activity (NORDA), Bay St. Louis, MS.

Weisburd, S., 1987, Cloud Conundrums: The Soviet Island Mystery Plumes, Science News, 131, 13, 204-206.

EOS

Transactions, American Geophysical Union
Vol. 64 No. 20 May 17, 1983

Large Plume Events in the Soviet Arctic

Figure 1. Bennett Island Plume event observed from a satellite. This report raised interest in the phenomenon.

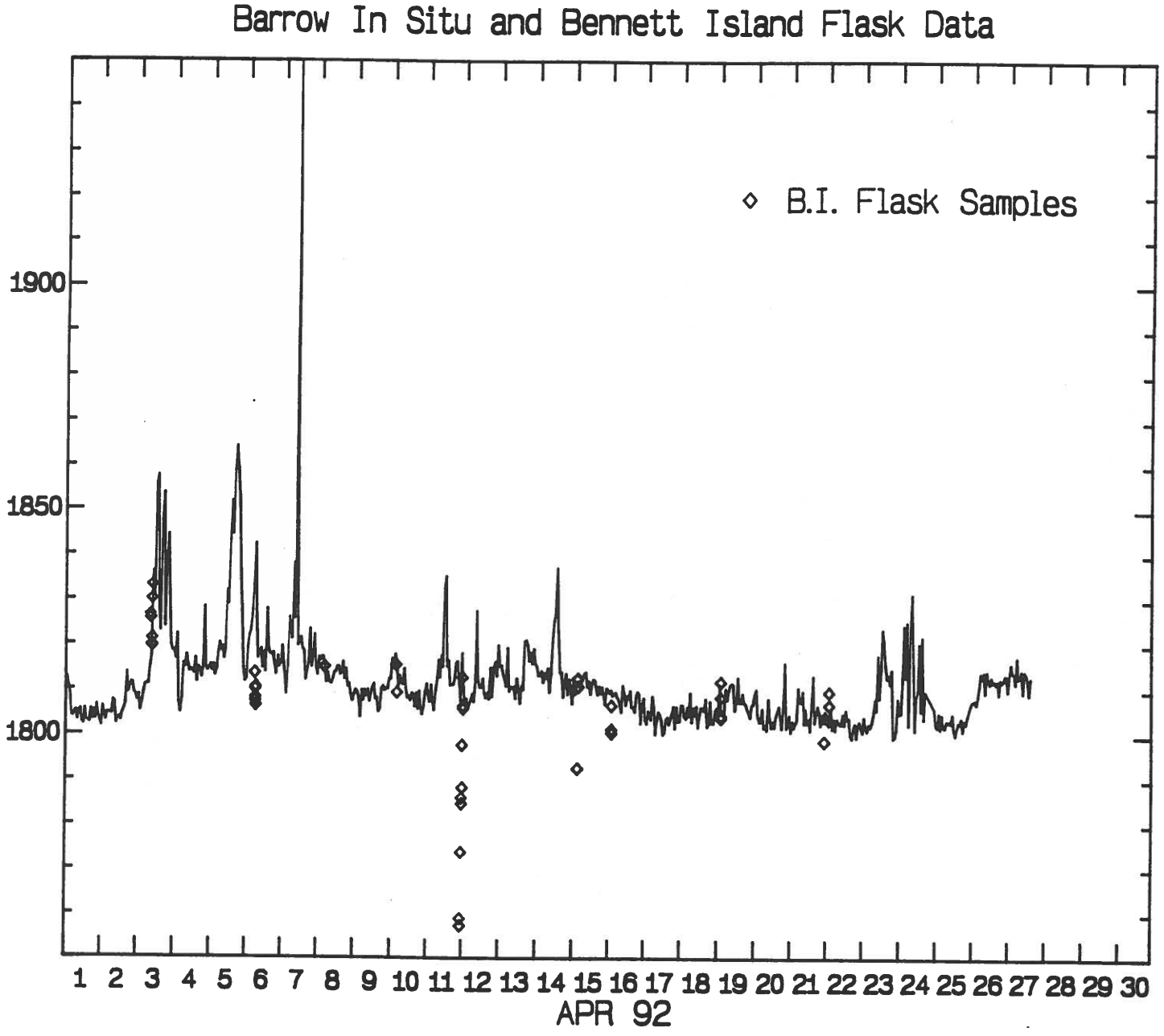

Figure 2. Methane measurements from a gas chromatograph at Barrow, Alaska (continuous trace) and flask samples over and around Bennett Island (open squares). The CH_4 concentrations from within the plume (April 18) are similar to those measured at Barrow and on other days around Bennett Island. The lower CH_4 concentrations measured on April 11 are from a profile up to the operating ceiling of the aircraft and exhibit the normal decrease of CH_4 concentrations with altitude observed in the Arctic.

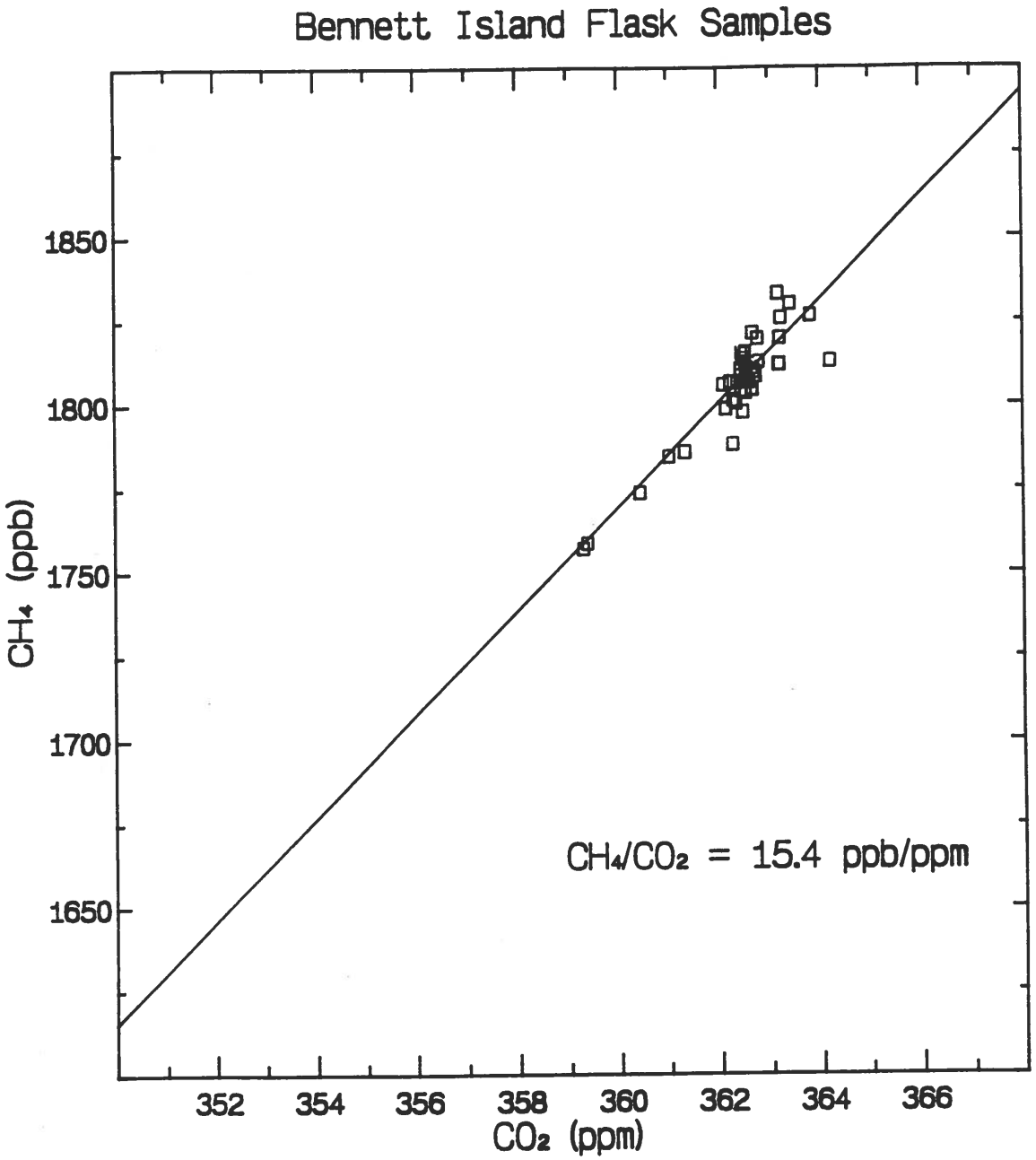

Figure 3. Correlation between CH_4 and CO_2 concentrations for the Bennett Island samples. The slope equals 15.4 ppb CH_4/ppm CO_2 with a r^2 = 0.82. The ratios are indistinguishable from flask measurements from the NOAA WP-3D in the Alaska Arctic and from the Barrow baseline station for the same period.

PROPERTIES OF ARCTIC HAZE USING AIRBORNE RADIATION MEASUREMENTS.

Irina N. Sokolik,
CIRES, University of Colorado, Boulder, USA.

Francisco P.J. Valero,
NASA Ames Research Center, Moffett Field, USA.

During the AGASP experiments the measurements of vertical profiles of upwelling and downwelling solar hemispherical fluxes for several wavelengths were carried out (Valero 1989). Using these measurements a technique to estimate the vertical profiles of Arctic haze optical properties was developed. This tecnique allows us to obtain the spectral values of τ, optical depth, ω, single scattering albedo, and g, asymmetry parameter of scattering phase function.

First, the initial profiles of optical parameters are obtained using the measurements of spectral downwelling fluxes and the parameterization formula for transmission in aerosol layer, constructed by Sokolik (1989). Next, by iteration method the initial profiles are corrected using measurements of upwelling fluxes. The resulting, data of τ, ω and g versus wavelengths for several aerosol layers in the atmosphere are estimated. Obtained optical parameters reproduce the spectral upwelling and downwelling hemispherical fluxes with an estimated relative error of not more than 5%.

Valero F.P.J., Ackerman T.P. and Gore W.J.Y. The effects of the Arctic haze as determined from airborne radiometric measurements during AGASP II. J.Atm.Chem. 1989, 9, 225-244.

Sokolik I.N. Investigation of optical and radiative-climatic effects of absorbing aerosols. PhD thesis. Institute of Atmospheric Physics, USSR Acad.Sci., Moscow, 1989, 116p.

Session 4

Icecores

Chairman:
J. Dibb

Continuous High Resolution Dust Measurements along Greenland Ice Cores.

by

C.U. Hammer and P. Iversen

Glaciological Dept., Geophysical Inst., University of Copenhagen.

Abstract:

Among the trace substances, which presently can be measured continuously and with high resolution along Greenland ice cores, the dust concentration is of particular interest: It can be measured with 0.5-1 mm resolution; does nearly not diffuse during the ice flow; shows a seasonal though irregular cycle, which can be used for dating old annual ice layers; its origin is continental even though the contribution from various continents needs to be investigated e.g. by isotopic analysis.
The instrumental measuring technique was applied on the South Greenland Dye 3 deep ice core (drilled 1979-1981), but has recently been strongly improved: It is now possible to analyze in situ approximately 50-60 meter of ice core per day (0,5-1 mm resolution).
The data were obtained during the EUROCORE 1989 300 m drilling in Central Greenland at the Summit location. The dust concentration profiles presented are typical for the Holocene i.e. the past 11500 years. The resolution is approx 3-5 mm as the high resolution combined with a high daily rate of core processing was first accomplished in 1991 and 1992.
The interpretation of the data in terms of seasonal variations is discussed; especially the effect of variable seasonal snow accumulation and year to year changes in the seasonal weather conditions.

Introduction

The dating of polar ice cores by seasonal variations of the dust concentration in the ice is a well established stratigraphic dating technique[1,2]. In most cases, however, the sole use of the dust concentration profile is not sufficient to secure a high dating accuracy and other seasonally varying parameters must be included in the analysis[3]. Even though the seasonal variations of the dust concentration in Greenland ice cores can be quite irregular and often less pronounced, than similar variations in e.g. $\delta(^{18}O)$ and nitrate, dust profiles along the cores offer special advantages:

a) The dust concentration can be measured continuously and with a very high resolution, 0,5-1 mm, along the core: At some locations on the ice sheet, this allows individual snow-fall/storm events to be detected in the ice[3].

b) Dust diffuse very little in the ice during the ice flow and the seasonal signal can be traced to the oldest ice at deeper strata of the core.

c) The most likely sources of the dust is known, at least for the past 8000 years, even though the average contribution from the various source regions needs to be investigated by isotopic analysis of the dust.

d) Under the meteorological conditions existing in e.g. Central Greenland it can be assumed, that the dust concentration in the deposited snow, on the average, mirrors the concentration in the precipitating air-mass[4].

Point c and d need of course to be verified by experimental studies, but are better fulfilled for dust, than for many other chemical substances of the atmosphere.

In practice, however, the seasonal character of the dust concentration in the ice is strongly dependent on the seasonal snow-fall and the atmospheric meteorological pattern, which reigned during the year in question.

Seasonal variation and annual snow deposition

Contrary to the more central parts of Antarctica most of the snow accumulating on the Greenland Ice Sheet is brought to the ice sheet by cyclonic activity and it is possible to identify individual snow-falls/storms in the upper snow pack of the ice sheet.

This possibility of identifying individual snow-fall events is due to the relative high amount of snow-fall during a precipitation event and the pause until the next event: Characteristics like crystal size, crystal growth, and surface crusts are to some extent determined by the meteorological conditions prevailing during and after the snow deposition. In some cases the surface snow may be redistributed by storms which homogenize the first few cm of the ice surface; such layers can be identified in ice cores as sequences of constant impurity concentrations.

In a high accumulation area like Dye 3 (56 cm of ice/year) in South Greenland an average of 25 events a year can be identified in a snow pit, while at Summit (72° 23' 42'' N, 37° 28' 13'' W) in Central Greenland the number is only around 14.

The identification of seasonal $\delta(^{18}O)$ cycles in the Dye 3 core was relatively easy, because the annual accumulation was high: Diffusion of the water molecule was no hindrance to the stratigraphic dating of the core back to 8000 BP[5], but at older strata diffusion rapidly increased due to the thinning of annual layers caused by the ice flow.

At Summit the $\delta(^{18}O)$ profile is less helpful as a stratigraphic dating tool and already in the surface layers diffusive processes are complicating a straight forward identification of annual layers. Hence the use of the continuously measured highly resolved dust- and nitrate profiles as independent stratigraphic dating tools becomes important. The low number of individual precipitation events at Summit may in any case be a cause for misinterpretations. Missing snow deposition during any season complicates the interpretation. The nitrate profile, which is generally more smoothly varying than the dust profile, is easier to interpret in terms of seasonal cycles, however, also in this case the actual distribution of snow deposition during a year may obliterate some of the annual cycles.

The dust profile shown in *figure 1* is from the Central Greenland Summit core. From model calculations based on the average surface snow deposition/year an annual layer thickness of approximately 23 cm should exist at the relevant depth. Hence it is beyond doubt, that the dust profile in figure 1 shows seasonal variation, but it is not exactly clear how many seasonal cycles are present. The arrows mark some peaks, which could represent the maximum dust concentration in less pronounced years. It is, however, known from other Greenland ice cores that it is unlikely to observe annual snow depositions much less than half the annual average

deposition. Therefore these peaks are probably part of irregular seasonal variations and not caused by low snow deposition during some parts of the year. The seasonal varying nitrate profile in figure 1 confirms that the above conclusion is most likely correct.

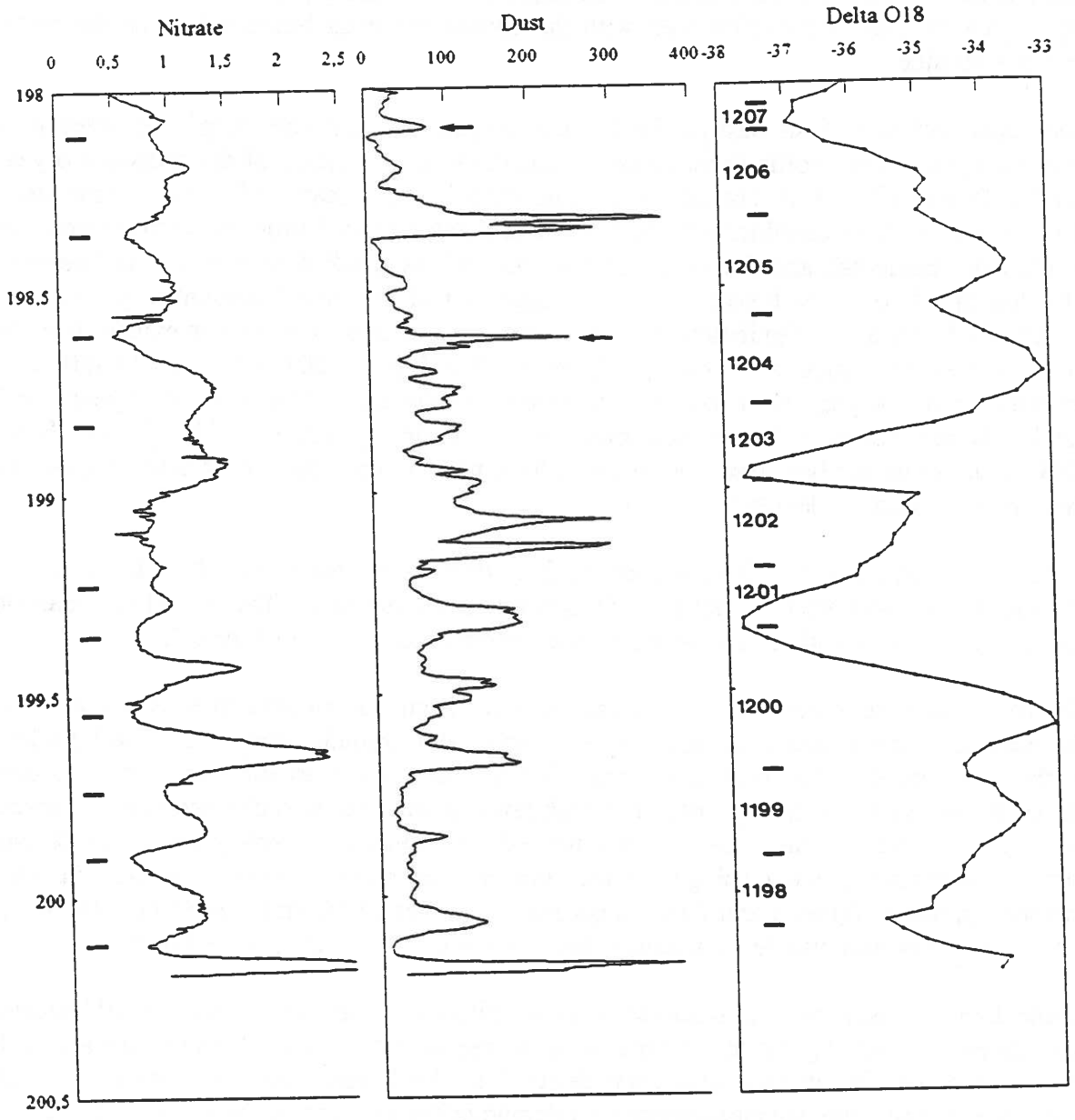

Figure 1 shows the continuous Nitrate dust and δ profiles over a 2,20 m ice core sequence from 198,00 - 200,20 m depth at the Summit drill-site. The nitrate concentration is given in μ equiv./kg of ice, the dust concentration in relative units and the isotopic composition of the ice in the δ scale ($\delta^{18}O$, the relative deviation of the ^{18}O concentration from that in Standard Mean Ocean Water; given in per mille)

It is possible to apply a mathematical back-diffusion technique in order to restore the original δ variations[6], but this technique requires detailed sampling and precise isotopic measurements over the ice sequence in question. The δ profile on figure 1 corresponds to a sampling frequency of 9 per calculated annual layer; the precision of the measurements is 0,005-0,1 °/oo, which is usually sufficient to "restore" most of the seasonal δ variations. The low annual

accumulation at Summit combined with the natural variability of the snows isotopic composition makes the back-diffusion technique less precise, when applied to the Summit core. Still the δ profile can be of some help to identify annual layers.

The annual divisions shown in figure 1 are based solely on the δ profile and, as can be seen, they agree in most cases fairly well with the annual divisions based solely on the nitrate profile (left side).

The upper half part of the dust profile is quite irregular and not very helpful for identifying seasonal cycles. The profile does, however, contribute to the dating of the proposed δ years 1200 A.D. and 1207 A.D. The annual accumulation in the δ year 1207 A.D. is quite small, the δ profile not very convincing (only a few data points and variability close to the precision of the measurements), and the nitrate profile around 1206-1208 A.D. not easy to interprete. The dust profile over the δ year 1207 A.D. suggests, that this "year" amount of precipitation consisted of only a few significant individual deposition events (this is more evident from the more detailed raw data; not shown in figure 1). The δ year 1207 A.D. may therefore not represent an actual year, but is rather an erroneous interpretation. The proposed δ years 1202-1201 A.D. are supported by the clear minimum in the dust profile in 1201 A.D. The δ year 1200 A.D. can hardly be correct because both the dust and nitrate profile strongly suggest, that this "year" should be devided into two.

In *figure 2* a sequence of δ, dust, and nitrate data covering the years 1280-90 A.D. are shown. (The high dust level around 1283-84 A.D. is due to contamination). The annual nitrate cycles are easy to identify and the annual dust cycles more regular than in figure 1.

On the average the lowest dust concentrations occur from late summer to early winter, while the minima in the nitrate concentration seems to cluster around winter time. The high level of the dust concentration apparently occurs between late winter to summer with the highest values in late winter to spring. Often this high level region of dust is characterized by several peaks of dust, which makes the identification of the annual cycle solely by use of the dust profile less certain than e.g. using the nitrate profile. The multi-parameter stratigraphic dating method applied to figure 1 and 2 can in general be applied to the entire Summit core, though the δ method is only usable, in practice, back to some 4000 years old ice layers.

A check of the resulting time scale can be accomplished by the use of a number of historical well dated volcanic signals in the core. Most of the well dated acid volcanic signals in the Dye 3 core has for instance also been detected in the Summit core; by using the multi-parameter dating approach and comparing volcanic reference horizons in the two cores a very high dating accuracy has been obtained.

Apart from the dating itself the identification of e.g. all the annual layers and their thicknesses over the past 1000 years offers the possibility of studying phase relations over the year between various atmospheric trace substances; it also opens the possibility of treating e.g. the seasonally varying dust concentration in a statistical way. It may be possible to detect significant changes in the seasonal deposition pattern of dust with time and analyze it in terms of climatic change. In case of the not too drastic climatic changes during the mid- and late Holocene the statistical approach looks promising. For such a procedure to be succesful we do also need much more detailed data on the present relation between air composition and meteorological conditions over and around the ice sheet.

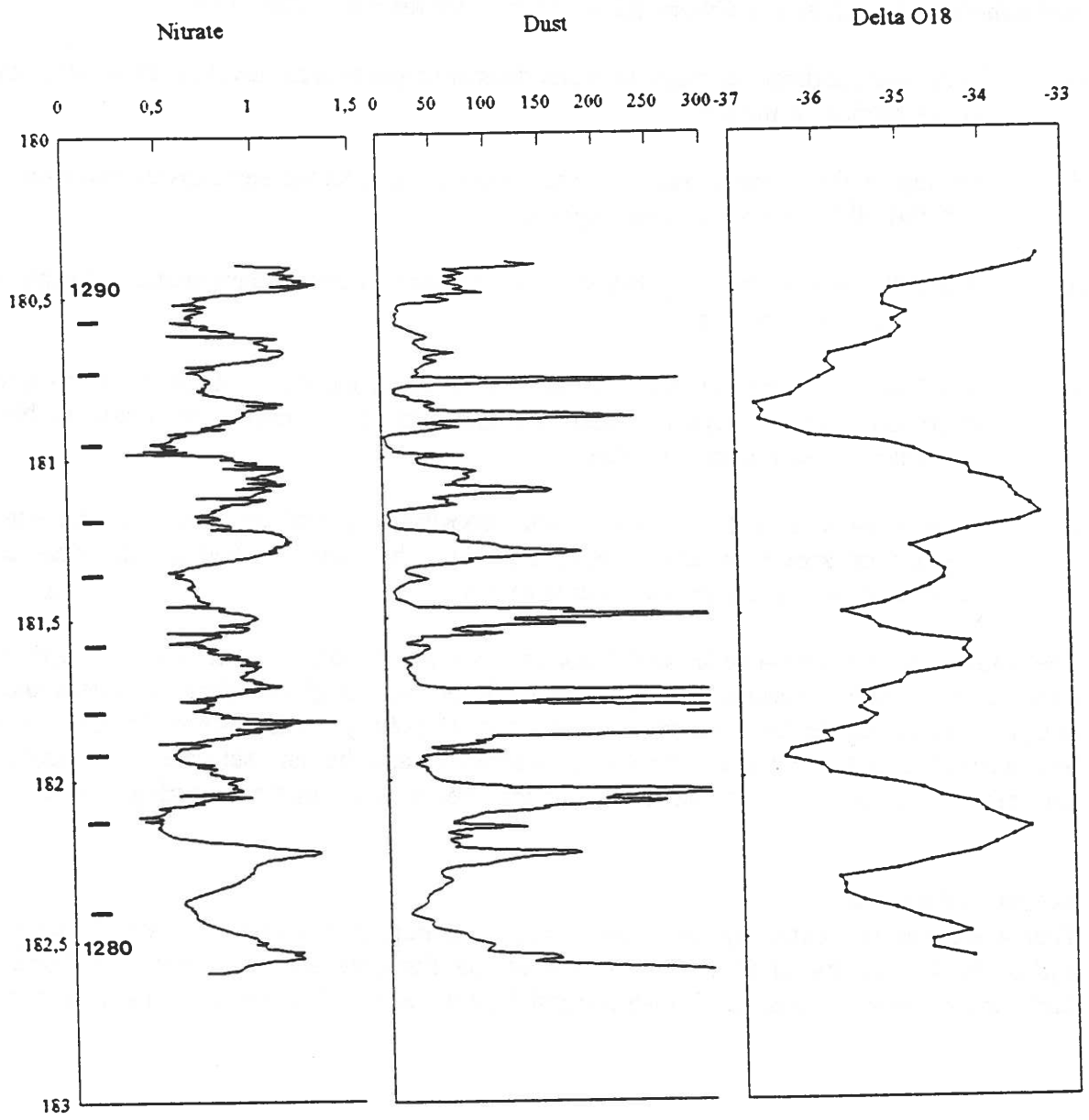

Figure 2 shows similar profiles as figure 1, but for the depth range 180,40 - 182,6 m of the Summit core.

Seasonal weather conditions

The dust concentration in Greenland ice cores has over longer time spans (more than 100 years) been analyzed by spectral analysis. The time series analyzed indicate that a considerable part of the power spectrum relates to frequencies which corresponds to 2-3 years, 5-8 years, and 20-35 years variation. The 5-8 years period can be associated with high dust concentrations in late winter to spring. This period also seems to determine, when dust concentrations vary in phase at different locations on the ice sheet. Contrary to this the 20-35

years period of the dust concentration does not indicate that such a phase relation exists; rather the variation of the dust concentration are out phase for the various ice sheet locations.

These findings and additional information on individual annual layers suggest the following working hyphotesis concerning the phenomena which determine the general features of the dust concentration profile in Greenland ice cores over the past 8000 years:

i) Persistent moderate climatic changes determine the general level of the average dust concentration in the ice.

ii) On top of the climatic induced dust concentration-change semi-cyclic variations of 5-8 and 20-35 years are superimposed.

iii) The 5-8 years period is probably associated with weather phenomena occuring due to the shift from winter to summer.

iv) The 20-35 years period affects all seasons and is associated with the transport tracks from the source regions to Greenland; the dust concentrations in South- to North Greenland need not vary in phase.

v) Exotic phenomena like volcanic ash deposition, special conditions at the source regions or special weather phenomena may be superimposed on the dust concentration as determined by point i) to iv).

The causes of the semi-cyclic variations are not at all known, but their strength and persistence through thousands of years clearly tell us, that the global climatic system and its internal feed-backs are far from being understood. Hopefully, in the future, the GCM's will be improved in order to explain the above phenomena and the data set based on continuous dust measurements along Greenland is cores may serve as a statistical "testing ground".

Acknowledgements
This work was supported by the Commission of European Communities and Switzerland within the framework of Cost 611 as part of the Eurocore program. We also thank the Carlsberg Foundation and the Danish Natural Science Research Council for their support.

References

1. Hammer, C.U. et.al.: Journal of Glaciology No. 20, p. 3-26, 1978.

2. Mosley-Thompson, E. and Thompson, L.G.: Quaternary Research No. 17, p. 1-13, 1982.

3. Hammer, C.U.: Dahlem Konferenzen 1988. Physical, Chemical, and Earth Sciences Research Report p. 99-121, 1989.

4. Junge, C.E.: IAHS-AISH publication No. 118, p. 63-77, 1977.

5. Hammer, C.U., Clausen, H.B., and Tauber, H.: Radiocarbon 28, No. 2A, p. 284-291, 1986.

6. Johnsen, S.J.: IAHS-AISH publication No. 118, p. 210-210, 1977.

5th International Symposium on

Artic Air Chemistry

Experimental techniques for icecore dust measurements.

Peter Iversen
Glaciological Department
Geophysical Institute
University of Copenhagen

(Oral presentation only)

Ongoing work on the size distribution of insoluble microparticles in Greenland ice cores from different climatic periods.

Jørgen Peder Steffensen
Geophysical Institute
University of Copenhagen

The insoluble fraction of the atmospheric aerosol is deposited on the surface of remote areas of large ice sheets along with precipitating snow by processes such as the particles acting as condensation nuclei, by scavenging or by gravitational fall-out. Assuming that the processes of deposition are more or less constant in time, changes in the microparticle content of ice cores reflect changes in the atmospheric aerosol, which implies changes in the atmospheric circulation or changes in the sources and sinks of the aerosol.

The bulk concentration of microparticles (given as the mass of particles larger than 0.5 μm radius in μg/kg) in ice exhibits a strong seasonal variation, with spring/summer high and autumn/winter low, which can be used for dating purposes (Hammer et al., 1979; Steffensen, 1987). Futhermore, microparticle concentrations varies with climate, e.g. in ice from both Greenland and Antarctica microparticle concentrations are 10 - 100 times higher in the cold periods of the last ice age than at present (Hammer, 1985; Petit et al.,1990; Thompson and Mosley-Thompson, 1981).

In contrast to the extensive work done on bulk concentrations not much work has been published on the size distributions of microparticles in ice cores. This is partly due to the fact that the Coulter Counting technique used for this type of work is rather cumbersome (no laser light techniques are feasible with present technology). There is however information to be gained from analyzing the size distributions of microparticles in ice cores, especially when the results are compared to the substantial amount of results from recent investigations on aerosol size distributions in the atmosphere itself.

In Antarctic ice, Petit et al, 1981, found relatively more large particles in ice from the last glaciation than than in recent ice. They ascribed this to higher storminess during the glacial period. Steffensen, 1985, analyzed the seasonal variation of the size distribution in recent snow from South Greenland, and found that the number distributions could be fitted to Junge distributions (Junge, 1963) with relatively more large particles in winter snow than summer snow.

With the advent of the Coulter Multisizer system it has become possible to expand the particle size interval to be analyzed from [0.5μm;5 μm] to [0.3μm;10μm] and to determine the size distribution with much higher precision. In a measurement program on the Dye-3 core from South Greenland, involving more than 600 samples, size distributions were measured in ice from the Holocene and different warm and cold periods from the last glaciation to compare the size distributions from different climatic periods. The measured volume distributions could be well fitted to a model distribution

consisting of one log-normal distribution in the interval [0.4μm;2.5μm] and approximated by a Junge distribution "tail" in the interval [2.5μm;6μm] (particles larger than 6μm radius are extremely scarce). The reason why the South Greenland results from 1985 could not be fitted by a log-normal distribution was that the mode of this distribution was not clearly defined in the size interval covered by the old Coulter Counting system and that the old techniques was less precise.

The model-fit allows for a parameterization of the measured distributions, by the mode and standard deviation and normalization factor of the log-normal distribution and the constant and exponent of the Junge distribution. Some of the more important parameters are given in Table 1.

TABLE 1:

Period:	Conc. (μg/kg)	L-conc. (μg/kg)	J-conc. (μg/kg)	mode μm	Std.dev.	no. of samples
Holoc. su.	38.8	37.8	1.0	0.79	1.66	64
Holoc. win.	9.1	8.3	0.8	0.72	1.82	83
Bølling	40.7	39.5	1.2	0.65	1.80	22
Warm 1	76.3	73.0	3.3	0.78	1.70	91
Warm 2	84.0	82.5	1.5	0.76	1.67	33
Warm 1 tr.	122	117	5	0.74	1.63	40
Cold 2	660	651	9	0.84	1.59	52
Cold 3	615	609	6	0.83	1.59	19
Cold 1	930	919	11	0.90	1.62	41
Young. dry.	278	276	2	0.79	1.59	20

Concentrations are given as total concentrations and the calculated contributions from the Log-normal and the Junge part of the distribution fit. The fits are made in the dV/d log r representation of the measured distributions, thus mode=mean=median of the Log-normal distribution. The exponent of the Junge distribution was between 3.1 and 6.8. A particle density of 2700 kg/m^3 is assumed in the mass calculations.

Unfortunately, the number of particles larger than 2.5 μm radius was so low in the Holocene samples(10 - 40 /ml), that the counting levels approached the levels of the "blank" samples, i.e. artificial clean samples measured to check the cleanlines of the laboratory and preparation procedures. Therefore, the results presented here, give less clear information on the Junge "tail" in the Holocene samples. A few examples of distributions are given in three different representations in the Figure, together with a mean "blank" sample for comparison.

The results show, that even though the particle concentrations vary almost two orders of magnitude in most of the different climatic periods, the mode and the standard deviation do not vary very much. The mode is slightly shifted towards larger particles in the cold periods of the glaciation though, and this is believed to be caused by higher storminess in these periods. The contribution of the Junge distributed part of the size distributions to the total concentration exhibits little variation between the different climatic periods (see columns 2 and 3 in Table 1). The observed variation in

the total concentration thus reflects the variation in the log-normal part of the size distribution.

In my interpretation, the "constant" modes (mean 0.75 μm) and standard deviations (mean 1.7 < 2) in the different periods indicate that it is the same mechanism that generates the insoluble fraction of the aerosol at the sources, i.e. the blowing of wind over arid land masses. The high concentrations in the cold periods could be explained as a consequence of larger and more effective sources and a more efficient transportation from the sources to the deposition site. The less varying Junge-fraction of the distribution could be the contribution from the atmospheric "background" aerosol, i.e. the aged aerosol found in the free troposphere even at remote sites. The size distribution of this background aerosol often resembles a Junge-distribution (Junge, 1963; Lechner et al., 1989).

In conclusion it appears, that during the cold periods of the last glaciation the aerosol load of the low troposphere was 10 times higher than in the warm periods, due to stronger/larger sources and a more vigorous transportation while the high tropospheric aerosol background was to a lesser degree affected by these climatic changes.

For future work it is planned to improve the laboratory and preparation techniques to gain information on the Junge-"tail" in Holocene ice. Sequences of EUROCORE and GRIP ice core samples from Central Greenland will be measured to establish a Holocene reference of microparticle size distributions, including the seasonal variation. The Holocene reference will be used to compare future findings in ice from earlier climatic periods in the newly drilled 3028 m deep ice core from Central Greenland. Ice from the upper part of EUROCORE will be analyzed to investigate if man-made pollution is visible in the microparticle size distributions.

Acknowledgements:

This work has been supported by the Danish Research Science Council and by the Commission of European Communities and Switzerland within the framework of Cost 611 as part of the Eurocore program.

References:

Hammer, C.U., H.B.Clausen, W.Dansgaard, N.Gundestrup, S.J.Johnsen and N.Reeh, 1979, Dating of Greenland ice cores by flow models, isotopes, volcanic debris and continental dust. Journal of Glaciology, 20, 82, p 3-26.

Hammer, C.U., H.B.Clausen, W.Dansgaard, A.Neftel, P. Kristinsdottir and E. Johnsen, 1985, Continuous impurity analysis along the Dye 3 deep core. Geophysical Monograph 33, C.C.Langway, jr., H.Oeschger and W.Dansgaard ed. American Geophysical Union, p 90-94.

Junge, C.E., 1963, Air chemistry and radioactivity. Academic Press, London.

Lechner, I.S., G.W.Fisher, H.R.Larsen, M.J.Harvey and R.A. Knobben, 1989, Aerosol size distributions in the Southwest Pacific, Journal of Geophysical Research, 94, D12, p 14893-14903.

Petit, J.R., M. Briat and A. Royer, 1981, Ice age aerosol content from east Antarctic ice core samples and past wind strength. Nature, 293, p 391-394.

Petit, J.R., L.Mounier, J.Jouzel, Y.S. Korodkevich, V.I. Kotlyakov and C.Lorius, 1990, Palaeoclimatological and chronological implications of the Vostok core dust record. Nature, 343, p 56-58.

Steffensen, J.P., 1985, Microparticles in snow from the South Greenland ice sheet, Tellus, 37B, p 286-295.

Steffensen, J.P., 1988, Analysis of the seasonal variations of dust, Cl^-, NO_3^- and SO_4^{--} in two Central Greenland firn cores. Annals of Glaciology 10, p 171-177.

Thompson, L.G. and E.Mosley-Thompson, 1981, Microparticle concentration variations linked with climatic change: Evidence from polar ice cores. Science, 212, p 812-815.

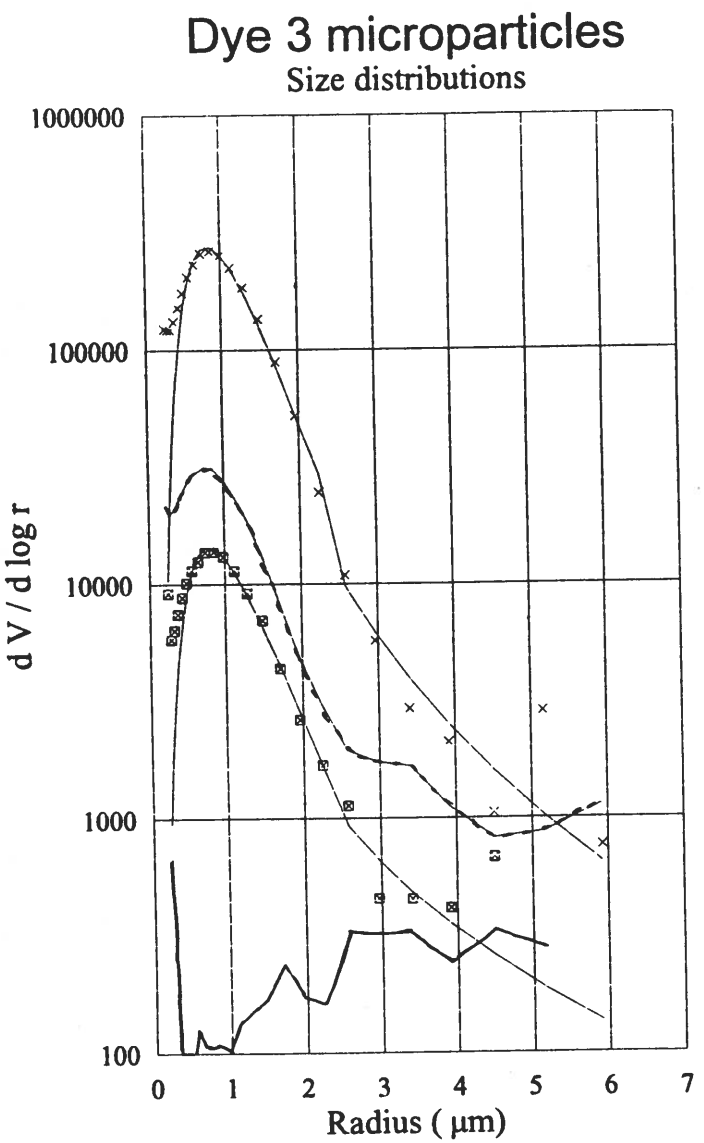
Dye 3 microparticles
Size distributions
1000000
100000
10000
1000
100
d V / d log r
0
1
2
3
4
5
6
7
Radius (µm)
Holocene summer data
Holocene summer fit
Wisc. warm periods data
Wisc. cold periods data
Wisc. cold periods fit
Mean blank sample

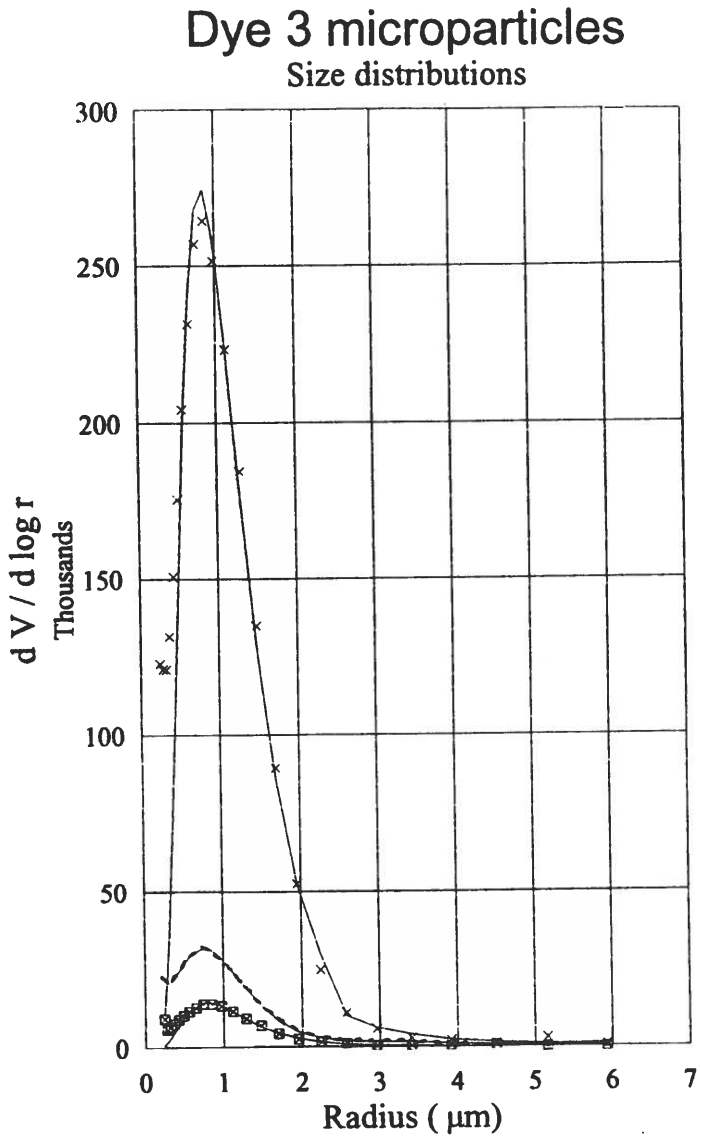
Dye 3 microparticles
Size distributions
300
250
200
150
100
50
0
d V / d log r
Thousands
0
1
2
3
4
5
6
7
Radius (µm)
Holocene summer data
Holocene summer fit
Wisc. warm per. data
Wisc. cold periods data
Wisc. cold periods fit
Mean blank sample

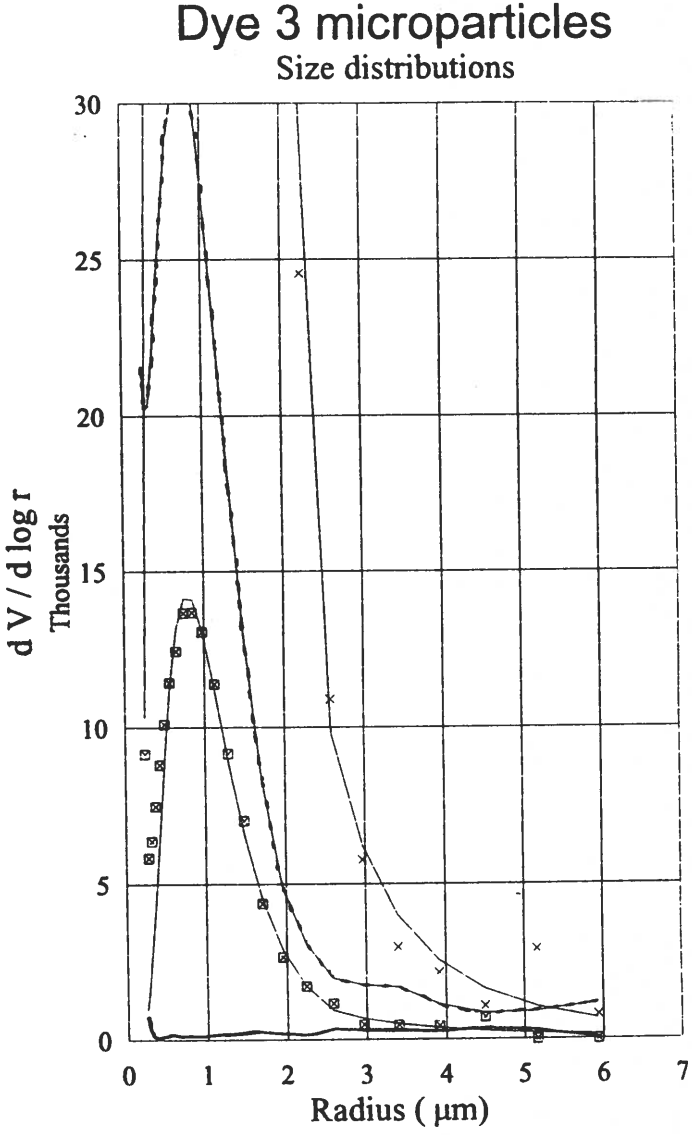
Dye 3 microparticles
Size distributions
30
25
20
15
10
5
0
d V / d log r
Thousands
0
1
2
3
4
5
6
7
Radius (µm)
Holocene summer data
Holocene summer fit
Wisc. warm per. data
Wisc. cold periods data
Wisc. cold periods fit
Mean blank sample

Session 5

Air-Snow Relationships

Chairman:
C. Hammer

SULFATE AND MSA IN AIR AND SNOW ON THE GREENLAND ICE SHEET

Jean-Luc Jaffrezo[1] and Cliff I. Davidson[2]

Prepared for the Proceedings of the Fifth International Symposium on Arctic Air Chemistry

Copenhagen, Denmark, 8-10 September 1992

[1]Department of Civil Engineering, Carnegie Mellon University, Pittsburgh, PA 15213 USA

Current address: Laboratoire de Glaciologie et Geophysique de l'Environnement du CNRS, Rue Moliere, Domaine Universitaire, BP 96, 38402 Saint Martin d'Heres, FRANCE

[2]Departments of Civil Engineering and Engineering and Public Policy, Carnegie Mellon University Pittsburgh, PA 15213 USA

I. INTRODUCTION

Two major multicomponent programs have taken place since 1988 to study the transport of chemical species from source regions to the Greenland Ice Sheet.

The Dye 3 Gas and Aerosol Sampling Program (DGASP) took place at Dye 3, a radar station located on the southern part of the Ice Sheet (65°, 11" N, 43°, 50" W, elevation 2479 m). This year-round program was conducted from August 1988 to July 1989 (Jaffrezo and Davidson, 1993). The program included the collection of near-daily aerosol samples together with fresh snow and snowpit samples analyzed for many chemical species. Samples of air for trace gas analysis were collected weekly. Studies of the climatology and the determination of source regions for the air masses arriving on site were also part of DGASP.

The second program, known as ATM, involves sampling of aerosols, gases, and snow at Summit (72° 20' N, 38° 45' W, elevation 3270 m). This program has been underway every summer since 1989 (Jaffrezo et al., 1991). The first three summer field seasons varied from 2 to 4 months each. The program began by being linked to the American and European deep drilling programs GISP II and GRIP that took place in the vicinity.

In this paper, we present the results of the DGASP and ATM sampling efforts for SO_4^{2-} and MSA. These species are particularly interesting: they represent a major fraction of the mass involved in the atmospheric sulfur cycle, and they are believed to play an important role in climate change (Charlson et al., 1987). We begin by discussing the experimental methods involved in the aerosol and snow collection during the two programs. We then present the data from both programs. Finally, we interpret and discuss the significance of the data.

II. EXPERIMENTAL

Aerosol samples for the determination of soluble ionic species were collected on Teflon Zefluor filters (pore size 1 μm, Gelman Sciences). The experimental set-up for the DGASP experiments enabled sampling for any wind direction: identical sampling equipment was located 300 m east and 300 m west of the radar station, with power provided by cables from the station. Details of the set-up have been described elsewhere (Jaffrezo and Davidson, 1993). For the ATM program, the experiments were conducted 28 km SSW from the main American drilling camp at GISP II (Jaffrezo et al., 1991; Dibb et

al., 1992). Electric power came from an array of solar panels that was upgraded from 1 kW to 7 kW between 1989 and 1991. A wind sector controller stopped the sampling when the wind came from the direction of the main drilling camp or from that of the local camp 500 m away. The remaining clean air sector encompassed 90° to 360° (true North). The local camp was managed in order to keep local contamination to a minimum: there were only 2-3 persons there, combustion sources were kept to a minimum, and the use of snowmobiles was limited.

During all of the experiments in both programs, extreme care was also taken to control direct contamination of the filters. No pre-washing was needed since the background for major anions and cations was very low for new filters. Filter holders were rinsed several times in Milli-Q water before loading. Handling of the filters took place under laminar flow benches, with personnel wearing disposable polyethylene gloves. The loaded filter holders were transported facing up, double-bagged in dust-free polyethylene between the field laboratories and the sampling locations. Filter holders were set in position for sampling by persons standing downwind of the filters and wearing full clean laboratory suits and disposable polyethylene gloves changed frequently.

After sampling, the filters were processed within 1 week (immediately in the case of DGASP) under a laminar flow hood in the field laboratories. Each filter was cut into several pieces using a stainless steel surgical knife and Teflon tweezers.

Fresh snow samples were collected from the surface immediately after each snowstorm. In some cases, older surface snow was also sampled. Collection took place at locations at least 1 km upwind of any local activity, with personnel dressed as described above. No tools were used; sample bottles were simply scraped along the surface.The goal was to sample the full depth of the fresh snow without collecting older snow underneath. Triplicate samples were collected in 125 ml polyethylene vials (Evergreen Scientific, Los Angeles) that had been extensively cleaned with Milli-Q water.

Several snowpits were also excavated during these experiments to assess the atmospheric signal in the accumulated snow. Similar contamination control procedures were implemented as in the aerosol and surface snow sampling. After excavation of a snowpit, several additional centimeters were shaved from the sampling wall just prior to collection of each sample. A sample consisted of six 30 ml polypropylene mailing tubes with screw caps; these were pushed directly into the wall to obtain the snow. These samples were handled similarly to the fresh snow samples.

The snowpit samples were not collected at fixed depth intervals below the surface. Rather, the stratigraphy of the layers was mapped and samples were collected from each stratigraphic layer. Layers were identified using a backlight pit: the main pit was covered with plywood (wrapped in clean polyethylene sheets) to minimize direct incidence of light, and another pit was excavated in the direction of the sun, 50 cm in front of the sampling wall. The light coming through this wall enabled the determination of stratigraphic features. Sampling in this manner allows collection of snow from discrete snowstorms rather than averaging over several storms.

All of the aerosol, surface snow, and snowpit samples were double-bagged in clean polyethylene and kept frozen in the dark until analysis. The analyses for SO_4^{2-} and MSA were performed with a Dionex 4500 ion chromatograph fitted with a PAX-100 column. The IC was programmed according to Dionex, using a 26 minute run with a gradient of sodium hydroxide and a constant concentration of methanol in the eluant. This allowed complete separation of the peaks of MSA and pyruvic acid, although the latter species was rarely present. Concentrations were calculated from the peak areas, using the ELAB-2 integration package (OMS Corp., Miami, FL). An injection loop of 700 µl was used. For these conditions, the typical detection limits were 0.20 ppb for MSA and 0.50 ppb for SO_4^{2}.

Preparation of the aerosol samples began with the extraction of a piece of filter in a Teflon beaker. The beaker had been thoroughly washed by rinsing with Milli-Q water in an ultrasonic bath. First, the filter was wetted with 1 ml of low-sodium grade methanol (JT Baker, Phillipsburg, NJ) before the addition of 14 ml of Milli-Q water. The beaker was shaken by hand at regular intervals for 10 minutes. The extract was then passed through a 0.45 µm pore size Teflon Zefluor filter to remove particles that might damage the IC column. Tests conducted in our laboratory have shown that retrieval of major anions and cations (including MSA and SO_4^{2-}) is always better than 95% for a single-step extraction.

Separate analyses were performed on two different pieces of each filter in order to obtain replicate data. Most of the results agree to within 10%. Field blanks for the determination of MSA in the aerosol are generally below the detection limit; average field blanks for SO_4^{2-} vary according to the different experiments, from 7.3 to 28.7 ppb. This translates into atmospheric detection limits of 0.1 ng/m^3 for MSA and 10 ng/m^3 for SO_4^{2-} for typical conditions encountered in this study.

Fresh snow and snowpit samples were thawed at room temperature in their collection vials under a laminar flow bench just before the analysis. They were not filtered or preconcentrated. Duplicate or

triplicate samples were analyzed using the same IC conditions as the aerosol samples. The results from analysis of these replicate samples generally agree to within 15%.

Aliquots of several samples were analyzed at the Laboratoire de Glaciologie et Geophysique de l'Environnement in Grenoble, France for quality assurance. Results of these analyses are generally within 15% of the CMU values.

III. PRESENTATION OF DATA

Figure 1 shows airborne concentrations of SO_4^{2-} and MSA corrected to STP conditions, as well as the molar ratio MSA/SO_4^{2-} at Dye 3 during the DGASP year. Values shown are arithmetic means of the analyses of the two filter halves. In this Figure and throughout the paper, total SO_4^{2-} concentrations uncorrected for seaspray have been used: based on the SO_4^{2-}/Na ratio in seawater, the fraction of marine SO_4^{2-} in the aerosol and snow at Dye 3 is small, almost always less than 10% of the total (Mosher and Jaffrezo, 1993).

Figures 2 and 3 show data for airborne SO_4^{2-}, MSA, and the ratio MSA/SO_4^{2-} for the 1990 and 1991 ATM field seasons, respectively. As in Figure 1, values shown are arithmetic means of two filter halves.

Figure 4 gives the concentrations of SO_4^{2-} and MSA, and the ratio MSA/SO_4^{2-}, in fresh snow at Dye 3. Similarly, Figures 5a, b, and c present the concentrations of SO_4^{2-} and MSA, and the ratio MSA/SO_4^{2-}, respectively, for a snowpit excavated on August 23, 1990. Sampling was conducted according to stratigraphy as described above; the horizontal lines on the Figures correspond to the boundaries observed between different layers.

The envelope in the MSA/SO_4^{2-} ratio in Figure 5c was calculated by determining the minimum and maximum values of this ratio. These were estimated using the range of values of MSA and SO_4^{2-} from one standard deviation below the mean to one standard deviation above the mean for each sample.

IV. DISCUSSION

A. SO_4^{2-} and MSA in Aerosols at Dye 3

Figure 1 shows that airborne concentrations of SO_4^{2-} at Dye 3 are very low in the winter. Episodic peaks begin in April and extend through May, with concentrations returning to background levels in June. Another period of relatively high concentrations occurs in October-November. This pattern is quite different from that observed at sea-level arctic sites, where high SO_4^{2-} concentrations are maintained from November-December through May. In contrast to the brief incursions of polluted air reaching Dye 3, where 1-2 day maximum values peak at 1000-2000 ng/m^3, weekly average values often exceed 2000 ng/m^3 at Alert in the Canadian Arctic (Barrie, 1986; Barrie and Barrie, 1990).

The shape of the SO_4^{2-} curve in Figure 1 can be explained on the basis of a combination of factors, similar to those responsible for seasonal variations in other chemical species at Dye 3 (Davidson et al., 1993 a, b; Dibb and Jaffrezo, 1993; Mosher and Jaffrezo, 1993). First, the source regions influencing Dye 3 vary with season, according to five-day backward air mass trajectories computed during the DGASP year (Davidson et al., 1993c). Source regions are mainly S and SW of Dye 3 during fall, W during winter, and NW during spring. There is no preferred direction in summer, when northward migration of the polar front greatly decreases the overall distances of transport for air masses reaching Dye 3. The source regions are thus over relatively clean areas of central Canada in winter; it is not until April that the source regions have move northward into the more polluted regions impacted by Arctic Haze, e.g. Barrow (Rahn and McCaffrey, 1979), Alert (Barrie and Barrie, 1990), and Nord and Thule, Greenland (Heidam, 1983 and 1984). The extent to which these trajectories are representative of other years is currently being investigated.

Second, strong temperature inversions are present over the Ice Sheet during much of the year (Putnins, 1970). These inversions limit air exchange between the free troposphere, where most of the long-range transport takes place, and the boundary layer where measurements are obtained. Dibb et al. (1992) have shown that aerosol concentrations greatly decrease during inversions, in part due to radiative fog events associated with the inversions which efficiently scavenge the aerosols. The inversions are weaker and less frequent during spring and fall, suggesting that better air exchange occurs between the surface and the free troposphere during April when the peak concentrations are observed.

Third, there is less precipitation in winter and early spring, leading to less scavenging of aerosols en route to Dye 3. Frequent precipitation as well as shorter transport distances overall are probably responsible for the low concentrations seen in summer and fall at Dye 3. However, lack of precipitation at a time when air masses were over populated regions of North America and western Europe may be responsible for the October-November peaks; this is suggested by the trajectories in Figure 6, corresponding to the date of the highest SO_4^{2-} peak in November.

The annual cycle of MSA in Figure 1 shows very low concentrations in winter and the first sizeable peaks in May. As with SO_4^{2-}, the pattern is episodic with brief periods of relatively high concentration. The highest values of the year are reached in June and July. There is also an October-November peak that is coincident with that for SO_4^{2-}.

Airborne concentrations of MSA are dominated by the marine biogenic production of DMS. Both production of DMS and oxidation of some fraction of the DMS to MSA are maximum during summer, leading to high MSA concentrations (Davison and Nicholas-Hewitt, 1992; Leck et al., 1990). However, Li et al. (1993) have hypothesized that some production of DMS may be occurring in the polar seas during the arctic winter, leading to a buildup of DMS in the absence of sunlight. Oxidation of this reservoir of DMS after polar sunrise might explain the increase of MSA in May shown in Figure 1. Alternatively, production of DMS around Iceland as early as April-May may be responsible for some of the brief episodes seen at Dye 3 (E. Saltzmann, personal communication). The dominant MSA peaks in June and July probably reflect short-range transport from biologically productive ocean areas surrounding Greenland. In contrast, the peak in October-November is more likely to reflect greater transport distances from warmer areas of the Atlantic, since DMS production in the northern latitudes have greatly decreased by this time (Davison and Nicholas-Hewitt, 1992; Watts et al., 1990; Leck et al., 1990), and atmospheric concentrations of MSA are known to be low in the northern regions during the fall (Savoie and Prospero, 1989; Li et al., 1993).

Figure 1 also shows that the MSA/SO_4^{2-} ratio is less than 1% for much of the year (late fall to mid-spring), but increases to 3-4% in May. Maximum values exceed 5-7% in summer, indicative of high biological productivity and oxidation to produce MSA, with low levels of anthropogenic SO_4^{2-}. These high ratios also imply local sources, since values above 5% are not generally found in mid or low latitude regions. There is no evidence of the October-November concentration increases in the curve of the MSA/SO_4^{2-} ratio, since both MSA and SO_4^{2-} vary in proportion. This is consistent with the trajectories

in Figure 8 from populated coastal areas where DMS production as well as anthropogenic SO_4^{2-} emissions are expected to be significant.

B. SO_4^{2-} and MSA in Aerosols at ATM

Figures 2 and 3 show that some of the patterns seen at Dye 3 also occur at ATM. For example, SO_4^{2-} concentrations are relatively low in mid summer, while MSA concentrations tend to be relatively high at that time. The MSA/SO_4^{2-} ratios thus show a pronounced increase in summer at both sites. However, the ATM data are more variable, and there are occasional incursions of polluted air during the summer. Because the Dye 3 and ATM data are for different years and only partially overlapping months, it is difficult to know if there are significant differences between the two sites.

MSA concentrations in both 1990 and 1991 show peaks early in the field season. Following those peaks, the concentrations are low until mid to late July, when there are additional concentration increases. The early peaks may indicate transport from the Arctic Basin where DMS has accumulated, as hypothesized for Dye 3. The elevated MSA levels in July and August probably reflect shorter range transport from the surrounding oceans as suggested for Dye 3, or transport from sources of production at high latitude. However, the MSA/SO_4^{2-} ratios at ATM peak much later than values of the ratios at Dye 3, due to the fact that SO_4^{2-} levels at ATM do not decrease substantially until August. It is noteworthy that the regular occurrence of two sets of MSA peaks, in spring and again in summer, have also been reported by Barrie (1992).

C. SO_4^{2-} and MSA in Fresh Snow at Dye 3

The fresh snow concentrations in Figure 4 are generally consistent with the aerosol data in Figure 1. However, some episodes in the air are missed because of lack of precipitation on the episode dates.

The overall variations in concentration in the snow are generally much smaller than variations in aerosol concentration. For example, the SO_4^{2-} concentration varies over one order of magnitude in the snow but over two orders of magnitude in the aerosol. Also, the MSA concentration varies over a factor of ~ 200 in the snow but over a factor of ~ 500 in the aerosol. The atmospheric variations are thus somewhat muted in the snow, as suggested previously by several authors (Rahn, 1981; Barrie et al., 1985; Davidson et al., 1987 and 1989).

The MSA/SO_4^{2-} ratios are quite similar in the snow and air. In both media, values are <1% in winter but over 5% in summer, with maxima at about 20%. This suggests that the air-to-snow transfer processes are acting in a similar manner on both SO_4^{2-} and MSA. Such a hypothesis is consistent with preliminary impactor measurements of SO_4^{2-} and MSA aerosol size distributions during ATM 1992, showing that both species are present primarily in sizes below 1 μm. This provides some confidence in using snow data for MSA/SO_4^{2-} ratios to reflect values of this ratio in the atmosphere.

D. SO_4^{2-} and MSA in the Snowpit at ATM

Figures 5a and b show that variations in concentration from one snowpit layer to the next are generally much greater than variations within a single layer. This indicates that there is little mixing between the layers, suggesting that the chemical information in a snowstorm is well preserved in the snowpit. Several factors are probably responsible, including the low occurrence of sastrugi at Summit, rapid development of crusts that protect the underlying layer, and a reasonably large accumulation (~24 g/cm^2 year).

Figures 5a, b, and c clearly identify the layers deposited in spring 1990 (between 30 and 45 cm), summer 1989 (between 65 and 80 cm), and spring 1989 (around 110 cm). There is good agreement between these depth values and the direct measurements of accumulation performed during the ATM field seasons by personnel at the camp, using a 100-pole accumulation network. Note that the accumulation during the fall and winter (October-late March) extends at most from 50 to 65 cm in the snowpit. This implies that less than 20% of the annual accumulation occurs in this six-month period, in agreement with results obtained with radionuclides measured in snowpits at the same location (Dibb et al., 1992). It is unknown whether this pattern results from substantial winter precipitation that is subsequently removed by wind or sublimation (perhaps leaving chemical constituents to remain in the snow pack) or whether there is simply little precipitation on-site; this is currently being investigated.

The dual MSA peaks in spring and summer 1989 are evident in Figures 5a, b, and c, consistent with the 1991 ATM aerosol data and the Dye 3 aerosol and snow data for 1989. It is also of interest that the concentrations of SO_4^{2-} in the snowpit range over a factor of 15, while concentrations of MSA range over a factor of 25. In comparison, aerosol SO_4^{2-} and MSA concentrations for ATM in 1991 range over factors of 50 and 80, respectively; if full-year aerosol concentrations were available, these ranges would be even greater. Thus, the atmospheric signals are somewhat muted in the snow. However, the

MSA/SO_4^{2-} ratio is reasonably well preserved, as evidenced by comparing the peak ratios in Figure 5c with those in the bottom curve of Figure 2: both curves indicate values above 20%, probably associated with high latitude air masses over Summit during summer.

CONCLUSIONS

This paper has summarized the results of SO_4^{2-} and MSA concentration measurements in aerosol, surface snow, and snowpit samples for two sites on the Greenland Ice Sheet. The data show that seasonal variations in atmospheric concentration are approximately reproduced in surface snow and preserved in snowpit records. The amplitudes of the variations over the year are smaller in the snow than in the air, but values of the ratios of MSA/SO_4^{2-} are comparable.

The seasonal variations for airborne SO_4^{2-} on the Ice Sheet are different from variations observed at sea-level arctic sites. Concentrations are much lower in winter on the Ice Sheet, with short episodes of elevated concentration in spring. In contrast, seasonal variations in airborne MSA are comparable on the Ice Sheet and at sea level, with a period of elevated concentrations in spring and a similar period in summer; MSA concentrations in winter are low at both categories of locations, due to reduced biogenic activity. The ratio MSA/SO_4^{2-} is indicative of high latitude sources during the summer, but the large impact of anthropogenic SO_4^{2-} precludes any conclusions based on the spring ratios.

The clear seasonal pattern observed for these species in a snowpit sampled according to stratigraphy indicates a deficit in the accumulation of winter snow at Summit, in agreement with results of others based on different different chemical species.

ACKNOWLEDGMENTS

The authors gratefully acknowledge the many participants in the Dye 3 Gas and Aerosol Sampling Program in field, laboratory, and data interpretation assistance. This work was funded by the following grants from the National Science Foundation: DPP-8618223, DPP-8821018, ATM-8922034, and DPP-9123082. The work conducted in France was funded in part by the French Ministry of the Environment and the Centre National de la Recherche Scientifique.

REFERENCES

Barrie LA (1986) Arctic air chemistry: an overview. In: Arctic Air Pollution, B. Stonehouse (ed), Cambridge Univ. Press, pp 5-23.

Barrie LA (1992) Presentation at the Fifth International Symposium on Arctic Air Chemistry, Copenhagen, Denmark, 8-10 September 1992.

Barrie LA and Barrie MJ (1990) Chemical component of lower tropospheric aerosol in the High Arctic: Six years of observations. J. Atm. Chem., 11, 211-226.

Barrie LA, Fisher D, and Koerner RM (1985) Twentieth century trends in Arctic air pollution revealed by conductivity and acidity observations in snow and ice in the Canadian High Arctic. Atm. Env., 12, 2055-2063.

Charlson RJ, Lovelock JE, Andreae MO and Warren SG (1987) Oceanic phytoplankton, atmospheric sulphur, cloud albedo and climate: A geophysiological feedback. Nature, 326, 655-661.

Davidson CI, Honrath RE, Kadane JB, Tsay RS, Mayewski PA, Lyons WB, and Heidam NZ (1987) The scavenging of atmospheric sulfate by arctic snow. Atm. Env., 21, 871-882.

Davidson CI, Harrington JR, Stephenson MJ, Small MJ, Boscoe FP, and Gandley RE (1989) Seasonal variations in sulfate, nitrate, and chloride in the Greenland Ice Sheet: Relation to atmospheric concentrations. Atm. Env., 23, 2483-2493.

Davidson CI, Jaffrezo JL, Mosher BW, Dibb JE, Borys RD, Bodhaine BA, Rasmussen RA, Boutron CF, Gorlach U, Cachier H, Ducret J, Colin JL, Heidam NZ, Kemp K and Hillamo R (1993a) Chemical constituents in the air and snow at Dye 3, Greenland. I: Seasonal variations. Atm. Env., in press.

Davidson CI, Jaffrezo JL, Mosher BW, Dibb JE, Borys RD, Bodhaine BA, Rasmussen RA, Boutron CF, Ducroz FM, Cachier H, Ducret J, Colin JL, Heidam NZ, Kemp K and Hillamo R (1993b) Chemical constituents in the air and snow at Dye 3, Greenland. II: Analysis of episodes in April 1989, Atm. Env., in press.

Davidson CI, Jaffrezo JL, Small MJ, Summers PW, Olson PM and Borys RD (1993c) Trajectory analysis of source regions influencing the South Greenland Ice Sheet during the Dye 3 Gas and Aerosol Sampling Program. Atm. Env., in press.

Davison B and Nicholas-Hewitt C (1992) Natural sulphur species from the North Atlantic and their contribution to the United Kingdom sulphur budget. J. Geophys. Res., 97, 2475-2488.

Dibb JE, Jaffrezo JL and Legrand M (1992) Initial findings of recent investigations of air-snow relationships in the Summit region of the Greenland Ice Sheet. J. Atm. Chem., 14, 167-180.

Dibb JE and Jaffrezo JL (1993) Beryllium-7 and Lead-210 in aerosol and snow in the Dye 3 Gas and Aerosol Sampling Program. Atm. Env., in press.

Heidam NZ (1983) Studies of the Aerosol in the Greenland atmosphere. Report MST LUFT-A73, NERI, Denmark, 169 pp.

Heidam NZ (1984) The components of the Arctic aerosol. Atm. Env., 18, 329-343.

Jaffrezo JL, Dibb JE and Davidson CI (1991) GISP 2 studies of the atmosphere and surface snow at Summit, Greenland. EOS, Transactions of the American Geophysical Union, 72, 250-251.

Jaffrezo JL and Davidson CI (1993) The Dye 3 Gas and Aerosol Sampling Program (DGASP): An overview. Atm. Env., in press.

Leck C, Larsson U, Bagander LE, Johansson S and Hajdu S (1990) Dimethyl sulfide in the Baltic Sea: Annual variability in relation to biological activity. J. Geophys. Res., 95, 3353-3363.

Li SM, Talbot RW, Barrie LA, Harriss RC, Davidson CI and Jaffrezo JL (1993) Seasonal and geographic

variations of methanesulfonic acid in the arctic troposphere. Atm. Env., in press.

Mosher BW and Jaffrezo JL (1993) Seasonal trends in aerosol chemistry at Dye 3, Greenland. Atmos. Env., in press.

Putnins P (1970) The climate of Greenland. In: Climates of the Polar regions, World Survey of Climatology. S Orvig (ed), Elsevier (pub), NY.

Rahn KA (1981) Atmospheric, riverine and oceanic sources of seven trace constituents to the Arctic Ocean. Atm. Env., 15, 1507-1516.

Rahn KA and McCaffrey RJ (1979) On the origin and transport of the winter arctic aerosol. Ann. N.Y. Acad. Sci., 338, 486-503.

Savoie DL and Prospero JM (1989) Comparison of oceanic and continental sources of non-sea-salt sulphate over the Pacific Ocean. Nature, 339, 685-687.

Watts SF, Brimbelcombe P and Watson AJ (1990) Methanesulfonic acid, dimethyl sulfoxide and dimethyl sulfone in aerosols. Atm. Env., 24A, 353-359.

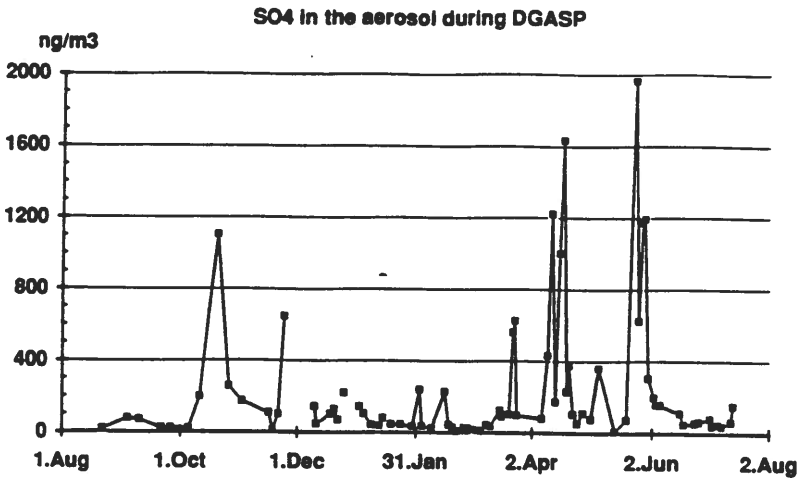
SO4 in the aerosol during DGASP
ng/m3
2000
1600
1200
800
400
0
1.Aug
1.Oct
1.Dec
31.Jan
2.Apr
2.Jun
2.Aug

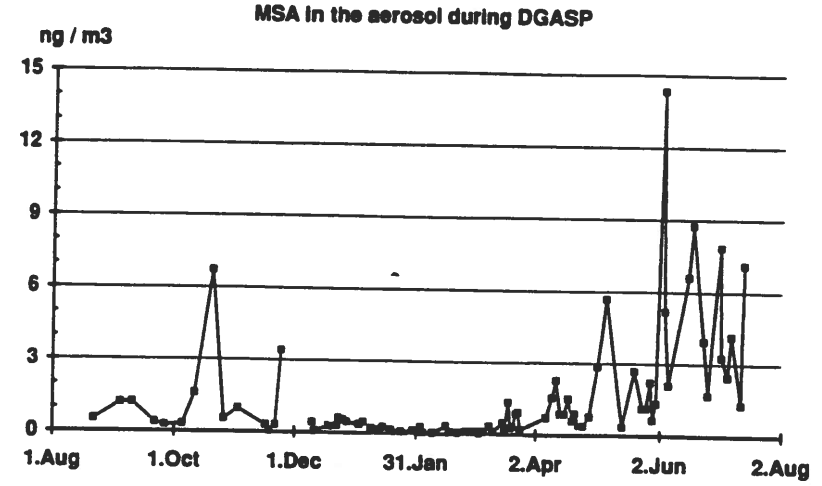
MSA in the aerosol during DGASP
ng / m3
15
12
9
6
3
0
1.Aug
1.Oct
1.Dec
31.Jan
2.Apr
2.Jun
2.Aug

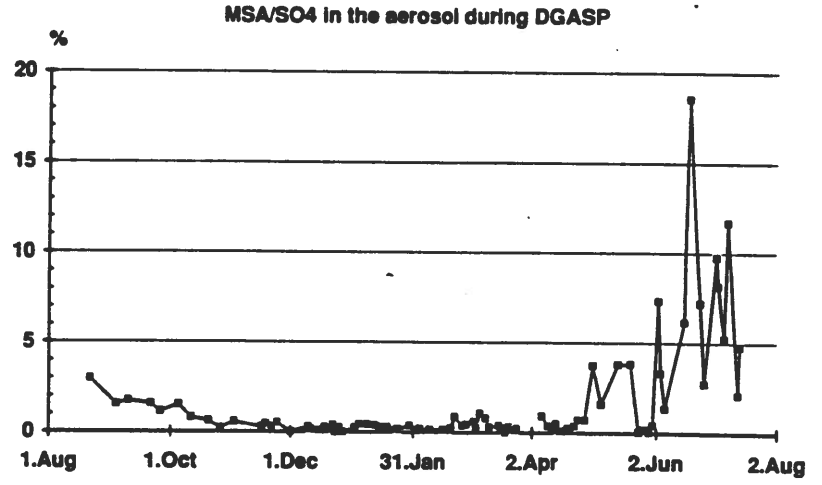
MSA/SO4 in the aerosol during DGASP
%
20
15
10
5
0
1.Aug
1.Oct
1.Dec
31.Jan
2.Apr
2.Jun
2.Aug

Figure 1

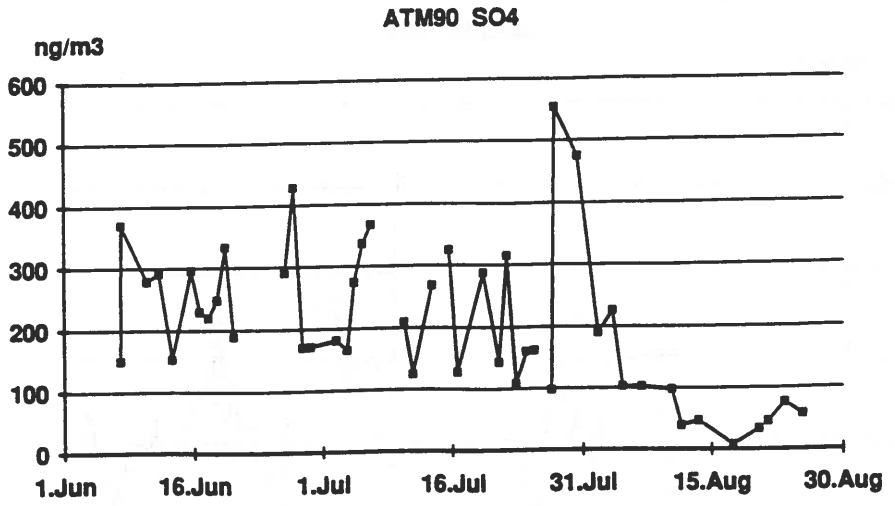

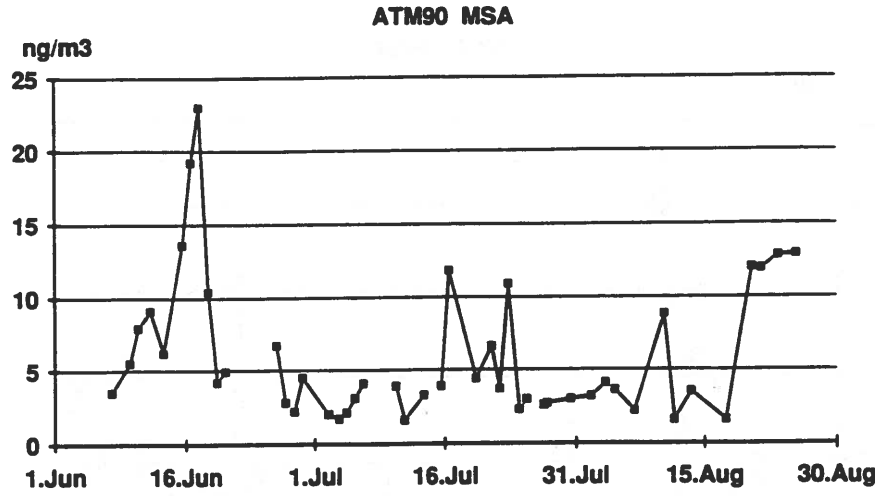

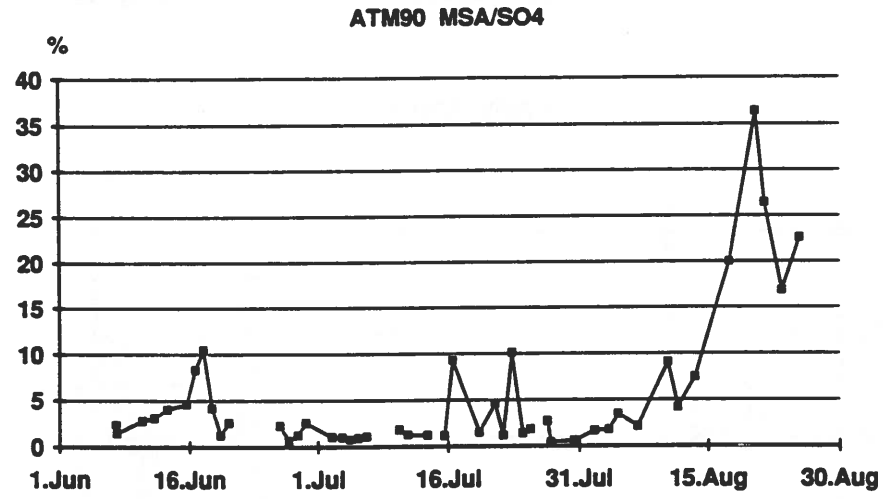

Figure 2 Concentrations in the aerosol

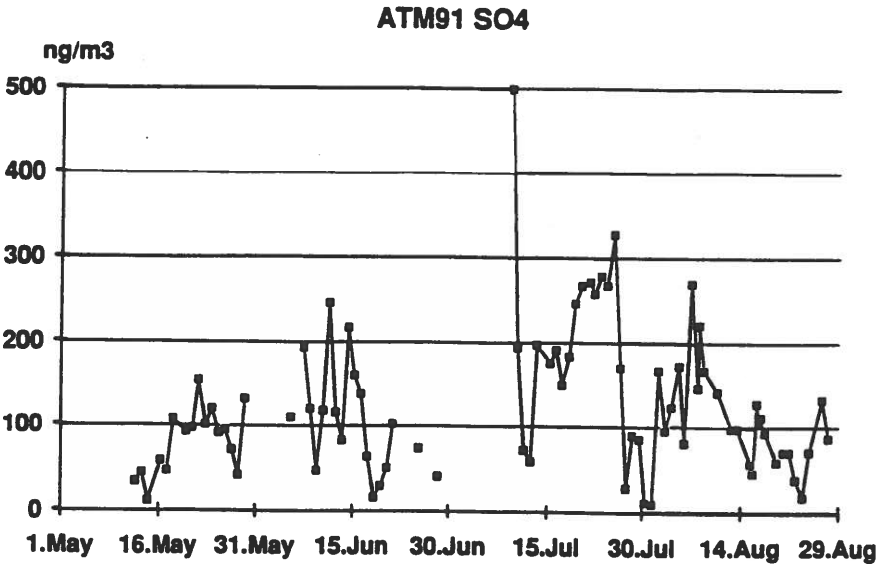

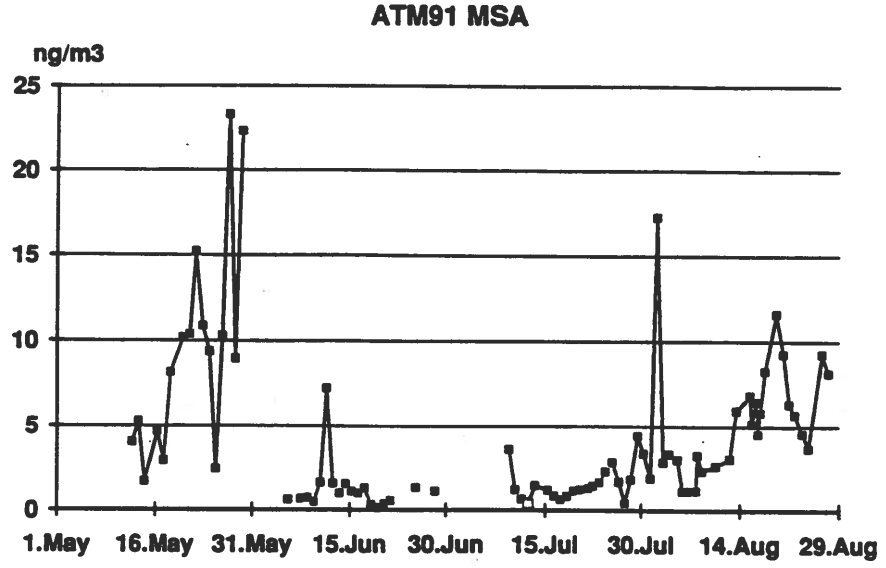

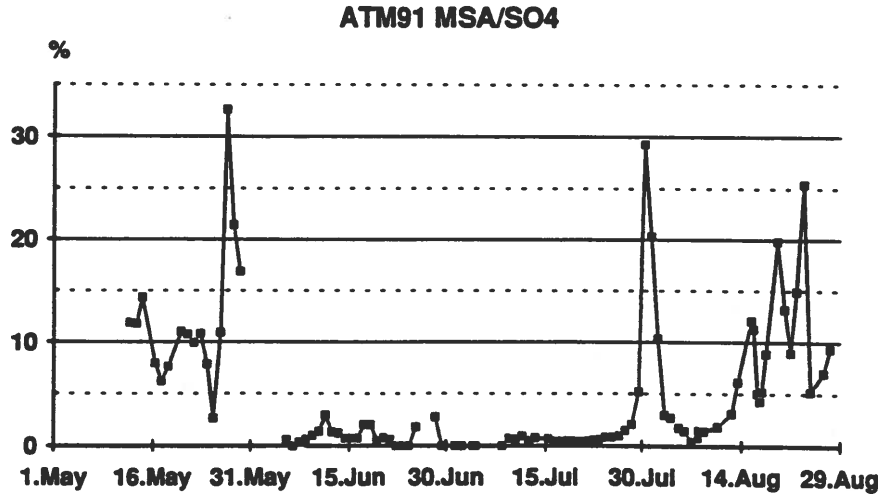

Figure 3 Concentrations in the aerosol

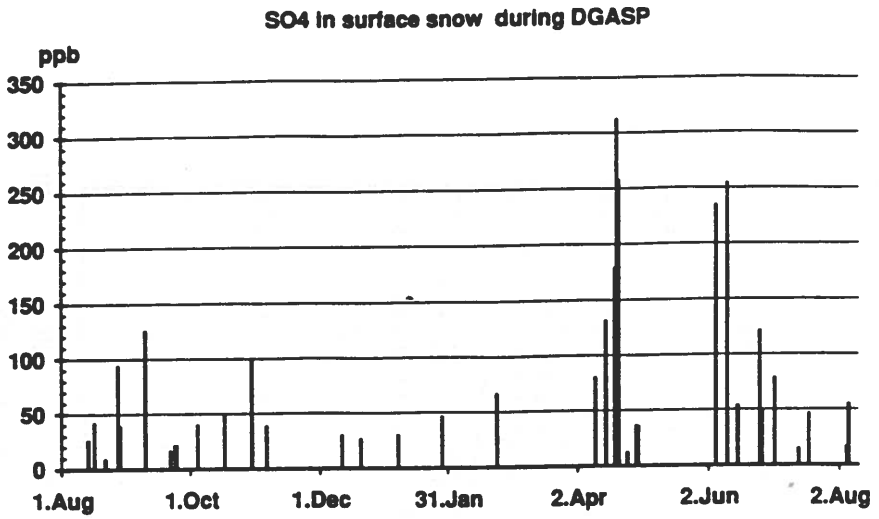
SO4 in surface snow during DGASP
ppb
350
300
250
200
150
100
50
0
1.Aug
1.Oct
1.Dec
31.Jan
2.Apr
2.Jun
2.Aug

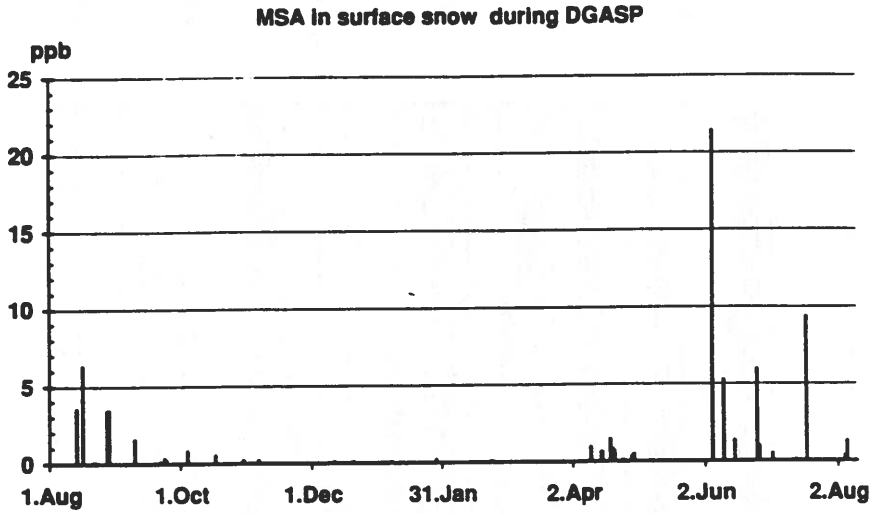
MSA in surface snow during DGASP
ppb
25
20
15
10
5
0
1.Aug
1.Oct
1.Dec
31.Jan
2.Apr
2.Jun
2.Aug

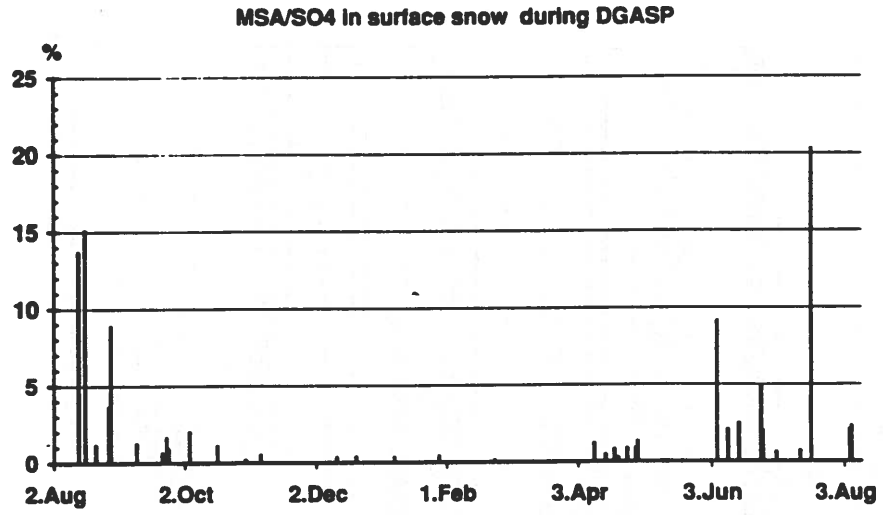
MSA/SO4 in surface snow during DGASP
%
25
20
15
10
5
0
2.Aug
2.Oct
2.Dec
1.Feb
3.Apr
3.Jun
3.Aug

Figure 4

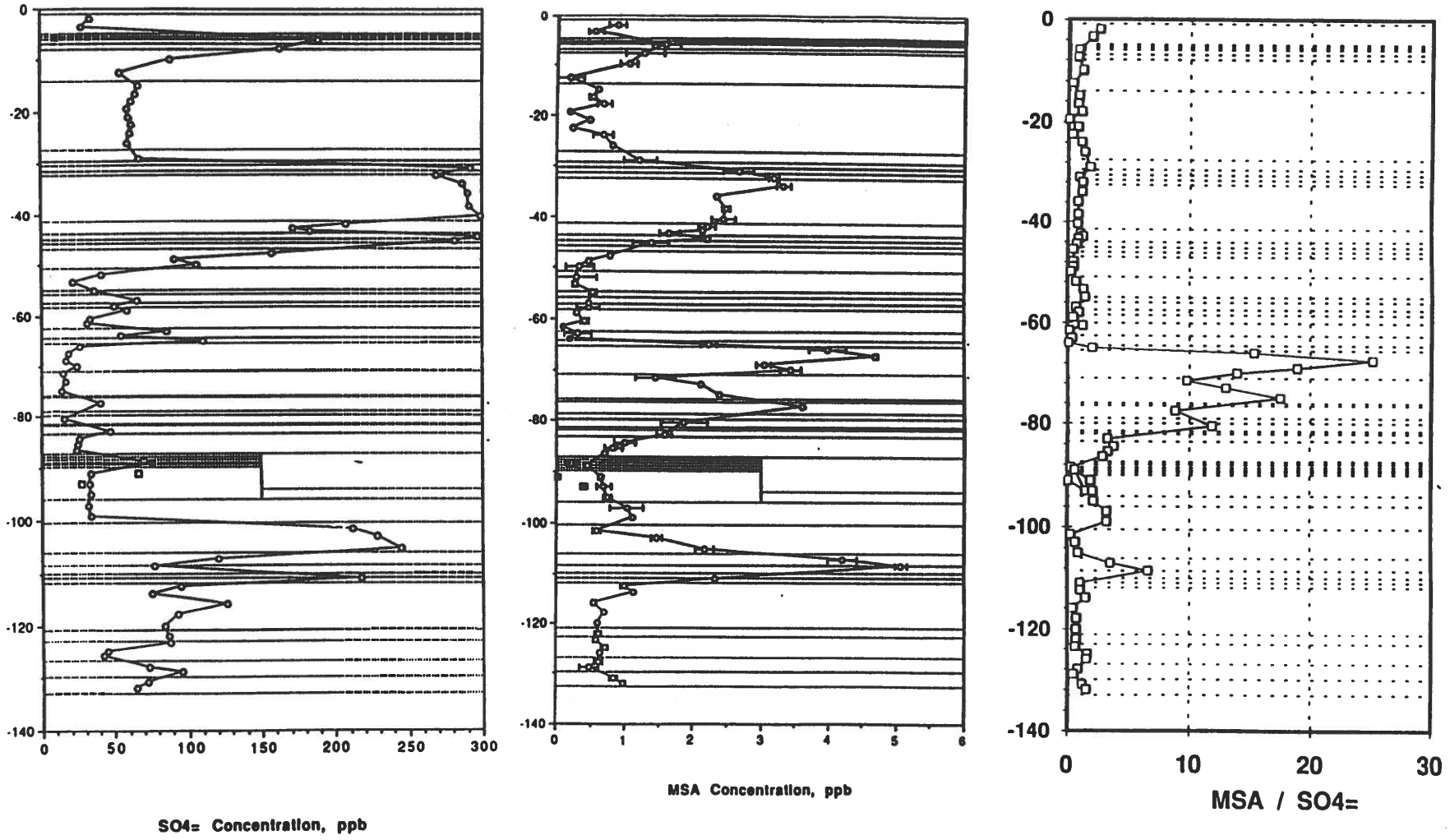

Figures 5a, 5b, 5c

Concentrations in a snowpit dug during ATM90
Surface (0 cm) as of 08-23-90

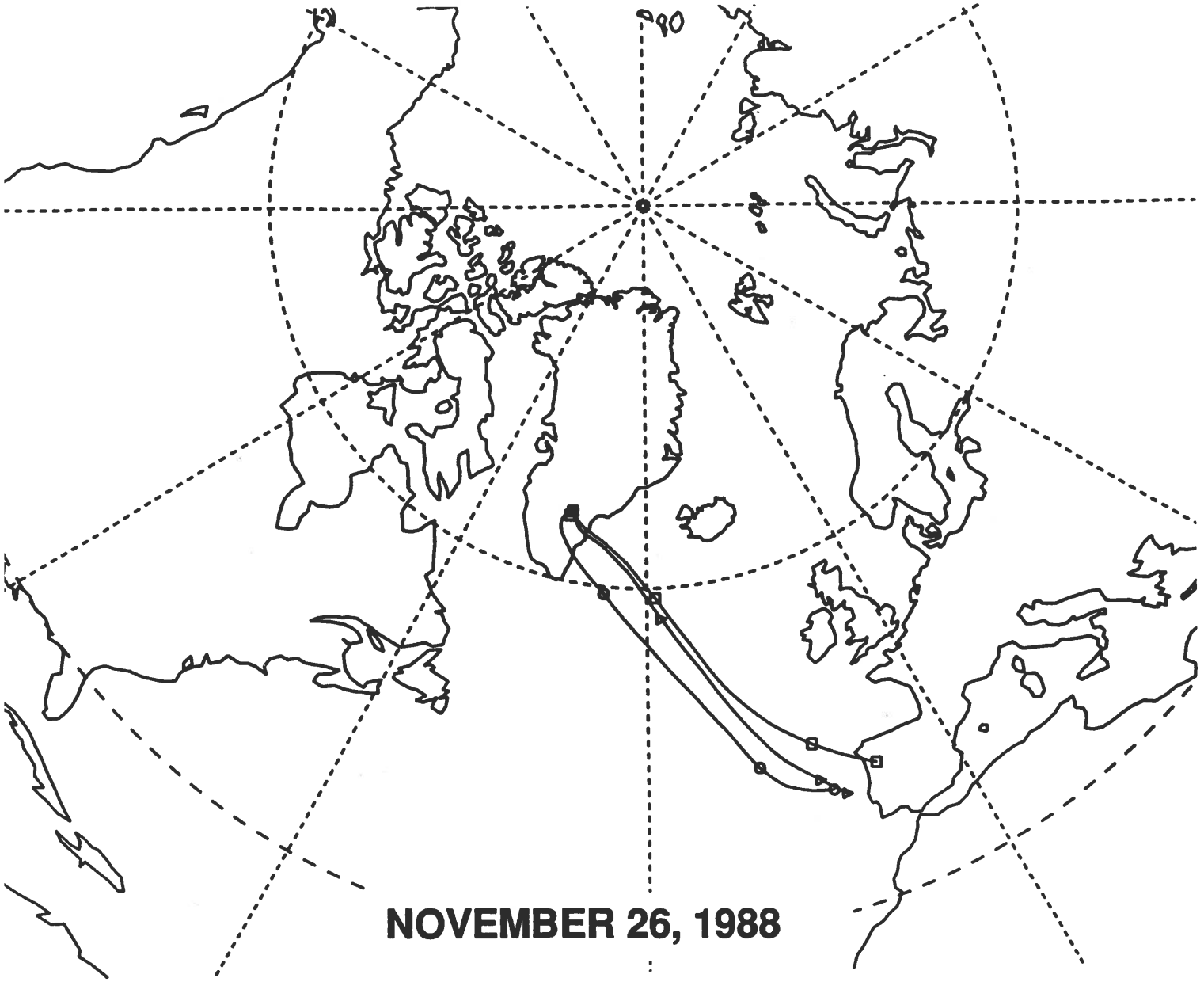

Figure 6

3-day backtrajectories ending at Dye3 on 11-26-88, 0000TU

○ 500 hPa
△ 700 hPa
□ 775 hPa

Further Insights into Air-Snow Relationships at Summit, Greenland from Beryllium-7 and Lead-210.

Jack Dibb, Glacier Research Group, UNH/EOS, Durham, New Hampshire, 03824 USA

Presented at the Fifth International Symposium on
Arctic Air Chemistry

8 - 10 September, 1992 Denmark

And Submitted for Proceedings

ABSTRACT

An ambitious, international, multi-parameter investigation into air to snow transfer processes has been associated with the GISP2 and GRIP deep drilling programs at Summit, Greenland. One aspect of this program has been the collection of daily (or more frequent) high volume aerosol samples, fresh and aged surface snow samples, and a series of shallow snowpit profiles for the determination of the natural radionuclides ^{7}Be and ^{210}Pb. Results for the 1989 and 1990 summer seasons have been previously reported (Dibb, 1990; Dibb et al., 1992). Key findings included the tendency for the concentrations of these radionuclides to covary in surface-level air (apparently in response to local-scale exchange between free tropospheric and boundary layer air), a general lack of clear relationships between the radionuclide concentrations in fresh snow and surface air during snowfall events, and the frequent detection of surprisingly high levels of the short-lived ^{7}Be (half-life = 53.3 days) at depths in the snowpack approaching the annual layer thickness (suggesting a strong bias toward spring and summer in the records preserved at this site).

The 1991 season was characterized by greater storminess than the first two seasons, with extended periods of surface winds exceeding 20 knots and considerably more snowfall. One result of these different weather patterns was lack of the "expected" covariance of ^{7}Be and ^{210}Pb aerosol concentrations, presumably due to vigorous larger-scale vertical mixing overriding the boundary layer processes that had dominated during previous summers. This suggests that surface level aerosol samples were more representative of the air aloft at snow formation height, as evidenced by scavenging ratios calculated for the fresh snow samples which tended to cluster (near 200 for ^{7}Be and 300 for ^{210}Pb). The increased snowfall nearly doubled the depositional fluxes of both radionuclides compared to 1989 and 1990. This increased scavenging of the radionuclides by snow also resulted in their average concentrations in surface-level aerosol being quite similar in all three summers, rather than showing an expected increase in 1991 due to the apparently greater downward mixing of free tropospheric air.

In 1991 direct knowledge of the structure of the lower atmosphere over Summit was obtained for the first time through tether sonde profiling. The period 13-19 August is of particular interest, with sonde profiles measured every three hours and aerosol filters changed every eight. ^{7}Be concentrations reached 500 fCi m^{-3} STP in two samples collected 16-17 August, nearly twice as high as the previous maximum observed in nine months of sampling over three seasons. Temperature profiles during this time showed rapidly descending air, which presumably originated in the upper troposphere or lower stratosphere.

INTRODUCTION

Chemical records recovered from polar glaciers are arguably the highest quality, high resolution, proxy records of past climate and atmospheric conditions over at least the last 100,000 years. Concern over the very real potential for large anthropogenic impacts on the operation of the coupled atmosphere-hydrosphere-climate systems has heightened interest in the past operation of these system and proportionately increased the value of glacial records to the "global change research" community. The high visibility of the Vostok deep coring effort, the coordinated US (Greenland Ice Sheet Project Two (GISP 2)) and European (Greenland Icecore Program (GRIP)) drilling programs currently underway at Summit, Greenland, and the advanced state of planning for a US deep core in West Antarctica, are prominent indications of the current scientific interest in long ice core records.

It is clear that the chemistry of glacial snow and ice largely reflects that of the atmosphere from which the snow was derived. However, nearly a decade ago, Lambert et al. (1983) observed that "***for lack of a transfer function between air and snow, it is yet impossible to deduce from firn measurements what the air concentration was at the time of deposition***" (p. 1289). Despite a number of recent studies attempting to

quantify air to snow transfer of a range of atmospheric constituents in both polar regions [(Rahn and McCaffrey, 1979; Ng and Patterson, 1981; Peel and Wolff, 1982; Borys, 1983; Davidson et al., 1985, 1987, 1989; Dick and Peel, 1985; Dick, 1988) (perhaps reflecting the fact that these studies were far from reaching a consensus on air-snow relationships)], the June, 1988, Ice Core Workshop at Durham, NH, concluded that quantification of air-snow transfer functions should remain a priority research objective to allow full interpretation of ice core records. This group also pointed out that post-depositional modification of snow may significantly alter some atmospheric signals before preservation as glacial ice, but that understanding of these processes is very limited. The international scientific community has also recently restated the importance, but current lack, of a quantitative understanding of air-snow and snow-glacial ice transfer processes.

The Polar Air-Snow Experiment (PASE), a planned project under IGAC, which is, in turn, a core project of IGBP, has as its ambitious, but simply stated, goal: "***to establish the relationships between atmospheric composition and the chemical composition of ice in the central polar areas***" (IGAC, 1990, p. 25). This goal was also central to the year long Dye 3 Gas, Aerosol and Snow Sampling Program (DGASP) and to ongoing atmospheric and snow sampling at Summit, Greenland in conjunction with the GISP2 and GRIP deep drilling programs. The author has participated in all of these recent campaigns, focusing on the use of the natural radionuclides ^{7}Be and ^{210}Pb as tracers of submicron aerosols in the atmosphere and upper layers of the snowpack.

Radionuclides as Tracers.

Although the short half-lifes of ^{7}Be and ^{210}Pb (53.3 d and 22.3 y, respectively) preclude their presence in polar glacial ice, they have attributes that make them well suited for studies of air-snow and snow-snowpack transfer processes. After formation from gaseous precursors in the atmosphere, mainly at low altitudes for ^{210}Pb and in the upper-troposphere and lower-stratosphere for ^{7}Be, both radionuclides quickly attach to ambient aerosol particles, predominantly those in the submicron size fraction (Turekian et al., 1989). (Lead-210 is a daughter of ^{222}Rn, while ^{7}Be is cosmogenic.) Thereafter, the fates of ^{7}Be and ^{210}Pb are those of the particles on which they reside, making them ideal tracers for the study of processes removing submicron aerosol particles from the atmosphere (Brost et al., 1991; Feichter et al., 1991). This very simple atmospheric chemistry also suggests that ^{7}Be and ^{210}Pb in fresh and surface snow will continue to be associated with submicron particles, hence their concentrations in the snow may be modified by physical, but probably not chemical, processes occurring after deposition.

Because of their presumed exclusive association with aerosol particles, ^{7}Be and ^{210}Pb alone can not provide insight into all of the processes determining air-snow and snow-snowpack transfer functions, but must be integrated into multi-parameter investigations like the recent and ongoing studies in Greenland. Interpretation of the radionuclide data for DGASP and the first two seasons at Summit has suggested the following major findings;

1) The atmosphere over Greenland is quite different than the better studied Arctic basin troposphere,
2) Surface-level air over the Greenland ice sheet is often a poor reflection of air aloft,
3) Because of 2), precipitation scavenging processes over the Greenland ice sheet will not generally be illuminated by direct comparisons between the chemistry of fresh snow and surface-level air, but high resolution aerosol sampling for ^{7}Be and ^{210}Pb can indicate when such comparisons will be more fruitful, and
4) Significant changes do occur in the chemistry of surface snow over relatively short time scales, and depth profiles of some species in the upper layers of the snowpack do not always directly reflect the history of their input to the site. The processes causing these changes remain unclear.

All data that is so far available on trace element and soluble ionic species concentrations in air and snow during DGASP and the first two seasons at Summit support these main radionuclide-

based findings. (Approximately 15 papers on DGASP will appear in a forthcoming special issue of Atmospheric Environment.) Results of sampling surface-level aerosols and fresh and surface snow at Summit for the determination of ^{7}Be and ^{210}Pb during 1991 continue to illustrate the complexity of air-snow and snow-snowpack transfers, the progress being made toward understanding the responsible processes, and the value of including these aerosol-associated radionuclides in studies of such questions.

METHODS

Aerosol and snow sampling protocols for radionuclides at Summit in 1991 were essentially unchanged from the previous two seasons (Dibb, 1990; Dibb et al., 1992). All aerosol and most snow sampling took place at the remote, solar-powered, camp (ATM). The nominal 24-hour aerosol collection interval was decreased to 12 and 8 hours for two intensive study periods during the 1991 season. Very few snowfall events resulted in identifiable new layers on the surface, but four ^{7}Be depth profiles were recovered from shallow pits excavated through the season.

Processing and analysis of aerosol samples was as previously described (Dibb, 1990). Snow samples were concentrated onto cation-exchange impregnated filters rather than by evaporation. Comparisons between the two concentration techniques using 1.0 - 1.5 liter splits of New Hampshire rainwater samples indicate that the exchange-filters collect 97$\pm$6% of both ^{7}Be and ^{210}Pb. Each snow sample was passed three times through a single filter, which was then pressed into a pellet in the same type polyethylene vials as the aerosol filters for gamma spectrometric determination of ^{7}Be and ^{210}Pb activities.

RESULTS

Aerosol.

The concentrations of aerosol-associated ^{7}Be and ^{210}Pb in surface-level air at Summit during summer 1991 were broadly similar to those in 1989 and 1990 (Table 1). Monthly average concentrations of both radionuclides increased from May - July, then decreased in August. A similar pattern was observed in 1990, while in 1989 concentrations were higher in June than July (Table 1).

There was substantial variability on a sample to sample (day to day) basis in the concentration of both radionuclides (Fig. 1). Such variability has characterized all recent sampling on the Greenland ice sheet (Dibb, 1990; Dibb et al., 1992; Dibb and Jaffrezo, in review). However, unlike these recent campaigns, there was essentially no correlation ($r = 0.2$) between the concentrations of ^{7}Be and ^{210}Pb in the 120 samples collected in 1991. The correspondence between ^{7}Be and ^{210}Pb was particularly lacking in May and June, with correlation coefficients of -0.11 and -0.12, respectively, suggesting a weak inverse relationship. Correlation improved to 0.69 in July and 0.32 in August (excluding the two samples with ^{7}Be near 500 fCi m^{-3} STP (Fig. 1)). Throughout the season the time series showed frequent switching between intervals where the two radionuclides were essentially in phase, then nearly perfectly out of phase (Fig. 1 and in discussion below).

As outlined above, we have come to feel that the tendency for covariance of ^{7}Be and ^{210}Pb in surface-level air over Greenland reflects the influence of local, perhaps predominantly boundary layer, processes. The distinct sources of ^{7}Be and ^{210}Pb suggest that their spatial and temporal distributions in the atmosphere should be controlled by different processes, hence any similarities in free tropospheric distributions would be fortuitous. However, on the Greenland ice sheet, these radionuclides appear to share a common free tropospheric proximal source, and isolation or communication between the surface and air aloft largely determines the concentrations observed in surface-level air (Dibb, 1990; Dibb et al., 1992; Dibb and Jaffrezo, in review). The fact that ^{7}Be and ^{210}Pb concentrations generally did not covary in 1991 was thus surprising, but provides insight into larger scale atmospheric dynamics impacting the chemistry of air over Greenland, as well as an opportunity to better quantify air-snow transfer functions.

Snow.

Fresh Snow. Although snow fall events were more common in 1991 (particularly in the first half of the summer) than in the 1989 and 1990 seasons, opportunities to collect samples of newly fallen snow were limited. High winds caused much drifting and blowing of surface snow, mixing aged snow with new and often preventing any appreciable accumulation of new snow on the surface. Snow falling during relatively calm conditions 25 - 26 May, 30 May - 3 June and 17 - 18 June did create identifiable layers of fresh snow that were sampled at the remote camp (Table 2). The event in mid-June resulted in more accumulation from a single storm than any of the GISP 2 field party members had ever experienced in Greenland. This layer was also sampled for ^{7}Be and ^{210}Pb within a few hours after the snow had stopped falling along a 60 km traverse from ATM to GISP 2 then on to GRIP (Table 3).

The concentrations of ^{7}Be and ^{210}Pb in fresh snow sampled at the remote camp (Table 2) were quite comparable to the averages for all fresh snow sampled in 1989 and 1990 (Dibb, 1990; Dibb et al., 1992). However, these samples were unusual in that calculated scavenging ratios (Table 2) tended to cluster fairly tightly compared to those for all recent sampling on the Greenland ice sheet (Dibb, 1990; Dibb et al., 1992; Dibb and Jaffrezo, in review). This is consistent with the hypothesis outlined above regarding greater mixing between free-tropospheric and surface-level air. The ^{210}Pb scavenging ratios were lower than previously reported values for a coastal Antarctic site, and less than half those at South Pole (Lambert et al., 1983). ^{7}Be ratios were consistently lower than those for ^{210}Pb; the significance of this trend is uncertain due to the very limited data set, but may also have been present in the widely scattered results for recent sampling on Greenland (Dibb, 1990; Dibb and Jaffrezo, in review).

Concentrations of both radionuclides along the 18 June fresh snow sampling traverse showed notably low variability (2-fold for ^{7}Be and 11-fold for ^{210}Pb (Table 3)), when compared to 50-fold and 20-fold variations in the concentration of ^{7}Be and ^{210}Pb, respectively, along the same traverse in the 1989 season (Dibb, 1990). Despite the relatively homogeneous composition of this particular snow fall in the Summit region, variations in layer thickness resulted in sizeable differences in the amount of ^{7}Be deposited along the traverse (maximum/minimum = 3.1 (Table 3)). In contrast, ^{210}Pb deposition varied less than concentration (maximum/minimum deposition = 5.4).

Shallow Pits. ^{7}Be was detectable in the deepest sample from each of the shallow pits that were sampled through the season (Fig. 2). The total measured inventory (including an estimate of 100 fCi ^{7}Be m^{-2} for the lost sample at 15 - 20 cm 18 July) (Table 4) ranged 1.4 - 2.2 times higher than the maximum inventory of 583 pCi ^{7}Be m^{-2} measured in 1990 (Dibb et al., 1992). The two 60 cm deep pits (25 May and 1 September) likely recovered the dominant portion of ^{7}Be present in the snowpack. Their inventories thus allow reasonable estimates of the steady-state flux required to support the inventory (Dibb et al., 1992). The calculated fluxes (11.0 and 16.4 pCi ^{7}Be m^{-2} d^{-1}, respectively) were also 2-fold higher than estimates for 1989 and 1990. The measured inventories in June and July clearly missed a significant fraction of ^{7}Be present by not including the 40 - 60 cm depth range, so similar flux estimates would be biased low. However, comparison of decay-corrected inventory changes in the upper 40 cm of successive pits yields estimated ^{7}Be fluxes over the respective time intervals (Dibb et al., 1992, Canuel et al., 1990; Dibb and Rice, 1989). These calculations indicate the addition of 14.7, 19.9 and 9.9 pCi ^{7}Be m^{-2} d^{-1} between 25 May and 14 June, 14 June to 18 July and 18 July through August, respectively.

DISCUSSION

Meteorologic Overview.

The 1991 GISP 2 field season began nearly a month earlier than the first two seasons, with put in flights on 15 April. As expected, the weather at Summit during the last half of April was severe, with a sequence of 2 - 4 day storms bringing winds in excess of 40 knots.

Surprisingly, this storminess continued through at least the middle of July. In May, only 14 days, in 1 - 6 day intervals, failed to have winds of 20 knots or more. The first 12 days of June were relatively fair, comparable to the fine weather of June, 1990 (Alley et al., 1990; Dibb et al., 1992), but another storm blew in 12 - 13 June and from 17 June to 3 July skies were mainly unbroken clouds with moderate to strong winds throughout. Many of the storms included intense snow squalls, resulting in higher than "usual" (compared to 1989 and 1990) early summer snowfall. A particularly notable snow event over 17-19 June led to surface accumulation up to 20 cm. High winds frequently reworked and eroded the surface of the snowpack, but net accumulation from 19 May to 26 June (measured on a 100 stake "forest" at the remote camp) averaged 10.6 cm. For comparison, the average accumulation measured on the same stakes was only 1.7 and 1.2 cm in June, 1989 and 1990, respectively. In contrast, measured accumulation during July and August, 1991 (7.0 cm) was not quite half that of the same two months in 1990 (15.9 cm).

The lack of the "expected" covariation of ^{7}Be and ^{210}Pb suggests that near-surface air may not have been isolated from air aloft during most of May and June; reflecting increased vertical mixing by the frequent storms. If so, comparisons between the chemistry of surface-level air and fresh snow will be more informative than comparisons made under more usual conditions with a distinct boundary layer immediately above the ice sheet. The fact that radionuclide scavenging ratios calculated for snow falling during this period make sense for the first time in recent experience certainly supports this suggestion. However, we have hypothesized that shorter periods when Summit is in free-tropospheric air can be identified by elevated concentrations of both ^{7}Be and ^{210}Pb (Dibb et al., 1992; Dibb and Jaffrezo, in review). This would imply that the radionuclide concentrations in May and June, 1991, should have been significantly higher than in previous years, which was clearly not the case (Table 1). This inconsistency does not necessarily invalidate the hypothesis, as the higher snowfall during the period increased scavenging enough to double ^{7}Be flux in spring 1991 compared to the same season in 1989 and 1990. Apparently the cleansing by snow reduced the free tropospheric inventory of ^{7}Be (and other aerosol-associated species) enough to negate increased concentrations in surface-level air expected from the greater vertical mixing.

Atmospheric Structure Over Summit.

The hypothesis that the chemistry of surface-level air over the Greenland ice sheet may often differ from that of air aloft was developed largely through examination of aerosol chemistry at the surface, with little or no independent information about atmospheric structure. A three-week deployment of an acoustic echo sounder in 1990 allowed detection of a low-level reflector most days from early morning to mid-afternoon. During two anomalous periods when the reflector persisted for longer periods the concentrations of several aerosol-associated species dropped sharply (Dibb et al., 1992). These results were qualitative since the atmospheric structures responsible for the reflectors could not be identified (though it was assumed they were related to temperature inversions). In 1991 a tether-sonde system was employed to measure temperature profiles in the bottom 1 km of the atmosphere over Summit.

The sounding campaign was plagued by equipment problems and forced curtailment during periods of high wind, but over 100 profiles were obtained. Relatively continuous (no more than 24 hours between flights) sequences of at least two daily flights were achieved 29 May - 10 June, 12 - 27 July and 5 - 19 August.

Soundings 29 May through 10 June. Sonde profiles were obtained at 10:00 and 22:00 (local time = GMT - 2 h) from 29 May through 10 June. Temperature inversions were observed in the bottom 500 m of the atmosphere on 23 of the 26 profiles obtained and inversion intensity (inversion intensity = $\Delta T^2/\Delta H$, after Stone and Kahl, 1991) was calculated (Fig. 3). This simple analysis revealed that near-surface inversions tended to be stronger under clear skies, particularly 3 - 7 June, and that inversions at 22:00 were generally much stronger than those present on the preceding or following morning flights. Beginning with the 3 June evening profile, all of the inversions through the evening of 6 June were surface-based. After this time,

all of the inversions except the two most intense ones observed the evenings of 7 and 9 June were lifted. The sequence of 7 flights showing surface-based inversions (3 - 6 June) suggests, but does not prove, that the inversion "persisted" (Kahl, 1990) throughout this period. It should be noted that even the strongest inversion observed during these two weeks (intensity of 2.1) was weaker than the average inversion under clear skies at South Pole in the winter of 1986 (Stone and Kahl, 1991).

Concentrations of ^{7}Be and ^{210}Pb during this period were not atypical, compared to the rest of the summer (Figs. 1 and 3). Both radionuclides varied widely from one sample to the next, these variations started out roughly in phase but shifted out of phase by 2 June and may have tended toward covariance again at the end of the interval (Fig. 3). However, any response of the concentrations of ^{7}Be and ^{210}Pb to the strength or persistence of near-surface inversions was far from clear.

Mid-July Soundings. From 12 - 27 July, 26 profiles were obtained on nearly the planned 10:00 and 22:00 schedule. Near-surface inversions were present on only half the flights, but 11 of these 13 cases were clustered between the 17 and 23 July, suggesting persistence through these 7 days. Again, inversions were always stronger in the nighttime flights. There was no consistent relationship between presence or intensity of inversions and the concentrations of ^{7}Be and ^{210}Pb; rather, both radionuclides generally increased in concentration from the 13th through the 23rd, then remained roughly constant. Neither trend was monotonic, and the excursions in radionuclide concentrations alternated between being in and out of phase.

It may be that none of these inversions were strong enough to significantly impede downward mixing of aerosols and associated species to the surface of the ice sheet, or the inversions may have been regularly disrupted on time scales too short to be resolved by twice daily soundings. Alternatively, inversion intensity, based only on temperature gradients, may be a poor index of the ability of inversions to isolate the surface from air aloft, as it neglects the potential for wind shear at the inversion to facilitate downward mixing through even the strongest inversion (J. Kahl, personal communication, August, 1991).

High Frequency Aerosol Sampling.

The echo-sounder deployment in 1990 indicated a diurnal pattern, with low-level reflectors present during the day more often than at night (Dibb, et al., 1992). The 1991 sonde profiles also revealed a diurnal pattern, but in this case temperature inversions were more frequent and stronger at night. This suggests that the echo-sounder was responding to turbulence structure that was not simply related to temperature. However, it does appear that, if these variations in atmospheric structure are impacting the composition of surface level air, they occur at too high a frequency to be resolved by 24-hour aerosol sampling intervals. To examine this possibility, aerosol collection intervals were reduced to 12 hours 16 - 21 June, and then to 8 hours 22 - 24 June. A second series of 8 hour long samples was collected 15 - 17 August.

June Intensive Aerosol Sampling. Unfortunately, no independent information on atmospheric structure is available for the June period of interest (due to previously noted equipment problems). Skies were overcast for all nine days, with frequent, intense snow squalls and moderate to high winds, predominantly from the southwest, throughout. Comparison to the conditions prevailing during the two weeks of tether-sonde profiling in early June suggests that any temperature inversions were probably not very well developed or persistent. ^{7}Be and ^{210}Pb concentrations in surface-level air showed variability from one 8 or 12 hour sample to the next (Fig. 4) that was comparable to the results of 24-hour sampling (Figs. 1 and 3). No consistent diurnal pattern was apparent during this nine day period (Fig. 4). Even with higher temporal resolution sampling, the concentrations of the two radionuclides seem to switch from being clearly out of phase early in the interval to roughly in phase toward the end. The reasons for the short-term variations of ^{7}Be and ^{210}Pb are not entirely clear at present. Results from the other sampling at ATM, continuous monitors, and meteorologic information (on both synoptic and local (from C. Stearns' AWS network around Summit) scales) should soon be available and may clarify this question.

August Intensive Aerosol Sampling. Beginning on the evening of 15 August, a series of profiles was obtained with the tether sonde at nominal three hour intervals. Increasing winds temporarily suspended flights at midday 17 August. The 22:00 flight 16 August was aborted when the balloon failed to ascend past 665 mb (5 mb above surface) due to He leakage, but repairs allowed the sequence to resume at 1:00 17 August. Over this same period, aerosol samples for radionuclide determinations were collected at higher frequency than the usual 24-hour interval. The intended sampling interval was 8 hours, but logistic constraints resulted in varied exposure times (approximately 6 - 15 hours, with a 7.5 hour gap early 16 August due to low power).

^{7}Be concentrations were more than 1.5-fold higher than the average for all of August throughout the three days, and peaked near 500 fCi m^{-3} STP in two eight hour samples (Fig. 1). Peak concentrations were observed in the two samples bracketing the break in sampling, suggesting that the higher concentrations persisted for nearly 24 hours (Fig. 5). The concentrations in these two samples were 2.4 times higher than that in the next highest sample for the entire 1991 season (Fig. 1), and 1.6 times higher than the previous maximum concentration in the 1989 and 1990 seasons (Dibb, 1990; Dibb et al., 1992). These ^{7}Be concentrations are high enough to suggest that upper-tropospheric and/or lower-stratospheric air was influencing the composition of surface-level air.

Soundings with the tether sonde during these three days penetrated only the bottom 400 - 750 m of the atmosphere over Summit. Surface pressure was essentially constant between 669 and 670 mb through the period. These pressures are below the 1991 summer mean at Summit, but are relatively high compared to the rest of August (eg., about 5 mb higher than the three day periods on either side of 15 - 17 August). Near-surface temperature inversions were present in all soundings at "night" (19:00 - 4:00), reflecting cooling by the ice, but had little or no impact on ^{7}Be concentrations (Fig. 5). However, inversions at higher levels, and their altitudinal progression, appeared to be related to the composition of surface-level air.

At the beginning of the interval temperature varied only slightly with height above the near-surface boundary layer, where a reasonably strong inversion had developed by 19:00. ^{7}Be concentrations were the lowest they would reach during the three days (Fig. 5a). Over the duration of the next aerosol collection, air very near the surface continued to cool, but the 22:05 profile revealed slightly increasing temperatures above 640 mb and by 1:25 a strong, shallow temperature inversion was present at 655 mb. This sample had the highest ^{7}Be concentration yet seen at Summit (Fig. 5b). Low power curtailed aerosol collection for the following 7.5 hours; the 4:00 sounding revealed a stronger inversion near 635 mb. Between 4:00 and 7:00 the surface-level air warmed by about 6°C, the distinct inversion at 635 mb disappeared but the air from about 650 to 625 mb reflected a general warming (Fig. 5c). At 10:00 on 16 August a weak near-surface inversion was reestablished, but the most prominent feature in this sounding was a 5°C temperature increase between 615 and 612 mb. This warm air appeared to descend and increase in temperature over the next 6 hours, with the base of the inversion at 630 mb at 16:00. ^{7}Be concentrations were also very high during this period (Fig. 5d). At 19:00 the inversion was based near 640 mb; the temperature increase was of the same magnitude as those in the four preceding flights, but occurred over about 30 mb rather than abruptly. None of the flights after balloon repair late on the night of 16 August reached 630 mb, but they all showed nearly isothermal temperature profiles from above the near-surface layer to the highest levels reached, similar to the bottoms of the first two profiles seen on the 15th (Fig. 5e and f). ^{7}Be concentrations rapidly decreased during the final two sampling periods (Fig. 5), and continued to decline in the next several samples (Fig. 1).

This series of soundings suggests that air warmed by compression during subsidence came near to or reached the surface at Summit through much of 16 August and perhaps as early as the night of 15 August. Surface air during this interval was also quite dry, with the water vapor mixing ratio sharply dropping from about 1.2 to 0.5 g kg^{-1} midday 15 August and returning to higher levels in the morning of 17 August. Over the same period there was divergence and negative (anticyclonic) vorticity in the boundary layer over Summit (C. Stearns, personal communication, August, 1992). Thus all of the local meteorological data is consistent with

significant downward motion, while the very high ^{7}Be concentrations implicate upper tropospheric/lower stratospheric influence on the composition of surface-level air. It is perhaps surprising that such ^{7}Be spikes have not been observed more often in the past three summers at Summit, as potential vorticity analyses indicate that the troposphere over Greenland should frequently be influenced by injections and downward transport of stratospheric air through tropopause folding (eg., Danielsen, 1968, 1980; Bachmeier et al., in review).

Snow.

Fresh Snow. The limited number of fresh snow samples precludes extensive analysis of air-snow relations at Summit. The previously noted clustering of scavenging ratios (in response to more vigorous vertical mixing early this season) is encouraging, but further examination of the five "fresh" snow samples reveals considerable complexity.

Concentrations of ^{7}Be and ^{210}Pb in the 31 May fresh snow sample (Table 2) were toward the high end of the concentration range for fresh snow samples collected during the 1989 and 1990 seasons (Dibb, 1990; Dibb et al., 1992). Snow flurries, heavy at times, continued through about mid-day 3 June. Accumulation after the time of sampling 31 May was not distinguishable from the earlier deposits, so samples collected 1 and 3 June were felt to contain the cumulative snowfall (i.e., the 1 June sample should contain snow falling after the 31 May sample mixed with the snow that was previously sampled). The successive samples (Table 2) suggest that the snow accumulating between 31 May and 1 June had ^{7}Be concentrations low enough to depress the average concentration to 14 pCi kg^{-1}, while snow accumulating 1 - 3 June apparently had concentrations even higher than the initial snow; resulting in a whole storm average of 28 pCi kg^{-1}. Failure to detect ^{210}Pb in 1 June snow imply that this sample probably did not contain all of the early snow sampled on 31 May (due to small-scale spatial heterogeneity in accumulation and/or sampling difficulty, as the layer sampled 31 May was only about 0.5 cm thick). However, the sequence of three samples also suggests elevated concentrations of ^{210}Pb early in the storm, "clean" snow falling between 31 May and 1 June, and a return to enhanced deposition of ^{210}Pb during the last two days of the storm (Table 2). Aerosol concentrations varied in rough accord with this scenario; ^{7}Be and ^{210}Pb dropped from 96 and 9 fCi m^{-3} STP to 64 and 6 fCi m^{-3} STP, respectively, between 31 May and 1 June. ^{210}Pb levels remained low (5 fCi m^{-3} STP) the following two days, while ^{7}Be recovered to 99 fCi m^{-3} STP.

Despite the high concentrations in some of the snow falling during this four day "event", the amounts of ^{7}Be and ^{210}Pb deposited (36 and 2.8 pCi m^{-2}, respectively) were not exceptionally high (Table 2). It is reassuring to note that the deposition series also reflects the apparent change in the composition of snow falling through the storm. Twenty three percent of the total ^{7}Be and 40% of the total ^{210}Pb deposition occurred in the first day, with 65 and 60%, respectively deposited over the last two days; while 24% of the total mass of snow delivered in the four days accumulated in the first day and only 29% in the last two days.

The concentration/deposition relationships for the radionuclides in snow on the 18 June traverse were also intriguing (Table 3). It was noted that ^{7}Be concentration varied little, with deposition apparently reflecting differences in snow accumulation along the traverse; while the deposition of ^{210}Pb varied 1/2 as much as concentration. This might imply nearly complete removal of the aerosol particles carrying ^{210}Pb from the overlying atmosphere early in the storm and incomplete removal or replenishment of those particles carrying ^{7}Be during the course of the storm (ie., ^{210}Pb deposition may have been limited by its availability in the air over Summit while ^{7}Be deposition was limited by snow available for scavenging it). It is interesting to note that ^{210}Pb in surface-level air dropped below detection limit in the sample collected during the storm, while ^{7}Be increased from 25 to 84 fCi m^{-3} STP. However, ^{210}Pb concentrations in the snow did not consistently vary inversely with the accumulation of snow and ^{7}Be, as they would if they were solely reflecting variable dilution of a roughly constant amount of ^{210}Pb by different amounts of snow.

Shallow Pits. Difficulties in sampling very light, but frequent, precipitation and occult deposition (hoar and rime), the previously noted tendency for heavier snowfalls to be accompanied by strong winds that mix new snow with varying amounts of older snow, and the uncertain contribution of dry deposition, represent serious obstacles to the construction of detailed time series of precipitation chemistry on the Greenland ice sheet. The snowpack integrates all of these inputs, such that the time history of the chemistry of the snow at the surface is probably already altered from the precipitation time series before any post-depositional processes begin to operate. In order to quantitatively link glacial ice chemistry to that of the atmosphere through precipitation chemistry, it will also be necessary to determine the transfer functions between snow delivered to the surface and that which is actually preserved. While surely not the only important factor, physical redistribution and mixing of surface snow by wind is an obvious, and potentially major, process impacting the atmospheric signals reflected in snow chemistry before they are preserved by burial.

The short (53.3 d) half-life and simple chemistry of ^{7}Be make it a powerful tracer of mixing processes in sedimentary systems (e.g., Rice, 1986). Preliminary investigations indicated potential for similar power in snowpack studies (Dibb et al., 1992). Two of four ^{7}Be profiles in shallow snowpits sampled in 1990 had prominent subsurface maxima that were interpreted as evidence of uneven accumulation of snow at Summit through the year (Dibb et al., 1992). None of the 1991 pits (Fig. 2) had prominent maxima at depth, but the presence of 2.0 pCi ^{7}Be kg^{-1} at 60 cm depth 25 May is consistent with the possibility that a disproportionate fraction of the annual snow accumulation occurs in spring and early summer. The average accumulation measured on 100 stakes between 28 May, 1990, and 19 May, 1991 was 84 ± 15 cm. If it is assumed that this accumulation was steady through the year, the age of the deepest sample in the 25 May pit would be 240 - 255 days. Back correcting the measured concentration for decay yields an estimated concentration of 45 - 55 pCi ^{7}Be kg^{-1} in this snow when it was at the surface, which is 1.3 - 1.6 times higher than the maximum concentration we have yet measured in any surface snow at Summit (Dibb, 1990; Dibb et al., 1992). Alternatively, if this layer were only 220 days old (or less), the presence of 2.0 pCi ^{7}Be kg^{-1} at this depth would be consistent with an initial concentration of 35 pCi kg^{-1} (the maximum concentration yet observed in surface snow at Summit), but would imply that 71% of the annual accumulation of snow had occurred in the past 60% (or less) of the year. Of course, the observed variability in snow accumulation over small spatial scales makes this analysis qualitative at best. If the actual accumulation at the snowpit site for this year was closer to 70 cm it would imply a much greater fraction of spring-summer snow (80 - 85% of annual layer less than 220 days old), while actual accumulation near 100 cm would make the ^{7}Be profile consistent with a roughly constant accumulation rate.

There is another, potentially more problematic, possible explanation for unexpectedly high ^{7}Be concentrations at depth and subsurface maxima in the snowpack. If submicron aerosols carrying ^{7}Be were emplaced at depth in the column, the apparent ^{7}Be age could generally be less than that of the associated snow. Note that this would imply that all aerosol-associated species could also be younger than the snow they are found in. The sequence of ^{7}Be depth profiles (Fig. 2) suggests that such a process does sometimes occur. For example, the ^{7}Be inventories in samples from 10 - 40 cm 14 June tend to be higher than those over the same depth range 25 May. If ^{7}Be were only added at the surface, the amount in any given deeper layer would have to steadily decline through decay.

In an attempt to quantify comparisons of successive ^{7}Be profiles, the first three profiles were decay corrected to the time of the next pit (ie., 20 days elapsed between 25 May and 14 June). The earlier profile from each pair was shifted down by the measured average accumulation over the interval (2 cm 25 May - 14 June, 12 cm 14 June - 18 July, 2.5 cm 18 July - 1 September) and the two profiles were superposed (Fig. 6). These comparisons suggest that about 200 fCi ^{7}Be m^{-2} was added to the 8 - 36 cm depth range of the snowpack from 25 May to 14 June, with an additional 70 fCi m^{-2} apparently added between 20 and 45 cm 14 June

- 18 July (these totals are simply the areas between the profiles over intervals where the later profile is consistently higher than the decay corrected earlier one (Fig. 6)). Between 18 July and 1 September the 2.5 - 17.5 cm depth range gained 240 fCi ^{7}Be m^{-2}, but this estimate is more ambiguous than the first two comparisons. Much of the apparent increase is in the 2.5 - 10 cm range and could very well reflect new snow mixed below 5 cm by wind. The rest of the apparent increase is due to relatively low ^{7}Be concentration at 10 - 15 cm 18 July, just above the sample that was lost during processing.

The apparent post-depositional addition of ^{7}Be to snow that may be as much six months old is provocative, but may not be real. Spatial variability in snow accumulation makes depth registration between successive profiles tenuous. Spatial variability in ^{7}Be accumulation also contributes uncertainty. Layer by layer comparison of duplicate profiles in a single pit separated by 2 m revealed up to 2-fold variations in 8 cm thick samples, but the total inventories over 40 cm agreed within 10% (Dibb et al., 1992). It is uncertain how much variability should be expected in inventories over 20 - 30 cm depth intervals in pits separated by tens of meters; but if spatial noise was impacting these comparisons it would seem that cases of apparent ^{7}Be deficits would be as likely as excesses, yet none have been seen in six comparisons so far (including the four 1990 pits discussed by Dibb et al., 1992). More work is clearly needed to assess the spatial and temporal variability of snow accumulation and the spatial variability of the radionuclides (and other aerosol-associated species) in the snowpack at Summit.

CONCLUSIONS

The "unusual" weather at Summit in May and June, 1991, seems to have resulted in more frequent and complete vertical mixing of the lower atmosphere than was the case in the 1989 and 1990 seasons. This meso- to synoptic-scale change in meteorological conditions greatly diminished the impact of local atmospheric processes on the chemistry of surface-level air. As a result, ^{7}Be and ^{210}Pb concentrations in surface-level aerosols generally did not display the covariance that has characterized all recent results from sites on the Greenland ice sheet (Summit and Dye 3, Dibb, 1990; Dibb et al., 1992; Dibb and Jaffrezo, in review). These storms resulted in nearly an order of magnitude increase in the accumulation of snow and 2-fold higher ^{7}Be fluxes to the snowpack compared to 1989 and 1990. The increased snowfall also appears to have scavenged enough of the aerosol-associated radionuclides from the free troposphere over Summit to negate the increased concentrations in surface-level air expected from more vigorous vertical mixing

The apparent increase in communication between the surface of the ice sheet and air aloft during the 1991 season also increased the probability that atmospheric samples collected at the surface were representative of the air masses "sampled" by newly forming snow. As an example, ^{7}Be and ^{210}Pb scavenging ratios calculated for fresh snow events this season were quite similar to each other and clustered in the 150 - 350 range. This is in stark contrast to results of similar calculations for the past two seasons at Summit and the year-long DGASP campaign, where extreme variability led to the conclusion that scavenging ratios based on concentrations measured in surface-level air are generally highly suspect for assessing precipitation scavenging over the Greenland ice sheet (Dibb, 1990; Dibb et al., 1992; Dibb and Jaffrezo, in review). It is thus likely that direct comparison between the concentrations of ionic species and trace elements in fresh snow and aerosol samples collected by other investigators at Summit in May and June, 1991, will provide less ambiguous insight into air-snow transfer functions than was possible in recent programs.

Comparisons between atmospheric temperature profiles and the concentrations of radionuclides in surface-level air revealed no clear relationship between near-surface temperature inversions and boundary layer air composition. A three day interval of frequent soundings and aerosol sampling in mid-August coincided with the highest ^{7}Be concentrations (500 fCi m^{-3}) yet measured on the Greenland ice sheet. The ^{7}Be spike suggests a significant upper-tropospheric or lower-stratospheric component in surface-level air at this time and the soundings provided clear evidence of subsiding motion. Further analysis of the existing

sounding data, and collection of additional data on atmospheric structure are ongoing and may resolve the impact of boundary layer dynamics on the chemistry of surface-layer air over Summit.

^{7}Be concentrations at depth (up to 60 cm) in the snowpack in late May were higher than expected, given the age at these depths inferred from the measured accumulation of snow. This finding is consistent with recent results suggesting that much more snow accumulates at Summit during spring and early summer than in winter (Dibb et al., 1992). These results, and apparent increases of ^{7}Be inventories in the 8 - 45 cm depth range in the snowpack over time, could also be interpreted as indicating that some of the aerosol particles with which ^{7}Be in the snowpack is associated are emplaced well after the snow has become part of the snowpack. At present, non-constant accumulation of snow through the year is the preferred explanation for deep penetration of ^{7}Be, but either case demands caution when detailed depth profiles of snow chemistry are converted to time series.

ACKNOWLEDGEMENTS

This work would not have been possible without the logistic and other support provided by the GISP2 Science Management Office and the Polar Ice Coring Office. Partial support of this research was provided by NSF Division of Polar Programs. We also gratefully acknowledge the Commission for Scientific Research in Greenland for granting access to, and the 109th Air National Guard for making it possible to reach, so remote a location as Summit. Special thanks are due all who assisted in the field and laboratory aspects of this research; particularly J.-L. Jaffrezo, N. Fuller, S. Weyenberg, E. Silvente, R. Schoen, G. Marek and S. Whitlow. This is contribution number 92-05 of the Greenland Ice Sheet Project Two (GISP2).

REFERENCES CITED

Alley, R.B., E.S. Saltzman, K.M. Cuffey and J.J. Fitzpatrick, 1990, Summertime formation of depth hoar in central Greenland; Geophys. Res. Lett., 17, 2393-2396.

Bachmeier, A.S., M.C. Shipham, E.V. Browell and J.M. Klassa, in review, Stratosphere/troposphere exchange affecting the northern wetlands region of Canada during summer 1990, submitted to J. Geophys. Res.

Borys, R.D., 1983, Snow crystal riming and arctic snowpack chemical composition; in Precipitation Scavenging, Dry Deposition, and Resuspension, Proceedings of the Fourth International Conference, Santa Monica, CA., 29 November - 3 December, 1982, vol. 2, 1281-1288.

Brost, R.A., J. Feichter and M. Heimann, 1991, Three-dimensional modeling of ^{7}Be in a global climate simulation model; J. Geophys. Res., 96, 22,423-22,445.

Canuel, E.A., C.S. Martens and L.K. Benninger, 1990, Seasonal variations in ^{7}Be activity in sediments of Cape Lookout Bight, North Carolina; Geochim. Cosmochim. Acta, 54, 237-245.

Danielsen, E.D., 1968, Stratospheric-tropospheric exchange based on radioactivity, ozone and potential vorticity; J. Atmos. Sci., 25, 502-518.

Danielsen, E.D., 1980, Stratospheric source for unexpectedly large values of ozone measured over the Pacific ocean during Gametag, August 1977; J. Geophys. Res., 85, 401-412.

Davidson, C.I., S. Santhanam, R.C. Fortmann and M.P. Olson, 1985, Atmospheric transport and deposition of trace elements onto the Greenland ice sheet; Atmos. Environ., 19, 2065-2081.

Davidson, C.I., R.E. Honrath, J.B. Kadane, R.S. Tsay, P.A. Mayewski, W.B. Lyons and N.Z. Heidam, 1987, The scavenging of atmospheric sulfate by Arctic snow; Atmos. Environ., 21, 871-882.

Davidson, C.I., J.R. Harrington, M.J. Stephenson, M.J. Small, F.P. Boscoe and R.E. Gandley, 1989, Seasonal variations in sulfate, nitrate, and chloride in the Greenland ice sheet: Relation to atmospheric concentrations; Atmos. Environ., 23, 2483-2494.

Dibb, J.E., 1990, Beryllium-7 and Lead-210 in the atmosphere and surface snow over the Greenland ice sheet in the summer of 1989; J. Geophys. Res., 95, 22,407-22,415.

Dibb, J.E., and J.-L. Jaffrezo, in review, Beryllium-7 and Lead-210 in aerosol and snow in the Dye 3 gas, aerosol and snow sampling program; submitted to Atmos. Environ.

Dibb, J.E., and D.L. Rice, 1989, Temporal and spatial distribution of beryllium-7 in the sediments of Chesapeake Bay; Est. Coast. Shelf Sci., 28, 395-406.

Dibb, J.E., J.-L. Jaffrezo and M. Legrand, 1992, Initial findings of recent investigations of air-snow relationships in the Summit region of the Greenland ice sheet; J. Atmos. Chem.

Dick, A.L., and D.A. Peel, 1985, Trace elements in Antarctic air and snowfall; Annals Glaciol., 7, 12-19.

Dick, A.L., 1988, Trace elements in simultaneously sampled aerosol and snow from the Antarctic Peninsula; Annals Glaciol., 10, 201 (abstract)

Feichter, J., R.A. Brost and M. Heimann, 1991, Three-dimensional modeling of the concentration and deposition of ^{210}Pb aerosols; J. Geophys. Res., 96, 22,447-22460.

IGAC, 1990, The International Global Atmospheric Chemistry (IGAC) Programme: A core project of the International Geosphere-Biosphere Programme, published by IAMAP-CACGP.

Kahl, J.D., 1990, Characteristics of the low-level temperature inversion along the Alaskan Arctic coast; Inter. J. Clim., 10, 537-548.

Lambert, G., B. Ardouin and A. Mesbah-Bendezu, 1983, Atmosphere to snow transfers in Antarctica; in Precipitation Scavenging, Dry Deposition, and Resuspension, Proceedings of the Fourth International Conference, Santa Monica, CA., 29 November - 3 December, 1982, vol. 2, 1289-1300.

Ng, A., and C.C. Patterson, 1981, Natural concentration of lead in ancient Arctic and antarctic ice; Geochim. Cosmochim. Acta, 45, 2109-2121.

Peel, D.A., and E.W. Wolff, 1982, Recent variations in heavy metal concentrations in air and firn from the Antarctic Peninsula; Annals Glaciol., 3, 255-259.

Rahn, K.A., and R.J. McCaffrey, 1979, Compositional differences between Arctic aerosol and snow; Nature, 280, 479-480.

Rice, D.L., 1986, Early diagenesis in bioadvective sediments: Relationships between the diagenesis of beryllium-7, sediment reworking rates, and the abundance of conveyor-belt deposit-feeders; J. Mar. Res., 44, 149-184.

Stone, R.S., and J.D. Kahl, 1991, Variations in boundary layer properties associated with clouds and transient weather disturbances at the South Pole during winter; J. Geophys. Res., 96, 5137-5144.

Turekian, K.K., W.C. Graustein and J.K. Cochran, 1989, Lead-210 in the SEAREX program: An aerosol tracer across the Pacific; in J.P. Riley and R. Chester, eds., Chemical Oceanography, vol. 10, 51-81, Academic Press.

Table 1. Monthly average concentrations (fCi m^{-3} STP) of ^{210}Pb and ^{7}Be in surface-level air at the ATM site at Summit, Greenland.

	^{210}Pb			^{7}Be		
	1989	1990	1991	1989	1990	1991
May			2.7			58
June	7.2	4.6	4.4	123	91	88
July	4.0	4.0	6.3	82	102	126
August		3.0	3.1		65	81

Table 2. Atmospheric radionuclides in fresh snow collected at Summit in 1991. (Uncertainties in parentheses.)

	Concentration pCi kg^{-1}		Areal Inventory pCi m^{-2}		Scavenging Ratio	
Date	^{210}Pb	^{7}Be	^{210}Pb	^{7}Be	^{210}Pb	^{7}Be
26 May	0.10 (0.04)	9.21 (0.44)	0.72 (0.28)	64.03 (3.06)	>300.[2]	202
31 May	3.59 (0.47)	26.84 (1.66)	1.12 (0.14)	8.33 (0.51)	355	246
1 June[1]	n.d.	13.76 (1.20)	n.d.	12.58 (1.10)		191
3 June[1]	2.16 (0.21)	27.88 (1.01)	2.77 (0.27)	35.82 (1.30)	420	252
18 June	n.d.	8.54 (0.56)	n.d.	42.36 (2.78)		140

1 Samples collected 6/1 and 6/3 are later samples of same storm sampled 5/31. All three samples included all snow above the surface existing at beginning of the storm.
2 No ^{210}Pb was detected in aerosol sample. Scavenging ratio calculated with an upper limit estimate of 0.3 fCi m^{-3}.

Table 3. Atmospheric radionuclides in a fresh snow sampling traverse conducted 18 June. (Uncertainties in parentheses.)

km from GISP2		Concentration pCi kg^{-1}		Areal Inventory pCi m^{-2}	
		^{210}Pb	^{7}Be	^{210}Pb	^{7}Be
ATM	29	n.d.	8.54(0.56)	n.d.	42.36(2.78)
	18	n.d.	6.08(0.49)	n.d.	18.94(1.53)
	12	0.76(0.22)	7.76(0.69)	1.76(0.51)	17.97(1.60)
	6	n.d.	11.07(0.62)	n.d.	27.23(1.53)
GISP	0	n.d.	9.52(0.51)	n.d.	35.91(1.92)
	3	1.55(0.15)	8.86(0.44)	4.29(0.41)	24.49(1.22)
	9	0.14(0.09)	8.76(0.54)	0.80(0.53)	51.58(3.18)
	15	0.58(0.10)	8.52(0.48)	3.82(0.65)	55.79(3.14)
	21	0.20(0.18)	7.28(0.52)	0.58(0.52)	21.22(1.51)
GRIP	27	0.48(0.17)	12.07(0.56)	1.93(0.71)	48.96(2.27)

Table 4. Measured ^{7}Be inventories (pCi m^{-2}) in shallow snowpits at Summit, 1991.

	25 May	14 June	18 July	1 September
Whole Pit	850	835	1285	1260
0 - 40 cm	702	835	1212	1123

FIGURE CAPTIONS

Figure 1) Time series of ^{210}Pb (solid line) and ^{7}Be (dotted line) concentrations (fCi m^{-3} STP) in surface-level air at Summit, Greenland; May - August, 1991.

Figure 2) Depth profiles of ^{7}Be in the snowpack at Summit, Greenland; summer 1991.

Figure 3) ^{210}Pb (solid line) and ^{7}Be (dotted line) activities in aerosol samples collected during the first two weeks of tether-sonde flights. Horizontal bars show duration of filter exposure. Intensities of surface-based or near-surface (below 300 m) inversions are shown as bars for 10:00 local (12:00 GMT) and 22:00 local (0:00 GMT) flights each day (after Stone and Kahl, 1991). No scale is shown for inversion intensity, but the strongest inversions on 7 and 9 June have values of 2.1 and 1.8, respectively. Uncertainties for ^{7}Be and ^{210}Pb average 6 and 20%, respectively.

Figure 4) ^{210}Pb (solid line) and ^{7}Be (dotted line) activities in higher frequency aerosol samples. Sample intervals (horizontal bars) were nominally 12 hours 16 - 22 June and 8 hours 22 - 24 June. Uncertainty of the ^{7}Be activity averaged 7%. For ^{210}Pb activities greater than 2 fCi m^{-3} STP uncertainty averaged 25%, increasing to approximately 100% for lower levels.

Figure 5) Temperature profiles from tether-sonde flights 15 -17 August, 1991. Flights are grouped to correspond to aerosol sampling intervals. Concentrations of ^{7}Be are also shown.

Figure 6) Comparison between successive ^{7}Be profiles in the snowpack. In each frame the profile on the indicated date is the solid line with filled circles and error bars at sample mid-depth, with the decay-corrected profile from preceding pit superposed (dotted line). See text for discussion.

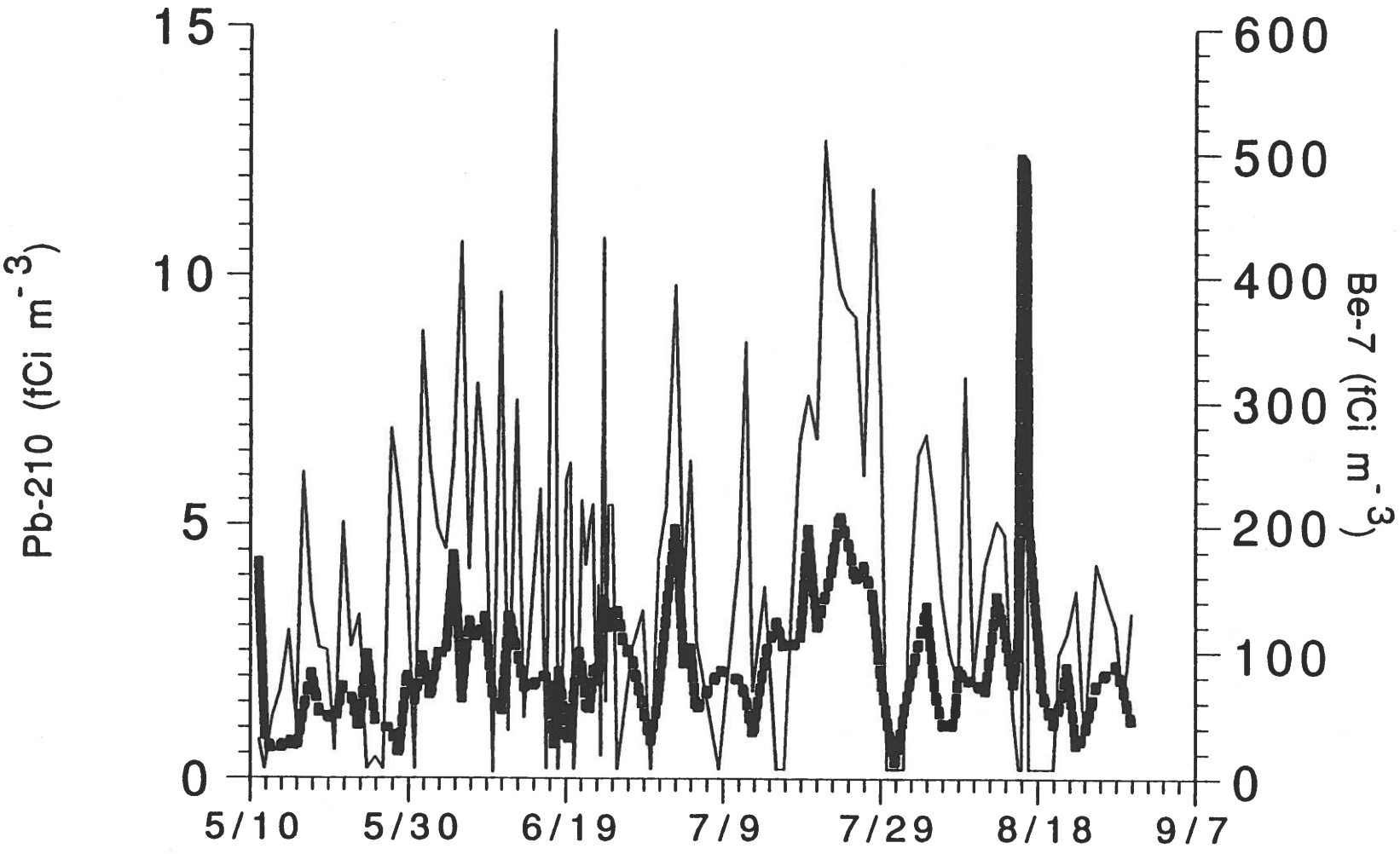
Pb-210 (fCi m-3)
Be-7 (fCi m-3)
15
10
5
0
600
500
400
300
200
100
0
5/10
5/30
6/19
7/9
7/29
8/18
9/7

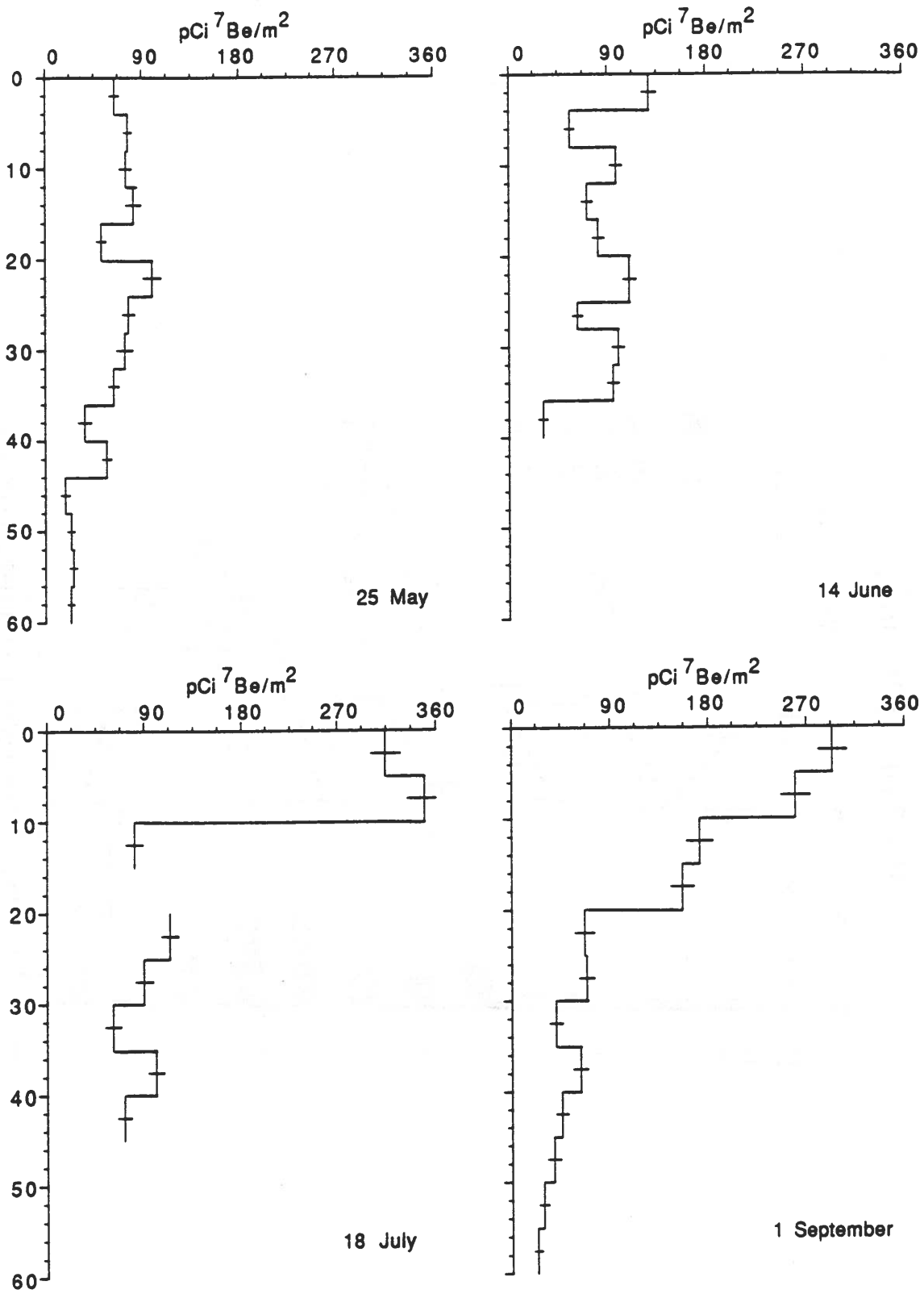
pCi ^{7}Be/m^{2}
0
90
180
270
360
0
10
20
30
40
50
60
25 May
14 June
18 July
1 September

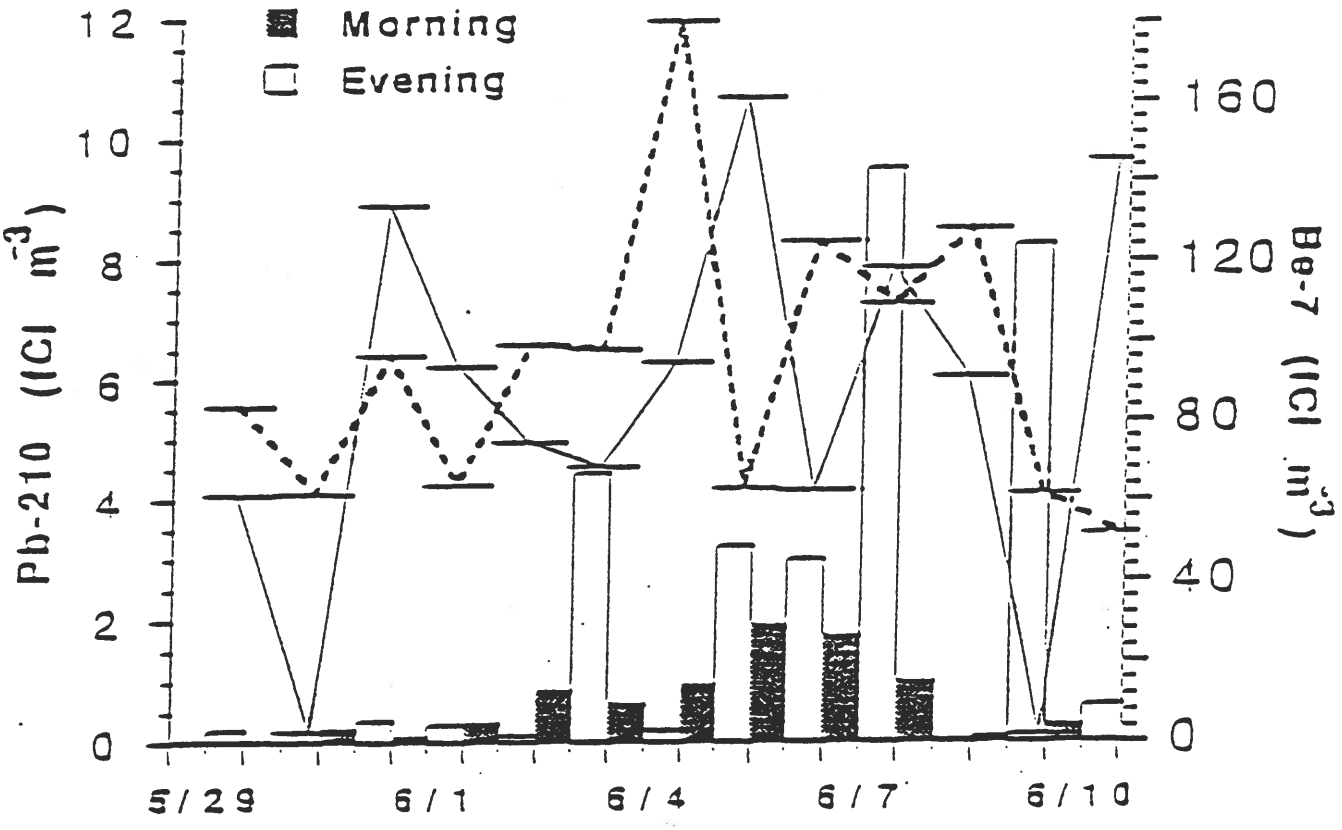
Morning
Evening
Pb-210 (ICI m-3)
Be-7 (ICI m-3)
0
2
4
6
8
10
12
0
40
80
120
160
5/29
6/1
6/4
6/7
6/10

Pb-210 (ICI m^{-3})
Be-7 (ICI m^{-3})
15
10
5
0
160
140
120
100
80
60
40
20
0
6/16
6/18
6/20
6/22
6/24

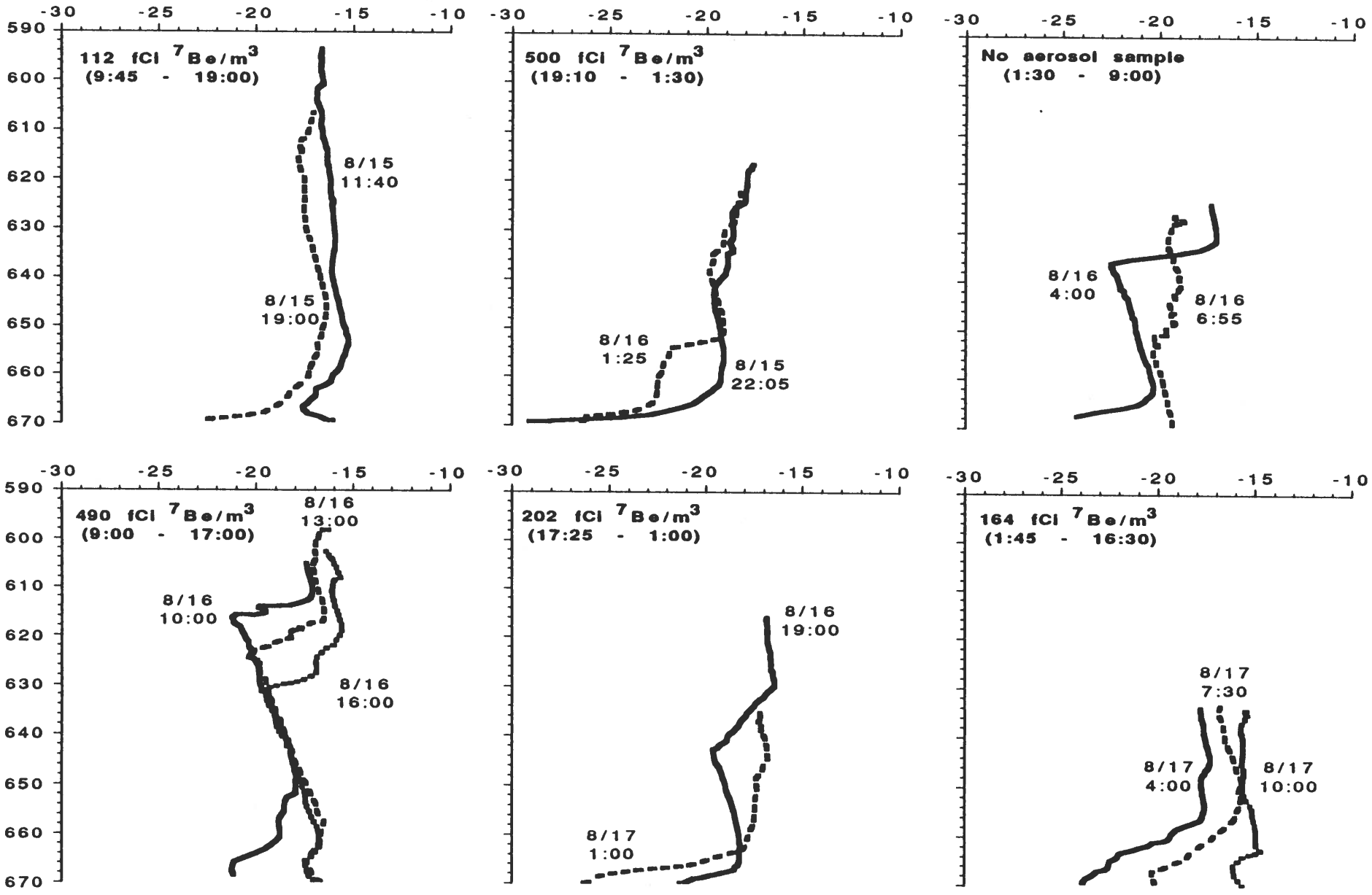
-30 -25 -20 -15 -10
590 600 610 620 630 640 650 660 670
112 fCi ^{7}Be/m^{3}
(9:45 - 19:00)
8/15
11:40
8/15
19:00
500 fCi ^{7}Be/m^{3}
(19:10 - 1:30)
8/16
1:25
8/15
22:05
No aerosol sample
(1:30 - 9:00)
8/16
4:00
8/16
6:55
490 fCi ^{7}Be/m^{3}
(9:00 - 17:00)
8/16
13:00
8/16
10:00
8/16
16:00
202 fCi ^{7}Be/m^{3}
(17:25 - 1:00)
8/16
19:00
8/17
1:00
164 fCi ^{7}Be/m^{3}
(1:45 - 16:30)
8/17
7:30
8/17
4:00
8/17
10:00

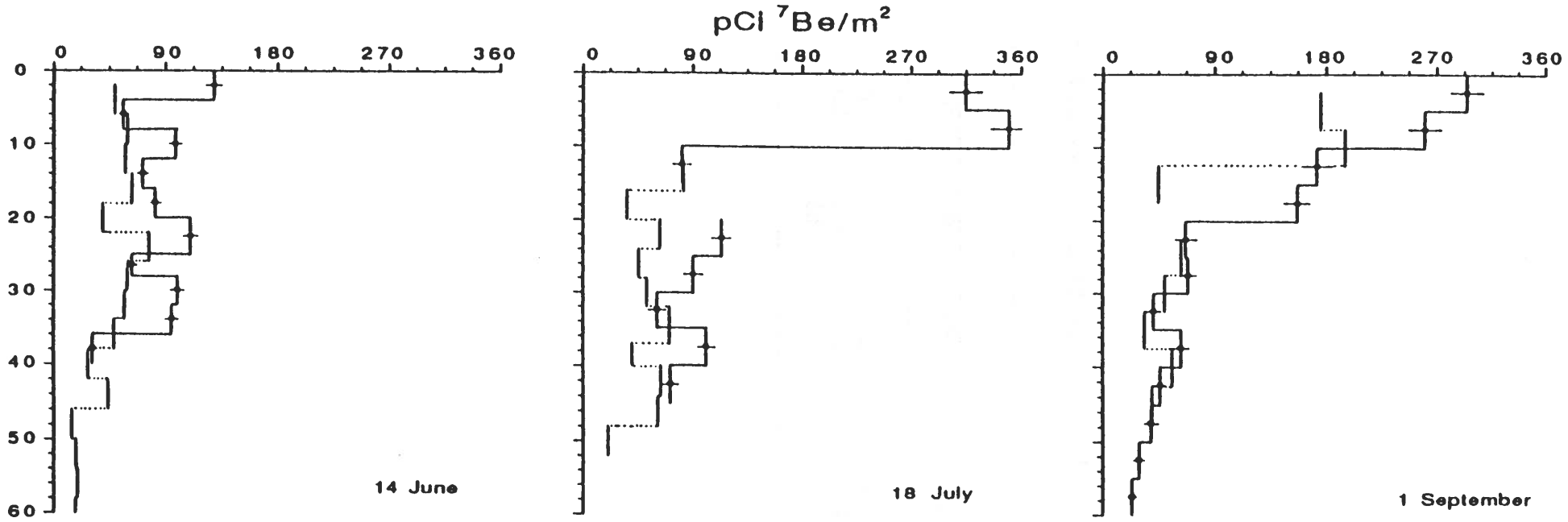
pCi ^{7}Be/m^{2}
0
90
180
270
360
0
10
20
30
40
50
60
14 June
18 July
1 September

Table 1. Monthly average concentrations (fCi m^{-3} STP) of ^{210}Pb and ^{7}Be in surface-level air at the ATM site at Summit, Greenland.

	^{210}Pb			^{7}Be		
	1989	1990	1991	1989	1990	1991
May			2.7			58
June	7.2	4.6	4.4	123	91	88
July	4.0	4.0	6.3	82	102	126
August		3.0	3.1		65	81

Table 2. Atmospheric radionuclides in fresh snow collected at Summit in 1991. (Uncertainties in parentheses.)

	Concentration pCi kg^{-1}		Areal Inventory pCi m^{-2}		Scavenging Ratio	
Date	^{210}Pb	^{7}Be	^{210}Pb	^{7}Be	^{210}Pb	^{7}Be
26 May	0.10 (0.04)	9.21 (0.44)	0.72 (0.28)	64.03 (3.06)	>300.[2]	202
31 May	3.59 (0.47)	26.84 (1.66)	1.12 (0.14)	8.33 (0.51)	355	246
1 June[1]	n.d.	13.76 (1.20)	n.d.	12.58 (1.10)		191
3 June[1]	2.16 (0.21)	27.88 (1.01)	2.77 (0.27)	35.82 (1.30)	420	252
18 June	n.d.	8.54 (0.56)	n.d.	42.36 (2.78)		140

1 Samples collected 6/1 and 6/3 are later samples of same storm sampled 5/31. All three samples included all snow above the surface existing at beginning of the storm.

2 No ^{210}Pb was detected in aerosol sample. Scavenging ratio calculated with an upper limit estimate of 0.3 fCi m^{-3}.

Table 3. Atmospheric radionuclides in a fresh snow sampling traverse conducted 18 June. (Uncertainties in parentheses.)

km from GISP2		Concentration pCi kg^{-1}		Areal Inventory pCi m^{-2}	
		^{210}Pb	^{7}Be	^{210}Pb	^{7}Be
ATM	29	n.d.	8.54(0.56)	n.d.	42.36(2.78)
	18	n.d.	6.08(0.49)	n.d.	18.94(1.53)
	12	0.76(0.22)	7.76(0.69)	1.76(0.51)	17.97(1.60)
	6	n.d.	11.07(0.62)	n.d.	27.23(1.53)
GISP	0	n.d.	9.52(0.51)	n.d.	35.91(1.92)
	3	1.55(0.15)	8.86(0.44)	4.29(0.41)	24.49(1.22)
	9	0.14(0.09)	8.76(0.54)	0.80(0.53)	51.58(3.18)
	15	0.58(0.10)	8.52(0.48)	3.82(0.65)	55.79(3.14)
	21	0.20(0.18)	7.28(0.52)	0.58(0.52)	21.22(1.51)
GRIP	27	0.48(0.17)	12.07(0.56)	1.93(0.71)	48.96(2.27)

Table 4. Measured ^{7}Be inventories (pCi m^{-2}) in shallow snowpits at Summit, 1991.

	25 May	14 June	18 July	1 September
Whole Pit	850	835	1285	1260
0 - 40 cm	702	835	1212	1123

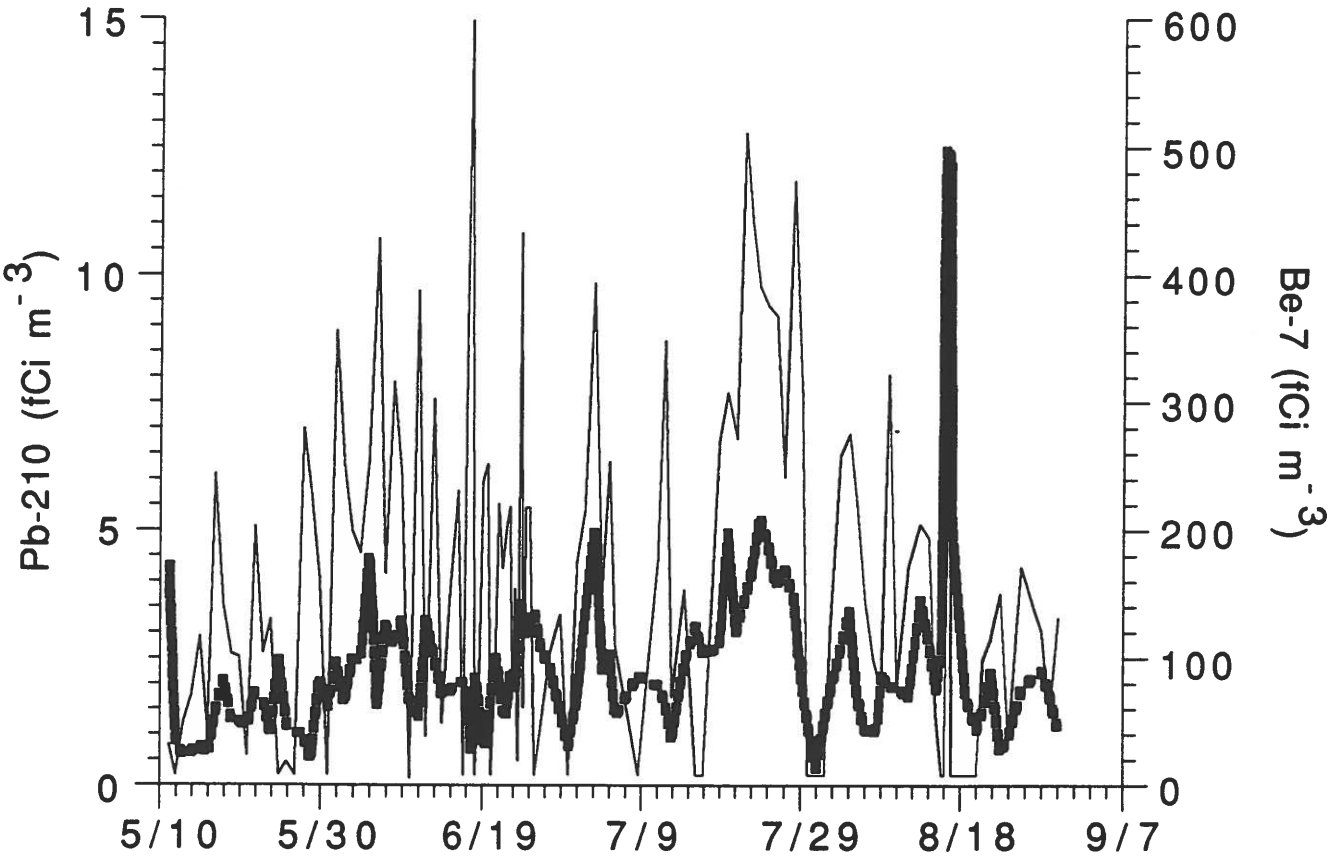

Figure 1) Time series of ^{210}Pb (solid line) and ^{7}Be (dotted line) concentrations (fCi m^{-3} STP) in surface-level air at Summit, Greenland; May - August, 1991.

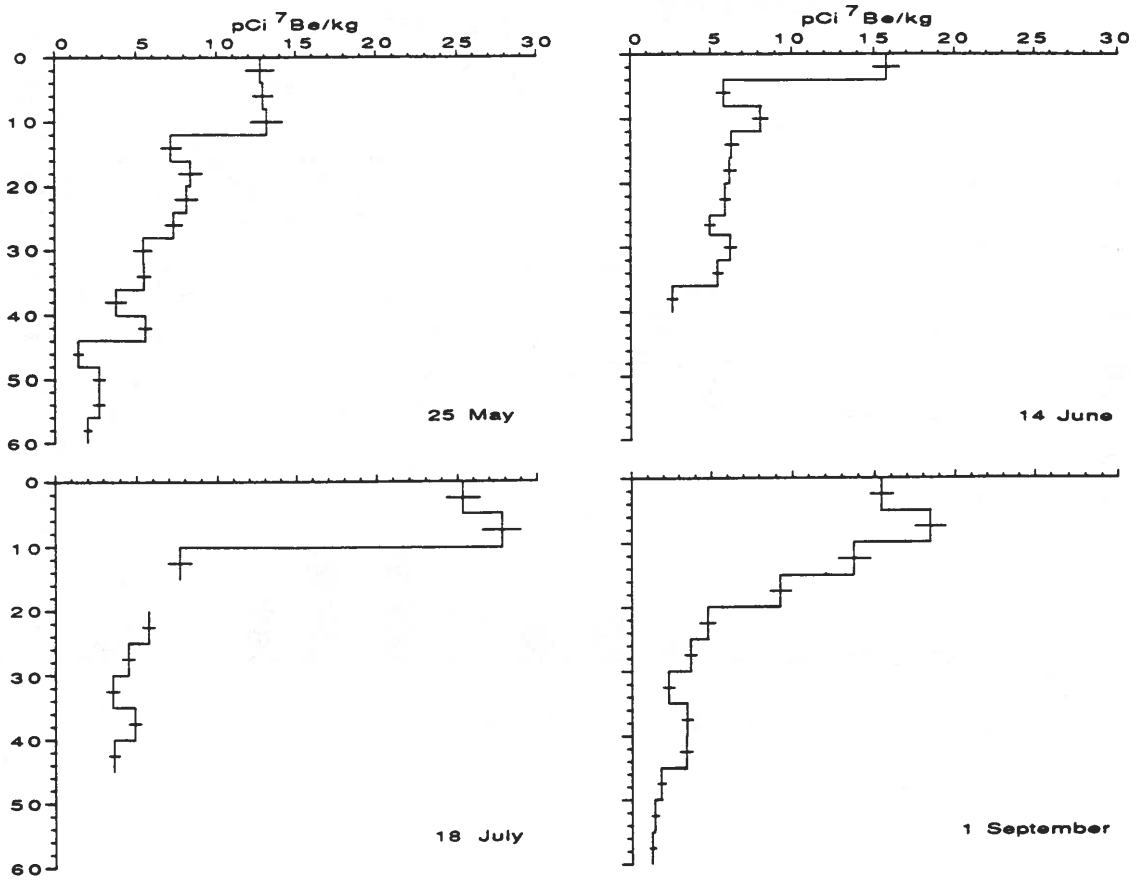

Figure 2) Depth profiles of ^{7}Be in the snowpack at Summit, Greenland; summer 1991.

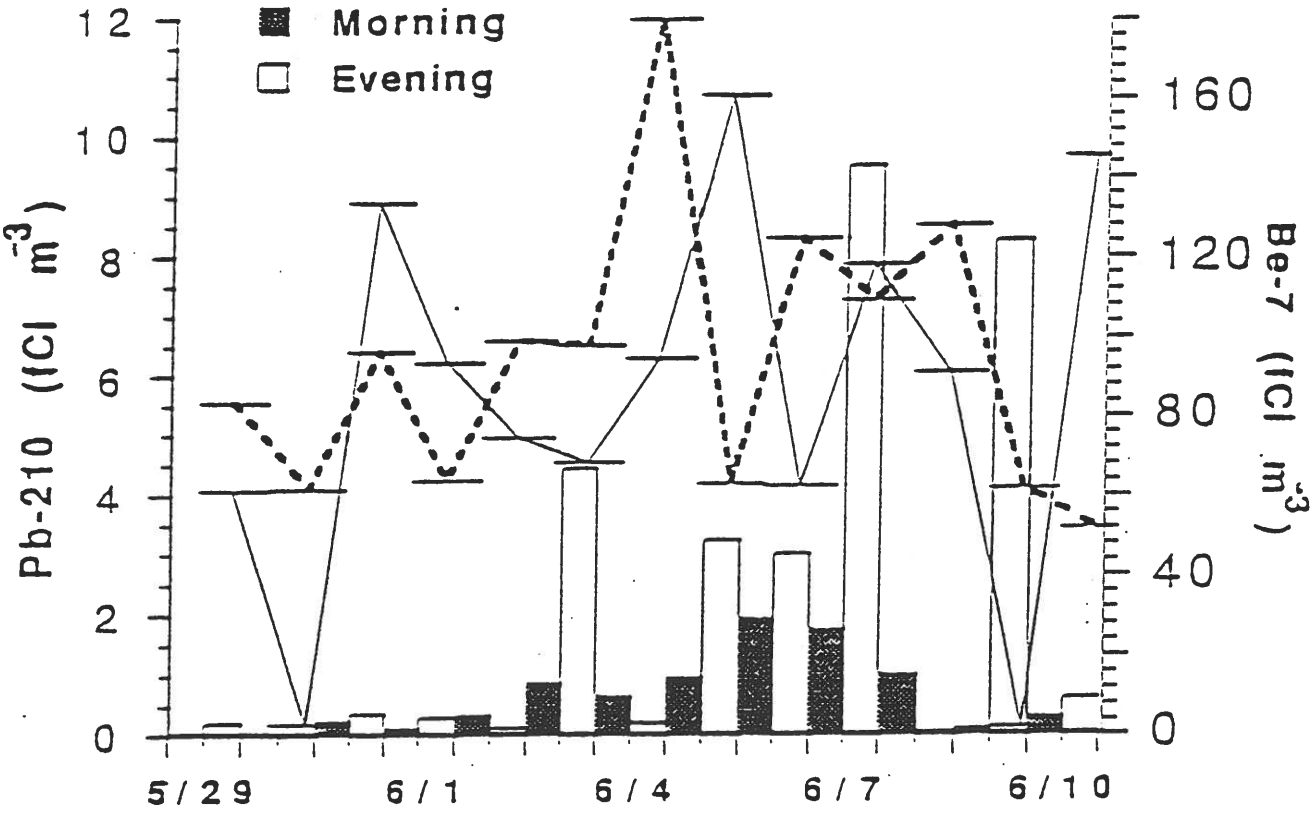

Figure 3) ^{210}Pb (solid line) and ^{7}Be (dotted line) activities in aerosol samples collected during the first two weeks of tether-sonde flights. Horizontal bars show duration of filter exposure. Intensities of surface-based or near-surface (below 300 m) inversions are shown as bars for 10:00 local (12:00 GMT) and 22:00 local (0:00 GMT) flights each day (after Stone and Kahl, 1991). No scale is shown for inversion intensity, but the strongest inversions on 7 and 9 June have values of 2.1 and 1.8, respectively. Uncertainties for ^{7}Be and ^{210}Pb average 6 and 20%, respectively.

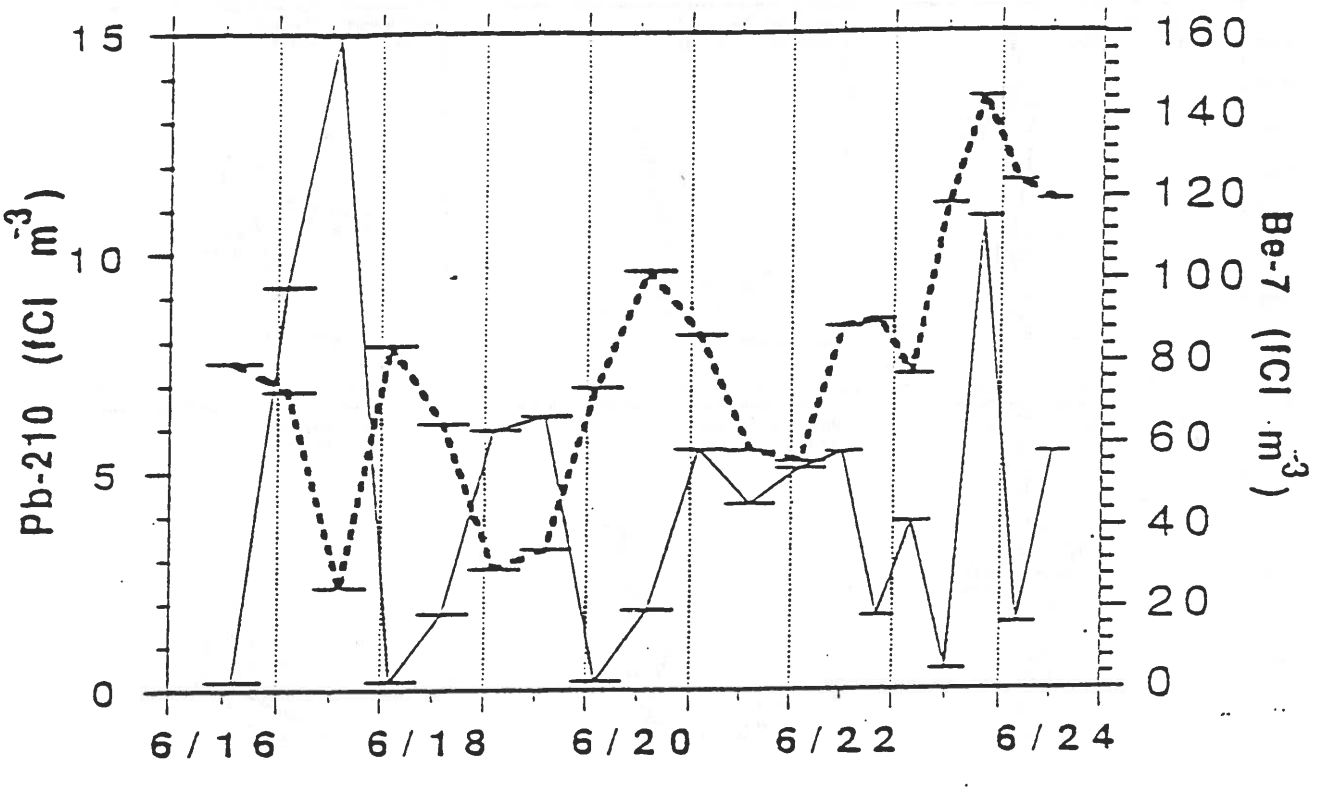

Figure 4) ^{210}Pb (solid line) and ^{7}Be (dotted line) activities in higher frequency aerosol samples. Sample intervals (horizontal bars) were nominally 12 hours 16 - 22 June and 8 hours 22 - 24 June. Uncertainty of the ^{7}Be activity averaged 7%. For ^{210}Pb activities greater than 2 fCi m^{-3} STP uncertainty averaged 25%, increasing to approximately 100% for lower levels.

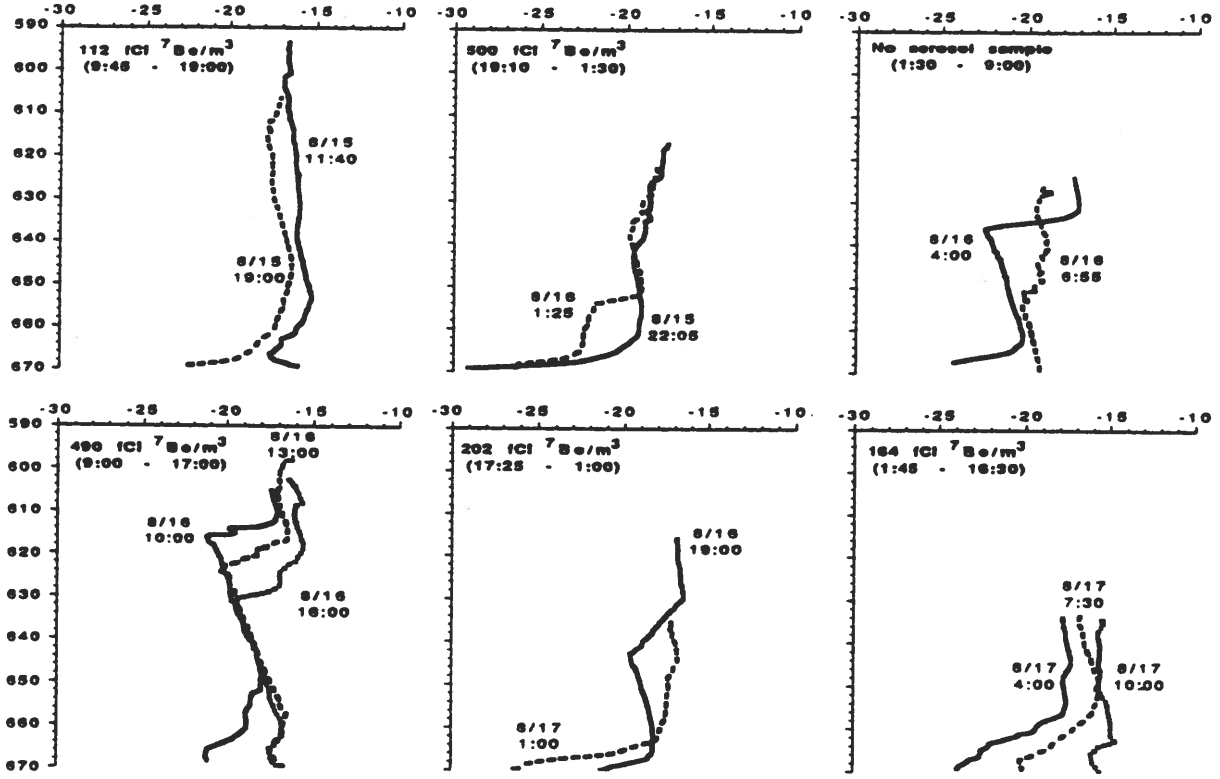

Figure 5) Temperature profiles from tether-sonde flights 15 -17 August, 1991. Flights are grouped to correspond to aerosol sampling intervals. Concentrations of ^{7}Be are also shown.

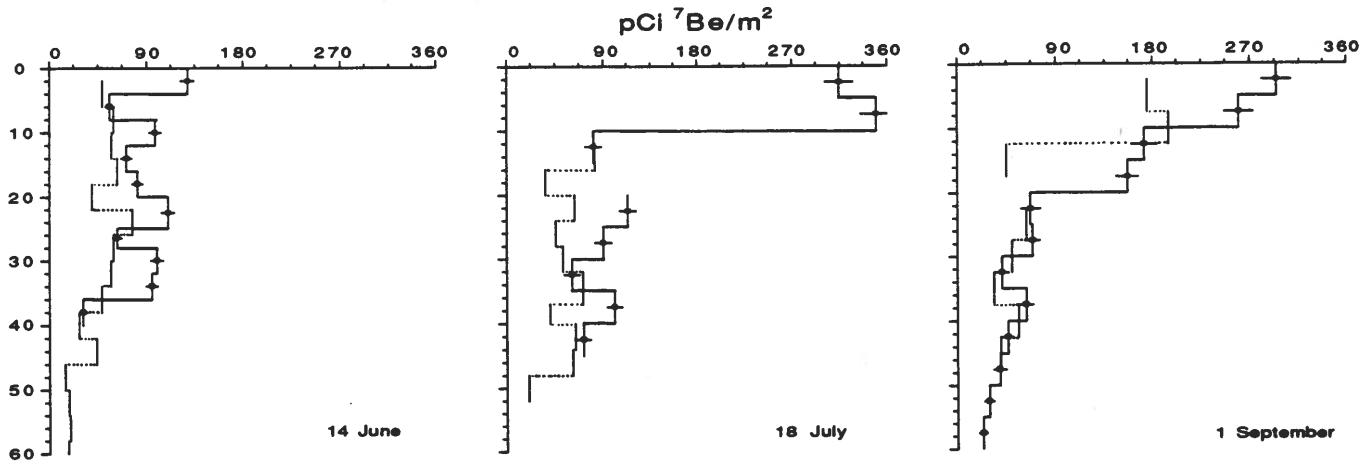

Figure 6) Comparison between successive ^{7}Be profiles in the snowpack. In each frame the profile on the indicated date is the solid line with filled circles and error bars at sample mid-depth, with the decay-corrected profile from preceding pit superposed (dotted line). See text for discussion.

Session 6

Model Applications I

Chairman:
L.A. Barrie

(Proceeding of the Fifth Conference on Arctic Air Chemistry)

Qualitative Determination of Source Regions of Long-Range Transported Aerosol Using Data Collected at Canadian High Arctic

by

Meng-Dawn Cheng[1], Philip K. Hopke[1], Leonard Barrie[2], Ann Rippe[1], Marvin Olson[2], and Sheldon Landsberger[3]
1. Department of Chemistry, Clarkson University, Potsdam, NY
2. Atmospheric Environment Services, Downsview, Toronto, Ontario, CANADA
3. Department of Nuclear Engineering, University of Illinois at Urbana-Champaign, Urbana, IL

ABSTRACT

Traditional receptor models use chemical composition data for airborne particles to infer the likely sources for an airshed and estimate the source contributions to the material collected at the receptor sites. In this article, a hybrid receptor method was employed to identify the possible source regions for various airborne particulate species observed at one of the Canadian High Arctic Aerosol Sampling Stations. This method explores the long-term statistical nature of the air parcel backward trajectories and used the ensemble properties of the trajectories to describe the long-range transport of atmospheric species. The Arctic air chemistry data collected at a ground station was matched with back trajectory locations in order to identify the possible source regions located in the northern hemisphere reached by the trajectories. In order to account for vertical transport of the species to the ground station, this model incorporates the concept of total probability directly into the calculation of the potential source contribution function. The analyses for the data collected during the periods of November 1 to March 20 annually from 1982 to 1987 are presented. This time period was selected since samples taken from the remaining periods include a large number of analyses with values below detection limit. Results of the analyses appear to be consistent with those reported in the literature for trace elements and non-marine sulfate. Major geographical source areas for the chemical species examined in this work were identified. The elemental ratios previously suggested to be used as a discriminatory tracers for source regions around the Arctic were found to be ineffective.

INTRODUCTION

The Arctic is quite distant from most major sources of pollution and had been traditionally considered a remote region where the air and water were pristine. However, this is not the case. After 20 years of measurements and a number of intensive studies, it has been shown that between October and May, the Arctic troposphere is filled with airborne particles commonly called "Arctic Haze" (1,2,3,4).

During the mid-1970s, the haze was thought to consist of mostly soil particles originating in the deserts of eastern China and Mongolia. The limit number of ground measurements, however, indicated that particles collected at ground level stations were enriched in vanadium, aluminum, and other elements of anthropogenic origin. Discovery of anthropogenically enhanced chemical species such as $SO_4^=$, V, Ni, In, Pb, etc. (2,3), man-made organic compounds such as light hydrocarbons (5) as well as a large number of polycyclic aromatic hydrocarbons, polychlorinated dibenzo-p-dioxines and pesticides (6) in the Arctic raises a series of questions about the long-range transport and transformation of airborne chemicals through the atmosphere, the impact of the man-made "foreign" chemicals on fragile Polar ecosystems, the atmospheric chemistry that occurs in the cold Polar region, and so on.

A major question in the Arctic Haze problem is what sources contribute to the measured chemical species and where do those sources exist geographically. Multivariate statistical techniques such as factor analysis have been used to identify possible source types (7,8,9,10). Measured air pollutant concentrations have been related to sources in the industrialized areas surrounding the Arctic using backward air parcel trajectories (11).

Lowenthal and Rahn (L&R) (12) first applied a simple linear mass balance system similar to the chemical mass balance model (13) with 7 chemical tracers to the Arctic aerosol mass on an hemispheric scale. Traditional receptor models have been used less frequently at scales larger than regional because over longer distances diffusion and removal processes as well as chemical transformations confound the relationship between emission and concentrations. In other words, long-range transport, removal and chemical/physical transformation processes can modify and substantially reduce the strength of source-receptor relationship. Gordon (14) has provided an excellent review of current research and developments in receptor-oriented models for studying global and regional air pollution problems.

The simultaneous use of chemical and meteorological data has often been applied to qualitatively understanding the source of pollutants to a region. For instance, particulate

concentrations of 14 elements measured in Sweden were related to air mass trajectories (15) that were classified into five pre-determined directional sectors. They have found a strong dependence of the elemental concentration variations with air mass history. Similarly, Hopper, *et al.* (16) used lead isotope observations in Sweden with trajectories to characterize European sources for lead and thereby assist in the identification of the origins of Arctic lead (17). Davies *et al.* (18) employed Lambert weather type classification system to facilitate categorizing chemical composition observed in precipitation in Scotland. Several studies have examined the origin of atmospheric CO_2, particles and O_3 concentrations observed in the Arctic by classifying trajectories that are associated with "episodic events" (19,20) . These are examples in which chemical concentrations observed at the receptor site are qualitatively related to the source locations through meteorological information.

However, there is a need to identify more precisely the sources that contribute pollutants to remote sampling sites. This modeling has been done on a regional scale (21,22), but not on a large enough scale to be suitable for the Arctic. The potential for using trajectories over long distances has been demonstrated by studies of dust transport from the deserts of Asia to the mid Pacific (23). A receptor model that explicitly incorporates meteorological information directly in the analysis scheme called potential source contributions function (PSCF) analysis may be suitable for such a task (24,25). This paper explores the use of PSCF analysis to study the long-range transport of chemical species to the Arctic using data collected at the Alert sampling site in the Canadian High Arctic. The samples were taken continuously over a six year period from 1982 to 1987. The approach of Cheng, *et al.* (25) was employed to account for the total source potential contributed of material arriving at three altitudes directly above the ground level sampling site.

DESCRIPTION OF DATA

Chemistry Data

Airborne particle samples were collected at Alert, Northwest Territories (latitude=82.3°N, longitude=62.5°W) by the Atmospheric Environment Services of Canada (AES). Sampling operations began in July, 1980 and the station is still operating. However, only the samples taken between January, 1982 and May, 1987 were used in this analysis. Details of the sampling and analytical procedures for ionic species are given by Barrie and Hoff (26). Additional elemental data were obtained using instrumental neutron activation analysis performed at University of Illinois at Urbana-Champaign as described by Landsberger, *et al.* (27,28).

Detailed summary statistics are reported and a comprehensive analysis of the frequency distributions of these chemical species shows that most of them are lognormally distributed (29).

Because of a number of differences in meteorology and atmospheric chemical activities between Arctic summer and winter, the samples were divided into two groups. Since Polar sunrise is around March 21 each year, the period from March 21 to October 31 was designated the LIGHT period and the DARK period was defined as November 1 to March 20. The choice of these dates is somewhat arbitrary and the adjustment of these dates by a month in either directions did not significantly alter the results of the PSCF analysis. Only the DARK data were analyzed in this study since a large number of LIGHT data points were below detection limits.

Trajectory Data

The AES trajectory model (30) was used in this study to calculate the air parcel movement in terms of trajectory segment endpoints by latitude and longitude every six hours backwards in time up to 5 days. The model used three-dimensional objectively-analyzed wind fields at four pressure levels: 1000, 850, 700, and 500 hPa. Height and temperature fields are inputs to compute vertical motion in the atmosphere. Upper air analyses are available every six hours from the Canadian Meteorological Centre. Cubic interpolation was used to obtain winds at intermediate levels in the vertical direction and between horizontal grid points. The computations were performed on the standard Canadian Meteorological Centre grid of 381 km. This grid size is considered as the maximum spatial resolution in the TPSCF analysis. A grid size of 5° in latitude by 5° in longitude was subsequently used for the TPSCF to reduce the statistical counting uncertainty in the analysis.

Air parcel back trajectories were calculated starting at Alert, Canada at the 1000, 925, and 850 hpa levels. It is important to note that the back trajectories moved in the horizontal as well as vertical directions. Each backward wind trajectory was computed 4 times a day (00, 06, 12, and 18 UTC) at 6-hour intervals for a 120-h transport time.

TOTAL POTENTIAL SOURCE CONTRIBUTION FUNCTION

The PSCF was initially introduced to identify geographical regions that might have high probabilities of being source areas for airborne sulfate in the southwestern United States (31). Zeng and Hopke (24) explored the use of 1000 hPa pressure level 2-day back trajectory data in the PSCF analysis based on both principal component scores and individual species

concentrations, and noted differences in the PSCF patterns between sulfate and nitrate. Using only surface trajectories may not be reliable because of the substantial vertical movement of a trajectory travelling across a variety of terrains and surfaces over long distance to reach Alert.

It is assumed that the weekly mean concentration of air pollution measured at ground level at Alert is the result of an ensemble of transport events from mid-latitudes through all levels of the atmosphere represented by trajectories ending at Alert at the 1000, 925, and 850 hPa levels. Despite a climatologically persistent surface-based inversion height of 500-1000 m in the Arctic, the vertical mixing of air from aloft to the ground can be affected by mesoscale katabatic winds in areas of orography or by mechanical turbulence in situations of high winds. At the Alert site, 800 hPa hills in the region ensure that katabatic winds deliver free tropospheric air to the site during frequent calm periods.

The integration of airborne transport at all three levels is provided by the total potential source contribution function (TPSCF). TPSCF is based on the assumption that A^k, {k = 1, 2, and 3} constitute a set of nearly exhaustive events for the arrival of trajectories at the three pressure levels, i.e. 1000, 925, and 850 hPa. From the hydrostatic equation, it can be estimated that 850 hPa is at a pressure level approximately 1.3 km above the ground. Based on this estimate and the pressure level of inversion layer, the 850 hPa level was assumed to represent the maximum pressure level of atmospheric mixing above which material cannot be collected at the ground station. The major question in this approach is whether the probabilities of downward transfer of chemical species are approximately identical from all three levels over a week long sampling period. At the present time, all three layers are assumed equally likely to contribute material to the ground level samples.

If an event occurs where a trajectory endpoint terminates at a cell of address (i,j), the trajectory is assumed to collect material emitted in the cell (i,j). The built-in assumption of the TPSCF analysis is that once the material is incorporated into the air parcel, it will be transported along the trajectory to the receiver. If the total number of endpoints in the kth pressure level that fall in the cell is n_{ij} over entire modeling period, the cumulative probability of these events, A_{ij}, is given by

$$P[A^k_{ij}] = \frac{n_{ij}}{N} \quad (1)$$

where k indicates the pressure level number. Event A^k is the arrival of an air parcel at Alert at pressure level index k without regard to the composition of the associated particulate matter.

There will be m_{ij} endpoints for the same cell for which the measured concentration exceeds a criterion value selected for a target species. The cumulative probability of these high concentration selected events, B_{ij}, over the same modeling period is given by

$$P[B^k_{ij}] = \frac{m_{ij}}{N} \quad (2)$$

Event B^k is then the arrival of an air parcel at Alert at pressure level k carrying concentration of a chemical species above a certain level. The conditional probability, PSCF, for the cell of address (i,j) can then be defined as:

$$PSCF^k_{ij} = P[B^k_{ij}|A^k_{ij}] = \frac{P[B^k_{ij}]}{P[A^k_{ij}]} = \frac{m_{ij}}{n_{ij}} \quad (3)$$

$P[B^k|A^k$, k=1, 2, and 3] is the conditional probability of the occurrence of the event B^k as the individual event A^k occurs, and $P[A^k$, k=1, 2, and 3] is the probability of the occurrence of the event A^k. The conditional probability of a single level, $P[B^k|A^k]$, is the PSCF probability calculated for the pressure level index k.

The PSCF is interpreted as a conditional probability function describing the spatial distribution of contributing probabilities of geographical origins inferred by using trajectories arriving at the kth pressure level. Cells for which high PSCF values are calculated are identified as "**potential**" sources areas.

Let B denote the selected subset events of A_t in which the concentration of a given chemical constituent exceeds a criterion value. The probability of B is given by

$$P[B_{ij}] = \sum_{k=1}^{3} P[B^k_{ij}|A^k_{ij}]\, P[A^k_{ij}] \quad (4)$$

In other words, P[B] is the total probability of the occurrence of an event B as calculated for the concentration of a species collected at the ground station based on the arrival of material at all three pressure levels. The TPSCF can then be defined for a grid cell (i,j) as follows:

$$TPSCF_{ij} = PSCF_{ij} = \frac{P[B_{ij}]}{\sum_{k=1}^{3} P[A^{k}_{ij}]} = \frac{\sum_{k=1}^{3} P[B^{k}_{ij}|A^{k}_{ij}]\ P[A^{k}_{ij}]}{\sum_{k=1}^{3} P[A^{k}_{ij}]} \quad (5)$$

PSCF and TPSCF value falls within a numeric range of 0 and 1. A grid cell of the probability value of 0 is unlikely to be a source region where a value of 1 is likely to be a source region.

Since PSCF or TPSCF for a grid cell is computed as a ratio of the counts of selected events (m_{ij}) to the counts of all occurred events (n_{ij}), it is likely that a small but non-zero m_{ij} ($\leq n_{ij}$) may result in a $PSCF_{ij}$ in the class of 0.8 to 1.0. For instance, $n_{ij} = 2$ and $m_{ij} = 2$ would result in $PSCF_{ij} = 1.0$. However, if $n_{ij} = 300$ and $m_{ij} = 300$, $PSCF_{ij}$ would end up equal to unity. The latter case has more significance than the former one. To discriminate the two ones, a weighting function of n_{ij} is fabricated, although choice of the weights is arbitrary. The weight function is defined as follows:

$$W(n_{ij}) = \left\{ \begin{array}{l} 1.00,\ if\ n_{ij} \geq 4 \\ 0.85,\ if\ n_{ij} = 3 \\ 0.65,\ if\ n_{ij} = 2 \\ 0.50,\ if\ n_{ij} = 1 \end{array} \right\} \quad (6)$$

The maps shown in the next section displayed weighted TPSCF values.

RESULTS AND DISCUSSION

The chemical species selected from the 38 measured constituents for presentation in this paper are non-marine SO_4(N.M.SO_4), Pb, Ni, In, As/Sb, excess V/Sb (Exs_V/Sb), and Zn/Sb. These elements are typically of anthropogenic origins and have been used as "tracers" of man-made sources in previous receptor modeling studies (32). Sodium (Na) which is of natural origin was used to evaluate the methodology by comparison with the literature results (33). The Non-Marine Sulfate (N.M. SO_4) is calculated as

$$[N\_M.SO_4]_a = [SO_4]_a - 0.25*[Na]_a \quad (7)$$

where "a" denotes aerosol concentration. The ratio of SO_4 to Na is 0.25 for sea water (34). The Exs_V is the excessive vanadium concentration calculated as above the background soil level;

$$[ExsV]_a = [V]_a - 1.3*10^{-3}\,[Al]_a \quad (8)$$

The ratio of average [V] to the average [Al] for the local soil is about 1.35 E-3 (35) and is similar to that in average crustal rock (34).

Although the grid size chosen for the TPSCF computation is adequate to assimilate the uncertainty associated with the trajectory endpoints, Kahl, *et al.* (36) noted the uncertainty after 120 hours of travel could be on the order of 1,000 km. In other words, the accuracy of source region identification by using trajectory analysis is limited primarily by the precision in the trajectory endpoints. A 5° by 5° grid size corresponds to about 500 km in the latitudinal direction and about 48 - 355 km in the longitudinal direction depending on where the grid cell is located between 50°N and the North Pole. A trajectory endpoint calculated at 120 hours or longer travelling time could, therefore, terminate at cells adjunct to it with some probability due to the uncertainty in the calculation (30).

It should be emphasized that PSCF analysis identifies source areas that are likely to have contributed to the high concentrations measured at Alert. The PSCF maps provide an indication of where likely sources exist, but do not provide quantitative estimates of the contributions of those locations to the measured concentrations. Thus, PSCF maps should not be interpreted as surrogates for emission inventory maps.

Individual Chemical Species

It is generally believed that concentrations of airborne particulate N.M.SO_4 observed in remote areas is related to both the anthropogenic emission of SO_x and the biogenic emission of sulfur-containing compounds, DMS (dimethyl sulfide) or DMDS (dimethyl disulfide) from the surface of the ocean (37). Yin, *et al.* (38) have outlined a detailed photooxidation mechanism for DMS and DMDS. These reduced organosulfur compounds are the precursors of atmospheric sulfate production in a natural environment. DMS was found to be the major species (more than

80% relative abundance) among various sulfur emitted from ocean surface in North Sea (39). Li and Barrie (40) have measured aerosol oxidation products over a decade at Alert. On the basis of their work, it can be concluded that biogenic contribution to N.M.SO_4 is negligibly small during the DARK period studied here. The criterion value selected in the TPSCF analysis for N.M.SO_4 was 330 ng m^{-3}. This average value over entire sampling period is sufficiently large that concentration of the N.M.SO_4 can be considered to result from anthropogenic sources.

In Figure 1 grid cells with PSCF values larger than 0.8 are identified in eastern Europe, the areas around the Kola Peninsula, the Pechora basin, and the St. Petersburg area and the Noril'sk area, one area adjunct to Alaska, and areas in the Atlantic Ocean. The major source cluster at 60-75°N and 30-50°E is likely to be a result of regional transport of SO_x from industrial complex located further south in area such as eastern Europe. Comparing with the source emission map of SO_2 in Figure 2, the location of potential source in eastern Europe as identified for non-marine sulfate in Figure 1 appears to be displaced toward northeast. The displacement could be due to chemical transformation from sulfur dioxide to sulfate particles during the time of transport. Several areas in the Baltic states have calculated PSCF values between 0.6 and 0.8. Identified sources of SO_x emission from fossil fuel combustion in these areas are in good agreement with those shown in Figure 2 (41,42). The cells close to the proximity of North America in Atlantic Ocean are likely to be related to the emissions in eastern North America (41,42). Grid cells located in far eastern Siberia could result from regional sulfate transport from Southeastern Asia.

Figure 3 shows the TPSCF map for Pb where the study period average concentration of 0.87 ng m^{-3} was used as the criterion value. The locations of Pb emission sources identified in this map are in a good agreement with those of Pacyna, *et al.* (11). A single cell is found in the Atlantic Ocean and another at the south of Anchorage in the Gulf of Alaska. Since the ocean is not a significant source of Pb (34) and the trajectory segment endpoints fall in the region are typically associated with the trajectories traced across Greenland (average about 3000 meters in height), the uncertainties of the endpoints in the region could be substantial. Thus, the Atlantic cell values could be considered highly unreliable. There could be local emission source around the Gulf of Alaska that contributes to the high cell value.

Figure 4 shows the TPSCF map for Ni in which the criterion value was chosen as 0.35 ng m^{-3}. Pacyna (43) indicates that nickel production is the major emission source of Ni located at Urals, Norilsk, and Kola areas in the former USSR. Based on the TPSCF analysis, the Urals and

Norilsk are identified as potential source areas of Ni in addition to the Kuznetsk area which Pacyna did not indicate as a source area. The Kola area was however found as a minor source of Ni in the TPSCF map with its PSCF values in the range of 0.6 to 0.8. The Donetsk and Moscow areas are identified as potential sources. Again, a number of "pseudo-source" areas are identified in Atlantic Ocean and around Alaska as those found in the non-marine sulfate and Pb maps. Jaffe (44) indicated that a large industrial complex is located in the Prudhoe Bay area in the Arctic. The cells at the border of Alaska and Canada where the Prudhoe Bay is located may be an indication of the industrial complex.

Figure 5 shows the result of TPSCF analysis for indium with 0.001 ng m^{-3} selected as the criterion value. Several grid cells were identified as potential areas by the criterion concentration level defined at 0.001 ng m^{-3}. These cells are found to locate in Spain, the border of France and Germany, the Donetsk and Moscow areas of former USSR, the Urals and Kuznetsk areas in central Russia, Prudhoe Bay, and areas in the south of Alaska. These locations are quite similar to those identified for Ni with differences in two locations. The first location is found in central Canada in the vicinity of Thompson, Manitoba and Flin Flon, Saskatchewan, well-known metal smelting regions. The other major source area (considering PSCF of values higher than 0.6) is in Europe from the border of France and Germany to the Moscow area of former USSR. The European area is not found in the Ni map.

The marine aerosol is highly enriched in Na and has been used frequently as the tracer element for the transport of sea salt particles (45). Figure 7 shows the TPSCF map for Na produced with a criterion value chosen at 251 ng m^{-3}, i.e. the 75th percentile point of the annual data. Using the average value, which is smaller than the 75th percentile, yields too many large regions of high source potential. A lower criterion value leads to the identification of source areas of both marine Na and soil-derived Na. High potential source clusters were mostly found in the western hemisphere. Major source regions lie in Atlantic Ocean close to Newfoundland and Europe. Another area is located in the Bering Sea area. These three regions are in good agreement with the distribution of sea-salt concentration measured during the boreal winter (December-January-February) (33). There were potential source regions in Hudson Bay and several other places in North America. One interesting land source area in Canada overlaps that found in the In map in Figure 5.

Concentration Ratios of Trace Elements

Lowenthal and Rahn (12) suggest that the ratios of the form X/Sb were useful in inferring the sources of particles collected at Barrow, Alaska, where X are the trace elements As, Zn, and Excess_V. To explore the utility of these ratios, the range of elemental ratios reported in the literature (12,35) for As/Sb, Excess-V/Sb, and Zn/Sb are presented in Figures 7, 9, and 11, respectively. The calculated ratios for the data used in the present studies are also displayed.

In these figures, data taken from L&R (12) and Barrie *et al.* (35) were used to construct the ranges. The L&R data were based on the samples collected in winter of 1979-1980, while Barrie's were collected in April, 1986 during the AGASP-II study. It should be noted that several factors, for instance, trace element emissions changing over time, different sampling locations and periods, and so on, all could cause the variations in the ratios. However, these values have been used to suggest that certain geographical areas are predominant source locations and thus, the utility of these ratios warrants further investigation. PSCF analysis can be performed using the elemental ratio values to choose the samples that have values above or below a criterion value. It must be emphasized that although PSCF analysis can provide direct source-receptor information, its range is limited by the finite length of reliable trajectories; in this case, five days.

Figure 7 shows the ratios of Arsenic to Antimony, Sb. Values larger than 5.0 should produce potential areas mainly in CUSSR in TPSCF analysis, since this area has the highest ratio, assuming that L&R (12) had correctly identified the ratio for these sources. Figure 8 presents the result for As/Sb using the criterion value of 6.5 which was considered adequate to isolate CUSSR from the other source areas. The map in Figure 8 shows that potential source regions were found primarily in Siberia in Russia. The northwestern Spain is also identified as the source area. Areas around Alaska (the Prudhoe Bay and the south of Alaska) as well as the central Canada are also identified in this map. It is important to mention that although CUSSR was found to be a potential source, identifying multiple source regions in the map suggests that the As/Sb ratio may not be as an efficient location indicator as initially suggested (12).

Figure 9 shows the ratios of Excess_V to Sb. The ratio range for the Central East Coast (CEC) region of North America from L&R is much larger than any of the other reported values. Excess vanadium is generally a good tracer for residual or fuel oil combustion. It appears that using a criterion value of 16 could separate the central coastal area of the U.S. from the rest. The 75th percentile value in the data is less than one half of 16; thus, using the value 16 will results in substantially small numbers of counts, i.e. m_{ij}, for each cell. Therefore, the median value

in the annual data was chosen in the analysis. Figure 10 shows the result for Excess V/Sb ratio using the criterion value of 6.5. A number of source areas are found in this map. These areas include 1) the northwestern Spain, 2) area from France, Germany, Poland, to the Donetsk and Moscow areas, 3) the Kuznetsk area in central former USSR, and 4) the two areas around Alaska. The area in Canada at about 60°N and 120°W is unknown at this point. By Figure 9 UKS, EUR, and CUSSR should be identified as source regions using the criterion value of 6.5 but this is not the case in Figure 10. Instead, the UKS region has PSCF values in the range of 0.0 to 0.2 indicating it was not a source area using Excess_V/Sb ratios calculated for Alert. CEC was found with PSCF values in between 0.6 to 0.8 not in the range of 8.0 to 1.0. Again, this result indicates the inefficacy of the ratio in identifying the geographical location of the sources.

Figure 11 shows various reported ranges for Zn/Sb ratios. Zn can be emitted from non-ferrous metal production processes such as copper-nickel production (43). A value of 70 was initially considered as the criterion value in the analysis since this value could provide an adequate separation for EUR from the other source regions. However, it was later found from the analyses that a higher value was needed. Figure 12 shows the map with the criterion value set at one hundred. Four major potential source areas were identified (1) in Siberia close to Bering Sea, (2) in the Alaska area, (3) the northeastern Canada, and (4) the Moscow area. Sources located at Sudbury, Ontario and Noranda, Quebec in Canada could have contributed to the high Zn source regions identified in the northeastern Canada. There is a grid cell in the Prudhoe Bay area having high PSCF value. The potential grid cells over Bering Sea in the Russia side were of unknown sources at this point; they could be resulted from regional transport from the source region further south. However, this result once again indicates the ratio of Zn to Sb is not an efficient discriminator of pollution source in the Arctic.

CONCLUSIONS

The geographical distribution of emission sources that contribute to trace metals and non-marine sulfate concentrations measured at the Canadian high Arctic was constructed by using a statistical receptor climatology approach. This approach explores the long-term statistical nature of the air parcel backward trajectories and used the ensemble properties of the trajectories to describe the long-range transport of atmospheric species to the Arctic. Identified geographical locations of sources for non-marine sulfate, Na, Pb, Ni, In, As/Sb, Exs_V/Sb, and Zn/Sb generally agree well with the previous studies and known emission inventories. Source locations identified

are repeated for these variables in the maps. These areas include 1) Moscow, 2) Donetsk, 3) Urals, 4) Kuznetsk. 5) Norilsk. 6) eastern Europe including the area at the border of France and Germany. and 7) the northwestern Spain. Central Canada was found to be the source areas of In, As/Sb. and Zn/Sb. Locations around Alaska have been repeatedly observed in a number of maps. The Prudhoe Bay area was identified as a source area for N.M.SO_4, Ni, In, Na, As/Sb, and Zn/Sb. It appears that a wide range of industrial processes could be found in this area. The two source regions in Bering Sea and Gulf of Alaska could not be asserted with known emission sources in the region.

There appear to be some artifacts near the end of the range of 5-day trajectories over an area such as Atlantic Ocean where meteorological sampling stations are sparse. Improvement of the analysis can be achieved depending upon the accuracy of the trajectories used.

ACKNOWLEDGEMENTS

This research was supported by the National Science Foundation under the grant numbers ATM 8996203, DPP 8821918, and NSF REU CHEM-9101219. Mention of trade names or commercial products does not constitute an endorsement or recommendation for use.

LITERATURE CITED

(1) Rahn. K.A. and McCaffrey, R.J., *Proc. WMO Symp.*, Sofia, 1979, WMO, NO. 538, pp. 25.
(2) Rahn. K.A. and McCaffrey, R.J., *New York Acad. Sci.*, 1980, pp. 486-503.
(3) Barrie. L.A., *Atmos. Environ.*, 1986. 24, 643.
(4) Ottar. B., *Atmos. Environ.*, 1989, 23, 2349.
(5) Hov. O. Penkett. S.K., Isaksen, I.S.A., and Semb. A., *Geophys. Res. Letter*, 1984, 11, 425.
(6) Oehme. M., Furst. F., Kruger, C., Meenken. H.A., and Groebel. W., *Chemosphere*, 1988,17,1291.
(7) Heidam. N.Z., *Atmos. Environ.*,1981.15.1421.
(8) Heidam. N.Z., *Atmos. Environ.*,1984.18.329.
(9) Barrie. L.A. and Barrie. M.J.*J. Atmos. Chem.*.1990.11.211.
(10) Li. S.M. and Winchester. J.W., *J. Geophys. Res.*,1990.95.1797.
(11) Pacyna. J.M., Ottar. B., Tomza. U., and Maenhaut. W., *Atmos. Environ.*, 1985.19,857.
(12) Lowenthal. D.H. and Rahn. K.A., *Atmos. Environ.*.1985.19,2011.
(13) Friedlander. S.K., *Environ. Sci. & Technol.*.1973.7,235.
(14) Gordon. G.E., *Environ. Sci. & Technol.*.1991.25.1822.
(15) Öblad. M. and Selin. E., *Atmos. Environ.*.1986.20.1419.
(16) Hopper. J.F., H.B. Ross. W.T. Sturges. and L.A. Barrie. *Tellus*. 1991,43B.45.
(17) Sturges. W.T. and L.A. Barrie. *Atmos. Environ.*. 1989.23.2513.
(18) Davis.T.D..Farmer.G..Barthelmie.R.J.*Atmos.Environ.*.1990.24A.63.

(19) Higuchi,K.,Trivett,N.B.A.,Daggupaty,S.M.,*Atmos.Environ.*,1987,21,1915.
(20) Peterson, J.T., K.J. Hanson, B.A. Bodhaine, and S.J. Oltmans, *Geophys. Res. Lett.*, 1980,7,349.
(21) Keeler, G.J., *A Hybrid Approach for Source Apportionment of Atmospheric Pollutants in the Northeastern United States*, Ph.D. Thesis, University of Michigan, Ann Arbor, 1987.
(22) Barrie, L.A., *J. Geophys. Res.*, 1988,93D,3773.
(23) Duce, R.A., Unni, C.K., Ray, B.J., Prospero, J.M., and Merrill, J.T., *Science*,1980,209,1522.
(24) Zeng,Y;Hopke,P.K.,*Atmos.Environ.*,1989,23,1499.
(25) Cheng,M.D.;Hopke,P.K.;Landsberger,S;Barrie,L.A.,*Applications of Air Pollution Meteorology*,1991,Boston,MA.
(26) Barrie,L.A.;Hoff,R.M.,*Atmos.Environ.*,1985.19,1995.
(27) Landsberger,S.;Hopke,P.K.;Cheng,M.D.,*Nuclear Sci. and Engr.*,1992,110,79
(28) Landsberger, S., Hopke, P.K., Cheng, M.D., Barrie, L.A.,*Environ. Pollution*.1992,75,181.
(29) Cheng,M.D.;Hopke,P.K.;Landsberger,S.;Barrie,L.A.,*Atmos.Environ.*,1991,25A,2903.
(30) Olson,M.P.;Oikawa,K.K.;Macafee,A.W.,*A Trajectory Model Applied to The Long-Range Transport of Air Pollutants*,Report of Atmos. Environ. Services, Canada, 1978.
(31) Malm,W.C.;Johnson,C.E.;Bresch,J.F.,*Receptor Methods for Source Apportionment*, Pace, T. ed., Air Pollution Control Association, Pittsburgh, PA, pp. 127-148, 1986.
(32) Hopke, P.K. (ed.), *Receptor Modeling for Air Quality Management*, Elsevier Sc. Pub., 1989.
(33) Erickson, D.J., Merrill, J.T., and Duce, R.A., *J. Geophysical Research*, 1986,91(D1),1067.
(34) Mason, B., *Principles of Geochemistry*, 3rd ed., John Wiley & Sons, 1966.
(35) Barrie,L.A.;den Hartog, G.;Bottenheim,J.W.;Landsberger,S., *J. Atmos. Chem.*,1989,9,101.
(36) Kahl,J.D.;Harris,J.M.;Herbert,G.A.;Olson,M.P.,*Tellus*,1989,41B,524.
(37) Erickson, D.J., Ghan, S.J., and Penner, J.E., *J. Geophys. Res.*, 95(D6):7543-7552, 1990.
(38) Yin,F.;Grosjean,D.;Seinfeld,J.H., *J. Atmos. Chem.*,1990,11,309.
(39) Leck, C. and Rodhe, H., *J. Atmos. Chem.*, 12:63-86, 1991.
(40) Li, S.M. and Barrie, L.A., Ten years of methane sulfonic acid observations in the high Arctic, Proceedings of the Fifth Conference on Arctic Air Chemistry, Copenhagen, Denmark, 1992.
(41) Hameed, S. and Dignon, J.,*J. Air & Waste Management Assoc.*,1992,42,159.
(42) Dignon, J.,*Atmos. Environ.*,1992,26A,1157.
(43) Pacyna, J.M. (1991), Pollution of The Arctic Atmosphere, Chapter 4 in W.T. Sturges, ed., Elsevier Science Publishers, New York, NY.
(44) Jaffe, D.A. (1991) in Pollution of the Arctic Atmosphere, ed. by W.T. Sturges, Elsevier Science Publishers, New York, NY.
(45) Warneck, P., Chemistry of the Natural Atmosphere, Academic Press, New York, NY, 1988.

CAPTION OF FIGURES

Figure 1. TPSCF map for N.M.SO_4 during the DARK periods

Figure 2. SO_2 emission from 5° by 5° (latitude by longitude) cells.

Figure 3. TPSCF map for Pb during the DARK periods

Figure 4. TPSCF map for Ni during the DARK periods

Figure 5. TPSCF map for In during the DARK periods

Figure 6. TPSCF map for Na during the DARK periods

Figure 7. As/Sb ratios from various data sources

Figure 8. TPSCF map for As/Sb during the DARK periods

Figure 9. Excess V/Sb ratios from various data sources

Figure 10. TPSCF map for Excess_V/Sb during the DARK periods

Figure 11. Zn/Sb ratios for various data sources

Figure 12. TPSCF map for Zn/Sb during the DARK periods

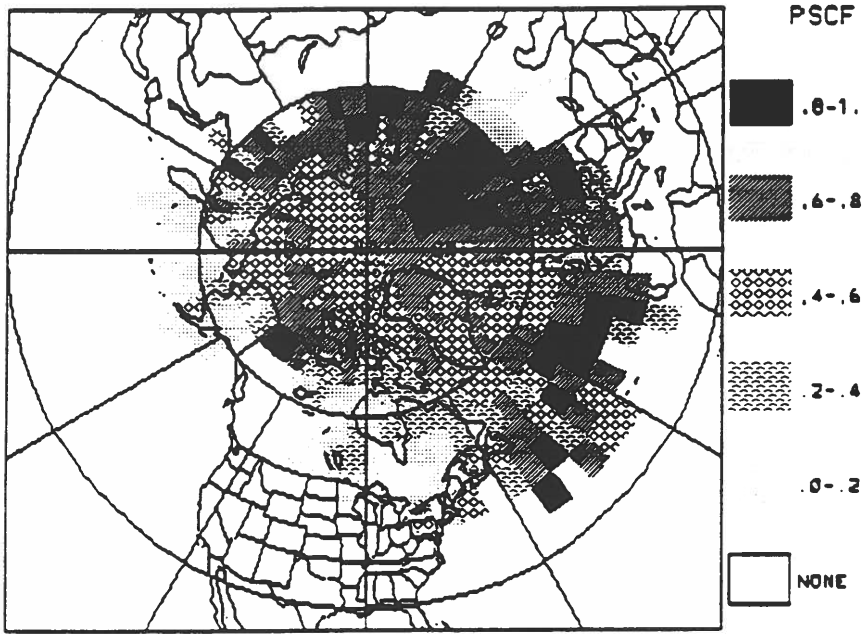
PSCF
.8-1.
.6-.8
.4-.6
.2-.4
.0-.2
NONE

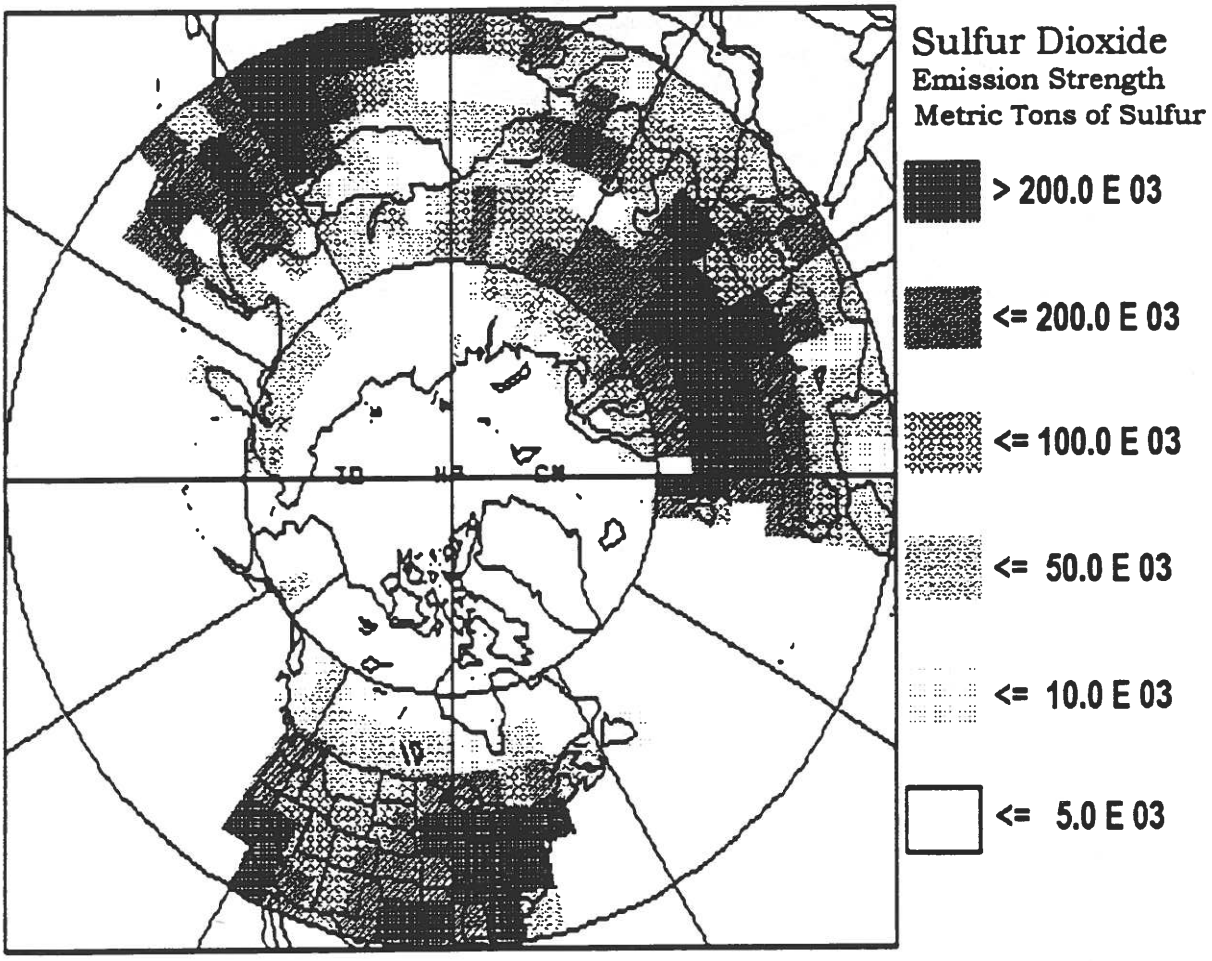
Sulfur Dioxide
Emission Strength
Metric Tons of Sulfur
> 200.0 E 03
<= 200.0 E 03
<= 100.0 E 03
<= 50.0 E 03
<= 10.0 E 03
<= 5.0 E 03

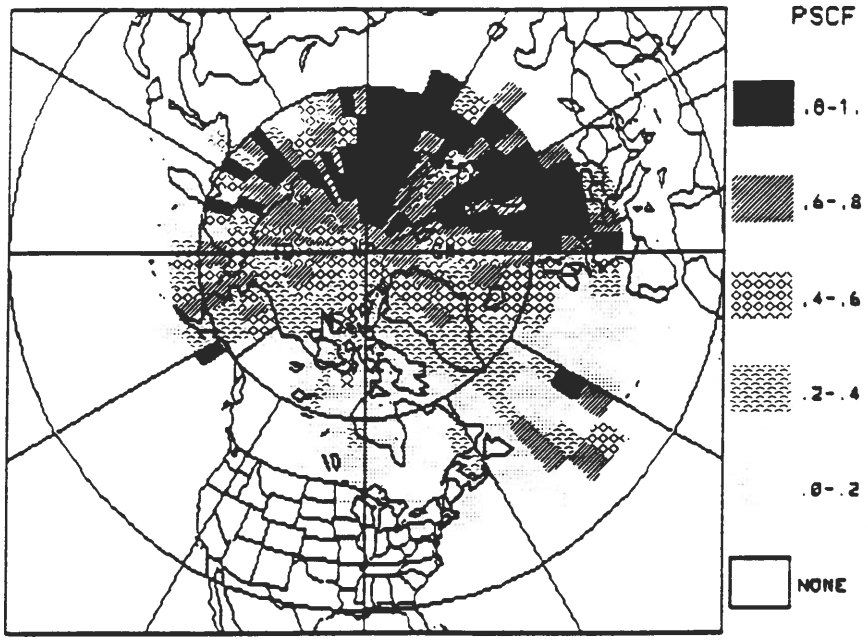

Pb

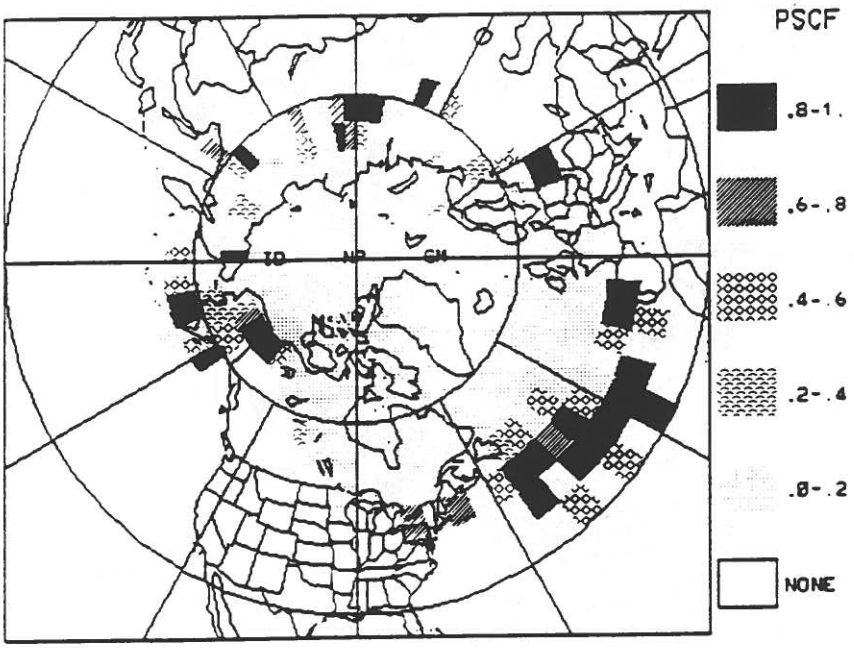

Ni

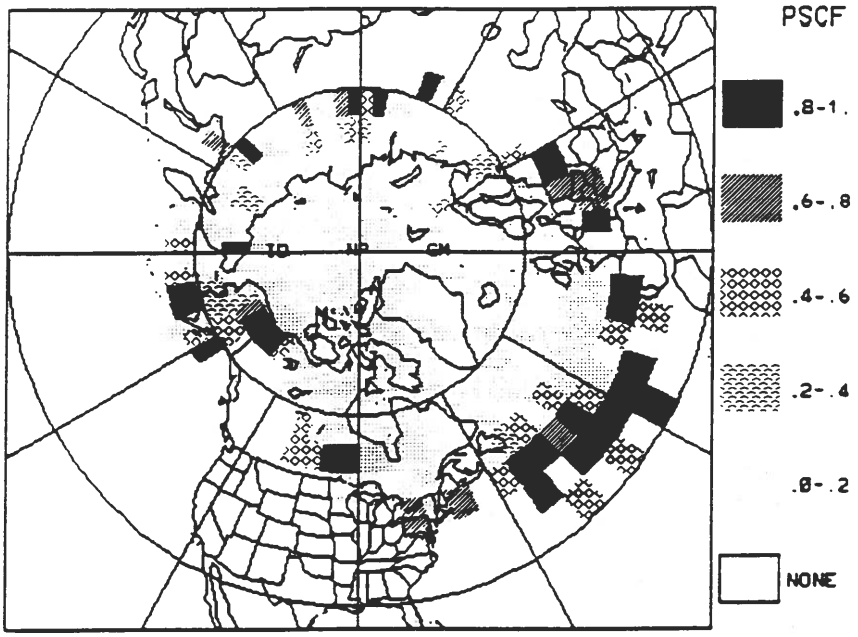

In

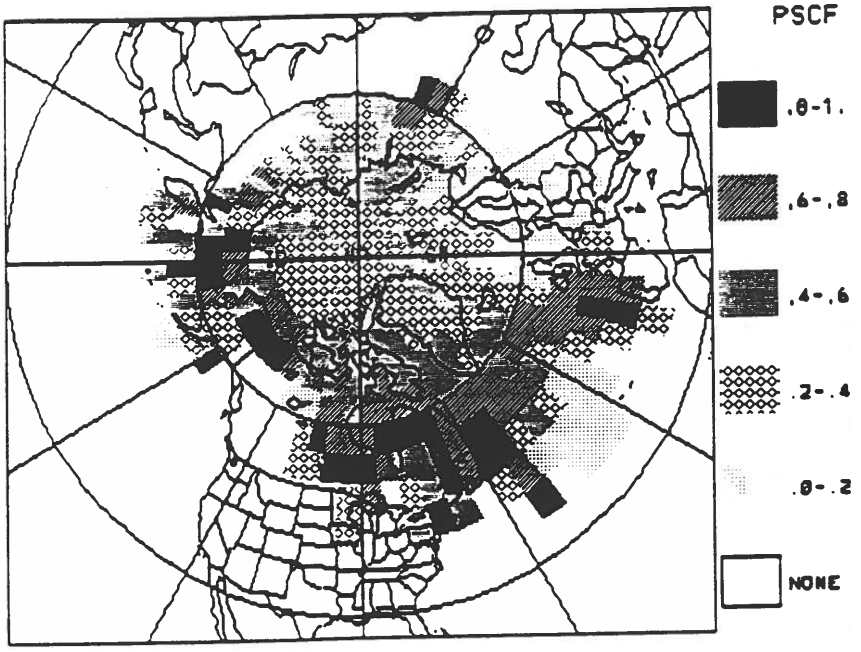

Na

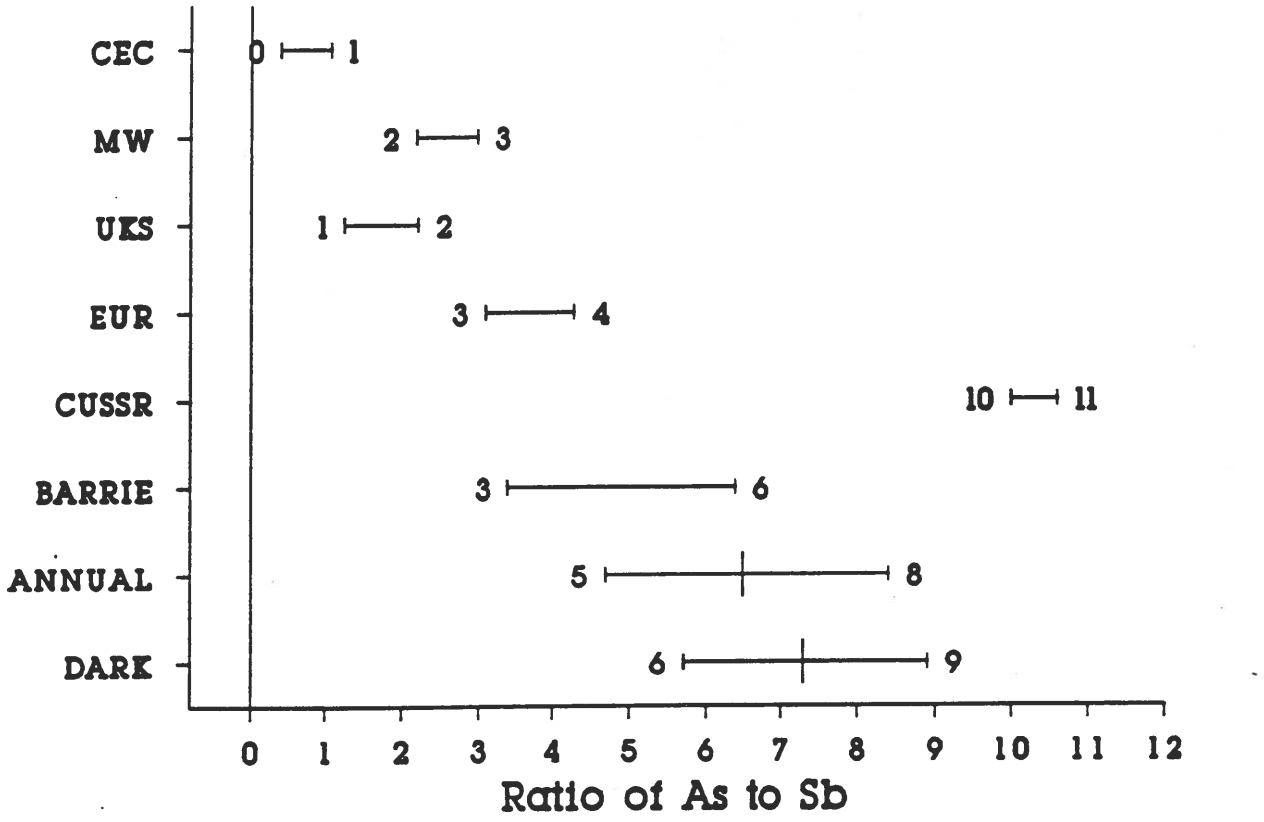

The top bar of a range corresponds to the mean + 1*standard deviation for a region, and the bottom bar is the mean - 1*standard deviation in the L&R data.

The range for Barrie is chosen from Barrie, *et al.* (35).

For ANNUAL and DARK, the 75 percentile sets the top and the 25 percentile points sets the bottom of a range. The vertical line in between these two ranges indicates the median value.

CEC (Central East Coast of U.S.), MW (Midwest of U.S.), UKS (United Kingdom), EUR (Europe and W. Russian Republic), and CUSSR (Central Russian Republic) are those taken from L&R (12).

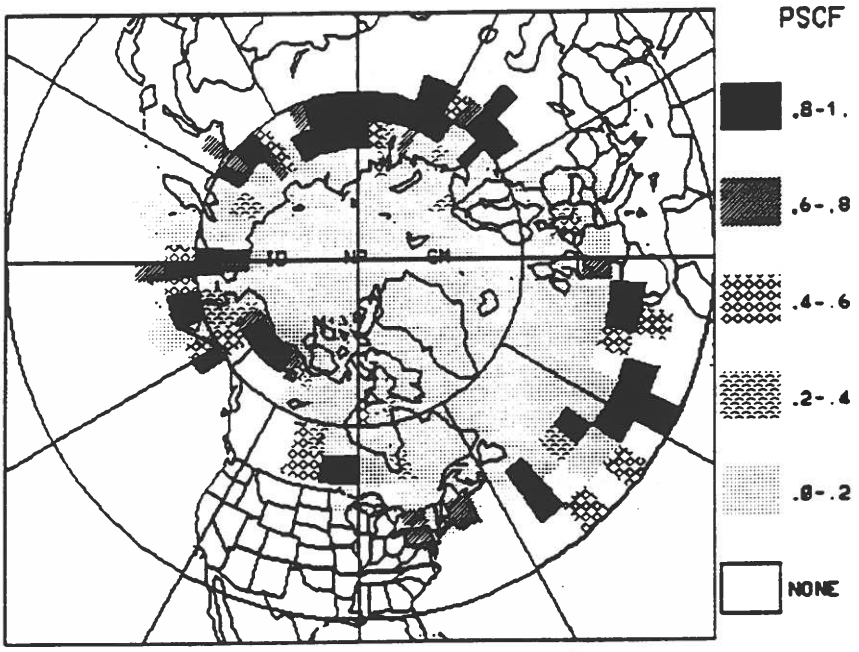

As/Sb

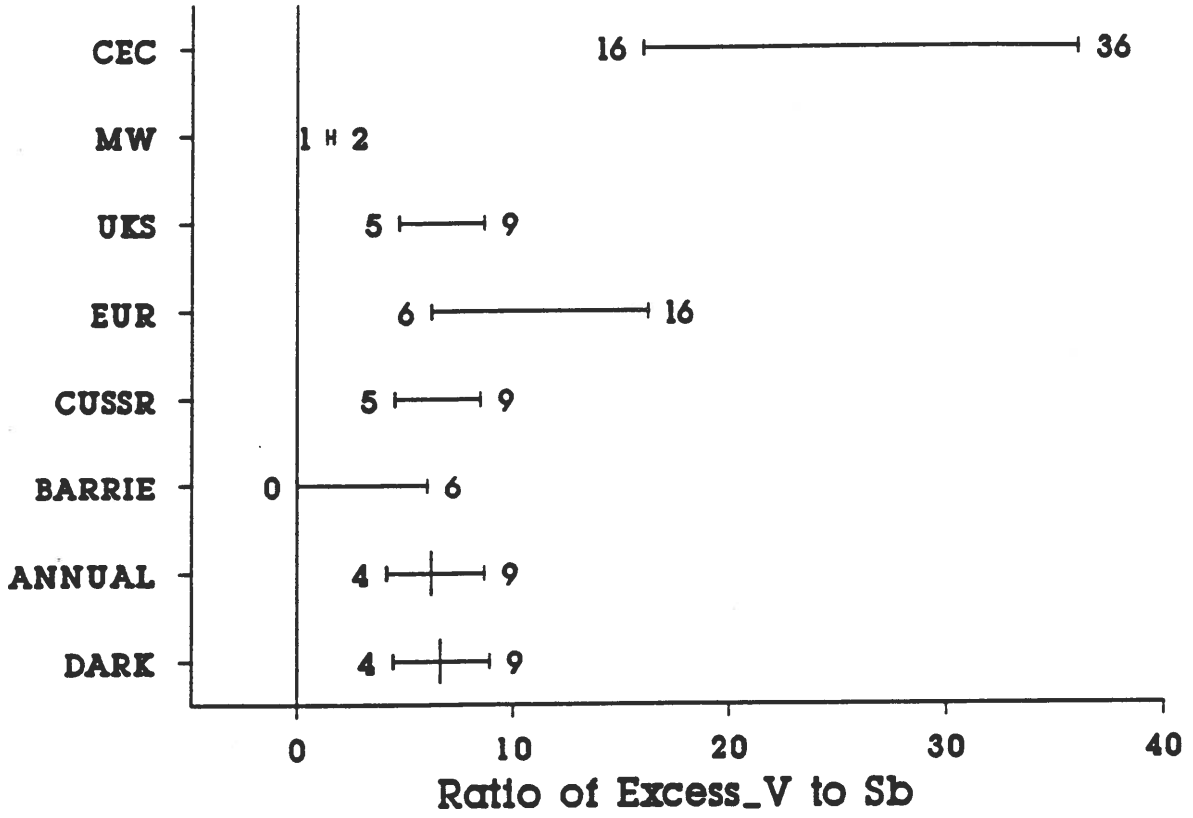

The top bar of a range corresponds to the mean + 1*standard deviation for a region, and the bottom bar is the mean - 1*standard deviation in the L&R data.

The range for Barrie is chosen from Barrie, *et al.* (35).

For ANNUAL and DARK, the 75 percentile sets the top and the 25 percentile points sets the bottom of a range. The vertical line in between these two ranges indicates the median value.

CEC (Central East Coast of U.S.), MW (Midwest of U.S.), UKS (United Kingdom), EUR (Europe and W. Russian Republic), and CUSSR (Central Russian Republic) are those taken from L&R (12).

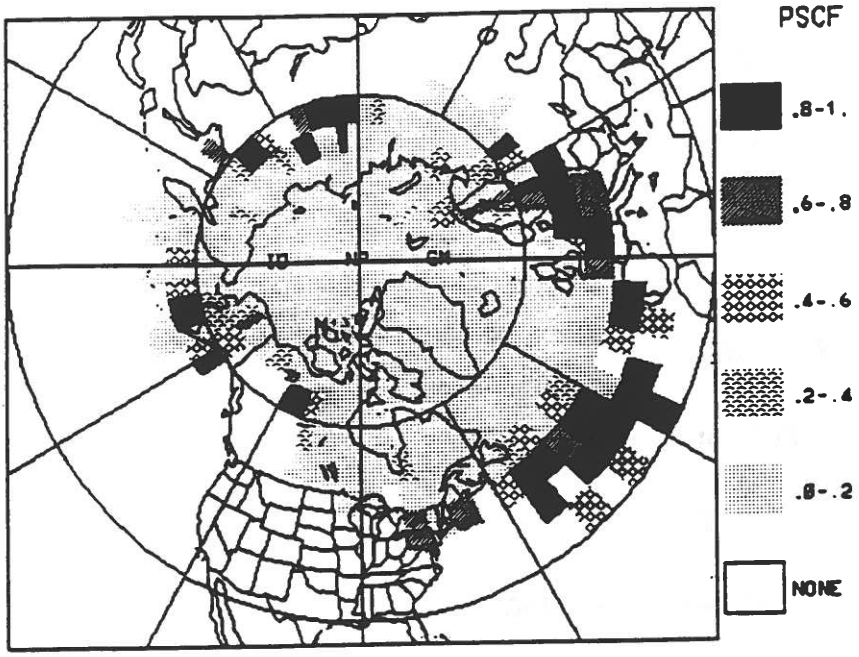

Exs_V/Sb

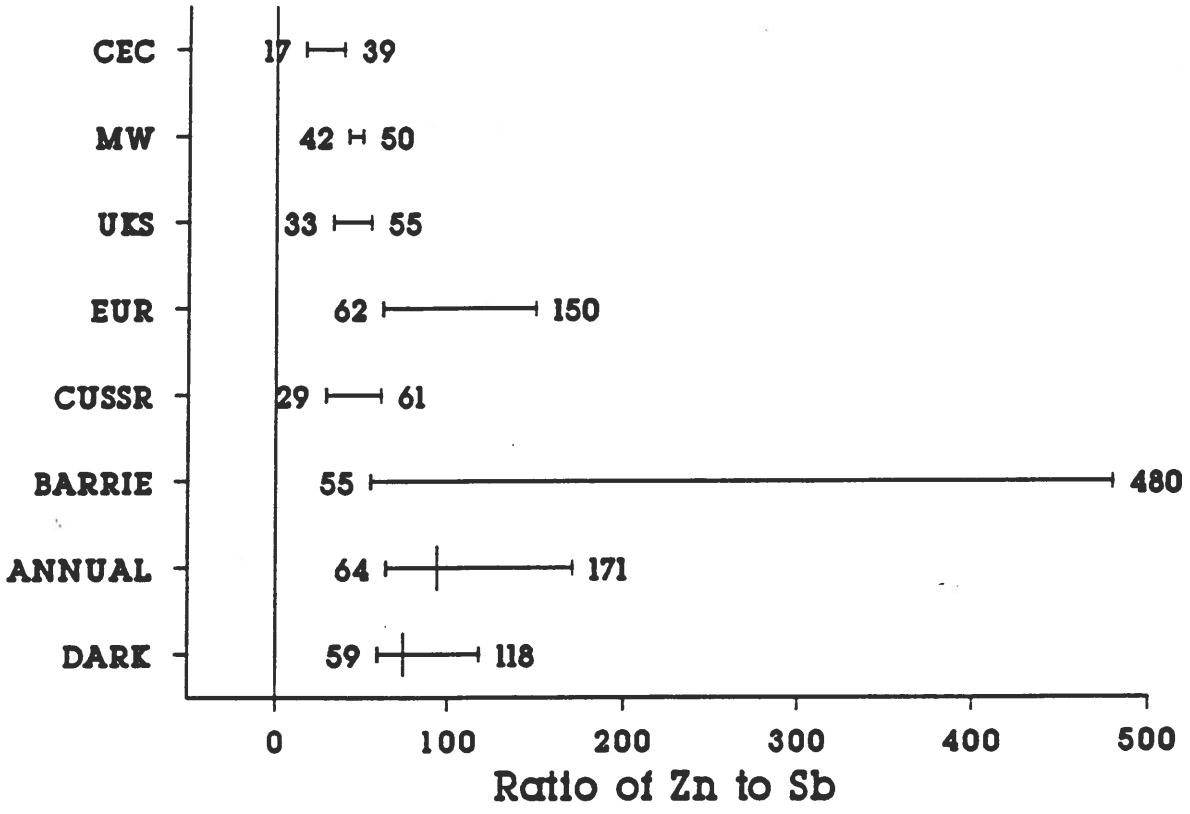

The top bar of a range corresponds to the mean + 1*standard deviation for a region, and the bottom bar is the mean - 1*standard deviation in the L&R data.

The range for Barrie is chosen from Barrie, *et al.* (35).

For ANNUAL and DARK, the 75 percentile sets the top and the 25 percentile points sets the bottom of a range. The vertical line in between these two ranges indicates the median value.

CEC (Central East Coast of U.S.), MW (Midwest of U.S.), UKS (United Kingdom), EUR (Europe and W. Russian Republic), and CUSSR (Central Russian Republic) are those taken from L&R (12).

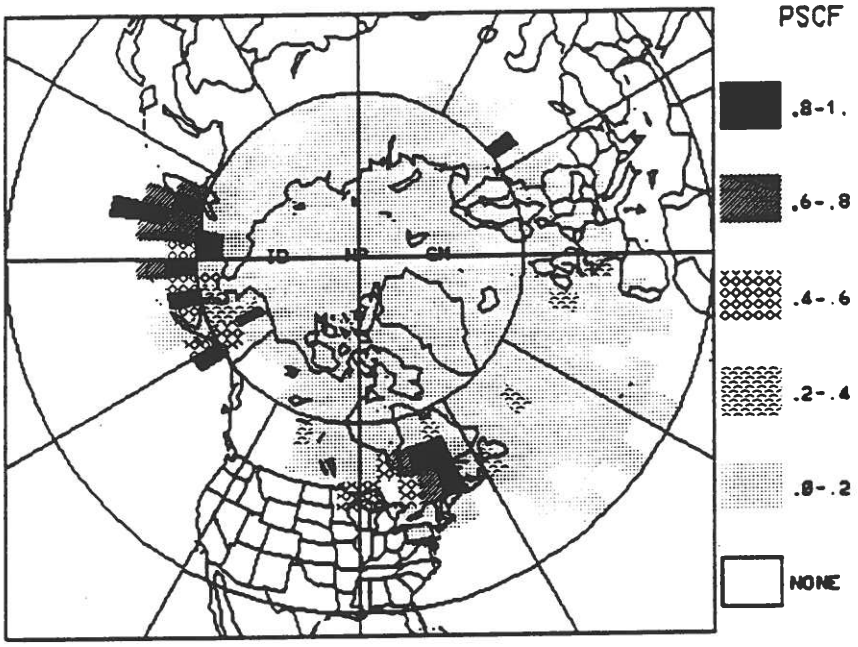

Zn/Sb

ATMOSPHERIC AEROSOL AT NY ÅLESUND DURING WINTER 1989: MULTIELEMENT COMPOSITION, RECEPTOR MODELING, AND COMPARISON WITH DATA FROM PREVIOUS WINTERS

Willy Maenhaut[1], Geert Ducastel[1] and Jozef M. Pacyna[2]

[1]Institute for Nuclear Sciences, Proeftuinstraat 86, B-9000 Gent, Belgium
[2]Norwegian Institute for Air Research, P.O. Box 64, N-2001 Lillestrøm, Norway

Abstract - A suite of over 100 daily filter samples of <2.5 μm aerosol was collected at Ny Ålesund, Spitsbergen, between January 1 and April 30, 1989. The samples were analyzed by instrumental neutron activation analysis and particle-induced X-ray emission analysis for a total of 42 elements. The data set was examined by receptor modeling, including absolute principal component analysis (APCA), chemical mass balance (CMB) and multiple linear regression (MLR) techniques. In the CMB analysis use was made of Rahn and Lowenthal's 8-element tracer system (with noncrustal V, noncrustal Mn, Zn, As, Se, In, Sb and Pb) to apportion the tracers to Eurasian source regions. In a separate MLR analysis, sulfate was also apportioned to these source regions. The results from the various receptor modeling approaches were related to the origin of the air mass, as deduced from 850 mb air mass back trajectories. Furthermore, the atmospheric aerosol data and receptor modeling results from the 1989 winter campaign were compared with similar results obtained in winter sampling campaigns of 1983, 1984, 1986, and 1987. Like for the combined data set from the previous 4 winter campaigns, the APCA on the 1989 data set gave rise to four components, which were identified as a general pollution component, crustal dust, sea-salt, and a halogen (Br,I) component. It appeared that the pollution component was largely responsible for the observed levels of the elements V, Mn, Ni, Zn, As, Mo, In and Sb. And as in the 4-winter data set, the pollution component was predominantly associated with air masses that originated in the Asian part of the former Soviet Union. The CMB fit indicated that on the average 70% of the concentration of the 8 tracer elements was attributed to Asian source regions (CUSSR) versus 30% to European sources (EURAVE). As to the source regions for particulate fine sulfur, the MLR analysis apportioned this sulfur for 66% to EURAVE and for 34% to CUSSR. This 66/34 ratio is in very good agreement with the 63/37 ratio observed in the 4-winter data set.

INTRODUCTION

The study of the aerosol composition of the Arctic atmosphere, the quantification of the manmade and natural contribution to the concentration of the various aerosol constituents, and the assessment of the possible alterations in the Arctic aerosol burden, composition and sources over the years are essential components of the study of regional and global change in atmospheric chemistry.

In this paper we present the results from a 4-month aerosol sampling campaign in the winter of 1989 at Ny Ålesund, Spitsbergen. The aerosol samples were analyzed for up to 42 elements, and the data set was examined by various receptor modeling techniques. The results were related to the origin of the air mass, as deduced from 850 mb air mass back trajectories. Furthermore, the atmospheric aerosol data and receptor modeling results from the 1989 winter campaign were compared with similar results obtained in winter sampling campaigns of 1983, 1984, 1986, and 1987.

EXPERIMENTAL AND METHODS

Sampling and analysis

The aerosol collections were carried out at the Norwegian Institute for Air Research (NILU) NILU II sampling station (at sea level) in Ny Ålesund (78°55' N, 11°57' E), Spitsbergen. The airborne particles were collected on a 400 cm^2 Whatman 41 filter, using an

in-line high-volume sampler, which was equipped with a pre-impaction stage (50% equivalent aerodynamic cut-off diameter (EAD): 2.5 μm) to discriminate against large particles. The flow rate through the sampler was about 1 m^3 min^{-1}. A total of 109 aerosol filter samples were collected from January 1 until April 30, 1989 (No samples were taken from March 21 until March 29). Virtually all samples were daily samples, and the filters were typically changed at 8 a.m. universal time.

The samples were analyzed at Gent for up to 42 elements by instrumental neutron activation analysis (INAA) and particle-induced X-ray emission analysis (PIXE). Details on the analytical procedures used were given by Maenhaut et al. (1989).

Receptor models

Three different types of receptor models were applied, i.e., absolute principal component analysis (APCA), chemical mass balance (CMB) and multiple linear regression (MLR). The APCA model used has been described in detail by Maenhaut and Cafmeyer (1987). In the CMB analysis use was made of Rahn and Lowenthal's 8-element tracer system with noncrustal V, noncrustal Mn, Zn, As, Se, In, Sb and Pb (Rahn and Lowenthal, 1984, 1985; Lowenthal and Rahn, 1985) in order to apportion the tracers to Eurasian source regions. We essentially followed the same CMB approach as described by Lowenthal and Rahn (1985) and Lowenthal et al. (1987). The MLR was carried out to apportion sulfur among the regional signatures (Rahn and Lowenthal, 1984, 1985; Lowenthal and Rahn, 1985). This was done by regressing the sulfur concentration in the series of 109 samples against the regional coefficients in these samples.

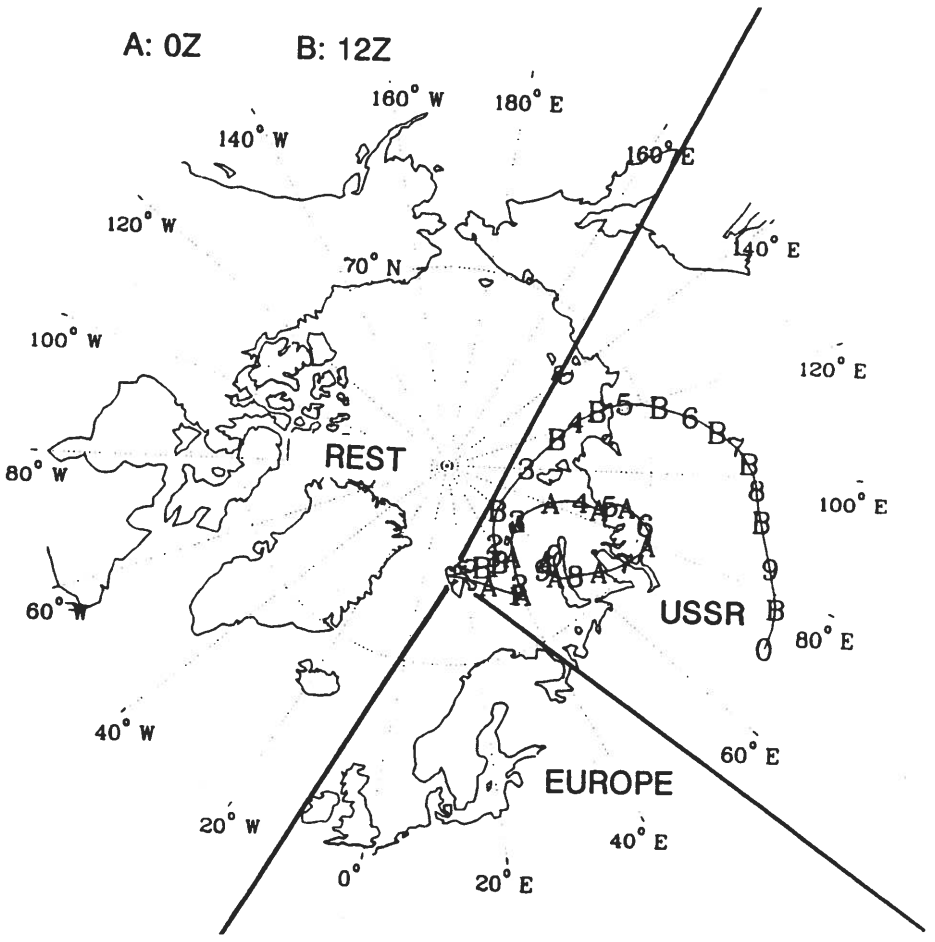

Fig. 1. Sectors used to classify the Ny Ålesund 850 mb 10-day back trajectories, with examples of such trajectories.

Air mass back trajectories

850 mb 10-day back trajectories were calculated with the GMCC trajectory program (Harris, 1982) for 0Z and 12Z of each day of the 4-month sampling campaign. These trajectories were used to classify the samples into one of the 3 sectors shown in Fig. 1, i.e., Europe (this sector includes the European part of the former USSR), the Asian part of the former USSR, and a so-called rest sector. However, when the trajectories for a sample covered more than one sector, this sample was left unclassified. The back trajectories were also used to determine NS and EW wind directional data for each sample, so that the origin of the air mass could be entered as two numerical data for each sample in the APCA calculation. The approach followed to obtain such NS and EW data was described by Tuncel et al. (1985). We determined the values of the NS and EW data from the intersection of the air mass back trajectories with a 2000-km radius circle around Ny Ålesund.

ATMOSPHERIC CONCENTRATIONS, TIME TRENDS, AND COMPARISON WITH DATA FROM PREVIOUS WINTER CAMPAIGNS

The temporal variability of selected elements over the 1989 winter sampling campaign is shown in Fig. 2. The time trend for Na illustrates the variability in the sea-salt component of the aerosol. Al, Sc and Fe are marker elements for soil dust. V, Zn, As and Sb are used to indicate the variation in the pollution component, and, finally, S and Se are elements which are of anthropogenic origin in winter, but not necessarily in summer (Maenhaut et al., 1989). It is evident from Fig. 2 that S and Se are well correlated with each other and that they exhibit less variability than the other elements. The trend for Na is clearly quite different from those of the other elements, and, in general, the Na levels tend to be high when the levels of the crustal and pollutant elements are low. All these observations are qualitatively identical to those for our four previous winter sampling campaigns, i.e., of 1983, 1984, 1986, and 1987 (Maenhaut et al., 1989; Cornille, 1991).

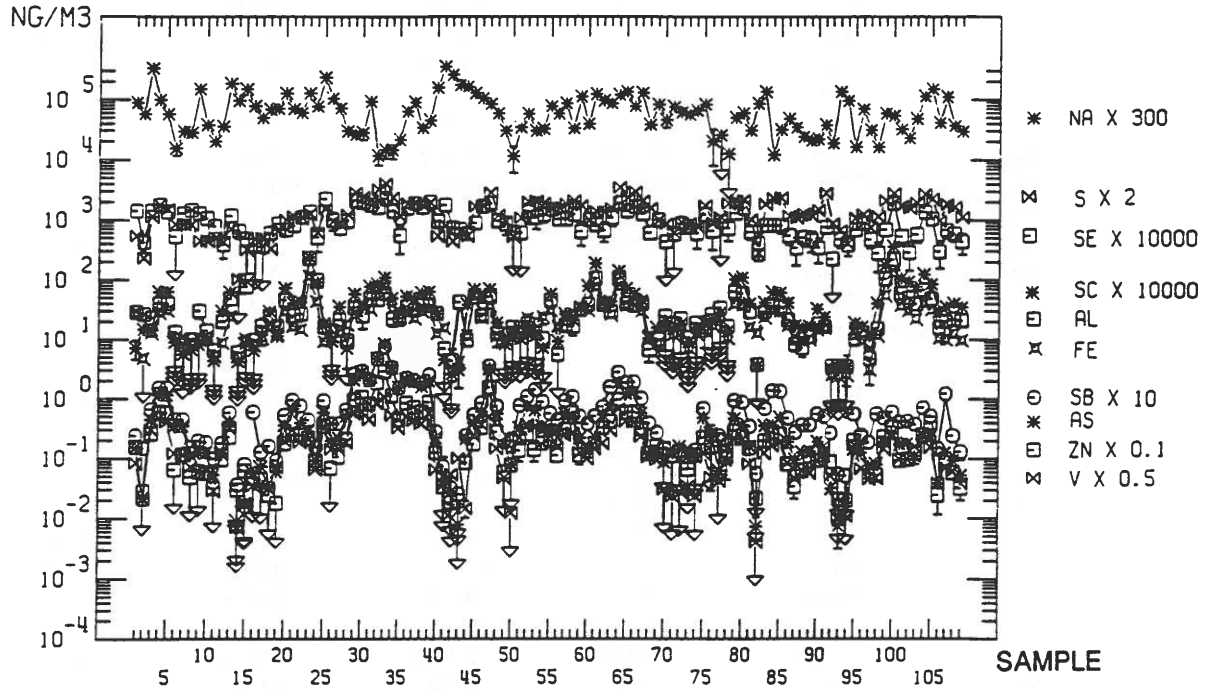

Fig. 2. Temporal variability of selected elements over the Ny Ålesund 1989 winter sampling campaign. Error bars indicate the analytical standard deviation, including the contribution from blank correction. Upper limit values are indicated by arrows.

Table 1 presents the median atmospheric concentrations (in ng/m^3) for 42 elements in the Ny Ålesund 1989 winter campaign. The table also gives, for comparison, the median values in the winter campaigns of 1983, 1984, 1986, and 1987 (Maenhaut et al., 1989; Cornille, 1991). The median values in the 1989 campaign are generally of the same order as those in the previous winter campaigns, but for the anthropogenic element group they are clearly systematically lower.

Table 1. Median atmospheric concentrations (in ng/m^3) for Ny Ålesund 1989 winter (this work) and comparison with medians from four previous winter campaigns (Maenhaut et al., 1989; Cornille, 1991). All data pertain to the <2.5 μm aerosol size fraction.

Elem.	1983	1984	1986	1987	1989
Sea-salt elements (including halogens)					
Na	210	310	192	210	197
Mg	66	55	30	42	40
Cl	85	105	30	49	140
K	44	26	28	39	21
Ca	41	15	36	45	32
Br	8.0	7.1	11.6	4.0	5.9
Sr	<1	<1.0	<1.4	<0.9	<1.4
I	1.41	0.75	0.92	0.53	0.56
Sulfur and selenium					
S	1480	570	990	740	620
Se	0.20	0.146	0.155	0.24	0.083
Crustal elements					
Al	43	28	49	44	22
Si	220	96	<200	134	190
P	<14	<14	<18	<9	<19
Sc	0.0059	0.0034	0.0049	0.0061	0.0029
Ti	2.2	1.0	<1.5	1.82	2.0
Fe	41	13.4	16.7	31	15.5
Co	0.031	0.0084	<0.007	0.024	0.0102
Ga	<0.2	<0.2	0.073	<0.11	<0.06
Rb	0.170	<0.15	0.119	0.115	<0.15
Cs	0.0164	0.0063	0.0085	0.0102	0.0070
Ba	1.12	<2	0.80	0.98	0.80
La	0.030	0.0129	0.0177	0.021	0.0109
Ce	<0.03	<0.05	<0.06	<0.06	<0.08
Sm	0.0030	0.0024	0.0028	0.0054	0.0040
Eu	0.00096	<0.002	0.0021	0.00123	<0.0012
Lu	<0.003	<0.003	<0.0014	<0.0006	<0.0014
Th	0.0057	0.0024	0.0056	0.0054	0.0030
Anthropogenic elements					
V	1.99	0.42	0.47	0.75	0.25
Cr	0.94	<0.5	<0.3	0.56	0.60
Mn	2.2	0.51	0.78	0.91	0.51
Ni	0.95	0.38	<0.3	0.48	0.110
Cu	<1.5	<0.9	<0.7	<1.3	<1.2
Zn	9.6	2.3	4.0	6.5	1.36
As	1.49	0.32	0.52	0.78	0.22
Mo	<0.6	<0.15	<0.05	0.045	0.030
Ag	0.0178	<0.02	0.0097	0.0091	<0.015
Cd	0.126	<0.3	<0.15	<0.10	<0.11
In	0.0048	0.00154	0.00132	0.00191	<0.002
Sb	0.22	0.048	0.108	0.125	0.048
W	<0.08	<0.050	0.0154	0.024	<0.03
Au	<0.009	<0.0008	0.00044	<0.0002	<0.0003
Pb	8.2	1.76	2.6	4.4	<3.0

Table 2. Principal component analysis of the Ny Ålesund 1989 winter data set with 97 samples and 26 elements. VARIMAX rotated loadings, communalities, standard deviations of the loadings (s_b) and the variance explained by each component after rotation.

Elem.	Rotated loadings[a] Comp.1 Pollut.	Comp.2 Crust	Comp.3 Sea-salt	Comp.4 Halogen	Comm.	s_b
Na	(-0.10)	(-0.02)	0.94	(-0.09)	0.90	0.033
Mg	(0.05)	0.12	0.93	0.12	0.90	0.033
Al	0.13	0.95	0.09	(-0.05)	0.93	0.028
Si	0.20	0.82	(0.06)	(-0.03)	0.71	0.055
S	0.73	0.31	(-0.15)	0.42	0.83	0.043
Cl	(-0.10)	(-0.17)	0.90	(-0.18)	0.89	0.035
K	0.37	0.64	0.55	0.22	0.90	0.034
Ca	(0.02)	0.56	0.66	(0.09)	0.76	0.051
Sc	0.19	0.96	(-0.02)	0.09	0.96	0.020
V	0.96	0.12	(0.00)	(-0.02)	0.93	0.026
Mn	0.85	0.46	(-0.04)	(0.06)	0.94	0.024
Fe	0.43	0.86	(0.00)	(0.03)	0.93	0.028
Co	0.66	0.68	(0.00)	0.10	0.91	0.031
Ni	0.89	0.30	(-0.01)	(0.03)	0.88	0.037
Zn	0.97	0.08	(-0.07)	(-0.00)	0.96	0.022
As	0.96	(0.01)	(-0.09)	(-0.06)	0.94	0.026
Se	0.75	0.20	0.29	(0.02)	0.69	0.058
Br	(-0.04)	(-0.03)	0.20	0.83	0.73	0.054
Mo	0.82	0.24	(0.00)	(-0.08)	0.74	0.053
In	0.94	(0.00)	0.10	(-0.08)	0.90	0.033
Sb	0.98	(0.04)	(-0.11)	0.06	0.97	0.018
I	(0.04)	(0.10)	(-0.28)	0.80	0.73	0.054
Cs	0.69	0.61	(-0.05)	(0.11)	0.85	0.040
La	0.12	0.97	(0.02)	0.08	0.97	0.018
Sm	(0.06)	0.94	(0.04)	(0.01)	0.89	0.035
Th	0.08	0.97	(-0.01)	(0.01)	0.95	0.022
Var.	9.3	8.1	3.6	1.7		
NS[b]	0.50	(0.23)	(-0.19)	(-0.08)	0.35	0.084
EW	(0.25)	0.31	(-0.11)	(-0.12)	0.18	0.094

[a]Loadings that are less than 3 standard deviations are placed in parentheses.
[b]The loadings for NS and EW were obtained from the PCA with the wind directional data included.

ABSOLUTE PRINCIPAL COMPONENT ANALYSIS (APCA)

The first part of the APCA procedure (i.e., the PCA and VARIMAX rotation of the principal component loading matrix) was carried out on both a data set with the NS and EW wind directional data excluded and one with those directional data included. Otherwise, the two data sets were identical and comprised the concentrations of 26 elements in 97 samples. Selection of the elements and exclusion of certain samples was done on the basis of criteria described by Maenhaut et al. (1989) and Maenhaut and Cafmeyer (1987). The first seven eigenvalues of the correlation matrix for the data set with the wind directional data excluded were 12.6, 5.2, 3.3, 1.58, 0.59, 0.55 and 0.35. As only the first 4 eigenvalues are greater than 1, four components were retained and subjected to VARIMAX rotation. The rotated loadings are presented in Table 2, together with the communalities, the standard deviations of the loadings for each element (s_b, calculated according to Heidam, 1982) and the variance ex-

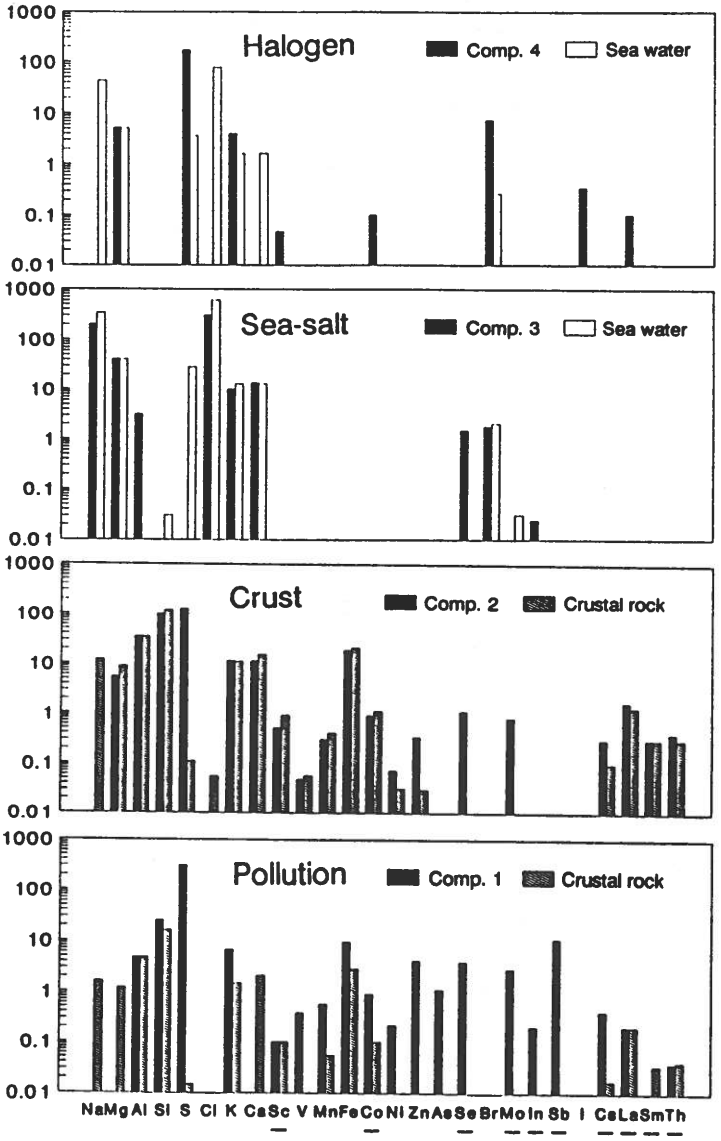

Fig. 3. Source profiles (in relative concentration units) for the Ny Ålesund 1989 winter aerosol, as obtained by APCA. The source profiles are compared with the average crustal rock composition of Mason (1966) and with the sea water composition of Riley and Chester (1971). Al and Mg were used as normalizing elements in the profile comparisons. For the underlined elements the relative concentration was multiplied by 100.

plained by each component after rotation. The PCA on the data set with the NS and EW wind directional data included resulted in very similar VARIMAX rotated loadings for the various elements as those listed in Table 2. The last two rows in Table 2 present the rotated loadings for the NS and EW variables for that data set with the wind directional data inserted.

The rotated loadings of Table 2 were converted into source profiles with the elemental concentrations in relative concentration units (see Fig. 3). Relative elemental concentrations that are less than three times their associated standard deviation are not retained in Fig. 3. The interpretation of the four components in terms of physical aerosol sources is rather straightforward. The first component has high loadings for the elements S, V, Mn, Ni, Zn, As, Se, Mo, In, Sb and Cs, and is clearly a pollution component. Considering the variety of elements that are loaded on this pollution component, it must represent a mixture of

combustion processes, industrial emissions (including smelters) and other anthropogenic activities. A further differentiation of this pollution component was not possible by APCA, even not when the number of retained components was increased. Component 2 exhibits high loadings for the typical crustal elements (Al, Si, Sc, Fe, La, Sm, and Th). The median crustal enrichment factors (EFs), relative to Al and the average crustal rock composition of Mason (1966), in the collected aerosol are 1.3 for Si, 0.6 for Sc, 1.2 for Fe, 1.5 for La, 1.4 for Sm, and 1.8 for Th. Furthermore, Fig. 3 indicates that the crustal EFs for Mg, Si, K, Ca, Sc, V, Mn, Fe, Co, La, Sm and Th in component 2 are close to 1. This component can thus unambiguously be identified as crustal material. The third component exhibits a composition that is similar to that of the bulk sea water composition of Riley and Chester (1971), at least for the typical sea-salt elements Na, Mg, Cl, K, Ca and Br, thus indicating that this component is essentially sea-salt. The fourth and last component has high loadings for only two elements (i.e., Br and I). Most likely, this component is also a marine component, but unrelated to sea-salt. It almost certainly includes the non-sea-salt bromine that has been observed in the Arctic by various investigators at polar sunrise (e.g., Berg et al., 1982; Barrie et al., 1988; Sturges and Barrie, 1988). This fourth component will be termed an "halogen component".

The loadings of the two wind directional variables (NS and EW) on the four components of Table 2 are rather low. Moreover, only a small fraction of the variance of these two variables is explained by the 4-component model. In order to obtain high communalities for the NS and EW variables six components had to be retained. However, the two additional components in the 6-component model appeared to be nearly unique vectors, i.e., one for NS (Se had a loading of 0.32 on this component) and one for EW. This all seems to indicate that the four components of Table 2 and Fig. 3 are not associated with a well-defined direction of air mass origin. Nevertheless, the fact that the pollution component exhibits a moderate loading for NS (and a weak loading for EW) suggests that this component is mainly advected with northerly to northeasterly air masses, which most likely originated in the Asian part of the former USSR (as shown for the 12Z trajectory of Fig. 1). Similarly, the loadings of EW and NS on the crustal component point to an eastern (northeastern) soil dust source origin, which may also be inside the former USSR and/or in Mongolia and China.

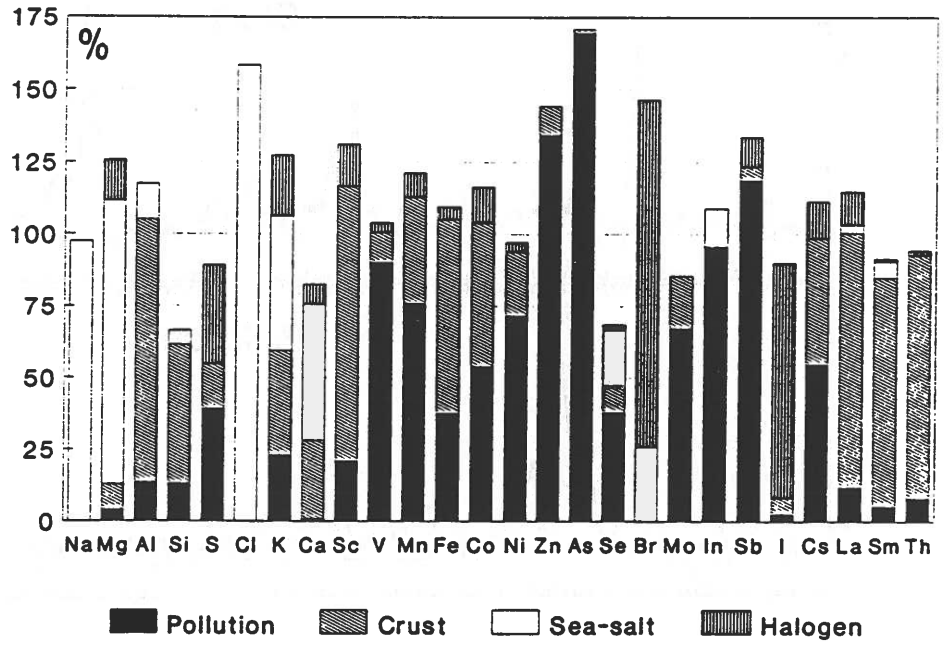

Fig. 4. Average contributions from the 4 sources to the atmospheric concentrations of the elements in the Ny Ålesund 1989 winter samples. The source contributions are expressed as percentages of the average observed atmospheric concentrations. Contributions are not shown when the VARIMAX rotated loading of the element in the component was less than 3 standard deviations.

The average apportionments for the 26 elements in the Ny Ålesund 1989 winter aerosol are presented in Fig. 4. The contributions of the four components are for each element expressed as percentages of the mean observed concentration. The pollution component dominates for V, Mn, Ni, Zn, As, Mo, In and Sb. The typical soil dust elements Al, Si, Sc, La, Sm and Th are mainly attributed to the crustal component. The sea-salt component is essentially the only one which contributes to the Na, Mg, and Cl levels. In addition, it provides the largest contribution to the K and Ca levels. The halogen component dominates for only two elements (Br and I), but is also responsible for a sizable fraction of the S.

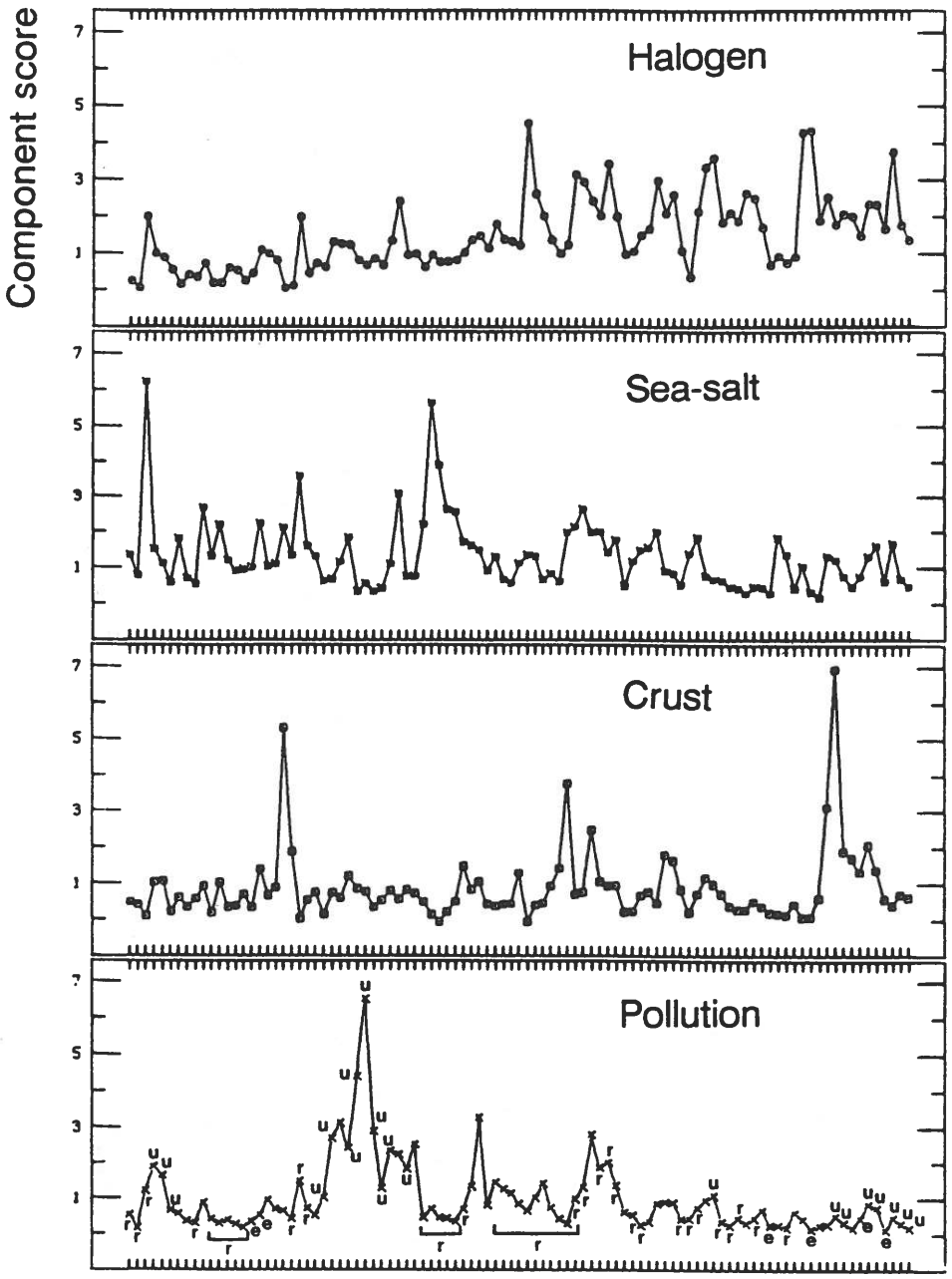

Fig. 5. Absolute principal component scores of the 4 components in each of the 97 samples of the data set subjected to APCA. The score plot for component 1 also denotes the sector in which the sample was classified (e: Europe, u: Asian part of former USSR, r: rest sector, see Fig. 1); unclassified samples are left unmarked.

Fig. 5 displays the absolute principal component scores for the 4 components in each of the 97 samples included in the APCA. These scores provide an indication of the strength of each component in each sample. The score plot for the pollution component also denotes the sector in which the sample was classified (e: Europe, u: Asian part of former USSR, r: rest sector, see Fig. 1); unclassified samples are left unmarked. It is evident that high scores for this component are related to air masses that originated from the Asian part of the former USSR. This observation is entirely consistent with what was suggested above on the basis of the NS and EW wind directional variable loadings on the pollution component.

CHEMICAL MASS BALANCE (CMB) FOR SOURCE REGION APPORTIONMENT

In the CMB regional source apportionment for the elements of Rahn and Lowenthal's 8-element tracer system we used the same two regional signatures as in the final apportionment of Maenhaut et al. (1989). These signatures were a combined western/eastern European signature (EURAVE) and a signature for the central former USSR (CUSSR). The relative concentrations of the 8 tracer elements in these two signatures are found in Table 10 of Maenhaut et al. (1989).

The CMB apportionment was done for each of the 109 samples of the campaign. The average regional apportionments are presented in Table 3. The last column of Table 3 gives the ratio of the mean predicted to the mean observed concentration for each element. These ratios indicate how well the average elemental concentrations are modeled. The mean predicted to observed concentration ratio and associated standard deviation, as obtained by averaging over all samples, are given in the last but one column of Table 3. These data provide an indication of the quality of the CMB apportionment for each element in the individual samples.

Table 3 shows that the apportionment to the CUSSR signature dominates for each of the elements. It varies from 56% for noncrustal Mn up to 89% for In. When averaging over all 8 elements, 71% of the mean predicted concentration is attributed to CUSSR, versus only 29% to EURAVE. This 30/70 ratio for EURAVE/CUSSR is similar to that for the Ny Ålesund winter campaigns of 1983 and 1984 (Cornille, 1991). However, in 1986 winter a 50/50 ratio was observed, and in 1987 winter a 70/30 ratio (Cornille, 1991).

Table 3. Average regional apportionments for the tracer elements in the Ny Ålesund 1989 winter aerosol.

Elem.	Apportionment, percent of mean predicted concentration		Mean (predicted/ observed conc.)	Mean predicted/ mean observed concentration
	EURAVE	CUSSR		
As	18	82	1.19±0.30	1.02
Sb	31	69	0.99±1.08	0.87
Se	30	70	0.65±0.56	0.76
VX[a]	30	70	1.50±0.99	1.37
Zn	31	69	1.27±0.40	1.17
MnX[a]	44	56	1.56±1.92	1.11
In	11	89	0.87±0.32	1.06
Pb	33	67	1.04±0.28	1.02
Average	29	71		

[a]VX and MnX indicate noncrustal V and noncrustal Mn, respectively.

The last two columns of Table 3 show that the elemental concentrations of the various elements are rather well modeled by our CMB fit. Se is clearly underpredicted, though. Furthermore, the average predicted to observed concentration ratios for noncrustal V and noncrustal Mn are about 50% higher than 1, and, in addition, they have large associated standard deviations. The poorer results for noncrustal V and noncrustal Mn are to a large extent caused by applying a correction for the crustal contribution. This correction was often fairly significant (particularly for Mn), so that the noncrustal concentration was very low or even sometimes negative. The underprediction of Se is harder to explain. During summer, a very significant fraction of the Se at Ny Ålesund is most likely from marine biogenic origin (Maenhaut et al., 1989), but it is doubtful that this is also so during winter. Perhaps, the Se concentration in the EURAVE and/or CUSSR signatures needs to be revised.

REGIONAL APPORTIONMENT FOR SULFUR

The S/Na ratio in our Ny Ålesund 1989 winter samples is almost two orders of magnitude larger than that in sea water. Consequently, the particulate sulfur cannot be attributed to sea-salt, but has to be of secondary origin (i.e., the product of oxidation reactions and of gas-to-particle conversion). During winter, virtually all non-sea-salt sulfur is present in the form of sulfate and undoubtedly results from the oxidation of anthropogenic SO_2. That the sulfur is indeed pollution-derived is confirmed by the fact that it is very highly loaded on the same PCA component as the other typical anthropogenic elements. Furthermore, the correlation coefficient between S and the elements V, Mn, Zn, As and Sb was on the average 0.75.

We apportioned the sulfur among the EURAVE and CUSSR source regions by resorting to the MLR approach of Rahn and Lowenthal (Rahn and Lowenthal, 1984, 1985; Lowenthal and Rahn, 1985). It turned out that the aerosol sulfur was on the average for 66% attributed to EURAVE and for the remaining 34% to CUSSR. This 66/34 ratio for EURAVE/CUSSR is in very good agreement with the results from a similar apportionment for the combined Ny Ålesund data set of the 1983, 1984, 1986, and 1987 winter campaigns (Cornille, 1991). For this 4-winter data set a 63/37 ratio was observed for EURAVE/CUSSR. The quality of the MLR analysis was assessed by calculating the ratio of the modeled to the observed S concentration for each of the 106 samples that were included in the MLR. The average ratio and associated standard deviation were 1.15 ± 0.65 (N=106), thus indicating that the model reproduced the experimental data reasonably well.

Acknowledgments - W.M. and G.D. acknowledge support from the Belgian "Nationaal Fonds voor Wetenschappelijk Onderzoek", the "Interuniversitair Instituut voor Kernwetenschappen", the "Instituut tot Aanmoediging van het Wetenschappelijk Onderzoek in Nijverheid en Landbouw", and the Impulse Programme "Global Change" supported by the Belgian State - Prime Minister's Service - Science Policy Office. The authors are very much indebted to Dr. J.M. Harris (NOAA/GMCC, Boulder, Colorado) for her calculations of the air mass trajectories. Thanks are also due to J. Cafmeyer for technical assistance.

REFERENCES

Barrie L.A., Bottenheim J.W., Schnell R.C., Crutzen P.J. and Rasmussen R.A. (1988) Ozone destruction and photochemical reactions at polar sunrise in the lower Arctic atmosphere. *Nature* **334**, 138-141.

Berg W.W., Sperry P., Rahn K.A. and Gladney E.S. (1983) Atmospheric bromine in the Arctic. *J. geophys. Res.* **88**, 6719-6736.

Cornille P. (1991) *Chemische karakterisering en brononderzoek van het atmosferisch aerosol.* Ph. D. thesis, University of Gent.

Harris J.M. (1982) *The GMCC atmospheric trajectory program.* NOAA Technical Memorandum ERL ARL-116, Air Resources Laboratories, Rockville, Maryland, November 1982.

Heidam N.Z. (1982) Atmospheric aerosol factor models, mass and missing data. *Atmos. Environ.* **16**, 1923-1931.

Lowenthal D.H. and Rahn K.A. (1985) Regional sources of pollution aerosol at Barrow, Alaska during winter 1979-80 as deduced from elemental tracers. *Atmos. Environ.* **19**, 2011-2024.

Lowenthal D.H., Hanumara R.C., Rahn K.A. and Currie L.A. (1987) Effects of systematic error, estimates and uncertainties in chemical mass balance apportionments: Quail Roost II revisited. *Atmos. Environ.* **21**, 501-510.

Maenhaut W. and Cafmeyer J. (1987) Particle induced X-ray emission analysis and multivariate techniques: An application to the study of the sources of respirable atmospheric particles in Gent, Belgium. *J. Trace Microprobe Techn.* **5**, 135-158.

Maenhaut W., Cornille P., Pacyna J.M. and Vitols V. (1989) Trace element composition and origin of the atmospheric aerosol in the Norwegian Arctic. *Atmos. Environ.* **23**, 2551-2569.

Mason B. (1966) *Principles of Geochemistry,* 3rd Edn. Wiley, New York.

Rahn K.A. and Lowenthal D.H. (1984) Elemental tracers of distant regional pollution aerosols. *Science* **223**, 132-139.

Rahn K.A. and Lowenthal D.H. (1985) Pollution aerosol in the Northeast: Northeastern-Midwestern contributions. *Science* **228**, 275-284.

Riley J.P. and Chester R. (1971) *Introduction to Marine Chemistry,* Academic, New York.

Sturges W.T. and Barrie L.A. (1988) Chlorine, bromine and iodine in Arctic aerosols. *Atmos. Environ.* **22**, 1179-1194.

Tuncel S.G., Olmez I., Parrington J.R., Gordon G.E. and Stevens R.K. (1985) Composition of fine particle regional sulfate component in Shenandoah Valley. *Environ. Sci. Technol.* **19**, 529-537.

Fifth International Symposium on Arctic Air Chemistry
September 8-10, 1992

A RECEPTOR MODEL APPLIED TO AEROSOL DATA FROM NORTHEASTERN GREENLAND

Peter Wåhlin
National Environmental Research Institute
Division of Emissions and Air Pollution
Frederiksborgvej 399, DK-4000 Roskilde, Denmark.

Introduction

The physical receptor model described by Wåhlin (1992) has been applied to aerosol data from Station Nord in Northeastern Greenland (fig. 1) with the purpose of testing its ability to give a useful description of source profiles and source strengths. Actually, the physical receptor model was developed with the object of obtaining a better description of those data than could be obtained with ordinary factor analysis.

In the model,

$$x_{ij} \equiv \sum_k a_{ik} f_{kj} \ , \qquad (1)$$

x_{ij} are the measured chemical variables in a series of samples. Index i refers to the chemical variables, index j refers to the samples. The source profiles a_{ik} are constants representing the relative chemical composition of the sources, and f_{kj} are the source strengths found in the samples. Index k refers to the sources.

The physical receptor model uses an iterative method in which the total chi-square,

$$\chi^2 = \sum_j \sum_i \frac{(x_{ij} - \sum_k a_{ik} f_{kj})^2}{\sigma_{ij}^2}, \qquad (2)$$

is minimized within the limits imposed by constraints. In (2) σ_{ij} denotes the uncertainties. Built-in model constraints exclude non-physical solutions (negative components in the source profiles and negative source strengths), and additional constraints can, by means of a form matrix, be included to fix profile component ratios, partly or entirely. An initial profile matrix is set up in which the source vectors are chosen freely.

Methods and results

Samples were collected at a site 2 km north of Station Nord as small spots on one single grease-coated impaction foil and one single 0.4 μm Nuclepore filter on a weekly basis from August 1990 to April 1991 with an automatic two-stage discrete streaker designed for PIXE analysis (Kemp and Wåhlin, 1992). The 35 coarse fraction samples (aerodynamic cut-off diameter $\cong$ 2.0 μm) and 35 fine fraction samples were analyzed for elemental contents by PIXE, and weekly mean concentrations were calculated using measured air volumes. Background corrections were performed using measured values on non-exposed areas on the impaction foil and the filter. Twenty elements (Si, S, Cl, K, Ca, Ti, V, Cr, Mn, Fe, Ni, Cu, Zn, As, Se, Br, Rb, Sr, Zr, and Pb) were detected with uncertainties down to 5%. Some elements in some samples were below detection limits, and background corrections produced some negative concentrations, but no special handling of this was needed in the fitting process thanks to the consistent use of absolute uncertainties.

The weekly mean concentrations were fitted with an initial profile matrix (table 1) containing four source vectors : A soil profile, a sea salt profile, a general anthropogenic profile (in this paper called the urban profile), and an additional anthropogenic profile containing only Cu and Ni (in this paper called the metal profile). As soil and sea profiles were used the proportion by weight in ppm of the elements occurring in igneous rocks of the continents and the average composition of sea water in ppm, both quoted by Kaye and Laby (1959). In the soil column of the corresponding form matrix (table 2) Ti was defined as soil tracer by fixing the mass ratios of the essential non-crustal elements S, Cl, Cr, Ni, Cu, Zn, As, Se, Br, and Pb to this crustal element, while the ratios of the remaining crustal elements K, Ca, V, Mn, Fe, Rb, Sr, and Zr were allowed to vary freely. The elements S, Cl, and Br could not be satisfactorily fitted into the four-vector space, and they were excluded by introducing infinite uncertainties in the data matrix (table 3). With S, Cl, and Br missing only K, Ca, and Sr were left as important sea source markers, and therefore the sea profile was fixed by a null sea column in the form matrix to preserve the initial average sea water composition. Pb was used as tracer in the urban profile with fixed initial ratios of S, Cl, Br, and Cu to Pb. Because S, Cl, and Br were of no importance in the fitting process, the mass ratios of these elements were arbitrarily fixed to values to be discussed later in this paper. The mass ratio of Cu to Pb was fixed after some attempts at a value that assigned maximum contributions of Cu and Ni to the urban source and minimum contributions to the metal source. A slightly better fit could have been achieved if Cu was allowed to be totally assigned to the metal source, but incidents of high metal source strengths were easier to discriminate with minimum contributions. The other elements in the urban profile were allowed to vary freely with over-estimated initial values of the crustal elements.

The resulting profile matrices were calculated independently for the fine and the coarse samples and are summarized in Table 4. The goodness of the single element fits and the total fit are expressed by the reduced chi-square values in table 5. Also summarized in table 5 are the results of a multiple linear regression analysis performed on the residuals suggesting a weak fine fraction V/Ni source. The residual profiles have been normalized to unity source strength variance. It can be seen that the fits are very good, which indicates a remarkable constancy of the anthropogenic profiles during the period. The coarse fraction fit (reduced chi-square, $\chi^2/\nu = 1.27$) is so close that the deviations can be explained by the statistics alone. The fine fraction fit is slightly more deviant ($\chi^2/\nu = 1.87$) mostly due to the correlated divergences of V and Ni.

The resulting profile matrix elements were normalized to arithmetic mean concentrations and could be used to calculate the coarse mass fraction for each variable/source combination (fig. 2). It can be seen clearly from the figure that aerosol particles from the soil source have the coarsest size distribution, while the long-range urban and metal aerosol particles have the finest size distribution (see also fig. 8). Although profile element uncertainties are not estimated in the model, it is also evident that the crustal chemical elements in the urban part of the aerosol (Si, Ca, Ti, Fe) are displaced towards coarser particle sizes, but not so far as they are in the soil part of the aerosol.

The source strength time series are plotted in figs. 3 – 7. As far as can be deduced from the fine and the coarse soil signals the soil aerosol seems to have a rather constant size distribution in the period. The strengths decrease in the winter to almost zero, which is natural because of the snow cover. The sea aerosol size distribution is much more varying, and the signals do not show a clear seasonal tendency. The urban and the metal signals seem to have nearly constant size distibutions, and they both show the typical winter appearance of the long range anthropogenic pollution in the Arctic (arctic haze). The rapid variation of the metal source strength signals suggests that Cu and Ni are emitted from a strong point source positioned in a larger urban source area. The "ravines" between the peaks in the urban signal also appear in the metal signal but not in the sea signal, so they probably reflect injections of non-polluted air from south. The fine residual source strength signal shows an overall change indicating a small enhancement of the V/Ni content in the fine urban source profile during the winter.

The fitted concentrations are obtained from the calculated source profiles and source strengths. I fig. 8 this is done for Si and the result is plotted together with the measurements. As can be seen from the chi-square values in tabel 5 the goodness of the silicon fits is representative of all the fitted variables apart from fine fraction V and Ni, which, as recognized by the analysis on the residuals, both display a distinct growth during the winter compared with the fits (fig. 9).

The misfits Sulphur, Chlorine and Bromine

It was a necessity to exclude S, Cl, and Br from the analysis to get good fits, but calculated concentrations of these elements could be obtained by giving them reasonable values in the source profiles. The average composition of sea water was used throughout as the sea source profile, and the contributions from the sea source to S, Cl, and Br were on this basis obtained as a direct result of the calculations. The mass ratios of S to Pb in the urban profiles were arbitrarily fixed by inspection of the plots to values that looked reasonable (fig. 10), when it was taken into account that a large fraction of total sulphur was in a gaseous state in midwinter. Simultaneous, but two days displaced, filter-pack measurements of sulphur dioxide and sulphate at Station Nord demonstrate this, and the total-sulphur plot (fig. 11) of the filter-pack measurements has indeed some resemblance to the "fits" in fig. 10, but a still unexplained occurrence of sulphur, especially in the coarse fraction, in August and September might be of marine biogenic origin. The chemical elements Cl and Br were modeled with zero contributions from the anthropogenic sources, but even in this case, regarding sea salt as the only important source, the calculated values were generally too large (fig. 12 and fig. 13). In many samples, especially in the fine fraction samples, Cl was totally absent, so it may be assumed that it was lost from the filter by the reaction between chloride and sulphuric acid (and, probably, ammonium hydrogen sulphate):

$$H_2SO_4 + 2Cl^- \rightarrow SO_4^{2-} + 2HCl(g) \ ,$$
$$NH_4HSO_4 + 2Cl^- \rightarrow SO_4^{2-} + NH_3(g) + 2HCl(g) \ .$$

This hypothesis is supported by fig. 14, in which measured and calculated Cl concentrations (in nmol/m^3) are compared with the concentration of S multiplied by 2. The stoichiometrical correspondence between S and missing Cl is good, especially on the filter stage. Br may be lost by similar reactions, and it was confirmed that Br to some extent disappeared during the PIXE analysis itself. The blank correction was obtained by PIXE analysis of five consecutive spots on the non-exposed parts of the Nuclepore filter and the impaction foil, and it was hereby shown that the Br content in the Nuclepore filter material was rather high (0.016+/-0.001 μg/cm^2). The PIXE values of Br on the exposed part of the filter were in the range 0.010 – 0.053 μg/cm^2, indicating by comparison with the blank values that Br was much more unevenly distributed on the blank filter than recognized by the blank values alone, and the discrepancy between the measured and calculated fine fraction concentrations of Br seems to some extent to be a consequence of that.

Conclusion

It is clear from the chi-square values that good fits could be obtained for most chemical elements when the physical receptor model was applied. A soil source profile, a sea source profile, and an urban source profile were upon the whole sufficient for the description. Episodes of enhanced Cu/Ni contents could be described by an additional metal source profile, and a slow increase in the fine fraction V/Ni content during the winter was described by a residual profile.

The elements S, Cl, and Br presented a singular behaviour and could not be fitted, but it was possible by application of the model to calculate expected S, Cl, and Br concentrations. In this way the model could give input to a discussion about the reasons for the deviant behaviour.

References

Wåhlin P. (1992) A multivariate receptor model with a physical approach. *Proceedings of 5th International Symposium on Arctic Air Chemistry.*

Kemp.K. and Wåhlin P. (1992) Aerosol sampler for all-year sampling at remote sites. *Proceedings of 5th International Symposium on Arctic Air Chemistry.*

Kaye G.W.C and Laby T.H. (1959) Abundances of the elements. *Physical and chemical constants*, pp. 108-110. Longmans, London.

Table 1. Initial profile matrix used in fitting the fine and coarse fraction samples. Figures in brackets are deviant coarse fraction values.

	Soil	Sea	Urban	Metal
Si	277200	0.02	20	0
S	520	884	400 (190)	0
Cl	480	18980	0	0
K	25900	380	7	0
Ca	36300	400	3	0
Ti	4400	0	0.3	0
V	300	0.0003	0.4	0
Cr	100	0	0	0
Mn	1000	0.001	0.4	0
Fe	50000	0.002	6	0
Ni	64	0.0001	0	1
Cu	70	0.001	0.11 (0.12)	1
Zn	80	0.005	0	0
As	5	0.01	0	0
Se	0.09	0.004	0	0
Br	2.5	65	0	0
Rb	310	0.2	0.04	0
Sr	150	13	0	0
Zr	220	0	0.01	0
Pb	16	0.004	1	0

Table 2. Form matrix used to define constraints in fitting the fine and coarse fraction samples. The zeros in a column freeze the corresponding ratios in the profile matrix.

	Soil	Sea	Urban	Metal
Si	1	0	1	0
S	0	0	0	0
Cl	0	0	0	0
K	1	0	1	0
Ca	1	0	1	0
Ti	0	0	1	0
V	1	0	1	0
Cr	0	0	1	0
Mn	1	0	1	0
Fe	1	0	1	0
Ni	0	0	1	1
Cu	0	0	0	1
Zn	0	0	1	0
As	0	0	1	0
Se	0	0	1	0
Br	0	0	0	0
Rb	1	0	1	0
Sr	1	0	1	0
Zr	1	0	1	0
Pb	0	0	0	0

Table 3. Part of fine fraction data matrix. Figures in ng/m^3. Negative uncertainties are interpreted as infinite. The original uncertainties of S, Cl, and Br have been replaced by negative numbers in order to exclude the measurements from the fitting process.

Date	Si	σ(Si)	S	σ(S)	Cl	σ(Cl)	K	σ(K)	etc...
22-8-90	11.6	0.869	36.16	-1	2.685	-1	2.496	0.175	
29-8-90	257.7	13.26	32.37	-1	17.48	-1	31.25	1.605	
5-9-90	143.8	7.469	34.34	-1	26.78	-1	18.95	1.022	
12-9-90	20.15	1.236	82.84	-1	18.29	-1	4.975	0.314	
19-9-90	33.85	2.002	135.6	-1	6.817	-1	5.655	0.355	
26-9-90	24.94	1.507	42.24	-1	63.53	-1	6.618	0.408	
3-10-90	13.58	0.912	30.83	-1	14.49	-1	3.443	0.192	
10-10-90	17.51	1.109	46.45	-1	21.28	-1	6.365	0.395	
17-10-90	25.15	1.52	67.66	-1	11.85	-1	7.009	0.427	
2-1-91	20.89	1.318	270.4	-1	-1.12	-1	10.46	0.584	
9-1-91	40.01	2.425	516.7	-1	-2.23	-1	16.84	0.953	
etc...									

Table 4. Resulting profile matrices normalized to arithmetic mean concentrations (in ng/m^3) in the sampling period.

	Fine fraction				Coarse fraction			
	Soil	Sea	Urban	Metal	Soil	Sea	Urban	Metal
Si	20.6746	0.000281	10.9338	0	20.9741	0.00026	4.0912	0
S	0.05075	12.4188	497.814	0	0.07458	11.6312	88.3206	0
Cl	0.04684	266.638	0	0	0.06884	249.729	0	0
K	2.49422	5.33838	5.46904	0	3.25616	4.99985	1.60903	0
Ca	4.65952	5.61935	2.27365	0	5.66968	5.263	1.51443	0
Ti	0.42942	0	0.15977	0	0.63108	0	0.13024	0
V	0.02022	4.21E-06	0.25924	0	0.03739	3.95E-06	0.03830	0
Cr	0.00976	0	0.13182	0	0.01434	0	0.07166	0
Mn	0.06759	1.40E-05	0.2669	0	0.09365	1.32E-05	0.12250	0
Fe	5.56765	2.81E-05	4.33886	0	7.23842	2.63E-05	2.76546	0
Ni	0.00625	1.40E-06	0.12042	0.03092	0.00917	1.32E-06	0.03474	0.01397
Cu	0.00683	1.40E-05	0.13689	0.11869	0.01004	1.32E-05	0.05578	0.08248
Zn	0.00780	7.02E-05	1.63484	0	0.01147	6.58E-05	0.62891	0
As	0.00048	0.00014	0.14297	0	0.00071	0.00013	0.08143	0
Se	8.78E-06	5.62E-05	0.02538	0	1.29E-05	5.26E-05	0.01016	0
Br	0.00024	0.913144	0	0	0.00035	0.85523	0	0
Rb	0.01491	0.00281	0.02522	0	0.02225	0.00263	0.01648	0
Sr	0.01299	0.182629	0.03061	0	0.02992	0.17104	0.03284	0
Zr	0.01997	0	0.00644	0	0.03011	0	0.00832	0
Pb	0.00156	5.62E-05	1.24454	0	0.00229	5.26E-05	0.46484	0

Table 5. Chi-square and degrees of freedom. Results of "one-factor" analysis on the residuals are expressed as source profiles in ng/m^3 normalized to unity source strengths variance.

	Fine fraction			Coarse fraction		
	Residue profile	χ^2	ν	Residue profile	χ^2	ν
Si	-2.81E-05	56		1.37E-05	39	
S	0	0		0	0	
Cl	0	0		0	0	
K	-0.00022	67		-0.00032	32	
Ca	4.34E-05	34		0.000139	19	
Ti	0.003484	63		0.013545	95	
V	0.041391	183		0.003371	9	
Cr	0.001156	46		-0.01903	33	
Mn	-0.00993	70		-0.02683	68	
Fe	-0.00016	24		-0.00068	44	
Ni	0.026623	140		-0.01314	61	
Cu	-0.01394	28		-0.0959	54	
Zn	-0.00343	60		-0.00232	13	
As	0.004625	57		0.0844	29	
Se	0.00835	42		0.051044	35	
Br	0	0		0	0	
Rb	0.001166	26		-0.00918	75	
Sr	0.005191	46		0.005232	37	
Zr	-0.00086	10		0.004851	11	
Pb	-0.00275	71		-0.01221	48	
Total		1022	545		701	552

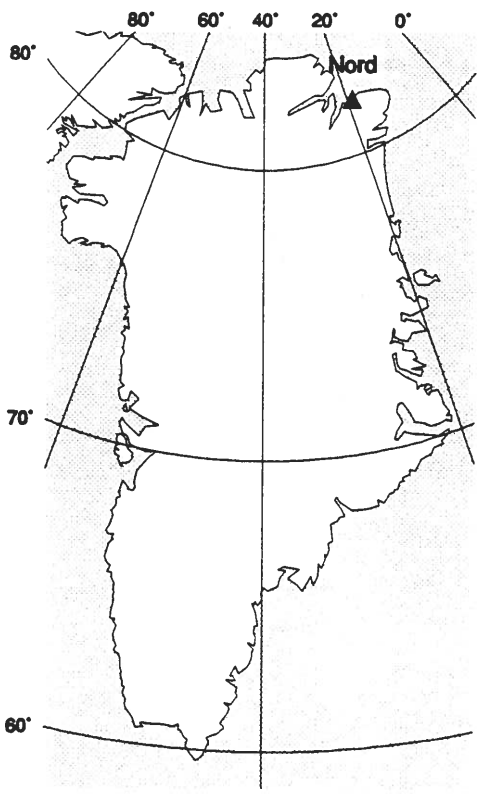

Fig. 1. The position of Station Nord in Greenland.

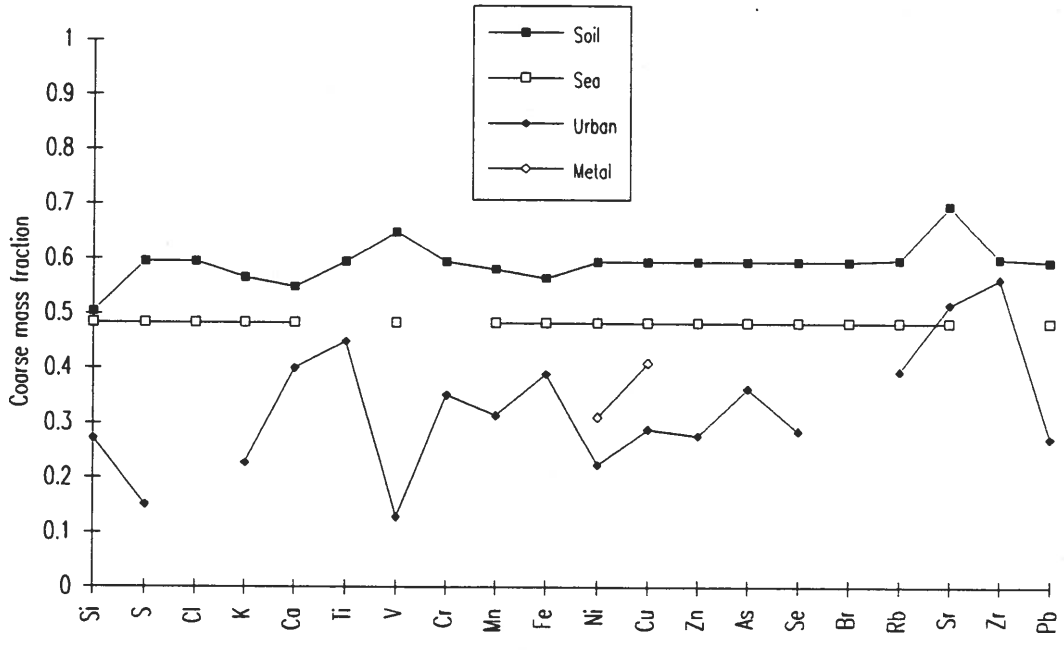

Fig. 2. Result of model calculations: Fractions of mass collected in the coarse fraction samples.

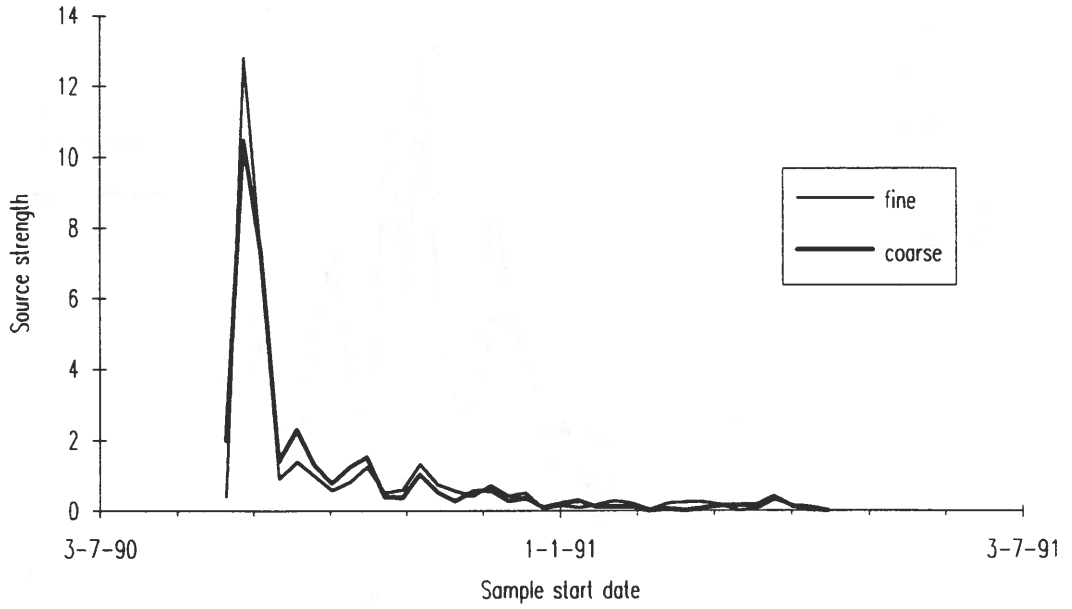

Fig. 3. Soil source strength signals at Station Nord.

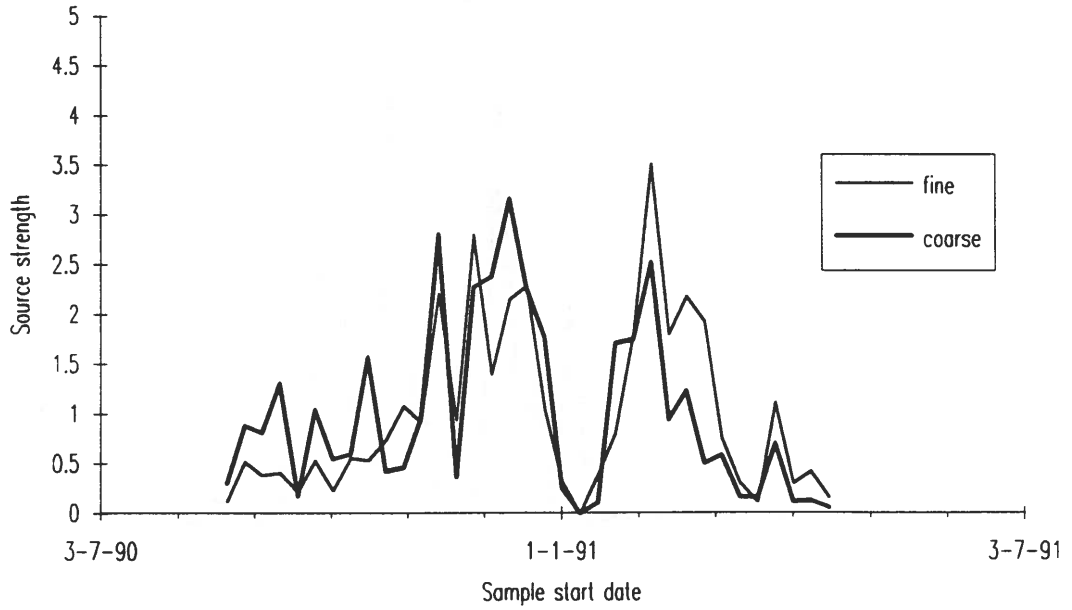

Fig. 4. Sea source strength signals at Station Nord.

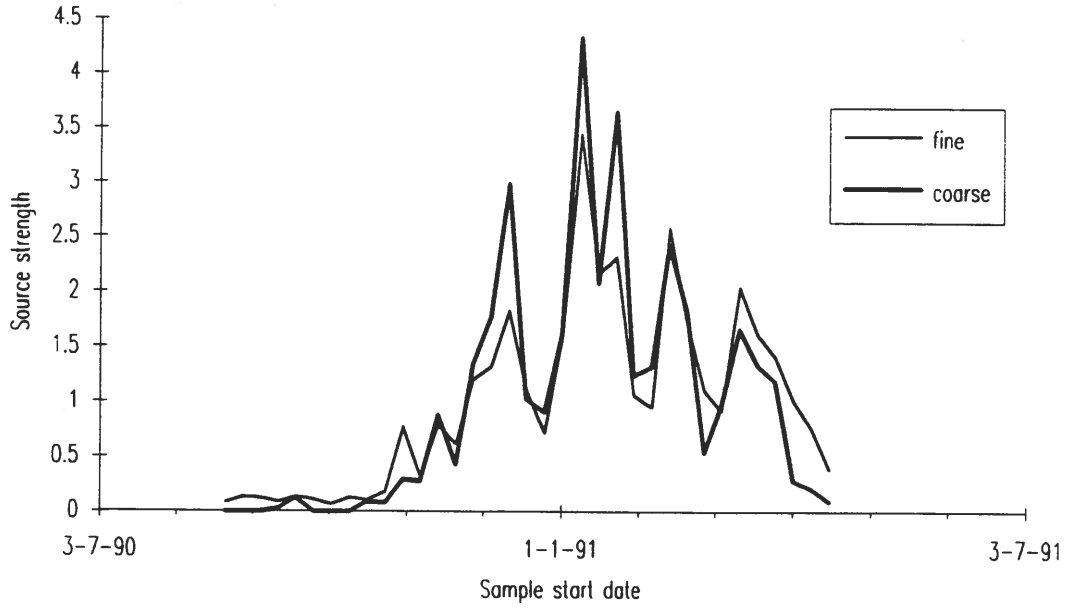

Fig. 5. Urban source strength signals at Station Nord.

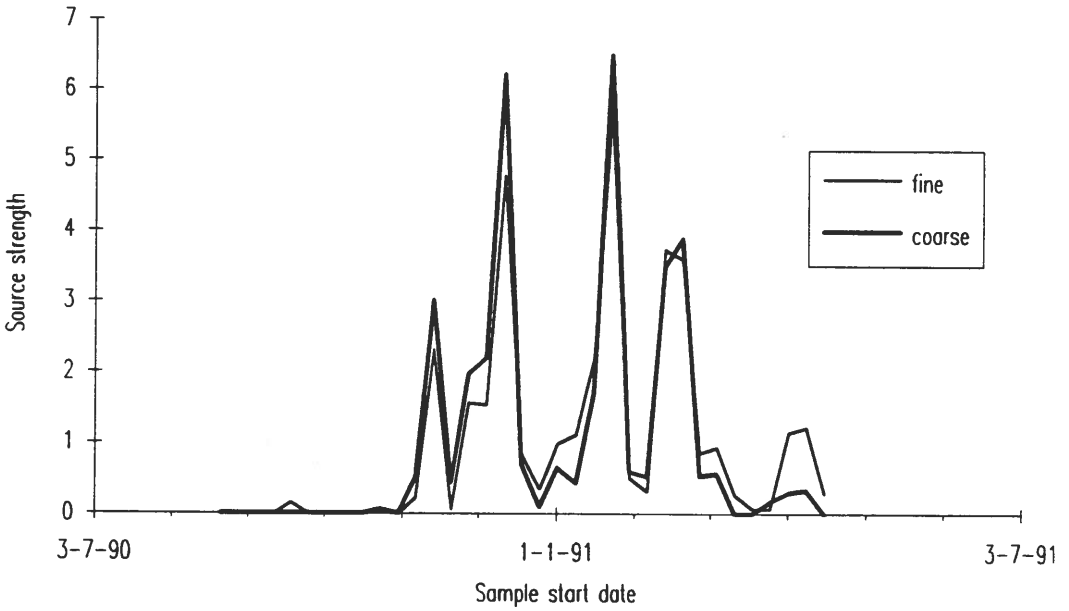

Fig. 6. Metal source strength signals at Station Nord.

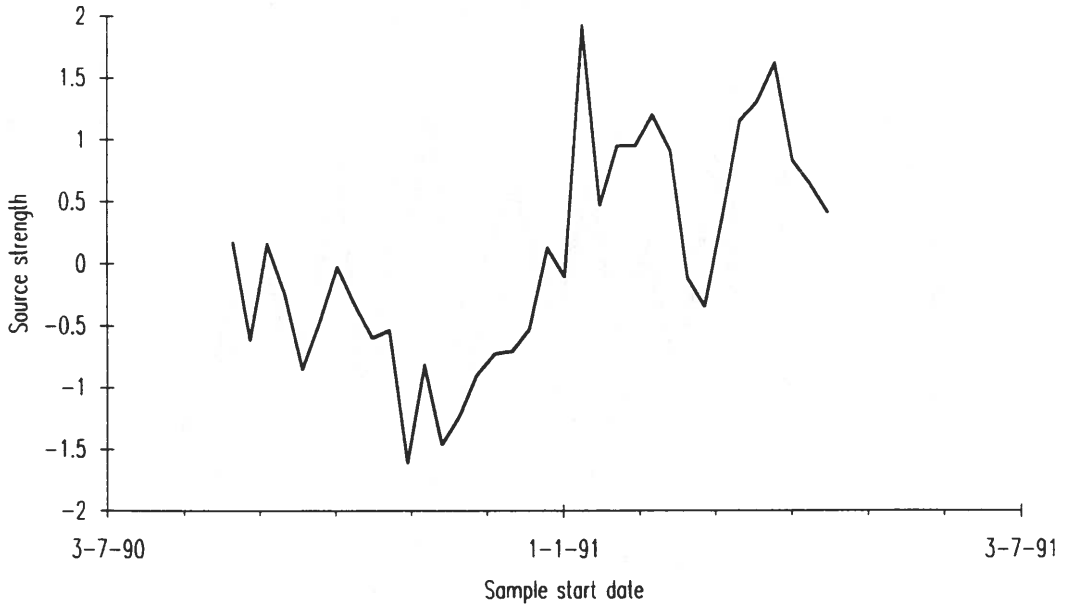

Fig. 7. Fine residual source strength signal at Station Nord.

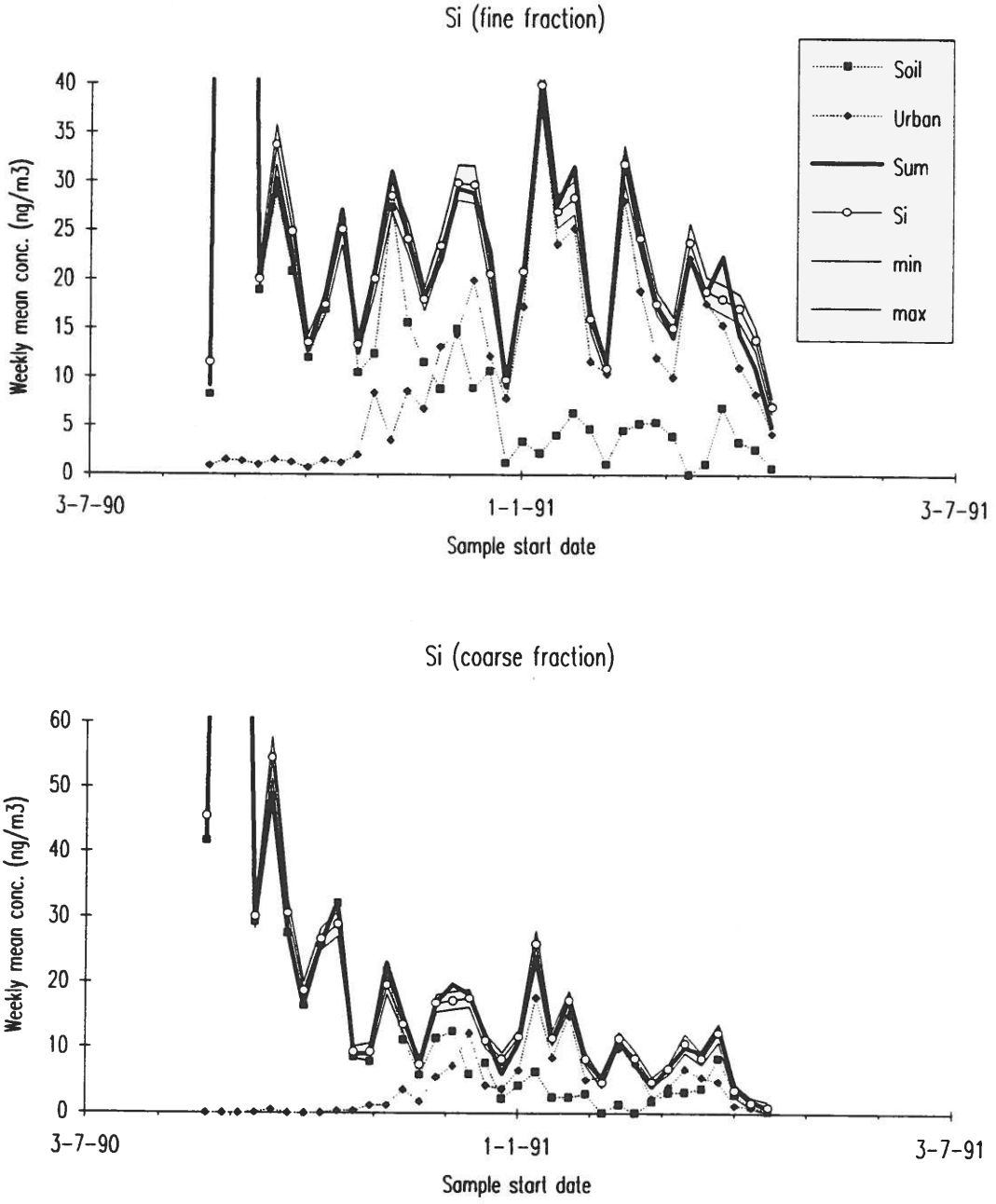

Fig. 8. Fine and coarse fraction fits for silicon. The smaller size of the long range transported aerosol particles compared with the soil aerosol particles appears clearly. Min and max indicate the analytical uncertainty interval.

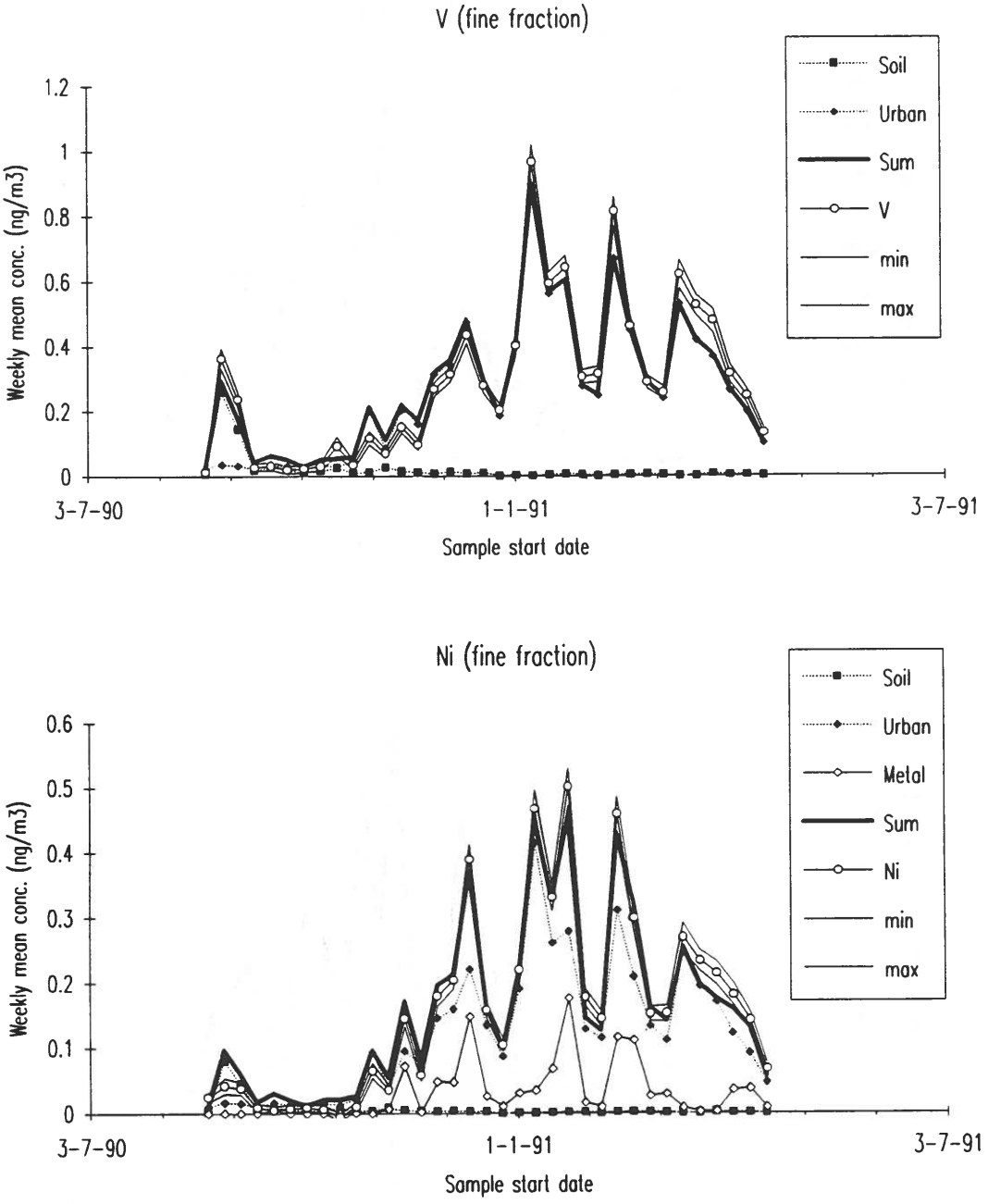

Fig. 9. Poor fine fraction fits for vanadium and nickel.

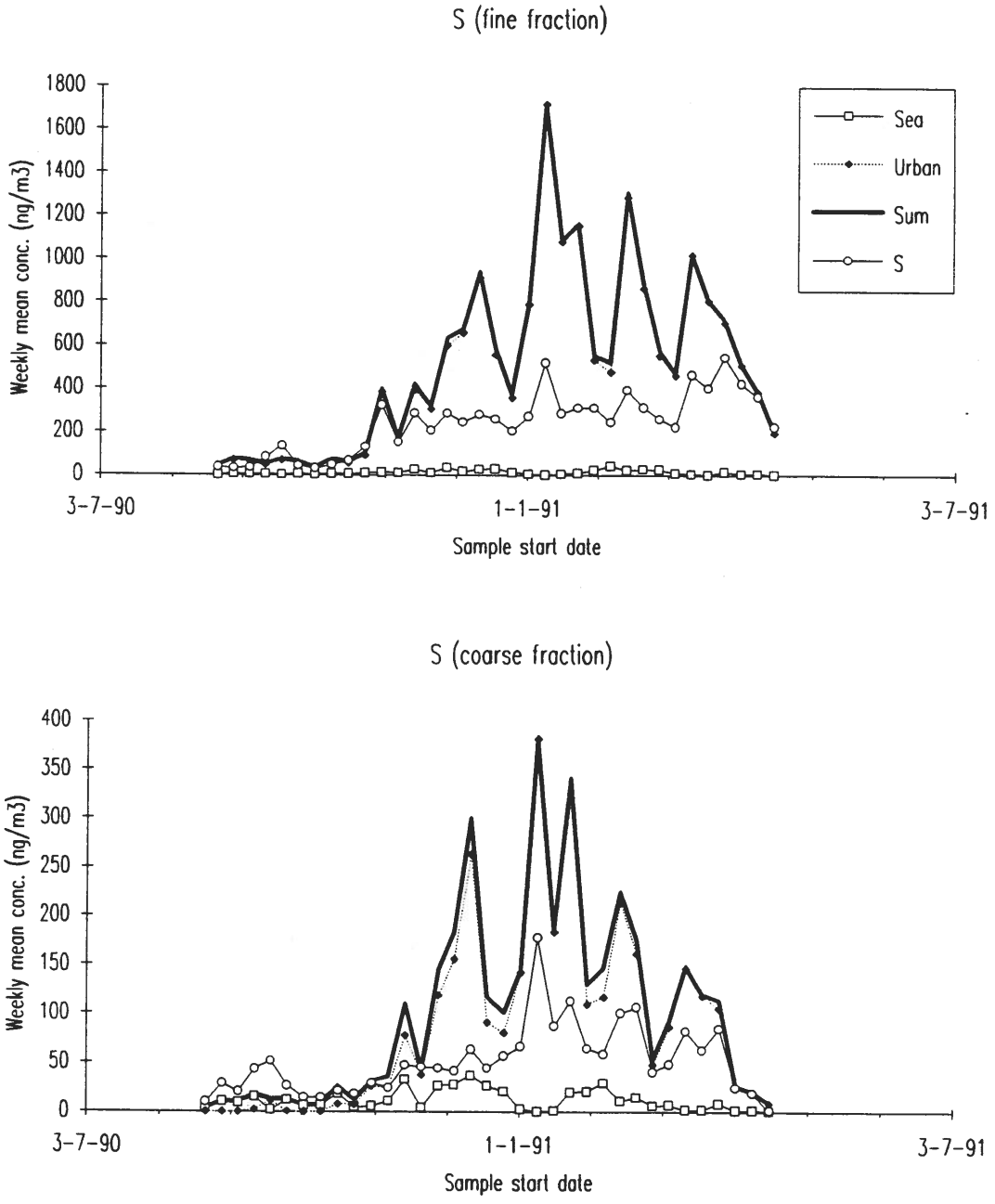

Fig. 10. Sulphur fitted by eye using the average composition of sea water and an arbitrary S-component in the urban source profile.

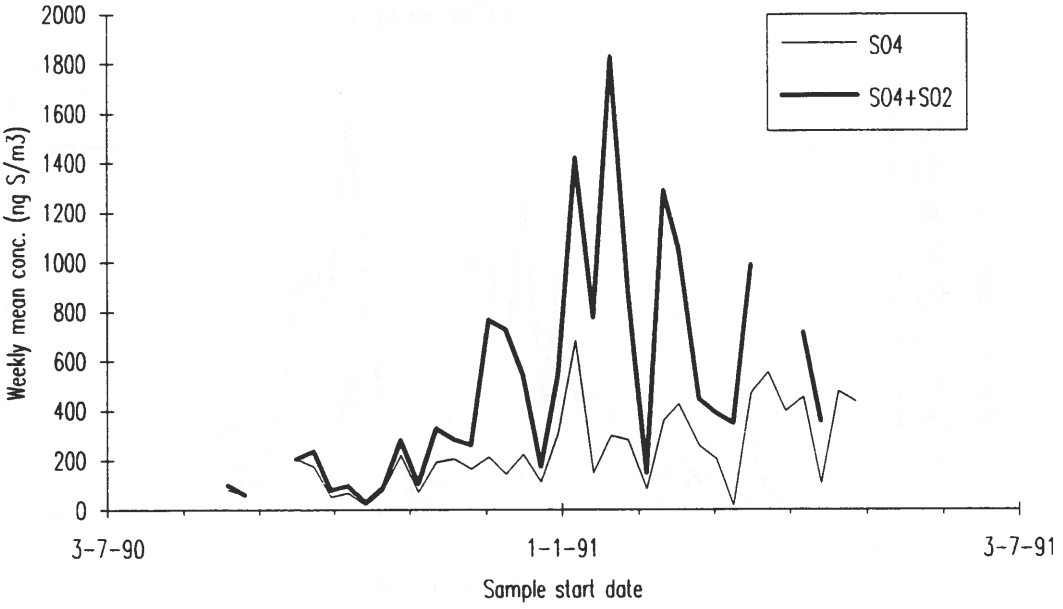

Fig. 11. Filter-pack measurements of SO_2 and SO_4^{2-} at Station Nord. The plots represent the mass of S in SO_4^{2-} and SO_2 + SO_4^{2-}.

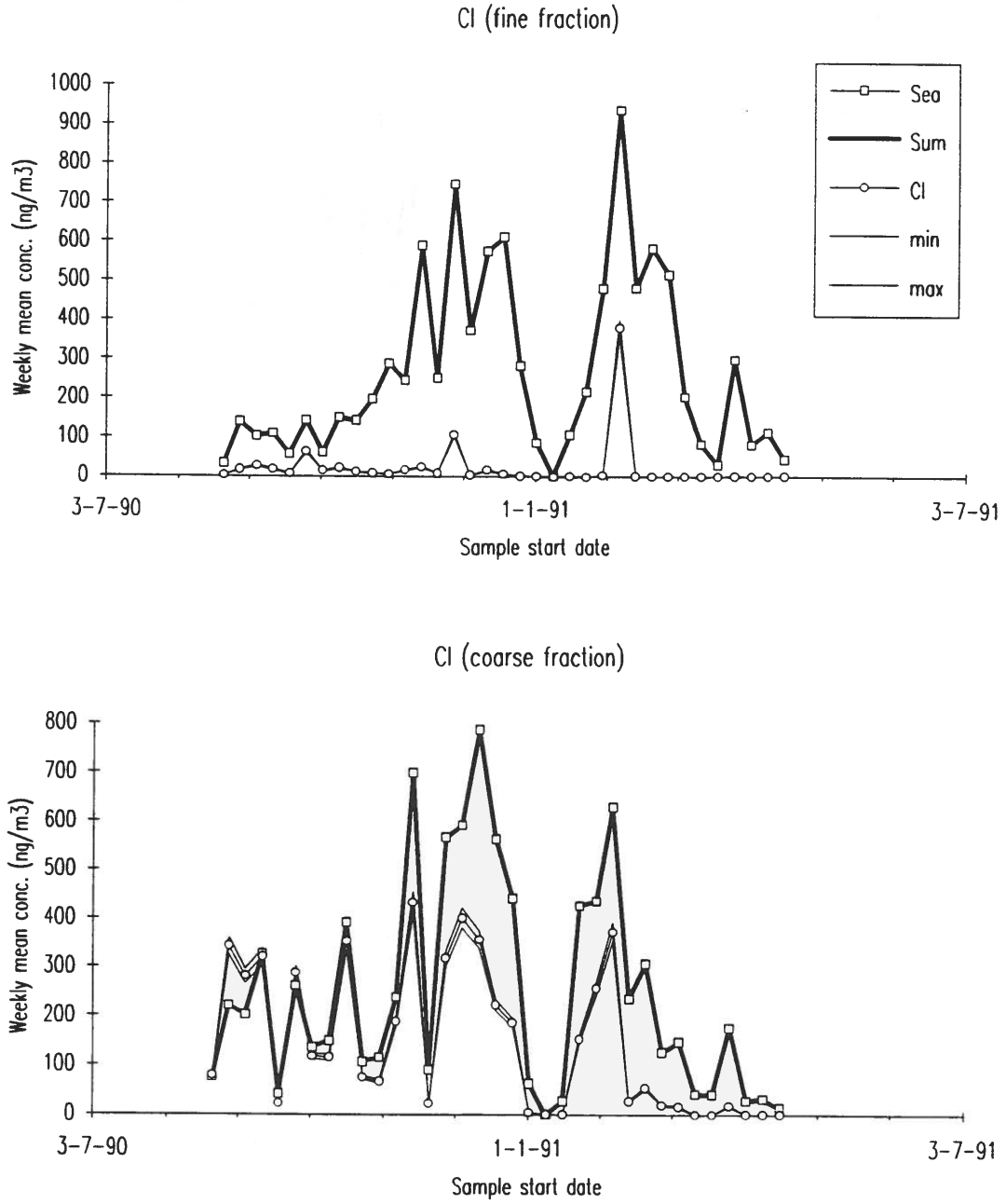

Fig. 12. Fine and coarse fraction measurements of chlorine concentrations compared with model calculations.

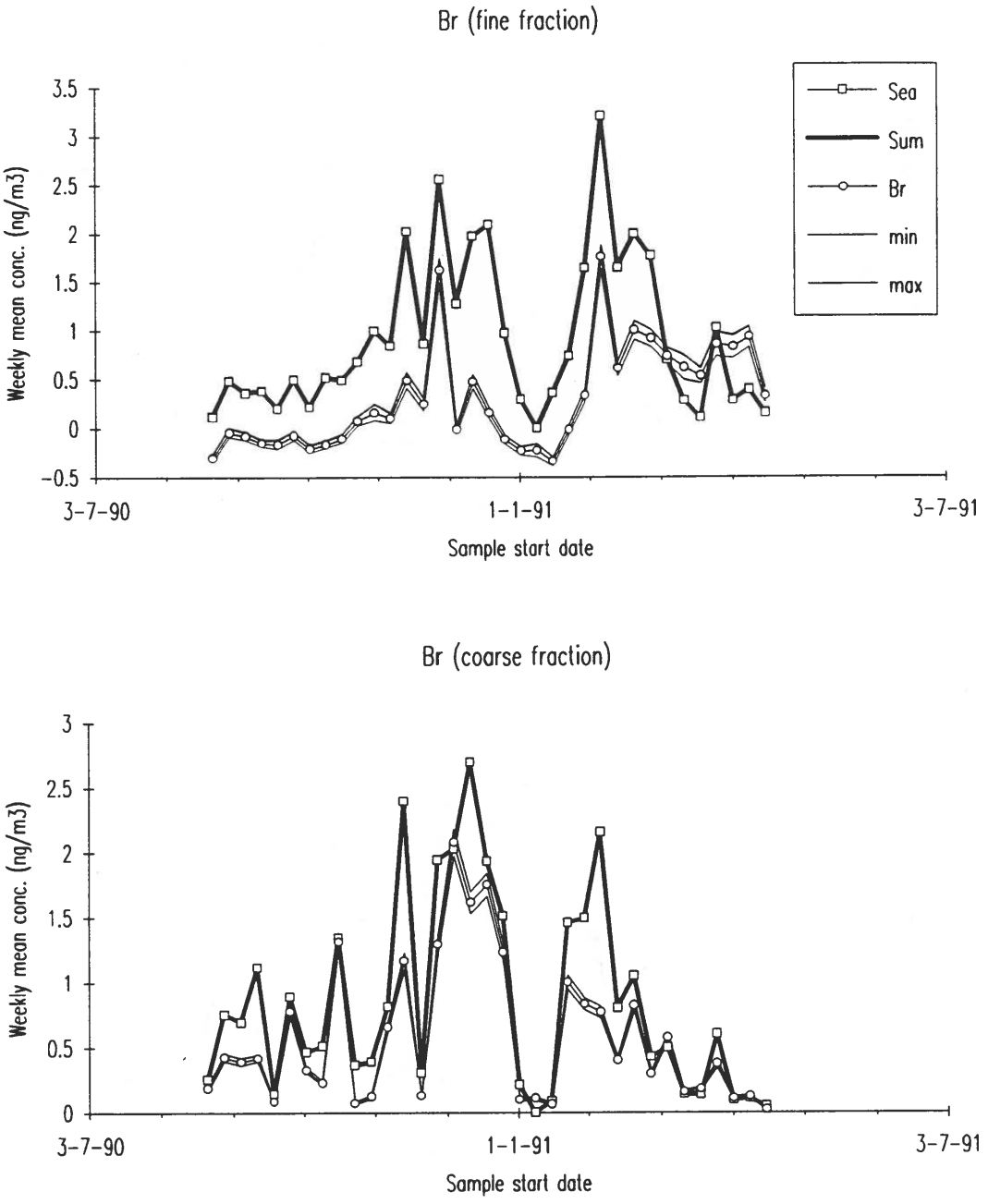

Fig. 13. Fine and coarse fraction measurements of bromine concentrations compared with model calculations.

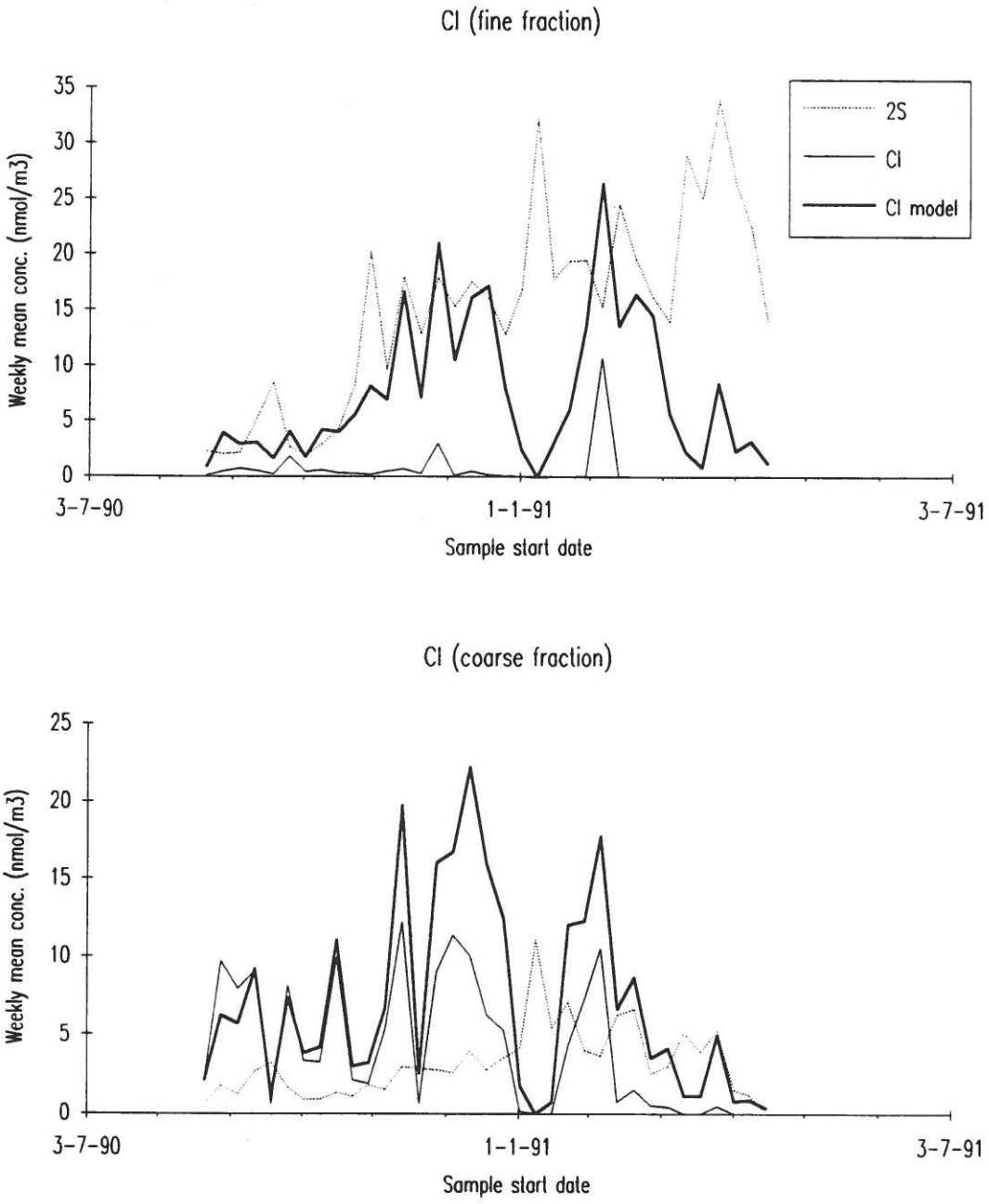

Fig. 14. The measured and calculated chlorine concentrations (in nmol/m^3) compared with the concentration of sulphur multiplied by 2.

Session 7

Model Applications II

Chairman:
P.K. Hopke

NATIONAL ENVIRONMENTAL RESEARCH INSTITUTE
Division of Emissions and Air Pollution
Roskilde, DENMARK

25.08.1992

Fifth International Symposium on Arctic Air Chemistry

Rarely Occuring Elements in the Arctic Aerosol

Niels Z. Heidam
National Environmental Research Institute
Frederiksborgvej 399
DK 4000 Roskilde
Danmark

Abstract

Aerosol samples collected in Northeast Greenland in the period 1979-1983 were analyzed by PIXE and found to contain a large number of elements. The more abundant elements were subjected to factor analysis. This modelling of the data led to a description of the Arctic aerosol as composed of a small number of source-related components of both natural and antropogenic origin in remote midlatitude regions.

Unfortunately a fairly large number of elements detected infrequently by PIXE had to be ignored in these studies which do not handle missing values well. In this investigation these rarely occurring elements are studied in the context of the source-related components in order to elucidate their origin. Results of correlation analyses between the elements and the factor scores are presented. The similarity of temporal behaviours is used in a discussion of tentative source apportionments.

Keywords: aerosols, arctic haze, elements, factor analysis, Greenland

Introduction

Arctic air pollution research in Greenland has over the recent decade been focused on the tropospheric aerosols occurring in this remote region. These and other investigations have revealed that the arctic troposphere is recurrently burdened with a significant pollution load, particularly during the winter (Arctic Air Chemistry, 1977, 1981, 1985, 1989; AGASP, 1984; Arctic Air Pollution, 1986; Heidam, 1984, 1985; Ottar et al 1986).

Many of these investigations, including the Danish measurements in Greenland, have incorporated studies of the composition and seasonal variations of arctic aerosols and they have been particularly useful in increasing our understanding of the mid-latitude origin of arctic air pollution and of the meteorological conditions leading to the phenomenon of Arctic Haze which regularly afflicts the Polar region. In this context hitherto neglected results on rarely occurring elements in the Arctic aerosol are presented. The aim is to use the supplementary data on the rarely occurring elements (to be termed ROZ, where Z refers to the atomic number) to extend and generalize the previouly described results and conclusions.

Arctic Haze Aerosols

The SAGA project.

The purpose of Danish programme SAGA, Studies of Aerosols in the Greenland Atmosphere, was to determine the levels, composition and seasonal variations of Arctic aerosols in Greenland for elucidating the origins and transport routes of arctic air pollution. The SAGA-project cover the period from autumn 1979 to spring 1983 and the results considered here have been obtained from aerosol filter samples collected at the two coastal stations THUL (Qaanaaq) and NORD shown in Figure 1.

At these stations membrane filter samples representing about 200 m^3 of air were collected on a semi-weekly basis and shipped to our laboratory for elemental analysis by the PIXE-method. By this method elemental concentrations can in most cases be determined with an accuracy of 10 - 15 % and as many as 25 elements can be detected. After screening for outliers and for elements frequently below detection limits data contain concentrations for about 15 elements with about 100 annual values for 3½ years at 4 stations.

Data analysis and interpretation.

In previous reports detailed results for these more abundant elements have been presented and detailed interpretations were given in terms of source related aerosol components originating mainly in distant midlatitude source areas (Heidam, 1984, 1985).

The large amount of concentration data were subjected to Factor Analysis (Harman, 1976; Heidam, 1982, 1984). Factor Analysis is a statistical modelling technique by which a large number of intercorrelated variables are replaced or described by a much smaller set of uncorrelated fictive variables. These factors

are subsequently subjected to a stiff (varimax-) rotation which leaves the descriptive powers of the model unaffected but may render the model more easy to interprete. Due to the approximate lognormality of air pollution concentations, the logarithms of the elemental concentrations were used as input variables, standardized so as to possess zero mean and unit variance.

Examples of factor models obtained with data from 2 complete and separate years and rotated by the Varimax-criterion are shown in Tables 1 and 2. The models are valid for the concentrations at NORD and THUL, respectively.

In both cases the variations and intercorrelations of 14 - 16 variables appear to be explainable in terms of 3-4 independent factors. The composition of the various groups of elements most strongly coupled to a factor permits an interpretation of the factor as representing a source-related component of the aerosol.

Thus the model in Table 1 shows that the aerosol is composed of an Erosion component - factor 1, a Metallic component - factor 2, and a LRT_anthropogenic Combustion component - factor 3. The model explains 84 % of the system's total variance which is distributed over the factors as shown. From the column of communalities, which are the fractions of variance for each variable explained by the model, it is seen that all variables have about 70 % or more of their variance attributed to the variation of these three aerosol components. The exception is Pb for which the modelling quality is not too good as only 50 % of it's variance is accounted for.

In a similar way the aerosol measured at THUL in the last period of the SAGA project contains 4 components where the first three are the same LRT components as at NORD, Erosion, Metals, and Combustion, and the fourth is a LRT_Marine component, presumably not found at NORD because of a permanent and extensive ice cover of the ocean. This model account for 89 % of the total variance.

These models are mutually quite similar and of a high quality in terms of variance explained despite the fact that they describe aerosols separated in time by a year and in space by more than 1000 km. It can therefore be concluded that this simple source-related composition is a general characteristic of the Arctic aerosols in Greenland. Since the potential source areas are very distant and the seasonal variations of the source-related factors and of the associated aerosol concentrations are also systematically similar (Heidam, 1984, 1985) it is evident that North Greenland is exposed to a recurrent atmospheric pollution transport on a hemispheric scale.

In the original investigations (*op. cit.*) it was concluded that the crustal component was of indigeneneous origin in summer but that it was an LRT-component in winter. The marine component appeared to contain aerosols transported by both mesoscale and longrange mechanisms. The anthropogenic combustion component was allocated to extended source areas in the Euro-Asian region whereas the metallic component seemed to originate in the industrial complex in the Urals.

Rarely Detected Elements

Definition and Basic Characteristics

As a statistical technique factor analysis does not handle missing data well. In some software packages missing data cannot be tolerated at all. This can be circumvented to some extent by using the modelling capability of the technique iteratively to produce artificial input data as substitutes for missing values. Iterations are started with some guessed values and stopped when the changes are sufficiently small.

To avoid producing a self-affirming model the number of missing concentrations treated in this way should be kept at a reasonable level, say maximum 30 %. Also the criterion for terminating the iterations must not be too strict, a value of 10 % or some similar figure comparable to the analytical error can be used. The data analyzed and modelled as described have been selected according to these criteria with the result that concentration data on 14 - 16 elements could be used.

The experimental data do, however, contain a fairly large number of additional results on Rarely Occurring Elements, ROZ. The ROZ are defined instrumentally to be those elements for which concentrations are below the detection limit of the PIXE method in more than 30 % of the samples.

By this definition the ROZ studied here are listed together with some characteristics in Table 3. In general the concentrations at THUL are lower than at NORD which supports earlier conclusions that NORD is the more exposed site for long range transport. Elements detected in less than 10 % of the samples or only intermittently in less than 30 % of the cases will not be studied further.

Correlation Analysis

To study the relation beteween the ROZ and the source-related models an analysis of correlation between the factor scores and the ROZ was carried out. As shown in a previous work (Heidam, 1982) these correlation coefficients are identical to the factor loadings that would be obtained in a fictive factor model that includes the ROZ, provided this enhancement of the input data does not lead to a different pattern of eigenvalues of the correlation matrix.

Therefore the correlation analysis gives indications as to where the ROZ would fit into the model-space if they could have been included. Such an indication is however only valid if the measured fraction of samples contains concentrations which are representative of the whole period. Because of the missing values the correlation coefficients can at best be considered as semi-quantitative estimates of the potential factor loadings of the ROZ.

The results on the correlation coefficients, their significance and the number of observations are given in tables 4 - 5. The correlations significant at less than 5 % are marked with an asterisk. When viewed in the context of factor analysis only factor loadings larger than about 0.5 are of any importance. In fact a loading of at least 0.7 is required for an ROZ to be considered a major member of the factor since such a

loading will contribute with 0.7^2, i.e. at least half of the communality which excludes any stronger couplings to other factors. These values are printed in bold type.

Discussion

Source allocation of ROZ

From these results it is noted that Cl_17 which is a ROZ at NORD appears within the source space avilable to be classified as mainly of combustion origin. Clearly a marine dimension is lacking.

The well-known anthropogenic elements V_23 and Ni_28 appearing as ROZ at NORD are allocated to the metal factor. Whereas this appears reasonable for Ni_28 it is against expectations that V_23 is not classified as a combustion component. This may be a consequence of the sparse data basis. At THUL however V_23 has the strongest correlation with the combustion factor.

At both sites Rb_37 and Zr_40 are classified as elements of a natural origin in crustal erosion processes. Since Zr_40 is chemically similar to the well-known crustal element Ti_22 that conclusion appears reasonable but whether the same is true for Rb_37, which is only represented in 15 - 20 % of the samples, is more uncertain. However, Rb_37 is chemically similar to K_19 which is a member of the crustal component at both stations.

The remaining important correlations concern As_33 and Sn_50 which are classified as members of the metal factors at THUL and NORD, respectively. As_33 is not considered at NORD and at THUL Sn_50 cannot be fitted within the available source categories.

A similar non-conclusive allocation is seen for the remaining two elements Mo_42 and Ba_56. There are either too few observations or the correlations (loadings) are less than 0.7, i.e. not sufficiently large to exclude other source type allocations. At THUL the metal Mo_42 has a fairly strong correlation with the combustion component and the same is true of Ba_56 with respect to the erosion component. In view of the chemical similarity with other crustal elements such as Sr_38 and Ca_20 this appears reasonable.

Seasonal variations of factors and selected ROZ

In Figure 2 the concentrations of Sn_50 at NORD are shown logarithmically together with the linear variations of the Metal factor. The number of observations is quite small and only the dozen consequtive samples in February 1982 indicates that the correlation is not spurious but corresponds to a significant loading that places Sn_50 with an origin in remote smelters, presumably Russian.

The concentrations of As_33 and the Metal factor at THUL are shown together in Figure 3. The metallic origin of this element seems fairly convincing. Some coincidences are seen in the summer months of 1982 but especially the winter-spring period of 1983 shows a high degree of consequtive covariation.

The apparently crustal ROZ Zr_40 is illustrated in Figure 4 in a comparison with the crustal factor at THUL. With a basis of 61 % of the samples there is not much doubt that this element is indeed a crustal one. Because of the rather high factor values in the summer period the erosion component has previously (Heidam, 1984) been interpreted as having an indigeneous origin in Greenland and only in winter-spring is it of a remote origin. These are also the periods of frequent detection of Zr_40.

Conclusions

This study of rarely occurring elements (ROZ) in the Arctic aerosol has confirmed the structure of the aerosol in terms of remote source types found previously by analysis of the more abundant elements. In addition there are strong indications that the Arctic aeosol contains a richer source spectrum since some of the ROZ could not be fit into the available source space.

A study of this wider source spectrum requires a wider range of analytical methods that are able either to reduce the number of instrumentally defined ROZ or to increase the range of components by, e.g., gaseous and organic pollutants. But even under such circumstances it is highly probable that some compounds occur only rarely and in these cases the ROZ-technique presented here could help extract additional relevant information.

Ackowledgements

The SAGA project has in variuos phases been partly supported by grants from the Nordic Ministerial Council and the Danish Natural Science Research Council.

References

AGASP (1984). Arctic Gas and Aerosol Sampling Program.
Geophys. Res. Letters, **11**, No. 5.

ARCTIC AIR CHEMISTRY (1977). Sources and Significance of Natural and Man-made Aerosols in the Arctic. Proceedings of the I. International Symposium. June 1977, NILU, Norway.

ARCTIC AIR CHEMISTRY (1981). Proceedings of the II. International Symposium 1980. Atmospheric Environment **15**, No. 8, Special Issue.

ARCTIC AIR CHEMISTRY (1985). Proceedings of the III. International Symposium 1984. Atmospheric Environment **19**, No. 12, Special Issue.

ARCTIC AIR CHEMISTRY (1989). Proceedings of the IV. International Symposium 1987. Atmospheric Environment **23**, No. 11, Special Issue.

ARCTIC AIR POLLUTION (1986). Proceeding of a Symposium 1985. Ed. B. Stonehouse, Cambridge University Press, Cambridge.

Harman, H. H. (1976). Modern factor Analysis. (3rd rev. Edition). The University of Chicago Press, Chicago.

Heidam N. Z. (1982). Atmospheric Aerosol Factor Models, Mass and Missing Data. Atmospheric Environment, **16**, 1923-1931.

Heidam N. Z. (1984). The Components of the Arctic Aerosol. Atmospheric Environment, **18**, 329-343.

Heidam N. Z. (1985). Crustal Enrichments of the Arctic Aerosol. Atmospheric Environment, **19**, 2083-2097.

Ottar B., Gotaas Y., Hov Ø., Iversen T., Joranger E., Oehme M., Pacyna J., Semb A., and Vitols V. (1986). Air Pollutants in the Arctic. NILU Report OR 30/86.

Table 1. Varimax rotated 3-factor model for the Arctic aerosol.
NORD June 1981 - May 1982.

	FACTOR1 EROSION	FACTOR2 METALS	FACTOR3 COMBUSTION	COMMU-NALITY
AL_13	0.977	0.012	-0.004	0.954
FE_26	0.968	0.153	0.062	0.965
TI_22	0.941	0.067	0.013	0.891
SI_14	0.871	-0.014	-0.262	0.826
CA_20	0.870	0.206	0.227	0.850
K_19	0.834	0.417	0.206	0.912
MN_25	0.811	0.514	0.206	0.964
SR_38	0.566	0.472	0.410	0.710
ZN_30	0.202	0.831	0.345	0.850
CU_29	0.002	0.763	0.449	0.785
CR_24	0.503	0.634	0.274	0.730
BR_35	0.016	0.228	0.973	0.999
S_16	-0.151	0.456	0.754	0.799
PB_82	0.191	0.259	0.640	0.513
Variances explained	6.317	2.732	2.698	11.747 83.9 %

Table 2. Varimax rotated 4-factor model for the Arctic aerosol.
THUL May 1982 - May 1983.

	FACTOR1 EROSION	FACTOR2 COMBUSTION	FACTOR3 METALS	FACTOR4 MARINE	COMMU-NALITY
TI_22	0.971	0.029	0.154	0.135	0.986
SI_14	0.966	-0.065	0.163	0.094	0.973
AL_13	0.961	0.095	0.166	0.106	0.972
FE_26	0.957	0.138	0.214	0.114	0.995
MN_25	0.853	0.310	0.354	0.104	0.959
K_19	0.609	0.386	0.348	0.506	0.897
S_16	-0.085	0.919	0.207	-0.171	0.923
BR_35	0.055	0.847	0.385	0.149	0.890
NI_28	0.138	0.823	0.289	0.019	0.781
CA_20	0.410	0.623	0.369	0.438	0.885
PB_82	0.230	0.397	0.804	0.060	0.860
CU_29	0.317	0.257	0.778	0.149	0.794
ZN_30	0.230	0.485	0.765	0.089	0.881
CR_24	0.363	0.527	0.546	0.090	0.715
CL_17	0.080	-0.117	0.032	0.844	0.734
SR_38	0.491	0.503	0.310	0.633	0.990
Variances explained	5.599	3.908	3.012	1.717	14.234 89.0 %

Table 3. Rarely Occurring Elements: Number of samples above detection limit, sample geometric mean (in ng m^{-3}) and geometric standard deviation.

	NORD 81-82	THUL 82-83
Total samples	100	100
CL_17	40 62.74 4.89	72
V_23	63 0.691 3.08	53 0.305 2.15
NI_28	59 0.383 3.13	71
AS_33	15 * 0.745 3.49	42 0.314 2.58
RB_37	15 0.363 2.70	21 0.162 2.35
ZR_40	31 0.237 2.81	61 0.179 2.37
NB_41	7 * 0.134 2.24	0
MO_42	7 * 0.161 1.37	16 0.075 1.29
CD_48	8 * 0.835 1.33	11 * 0.191 1.33
SN_50	16 0.785 1.37	31 0.429 1.48
SB_51	3 * 0.877 1.27	19 * 0.520 1.78
BA-56	18 4.698 3.45	22 1.698 1.38

* Excluded because of too few samples or predominantly non-sequential samples.

Table 4. Correlation coefficients of ROZ and factors, significance level and number of samples.
NORD June 1981 - May 1982.

	FACTOR1 EROSION	FACTOR2 METALS	FACTOR3 COMBUSTION
CL_17	0.28 0.082 40	0.17 0.31 40	0.474 * 0.002 40
V_23	0.20 0.13 63	**0.701** * 0.0001 63	0.20 0.12 63
NI_28	0.474 * 0.0001 59	**0.811** * 0.0001 59	0.24 0.07 59
RB_37	**0.981** * 0.0001 15	0.550 * 0.034 15	0.07 0.81 15
ZR_40	**0.912** * 0.0001 31	0.02 0.90 31	-0.14 0.44 31
SN_50	0.04 0.87 16	**0.703** * 0.002 16	0.33 0.22 16
BA_56	0.14 0.58 18	0.11 0.67 18	-0.09 0.72 18

Table 5. Correlation coefficients of ROZ and factors, significance level and number of samples.
THUL May 1982 - May 1983.

	FACTOR1 EROSION	FACTOR2 COMBUSTION	FACTOR3 METALS	FACTOR4 MARINE
V_23	0.354 * 0.009 53	0.675 * 0.0001 53	0.364 * 0.007 53	-0.05 0.71 53
AS_33	0.29 0.062 42	0.453 * 0.003 42	**0.818** * 0.0001 42	-0.112 0.48 42
RB_37	**0.946** * 0.0001 21	0.11 0.63 21	0.615 * 0.003 21	0.591 * 0.005 21
ZR_40	**0.901** * 0.0001 61	-0.17 0.20 61	0.25 0.052 61	0.45 * 0.0003 61
MO_42	0.33 0.22 16	0.576 * 0.020 16	0.33 0.21 16	0.22 0.42 16
SN_50	0.12 0.51 31	-0.26 0.16 31	0.34 0.058 31	0.07 0.72 31
BA_56	0.505 * 0.017 22	-0.18 0.43 22	0.12 0.60 22	0.33 0.13 22

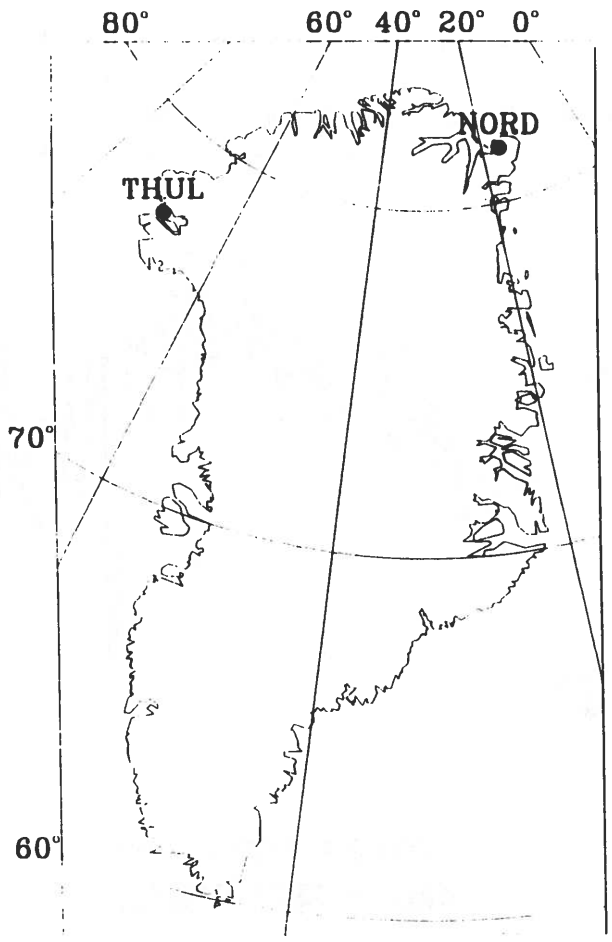

Figure 1. Location of Station Nord and Thule/Qaanaaq in North Greenland.

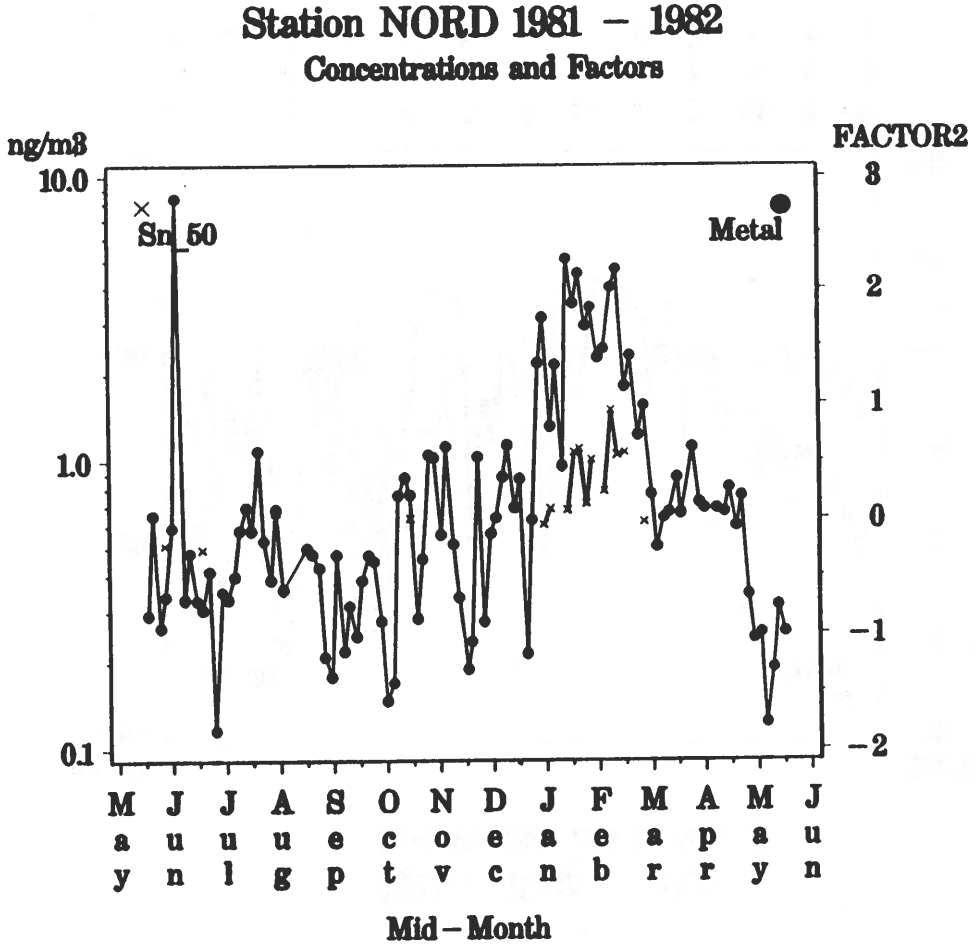

Figure 2. Time variations of ROZ concentrations and source related factors. Sn_50 and Metal factor 2. NORD June 1981 - June 1982.

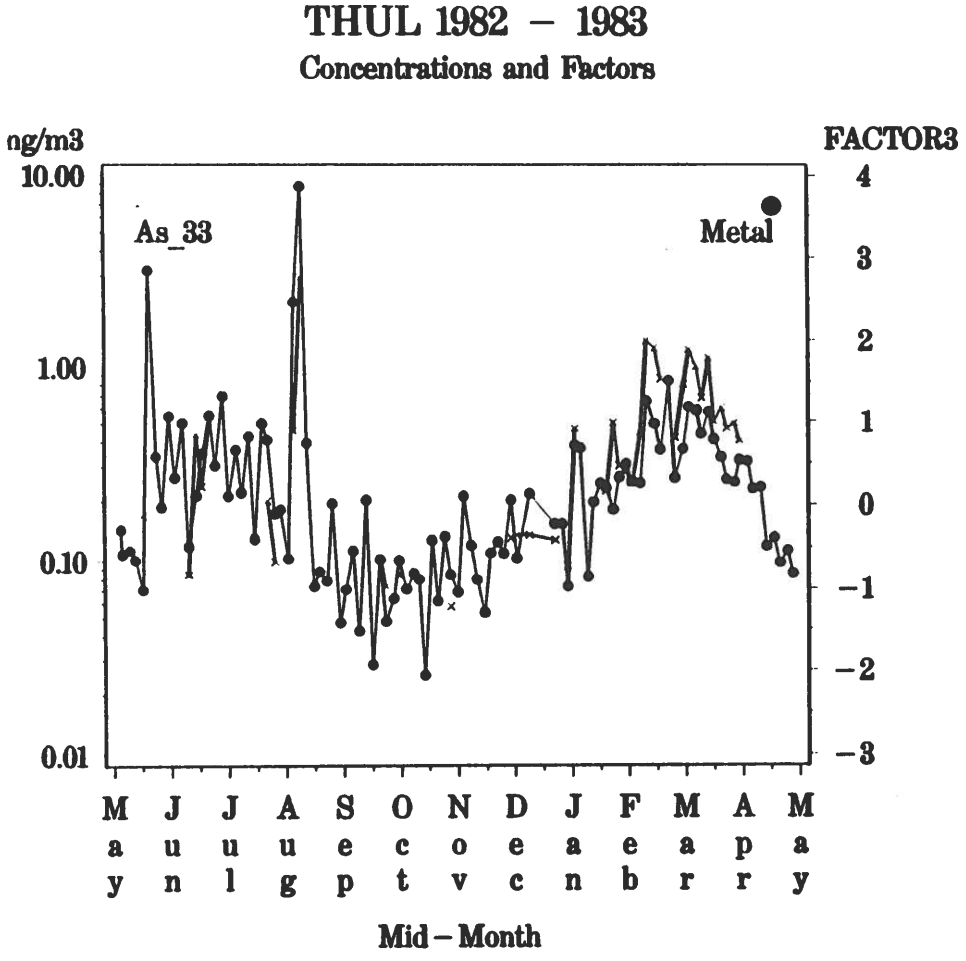

Figure 3. Time variations of ROZ concentrations and source related factors. As_33 and Metal factor 2. THUL May 1982 - May 1983.

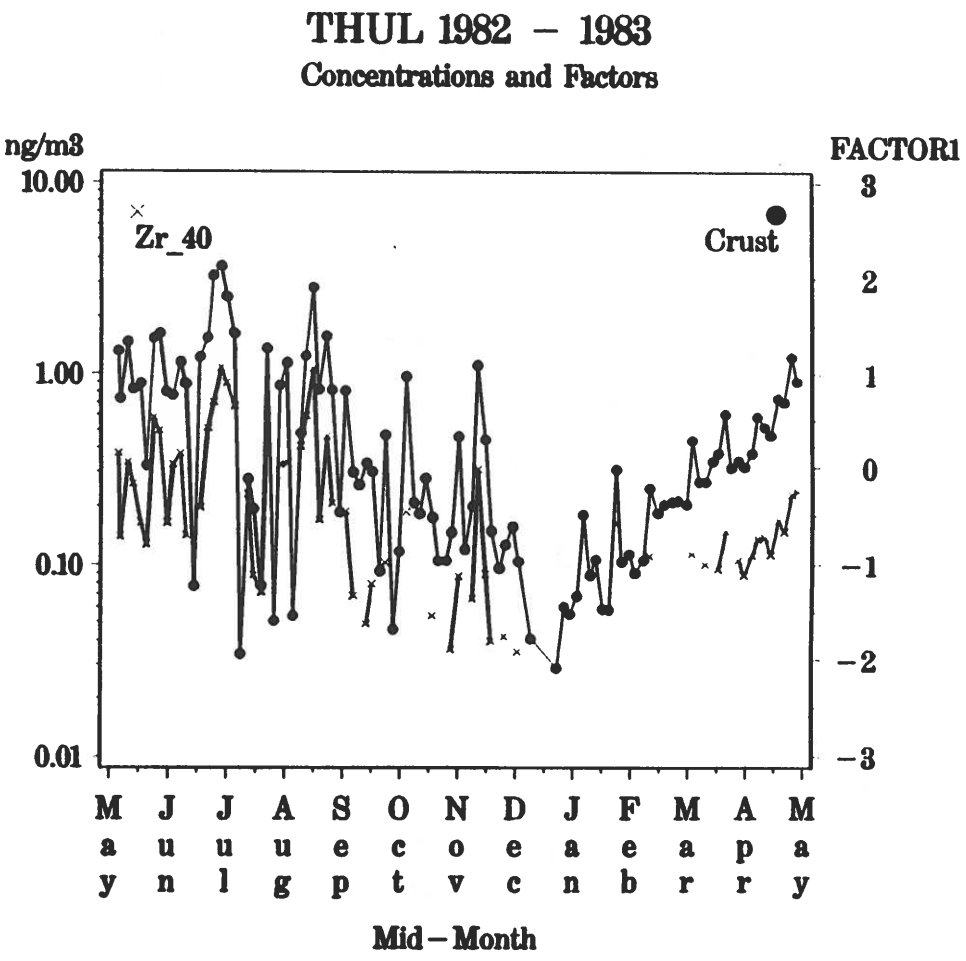

Figure 4. Time variations of ROZ concentrations and source related factors. Zr_40 and Crustal factor 1. THUL May 1982 - May 1983.

A three dimensional hemispheric air pollution model used for the Arctic

Jesper Christensen
National Environmental Research Institute
Frederiksborgvej 399
4000 Roskilde
Denmark

Abstract

A three dimensional air pollution model is in process of development at the National Environmental Research Institute. The model will be used to study long-range transport from the industrial areas in Europe, Asia and North-America to the Arctic. The model covers most of the Northern Hemisphere. The present version of the model includes only the long-range transport of sulphur di-oxide and particulate sulphate.

The transport process (advection and diffusion) is calculated by a pseudospectral method for the horizontal direction and by a Galerkin finite elements method for the vertical direction. The chemistry in the model is described by a simple linear oxidation of sulphur di-oxide (SO_2) to particulate sulphate ($SO_4^=$), where the reaction rate have both a temporal and spatial variation. The mixing layer, in which the emissions and dry depositions take place, is parameterized by simple models for the mixing layer height and the vertical diffusion. The model includes both dry and wet deposition processes. Emission are taken from Spiro et al. (1992), Semb (1985) and the EMEP emissions (Iversen et al., 1989). The model will be run for January 1991.

This work has been partly supported by the Danish Research Academy and the Danish Natural Science Research Council.

1. Introduction

There have been a considerably scientific interest of the air pollution in the Arctic. The reason for this is that the arctic area is rather sensitive to the pollution, and the pollution there is a finger print of the air pollution for the whole Northern Hemisphere. In the last 20 years several groups have done measurements in the arctic (see, for example, AGASP, 1984; Arctic Air Chemistry, 1985; Arctic Air Chemistry, 1989). All these measurements shows that the air pollution have a great seasonally variation with relative high concentrations during the winter and the early spring with a maximum normally in march and very low concentrations during the summer. The air pollution is also characterized by an episodic nature, because the origin of the pollution is only due to the long-range transport, and a deep vertical distribution, because of the very cold and stable Arctic atmosphere.

In this paper a hemispheric model, that is in progress of development at the National Environmental Research Institute (NERI), will be described. This model is an extension of the regional long-range transport models, that have been developed at NERI, see Zlatev and Christensen, 1989, where a simple sulphur model, covering the whole Europe, is discussed, and Zlatev et al., 1992, where a big model, including many photochemical non-linear reactions, is discussed. These models is not directly applicable to describe the transport on a hemispherical scale, because of the vertical structure (only 2-d boundary layer models). Therefore one of the first goals in this project was to define the vertical structure of the model.

There have been done some 3-dimensional models for the Arctic air pollution, see, for example, Iversen (1989). In his model the vertical structure is defined by isentrop levels. By doing this the vertical velocities became very small, and therefore the numerical errors due to the vertical transport are also very small. A big problem with this vertical structure is that some of the isentrop levels are going through the surface of the earth, which for example means that it is possible to have a transport through the surface. The chemistry in this model is simple linear and the grid-resolution is 300 km at 60° latitude.

A different vertical structure is used in other models as, for example, the hemispheric model developed by Pudykiewicz (Pudykiewicz, 1991). Here there is used the terrain-following coordinate system σ (Phillips, 1957). By doing this the lower boundary is the surface of the earth and effects due to the topographic of the surface (mountains, etc) should be minimized. This model is a tracer model with a grid-resolution of 75 km at the 60° latitude.

It was decided to use the terrain-following coordinates σ in the model. The grid resolution is 150 km at 60° latitude and the present version of the model includes only linear sulphur chemistry (SO_2 to sulphate).

2. Description of the model

The model is based on a set of coupled continuity equations for each species, where the coupling is through the chemical reactions. Each equation is derived by the assumption that the pure advection cannot change the mass mixing ratio for a species, i. e.

$$\begin{aligned}\frac{Dq_i}{Dt} &\equiv \frac{\partial q_i}{\partial t} + \frac{dx}{dt}\frac{\partial q_i}{\partial x} + \frac{dy}{dt}\frac{\partial q_i}{\partial y} + \frac{d\sigma}{dt}\frac{\partial q_i}{\partial \sigma} \\ &= \frac{\partial q_i}{\partial t} + u\frac{\partial q_i}{\partial x} + v\frac{\partial q_i}{\partial y} + \dot{\sigma}\frac{\partial q_i}{\partial \sigma} = 0\end{aligned} \qquad (1)$$

where x and y is the horizontal coordinates in the east and north direction respectively. The vertical coordinate σ is a terrain following coordinate and is defined by $\sigma = p/p_s$, where p is the pressure and p_s is the pressure at the ground. The total continuitets equation (see, for example, Pudykiewicz, 1991) for each species is

$$\begin{aligned}\frac{\partial q_i}{\partial t} &= -u\frac{\partial q_i}{\partial x} - v\frac{\partial q_i}{\partial y} - \dot{\sigma}\frac{\partial q_i}{\partial \sigma} \\ &+ \frac{\partial\left(K_x\frac{\partial q_i}{\partial x}\right)}{\partial x} + \frac{\partial\left(K_y\frac{\partial q_i}{\partial y}\right)}{\partial y} + \frac{\partial\left(\Gamma^2 K_z\frac{\partial q_i}{\partial \sigma}\right)}{\partial \sigma} \\ &- W_i q_i \\ &+ E_i \\ &+ Q(c_1, c_2, \cdots, c_{nq}) \qquad , \quad i=1,nq\end{aligned} \qquad (2)$$

where nq is the number of species; the first term is the advection term, where u and v is the horizontal wind fields in east and north direction respectively and $\dot{\sigma}$ is the vertical velocity. The second term is the diffusion, where K_x and K_y are the horizontal diffusion coefficient and K_z is the vertical diffusion; $\Gamma = g\sigma/RT$, where g is the acceleration due to the gravity, R is the gas constant and T is the temperature. The third term is the wet deposition term, and the last two terms are the emissions and the chemistry. In the present version nq=2, where the two species are SO_2 and sulphate.

3. Numerical solution of the transport equation

The Northern Hemisphere was transformed to a plane, by using the polar stereographic projection system true at 60° North (see, for example, Haltiner and Williams, 1980; Iversen, 1989; Pudykiewicz,

1991). Then the time integration is done by splitting (2) into four sub-models:

1. Horizontal advection

2. Horizontal diffusion

3. Vertical advection and diffusion (and dry deposition)

4. Emission, chemistry and wet deposition

After this splitting the time integration of the (2) is obtained by doing a time integration on each of the four sub-models. This procedure make it much more easy to find a numerical solution for the whole model, because it is possible to find an efficient numerical solution for each sub-model. Splitting is commonly used in air pollution models (see, for example, Mcrae et al., 1982).

The horizontal space of the model is define on a regular 96x96 grid (see fig. 1), that covers most of the Northern Hemisphere, with a grid-distant of 150 km at 60° latitude. The vertical grid is an irregular grid with 12 grid-points, which cover the whole troposphere, see table 1.

Table 1. Vertical structure used in the model

level no.	σ
1	0.100
2	0.308
3	0.472
4	0.602
5	0.705
6	0.787
7	0.851
8	0.902
9	0.935
10	0.960
11	0.980
12	1.000

The horizontal transport equations is solved by using a pseudospectral algorithm (see Bartnicki et al., 1990; Christensen, 1992a,b). The pseudospectral algorithm demands periodical boundary conditions, which are imposed by some artificial sinks on the horizontal boundaries (Zlatev et al., 1992; Christensen, 1992a,b), so that the concentrations are close to zero at the boundaries.

The vertical transport equation is solved by applying an finite element algorithm; see Pepper et al., 1979, and Christensen, 1992a,b. This algorithm is also used for the horizontal transport in some air pollution models, see, for example, Carmichael and Peters, 1984, and Piedelievre et al., 1990. The boundary conditions at the lower boundary (at the ground) is defined by that the flux out of the model domain is only due to the dry deposition. At the upper boundary there are free boundary conditions.

The sub-model, which includes emission, chemistry and wet deposition, could be rewritten to an equation of the following

type: $dc_i/dt = P_i - L_i c_i$, where P_i is the production of the i'te species, due to the emissions and chemistry, L_i is the loss term of the i'te species, due to the chemistry and the wet deposition. By assuming that P_i and L_i is constant during a timestep it is possible to find an analytical solution of the problem.

It should be emphasized that for a long-range transport model on hemispheric scale, used to study the transport to the Arctic, it is very important, that one choose numerical schemes, which are efficient and give small numerical errors, because the atmospheric transport is the only reason for the air pollution in the Arctic. The numerical schemes used in this paper is tested carefully (see Christensen, 1992a,b) and was found to work satisfactory well concerning numerical efficiency and numerical errors.

4. Physical parameters

In this section the main physical processes will be described. All the meteorological inputs are obtained from the European Centre for Medium-range Weather Forecasts (ECMWF), ECMWF/TOGA Basic Level III data sets. The windfields are transformed to the projection, used in the model. All the meteorological data are interpolated to the grid, used in the model. The time resolution is 6 or 12 hours.

4.1 Advection

The advection depends on the 3-d windfields. These windfields are meteorological inputs to the model.

4.2 Horizontal diffusion

In the model it is assumed that the horizontal diffusion is constant: $K_x=K_y=3\cdot 10^4$ m^2/s. This diffusion is some artificially compared with implicit diffusion due to the grid-resolution, but it smooths the numerical solution of the advection.

4.3 Vertical diffusion

The expressions for the K_z profile in the surface layer is based on Monin-Obukhov similarity theory (see Seinfeld, 1986)

$$K_z = \frac{\kappa u_* z}{\phi(z/L)} \tag{3}$$

where $\phi(z/L)$ is given by

$$\phi(z/L) = \begin{cases} 1+4.7\,z/L & z/L > 0 \quad stable \\ 1 & z/L = 0 \quad neutral \\ 1-15\,z/L & z/L < 0 \quad unstable \end{cases} \tag{4}$$

u_* is the friction velocity which are calculated by the relation $\tau = \rho\, u_*^2$ where τ is the surface layer stress (input from the meteorological data) and $\rho = p_s/RT_2$ is the density at the surface (surface pressure, p_s, and surface temperature, T_2, are both input from the meteorological data). L is the Monin-Obukhov lenght, calculated by

$$L = \frac{(\tau/\rho)^{3/2} T_2}{\kappa g(-H_d/c_p\rho)} \tag{5}$$

where κ is von Karman constant (=0.35), g is the acceleration due to the gravity, c_p is the heat capacity and H_d is the upward heat flux (input from the meteorological data).

The K_z profile for the surface layer is extended to the whole vertical by the following expression which ensures that vertical diffusion is small (0.1 m^2/s) above the mixing-layer

$$K_z = \max\left(\frac{\kappa u_* z}{\phi(z/L)}(1 - z/z_{mix}), 0.1\ m^2/s\right) \tag{6}$$

The height of the mixing layer, z_{mix}, is calculated by using a model for the boundary layer, which are described in Berkowicz and Olsen, 1990, and Gryning and Batchvarova, 1990. This model is based on a simplified energy balance equation for the internal boundary-layer, which could have following expression:

$$\left(N^2 z_{mix} + 1.9\frac{u_*^2}{z_{mix}}\right)\frac{dz_{mix}}{dt} = \frac{g}{T}\max(H_d, 0) + 2.5\frac{u_*^3}{z_{mix}} - 1.9\frac{u_*^2}{550s} \tag{7}$$

where N is the Brunt-Vaisala frequency, $N=\sqrt{\gamma g/T}$ (γ is the lapse rate).

4.5 Emission

The emissions used in the model are shown on Fig. 2. They are based on the global inventory of sulphur emissions described in Spiro et al., 1992, the EMEP emissions for Europe (Iversen et al., 1989) and the circumpolar emissions survey by Semb, 1985. For some regions (Europe and Asia) there are imposed a seasonal sine-variation from 1.33 in January to 0.67 in July. 5 % of the emissions are directly emitted as sulphate. The emissions are distributed evenly up to 500 m above the surface.

4.6 Chemistry

It is assumed that the oxidation rate of SO_2 to sulphate is linear, where the rate depends on the time of the year and the latitude (see, for example, Iversen, 1989, and Iversen et al., 1991):

$$k_{ox}(Lat,t) = (a(t) + b(t)\,(1 - 2\,Lat/180^{o}))\,k_{max} \qquad (8)$$

where $a(t)=\sin^2(2\pi t/365)$ and $b(t)=\cos^2(2\pi t/365)$. This spatial and temporal variation of the oxidant rate try to take into account the variations of OH in the gas phase and H_2O_2 and O_3 in the liquid phase. k_{max} is equal $5\cdot10^{-6}$ s^{-1}.

4.7 Dry deposition

Also the dry deposition for SO_2 have a temporal and spatial variation due to the low deposition of SO_2 over non-melting snow and the variation of the biochemical uptake of the vegetation which also have a diurnal cycle. Over the open water the dry deposition is very effective. The total expression for the dry deposition of SO_2 is (Iversen et al.,1991)

$$v_d(Lat,t,\tau) = (A_{ow} + (1-A_{ow})\,(a(t)\,\Delta(\tau) + b(t)\,(1 - 2\,Lat/180^{o}))\,v_{dmax} \qquad (9)$$

where $a(t)=\sin^2(2\pi(t-32)/365)$ and $b(t)=\cos^2(2\pi(t-32)/365)$, A_{ow} ratio of open water, $\Delta(\tau)$ is 0.25 in the night time and else 1. The maximal dry deposition velocity is 0.8 cm/s.

The dry deposition for sulphate is 0.1 cm/s over the whole area (see Zlatev et al., 1992).

4.8 Wet deposition

The wet removal is an important removal process for sulphur, therefore it is very important to threat this process properly. But the wet deposition is more difficult to handle, because the meteorological information about the precipitation is rather

coarse. In fact there are no precipitation fields in the meteorological input. One have to diagnosticate the precipitation by calculate the transport of humidity (the transport equation for the humidity is the same as for SO_2 and sulphate and the humidity is also a meteorological input), see, for example, Iversen, 1989. The removal of SO_2 and sulphate is estimated by using simple linear scavenging coefficients. The scavenging ratio for SO_2 have seasonally variation due to the variation of H_2O_2, see Iversen et al., 1991:

$$\Lambda_{SO_2} = 3 \cdot 10^5 + 1 \cdot 10^5 \sin(2\pi(t-80)/365) \qquad (10)$$

and for sulphate the scavenging ratio have no seasonally variation:

$$\Lambda_{sulphate} = 1 \cdot 10^6 \qquad (11)$$

In the model it is assumed that the wet removal process only exist in the planetary boundary layer.

5. Numerical results

The model will be run for January 1991 and in the beginning only compared with measurements done by NERI in Greenland.

6. Future work

The future work will first and foremost be concentrated in a better model evaluation by doing two thing:

1. Using much more measurements, not only from the Arctic, but also from other background measurement stations in the other part of the Northern Hemisphere.

2. Run the model for a longer period (one year from August 1990 to July 1991) and study the seasonally variations of the sulphur concentrations, if it is possible to get meteorological data for the whole period.

There are also plans about model comparison with the hemispherical model by Tarrason and Iversen, 1992, and the regional model for Europe by Zlatev et al., 1992. The last comparison includes also an evaluation of the sub-models for the mixing heights and the precipitation by comparing the model results with observations of the mixing-height and precipitation.

In the light of these model evaluations the parameterization of the different physical processes could be improved. A more realistic cloud parameterization scheme could be used (see, for

example, Sundqvist et al., 1989) so that one not only get a better estimates of the precipitation, but also prepared the model for a more sophisticated cloud chemistry and removal process. A another improvement could be by including much more chemical species, so one get a more realistic chemical scheme. This will not improved the sulphur results very much because the assumption about the linear chemistry is a good approximation. But then the model could be used to described other species than SO_2 and sulphate, for example, O_3, NO_2, PAN, VOC etc.

After the model evaluation and improvement of the physical parameterization, the model will be used study the transport of air pollution to the Arctic. The model could also be used to study intercontinental long-range transport, for example from North America to Europe.

7. Concluding remarks

There are not many concluding remarks yet. In this paper a new hemispherical transport model for SO_2 and sulphate is described. The hope is that the model will give rather good results, when it is run with real meteorological data, and therefore the model could be useful to study the transport of air pollution on a hemispheric scale.

References

AGASP (1984): Special issue edited by R. C. Schnell. Geophys. Res. Lett., 11, 359-472.

Arctic Air Chemistry (1985): Special issue edited by K. A. Rahn. Atmos. Env., 19, 1987-2208.

Arctic Air Chemistry (1989): Special issue edited by K. A. Rahn. Atmos. Env., 23, 2345-2638.

Bartnicki, J., K. Olendrzynski, K. Abert, P. Seibert and B. Morariu (1990): Numerical Approximation of the Transport Equation: Comparison of Five Positive Definite Algorithms. IIASA Working Paper WP-90-10, International Institute for Applied System Analysis, Laxenburg, Austria.

Berkowicz, R. and H. R. Olsen (1990): Modelling the Internal Boundary Layer at a Coastal Site. In: "Preprint from Ninth Symposium on Turbulence and Diffusion, April 30 - May 3, 1990, Risø, Denmark".

Carmichael, G. R. and L. K. Peters (1984): An Eulerian Transport/transformation/removal Model for SO_2 and Sulphate - I. Model Development. Atmos. Env., 18, 937-952.

Christensen, J. (1992a): Development and Testing Advection-diffusion Schemes in a Three Dimensional Air Pollution Model. Internal Report. National Environmental Research Institute, Roskilde, Denmark.

Christensen, J. (1992b): Testing Advection schemes in a Three Dimensional Air Pollution Model. Accepted by Mathl. Comput. Modelling.

Gryning, S. E. and E. Batchvarova (1990): Analytical for the Growth of the Coastal Internal Boundary Layer During Onshore Flow. Q. J. Meteorol. Soc., 116, 187-203.

Haltiner, G. J. and R. T. Williams (1980): Numerical Prediction and Dynamic Meteorology. John Wiley & Sons, New York.

Iversen, T (1989): Numerical Modelling of the Long Range Atmospheric Transport of Sulphur Dioxide and Particulate Sulphate to the Arctic. Atmos. Env., 23, 2571-2595.

Iversen, T., N. Halvorsen, S. Mylona and H. Sandnes (1991): Calculated Budgets for Airborne Acidifying Components in Europe, 1985, 1987, 1988, 1989 and 1990. Report No 1/91. EMEP Meteorological Synthesizing Centre - West, Norwegian Meteorological Institute, PO Box 43, Blindern, N-0313 Oslo 3, Norway.

Iversen, T., J. Saltbones, H. Sandnes, A. Eliassen and Ø. Hov (1989): Airborne Transboundary Transport of Sulphur and Nitrogen over Europe - Model Description and Calculations, Report No 2/89. EMEP Meteorological Synthesizing Centre - West, Norwegian Meteorological Institute, PO Box 43, Blindern, N-0313 Oslo 3, Norway.

Mcrae, J., W. R. Goodin and J. H. Seinfeld (1982): Numerical Solution of the Atmospheric Diffusion Equation for Chemical Reaction Flows. J. Comput. Phys., 45. 1-42.

Pepper, D. W., C. D. Kern and P. E. Long, Jr, (1979): Modelling The Dispersion of Atmospheric Pollution Using Cubic Spline and Chapeau Functions. Atmos. Env., 13, 223-237.

Phillips, N. A. (1957): A Coordinate System Having some Special Advantages for Numerical Forecasting. J. Meteorol., 14, 184-185.

Piedelievre, J., L. Musson-Genon and F. Bombay (1990): MEDIA - An Eulerian Model of Atmospheric Dispersion: First Validation on the Chernobyl Release. Mon. Wea. Rev., 29, 1205-1220.

Pudykiewicz, J. (1991): Environmental Prediction Systems: Design, Implementation Aspects and Operational Experience with Application to Accidental releases. In: "Air Pollution Modelling and its Applications VIII". (H. van Dop and D. G. Stein, eds), Plenum Press, New York, 145-159.

Seinfeld, J. H. (1986): Atmospheric Chemistry and Physics of Air Pollution. John Wiley & Sons, New-York.

Semb, A. (1985): Circumpolar SO_2 Emission Survey. Proj. No. 0-8516, Norwegian Institute for Air Research, Lillestrøm, Norway.

Spiro, P. A., D. J. Jacob and J. A. Logan (1992): Gloabl Inventory of Sulphur Emissions With 1° x 1° Resolution. J. Geophys. Res., 97, 6023-6036.

Sundqvist, H., E. Berge and J. E. Kristjansson (1989): Condensation and Cloud Parametrization Studies with a Mesoscale Numerical Weather Prediction Model. Mon. Wea. Rev., 117, 1641-1657.

Tarrason, L. and T. Iversen (1992): The Influence of North American Anthropogenic Sulphur Emissions over Western Europe. Tellus, 44B, 114-132.

Zlatev, Z. and J. Christensen (1989): Studying the Sulphur and Nitrogen Pollution over Europe. In: "Air Pollution Modelling and its Applications VII". (H. van Dop, ed), Plenum Press, New York, 1989, 351-360.

Zlatev, Z., J. Christensen and Ø. Hov (1992): An Eulerian Model for Europe. J. Atmos. Chem., 15, 1-37.

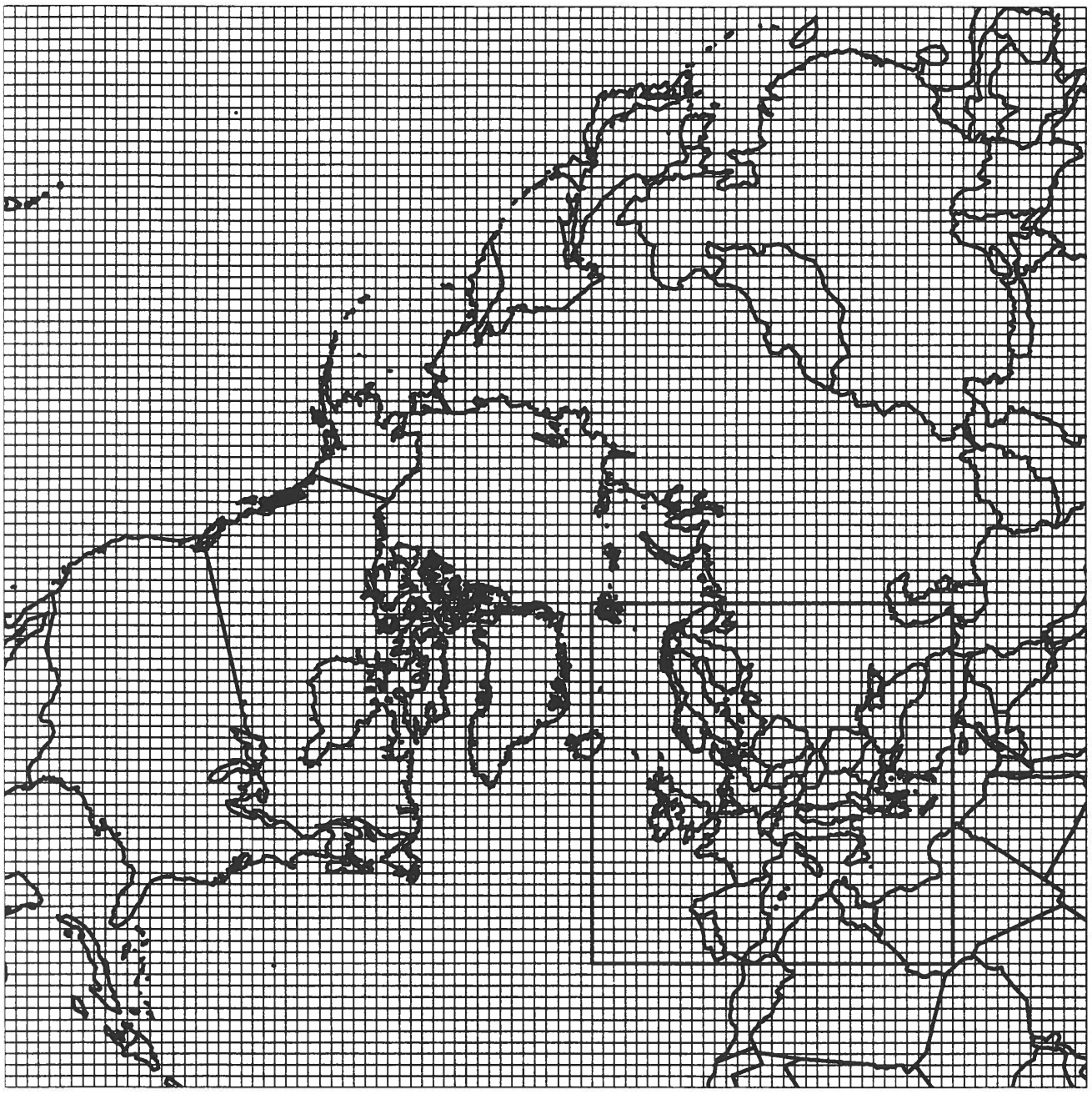

Figure 1.
The model area and the grid. The grid distance is 150 km at the 60° latitude. The window over Europe is the model area of the regional model by Zlatev and Christensen, 1991

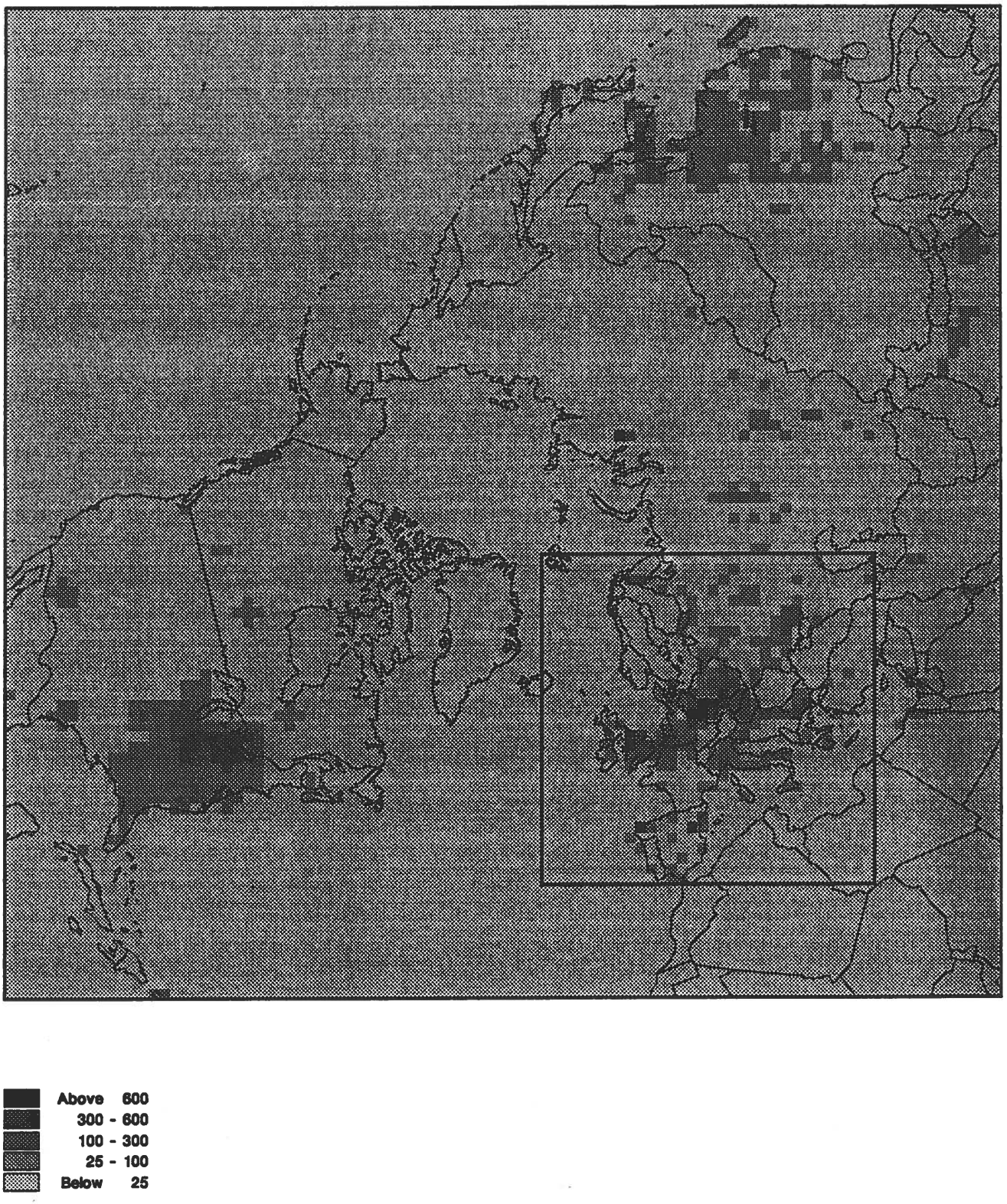

Figure 2.
The emissions of Sulphur in kt S/year for each grid-square.

Session 8

Transformation and Transport

Chairman:
N.Z. Heidam

ELEVEN YEARS OF METHANE SULPHONIC ACID OBSERVATIONS IN THE HIGH ARCTIC

S.-M. Li and L.A. Barrie
Atmospheric Environment Service, 4905 Dufferin St. Downsview
Ontario Canada M3H 5T4 Fax 416 739-5704

ABSTRACT

Methane sulphonic acid(MSA) is an aerosol end-product of the oxidation of dimethylsulphide(DMS) in the atmosphere. DMS is the main source of marine biogenic sulphur to the atmosphere. It is mainly marine in origin and is potentially important for its role in tropospheric chemistry, climatic forcing and acidification of the terrestrial biosphere. Archived aerosol samples collected at Alert N.W.T. Canada on a routine weekly basis during the 1980s have been analyzed by ion chromatography for MSA. The insight that these analyses - together with previously determined $SO_4^=$, Na^+ and S-isotopes of $SO_4^=$ - yield into natural sources of sulphur in high Arctic is discussed. MSA at Alert has a distinct bimodal seasonal distribution with the first peak in spring between March and May(~20 ng m^{-3}) and the second in summer between June and August(~10 ng m^{-3}); both decreased significantly by about 26% during the 11.3 year period. Whether this decrease is real or due to artifact MSA formation in archived filters remains to be determined. The determination of relative contributions of biogenic, sea salt and anthropogenic sources to total sulphate was possible in summer using previously determined Na^+ and S-isotopes of $SO_4^=$ data. Biogenic sources contribute from 25 to 30% while sea salt contributes only 1 to 8%. The remainder is from anthropogenic sources. Throughout the rest of the year, all that can be said is that sea salt contributes 2 to 7%, biogenic less than 15% and anthropogenic sources the rest. The ratio of MSA/biogenic $SO_4^=$ in summer was determined to be in the range 0.2 to 0.9 while in winter it was lower than this range.

Proc. of the Fifth International Symposium On Arctic Air Chemistry
8-10 September 1992 Copenhagen Denmark

INTRODUCTION

Sulfur compounds are of interest because of their role in tropospheric chemistry, climatic forcing and acidification of the terrestrial biosphere. Sources of atmospheric sulfur include emission of biogenic organo-sulphur compounds to organic gases such as dimethyl sulfide (DMS) and carbonyl sulfide (COS), sea spray, volcanoes, and the anthropogenic sources of fossil fuel combustion and sulfide ore smelting. On a global basis, approximately 15% of the total sulfur flux to the atmosphere originates from marine biogenic sources, mainly as DMS [Bates et al., 1992]. Considering that biogenic sources are highly seasonal and regional in nature, the contribution of biogenic sources in certain regions can dominate the atmospheric sulfur cycle.

Oxidation of DMS in the atmosphere mainly leads to aerosol sulfate and methanesulfonic acid (MSA). Like anthropogenic sulphur aerosols, these DMS products are in fine particles less than 1 micrometre in diameter. It has been proposed that fine particles dominated by sulphates affect the radiative balance of the atmosphere directly as scatterers of solar radiation [Shaw, 1987; Charlson et al., 1991] or indirectly through cloud albedo as cloud condensation nucleii [Charlson et al., 1987, 1992], and have a radiative forcing that may be comparable and opposite in sign to the current greenhouse gas forcing of carbon dioxide.

To date, only a few measurements have been reported of the marine biogenic sulfur product MSA in the northern polar atmosphere even though northern oceans have been shown to be highly productive sources of DMS during spring and summer [Turner and Liss, 1985; Bates et al, 1987b; Burgermeister et al, 1990; Erickson et al, 1990; Leck and Rodhe, 1991; Tarrason, 1991]. What evidence exists on northern polar spatial and temporal variation of MSA prior to 1991 has been reviewed by Li et al. [1993a]. This paper augments the previously limited observations with an 11 year record of aerosol MSA measurements at ground level at Alert, NWT (82.5°N, 62.3°W) between July 1980 and August 1991. In addition, analyses of $SO_4^=$, Na and sulphur isotopes of $SO_4^=$ as well as of air parcel trajectories are used to investigate biogenic $SO_4^=$ in the Arctic, its origin and contribution to total $SO_4^=$. Further details can be obtained elsewhere(Li and Barrie, 1993; Li et al, 1993b).

EXPERIMENTAL

Atmospheric filter samples have been routinely collected since July 1980 at Alert, Northwest Territories, Canada in an ongoing effort. For details of this sampling program and the sampling site, see Barrie and Hoff [1985] and Barrie et al. [1989]. Briefly, the samples from approximately 16000 m^3 of air are collected by hi-volume samplers at a face velocity of 50 cm s^{-1} on 20x25 cm^2 Whatman 41 filters on a weekly basis. One field blank is collected every four weeks following the same procedure as the samples but no air is drawn through them. Samples are then shipped to AES central laboratory and are divided into 8 parts for analyses for many different chemical species. Unused parts of the samples are archived at room temperature in sterile whirlpak bags. Sampled air volumes are at 1 atm pressure and 20°C after corrections for pressure and temperature changes during the period of each sample.

A Dionex 4500i ion chromatograph was used in the analysis of MSA with an AS4A column, a conductivity detector, and a 200 μl injection loop(Li and Barrie, 1993b). All but three samples had MSA concentrations higher than our analytical detection limit of about 0.02 μmol L^{-1}, while essentially all blanks showed no detectable amount of MSA.

$SO_4^=$ and Na^+ are determined routinely also by ion chromatography. In addition, samples for the period 1983-1986 were analyzed for their stable sulfur isotope composition $\delta^{34}S$ [Nriagu et al., 1990].

All data, including those of MSA, are considered quantifiable when they are more than 3 standard deviations above the mean field blanks. Otherwise, the data are reported as below detection limit. The operational detection limit is chosen to yield a final data set that is not affected much by blanks. The blanks for MSA were not above the instrumental analytical detection limit, so that the operational detection limit is essentially the same as the instrumental detection limit. Overall, the random errors in the data sets, from both sampling in the field and laboratory handling and analysis should be comparable to those of $SO_4^=$ (<13%) of the mean [Barrie et al., 1989], and roughly 5 ng m^{-3} for MSA.

A test of stability of the archived samples was carried out by comparing results obtained when the samples were extracted and analyzed right after they were received from the field and results obtained from extracting aliquots from the samples archived for

over 2 years. The results show that these two sets of results were not significantly different from each other by two-sample tests on the data and further by regression. The residuals from the one-to-one response are normally distributed with a zero mean and can be accounted for by analytical noise. In other words, there was no significant MSA decay occurring while the samples were archived. This is confirmed by Savoie (University of Miami, personal communication) who found MSA on W41 filter samples stable under long term storage. We conclude that MSA concentrations changed by less than 10% after two years of storage.

RESULTS AND DISCUSSION

Time Series Of MSA

The observed MSA time series is shown in Figure 1a. Overall, the time series has approximately 5% data missing which are replaced by using the cubic spline interpolation subroutine, ICSCCU, of the IMSL [IMSL, 1982] library. This procedure provides continuous first and second derivatives of the data sequence to the missing data points while preserving the shape of the original data.

Several features stand out in the time series of MSA(Fig. 1a): (i) a distinct seasonal cycle with spring (April to May) and summer (July to August) maxima, which is repeatable from year to year but is not a purely sinusoidal function; (ii) concentration fluctuates significantly from one sample to the next and over a span of several weeks, which probably reflect local and regional influences on DMS transport and transformation to MSA as well as atmospheric mixing processes. In addition, MSA also increases drastically from early spring to late summer; (iii) concentration remains relatively constant and low in the cold months of October to February; (iv) the maximum concentration in a year, usually occurring in spring, appears to peak in 1984 and decreases afterwards. These features of the seasonal variation are apparently widespread in the troposphere in the Arctic [Li et al., 1993a].

Spectral analysis techniques including digital filtering were used to first remove the short term variations from the record, and then to separate the longer-term variations and trends (Fig. 1b) from the annual and seasonal cycles(Fig. 1c). For details see Li et al(1993b) in which the log-transformed MSA series has been analyzed. Based on the untransformed MSA series, there is a

statistically significant decrease in the deseasonalized data amounting to -0.20 ± 0.06 ng m^{-3} yr^{-1}. In other words during the 11.3 year period of record, MSA decreased by 2.1 ng m^{-3} or 26% from its initial level in July 1980. This decrease is apparent in both spring and summer peaks of MSA. There are two explanations for the trend. The first is that MSA has been produced on the archived filters at a rate of about 2.3% per year. Analytical data from ourselves and others(see experimental section) rule out large production(>5% yr^{-1}) but we cannot preclude rates of this magnitude. A re-analysis of archived filters in several years time will allow us to test this explanation. The second explanation which we are inclined to believe at the moment is that these changes are real and reflect a change in the processes that control MSA concentrations in the atmosphere at Alert.

The seasonal variations of MSA at Alert during the 11-year period, obtained from smoothing the detrended MSA series given in Figure 1c, show clearly two major seasonal peaks in spring and summer and a minor third peak at New Years. Table 1 shows these characteristics of these seasonal MSA peaks at Alert. Earlier, we hypothesized that the summer peak is governed by different sources and/or transport and transformation processes from the spring peak based on the climatology of the Arctic front [Li et al., 1993a], with the spring peak most likely owing to a combination of photochemistry and transport from mid-latitude source areas and the summer peak due to regional or high latitude northern ocean sources. This hypothesis may now be tested with the present results.

Both the spring and the summer peak MSA concentrations at Alert are lower than summer peak values from the eastern North Atlantic [Prospero and Savoie, 1990; Watts et al., 1990] by about one order of magnitude. The multi-year measurements at Mawson on the periphery of Antarctica [Prospero et al., 1991] show an austral summer peak of between 30-40 ng m^{-3}. The high Antarctica summer MSA concentration may be in part attributed to the higher DMS air concentrations over the Southern Ocean, as shown by a 3-D global circulation model [Langner and Rodhe, 1991], for which the austral summer DMS air concentration is about 50% higher than over the high latitude northern oceans in summer, and in part due to the relative distance of Alert and Mawson from open ocean waters.

An examination of the time series of the spring and summer

maximum MSA concentrations (Table 1) for the 11-year period shows that there is no relationship in time between the spring and the summer MSA maximum. Spring maximum MSA shows a significant year-to-year variation, changing by as much as 60%, and displays a cyclic pattern of 2 years (with the exception of 1986). In contrast, the summer maximum is relatively stable, with inter-year changes of less than 20% (exception 1985). In addition, there is no evidence of 2-year cycles in the summer maximum. This is a good indication that these two peaks are not related.

A further examination of the seasonality in MSA is given below. The mean MSA concentration for each month during the 11-year period was derived based on the original MSA data (Fig. 1a), enabling the calculation of the correlation matrix between the MSA monthly means in different months. The correlation coefficients with significance levels $p < 0.05$ are shown in Table 2. It shows that MSA means in the months of February, March, April, and May are intercorrelated (thus defining the spring maximum), but are not correlated with the monthly means of other months including June, suggesting that MSA in June is not part of the spring peak. July and August MSA means are correlated and define the summer peak. However, they are not correlated with the rest of the months including June, September, and October. The monthly means of MSA in September and October (and less significantly November) are intercorrelated and are also curiously correlated with those in January. Apparently, these results represent different time variation patterns and suggest different processes in controlling MSA in the Arctic troposphere.

To explain why the spring and summer peaks of MSA are not related we have to consider all of the processes that deliver this compound to Alert near the North Pole. These include the spatial and temporal distribution of DMS emissions, its transformation to MSA, transport from source areas to Alert, and removal by wet and dry deposition processes. It is our contention that the spring peak is caused by transport from oceanic sources in the North Atlantic and North Pacific and possibly accelerated DMS oxidation in the northern atmosphere as spring solar irradiation increases in intensity, while the summer peak is due to DMS from more local Arctic sources as well as from northern oceans.

There are several reasons for postulating this. First, during the spring peak, the Arctic is still quite frozen and DMS

production is rising in the northern oceans peripheral to the Arctic [Turner and Liss, 1985; Bates et al., 1987; Leck and Rodhe, 1991]. Second, in the Arctic air mass, the lifetime of aerosols is much longer in spring than in summer because precipitation is much higher then than at other times of year [Barrie, 1986]. Thirdly, algae blooms in open waters of the Arctic Ocean occurs in summer not in spring. Finally, south to north transport is stronger in spring than in summer as indicated by winter-spring maxima and summer minima in long-lived anthropogenic tracers such as Freon-22 and CH_3CCl_3 in the Arctic atmosphere [Khalil and Rasmussen, 1983].

This contention is supported by a study of origin of air on high MSA concentration weeks at Alert during the spring and summer peak periods in 1982 to 1987 using air parcel back trajectories and a technique developed by Zeng and Hopke [1989] and applied to the Arctic by Cheng et al. [1993]. It is called potential source contribution function analysis, which is essentially the spatial probability density function of air within five days upwind of Alert during days when air concentrations were higher than average divided by those on all days. The result is a pattern with high values indicating source regions or at least favored pathways. The distributions for spring and summer periods are shown in Figures 2a and 2b, respectively. The difference in the origin of air with elevated MSA concentrations is significant between the two periods even when the limitations of this technique associated wih uncertainties in trajectories are taken into account. In spring, air comes from much further south than in summer when local sources in the Arctic Ocean are indicated.

Marine Biogenic Contributions to the Aerosol Sulfate

Two approaches were taken involving: (i) an isotopic mass balance approach and (ii) a source apportionment technique, the absolute principal component analysis (APCA).

(i) Sulphur Isotope Approach

Sulfur isotopic composition of $SO_4^=$ is expressed as $\delta^{34}S$ which is the relative deviation of the ratio of ^{34}S to ^{32}S in sample $SO_4^=$ to that in a standard(Canyon Diablo) expressed in per mil units. The maximum values of $\delta^{34}S_T$ for total(T) aerosol $SO_4^=$ in summer at Alert are about 9.5‰ (Fig. 3), much less than that expected from marine biogenic $SO_4^=$ of 15-19‰ [Calhoun et al., 1991; Wagenbach, personal communication]. This indicates that marine emissions of

DMS are not the only sources of aerosol $SO_4^=$ at Alert in summer. In other words, the ratio MSA/biogenic $SO_4^=$ must be higher than MSA/nss$SO_4^=$ (0.20 in summer, see below). On the other hand, even in the winter-spring season when anthropogenic $SO_4^=$ dominates aerosol $SO_4^=$, on occasions $\delta^{34}S_T$ is much higher than 6.3‰ (which may be considered the upper limit for $\delta^{34}S_a$ from European sources [Nriagu et al., 1991]), suggesting that biogenic contribution may be significant. The isotopic composition $\delta^{34}S_T$ of aerosol $SO_4^=$ (Fig. 2) can be used to determine the fractions of $SO_4^=$ contributed by (i) anthropogenic $SO_4^=$ with a $\delta^{34}S_a$ of 3.8-6.3‰ [Nriagu et al., 1991] (f_a), (ii) sea salt $SO_4^=$ with a $\delta^{34}S_s$ of 21‰ (f_s), and (iii) biogenic MSA and $SO_4^=$ with a $\delta^{34}S_b$ of 15-19‰ (f_b). These provide enough input parameters for the determination of the individual fractions of $SO_4^=$ from each source using the three-source model for aerosol $SO_4^=$ at Alert expressed with the following equations:

The mass balance equation:

$$f_a + f_b + f_s = 1 \tag{1}$$

The sulfur isotope balance equation:

$$\delta^{34}S_T = f_a\,\delta^{34}S_a + f_b\,\delta^{34}S_b + f_s\,\delta^{34}S_s \tag{2}$$

The fraction of sea salt equation:

$$f_s = \left[\frac{SO_4^=}{Na^+}\right]_s \cdot \left[\frac{Na^+}{SO_4^=}\right]_T \tag{3}$$

The fraction of biogenic $SO_4^=$, f_b, is then given by:

$$f_b = \left[\frac{\delta^{34}S_T - \delta^{34}S_a - f_s\,(\delta^{34}S_a + \delta^{34}S_s)}{\delta^{34}S_b - \delta^{34}S_a}\right] \tag{4}$$

R is then:

$$R = \frac{MSA}{biogenic\ SO_4^=} = \left[\frac{MSA}{Total\ SO_4^=}\right] \cdot \frac{1}{f_b} \tag{5}$$

Using observed concentrations of MSA(Fig.1a), total $SO_4^=$(Fig 4a) , Na^+(Fig.4b) and the $\delta^{34}S$ values of sample, sea salt and biogenic $SO_4^=$, these equations can be solved for f_a as well as f_b or R. In order to assess the uncertainty in the estimates a Monte-Carlo solution of the equations was undertaken. Over 2000

solutions of the equations for R are run using values for input parameters taken from a normal distribution whose first moment represents the uncertainty in the input parameter. By choosing a subset of samples where the $\delta^{34}S_T$ values are greater than 6.5‰, we are assured of non-zero f_b values which can be used in Equation (5) to determine R. We applied the Monte-Carlo approach to determine the values for R for this subset of samples(Fig. 5a). It can be seen that for several of the months there are no $\delta^{34}S_T$ values >6.5‰(Fig. 3), and therefore no determination of R could be made with confidence. In June, August and September, the best estimate of R(the median) is 0.16, 0.6 and 0.21, respectively. The summer peak in this ratio is based on all samples, while the winter-spring ratios are from a subset of the monthly values corresponding to $\delta^{34}S_T$ > 6.5‰.

As shown next, the picture given above from the sulfur isotopic composition of aerosol $SO_4^=$ is in agreement with the results from the second approach, the multivariate statistical method of APCA. The high ratio for R(i.e.MSA/biogenic $SO_4^=$) in summer is about a factor of 3 higher than MSA/nss$SO_4^=$. Such high ratios have been reported in the austral summer from the Southern Ocean [Berresheim, 1987] and more recently by Savoie et al. [1992], where anthropogenic $SO_4^=$ is expected to be minimal. The high ratio of 0.6 for R suggests that DMS oxidation yields relatively high MSA in the high latitude northern marine troposphere.

(ii) R From Source Apportionment of $SO_4^=$ and MSA using APCA.

The second approach using the multivariate statistical technique of APCA [Thurston and Spengler, 1985] is based on the temporal correlation among measured chemical species. In an earlier study, the technique was applied to semi-daily measurements of aerosol chemistry at Barrow, Alaska in spring in an attempt to separate the contribution of pollutant nss$SO_4^=$ from that of marine biogenic origin [Li and Winchester, 1989], resulting in ratio of 0.06 for MSA/nss$SO_4^=$ in an aerosol component attributed to biogenic origin. The same approach is again applied here, using data for Cl^-, Br^-, NO_3^-, $SO_4^=$, H^+, Na^+, NH_4^+, K^+, MSA, Al, I, Ca, and Mg in the APCA for the whole 10-year period. Based on the criteria used in the previous studies [Li and Winchester, 1989; Barrie and Barrie, 1990] combined with the additional test to determine whether an eigenvalue is derived from a normally distributed random data

matrix [Preisendorfer, 1988].

APCA is applied to individual months, for which the number of available data ranges from 43 to 48. These APCA applications usually yield 4 similar components for a given month (but 5 components are necessary for March, August, September, and October). Monthly estimates of R from the APCA approach are plotted in Figure 5b. It should be emphasized that R values in winter-spring months are influenced by anthropogenic $SO_4^=$, they can only be regarded as the lower limit of R while in the summer months while in the summer months we feel they are less biased estimates of R. Median R is 0.17, 0.55 and 0.86 in June, July and August, respectively. Considering the uncertainty, they are consistent with results obtained based on the sulfur isotopic measurements which are 0.16 in June and 0.6 in August.

Based on isotopic mass balance(equation 4), it was also possible to estimate with some confidence the median fractional contribution of biogenic sources to total $SO_4^=$(f_b) for the months of June, August and September to be 35, 31 and 29%, respectively with 90% confidence limits of approximately 18 absolute percentage points(Fig. 6). In the same months, the median of the sea salt contribution(f_s) was 1, 8 and 5 % respectively(in the remainder of the year it was 1.8 to 6.6 %). Estimates of f_b in other months, are possible for only a small fraction of the time and are biased high because they are for situations when isotopic composition is closer to that of marine sulphate sources and therefore the fraction of anthropogenic sulphates are low. All that can be said is that for other times of year, based on isotopic data, f_b is <15%(Fig 6).

CONCLUSION

An 11.3 year record of MSA in aerosols at Alert Canada(82.5 N, 62.3 W) has been recovered from an archive of samples at the Atmospheric Environment Service that dates back to July 1980. Together with other chemical analyses done on the same samples previously for $SO_4^=$ and its sulphur isotopes, Na^+, and multiple elements the data has yielded the following insights into Arctic biogenic aerosol sulphur:

1. There is a distinct seasonal variation in MSA with two peaks one in spring(March to April) and one in summer(July-August). the first is likely related to long range transport of marine biogenic emissions from the north Atlantic ocean while the second is caused by emissions closer to Alert in the Arctic seas.
2. There is a significant long term decrease in this MSA record amounting to 26% in 11.3 years. It is apparent in both spring and summer peaks. Whether this decrease is real or an artifact of archive storage remains to be determined.
3. Based on sulphur isotopic data the biogenic component of total $SO_4^=$ can be determined with confidence for only the summer period. It is 29 to 35%. Sea salt contributes 5 to 8 % and the rest is anthropogenic. For the rest of the year, all that can be said is that DMS sources contribute < 15%, sea salt 2 to 7 % and anthropogenic the rest.
4. The ratio of MSA/biogenic $SO_4^=$ which is important in estimating biogenic $SO_4^=$ from MSA observations and insightful to DMS oxidation pathways has been estimated by two independent methods based on sulphur isotopes of $SO_4^=$ and on absolute principle component analysis to be in the range 0.2 to 0.9 in summer. Isotope data suggests that the ratio is lower at other times of year.

ACKNOWLEDGMENTS

The authors wish to thank Dr. M.-D. Cheng for running the PSCF analysis and Dr. J. Nriagu for the sulphur isotope data as well as the Atmospheric Environment Service of Environment Canada for financial support.

REFERENCES

Barrie, L.A., Arctic air pollution: an overview of current knowledge, *Atmos. Environ., 20,* 643-663, 1986.

Barrie, L.A., and R.M. Hoff, The oxidation rate and residence time of sulphur dioxide in the Arctic atmosphere, *Atmos. Environ., 18,* 2711-2722, 1984.

Barrie, L.A., G. den Hartog, J.W. Bottenheim, and S. Landsberger, Anthropogenic aerosols and gases in the lower troposphere at Alert Canada in April 1986, *J. Atmos. Chem., 9,* 101-127, 1989.

Barrie, L.A., and M.J. Barrie, Chemical components of lower tropospheric aerosols in the high Arctic: Six years of observations, *J. Atmos. Chem., 11,* 211-246, 1990.

Bates, T.S., J.D. Cline, R.H. Gammon, and S.R. Kelly-Hansen, Regional and seasonal variations in the flux of oceanic dimethylsulfide to the atmosphere, *J. Geophys. Res., 92,* 2930-2938, 1987.

Berresheim, H., Biogenic sulfur emissions from the subantarctic and Antarctic oceans, *J. Geophys. Res., 92,* 13,245-13,262, 1987.

Bates, T.S., B.K. Lamb, A. Guenther, J. Dignon, and R.E. Stoiber,Sulfur emissions to the atmosphere from natural sources, *J. Atmos. Chem., 14,* 315-337, 1992

Bürgermeister, S., R.L. Zimmermann, H.-W. Georgii, H.G. Bingemer, G.O. Kirst, M. Janssen, and W. Ernst, On the biogenic origin of dimethylsulfide: relation between chlorophyll, ATP, organismic DMSP, phytoplankton species, and DMS distribution in Atlantic surface water and atmosphere, *J. Geophys. Res., 95,* 20,607-20,615, 1990.

Calhoun, J.A., T.S. Bates, and R.J. Charlson, Sulfur isotope measurements of submicrometer sulfate aerosol particles over the Pacific Ocean, *Geophys. Res. Lett., 18,* 1877-1880, 1991.

Charlson, R.J., J.E. Lovelock, M.O. Andreae, and S.G. Warren, Oceanic phytoplankton, atmospheric sulphur, cloud albedo and climate: A geophysiological feedback, *Nature 326,* 655-661, 1987.

Charlson, R.J., J. Langner, H. Rodhe, C.B. Leovy, and S.G. Warren, Perturbation of the northern hemispheric radiative balance by backscattering from anthropogenic sulfate aerosols, *Tellus, 43B,* 152-163, 1991.

Charlson, R.J., S.E. Schwartz, J.M. Hales, R.D. Cess, J.A. Coakley Jr., J.E. Hansen, and J.D. Hofman, Climate forcing by anthropogenic aerosols, *Science, 255,* 423-430, 1992.

Cheng, M.-D., P.K. Hopke, L.A. Barrie, A. Rippe, M. Olson and S. Landsberger, Qualitative determination of source regions of long range transported aerosol using data collected in the Canadian high Arctic, *Environ. Sci. Tech.,* submitted 1993

Erickson, D.J., S.J. Ghan, and J.E. Penner, Global ocean-to-atmosphere dimethyl sulfide flux, *J. Geophys. Res., 95,* 7543-7552, 1990.

IMSL, *Reference Manual* to IMSL Library, Edition 9, IMSL Houston, TX, 1982

Khalil, M.A. K., and R.A. Rasmussen, Gaseous tracers of arctic haze, *Environ. Sci. Tech., 17,* 157-164, 1983.

Langner, J., and H. Rodhe, A global three-dimensional model of the tropospheric sulfur cycle, *J. Atmos. Chem., 13,* 225-263, 1991.

Leck, C., and H. Rodhe, Emissions of marine biogenic sulfur to the atmosphere over northern Europe, *J. Atmos. Chem., 12,* 63-86, 1991.

Li., S.-M. and L.A. Barrie, Biogenic sulphur aerosols in the Arctic troposphere: I. Contributions to total sulphate., *J. Geophys. Res.,* (submitted), 1993.

Li, S.-M., and J.W. Winchester, Geochemistry of organic and inorganic ions of late winter Arctic aerosols, *Atmos. Environ., 23,* 2401-2415, 1989.

Li, S.-M., R.W. Talbot, L.A. Barrie, R.C. Harriss, C.I. Davidson, and J.-L. Jaffrezo, Seasonal and geographic variations of methanesulfonic acid in the Arctic troposphere, *Atmos. Environ.* (in press), 1992.

Li, S-M., L.A. Barrie, and A. Sirois, Biogenic sulfur aerosols in the Arctic troposphere: II. Trends and seasonal variations, *J. Geophys. Res.,* (submitted), 1993.

Nriagu, J.O., R.D. Coker, and L.A. Barrie, Origin of sulphur in Canadian Arctic haze from isotope measurements, *Nature, 349,* 142-145, 1991.

Preisendorfer, R.W., *Principal Component Analysis in Meteorology and Oceanography,* Edited by C.E. Mobley, Developments in Atmospheric Science 17, Elsevier, New York, 1988.

Prospero, J.M., and D.L, Savoie, Temporal and spatial variations of methanesulfonate concentrations and assessments of the impact of the biogenic source on non-sea-salt sulfate over the North Atlantic Ocean, *EOS Trans. AGU., 71,* 1234, 1990.

Prospero, J.M., D.L. Savoie, E.S. Saltzman, and R. Larsen, Impact of oceanic sources of biogenic sulphur on sulphate aerosol concentrations at Mawson, Antarctica, *Nature, 350,* 221-223, 1991.

Savoie, D.L., J.M. Prospero, R.J. Larsen, H. Fen, M. Izaguirre, H. Tao, and T. Snowdon, Nitrogen and sulfur species in Antarctic aerosols at Mawson, Palmer Station, and Marsh (King George Island), *J. Atmos. Chem.,* (in press), 1992.

Shaw, G.E., Aerosols as climate regulators: a climate-biosphere linkage?, *Atmos. Environ. 21,* 985-986, 1987.

Tarrason, L., Biogenic sulphur emissions from the North Atlantic Ocean, EMEP/MSC-W Note 3/91, Meteorological Synthesizing Centre-West, The Norwegian Meteorological Institute, Oslo, Norway, 1991.

Thurston, G.D. and J.D. Spengler, A quantitative assessment of source contributions to inhalable particulate matter pollution in metropolitan Boston, *Atmos. Environ., 19,* 9-25, 1985.

Turner, S.M., and P. S. Liss, Measurements of various sulphur gases in a coastal marine environment, *J. Atmos. Chem., 2,* 223-232, 1985.

Watts, S.F., P. Brimblecombe, and A.J. Watson, Methanesulfonic acid, dimethyl sulphoxide, and dimethyl sulfone in aerosols,

Atmos. Environ., 24A, 353-359, 1990.

Zeng, Y., and P.K. Hopke, A study of the sources of acid precipitation in Ontario, Canada, *Atmos. Environ., 23,* 1499-1509, 1989.

Table 1. Characteristics of the MSA concentration of seasonal peaks. Maximum concentrations in ng m^{-3}.

	Spring Peak		Summer Peak	
	Max. Conc.	Week	Max. Conc.	Week
1980			11.8	29
1981	16.2	19	13.4	31
1982	25.2	16	12.8	31
1983	16.6	18	9.6	35
1984	24.5	17	12.4	32
1985	14.6	18	20.4	28
1986	13.8	18	12.7	35
1987	23.1	19	8.4	36
1988	16.6	24	9.6	29
1989	18.8	18	6.8	31
1990	13.9	18	10.9	32
1991	12.9	22	10.6	30

Table 2. Correlation matrix among the different MSA monthly means of year. Only correlation coefficients with significance level $p < 0.05$ are shown.

	Jan	Feb	Mar	Apr	May	Jun	Jul	Aug	Sep	Oct	Nov	Dec
Jan	1.0											
Feb		1.0										
Mar		0.77	1.0									
Apr		0.53	0.52	1.0								
May				0.81	1.0							
Jun		-0.61			1.0							
Jul							1.0					
Aug							0.63	1.0				
Sep	0.71								1.0			
Oct	0.71								0.73	1.0		
Nov	0.63										1.0	
Dec											0.6	0.8

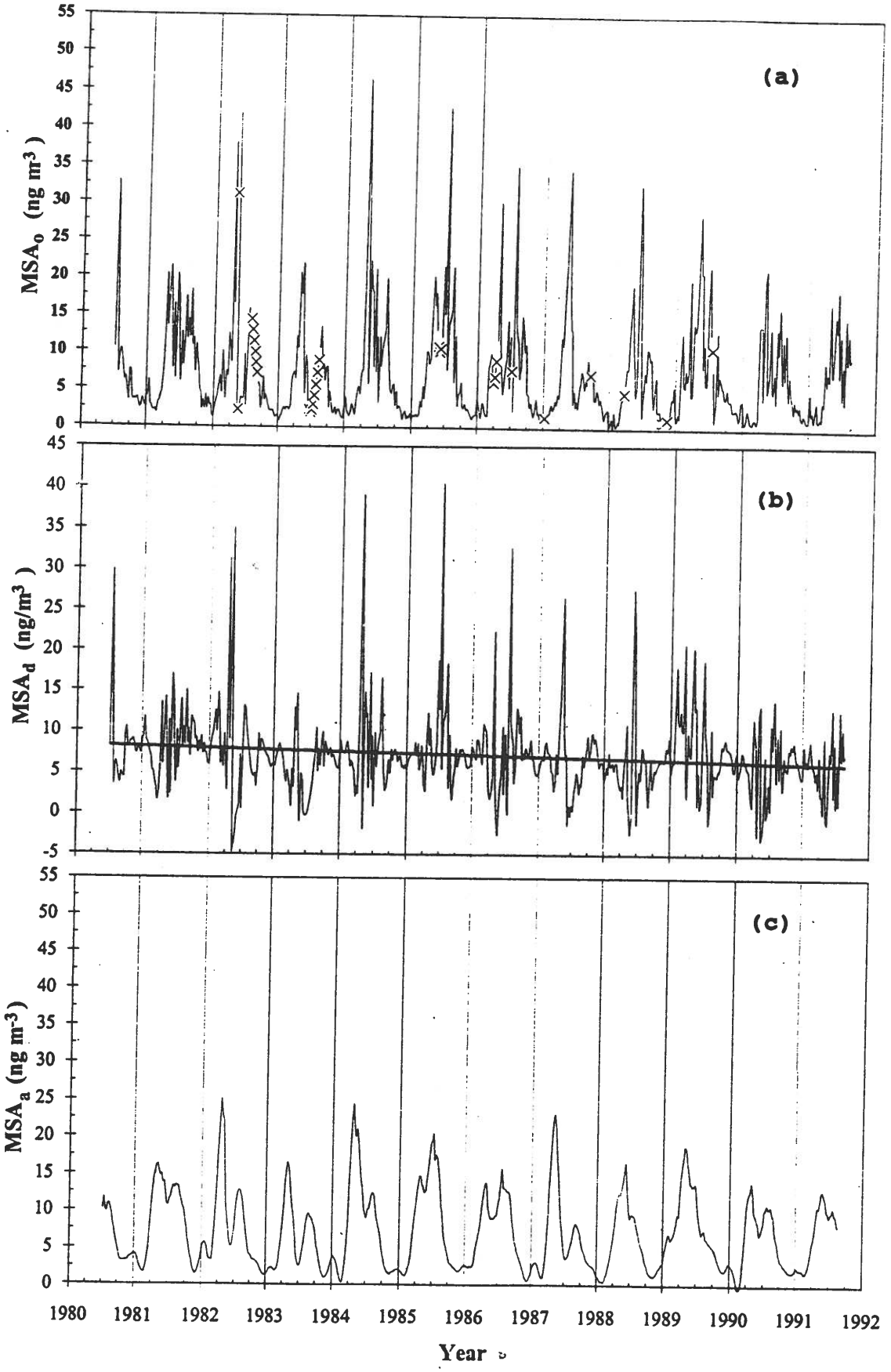

Figure 1.

Time series of: a) weekly average observed MSA data with interpolated data marked as "x" b) the data in a) de-seasonalized using spectral analysis techniques to emphasis long term variations and fitted with a linear regression line and c) the data in a) detrended and smoothed to emphasis the seasonal variations.

(a)

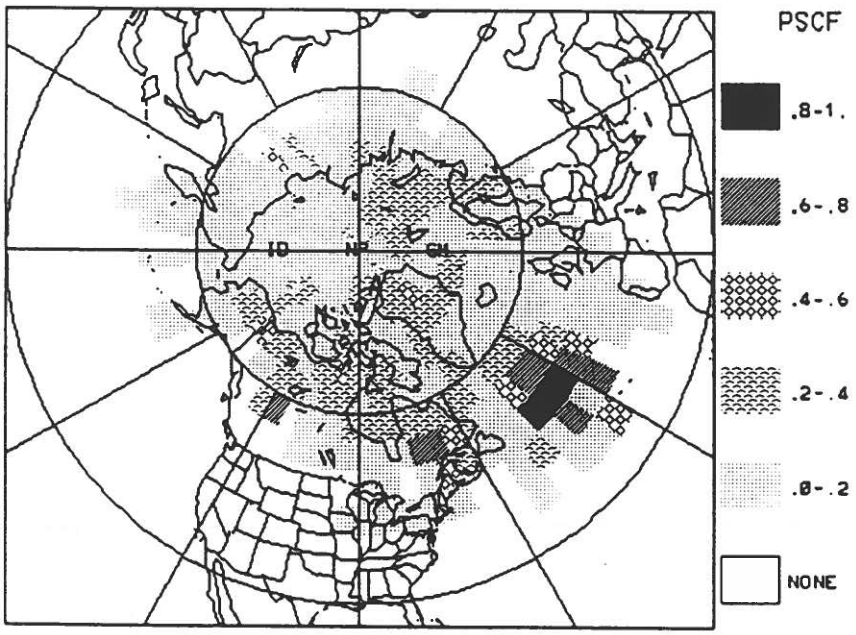

MSA April-May (C=10) 3L

(b)

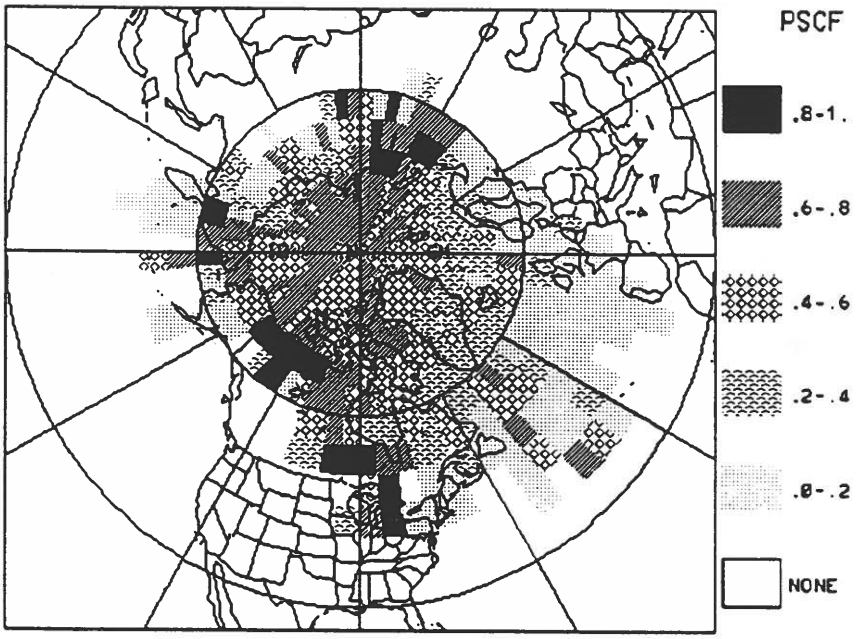

MSA July-August (C=10) 3L

Figure 2.
Potential source contribution analyses(see text) for the spring(a) and summer(b) periods for MSA showing the origin of air on weeks with exceptionally high MSA data.

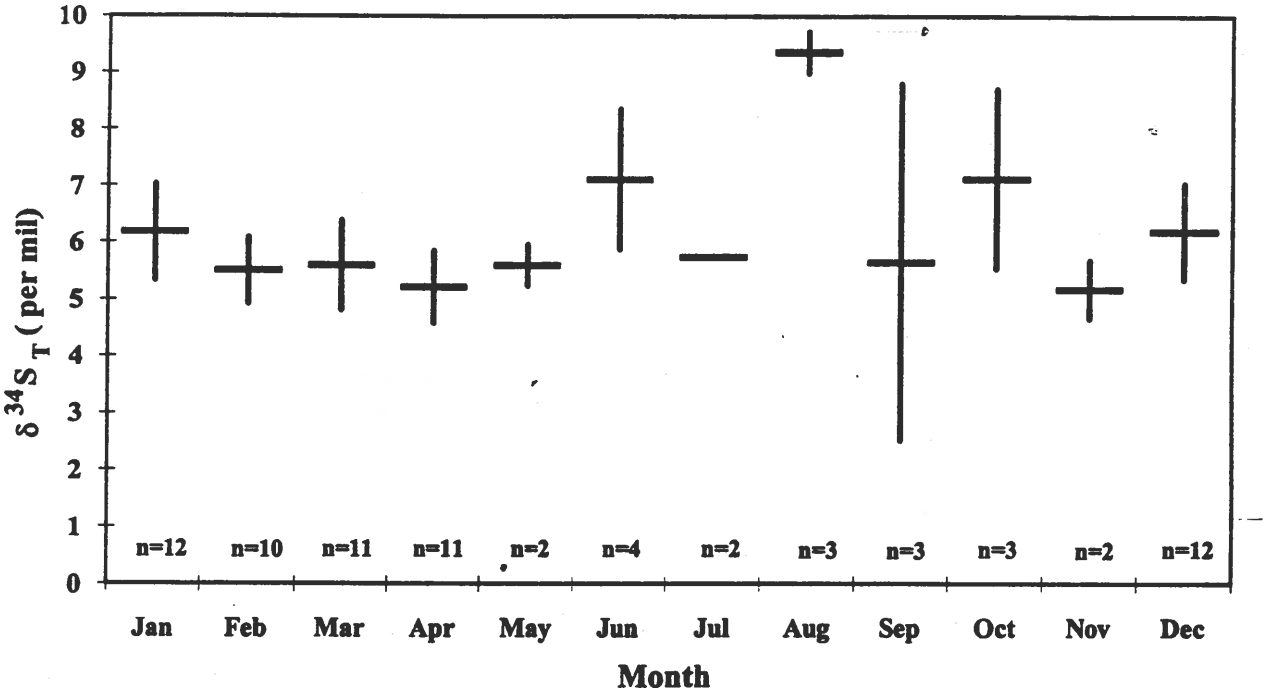

Figure 3.
Seasonal variations of $\delta^{34}S$ at Alert. Horizontal bars represent mean, vertical bars represent 1 standard deviation. Numbers of data points are indicated for each month. Data from Nriagu et al. [1991].

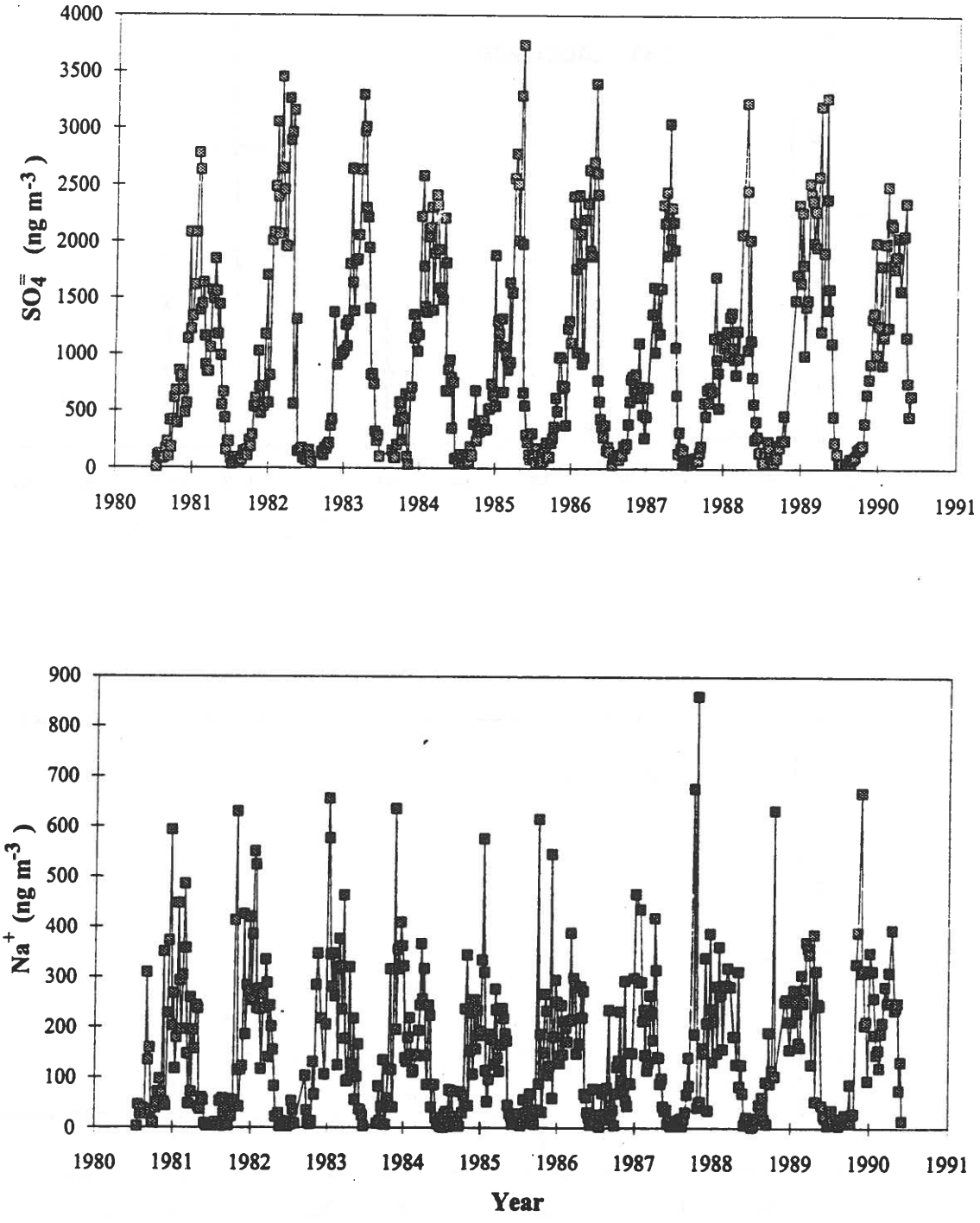

Figure 4.
Time series of weekly average observed $SO_4^=$ and Na^+ at Alert for the same samples as MSA in Fig. 1a.

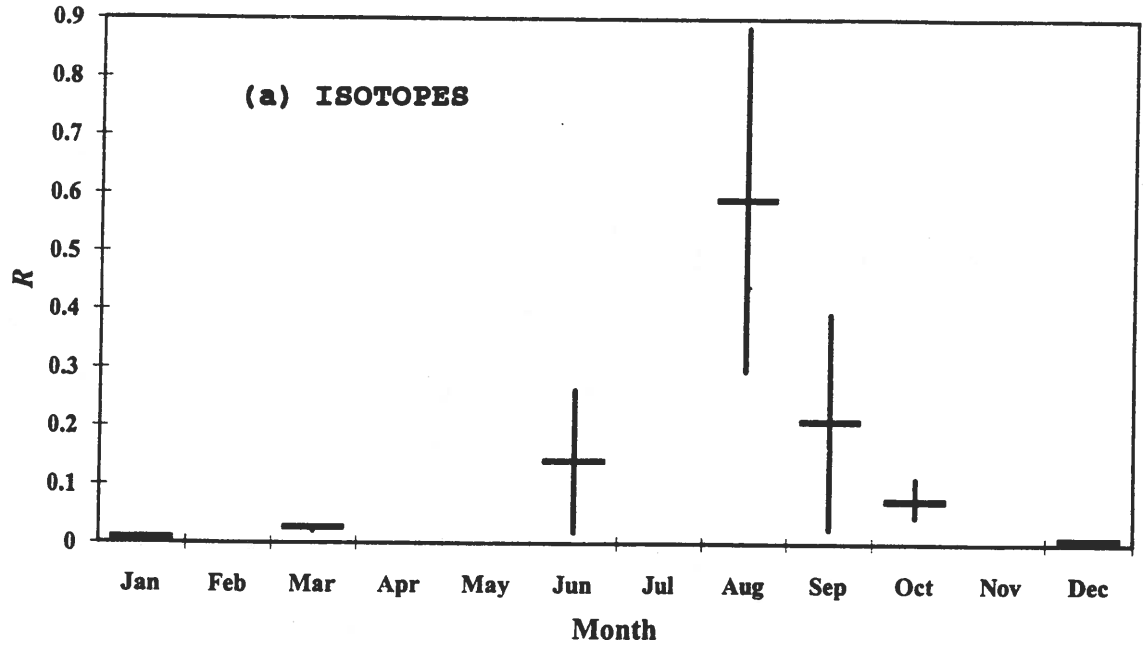

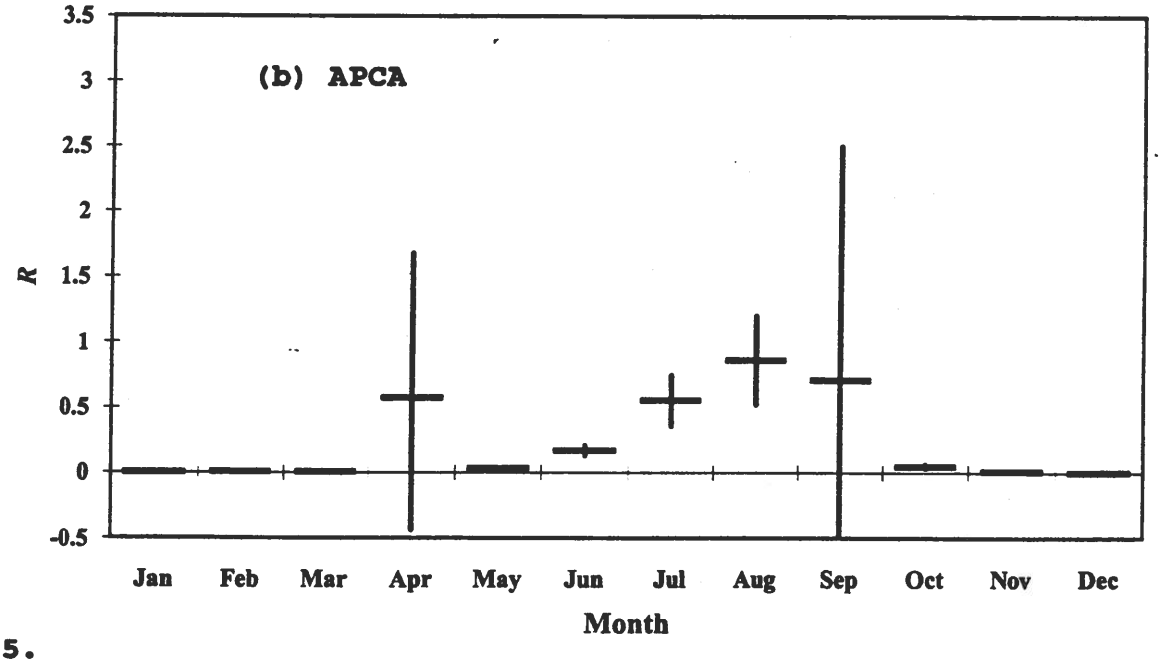

Figure 5.
(a) MSA/biogenic $SO_4^=$ ratios(R) from the sulfur isotope measurements with $\delta^{34}S_T$ >6.5‰ for each month. Medians with 90% confidence limits determined by Monte Carlo error propagation are shown. (b) MSA/$SO_4^=$ mass ratios for the APCA biogenic components as function of month. Note that only the ratios for summer months from June to August are deemed good estimates of the MSA/biogenic $SO_4^=$ ratio (see text). Horizontal bars represent mean, vertical bars represent 1 standard deviation.

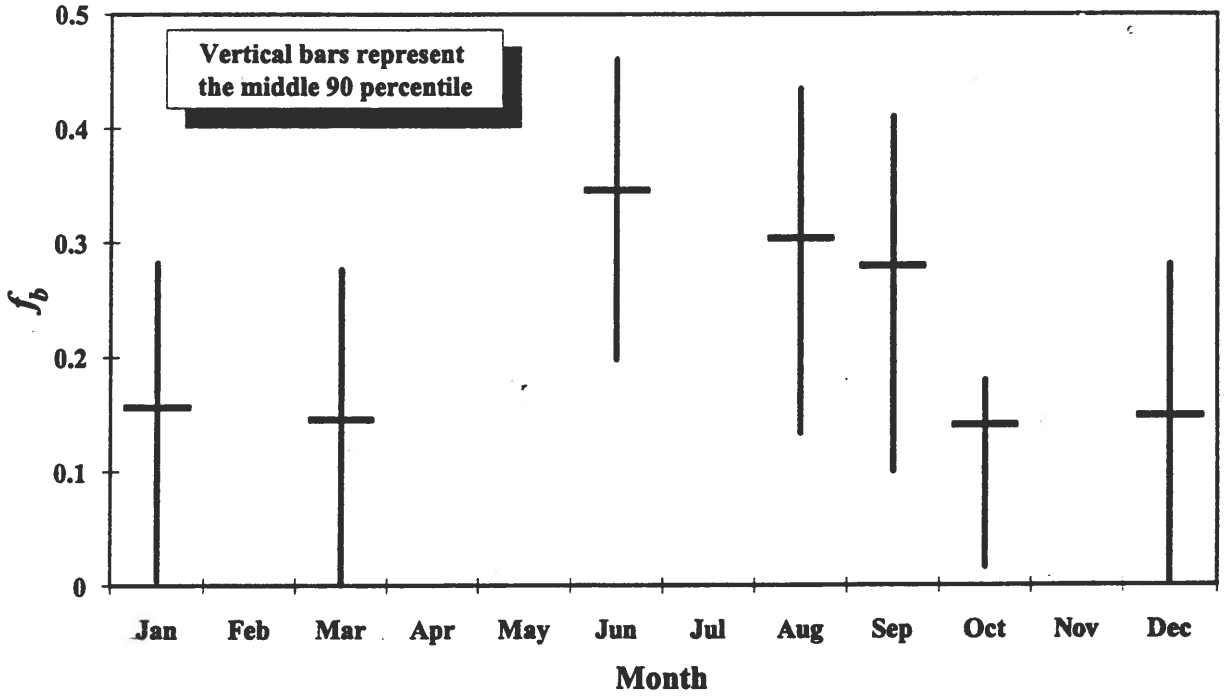

Figure 6.

The fractional contribution f_b to aerosol sulfate from biogenic sources determined from sulphur isotope measurements with $\delta^{34}S_T > 6.5$. Medians with 90% confidence limits determined by Monte Carlo error propagation are shown. This corresponds to data in Fig. 5a. Data in winter are for only a small fraction of the samples and therefore are biased high(see text). In contrast estimates from June to September represent most of the samples and are therefore representative.

Revisiting the Cold Condensation Effect

F. Wania and D. Mackay
Department of Chemical Engineering and Applied Chemistry, University of Toronto
Toronto, Ontario, Canada M5S 1A4

Introduction

The widespread occurrence of organochlorines (OCs) such as the PCBs and the organochlorinated pesticides in the Arctic has become a major concern in the late 1980s and early 1990s. But as early as the Second Arctic Air Chemistry Symposium in 1980, B. Ottar had speculated on the nature of the transport of these chemicals into the remote northern regions (1). Now after a decade of measuring OC concentrations in Arctic air, vegetation and wildlife it is worth taking a closer look at these speculations.

Ottar stressed that the OCs, unlike the sulphur and nitrogen pollution, can be re-emitted or evaporated after being deposited to the ground. Because rates of deposition and re-emission are controlled by temperature, he suggested "a systematic transfer of the more persistent compounds from warmer to colder regions"(1). With respect to the time span of this process he speculated that "no equilibrium has probably yet been established between prevailing air concentrations and the amounts deposited in the environment. In the long term this may lead to an accumulation of these substances in the temperate and Arctic regions"(1). This effect of emission and evaporation in warm areas, repeated cycles of atmospheric transfer, deposition and re-emission, and final deposition in cold areas, has since been termed the "cold finger" (2), "cold trap" (3), "cold condensation effect" or "global distillation" (4).

In the same paper, Ottar indicated that "a study of this effect will require a dispersion model which takes into account variations of the deposition and re-emission rates" (1). We are currently attempting to develop such a model of pollutant distribution and in this paper we present a short account of some of its features. Some preliminary results will be discussed and compared with measured environmental distributions.

Description of Global Distribution Model

The model is a global, meridional box model based on previous multimedia models of pollutant fate in the environment (5). These describe the environmental behaviour of a chemical in terms of its partitioning characteristics between separate environmental phases such as water and sediment. These compartments are considered well-mixed and homogeneous and only the transport processes between compartments have to be taken into consideration.

The basic building block of the global distribution model is a four media "unit world" environment featuring an air, soil, water and sediment compartment. The model allows chemical transformations in each of the phases, emission of chemical into each compartment and exchange of chemical between them by means of various intermedia transfer processes (5, 6). Several of these unit world environments can be connected by defining advective exchange rates between

them (7).

Following Troll (8) we divided the earth into nine climatic zones: N-polar, N-boreal, N-temperate, N-subtropic, N-tropic, S-tropic, S-subtropic, S-temperate, and S-polar. Each zone is represented by a "unit world" type environment. These building blocks are arranged sequentially from pole to pole and interconnected through atmospheric exchange (Figure 1).

For each of the 36 compartments (9 climate zones x 4 media) a chemical mass balance equation can be formulated. The mass balances are expressed in terms of fugacity (5). In the case of a steady-state assumption, the resulting system of linear equations can be solved algebraically. If concentration change in time is allowed, the system of differential equations has to be solved numerically with a finite difference iteration.

The required chemical property data are molecular weight, melting point, vapour pressure, water solubility, octanol-water partitioning coefficient K_{ow} and reaction half lives in each of the compartments. The points and the quantities of release of the chemical into the global environment also have to be specified. Because vapour pressure and, to a smaller degree, solubility and K_{ow} are functions of temperature, these properties have to be supplied for each climate zone separately. The same applies to the reaction half lives, which are strongly influenced by climatic parameters.

The parameters required to describe the environment in the nine climate zones are listed in Table 1. The areas and the land-ocean distribution in the zones were calculated from Troll's map (8). Following Czeplak and Junge (9) the height of the tropopause, which constitutes the upper limit of the air compartments, is assumed to increase from 8 to 10 km for φ=90° to φ>30° and to be constant at 16 km for latitudes smaller than 30°.

The advective atmospheric exchange rates between the climate zones were estimated from latitude-dependent horizontal eddy diffusion coefficients K reported by Czeplak and Junge (9) and Keeling and Heimann (10), which are based on the variance of the meridional wind component. Values for K were estimated for the average latitudes separating two neighbouring climate zones. An average advective exchange rate G in m^3/s was then estimated by:

$$G=\frac{K \cdot A}{\Delta x}$$

with Δx being the average distance between two climate zones calculated as the distance between the average latitudes of these zones at sea level in m. A is the area of tropospheric exchange between the zones and is estimated by $\pi \cos\varphi \cdot h \cdot (2R+h)$. h is the height of the tropopause at the latitude separating the two climate zones and R is the radius of the earth.

During the current stage of model development, all other environmental input parameters such as organic carbon content or mass transfer coefficients are either given a generic value (6) or we guessed a reasonable value.

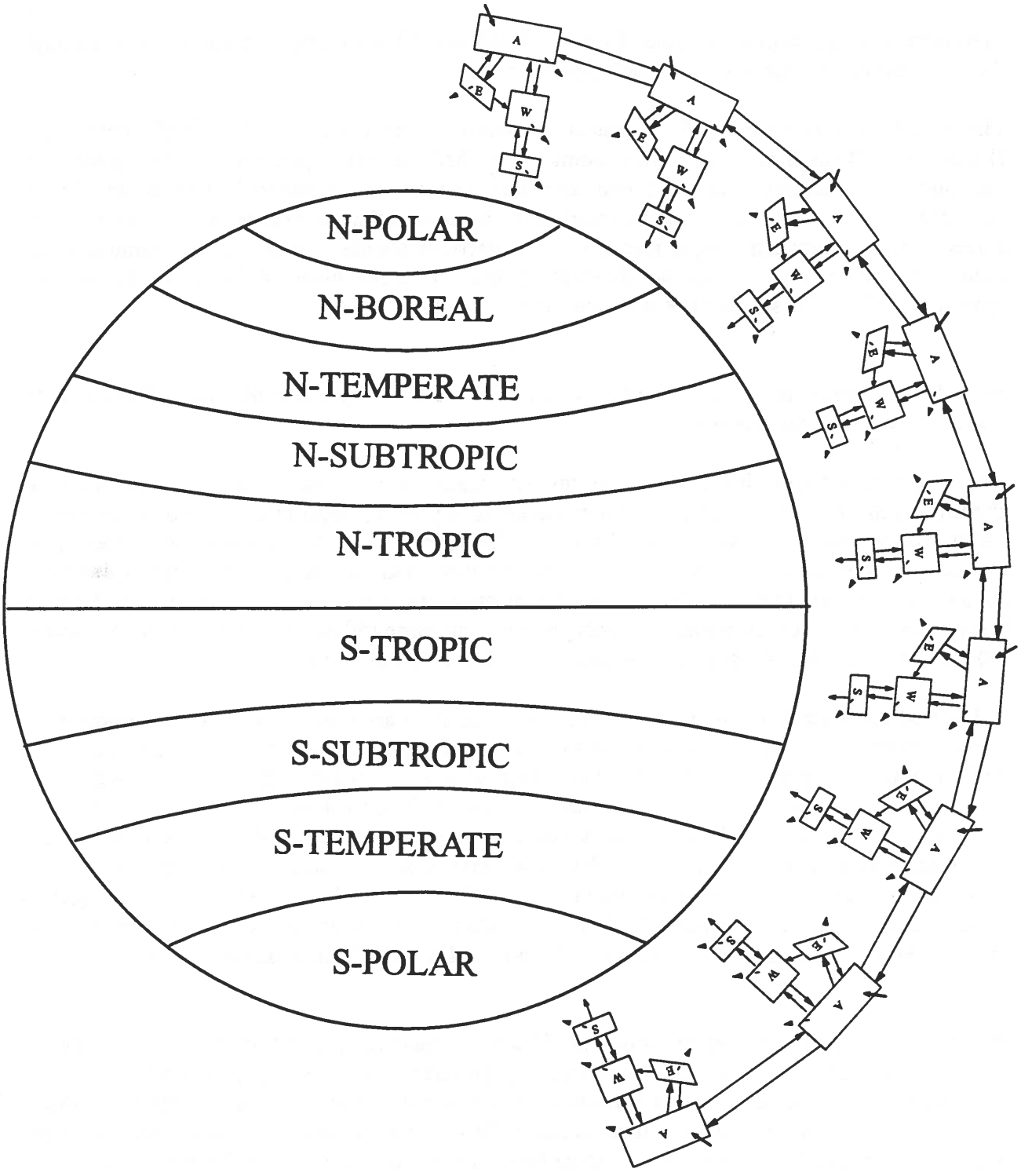

Figure 1: Schematic diagram of the global distribution model. Nine climate zones are represented by well-mixed 4-compartment units (A=Air, W=Water, E=Soil, S=Sediment), which are arranged sequentially and are interconnected by atmospheric air exchange.

The model is programmed in Visual Basic for Windows, allows interactive input of data through the user and can be run on a personal computer.

The model provides estimates for chemical concentration in air, water, soil and sediment in each climate zone. By assuming equilibrium being established between vegetation and air and between fish and water, estimates of biota concentrations can also be calculated. The model further provides rates for all transport and transformation processes, the percentage distribution between zones as well as between compartments and characteristic residence times of the chemical in the various climate zones. The non-steady state calculation further gives an indication of the time span required for the steady-state situation to be established.

Model Calculation for Hexachlorobenzene (HCB) and Comparison of Model Results with Environmental Measurements

We performed some preliminary calculations with hexachlorobenzene. How much and where the chemical is introduced into the global environment is of primary importance for the model results. Little information, however is available on the loadings of organochlorines. Often only approximate production estimates are available and little is known of the percentage which finds its way into the environment. We assumed that on average there occurs a release of 80 kg/h (i.e.approx. 700 t/a) of HCB into the northern temperate zone (50kg/h into air, 20kg/h into water, 10kg/h into soil). All other zones are assumed to have no direct emissions.

Calculated concentrations in air, water, fish and vegetation are compared with measurements in Arctic locations in Table 2. The agreement is very good in the case of air and fish concentrations, while the model appears to overestimate concentrations in water and vegetation. Figure 2 shows a mass balance diagram for the N-polar environment with the calculated steady-state transport and transformation rates. The model thus estimates a net transport of 44 tons per year into the Arctic environment. The calculated net deposition rate of approximately 15.4 $ng/m^2/a$ is close to previous estimates by Cotham et al. and Gregor, which were 56.7 $ng/m^2/a$ (11) and <10 $ng/m^2/a$ (12). Our model may overestimate the deposition into the water compartment, because it does not take into account the Arctic sea ice cover, which impedes the diffusive exchange between air and ocean.

Figure 3 shows the calculated latitudinal profiles of the relative distribution of HCB between the various media. The data illustrate how warm temperatures favour evaporation into the air-phase and cold temperatures result in condensation. While in the Tropics most of the HCB partitions into the air phase, in the colder climate zones HCB is mostly found in the water and sediment phase. The percentage in air decreases from 66% in the tropical to 3% in the polar zones.

Latitudinal profiles of HCB concentration in air, fish and leaves as calculated by the model are depicted in Figure 4. Measured environmental concentrations are superimposed. The air concentrations are relatively uniform in the three northernmost climate zones and steadily decline towards the South with a particularly sharp drop across the equator. Concentrations in the northern hemisphere are approximately four times higher than in the South. Although data on HCB concentration in air are limited, particularly for locations outside the northern temperate

dimensions	**intermedia transport parameters** in m/h
area	air-water mass transfer coefficient, air side
water coverage	air-water mass transfer coefficient, water side
height of atmosphere	rain rate
water depth	aerosol deposition rate
soil depth	soil-air phase diffusion mass transfer coefficient
sediment depth	soil-water phase transport mass transfer coefficient
volume fractions	soil-air boundary layer mass transfer coefficient
aerosols in air	sediment-water mass transfer coefficient
suspended solids in water	sediment deposition rate
water in soil	sediment resuspension rate
air in soil	soil-water run-off rate
water in sediment	soil-solids run-off rate
	sediment burial rate
organic carbon content in g/g	
in soil solids	**interzonal transport parameters** in m^3/h
in sediment solids	atmospheric exchange rate
in suspended solids	

Table 1: Required environmental input parameters. With the exception of the interzonal exchange rates the parameters have to be specified for each zone.

	Calculated	Measured	Location	Reference
Air	126 pg/m³	173 pg/m³	Ny Ålesund, Summer 1984	23
		153 pg/m³	Alert , Winter 1988	22
		210 pg/m³	Bering/Chukchi Sea, Summer 1988	21
Water	115 pg/L	105 pg/L	Lake Hazen, 1989	12
		28 pg/L	sea water at Ice Island, Summer 1986	20
"Fish"	2 ng/g wet	3 ng/g w.	Arctic cod muscle, Lancaster Sound 1984	26
	35 ng/g lipid	42.7 ng/g l.	Burbot liver, Mackenzie River, 1985+1986	14
		62-120 ng/g l.	Amphipods, Ice Island,Summers 1986 +1987	20
"Leaves"	5.4 ng/g dry	1 ng/g d.	lichens, mosses, Spitsbergen, 1985-88	13

Table 2: Comparison of calculated and measured HCB concentration levels in the northern polar zone.

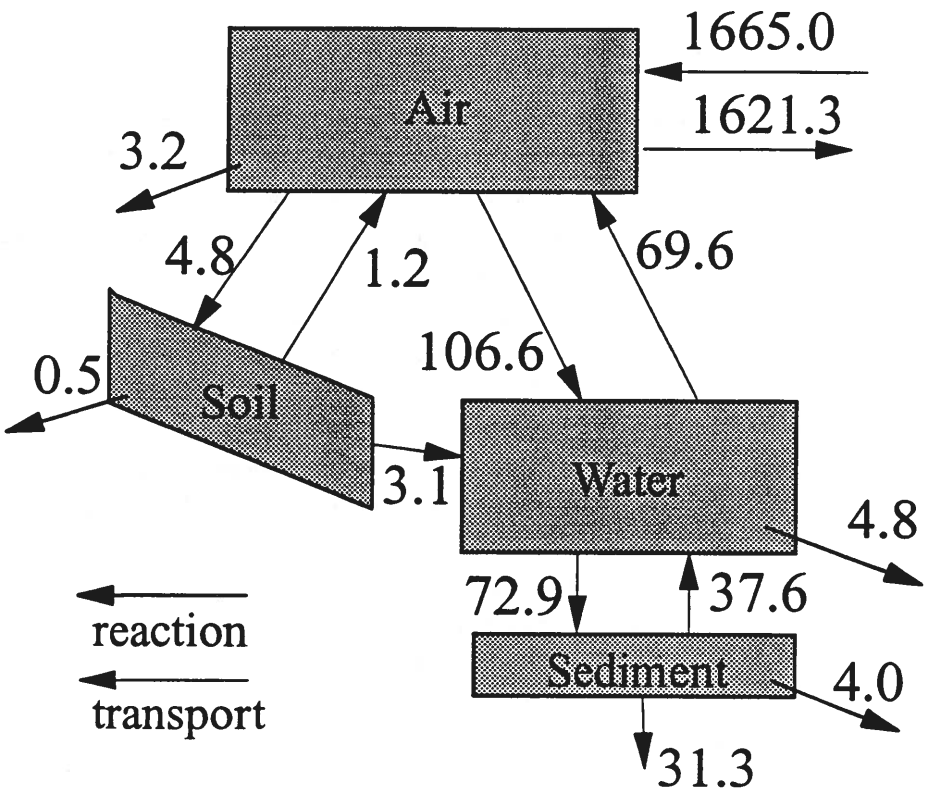

Figure 2: Mass balance diagram for HCB in the N-Polar climate zone at steady-state. Transport and transformation rates are given in t/a.

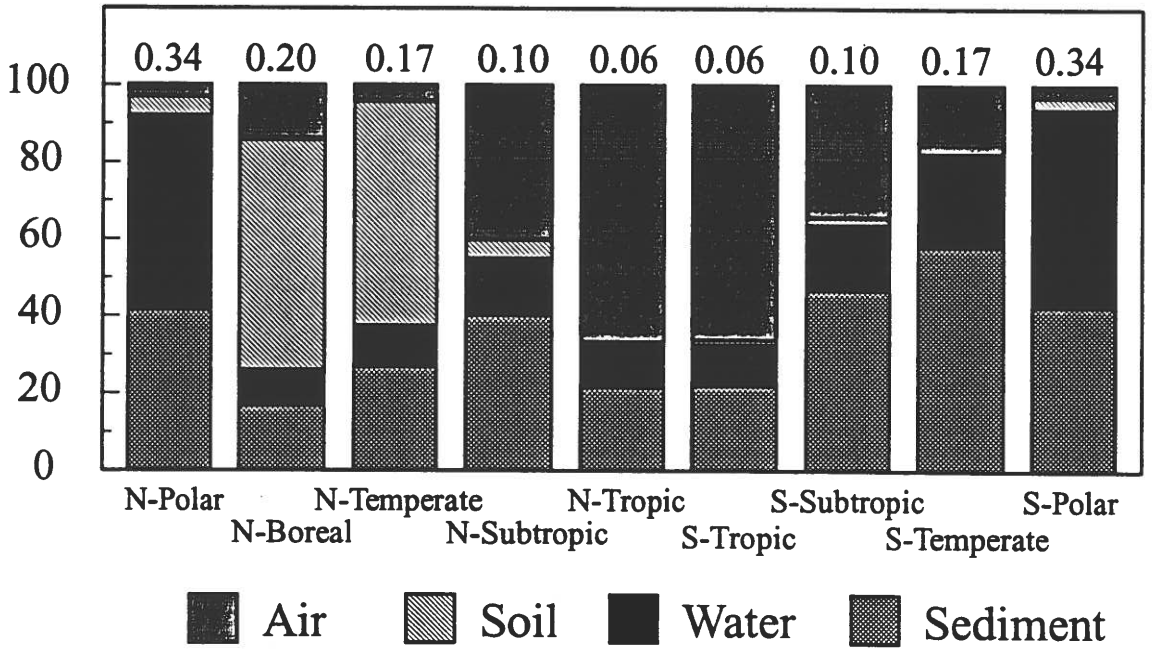

Figure 3: Percentage distribution of HCB between the four compartments at steady-state. The numbers above the bars give the percentage of HCB in air which is adsorbed to aerosols.

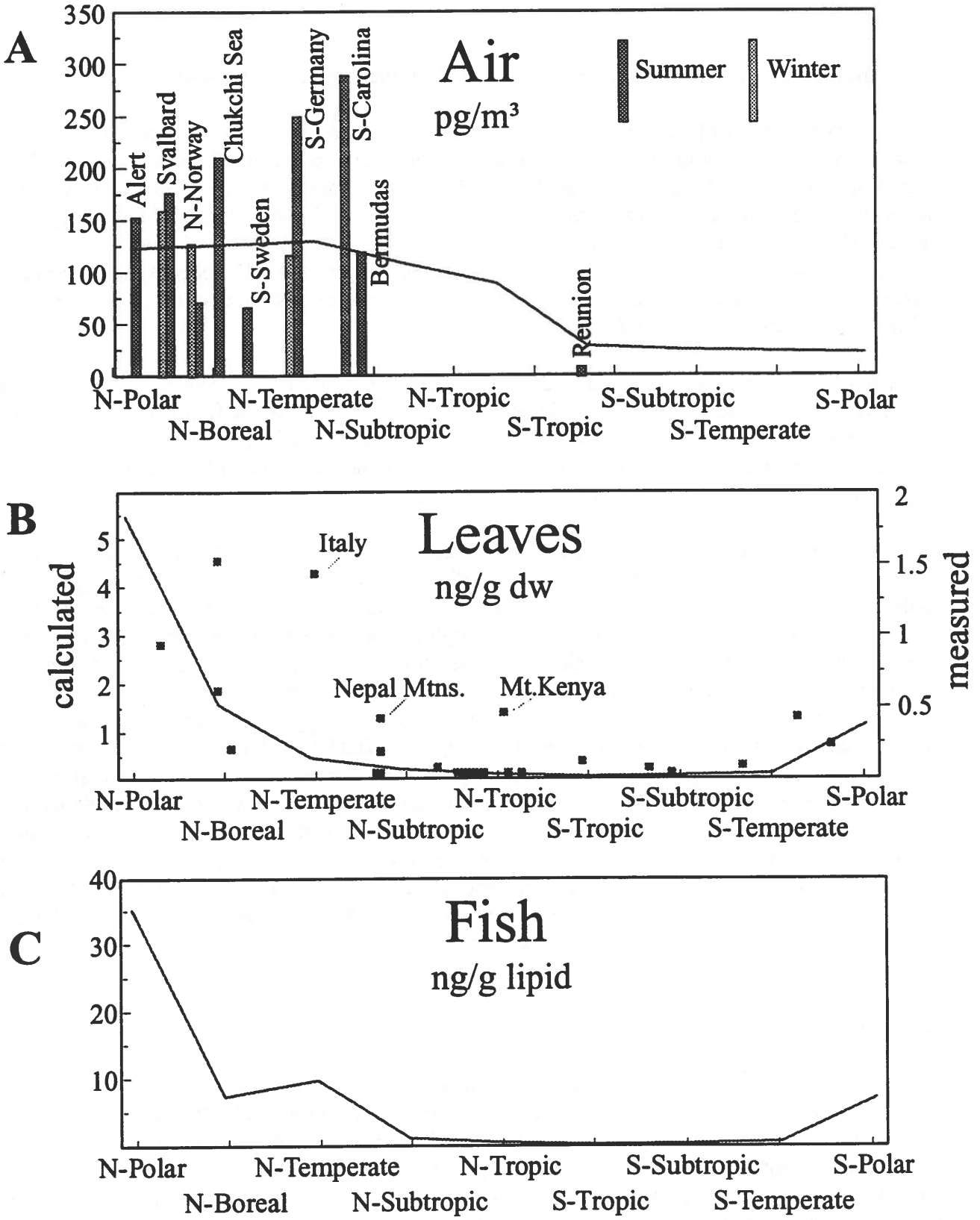

Figure 4: Latitudinal profiles of HCB concentrations in air, leaves and fish calculated for a steady-state situation , where all emission occurs into the northern temperate zone. The model results (lines) are compared with measured environmental concentrations (bars and points). Data taken from references 13, 17-19 and 21-25.

zone, they generally confirm the profile suggested by the model (Figure 4A).

The concentration profiles for leaves and fish are very different showing elevated levels in both polar environments, although the effect is much more pronounced in the northern hemisphere Figure 4B and 4C). The calculated profile for leaf concentrations matches very well with the HCB concentration pattern measured on plant leaves by Calamari et al. (13), although the measured concentrations are generally lower (Figure 4B). Latitudinal profiles of fish concentrations are rare. Burbot liver showed no clear trend of HCB concentrations along a latitudinal gradient across Canada (14), but all the sample locations were in the boreal zone and climate differences were limited.

Results of the non-steady-state calculation are depicted in Figure 5. These graphs give an indication of the time frame of the cold condensation effect. While HCB concentrations in air attain the steady-state concentrations relatively rapidly after a couple of years, the concentration increase is considerably delayed in water, fish and sediments of the polar zones. The model suggests that it takes several decades before steady-state levels are approached.

We have not yet calculated in detail the global distribution behaviour for chemicals other than HCB. Preliminary results of simulations with DDT, however, indicate that different OCs show different behaviour. Figure 6 shows the latitudinal dependence of air, leaf and fish concentrations for DDT, when the emission occurs into both tropical and the northern temperate climate zone. The air concentrations show a maximum in the tropical zone and decreasing concentrations towards the poles, while leaf concentrations show preferential condensation and accumulation in the northern boreal zone. The non-steady state calculation suggests that the time required to achieve steady state concentrations takes even longer for DDT than for HCB. This again agrees with earlier assertions by Ottar, that "depending on vapour pressure, ambient temperature and surface properties, an equilibrium will tend to be established between air concentrations and amounts adsorbed to the different surfaces. On this basis one would expect the more volatile substances to arrive first, while the least volatile substances may never reach the Arctic in appreciable amounts" (15). These differences between the condensation behaviour of various OCs may result in a process of global fractionation in which compounds become latitudinally fractionated, condensing at different temperatures dependent on their volatility (27).

Conclusion and Prospects

We believe that model calculations such as that described above can contribute to the simulation, understanding and interpretation of global chemical distribution patterns observed in the environment. The presented preliminary results of model calculations for HCB give further support to the hypothesis of a global distillation/cold condensation effect for organic compounds of low volatility. Reversed concentration profiles with latitude, i.e. increasing concentrations towards more northern, remote locations as observed e.g. for HCB on lichens (13), hexachlorocyclohexane (HCHs), pentachlorophenol and HCB on European pine needles (16) and HCB and HCHs in seals (27) can thus be explained. It also helps to explain "higher than expected" levels of the less volatile substances such as DDT and PCBs in remote polar ecosystems.

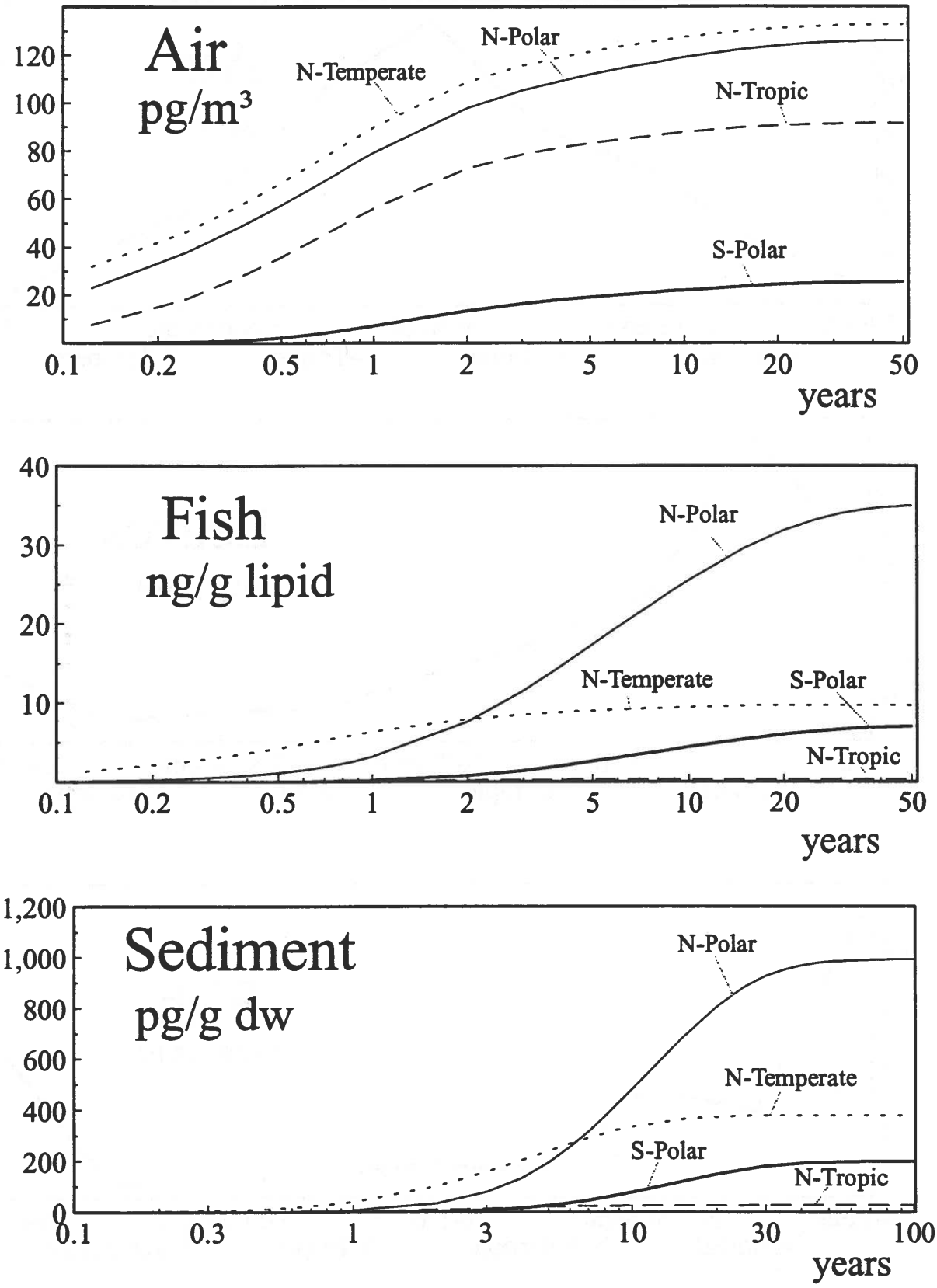

Figure 5: Increase of HCB concentrations in air, fish and sediment of four selected climate zones as calculated by the global distribution model. Emission occurs only into the nortern temperate zone.

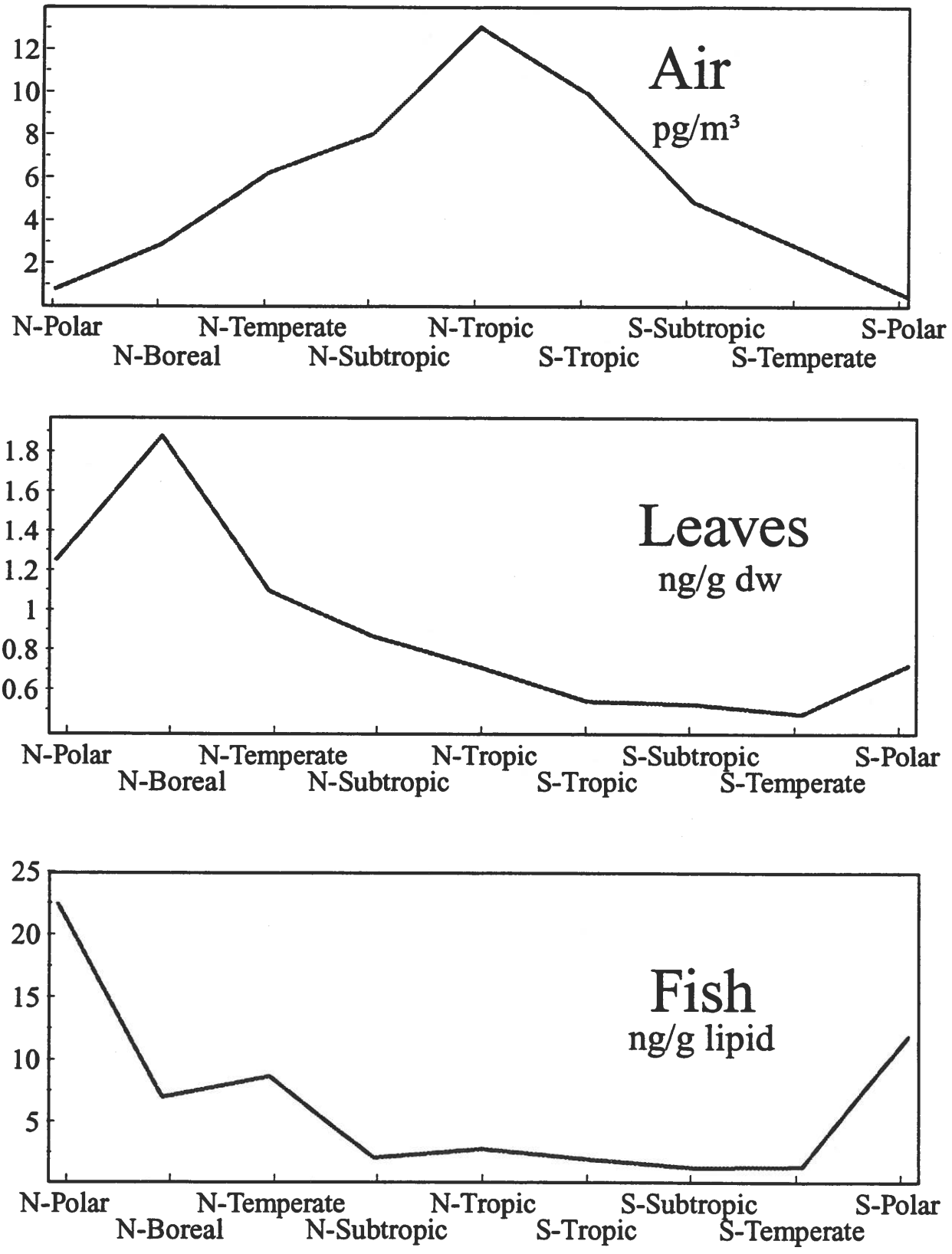

Figure 6: Latitudinal profiles of DDT concentrations in air, leaves and fish calculated for a steady-state situation, where discharge into the environment occurs in both tropical zones and the northern temperate zone.

We are planning to further develop this global distribution model. In particular the environmental input parameters and the identification of emission amounts requires considerable refinement. A major shortcoming of the model is the failure to include a snow and ice compartment, which should have a major impact on the environmental fate in polar regions. WE believe that high priority must be given to measuring air-snow equilibrium both in the atmosphere during snow-fall and on the ground when there is a possibility of evaporation from the fallen snow. It may also be necessary to allow for seasonal fluctuation of environmental parameters such as temperature and meridional air exchange.

A valuable feature of the model is that it becomes possible to run it with various temperature gradients from the equator to the poles, including the hypothetical case of an isothermal atmosphere. This enables the effect of temperature alone to be quantified, i.e. separated from other factors such as differences in environmental areas, volumes and precipitation characteristics. Obviously, what is needed are parallel efforts to measure environmental concentrations in a variety of media, determine the relevant environmental parameters and physical chemical properties of the chemicals of concern and synthesize these data into mass balance models. In this way a true picture of the nature of the cold condensation effect will become clearer. The results to date of our admittedly simplistic model indicates that Ottar's speculations were insightful and correct.

References

1. Ottar, B. 1981. The transfer of airborne pollutants to the Arctic region. *Atmos. Environ. 15*, 1439-1445.
2. Weschler, C. J. 1981. Identification of selected organics in Arctic aerosol. *Atmos. Environ. 15*, 1365-1369.
3. Rahn, K. A. and Heidam, N. 1981. Progress in Arctic air chemistry, 1977-1980: a comparison of the first and second symposia. *Atmospheric Environment 15*, 1345-1348.
4. Goldberg, E. 1975. Synthetic organohalides in the sea. *Proc. R. Soc. Lond. B 189*, 277-289.
5. Mackay, D. 1991. *Multimedia Environmental Models: The Fugacity Approach*, Lewis Publ., Chelsea, MI.
6. Mackay, D., Paterson, S. and Shiu, W. Y. 1992. Generic Models for Evaluating the Regional Fate of Chemicals. *Chemosphere* 24, 695-717
7. Wania, F. and Mackay, D. 1991. Temperature and the global distribution of low volatile organic compounds. In: Niimi, A. and Taylor, M. (ed.). *Proceedings of the Eighteenth Annual Aquatic Toxicity Workshop: September 30 - October 3, 1991, Ottawa, Ontario.* Can. Tech. Rep. Fish. Aquat. Sci. 1863: 381p.
8. Troll, C. 1966. Seasonal climates of the earth. The seasonal course of natural phenomena in the different climatic zones of the earth. In: Rodenwaldt, E. and Jusatz, H. (ed.). *World maps of climatology* by H.E.Landsberg, H.Lippmann, K.H.Paffen, C.Troll, Springer-Verlag, Berlin.
9. Czeplak, G. and Junge, C. 1974. Studies of interhemispheric exchange in the troposphere by a diffusion model. *Advances in Geophysics 18B*, 57-72.
10. Keeling, C. D. and Heimann, M. 1986. Meridional Eddy Diffusion Model of the Transport of Atmospheric Carbon Dioxide. 2. Mean Annual Carbon Cycle. *J. Geophys. Res. 91/D7*, 7782-7796.
11. Cotham Jr., W. E. and Bidleman, T. F. 1991. Estimating the atmospheric deposition of organochlorine contaminants to the Arctic. *Chemosphere 22*, 165-188.
12. Gregor, D. J. 1991. Trace organic chemicals in the Arctic environment: atmospheric transport and deposition. In: Sturges, W. (ed.). *Pollution of the Arctic Atmosphere*, Elsevier Science Publ., London.
13. Calamari, D., Bacci, E., Focardi, S., Gaggi, C., Morosini, M. and Vighi, M. 1991. Role of plant biomass in the global environmental partitioning of chlorinated hydrocarbons. *Environ. Sci. Technol. 25*, 1489-1495.
14. Muir, D. C., Ford, C. A., Grift, N. P., Metner, D. A. and Lockhart, W. L. 1990. Geographic variation of chlorinated hydrocarbons in burbot (*Lota lota*) from remote lakes and rivers in Canada. *Arch. Environ.*

Contam. Toxicol. 19, 530-542.

15. Oehme, M. and Ottar, B. 1984. The long-range transport of polychlorinated hydrocarbons to the Arctic. *Geophys. Res. Lett. 11*, 1133-1136.
16. Jensen, S., Eriksson, G., Kylin, H. and Strachan, W. 1992. Atmospheric pollution by persistent organic compounds: monitoring with pine needles. *Chemosphere 24*, 229-245.
17. Ballschmiter, K. and Wittlinger, R. 1991. Interhemispheric exchange of hexachlorocyclohexanes, hexachlorobenzene, polychlorobiphenyls, and 1,1,1-trichloro-2,2-bis(p-chlorophenyl)ethane in the lower troposphere. *Environ. Sci. Technol. 25*, 1103-1111.
18. Bidleman, T. F., Billings, W. N. and Foreman, W. T. 1986. Vapor-particle partitioning of semivolatile organic compounds: estimates from field collections. *Environ. Sci. Technol. 20*, 1038-1043.
19. Bidleman, T. F., Wideqvist, U., Jansson, B. and Söderlund, R. 1987. Organochlorine pesticides and polychlorinated biphenyls in the atmosphere of Southern Sweden. *Atmos. Environ. 21*, 641-654.
20. Bidleman, T. F., Patton, G. W., Walla, M., Hargrave, B., Vass, W., Erickson, P., Fowler, B., Scott, V. and Gregor, D. J. 1989. Toxaphene and other organochlorines in Arctic ocean fauna: evidence for atmospheric delivery. *Arctic 42*, 307-313.
21. Hinckley, D. A., Bidleman, T. F. and Rice, C. P. 1991. Atmospheric organochlorine pollutants and air-sea exchange of hexachlorocyclohexane in the Bering and Chukchi Sea. *J. Geophys. Res. 96/C4*, 7201-7213.
22. Patton, G. W., Walla, M., Bidleman, T. F. and Barrie, L. A. 1991. Polycyclic aromatic and organochlorine compounds in the atmosphere of Northern Ellesmere Island, Canada. *J. Geophys. Res. 96/D6*, 867-877.
23. Oehme, M. 1991. Further evidence for long-range transport of polychlorinated aromates and pesticides: North America and Eurasia to the Artic. *Ambio 20*, 293-297.
24. Wittlinger, R. and Ballschmiter, K. 1987. Global baseline pollution studies XI: congener specific determination of polychlorinated biphenyls (PCB) and occurrence of alpha- and gamma-hexachlorocyclohexane (HCH), 4,4'-DDE and 4,4'-DDT in continental air. *Chemosphere 16*, 2497-2513.
25. Knap, A. H. and Binkley, K. S. 1991. Chlorinated organic compounds in the troposphere over the Western North Atlantic Ocean measured by aircraft. *Atmos. Environ. 25A*, 1507-1516.
26. Muir, D. C., Norstrom, R. J. and Simon, M. 1988. Organochlorine contaminants in Arctic marine food chains: accumulation of specific polychlorinated biphenyls and chlordane-related compounds. *Environ. Sci. Technol. 22*, 1071-1078.
27. Wania, F. and Mackay, D. 1993. Global Fractionation and cold condensation of low volatility organochlorine compounds in polar regions. *Ambio* 22, 10-18.
28. We gratefuly acknowledge the financial support by the Gottlieb Daimler- und Karl Benz-Stiftung and the Natural Sciences and Engineering Research Council of Canada.

COMPARISON OF DATA ON PHYSICAL PROPERTIES OF ARCTIC AEROSOLS.

Irina N. Sokolik,

CIRES, University of Colorado, Boulder, USA.

Russ Schnell,

NOAA/CMDL, Mauna Loa Observatory, USA.

Analyses of experimental data on microphysical, optical and radiative properties of Arctic aerosols are presented. We have compared data obtained at different geographical ground-based locations in the Arctic as well as aircraft measurements to investigate the spatial and temporal structure of Arctic aerosol layers. For the first time, data from the Russian Arctic (Cape Chelyuskin, Dikson Island, Cape Shmidt) were included in the comparison with the Barrow station, Alaska.

We have found that experimental data are to sparse and incomplete to construct a microphysical and optical Arctic aerosol model. Thus the estimation of Arctic aerosol forcing in the atmosphere is still essentially an unresolved problem.

Session 9

Sources

Chairman:
W. Maenhaut

TRAJECTORY ANALYSIS OF SOURCE REGIONS INFLUENCING THE SOUTH GREENLAND ICE SHEET DURING THE DYE 3 GAS AND AEROSOL SAMPLING PROGRAM

Cliff I. Davidson[1], Jean-Luc Jaffrezo[1,2], Mitchell J. Small[1],

Peter W. Summers[3], Marvin P. Olson[3], and Randy D. Borys[4]

Submitted to Atmospheric Environment
Special Issue on Arctic Air and Snow Chemistry

January 8, 1993

[1]Department of Civil Engineering, Carnegie Mellon University, Pittsburgh, Pennsylvania 15213

[2]Laboratoire de Glaciologie et Geophysique de l'Environnement du CNRS, Rue Moliere, Domaine Universitaire, BP 96, 38402 Saint Martin d'Heres, France

[3]Atmospheric Environment Service, 4905 Dufferin Street, Downsview, Ontario, Canada M3H 5T4

[4]Atmospheric Sciences Center, Desert Research Institute, University of Nevada System, Reno, Nevada 89506

ABSTRACT

Backward air mass trajectories for Dye 3, Greenland (elevation 2.5 km) show source regions that vary with season: the direction of greatest transport distance is from the southwest in fall, west in winter, and northwest in spring; the trajectories in summer do not show a strong preferred direction. Based on five-day transit times, the trajectories in fall suggest the importance of northern U.S. and southern Canada as potential source regions, with occasional trajectories from western Europe. The trajectories in spring, especially in April, suggest Eurasia (transport over the Pole), eastern North America, and western Europe as potential source regions. Less transport of chemical constituents to Dye 3 is expected in summer when transport distances are shorter. Although some long-range transport to Greenland occurs in winter, the stability of the atmosphere over the Ice Sheet at this time of year is likely to limit the delivery of chemical constituents to the surface. Sources outside of these regions can also influence Dye 3 if transit times longer than five days are considered. These results are in contrast to trajectories reported by others for sea-level arctic locations such as Barrow, Alaska and Mould Bay, Canada, where transport over the Pole from Eurasia is responsible for high chemical species concentrations over much of the winter and early spring. Overall, the trajectories are consistent with aerosol chemical data for this time period at Dye 3 reported by several investigators, showing peak concentrations in spring and fall.

Key words: DGASP, Greenland, trajectories, meteorology, aerosols

INTRODUCTION

Several investigators have used backward airmass trajectories to identify mid-latitude source regions responsible for Arctic air pollution. For example, Miller (1981) has conducted a five-year climatology of back trajectories to determine source regions influencing Barrow, Alaska, at different times of the year. Bodhaine (1989) has used trajectories to identify source areas on days of high condensation nuclei concentration in Barrow. In order to assess source regions on days of high light scattering in the Canadian Arctic, Barrie et al. (1981) have computed trajectories for their sampling site at Mould Bay. Iverson and Joranger (1985) and Pacyna and Ottar (1985) have incorporated trajectory analysis into their studies in the Norwegian Arctic. Also, Harris (1984) and Herbert et al. (1989) report trajectories corresponding to aircraft sampling during the AGASP-I and AGASP-II campaigns.

The results of these studies suggest that Asia and eastern Europe are the major source regions when the arctic atmosphere experiences peak pollution levels. This typically occurs in the winter and early spring. The importance of these source regions has now been well-established through the use of chemical element tracers (Lowenthal and Rahn, 1985; Heidam, 1985; Maenhaut et al., 1989) and consideration of synoptic meteorology (Raatz and Shaw, 1984; Raatz et al., 1985 a,b,c; Bridgman et al., 1989).

Recent investigations of arctic air pollution have gone beyond studies of the atmosphere by documenting pollutants in the glacial record (e.g. Neftel et al., 1985; Mayewski et al., 1986; Finkel et al., 1986; see review by Davidson et al., 1991). These ice core and snowpit studies have the advantage of identifying changes in arctic pollution levels over time by determining concentrations of chemical species as a function of depth, and hence age, in the Ice Sheet. Results have shown generally increasing concentrations of sulfate, nitrate, and other pollutants in recent decades.

It is apparent that certain pollutants measured in the arctic atmosphere and also in arctic glaciers are the result of mid-latitude anthropogenic emissions. However, the relationship between airborne concentrations and the glacial record data is not straightforward. Many ice core and snowpit studies have been conducted in southern and central Greenland, at altitudes of 2.5-3.0 km and at locations far from sea-level atmospheric sampling sites in Alaska, the Canadian Arctic, coastal Greenland, and Scandinavia. Meteorological regimes for the Greenland Ice Sheet are quite different from those influencing the sea-level sites, possibly leading to different source regions. It is important to establish such differences: Greenland is a valuable resource for extracting glacial record samples to study global change.

Furthermore, the central plateau of the Ice Sheet is an excellent location for atmospheric studies of long-range transport, since it is remote from local influences of soil dust and seaspray.

The purpose of the present study was to determine a climatology of backward air mass trajectories for Dye 3 in southern Greenland as a receptor site. This work was designed as a component of the Dye 3 Gas and Aerosol Sampling Program (DGASP), covering the one year period August 1, 1988 - July 31, 1989 (Jaffrezo and Davidson, 1993; Davidson et al., 1993a). The computed trajectories have two functions. First, the full set of trajectories provides an indication of source regions influencing Dye 3 at different times of the year. Such information is valuable for interpreting time-integrated samples, e.g. layers in snowpits and ice cores that may encompass months or even years of data. This climatology can help establish overall differences in source regions and transport pathways influencing south Greenland compared with other arctic sites. Second, the trajectories are valuable on an individual basis for identifying source areas for specific air and snow samples collected during DGASP. The current paper focuses on the first function; several other papers deal with the second function (e.g., Boutron et al., 1993; Davidson et al., 1993b; Jaffrezo et al., 1993; Mosher et al., 1993).

METHODOLOGY

The trajectory model was developed by the Canadian Atmospheric Environment Service (AES) and described in detail by Voldner et al. (1981); the mathematical components of the model were assessed for accuracy by Walmsley and Mailhot (1983). The model incorporates a constant acceleration formulation of the trajectory equations. It is based on objectively analyzed windfields every six hours on a 381 km grid that are routinely prepared by the Canadian Meteorological Centre. Air parcel motions can be initiated at any pressure level between 1000 and 500 mb. As air parcels move, they can rise or fall depending on orographic and synoptic effects. The model contains a terrain pressure field which is used to compute orographic vertical motions to lift air parcels over mountains and ice sheets. Vertical motions due to synoptic high and low pressure systems are computed from the omega equation of Haltiner et al. (1963). Synoptic vertical motions can move an air parcel several hundred meters vertically during a five day travel time. The orographic effects can lift a parcel several thousand meters depending on the orographic scale.

In this study, the model was run at receptor pressure heights of 775, 700, and 500 mb in six-hour time steps going back five days. One trajectory was determined for each day for arrival at 00 GMT. Wind

components at a required pressure level, e.g. 775 mb, are cubically interpolated from the analyzed gridded winds at the mandatory pressure levels (1000, 850, 700, 500 mb). For the case of Dye 3, the two lowest wind levels of 1000 and 850 mb are extrapolated from the surface level winds of the Canadian numerical weather prediction spectral model and modified by any available observed data. Such data are from radiosondes, satellites, ships, and network coastal observation sites. Note that there will be differences between analyzed winds at a pressure level close to the Ice Sheet surface (max. 775 mb) and surface wind observations at Dye 3 which are not part of the observing network. The analyzed winds are considered to be a better representation of the large scale mean flow in and around Greenland than a surface measurement at one point in space and time. Surface winds are subject to local effects and local small scale fluctuations, and hence are not always suitable for long-range transport calculations.

After the trajectories were calculated, a procedure known as transit time analysis was applied to the 775 and 700 mb results (also called residence time analysis). Various forms of the method have been developed and used by Ashbaugh (1983), Poirot and Wishniski (1986), and Summers (1987). The method is used to identify regions where air masses spend most of their time over the period of the trajectory (e.g. five days) while en route to the receptor. The term "transit time" analysis is used here to describe the technique, since residence time often has another meaning, namely the lifetime of a constituent in the atmosphere.

The method of Summers (1987) has been used here. First, a simple linear interpolation was used to estimate the position of the air mass for each hour between the six-hour computed positions over the full 120 hours of the trajectory. This was done for each trajectory within a three-month period corresponding to a season of the year. In this case, the four seasons are defined for convenience as beginning on the first day of January, April, July, and October, respectively. The set of hourly trajectory points was then sorted by grid squares; the total number of hours corresponding to all trajectories was summed for each grid square. The cumulative density function (cdf) for these hourly values was then determined. For example, the cdf for winter at 775 mb showed that the 25th, 50th, and 75th percentile values were 54, 22, and 10 hours, respectively. Finally, isolines enclosing all grid squares containing values greater than these were drawn. Figures 1 and 2 show the results for the 775 and 700 mb trajectories, respectively. Using winter at 775 mb as an example, the black region contains grid squares that have at least 54 hours of total trajectory time, while the dark gray region contains grid squares with 22-53 hours. The light gray region contains grid squares with 10-21 hours. Note that the total number of hours for each map is 10,800 (120 hours per

trajectory x 90 trajectories for the 3-month period). Also note that the percentage of time that the air mass resided somewhere within the entire field (e.g. the entire map) during the five days prior to reaching Dye 3 is 100%.

The transit time analysis is useful for determining those regions where air masses spend most of their time over the period of the trajectories. For example, air masses have spent 75% of their time over the five day period somewhere within the regions of light gray, dark gray, and black on Figures 1 and 2. However, this analysis does not identify regions from which there are only occasional trajectories. This is an important issue: some of the chemical constituent flux to Greenland may be the result of infrequent transport from polluted areas. In most cases, these areas are further from Dye 3 than the shaded regions defined by the transit time analysis. Locating regions that are of concern only in occasional instances requires consideration of the individual trajectories.

To identify such regions, the locations of individual trajectory origins -- five days before reaching Dye 3 -- have been plotted for 775 and 700 mb for each season. These scatter plots are shown in Figures 3 and 4, respectively. Each plot includes roughly 90 points, one per day for each season. The circle indicates a distance of 2000 km from Dye 3.

Finally, the transit time analysis and scatter plots have been interpreted by examining synoptic scale weather charts for the DGASP year. Movements of cyclonic and anticyclonic systems on these charts have been studied to help explain the patterns observed in the trajectory analyses. Examples of these charts are shown in Figures 5a, 5b, and 5c.

RESULTS AND DISCUSSION

Transit Time Analysis

Figures 1 and 2 show that the regions defined at 700 mb cover wider areas than those at 775 mb. This is expected, due to stronger winds and hence greater transport distances at higher elevations. The 700 mb maps may be more relevant to Dye 3 during most of the year, based on surface pressure data for this site. However, there are many individual cases where the 775 mb trajectories may apply.

The patterns show a definite seasonal variation. During winter and spring, the trajectories appear to lie

along an east-west axis: the shaded regions extend westward into central Canada and, to a lesser extent, eastward toward Scandinavia. The spring trajectories for 700 mb show occasional transport from regions northwest of Dye 3. These northernmost regions, which lie within the Arctic Basin, regularly receive chemical constituents over the Pole from Asia and eastern Europe in winter and early spring. Such transport is the dominant pathway responsible for Arctic Haze observed at sea-level sites such as Barrow, Alaska (Rahn and McCaffrey, 1980) and Mould Bay, Canada (Barrie et al., 1981). The original trajectories indicate that Dye 3 can potentially receive these chemical constituents late in the Arctic Haze season, especially in April.

During the summer, there are still indications of transport from the west, but potential source regions are more uniformly distributed in all directions around Dye 3. Especially noteworthy is the smaller size of the shaded regions, indicating shorter transport distances over the five-day periods. Shorter-range transport in summer was also reported for Barrow and Mould Bay by Rahn and McCaffrey (1980) and Barrie et al. (1981), respectively.

During fall, the major direction of transport is from the southwest, clearly visible on the 700 mb map. The shaded regions extend into southeastern Canada and even New England.

Scatter Plots

The winter plots in Figures 3 and 4 show an abundance of points over the Canadian Arctic, with some trajectories extending into southern Canada and the U.S. Transport from the Arctic Basin north of Greenland is indicated by several points on the 775 mb map but is not apparent at 700 mb; the average surface pressure during the DGASP year averaged 710 in winter, but 730-740 in the other seasons, suggesting that the 700 mb trajectories are probably more reliable in winter. At both pressure heights, there is a virtual absense of transport from the Atlantic Ocean at distances greater than 2000 km.

The spring plots show some points over eastern North America and more over the Atlantic; a few points are within or close to western Europe. Several additional points are located over the Arctic Basin. Many of the trajectories from these different potential source regions occur on days of high airborne chemical constituent concentrations at Dye 3, as discussed below.

The plots in summer show more points within 2000 km of Dye 3, indicating shorter-range transport. North America is a potential source region, although there is some transport from all directions.

Finally, the fall plots show an abundance of points over North America, including populated areas of southern Canada and the U.S. There is also considerable transport from over the Atlantic and a few points over western Europe.

Synoptic Charts

Synoptic charts can be used to explain the underlying reasons for the patterns observed in Figures 1-4. The dominant influence of North America is due in part to the positions of cyclonic and anticyclonic systems in the northern latitudes. Transport from the west is driven by a major cyclonic system that frequently forms over the Canadian Arctic west of Greenland. The system typically persists over Baffin Island or Hudson Bay, but it is occasionally further south. This drives the airflow from the west toward Greenland, following a counterclockwise path south of the pressure center. On some occasions, the system is sufficiently large and extends to a sufficiently high altitude that it may affect all of Greenland, engulfing the entire island in clouds and precipitation (Putnins, 1970). Additional cyclonic systems over Iceland or over the Atlantic south of Greenland also play a role in directing the airflow to southern Greenland; Hogan et al. (1984) report that they are frequently responsible for bringing moist oceanic air and resulting precipitation to Dye 3.

Other cyclonic systems often form over the North American continent. Some of these systems last for several days; many of them eventually migrate eastward across the Atlantic. This pattern occurs with striking regularity: a new cyclone evolves and begins its migration every few days. The systems usually dissipate over the water but sometimes reach Europe. There are important seasonal differences to these patterns.

In winter, cyclones commonly form over central Canada, occasionally becoming quite strong before moving rapidly across the Atlantic. The tendency for strong cyclonic systems to persist over central Canada is responsible for trajectories showing predominant transport from the west in winter and continuing into spring. Figure 5a shows the positions of cyclonic systems during January 29-February 5, 1989 which are typical of this season, taken from the 700 mb synoptic maps. The individual 700 mb trajectories on these days show counterclockwise movement around the cyclones from the west to Dye 3.

In summer, cyclones often originate over southeastern Canada or northeastern U.S. and move slowly eastward. The cyclones persist over the Atlantic, pumping oceanic air toward Greenland. Figure 5b shows a sequence of typical summer cyclonic movement south of Greenland, in this case for August 2-12, 1988. The pattern is consistent with Figures 1-4 showing air mass transport from the south and west, with a considerable number of trajectories from the Atlantic, the Labrador Sea, and eastern North America. There is also frequent transport from the southeast and east as a result of persisting cyclones between Greenland and Iceland.

In fall, cyclones often originate over central North America and move slowly eastward. This allows air masses from populated areas of the U.S. and Canada to reach southern Greenland: the 700 mb transit time diagram for fall shows a strong tendency toward transport from the southwest, while the corresponding scatter plot shows points throughout Canada and the U.S. Figure 5c illustrates a sequence during November 1-8, 1988 which is typical of this time of year. The individual 700 mb trajectories on these dates show southeastern Canada and northeastern U.S. as major source regions.

A mitigating factor in all seasons is that precipitation associated with these cyclonic systems may efficiently scavenge aerosols. Thus the pathways suggested here must be considered merely as potential routes by which material can reach Dye 3.

These results suggest that the direction of the source areas furthest from Dye 3, based on five days of transport, has a distinct variation with season. In fall, the most distant source regions appear to be southwest of Dye 3. By winter, this has shifted to the west, and by spring the most distant source regions are northwest of Dye 3. Finally, the pattern is broken with the arrival of summer, as the polar front moves north and transport distances decrease overall. This "clockwise" shift in major source region from southwest through northwest is most easily seen on the 700 mb transit time diagrams and scatter plots. This pattern is quite different from that observed in Arctic Haze studies focusing on more northerly regions at sea-level, where anticyclones are expected to dominate overall long-range transport (Raatz, 1989).

Nevertheless, anticyclones can play a role in directing the airflow. Vowinckle and Orwig (1970) describe the persistence of a high pressure system over the Ice Sheet, caused by surface subsidence due to the heat capacity of the ice. This anticyclone is essentially a ridge which merely slows the air flowing over Greenland; it is not a closed high pressure system that can cause true stagnation conditions, such as that

occurring over Antarctica. Anticyclones can also assist in channeling mid-latitude air to the Arctic as described by Raatz and Shaw (1984). When a low pressure system approaches a high pressure system from the west, the northward airflow between the pressure centers may be accelerated, resulting in so-called "surge flow" of southern, often polluted air into the Arctic. Examination of the synoptic charts shows that several such events occurred during the DGASP year.

It is of interest to compare these results with the climatology for Barrow reported by Miller (1981). His work involved five-day backward trajectories in the 300-2000 m layer over the earth's surface for a period of five years, beginning February 1975. Four trajectories were calculated per day. The analysis considered the locations of the air masses five days prior to reaching Barrow, essentially the same type of analysis used in the scatter plots of Figures 3 and 4.

Overall, Miller's results show that most long-range transport (> 2000 km from Barrow over the five-day period) takes place during November - March, with a brief period of long-range transport in August. Roughly 40% of all trajectories year-round have traveled over 2000 km. The predominant directions of transport are from the north over the Pole, indicating Eurasia as a source region, and from the south indicating transport over the Pacific. Flow from the north peaks in March. Trajectories showing moderate and short transport distances (1000-2000 km and <1000 km, respectively) have much smaller seasonal variation than the long-range trajectories.

The results for Dye 3 also indicate that roughly 40% of all trajectories have transport distances > 2000 km (for 775 mb, the closest pressure height to Miller's analysis). The results similarly show more pronounced seasonal variations for long-range transport than for shorter distances. However, the predominant direction for trajectories > 2000 km is from the west.

Although these trajectories can provide information on potential source regions and long-range transport pathways, the delivery of airborne chemical species to Dye 3 also depends on local atmospheric mixing between the air aloft, where material is transported, and the surface. Such mixing is believed to be most prevalent in the spring and fall, when atmospheric stability over the Ice Sheet is minimal (Dibb and Jaffrezo, 1993; Putnins, 1970). Thus at times in winter when chemical constituents from the mid-latitudes reach Greenland, the constituents are less likely to be delivered to the surface. Considering both long-range transport and local mixing, the highest concentrations at Dye 3 are expected in the spring (when Eurasia, eastern North America, and western Europe are potential source regions) and in fall (when North

America and to a lesser extent western Europe are potential source regions).

Overall, these conclusions are consistent with seasonal variations in chemical species data reported by DGASP investigators. For example, Dibb and Jaffrezo (1993) report strong peaks in spring and fall for both ^{7}Be and ^{210}Pb in air. Mosher et al. (1993) show dominant spring peaks in several airborne trace metals, with secondary maxima in fall. Boutron et al. (1993) report high concentrations of trace metals in snow in the spring. Jaffrezo and Davidson (1992) report peaks for SO_4^{2-} in both air and snow that resemble those for the trace metals. These various datasets are summarized and compared to identify consistent patterns by Davidson et al. (1993a).

The results presented here are also supported by associations between individual episodes and daily trajectories in April, the month of highest average concentrations during DGASP (Davidson et al., 1993b). High airborne concentrations of chemical species during this month are often associated with trajectories from polluted regions, including the Arctic Basin, eastern North America, and western Europe. Similar comparisons for October-November show that elevated airborne concentrations are often associated with trajectories from North America, and less often from western Europe (Jaffrezo et al., 1993). High concentrations of trace metals in surface snow at Dye 3 during April have also been linked with source regions using these trajectories (Boutron et al., 1993). The filter sample containing the highest airborne concentrations of Al and other crustal species during the DGASP year (April 14-15, 1989) has been linked to trajectories from western Europe (Davidson et al., 1993b); Mosher et al. (1993) have conducted backward and forward trajectory analysis from a receptor site in Germany that strongly implicates Sahara dust for this sample, a hypothesis that is also supported by airborne particle concentration measurements in Germany. Although several episodes have been traced back to potential source regions in these studies, there are also instances where low airborne concentrations are associated with trajectories from populated areas at times of precipitation along the transport path. This suggests that the aerosols had been scavenged en route to Dye 3.

Limitations of the Results

There are several limitations to the analyses presented here. Most important, the calculated trajectories are subject to error: although the model accounts for vertical transport of air masses, it is likely that the true complexities of vertical motion around Greenland cannot be accurately represented due to the topography around the coast. The trajectories are also prone to error because of the limited windfield data available

for the Arctic: there are only 39 rawinsonde sites north of 70° N (Herbert et al., 1989). Kahl (1991) has shown that trajectories in the Arctic are very sensitive to receptor site because of the sparse input data available as well as other limitations.

Another problem is that the climatology presented here uses only one year of trajectory data. Miller (1981) has shown that substantial variations exist from year to year, although the same general pattern is apparent throughout the five years of his study. Work is currently underway to determine whether the DGASP year had typical meteorological conditions.

The trajectories presented here cover only five days of transport. Some of the chemical constituent material reaching Dye 3 probably came from regions traversed prior to this time period. One example is the April 14-15 sample believed to contain Sahara dust.

All trajectories must pass through the grid square containing the receptor site, and hence this square usually has the greatest number of hours. Similarly, all trajectories must pass through one of the eight grid squares immediately surrounding the receptor site. If one is interested in the relative probability of transit across a grid square associated with given air pollutant concentrations at the receptor site, a correction must be applied due to these geometric considerations. Poirot and Wishinski (1986) applied a $1/d^2$ correction factor for their analysis of trajectories reaching northern Vermont, where d is the distance from the receptor. When calculating source-receptor relationships, the concentration losses along trajectories have been corrected by applying a $1/t^2$ factor, where t is the travel time to the receptor (Strauss et al., 1986) or by using an empirical exponential decay factor (Summers, 1987). Because the purpose of the present study was to identify source regions influencing Dye 3 rather than to quantify source-receptor relations for specific pollutants, no correction factors have been applied.

Each point in the scatter plots represents the center of a probability field that is highly uncertain. Thus the points should be used merely as very rough indicators of air mass position five days prior to reaching Dye 3.

Finally, it should be cautioned that the results presented here apply only to Dye 3. Different source regions and transport pathways may influence central Greenland, e.g. the Summit site where the GISP-2 and GRIP ice coring efforts are underway, because of the spatial separation and differences in elevation. Additional trajectories are necessary to determine differences in possible source regions influencing

various ice coring sites in Greenland. Furthermore, the precise source regions for a given airborne constituent or snow sample depend on many other complexities; of particular importance is the coupling between the free troposphere and the boundary layer at the time of interest (Dibb and Jaffrezo, 1993) and nucleation scavenging, dry deposition, and other removal mechanisms en route to the sampling site (Borys, 1989; Borys et al., 1993; Davidson et al., 1985).

These uncertainties imply the need for reasonable caution when using these results. Nevertheless, the validity of the trajectories is supported by the aerosol and snow chemistry at Dye 3 in the studies cited above.

Although useful for interpreting atmospheric chemistry data, these findings also have implications for the glacial record. Dominant spring peaks in SO_4^{2-} and metals have been noted by many investigators in Dye 3 snowpits and ice cores (e.g., Beer et al., 1991; Davidson et al., 1987 and 1989; Finkel et al, 1986; Herron, 1982; Jaffrezo and Davidson, 1992; Langway et al., 1977; Mayewski et al., 1987; Wolff and Peel, 1988). Springtime peaks have also been noted in the Summit region of Greenland (Mayewski et al., 1990; Steffensen et al., 1988; Whitlow et al., 1992). The trajectory results suggest that the spring peaks at Dye 3 are due to material from a variety of source regions, including Eurasia (transported over the Pole), eastern North America, and/or western Europe. Work is underway to determine whether Summit is affected by similar potential source regions.

SUMMARY AND CONCLUSIONS

Five-day backward air mass trajectories have been computed for each day of the DGASP sampling year, August 1988 - July 1989, at 775, 700, and 500 mb. The trajectories at 775 and 700 mb have been used in a transit time analysis to identify those locations where air masses have spent the most time before arriving at Dye 3. This analysis is augmented by scatter plots showing the locations of air masses five days prior to reaching the receptor site.

Results show that potential source regions influencing southern Greenland vary with season. The most important source regions are southwest of Dye 3 in fall, west in winter, and northwest in spring; there is less long-range transport in summer.

When the lack of vertical mixing in winter and summer is taken into account, the results suggest that

much of the transport of chemical constituents to Dye 3 occurs in the spring and fall from a variety of source regions. Potential source regions in spring include Eurasia (transport over the Pole), eastern North America, and western Europe. Transport from these source regions is especially important in April, when maximum concentrations of many chemical species occur. North America is the dominant potential source region in fall, with western European sources also contributing on occasion. Other source regions greater distances from Dye 3 may also contribute chemical species, i.e., regions traversed by the air masses prior to the five-day period of the trajectories. For example, one of the aerosol samples collected during DGASP is believed to contain Sahara dust.

Overall, these findings suggest that the southern Greenland Ice Sheet is influenced by a different annual variation of source regions and transport pathways than sea-level arctic sites. This implies that it is tenuous to use the results of sea-level arctic studies to interpret Greenland glacial record data; rather, meteorological and chemical species data obtained near the sites of ice coring in Greenland must be used.

ACKNOWLEDGMENTS

We acknowledge Frank Boscoe, Siv Balachandran, Mike Bergin, and Ta-Chun Lin of Carnegie Mellon, and Balbir Sairi of Atmospheric Environment Service for assistance with the computation of trajectories and the statistical analyses. Meteorological data were obtained from the Danish Weather Service in Sondrestromfjord, Greenland. Suggestions on the manuscript were generously provided by Jack Dibb of the University of New Hampshire. This work was funded by National Science Foundation Grants DPP-8618223, DPP-8821018, and ATM-8922034.

REFERENCES

Ashbaugh L.L. (1983) A statistical trajectory technique for determining air pollution source regions. *J. Air Poll.Control Assoc.* **33**, 1096-1098.

Barrie L.A., Hoff R.M., and Daggupaty S. (1981) The influence of mid-latitudinal pollution sources on haze in the Canadian Arctic. *Atmospheric Environment* **15**, 1407-1420.

Beer J., Finkel R.C., Bonani G., Gaggeler H., Gorlach U., Jacob P., Klockow D., Langway, Jr. C.C.,

Neftel A., Oeschger H., Schotterer U., Schwander J., Siegenthaler U., Suter M., Wagenbach D. and Wolfli W. (1991) Seasonal variations in the concentration of ^{10}Be, Cl^-, NO_3^-, SO_4^{2-}, H_2O_2, ^{210}Pb, ^3H, mineral dust, and $\delta^{18}O$ in Greenland snow. *Atmospheric Environment* **25A**, 899-904.

Bodhaine B.A. (1989) Barrow surface aerosol: 1976-1986. *Atmospheric Environment* **23**, 2357-2369.

Borys R.D. (1989) Studies of ice nucleation by Arctic aerosol on AGASP-II. *J. Atmos. Chem.* **9**, 169-185.

Borys R.D., Del Vecchio D., Jaffrezo J.L., Davidson C.I., and Mitchell D.L. (1993) Assessment of ice particle growth processes at Dye 3, Greenland. *Atmospheric Environment* (in press).

Boutron C.F., Ducroz F.M., Gorlach U., Jaffrezo J.L., Davidson C.I., and Bolshov M.A. (1993) Variations in heavy metals concentrations in fresh Greenland snow from January to July 1989. *Atmospheric Environment* (in press).

Bridgeman H.A., Schnell R.C., Kahl J.D., Herbert G.A., and Joranger E. (1989) A major haze event near Point Barrow, Alaska: analysis of probable source regions and transport pathways. *Atmospheric Environment* **23**, 2537-2549.

Davidson C.I., Santhanam S., Fortmann R.C., and Olson M.P. (1985) Atmospheric transport and deposition of trace elements onto the Greenland Ice Sheet. *Atmospheric Environment* **19**, 2065-2081.

Davidson C.I., Honrath R.E., Kadane J.B., Tsay R.S., Mayewski P.A., Lyons W.B., and Heidam N.Z. (1987) The scavenging of atmospheric sulfate by Arctic snow. *Atmospheric Environment* **21**, 871-882.

Davidson C.I., Harrington J.R., Stephenson M.J., Small M.J.. Boscoe F.P., and Gandley R.E. (1989) Seasonal variations in sulfate, nitrate, and chloride in the Greenland Ice Sheet: relation to atmospheric concentrations. *Atmospheric Environment* **23**, 2483-2493.

Davidson C.I., Jaffrezo J.L., and Mayewski P.A. (1991) Arctic air pollution as reflected in snowpits and ice cores. In *Pollution of the Arctic Atmosphere*, W. T. Sturges, ed., Elsevier Science Publishers, London, pp. 43-95.

Davidson C.I., Jaffrezo J.L., Mosher B.W., Dibb J.E., Borys R.D., Bodhaine B.A., Rasmussen R.A., Boutron C.F., Gorlach U., Cachier H., Ducret J., Colin J.L., Heidam N.Z., Kemp K., and Hillamo R. (1993a) Chemical constituents in the air and fresh snow at Dye 3, Greenland: I. Seasonal variations. *Atmospheric Environment* (in press).

Davidson C.I., Jaffrezo J.L., Mosher B.W., Dibb J.E., Borys R.D., Bodhaine B.A., Rasmussen R.A., Boutron C.F., Ducroz F.M., Cachier H., Ducret J., Colin J.L., Heidam N.Z., Kemp K., and Hillamo R. (1993b) Chemical constituents in the air and fresh snow at Dye 3, Greenland: II. Analysis of episodes in April 1989. *Atmospheric Environment* (in press).

Dibb J.E. and Jaffrezo J.L. (1993) Beryllium-7 and Lead-210 in Aerosol and Snow in the Dye 3 Gas and Aerosol Sampling Program. *Atmospheric Environment* (in press).

Finkel R.C., Langway C.C., Jr. and Clausen H.B. (1986) Changes in precipitation chemistry at Dye 3, Greenland. *J. Geophys. Res.* **91**, 9849-9855.

Haltiner G.J., Clarke L.C. and Lawniczak G.E. (1963) Computation of large-scale vertical velocity. *J. Appl. Meteor.* **2**, 242-259.

Harris J.M. (1984) Trajectories during AGASP. *Geophys. Res. Lett.* **11**, 453-456.

Heidam N.Z. (1985) Crustal enrichments in the Arctic aerosol. *Atmospheric Environment* **19**, 2083-2097.

Herbert G.A., Harris J.M. and Bodhaine B.A. (1989) Atmospheric transport during AGASP-II: The Alaskan flights (2-10 April 1986). *Atmospheric Environment* **23**, 2521-2535.

Herron M.M. (1982) Geochemical dating techniques. In *Nuclear and Chemical Dating Techniques: Interpreting the Environmental Record*, L.A. Curry, ed., ACS Symposium Series No. 176, pp. 303-318.

Hogan A.W., Barnard S.C., Kebschull K., Townsend R. and Samson J.A. (1984) Aerosol variation in the Western Hemisphere Arctic. *J. Aerosol Science* **15**, 13-33.

Iversen T. and Joranger E. (1985) Arctic air pollution and large scale atmospheric flows. *Atmospheric*

Environment **19**, 2099-2108.

Jaffrezo J.L. and Davidson C.I. (1992) Sulfate in the air, surface snow, and snowpits at Dye 3, Greenland. In Schwartz S.E. and Slinn W.G.N., editors, *Precipitation Scavenging and Atmosphere-Surface Exchange, Volume 3*, Proceedings of the Fifth International Conference on Precipitation Scavenging and Atmosphere-Surface Exchange Processes, Richland, Washington, 15-19 July 1991, Hemisphere Publishing Company, Washington D.C., pp. 1693-1704.

Jaffrezo J.L. and Davidson C.I. (1993) The Dye 3 Gas and Aerosol Sampling Program: An Overview. *Atmospheric Environment* (in press).

Jaffrezo J.L., Davidson C.I., and Dibb J.E. (1993) Major ions in aerosols and surface snow during the Dye 3 Gas and Aerosol Sampling Program. Manuscript in preparation.

Kahl J.D. (1993) A cautionary note on the use of air trajectories in interpreting Arctic air chemistry measurements. *Atmospheric Environment* (in press).

Langway C.C. Jr., Cragin J.H., Klouda G.A., and Herron M.M. (1977) Seasonal variations in chemical constituents in annual layers of Greenland deep ice deposits. In *Isotopes and Impurities in Snow and Ice*, Proc. IUGG Symposium, Grenoble, August-September 1975, pp. 302-306. IAHS Publ.

Lowenthal D.H. and Rahn K.A. (1985) Regional sources of pollution aerosol at Barrow, Alaska during winter 1979-80 as deduced from elemental tracers. *Atmospheric Environment* **19**, 2011-2024.

Maenhaut W., Cornille P., Pacyna J.M., and Vitols V. (1989) Trace element composition and origin of the atmosphere in the Norwegian Arctic. *Atmospheric Environment* **23**, 2551-2569.

Mayewski P.A., Lyons W.B., Spencer M.J., Twickler M., Dansgaard W., Koci B., Davidson C.I. and Honrath R.E. (1986) Sulfate and nitrate concentrations from a south Greenland ice core. *Science* **232**, 975-977.

Mayewski P.A., Spencer M.J., Lyons W.B., and Twickler M.S. (1987) Seasonal and spatial trends in south Greenland snow chemistry. *Atmospheric Environment* **21**, 863-869.

Mayewski P.A., Spencer M.J., Twickler M.S., and Whitlow S. (1990) A glaciochemical survey of the Summit region, Greenland. *Annals of Glaciology* **14**, 186-190.

Miller, J.M. (1981) A five-year climatology of five-day back trajectories from Barrow, Alaska. *Atmospheric Environment* **15**, 1401-1405.

Mosher B.W., Winkler P., and Jaffrezo J.L. (1993) Seasonal aerosol chemistry at Dye 3, Greenland. *Atmospheric Environment* (in press).

Neftel A., Beer J., Oeschger H., Zurcher F. and Finkel R.C. (1985) Sulfate and nitrate concentrations in snow from South Greenland. *Nature* **314**, 611-613.

Pacyna J.M. and Ottar B. (1985) Transport and chemical composition of summer aerosol in the Norwegian Arctic. *Atmospheric Environment* **19**, 2109-2120.

Poirot R.L. and Wishinski P.R. (1986) Visibility, sulfate and air mass history associated with summertime aerosols in northern Vermont. *Atmospheric Environment*, **20**, 1457-1469.

Putnins P. (1970) The climate of Greenland, in *World Survey of Climatology*, Volume 14 of *Climates of the Polar Regions*, S. Orwig, ed., Elsevier, Amsterdam.

Raatz W.E. (1989) An anticyclonic point of view on low-level tropospheric long-range transport. *Atmospheric Environment* **23**, 2501-2504.

Raatz W.E. and Shaw G.E. (1984) Long-range tropospheric transport of pollution aerosols into the Alaskan Arctic, *J. Clim. Appl. Met.* **23**, 1052-1064.

Raatz W.E., Schnell R.C. Bodhaine B.A., Oltmans S.J. and Gammon R.H. (1985a) Air mass characteristics in the vicinity of Barrow, Alaska, 9-19 March 1983. *Atmospheric Environment* **19**, 2127-2134.

Raatz W.E., Schnell R.C. and Bodhaine B.A. (1985b) The distribution and transport of pollution aerosols over the Norwegian Arctic on 31 March and 4 April 1983, *Atmospheric Environment* **19**, 2135-2142.

Raatz W.E., Schnell R.C., Bodhaine B.A. and Oltmans S.J. (1985c) Observations of Arctic haze during polar flights from Alaska to Norway. *Atmospheric Environment* **19**, 2143-2151.

Rahn K.A. and McCaffrey R.J. (1980) On the origin and transport of the winter Arctic aerosol. *Annals of the N.Y. Academy of Sciences* **338**, 486-503.

Steffensen J.P. (1988) Analysis of the seasonal variation in dust, Cl^-, NO_3^-, and SO_4^{2-} in two central Greenland firn cores. *Annals of Glaciology* **10**, 171-177.

Strauss B., Martin D., and Criller C. (1986) Une methode nouvelle en climatologie de trajectoires de masses d'air. Proc. Seventh World Clean Air Congress, Sydney, Australia 25-29 August, Volume 1, pp. 326-333.

Summers P.W. (1987) Empirical source-receptor relationships in eastern Canada determined from monitoring data and airmass trajectory climatologies. EMEP Workshop on Data Analysis and Presentation, Cologne, Germany, 15-17 June.

Voldner E.C., Olson M.P., Oikawa K., and Loiselle M. (1981) Comparison between measured and computed concentrations of sulfur compounds in eastern North America. *J. Geophys. Res.* **86**, 5339-5346.

Vowinckle E. and Orwig S. (1970) The climate of the North Polar Basin, in *World Survey of Climatology*, Volume 14 of *Climates of the Polar Regions*, S. Orwig, ed., Elsevier, Amsterdam.

Walmsley J.L. and Mailhot J. (1983) On the numerical accuracy of trajectory models for long-range atmospheric transport. *Atmosphere-Ocean* **21**, 14-39.

Whitlow S., Mayewski P.A., and Dibb J.E. (1992) A comparison of major chemical species seasonal and accumulation at the South Pole and Summit, Greenland. *Atmospheric Environment* **26A**, 2045-2054.

Wolff E.W. and Peel D.A. (1988) Concentrations of cadmium, copper, lead, and zinc in snow from near Dye 3 in south Greenland. *Annals of Glaciology* **10**, 193-197.

FIGURE CAPTIONS

Figure 1. Regions defined by the cumulative density function for the number of hours that air masses spend in each grid square, based on 775 mb daily trajectories in each season. Air masses are within the black areas surrounding Dye 3 25% of the time, within the dark gray and black areas 50% of the time, and within the light gray, dark gray, and black areas 75% of the time.

Figure 2. Regions defined by the cumulative density function for the number of hours that air masses spend in each grid square, based on 700 mb daily trajectories in each season. Darkened areas are defined as in Figure 2.

Figure 3. Locations of air masses five days before reaching Dye 3 for the 775 mb daily trajectories in each season. Circles indicate a distance of 2000 km from Dye 3.

Figure 4. Locations of air masses five days before reaching Dye 3 for the 700 mb daily trajectories in each season. Circles indicate a distance of 2000 km from Dye 3.

Figure 5a. Positions of low pressure centers during the period January 29 - February 5, 1989 taken from 700 mb synoptic maps.

Figure 5b. Positions of low pressure centers during the period August 2-12, 1988 taken from 700 mb synoptic maps.

Figure 5c. Positions of low pressure centers during the period November 1-8, 1988 taken from 700 mb synoptic maps.

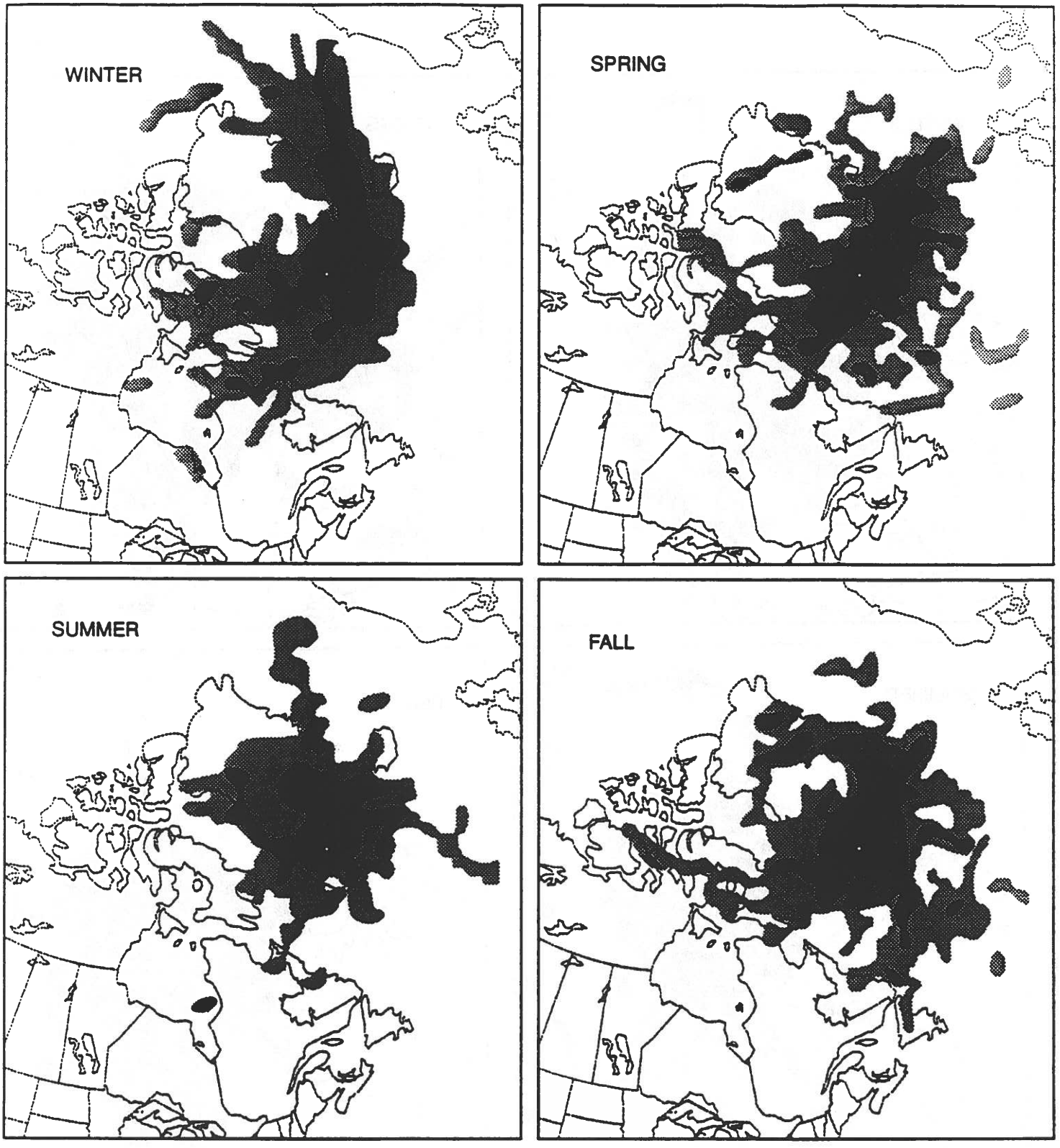

Figure 1

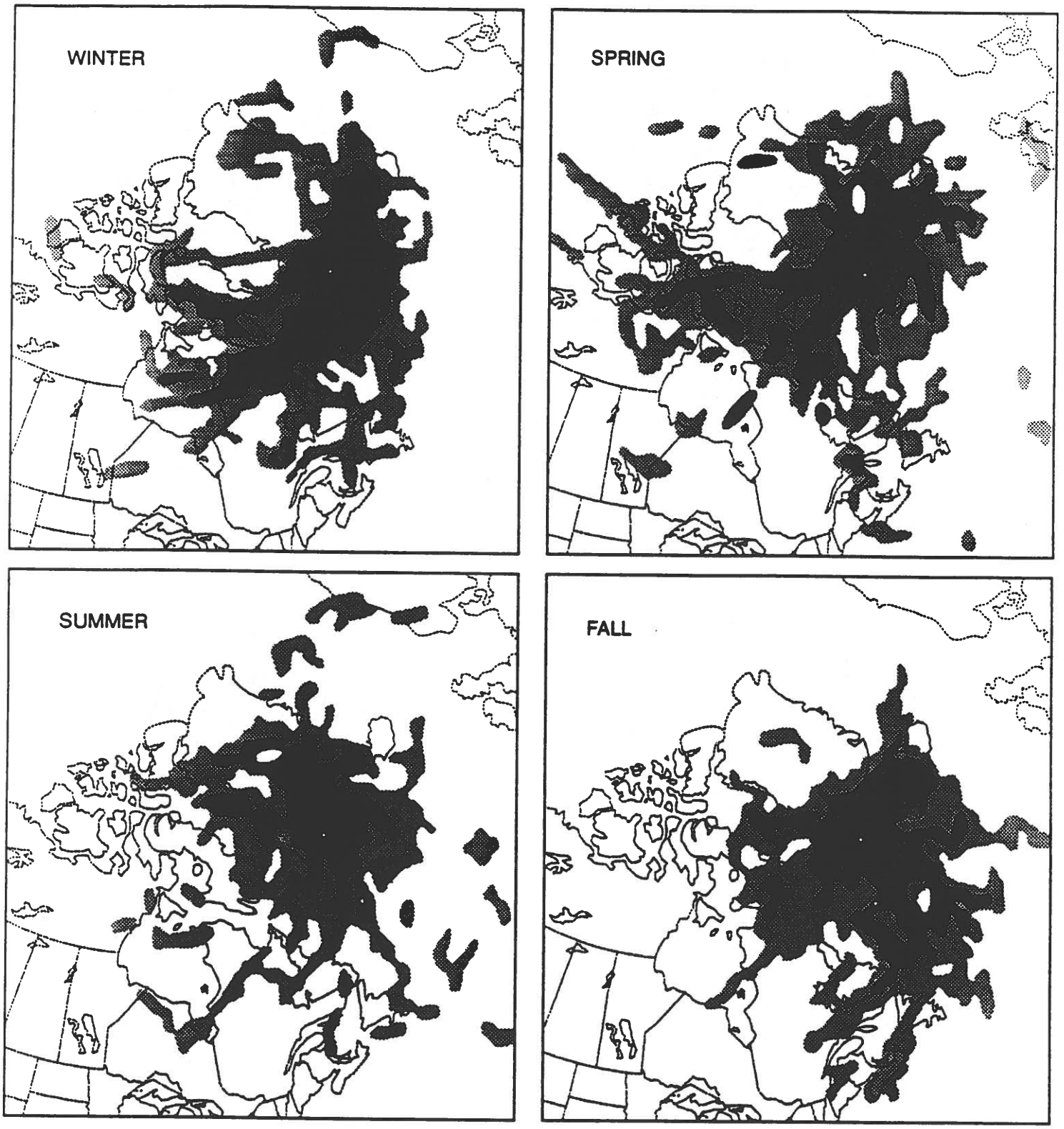

Figure 2

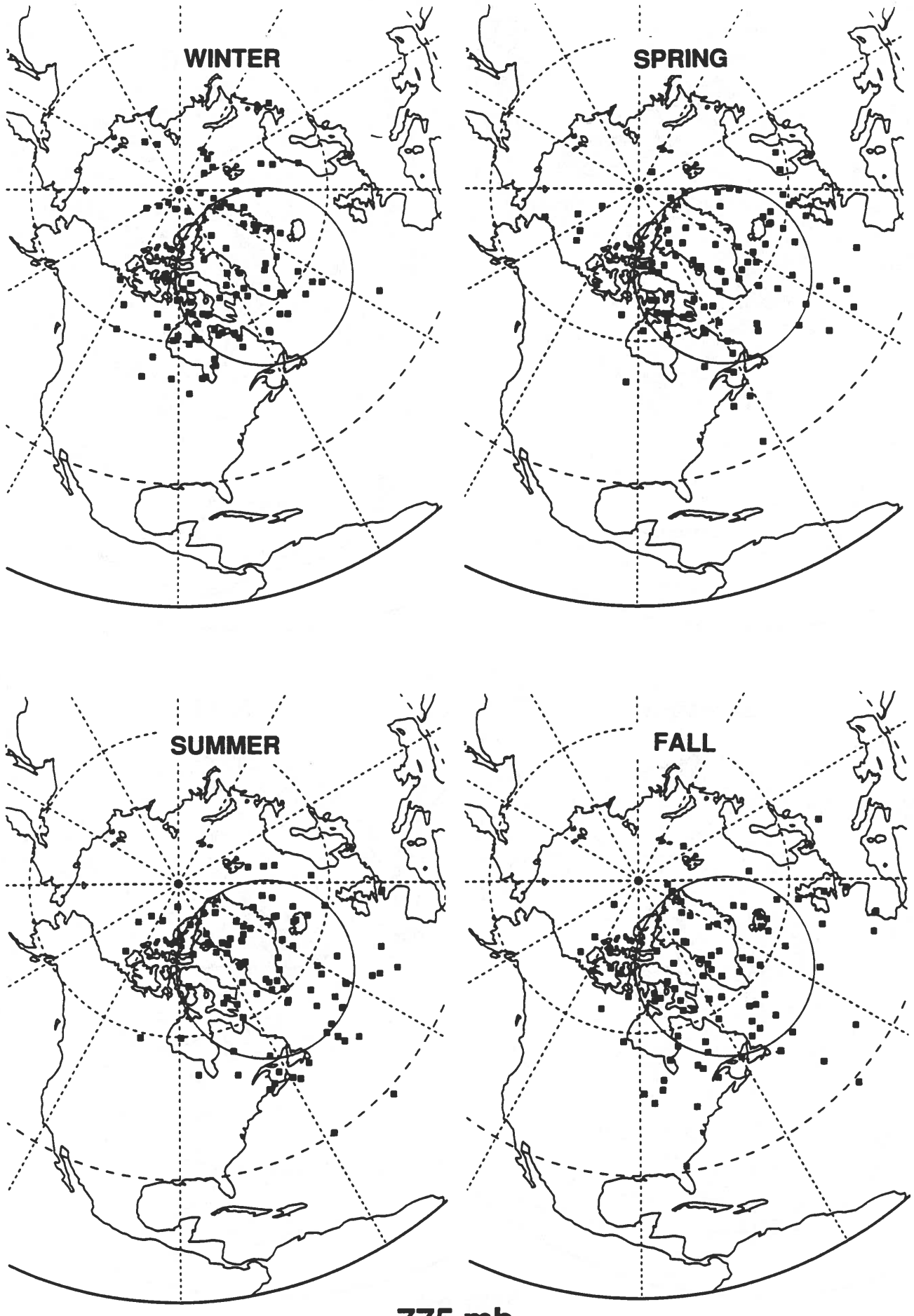

Figure 3

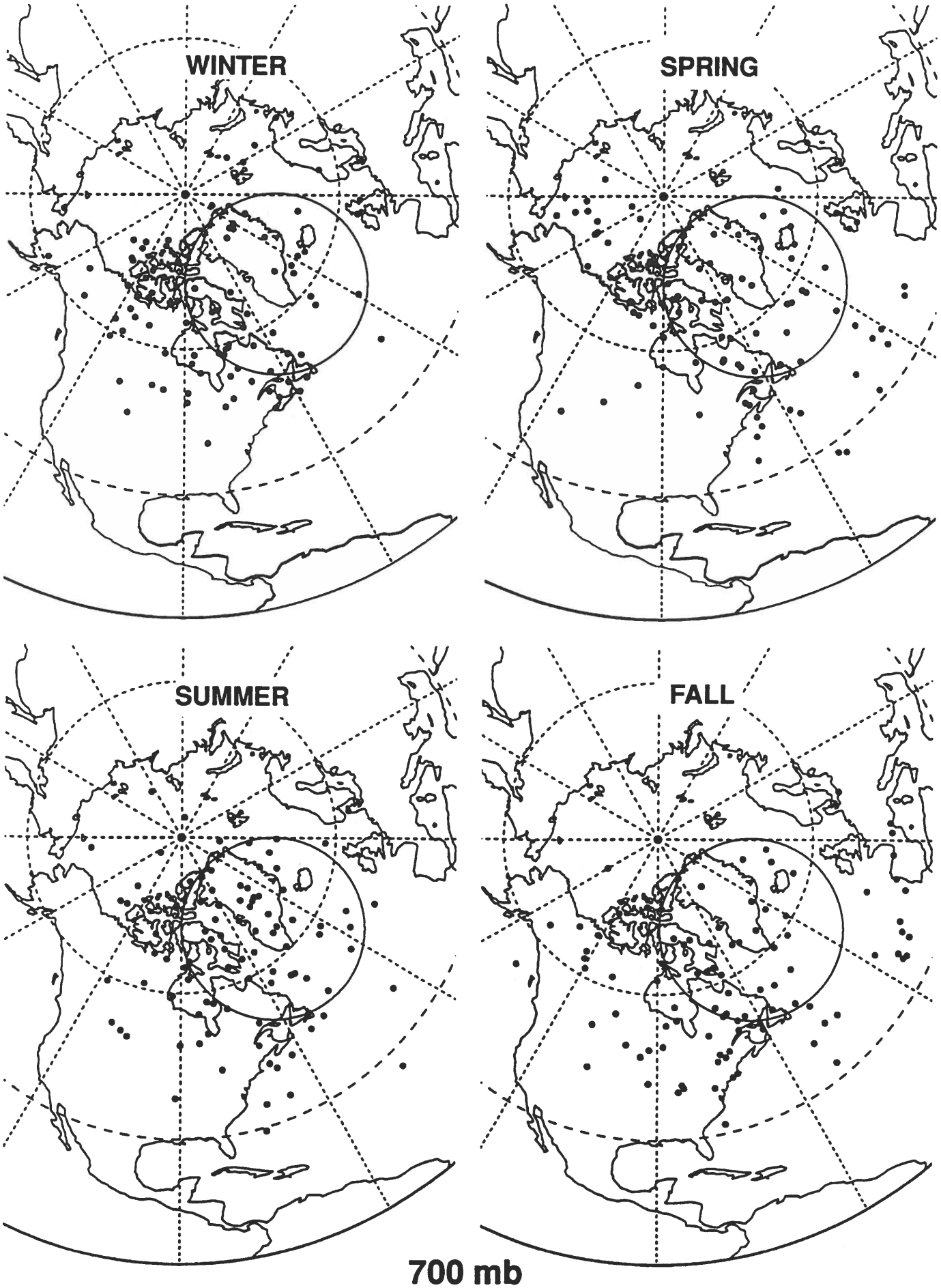

Figure 4

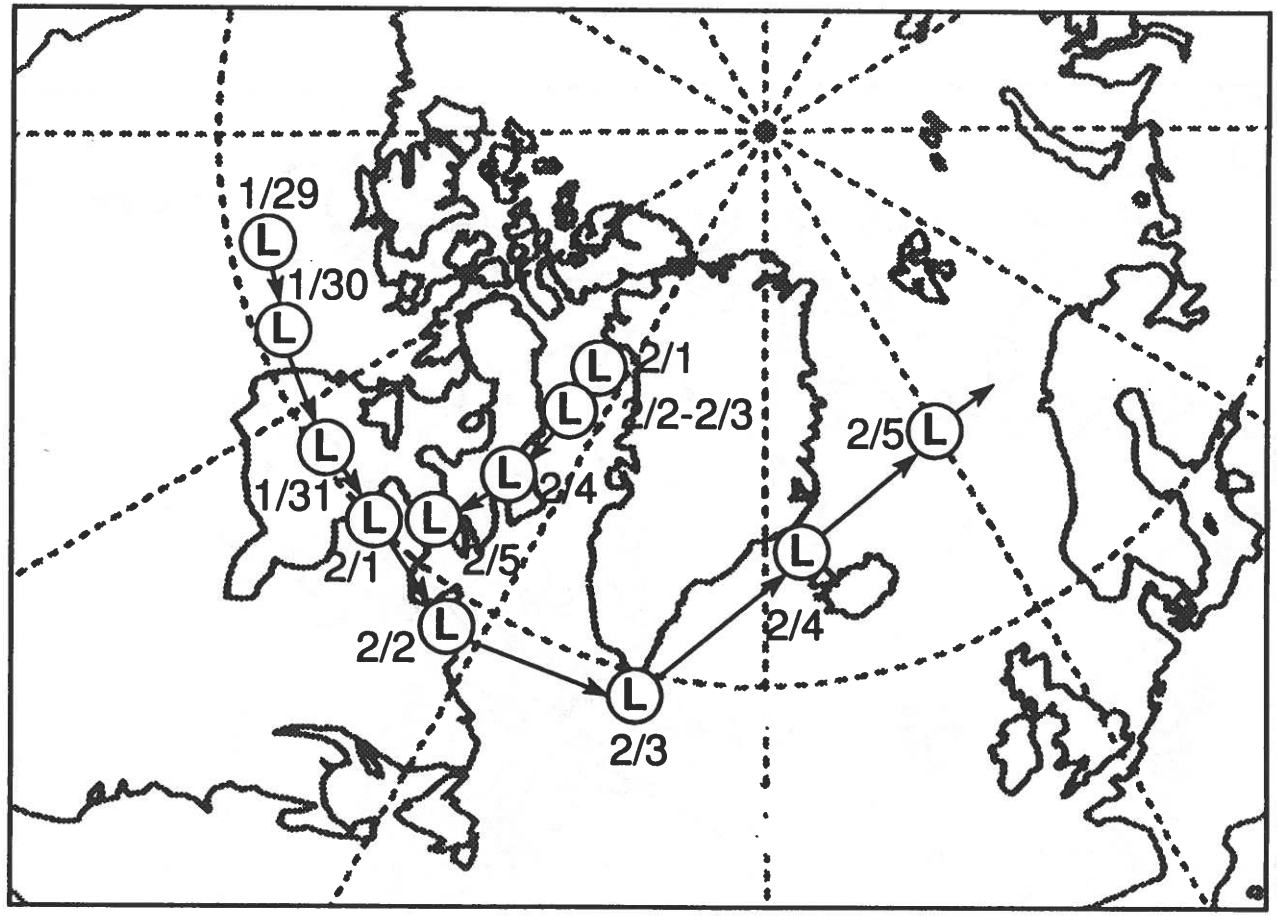

Figure 5a

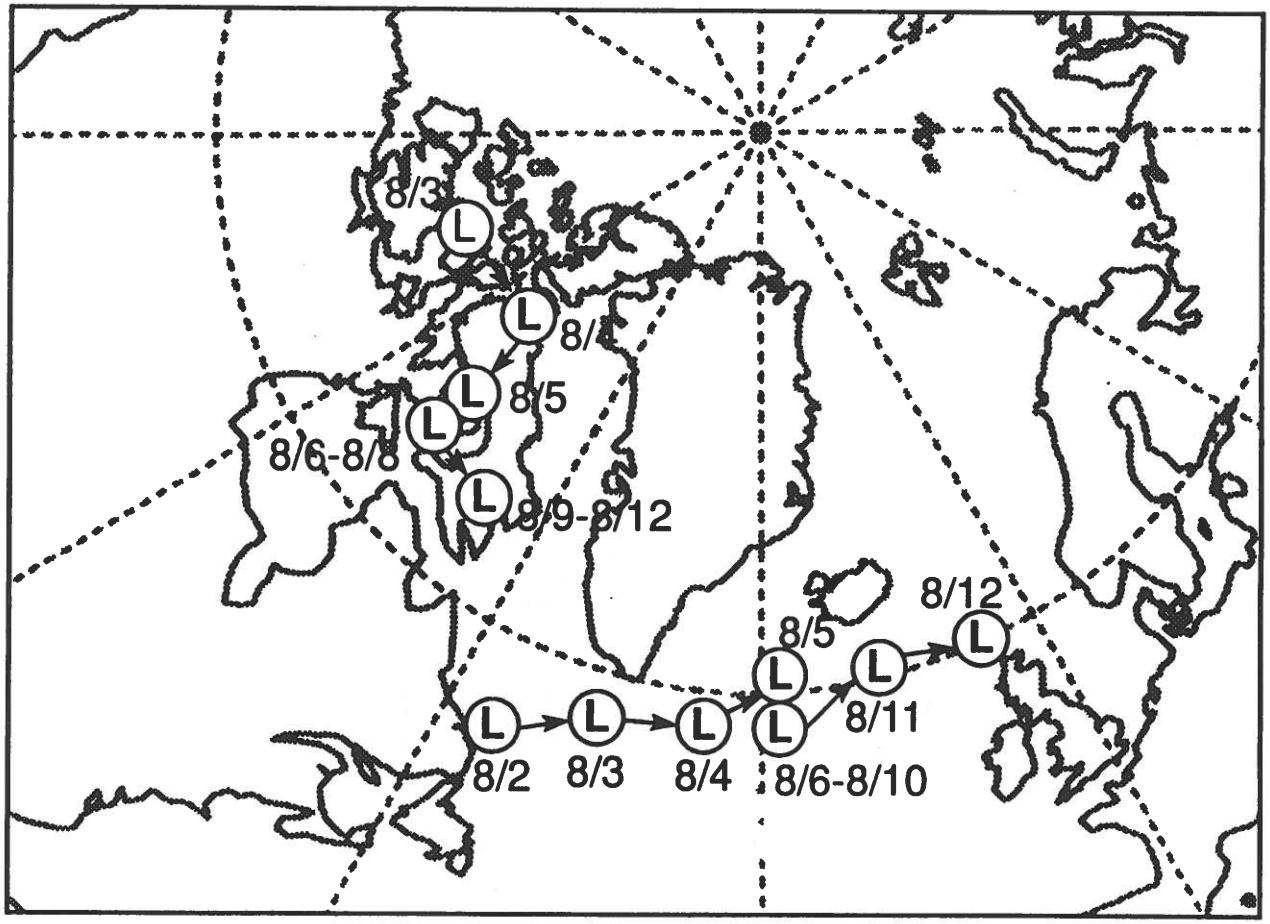

Figure 5b

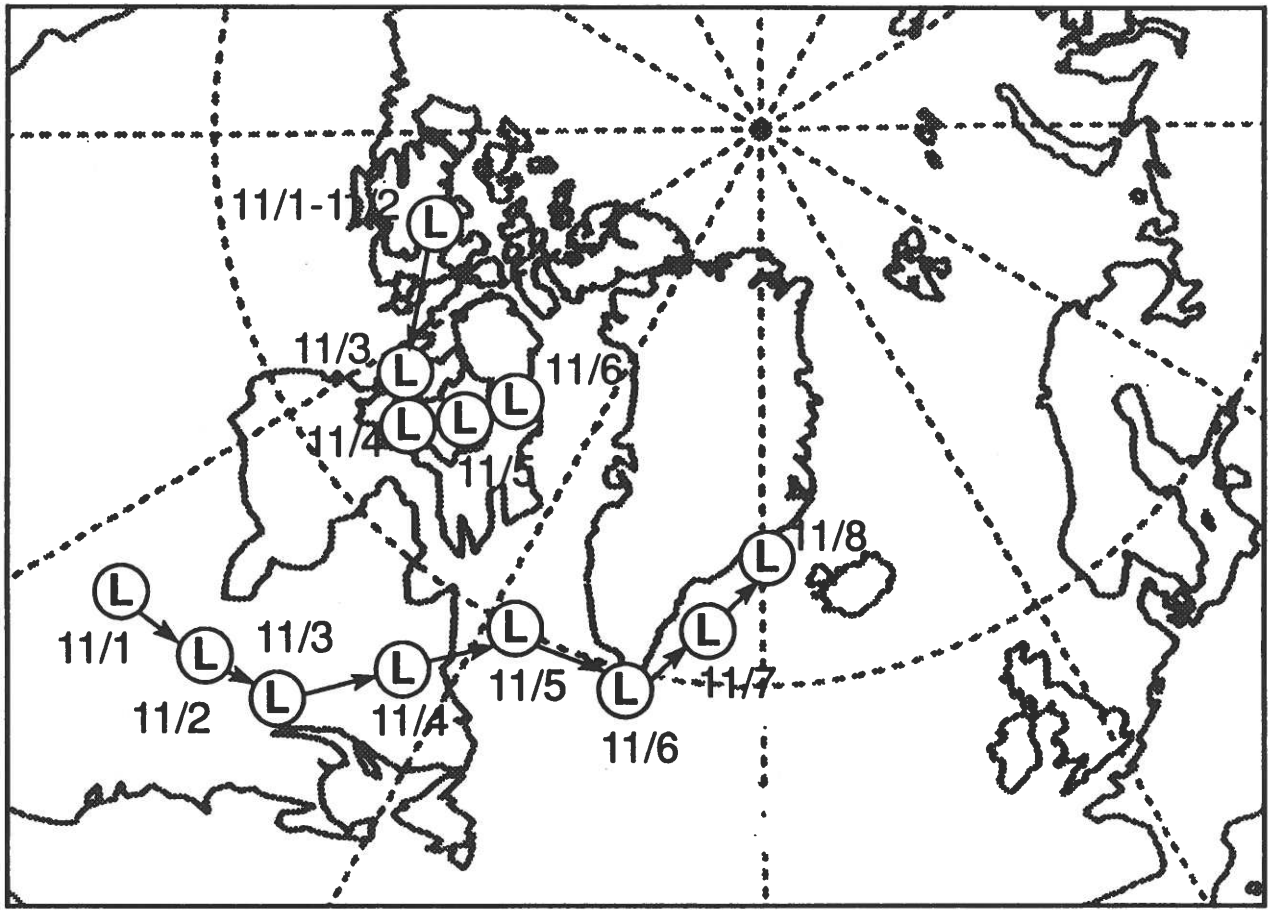

Figure 5c

EFFECTS OF STRATOSPHERIC AEROSOLS ON BREWER, SAOZ AND TOMS MEASUREMENTS

Arne Dahlback
Norwegian Institute for Air Research

Abstract: *A radiative transfer model in conjunction with aerosol profiles derived from lidar measurements at Sodankylä, Finland in 1991/92 are used to determine the stratospheric aerosol effect on total ozone inferred from Brewer, SAOZ and satellite (TOMS) measurements. Brewer direct sun or focused moon measurements are not affected. SAOZ zenith sky measurements are significantly affected by the aerosols. If airmass factors based on clear sky conditions are used SAOZ will underestimate the total ozone up to 30 %. TOMS measurements are also affected. For small solar zenith angles TOMS tends to overestimate the total ozone amount. For large solar zenith angles TOMS underestimate the total ozone significantly.*

The increased concentration of aerosols in the stratosphere due to the Mt. Pinatubo eruption in 1991 has led to increased scattering of solar radiation in the stratosphere. Therefore errors are introduced in the inferred total ozone from measurements by Brewer, SAOZ and TOMS.

The inferred total ozone from Brewer masurements is based on radiance measurements in the ultraviolet part of the spectrum: I_1=310.1 nm, I_2=313.5 nm, I_3=316.8 nm and I_4=320.0 nm. A combination of radiance ratios are formed [Brewer Manual, 1990]

$$N=\log(I_3/I_1)- 0.5 \log(I_3/I_2) - 1.7 \log(I_4/I_3)$$

This N-value is used to derive the total ozone. In addition to direct sun or moon measurements the above formula is also used on measured scattered sunlight from the zenith direction.

SAOZ utilizes absorption by ozone in the Chappuis band at 510 nm to infer the total ozone amount from zenith sky measurements when the sun is near the horizon [Pommereau et. al, 1990]. The instrument measures the ozone column along a slant path. In order to get the vertical ozone column the airmass factor (the slant column divided by the vertical) has to be calculated [Solomon et. al, 1987].

The total ozone derived from TOMS measurements is based on measurements of the backscattered solar ultraviolet radiation. A N-value is formed [WMO report no. 18, 1988]

$$N = 100 \log[(I_\lambda/F_\lambda) / (I_{\lambda'}/F_{\lambda'})]$$

I and F are respectively the measured backscattered radiance and irradiance of the incoming radiation at the top of the atmosphere. Three wavelength pairs, λ and λ' are used: 312.5 nm and 331.2 nm (A-pair), 317.5 nm and 339.8 (B-pair), 331.2 nm and 339.8 (C-pair). N_A, N_B and N_C are used to compute the total ozone. Over most of the globe the A-pair and the B-pair are used but in high latitude winters when the solar zenith angle is large the C-pair is given significant weight.

In the calculations a discrete ordinate radiative transfer for a vertically inhomogenous spherical atmosphere is used [Dahlback and Stamnes, 1991]. The model includes multiple scattering and absorption as well as reflection from the ground. The model can accommodate a general phase function (Mie scattering) implying that scattering by aerosol clouds can be included at any level in the atmosphere. The extinction coefficients, size distribution and phase functions for stratospheric aerosols are based on lidar measurements at Sodankylä in January 1992 and Mie theory.

Figure 1 shows the aerosol effect on Brewer zenith sky masurements. The ozone correction as a function of solar zenith angle has been calculated using two aerosol profiles (January 15 and January 25). The vertical optical depth is in both cases 0.1. The average height of the aerosol layer is 15 km on January 15 and 25 km on January 25. The figure shows the ozone correction as a function of solar zenith angle for these two aerosol profiles. To obtain the corrected total ozone the correction has to be added to the measured total ozone. For solar zenith angles in the range 20 - 50 degrees the ozone correction is less than 5 DU. For solar zenith angles greater than 50 degrees the error depends on the height of the Pinatubo cloud. The error increases with aerosol layer height and solar zenith angle.

The calculations show that the Brewer direct sun and focused moon measurements are not affected by the stratospheric aerosols. This is true for moon or solar zenith angles less than 75 degrees even if we in addition to the direct beam also take into account the diffuse component which is due to forward scattering of the direct radiation.

Figure 2 shows calculated airmass factors for SAOZ zenith sky measurements at 510 nm in three cases: No stratospheric aerosols, medium high (15 km) aerosol cloud and high aerosol cloud (25 km). When aerosols are introduced in the stratosphere the airmass factor will decrease. Since SAOZ zenith sky measurements are taken when the solar zenith angle are around 90 degrees the underestimastion in total ozone can be as large as 30 %.

Figure 3 shows the aerosol effect on inferred total ozone from TOMS. In the calculations the high aerosol cloud (25 km) has been used. The ozone correction has been calculated for the A, B and C wavelength pairs. We have assumed that the TOMS instrument is looking in the nadir direction. For solar zenith angles less than 60 degrees TOMS overestimates the total ozone by 0 - 10 DU. For solar zenith angles greater than 70 degrees TOMS underestimates the total ozone and the error increases rapidly for solar zenith angles greater than 80 degrees. Therefore TOMS data should not been used uncritically at high latitude winters when the aerosol loading in the stratosphere is high.

References:

Solomon, S., A.L. Schmeltekopf and R.W. Sanders, On the Interpretation of Zenith Sky Measurements, *J. Geophys. Res.*, **92**, 8311-8319, 1987.

UNEP/WMO, *Report of the International Ozone Trend Panel* (WMO Global Ozone Research and Monitoring Project. Report No. 18), 1988.

BREWER MKIV Spectrophotometer. *Operations Manual.* OM-BA-CO1/B, May 1, 1990.

Pommereau, J.P., F. Goutail, M. Pinharanda, J. Piquard, and A. Sarkissian, Ground-based total ozone measurements in the visible Chappuis band. *Proc. First European Workshop on Polar Ozone*, Schliersee, Germany, pp. 41-44, 1990.

Dahlback, A. and K. Stamnes, A new spherical model for computing the radiation filed available for photolyses and heating at twilight. *Planet. Space Sci.*, **39**, 671-683, 1991.

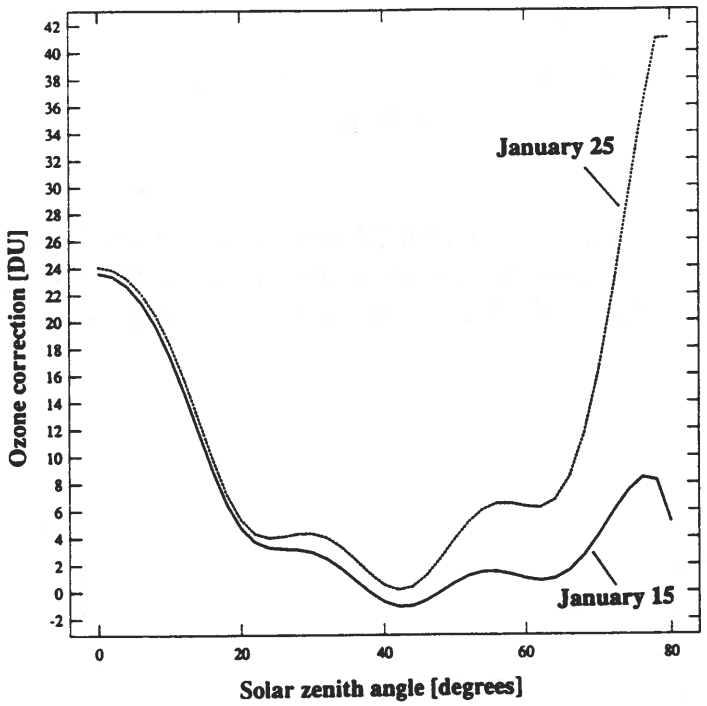

Figure 1. Effects of Pinatubo aerosols on Brewer zenith sky measurements as a function of solar zenith angle: The January 15 aerosol profile (medium high Pinatubo cloud) and the January 25 aerosol profile (high Pinatubo cloud). In order to obtain the corrected total ozone, the ozone correction has to be added to the measured (uncorrected) total ozone.

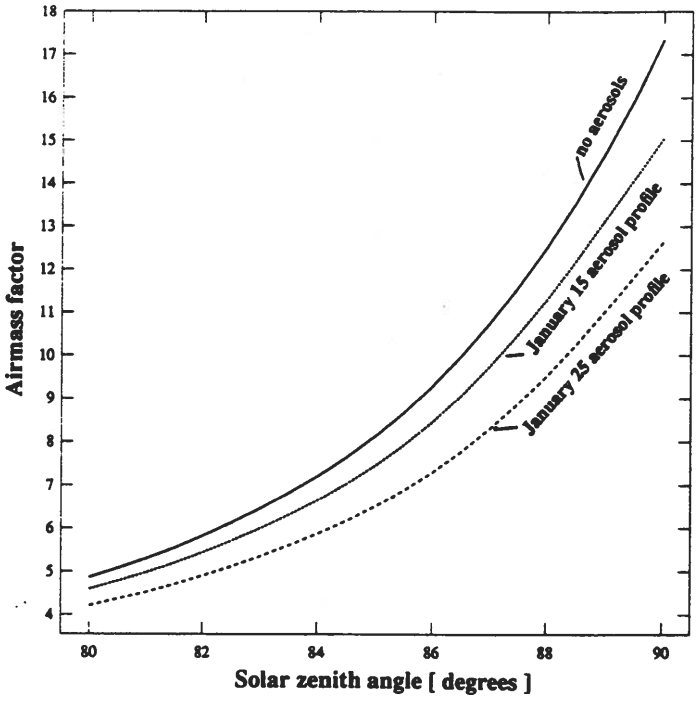

Figure 2. Effects of Pinatubo aerosols on SAOZ airmass factors as a function of solar zenith angle. The airmass factor for clear sky is compared with airmass factor using the medium high aerosol cloud on January 15 and the high aeosol cloud on January 15.

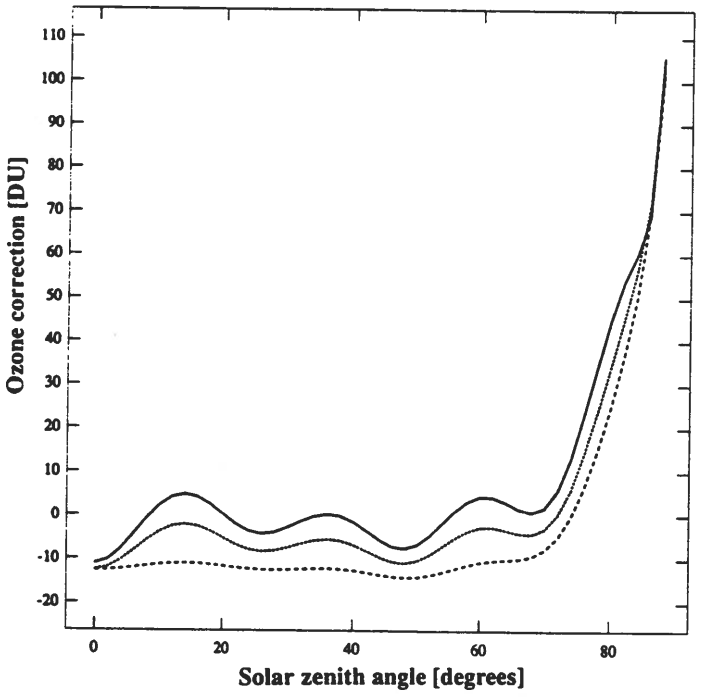

Figure 3. The effect of Pinatubo aerosols on TOMS total ozone measurements as a function of solar zenith angle for 0 - 88 degrees for the A, B and C wavelength pairs: A (solid line), B (dotted line) and C (dashed line). The aerosol optical depth is 0.1 and the average aerosol layer height is 20 km.

Posters

12

Arctic Measuring Stations

NILU F : 35/92
REFERENCE : O-8336
DATE : JANUARY 1993

Atmospheric Chemistry Research Station on the Zeppelin Mountain, Svalbard

G.O. Braathen and E. Joranger (Eds.)
Norwegian Institute for Air Research

POSTER PRESENTATION

5. International Symposium on
Arctic Air Chemistry
8-10 September, 1992, Denmark

NILU

NORSK INSTITUTT FOR LUFTFORSKNING
Norwegian Institute For Air Research
POSTBOKS 64 — N-2001 LILLESTRØM — NORWAY

Atmospheric Chemistry Research Station on the Zeppelin Mountain, Svalbard

G.O. Braathen and E. Joranger (Eds.)

Norwegian Institute for Air Research

A permanent Arctic mountain station was established in 1989 on the Zeppelin Mountain (78°54'29"N, 11°52'53"E), about 2 km from Ny-Ålesund and 475 m.a.s.l. An areal cableway of 1000 m length is constructed for the transportation between Ny-Ålesund and the Zeppelin station. A mountain site has been preferred in order to avoid influence of local pollutants on the measurement of trace gases. The station is most of the time situated above the inversion layer. The aim is to provide Arctic air chemistry and optical data, for the study of the greenhouse effect, the reduction of the ozone layer above Northern Europe, and the background level of inorganic and organic pollutants.

The construction of the station has been funded (11 M NOK) by the Ministry of the Environment (MD, Norway). The Norwegian Council of Scientific and Industrial Research (NTNF) has funded most of the instruments on the station (3 M NOK). The measurement programme is funded by the Norwegian State Pollution Control Authority (SFT) and the Norwegian Research Council for Science and the Humanities (NAVF). The daily operation of the station is carried out by the Norwegian Polar Research Institute (NPI) through funding from the Ministry of the Environment.

1. The greenhouse effect (CFC-gases, CH_4, N_2O, O_3),

Projects: TOR (Tropospheric Ozone Research),
GAW (Global Atmosphere Watch).

by F. Stordal, O. Hermansen, U. Pedersen, N. Schmidbauer and S. Solberg.

Methane

Methane has been measured by use of pressurized stainless steel canisters on the Zeppelin Mountain since September 1989. Normally are taken three measurement samples per week.

The observations show a seasonal cycle with the highest average concentrations in the winter, and the lowest in the summer. The average concentration in the months December-February (~1860 ppbv) was approximately 4% higher than the average concentration in the months June-August (~1790 ppbv). This seasonal difference seems to be consistent with the seasonal cycle in the OH concentration, controlling the chemical breakdown of methane. During the polar night the OH concentration is practically absent.

Compared to the North-European background station Birkenes at the south coast of Norway, the seasonal cycle in the CH_4 concentration was more pronounced at the Zeppelin Mountain.

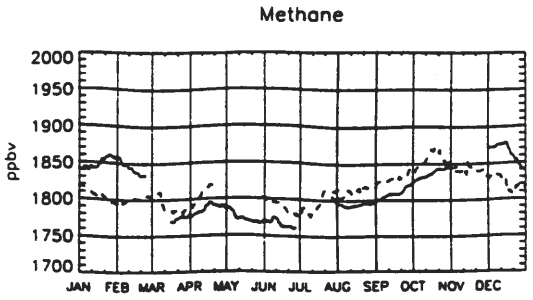

Figure 1.1: *Comparison of methane observed at the TOR stations Zeppelin Mountain (—) and Birkenes (---) (Southern Norway), 1990-1991. 30 days gliding mean values are applied.*

CFC

CFC-11 and CFC-12 are determined in the pressurized stainless steel flask samples taken at Zeppelin since 1991. The result of these measurements are compared with CFC-11 concentrations from Spitsbergen and Ny-Ålesund in 1982-1983 (Hov et al., 1984) in Figure 1.2. The difference corresponds to an annual increase of 10.8 ppt/a, which is close to the increase observed elsewhere, and when the annual increase is accounted for, the concentration level at Zeppelin is also close to the measured concentration level at other remote sites in the Northern Hemisphere (Sturges et al., 1990).

References

Ø. Hov et al. (1984) Geophys.Res.Lett.vol. 11, no. 5, p. 425-428.

W.T. Sturges et al. (1990) CMDL Summary Report, p. 63-71.

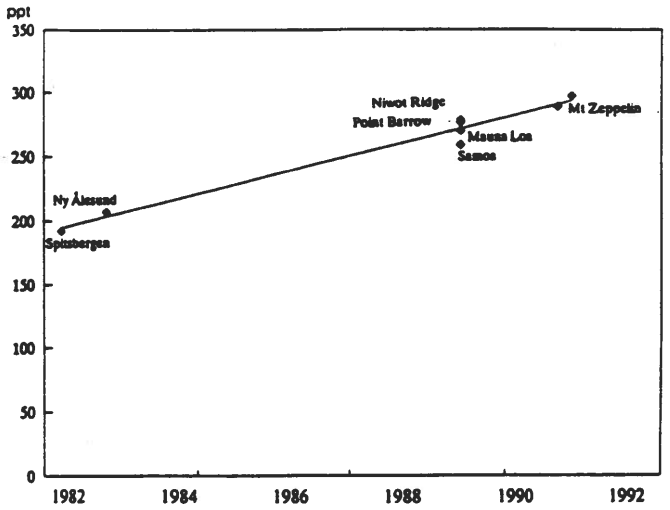

Figure 1.2: *CFC-11 trend since 1982.*

2. Photochemical oxidants at the surface level (ozone, HC, PAN).

Project: TOR.

by F. Stordal, U. Pedersen and S. Solberg.

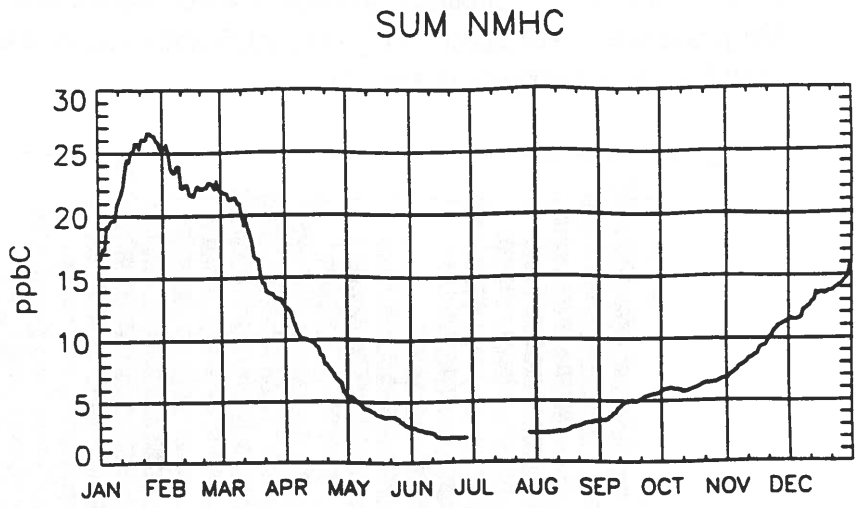

Figure 2.1: *Seasonal variation in the total amount of non-methane hydrocarbons (NMHC) at the Zeppelin Mountain, 1989-1991. 30 days gliding mean values are applied.*

Non-methane hydrocarbons (NMHC)

Individual C_2-C_5 hydrocarbons have been measured at the Zeppelin Mountain since October 1989, later extended up to C_9. Manual samples of pressurized air are taken in stainless steel bottles and are later analyzed in the laboratory with a gas-chromatography with a flame ionization detector.

The observations show a distinct seasonal cycle with a maximum in the winter and a minimum in the summer.

The average value of the sum of the nine C_2-C_5 components C_2H_6, C_2H_4, C_2H_2, C_3H_8, C_3H_6, n-C_4H_{10}, i-C_4H_{10}, n-C_5H_{12}, i-C_5H_{12}, was approximately 7 times higher in the months December-February (17.5 ppbC) than in the months June-August (2.4 ppbC), as shown in Figure 2.1.

The seasonal cycle of the short lived components except propane was most pronounced. This is discussed in an separate article in this compendium.

Ozone

Ozone has been measured on a continuous basis on the Zeppelin Mountain since September 1989, by use of uv-absorption.

Both the hourly (and daily) maximum and minimum concentrations occurred in the spring. Figure 2.2. shows that March 1991 and May 1990 were the months with the highest and lowest monthly average concentration, respectively.

In the autumn the monthly average ozone concentrations on the Zeppelin Mountain was 60-70 µg/m³, which is significantly higher than what is observed at most European background stations.

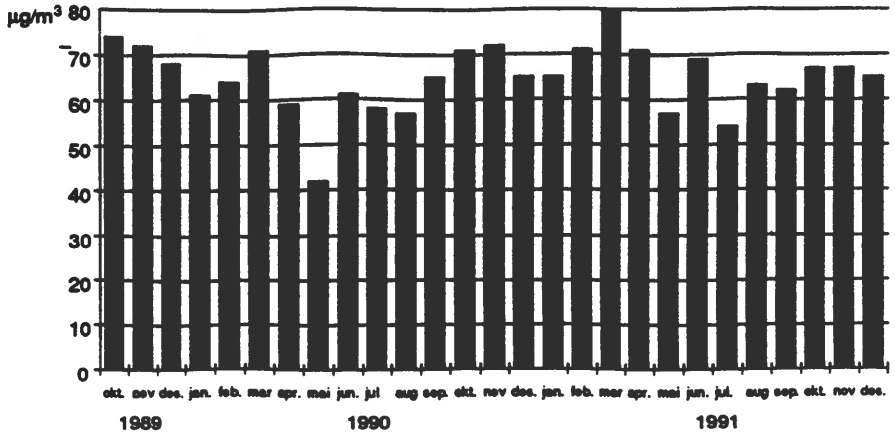

Figure 2.2: Monthly mean concentrations of surface ozone at the Zeppelin Mountain station.

3. Observation of total columns of O_3 and NO_2 with UV/visible spectrometry. Ozonesondes from Bjørnøya.

Projects: SFT,
EASOE (European Arctic Stratospheric Ozone Experiment),
NDSC (Network for Detection of Stratospheric Change),
ESMOS (European Stratospheric Monitoring Stations),
SCUVS (Stratospheric Climatology by UV-Visible Spectrometry).

by G.O. Braathen and B.A. Kaastad.

SAOZ

NILU operates a UV-visible spectrometer (SAOZ) at Ny-Ålesund. In addition, 1-2 ozonesondes/week are launched from Bjørnøya with the aid of the Norwegian Meteorological Institute (DNMI).

The SAOZ (System for Analysis of Observations at Zenith) is a diode array spectrometer which performs measurements of the total ozone column by looking at visible sunlight scattered at zenith. Ozone is calculated in the Chappuis band around 510 nm, which is free of temperature dependence, after removing interfering absorption by NO_2, O_4 and H_2O, by least squares correlation with laboratory ozone absorption cross sections. Slant columns are then converted into vertical columns, knowing the ratio of the actual slant path of the light scattered

through the atmosphere to the vertical path. This ratio is called the air mass factor and varies with the solar zenith angle. The airmass factors are calculated by using a multiple scattering model (Dahlback, et al., 1991).

While ultraviolet groundbased instruments like Dobson and Brewer spectrophotometers do not give reliable data at solar zenith angles larger than 80-82°SZA, SAOZ can operate at solar zenith angles up to 92°SZA. SAOZ makes observation of total ozone in polar regions possible almost throughout the year. In Ny-Ålesund the SAOZ instrument takes zenith measurements from early February to the end of October.

Figure 3.1. shows daily mean values obtained with SAOZ measurements in 1991 and 1992. Only measurements taken when the solar zenith angles were between 87-91°SZA are included in the mean values. The overall precision in total ozone measured with SAOZ at solar zenith angles between 87° and 91° is better than 8% (Pommereau et al., 1990). Total ozone values obtained from ozonesondes launched at Ny-Ålesund and Bjørnøya are also shown. The agreement between SAOZ and ozonesondes is satisfactory for 1991 and the beginning of 1992 when Ny-Ålesund is within the polar vortex. After the vortex breaks up around day 80 (20 March) SAOZ measures far too low total ozone values.

The eruption of Mt. Pinatubo in June 1991 has led to a large increase in the aerosol loading in the stratosphere. The presence of the aerosol layers results in increased attenuation of the direct sunlight and an increase in the diffuse solar flux. Both effects have implications for the UV-and UV/Visible-measurements of stratospheric ozone and result in an underestimation of total ozone. Aerosol lidar measurements at Ny-Ålesund show that the amount of stratospheric aerosols increases rapidly as the vortex breaks up in 1992. Also, the altitude of the aerosol layers is higher outside the vortex than inside. The volcanic aerosols cause a decrease in the airmass factors which increase with optical thickness and altitude of the aerosol layer (Dahlback et al., 1993). The SAOZ data will be corrected by calculating new airmass factors based on aerosol profile data from Ny-Ålesund.

References

Dahlback, A, Stamnes, K. (1991) A new spherical model for computing the radiation field available for photolysis and heating at twilight, *Planet.Space Sci.*, 39, 671-683.

Dahlback, A., Rairuox, P., Stein, B., Del Guasta, M., Kyrö, E., Stefanutti, L., Larsen, N. and Braathen, G.O. (1993) Effects of Stratospheric Aerosols from the Mt. Pinatubo on SAOZ, Brewer and TOMS Measurements at Sodankylä, Finland 1991/1992. To be published in Geophys.Res.Lett.

Pommereau, J.P, Goutail, F., Pinharanda, M., Piquard, J., Sarkissian, A. (1990) Ground-based total ozone measurements in the visible Chappuis band, *Proc. First European Workshop on Polar Stratospheric Ozone Research,* Schlieersee.

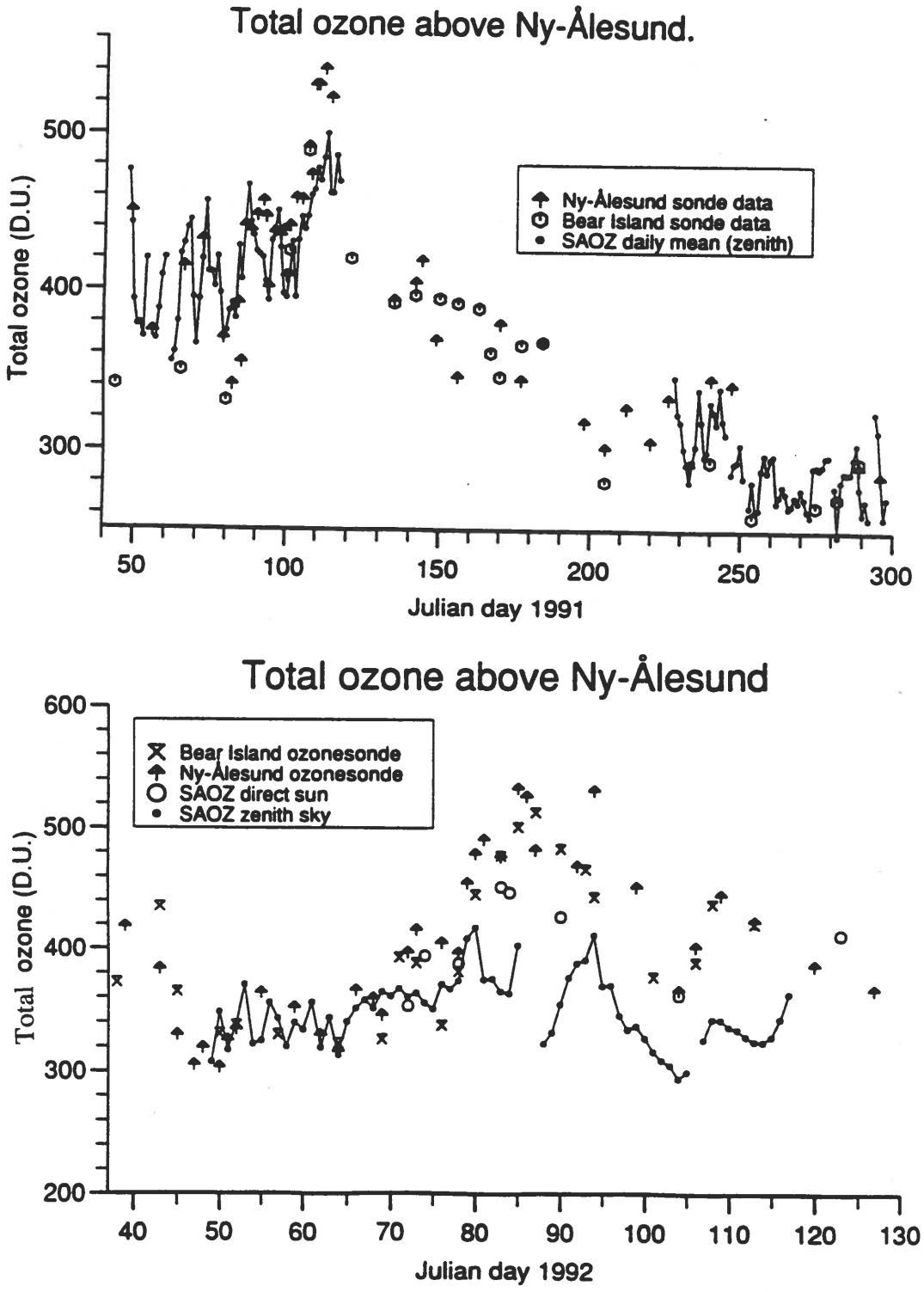

Figure 3.1: *Total ozone from SAOZ and ozone sondes in the period from a) February 1991 to October 1991. b) February 1992 to May 1992. The ozonsonde data from Ny-Ålesund have been provided by Dr. Rolf Fabian at the University of Bremen. The ozonsondes from Bjørnøya (Bear Island) are founded by grants from the State Pollution Control Authority (SFT), and the soundings are carried out by the Norwegian Meteorological Institute (DNMI).*

4. Background levels and transport of ozone, sulphur and nitrogen components in the air (O_3, SO_2, SO_4^{2-},NO_2, NO_3^- +HNO_3, NH_4^++NH_3). Precipitation chemistry.

Project: EMEP (European Monitoring and Evaluation Programme), SFT (The Norwegian State Pollution Control Authority).

by E. Joranger.

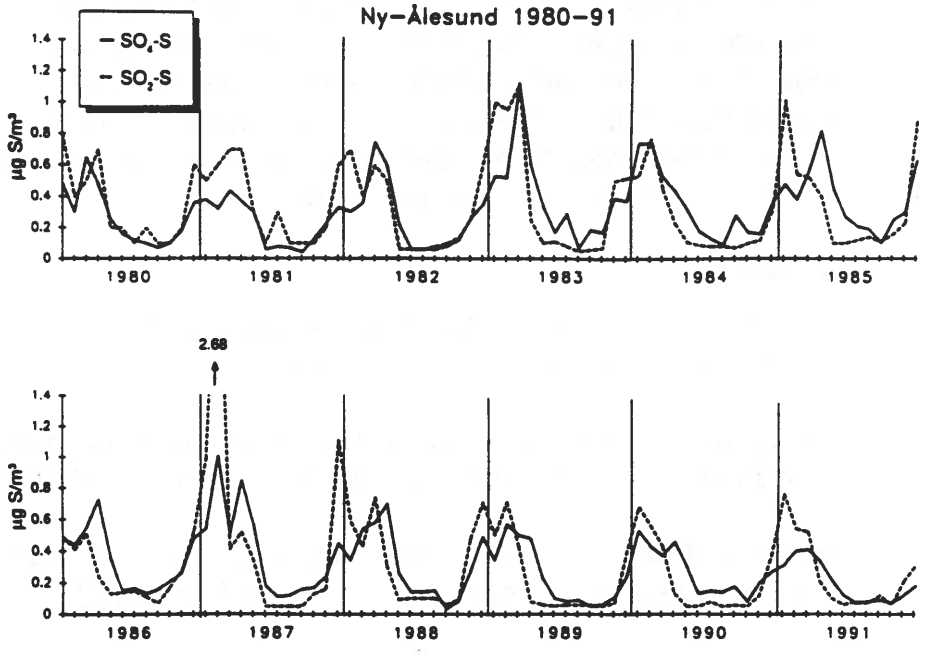

Figure 4.1: *Monthly mean concentrations of SO_2 and SO_4^{2-} at Ny-Ålesund 1980-1991.*

Particulate sulphate and sulphur dioxide are the dominating components of arctic haze and arctic gaseous air pollution, respectively. The monthly mean values are shown in Figure 4.1. The pronounced seasonal variation in the concentration of SO_2 and SO_4^{2-} results from a combination of strong meridional transport and low transformation and deposition rates during winter, conditions which are not present during the summer and autumn seasons.

The hypotesis "no trend" has been tested for the annual average concentrations of the sulphur components in the air at Ny-Ålesund since 1980 and at a number of measuring sites in Norway. The results indicate significant reductions for sulphur dioxide. The estimated decreases are 34% since 1980 at Ny-Ålesund, and 45% and 60% reductions respectively in Finnmark and in Southern Norway since 1979. For sulphate in aerosols there is, however, no significant trend at Ny-Ålesund, as well as in Finnmark, whereas the average reduction in Southern Norway was 37%.

5. Air concentrations of chlorinated hydrocarbons (PCB, HCH, Chlordanes, Toxaphenes, DDT, etc.) at Ny-Ålesund.

by M. Oehme.

Polychlorinated pesticides and aromatics with a long lifetime in the environment can be transported via the atmosphere from source areas to the Arctic. Figure 5.1. shows long range air transport episodes in March 1984. Chlordanes are pesticides which have been mainly used in North America and the Mediterranean countries. Increased levels were observed at March 10-11 and March 19-20. The 850 hPa trajectories (Figure 5.2.) indicate transport from the Iberian peninsula and North America, respectively. During the second episode, also elevated concentrations were found for α- and γ-hexachlorocyclohexane (HCH, part of a widely used technical pesticide mixture) and hexachlorobenzene (HCB, formed as a byproduct of chlorinated processes, by combustion sources and used as a fungicide). Further information has been published in the references.

References

Oehme, M. and Manø, S. (1984) The long-range transport of organic pollutants to the Arctic. *Fres.Z.Anal.Chem.* 319, 141-146.

Oehme, M. and Ottar, B. (1984) The long-range transport of polychlorinated hydrocarbons to the Arctic. *Geophys.Res. Letters*, 11, 1133-1136.

Pacyna, J.M. and Oehme, M. (1988) Long-range transport of some organic compounds to the Norwegian Arctic. *Atmos.Environ.*, 22, 243-257.

Oehme, M. (1991) Further evidence for long-range air transport of polychlorinated aromatics and pesticides from North America and Eurasia to the Arctic. *Ambio*, 20, 293-297.

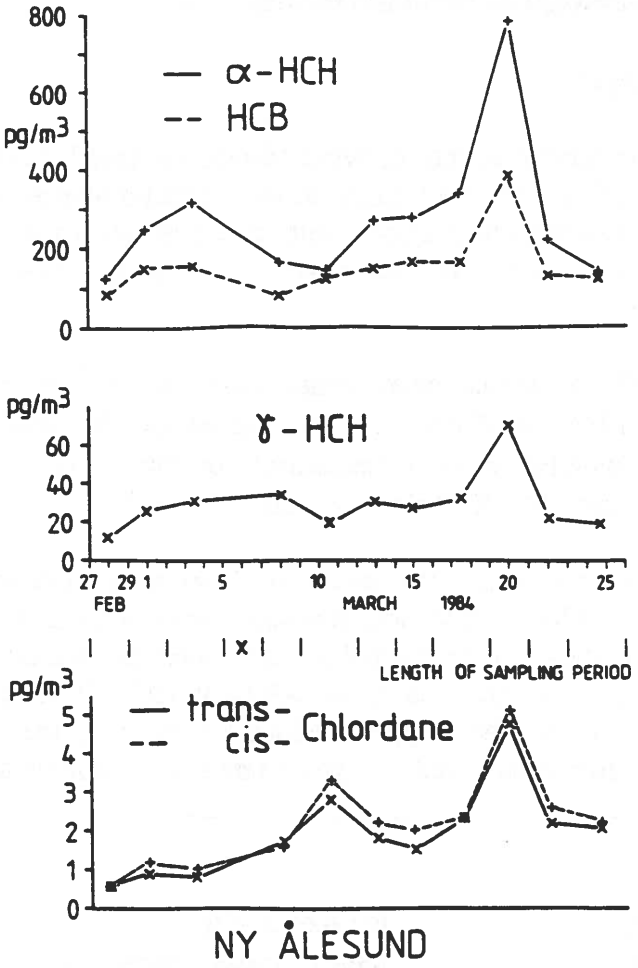

Figure 5.1: *Air concentrations of chlorinated hydrocarbons, measured February-March 1984 at Ny-Ålesund.*

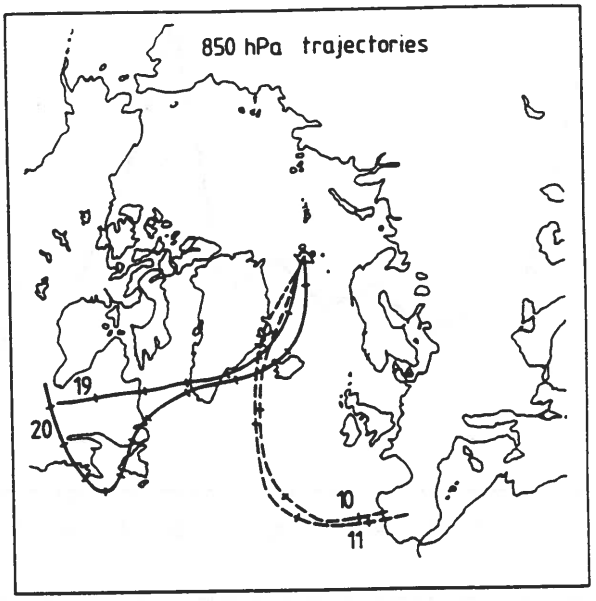

Figure 5.2: *Air trajectories at 850 mb-level March 10-11 and March 19-20, 1984.*

6. Meteorological measurements

by E. Joranger.

Continuous measurements of wind (direction, speed, gust), temperature and of relative humidity has been made at the Zeppelin station since September 1990. Synoptic weather observations with measurement of temperature and relative humidity are carried out at Ny-Ålesund by the Norwegian Meteorological Institute.

Since 1975 the annual mean temperatures at Ny-Ålesund has varied between -3.3°C in 1984 and -8.6°C in 1988, and no specific trend is discernible (Figure 6.1). The monthly mean temperatures for the period 1974-1991 (not shown) varied between -14.1°C (February) and 4.9°C (July).

The seasonal percentage frequencies of different wind directions and velocities at the Zeppelin Mountain station, measured since September 1990, has been fairly constant, as shown in Figure 6.2 for the winter-months December 1990-February 1991 and the summer-months June-August 1991. It is seen that the prevailing wind-direction on the Zeppelin Mountain is from the sector towards south-southeast. High wind speed is most common in the winter-months.

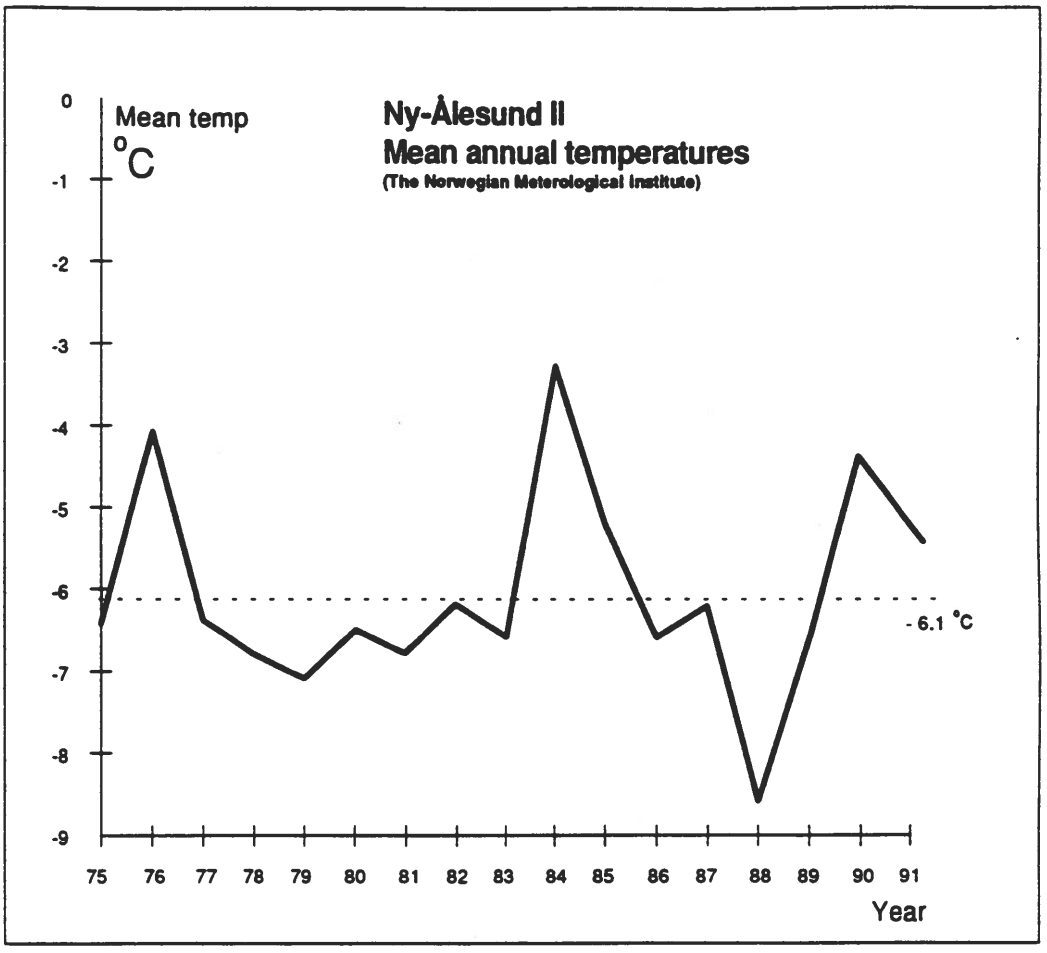

Figure 6.1: *Mean annual temperatures at Ny-Ålesund.*

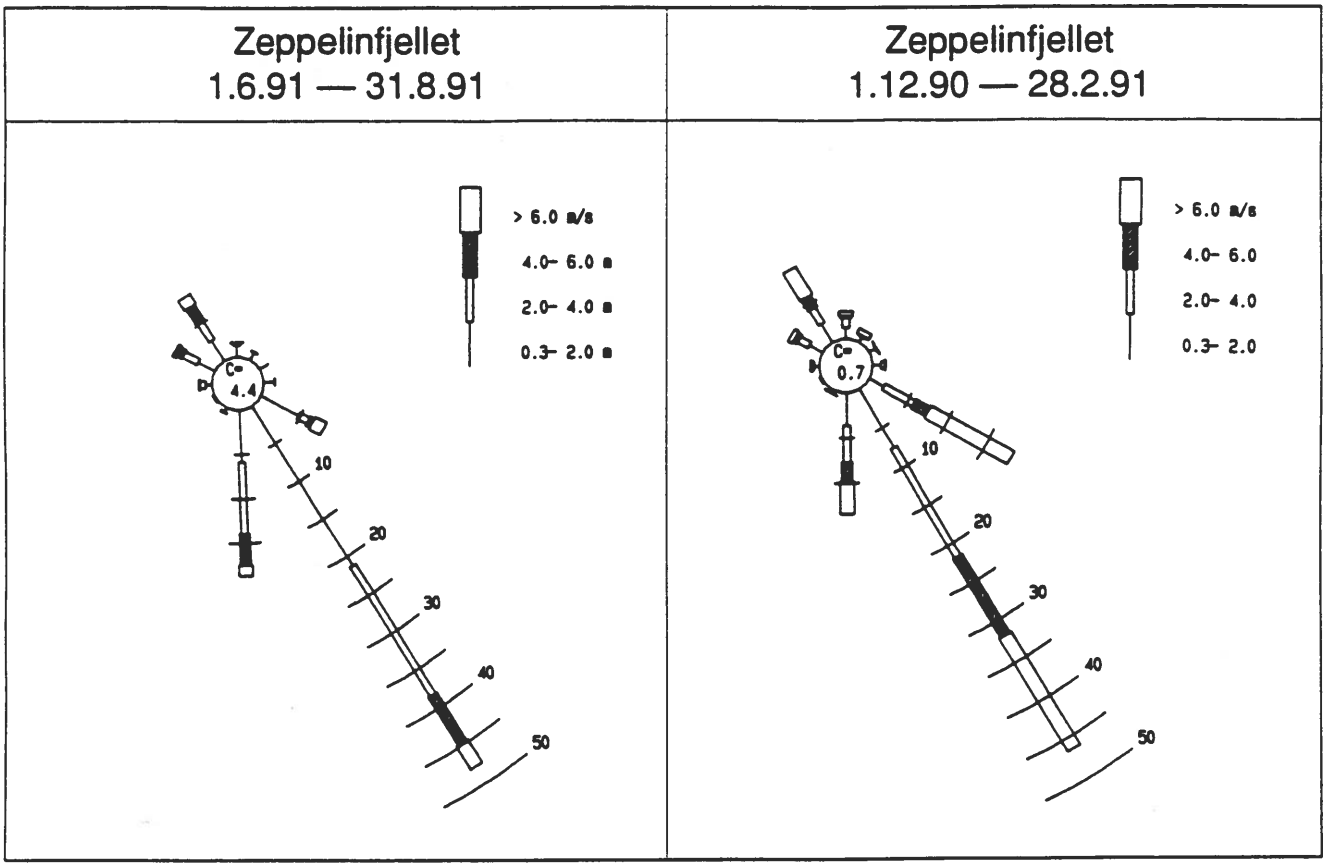

Figure 6.2: *Percentage frequencies of different wind directions of velocities at the Zeppelin Mountain station, summer and winter seasons 1990-91.*

Other measurements

In addition, the following air measuring programmes are presently in operation on the Zeppelin Mountain Research Station:

7. Air concentrations of CO_2 and aerosols (nephelometer, two condensation nuclei counters, filter sampling), wind, temperature, humidity, sensors and cloud detector. University of Stockholm (MISU).

8. Air concentrations of heavy metals. NILU, University of Gothenburg, University of Gent.

9. Radiation measurements. NPI (Norwegian Polar Research Institute).

10. NO_2 (University of Oslo, NILU). Chemiluminescence, photolytic $NO_2 \rightarrow NO$ conversion.

11. Radioactivity (gross gamma). NILU.

NATIONAL ENVIRONMENTAL RESEARCH INSTITUTE
Division of Emissions and Air Pollution
Roskilde, DENMARK 24.08.1992

Fifth International Symposium on Arctic Air Chemistry

The Danish Atmospheric Measuring Site Station Nord in the Greenland Arctic

Niels Z. Heidam
National Environmental Research Institute
Frederiksborgvej 399
DK 4000 Roskilde
Danmark

Abstract

Concerns for environmental and climatic impacts of air pollution in the Arctic have led to the establishment of an atmospheric measuring facility at Station Nord in Northeast Greenland. In view of the increasing international cooperation on atmospheric research and on monitoring within the Arctic Monitoring and Assessment Programme it is planned to develop the site into a full-fledged research and monitoring station.

The logistics of the site and the climatology of this region in the Arctic are presented.

Poster

Background

The Arctic is one of the last pristine regions on Earth but it is also an area very vulnerable to pollution. The environmental risk is particularly pronounced with respect to air pollution which may be transported long distances from industrial sources in the midlatitude regions of the northern hemisphere.

In addition the Arctic occupies a central position in the weather and climatic systems which dominate this hemisphere. Changes in the atmospheric conditions in the Polar area may produce widespread environmental and climatic consequences. It is thus a general, scientifically accepted opinion that the stratospheric ozone problem and the greenhouse effect will produce the largest - and possibly the first - consequences in the Polar regions. Other effects arising from the long range transport of air pollution are a modified radiation balance and changed precipitation patterns in the Arctic troposphere.

Such concerns have initiated efforts to develop the existing experimental facilities for air pollution measurements at Station Nord in Northeast Greenland into a permanent Atmospheric Research and Monitoring Station. The station will then become part of the network under the international Arctic Monitoring and Assessment Programme, AMAP. In order to promote international cooperation the station will be opened to other researchers who wish to perform relevant scientific or environmental investigations on a cooperative basis.

Location and Meteorology

Station Nord is a small danish military airbase in the farthest northeastern corner of Greenland at *81^0 36' N, 16^0 40' W* as shown on the map in *Figure 1*. It is located at an average height of about 30 m a.s.l. in the northern part of a 20 · 15 km^2 plain bordering on the Wandel Sea to the north and west and to a local icecap, Flade Isblink, to the east and south. The area is shown in *Figure 2*. In the snowfree season the ground surface is bare stony and moist soil with a sparse vegetation consisting mainly of scattered lichens

and mosses. With the exception of the military station proper the plain is part of the huge East Greenland National Park that occupies the whole northeastern quadrant of Greenland.

At this latitude the Arctic day lasts from April 10. to September 3. and Arctic night reigns from October 16. to February 26. The two first and two last weeks of the dark period are characterized by Arctic dusk. The extended periods of constant light and constant darkness makes the Arctic unique for studies of atmospheric processes such as physical transport mechanisms and chemical transformations.

This location has been chosen because Northeast Greenland is known from previous investigations to be systematically exposed to air pollution of distant midlatitude origin transported by seasonally governed, large scale atmospheric circulation patterns. That is illustrated by the average synoptic situation in January shown in *Figure 3*. In winter the dominant circulation brings air of Euro-Asian origin into the area between Northeast Greenland and Spitzbergen and very often it carries a heavy load of pollution emitted from the large industrial source areas in this continental region.

Experimental Facilities

Measurements at Nord has taken place in several periods since the late 1970's under the general heading 'Studies of Arctic Gases and Aerosols', **SAGA**. The measuring sites were and are to some extent still located at one of the more remote buildings of Station Nord proper, see *Figure 2*.

Thus weekly samples are presently collected of sulfate and ammonium aerosols and of the gases sulfurdioxide, ammonia, and nitrogen dioxide at the location 'LW hut' which houses a filterpack setup and an old long_wave transmitter. At the location 'LW streaker' an automatic streaker collects continuous weekly aerosol samples specially suited for PIXE-analysis. Similar sampling is taking place at the location labelled 'Knuth Streaker' on a 130 m high promontory at a distance of about 5 km from the cental building complex.

A new air measuring laboratory has been established at the site labelled 'New air lab'. This new SAGA-station is located in the National Park just outside the base area proper and about 2 km south of the central complex of buildings, see *Figure 2*.

The facility consists of a 6 · 4.5 m^2 well insulated wooden hut situated at the bank of a small lake that serves as a fresh water reservoir. A plan of building is shown in *Figure 4*. It contains a laboratory equipped with worktables along the walls. Ambient sample air is supplied centrally from an air intake 3 m above the roof and 6.5 m above the ground. The main air duct is a 10 $cm^{\varnothing}$ stainless steel tube with an airflow of 100 m^3/h that can be sampled internally. Air is returned to the outlet 1.5 m above the intake but can be diverted into the workspace for ventilation purposes. 220 V AC electricity is available but there is no running water.

Climatology

The temperature has an annual mean value of -17 °C and varies between winter minima below -50 °C and summer maxima around 15 °C. The monthly mean temperatures, shown in *Figure 5*, vary between -31 °C and 4 °C but the observed monthly maximum and minimum temperatures show that a large variation often occurs within the same month. The relative humidity is fairly constant around 80 % in winter but scatters between 50 % and 95 % from May to September which is the period when the mean temperature is above -10 °C.

The winds at Nord are usually moderate. The annual average velocity is about 4 m/s but velocities above 20 m/s do occur infrequently, less than 0.5 % of the time, and apparently mostly in autumn and early winter. Monthly mean and maximum wind velocities are shown in *Figure 6*.

The annual distribution of daily wind directions over 8 sectors of 45° around the compass is shown in *Figure 7*. The most frequent direction is from Southwest at a frequency of 30 %. Presumably these are catabatic winds from the main Icecap of Greenland so that Nord is also a good sampling point for clean air. Conditions of variable or no wind during the day, labeled 'Undecided' account for 40 % of the observations.

The annual distribution of 3h_observations of wind velocity over the 8 daily sectors is shown in *Figure 8*. It is seen that on the average the largest wind velocities occur in the S and NW directions.

Access and Logistics

Station Nord is only accessible by aircraft which makes for high costs of any facility requirements whether electric power or personal board and lodging. The runway at Station Nord is a 1.3 km long gravel airstrip which allows quite heavy aircraft to access the station. There is a fairly regular but infrequent air service with Hercules C-130 aircraft out of an airbase in the Copenhagen area. Regular flights usually take place in february, march, april, july, august (twice), september, and december.

Station Nord a.o. also serves as a radio beacon and a meteorological station. The permanent staff consists of 5 tecnically skilled military persons whose main duty is to keep the station and runway in operational order. There are about 25 wooden buildings serving as quarters for permanent and visiting personnel, mess hall, workshops, garages, storerooms and a 2 · 100 kW power station. Nord is affiliated to the Danish Defence Command and served by the Royal Danish Airforce. Access to Nord and the National Park is regulated and approval must be obtained from the authorities concerned.

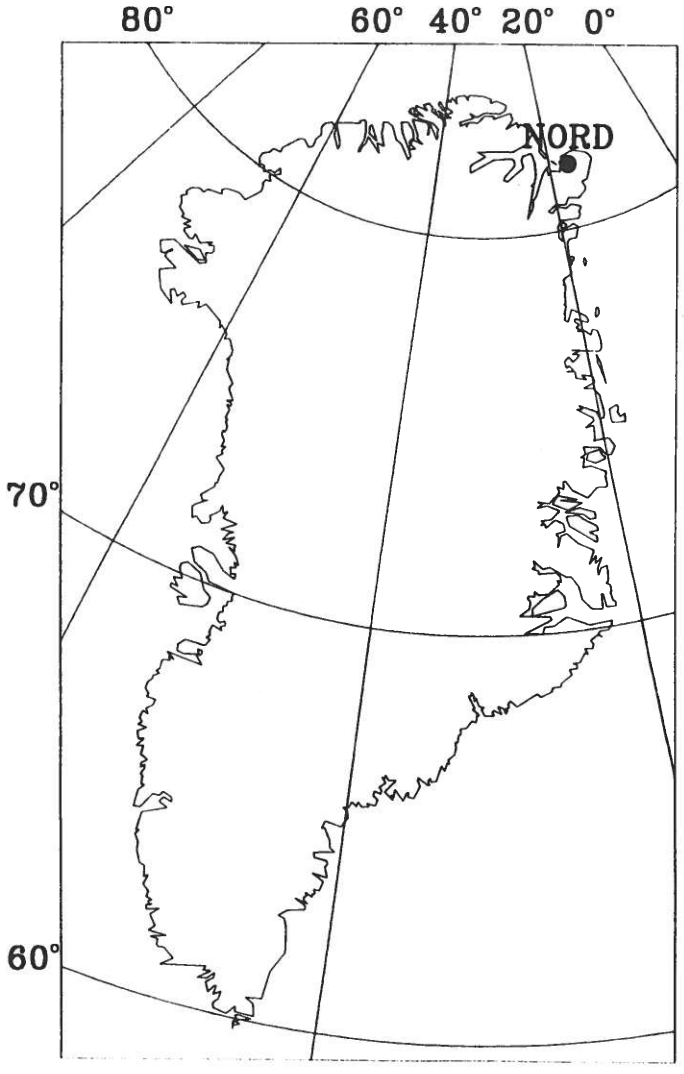

Figure 1. Station Nord in Northeastern Greenland.

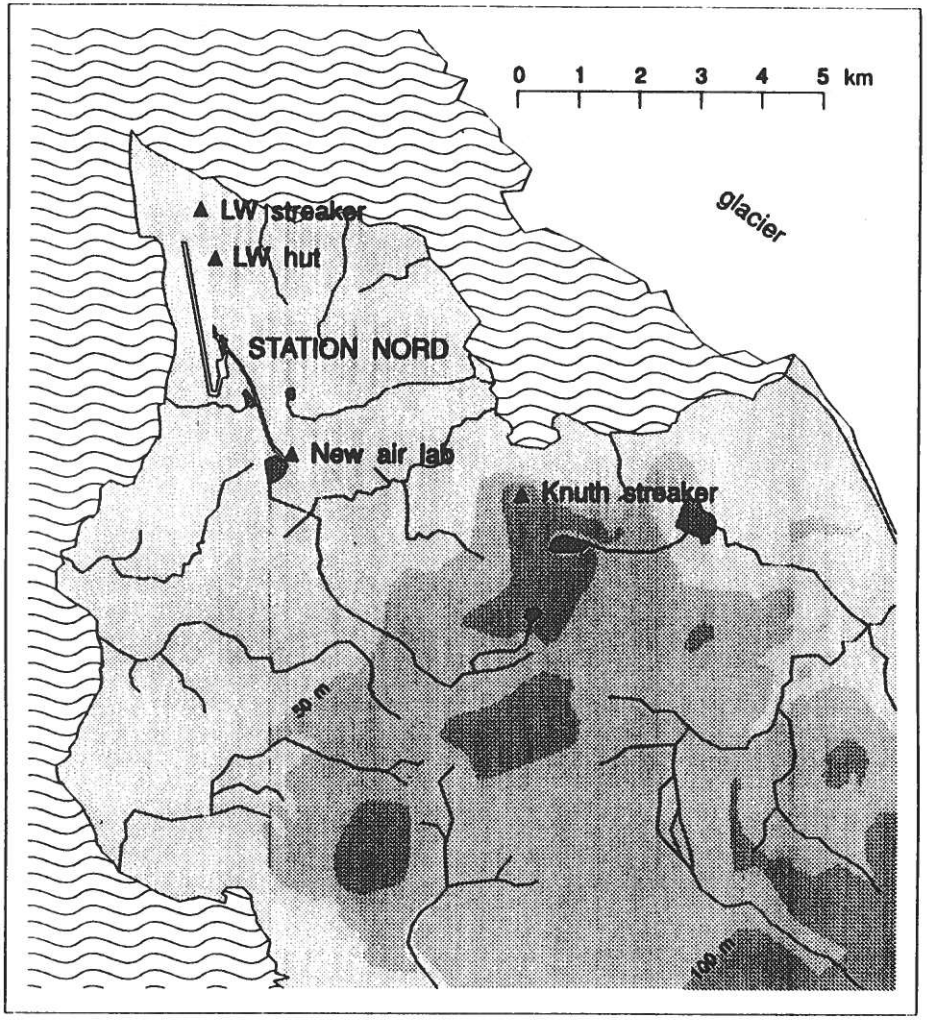

Figure 2. Station NORD. Location and surroundings.

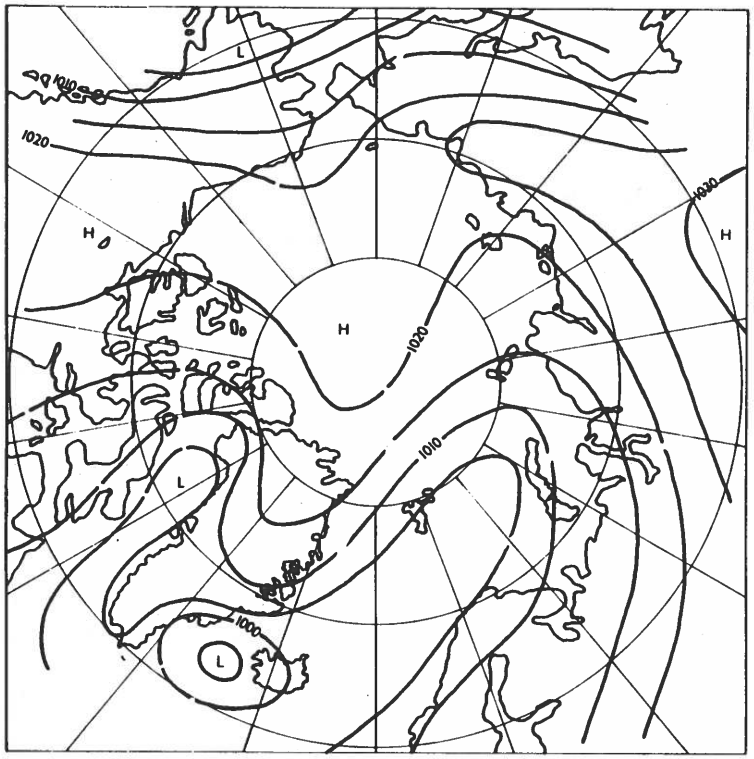

Figure 3. The average synoptic situation in the polar region in the month of January.

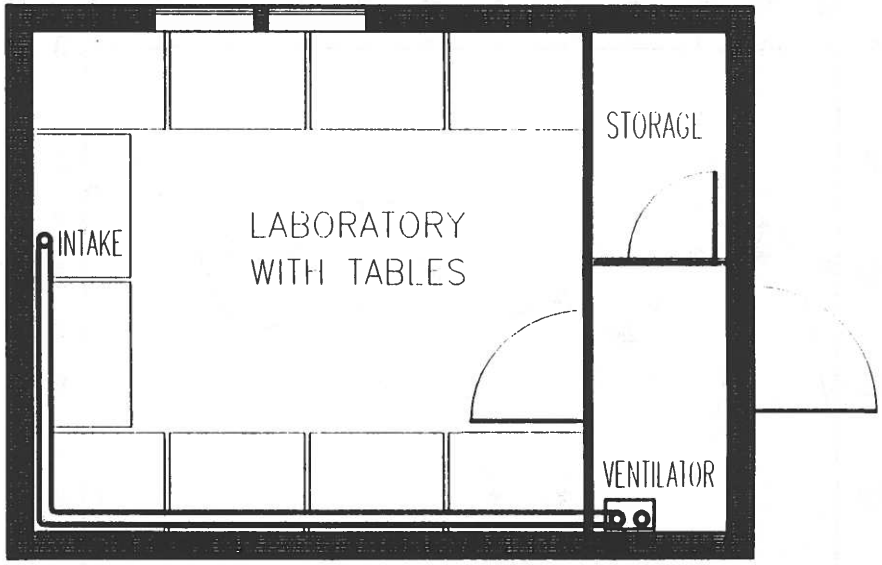

Figure 4. Plan of the new air laboratory at NORD. The gross area measures 6.0 * 4.5 m^2.

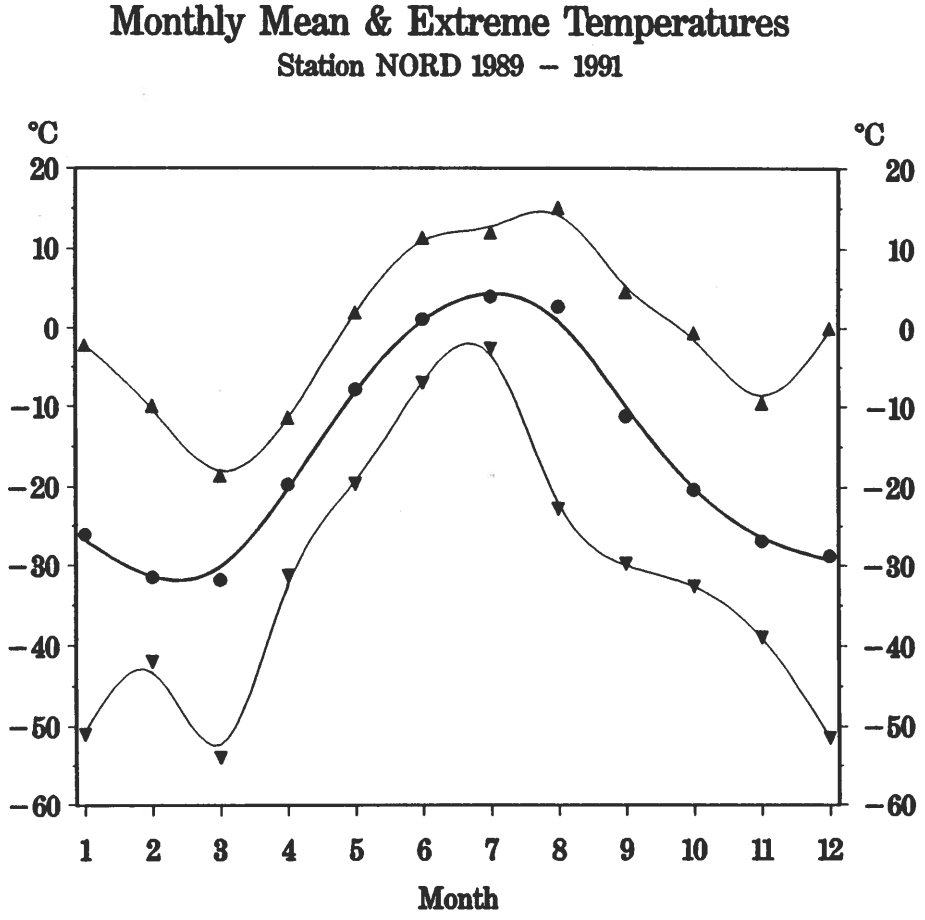

Figure 5. Monthly mean and extreme temperatures at NORD.

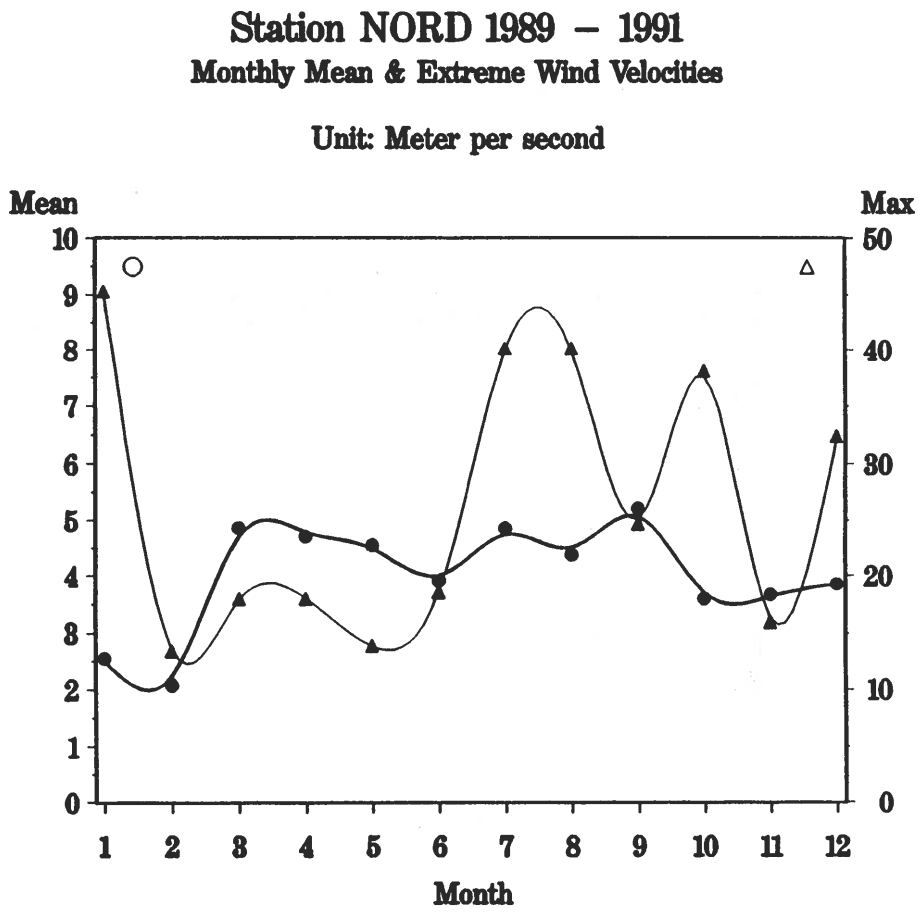

Figure 6. Monthly mean and maximum wind velocities at NORD.

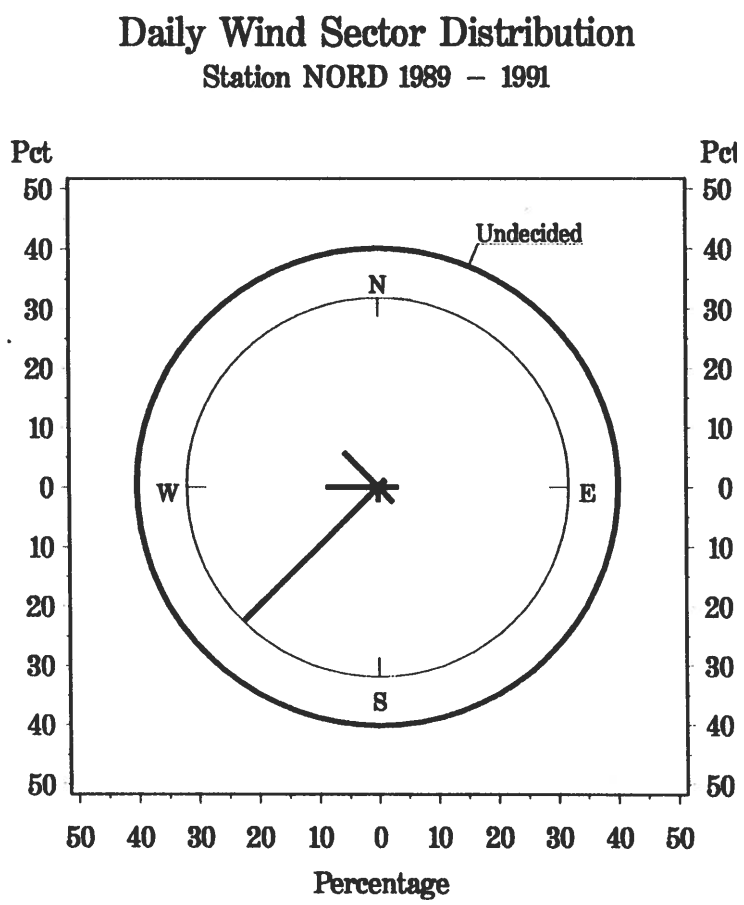

Figure 7. Annual distribution of daily wind sectors at NORD.

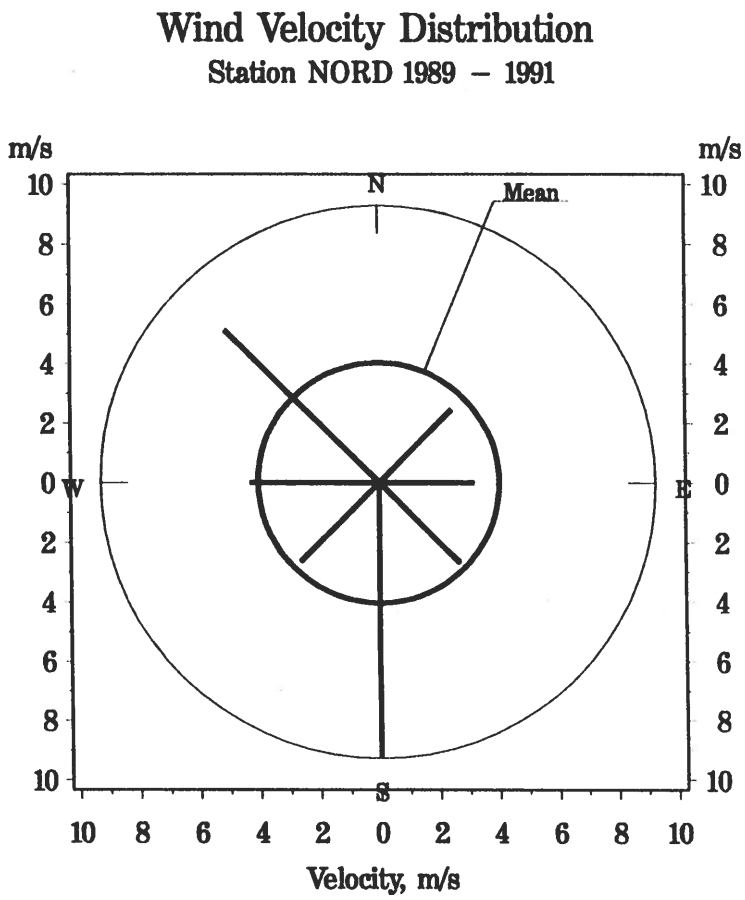

Figure 8. Annual mean wind velocities in wind sectors at NORD.

13

Sampling Techniques

Aerosol sampler for unattended all-year sampling at remote sites.

K. Kemp and P. Wåhlin
National Environmental Research Institute
Frederiksborgvej 399, DK-4000 Roskilde.

Introduction

Detailed information about the air pollution at remote sites is an important key in the description of transport and the global levels of the pollution. Due to the need for regular service and maintenance the sampling stations are usually by necessity connected to locations with human activity. This introduces of course a danger of local contamination of the samples and in some cases only sampling during the summer is possible.

It has been our intention to build a time sequential aerosol sampler, which could run continuously independent of external supplies and with service only once a year. A number of different species should be determined in order to characterize the emission sources that contribute to the pollution at the site. This gave rise to a number of theoretical and practical considerations. The only way to perform realistic tests was to place the sampler at the actual measuring location.

We decided to use a "streaker" sampler, which has been used in connection with PIXE analysis since the mid 70's (NELSON, 1977). The "discrete" streaker described by KEMP and MØLLER (1981) was used as starting point.

Limitations

The energy supply for the sampler could be either solar or wind power, or batteries. In any case the power consumption has to be modest. In the Arctic batteries have to constitute the main supply, since solar light is not available during winter and the low temperature impedes the use of wind energy. The practical limitation is the weight of the batteries, which should not exceed about 500 kg. Using Zn/air batteries, which are some of the most efficient, the average consumption of the sampler is thus limited to about 5 W.

The temperature inside the sampler must be above the freezing point in order to preserve the suppleness of the pump membranes, filter material etc. If the sampler is to be used on an ice sheet in the High Arctic the surrounding temperature may

fall to -70°C. Even if the sampler is placed approx. 2 m below the snow surface, where the temperature is close to the yearly mean, it may be necessary to maintain a temperature difference of up to 50°C between the inside of the sampler and the surroundings. An effective thermal insulation is obviously needed. A shield of insulation material between two concentric spheres with the radii r_o and r_i creates a temperature difference, due to the dissipation of the effect, P, in the inner sphere:

$$\Delta T = \frac{P}{4\pi\lambda} \cdot \left(\frac{1}{r_i} - \frac{1}{r_o}\right)$$

where λ is the thermal conductivity for the insulation material. λ is typically around 0.035 W/(m·°C) for some of the most efficient insulation materials like polystyrene or polyurethan foam. With P = 5 W this leads to a theoretical maximum diameter of about 0.5 m for the sampler. In practice it has to be restricted to 0.2-0.3 m.

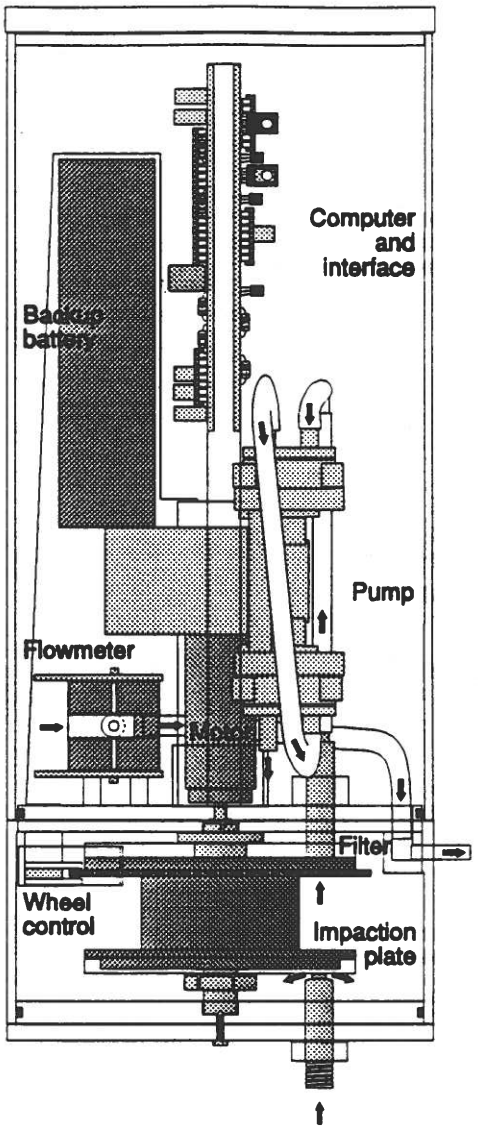

Fig. 1: Schematic drawing of the streaker.

The streaker

The discrete streaker (KEMP and MØLLER, 1981) was rebuilt to enable operation within the above limitations. A schematic drawing of the streaker is shown in fig. 1. It consists of a cylindric acryl tube with a diameter of 15 cm. There are two compartments in the tube. The smaller one contains the sampling system, while the larger on includes pumps, flowmeter and electronics.

Particles are collected in two size fractions on two coaxial discs. Coarse particles are deposited by means of impaction on an Apiezon coated (WESOLOWSKI et al., 1977) 12.5 μm thick mylar foil, while the fine particles are collected on a 0.4 μm pore size Nuclepore filter (cf. fig. 2). The size cut off for the impaction stage is approx. 2 μm (aerodynamical diameter). The samples are collected close to each other along a circle with a diameter of 7 cm on the foil/filter. The separation between the samples are 5°. The coarse particle spots are defined by the rectangular (0.25 cm x 0.025 cm) impaction orifice, while the fine fraction spots are defined by the 0.25 cm x 0.75 cm oval

orifice behind the filter. The foil and the filter are mounted on the same wheel, which is moved one step at each sample change.

The main power consumer is the pump. We have used Brailsford type TD-4S2X pumps, which enable an air flow of about 10 cm^3/sec through the sampling system at a power consumption of about 3 W. The pump is specified to run for at least 5000 hours without maintenance. Two pumps are included in the streaker and used by turns in order to ensure one year of continuous operation.

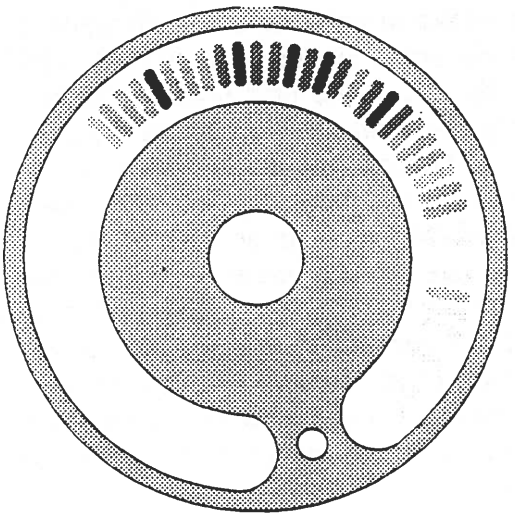

Fig. 2: A partly exposed Nuclepore filter used for collection of the fine fraction.

The air from the pumps is released directly to the larger compartment of the streaker, which apart from containing the pumps etc. also serves as a wind kettle before the flowmeter that is mounted in the outlet from the streaker. The position of the flowmeter ball is "read" by means of an array with 11 sets of LED/phototransistors. During sampling the flow is recorded with an uncertainty of about 1 cm^3/s.

The operation of the streaker is taken care of by a small computer. A built-in alarm clock ensures that the computer is turned on only in short intervals when recording and sample changes are in progress. The average power consumption of the computer is thus negligible. The flow rates and filter positions are stored in a RAM memory together with the corresponding dates and times. The information can at any time be dumped to an ordinary DOS/PC. The computer can be programmed in Basic. This enables the choice of any length of time between sample change and flow registration.

A 2 W heating element is automatically turned on if the temperature inside the streaker falls below 0 °C.

Sampling in the Arctic.

Insulation of the streaker is, as discussed above, necessary when the ambient temperature is expected to be low. Two blocks of polystyrene foam are fitted on top of each other into an Zarges aluminum box (170 cm long, 80 cm wide and 70 cm high) and a room for the streaker is hollowed out between the two blocks. Two co-axial tubes from the streaker to the end of the box act as heat exchanger between the outlet and inlet air. The heat exchanger prevents local cooling around the streaker intake. (Even without the heat exchanger the total effect carried away with the exhaust air would be less than 0.5 W). The batteries, 30 pieces of 1.5 V, 2000 Ah Zn/air cells, are placed in the same type of box as the streaker . The air intake is placed about 3 m above the soil/snow surface. A toy Frisbee is mounted at

the intake in order to avoid clogging of drifting snow (HALL and UPTON, 1988) (cf. fig. 3). A 0.5 $cm^{\varnothing}$ Nylon tube connects the intake with the heat exchanger in the box. Problems with rime in the inlet tube may arise if the temperature of the air is higher than of the snow. By using a wider tube just below the snow surface, it has been observed that the content of water in the modest amount of air, which is taken through the sampler, condensates on the wall of the tube without obstructing the air flow.

If the sampler is mounted at a location, which is permanently covered with snow it will be an advantage to bury it in the snow in order to obtain a near constant temperature. Each year it should be lifted a distance corresponding to the new snow layer. If the surface at the site is snow free in the summer the sampler can be placed directly on the soil. During the winter it will be shielded by snow, but during the summer the temperature may rise considerably above the freezing point. To prevent over-heating a slit is cut through the insulation material above the streaker. A water filled plastic back is placed in the slit. Usually the water will be frozen and the heat transport through the ice will be negligible. But if the temperature inside the sampler is to high, the water will melt and the heat will be removed by thermal convection in the water.

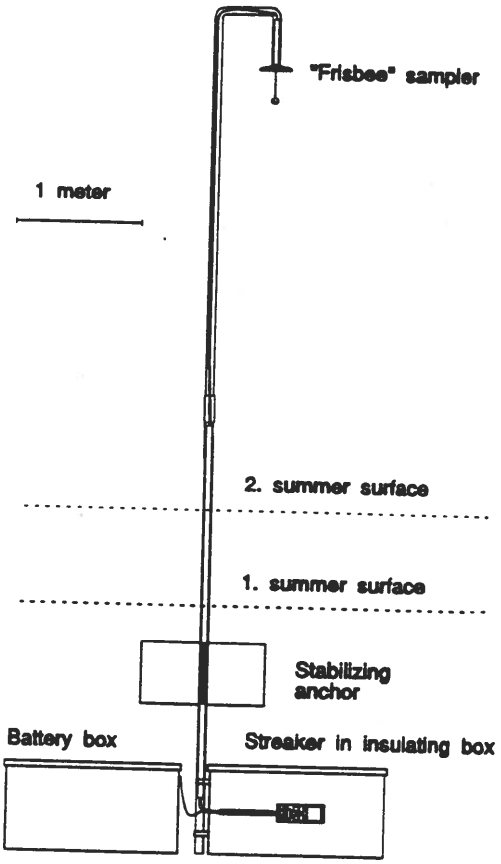

Fig. 3: The sampling system placed on the Greenland ice cap.

Species to be analysed

The streaker is primarily intended to be used in connection with elemental analysis by means of PIXE. The PIXE provides detection limits down to 10^{-10} - 10^{-11} g for the filters/foils used. For the about 6 m^3 of air, which is taken through the sampler during a one week sampling period, concentrations down to 0.02 ng/m^3 can be measured for several elements.

The very small amount of sample material makes other types of chemical analysis very difficult, but an estimate of the total weight of the fine particle fraction could be done by means of ß gauge measurements and the graphite or soot content may be determined with optic reflectometry. In both cases the variations of the filter background require an elaborate correction procedure. A very promising possibility

would be an analysis of single particles collected on the filters. This could be done either by SEM in connection with XRF or by means of μ-PIXE. Convincing examples of classification of aerosols on the basis of the elemental composition and size of single particles are given by ANDERSON et al. (1992).

Status

Up to now sampling have been performed in the Greenland High Arctic at Summit on the ice cap and at Station Nord in the far northeast. It is planned to start sampling at a mountain peak on the Faeroe Islands. The samplers have been wrecked several times, but as mentioned in the introduction realistic test can only be performed at the actual sampling place. We have corrected a number of errors and improved the construction at several points. It is our belief that the streaker itself is "reliable" now, which probably means that an all-year sampling usually will be successful.

A number of positive results has been obtained. The first of these are described by WÅHLIN, 1992.

References

Anderson, J.R, P.R. Buseck, D.A. Saucy and J.M. Pacyna (1992) Characterization of individual fine-fraction particles from the Arctic aerosol at Spitsbergen, May-June 1987. Atmospheric Environment **26A** 1747-1763.

Hall, D.J. and S.L. Upton (1988) A wind tunnel study of the particle collection efficiency of an inverted Frisbee used as dust deposition gauge. Atmospheric Environment **22** 1383-1394.

Kemp, K. and J. Tscherning Møller (1981) A two-stage "discrete streaker" compatible with high volume samplers. Nuclear Instruments and Methods **181** 481-485.

Nelson, J.W (1977) Proton-induced aerosol analysis: Methods and samplers. In X-ray fluorescence analysis of environmental samples (edited by T.G. Dzubay) pp 19-34. Ann Arbor Science. Ann Arbor.

Wåhlin, P. (1992) A receptor model applied to aerosol data from Northeastern Greenland. Proceedings from the 5th International Symposium on Arctic Air Chemistry, September 8-10, Copenhagen.

Wesolowski, J.J. et al. (1977) Collection surfaces of Cascade Impactors. In X-ray fluorescence analysis of environmental samples (edited by T.G. Dzubay) pp 121-131. Ann Arbor Science. Ann Arbor.

POSTER

Measurements of nitrogen and sulphur containing compounds in gas phase and in aerosols in the Greenland Arctic.

Lone Grundahl
National Environmental Research Institute
Emissions and Air Pollution
Denmark

Abstract

Measurements of gasses and aerosols have been carried out at Station Nord (Heidam, 1992) in North-east Greenland since the 1'st of august 1990. The method used for sampling NO_2 is KI-impregnated filters. A filterpack method is used for sampling SO_2, SO_4^{2-}, NH_3+NH_4^+, HNO_3+NO_3^- and a number of elements. Both methods are used in Danish monitoring programs. Because of different conditions in the Greenland Arctic and in Denmark, some tests have been done to verify the methods. The sampling efficiency has been investigated, and it has been tested if the KI-impregnated glassfilters and the impregnated filters in the filterpack are stable for half a year before exposure. Also the contribution from passive sampling is estimated.
For NO_2 the highest concentrations are found at about 110 ng-N/m^3 with no clear seasonal variation. For the other compounds the highest concentrations are found during winter. The maximum values are found about 1500 ng-S/m^3 for SO_2, about 550 ng-S/m^3 for SO_4^{2-} about 150 ng-N/m^3 for NH_3+NH_4^+ and about 130 ng-N/m^3 for HNO_3+NO_3^-.

Measuring methods.

The method for measuring NO_2.

The method used for sampling NO_2 is KI-impregnated filters. Sintered glass filters are impregnated with a methanol solution containing KI, $NaAsO_2$ and ethyleneglycol. The method is described by Ferm (1992). The interferences are HNO_2, which is absorbed 100 % and PAN which is absorbed about 25 %.

Each impregnated filter is exposed for a period of 7 days with a flow of about 0.6 l/min. The sampler is build for four filters, and with a sampling period of 7 days, it is necessary to change filters every third week. The sampler for sampling NO_2 on KI-impregnated filters is shown in figure 1.

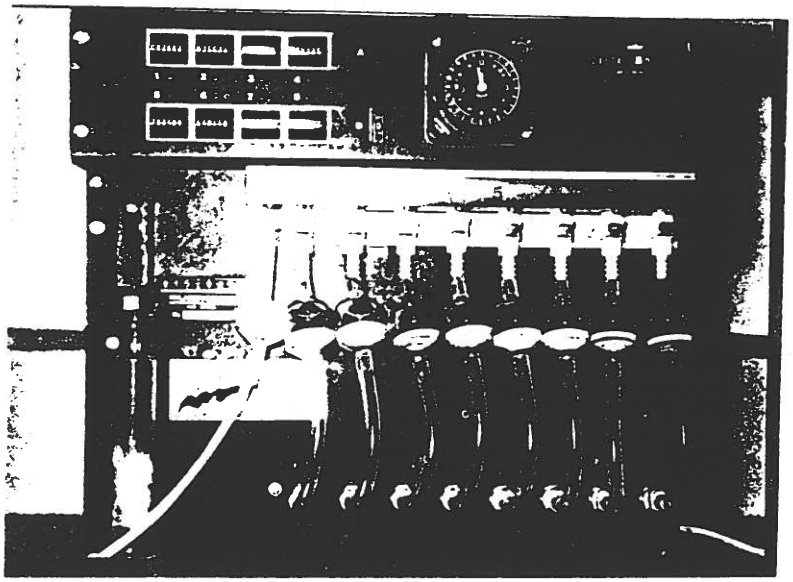

Figure 1. The sampler for sampling NO_2. The sampler at Station Nord is built for four glasfilters.

The method for measuring SO_2, SO_4^{2-}, the sum of NH_3 and NH_4^+, the sum of HNO_3 and NO_3^-, and a number of elements.

The method used for sampling gasses and aerosols is a filterpack method described by Fuglsang (1986). The filterpack consist of four filters in series: A particle filter (a cellulose acetate filter) for sampling the particles, followed by three impregnated filters for sampling the gaseous compounds.

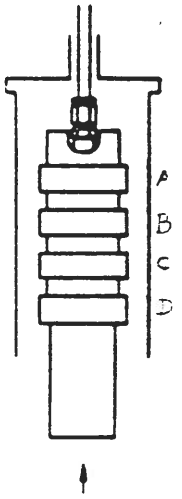

A. Whatman filter impregnated with $(COOH)_2$, analysed for NH_3
B. Whatman filter impregnated with KOH (and glycerol), analysed for SO_2
C. Whatman filter impregnated with NaF, analysed for HNO_3 and SO_2
D. Cellulose acetate filter (1,2 µm), analysed for SO_4^{2-}, NH_4^+, NO_3^- and a number of elements (by PIXE)

Flow 40 l/min (0°C)
The velocity at the filter inlet is 0.5 m/sec

Each filterpack is exposed for 7 days.
The sampler is built for four filterpacks, and with a sampling period of 7 days, it is necessary to change filterpacks every third week. On the sampler there is room for a fifth filterpack which serves as an outdoor blank to test passive sampling. The sampler for the filterpack is shown in figure 2.

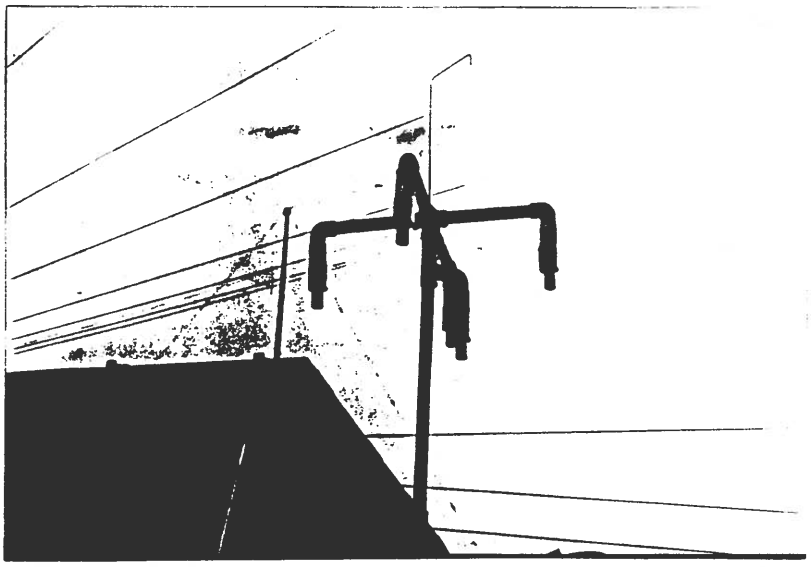

Figure 2. The sampler with the filterpack. The little funnel on top of the sampler is the inlet for the NO_2 sampler.

Test of methods

Sampling efficiency

Tests of sampling efficiency for SO_2 have been made for the Whatman filters impregnated with KOH and glycerol. Two identical filters have been placed in series after the particle filter. The first test made on two filterpacks showed about 100 % efficiency. More tests are planned in the period with the lowest relative humidity, where the efficiency is expected to be the lowest (Lewin, Zachau-Christiansen, 1977). The same test is running for the KI-impregnated glasfilters.

Stability of the impregnated filters

Because of rare flights to Station Nord, the filtermaterial is up to 8 months old before the exposed filters are back again. Similarly the filtermaterial can be up to 5 months old before exposure. 6 filterpacks and 6 glassfilters which have been at Station Nord for about 5 months without getting exposed, have been tested in Denmark against newly prepared filterpacks. The results are shown in figure 3.

The results show no systematically difference in concentrations obtained with new prepared and 5 month old filters.

The problems about stability of the exposed filters have not been tested!

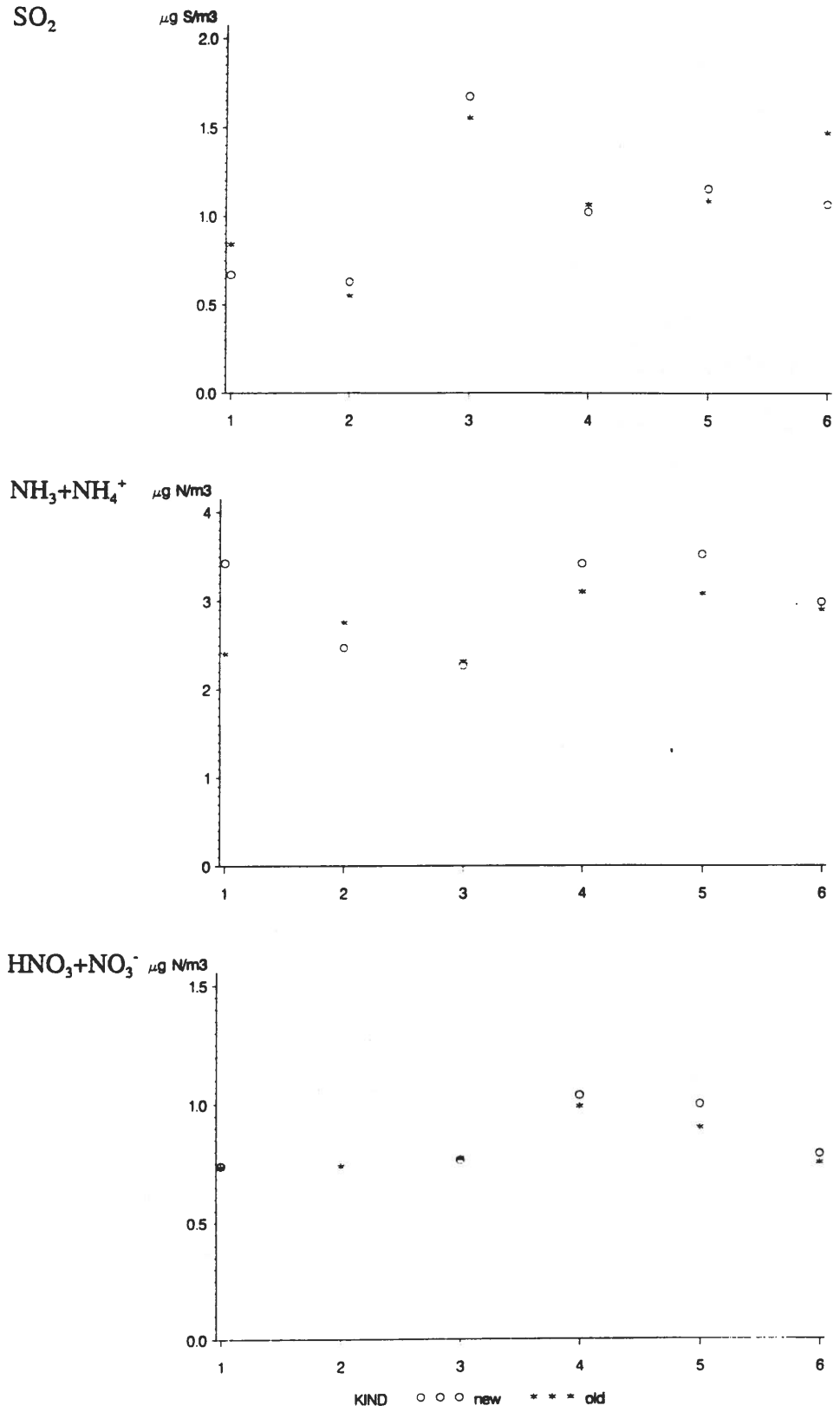

Figure 3. Results from sampling with newly prepared filters (0), and with filters stored at Greenland for about 5 months (*).

Passive sampling

For the filterpack method there might be a problem with passive sampling, during the time where the filterpacks are placed in the sampler without being actively exposed. Therefore a filterpack is placed in the sampler for six weeks as a passive sample. This outdoor blank is compared to the blanks placed in the dispatch box used. The boxblank is closed at both ends and represents filterpacks for six weeks sampling. Results from the passive sampling are shown in figure 4 a and b.

For the sum of HNO_3 and NO_3^-, the results show sometimes a contribution from passive sampling on the outdoor blank. For the other compounds there are no systematic differences between the boxblanks and the outdoor blanks. The comparisons continue on a routine basis.

The problem about passive sampling on exposed filterpacks have not been investigated.

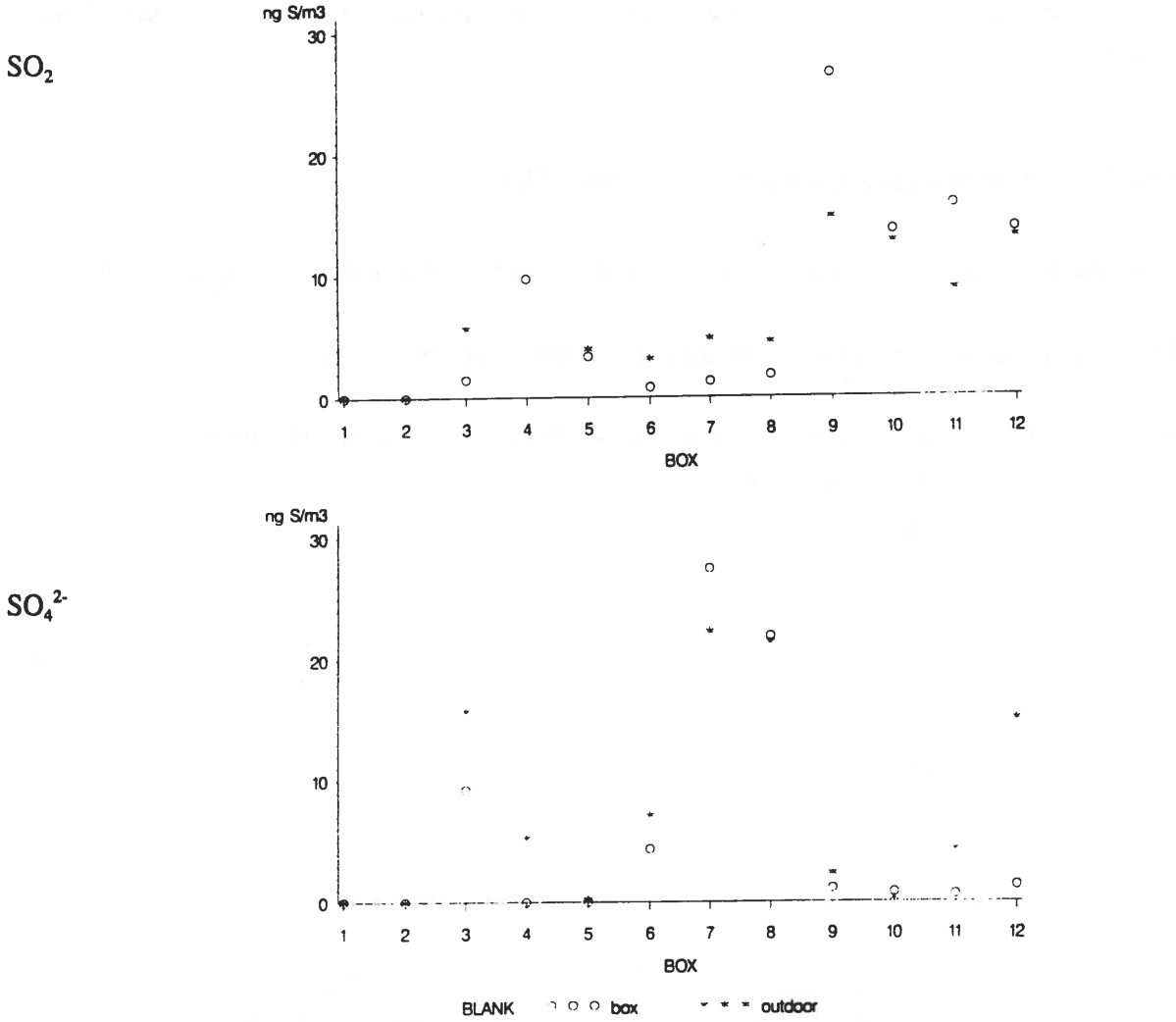

Figure 4a. Results for SO_2 and SO_4^{2-} from blanks placed in the boxes (0) and the blanks placed outdoor (*).

$HNO_3+NO_3^-$

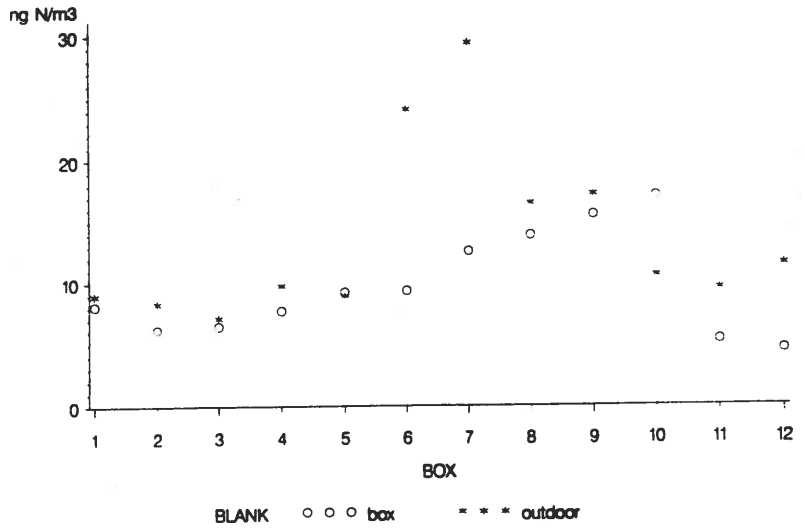

Figure 4b. Results for $HNO_3 + NO_3^-$ from blanks placed in the boxes (0) and the blanks placed outdoor (*).

Results from measurements at station Nord.

All results are based on a single sampling, and each result represent the mean of one week.

The results for all the measured compounds are shown in figure 5 a, b and c.

For NO_2 there is no clear seasonal variation, while for the other compounds the highest concentrations are found during winter.

SO_2

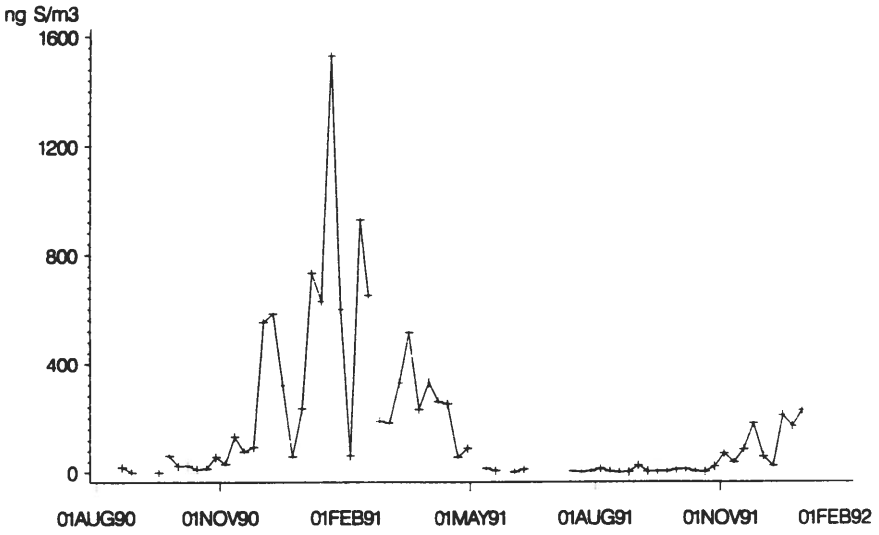

Figure 5a. The concentration of SO_2 in ng S/m^3.

SO_4^{2-}

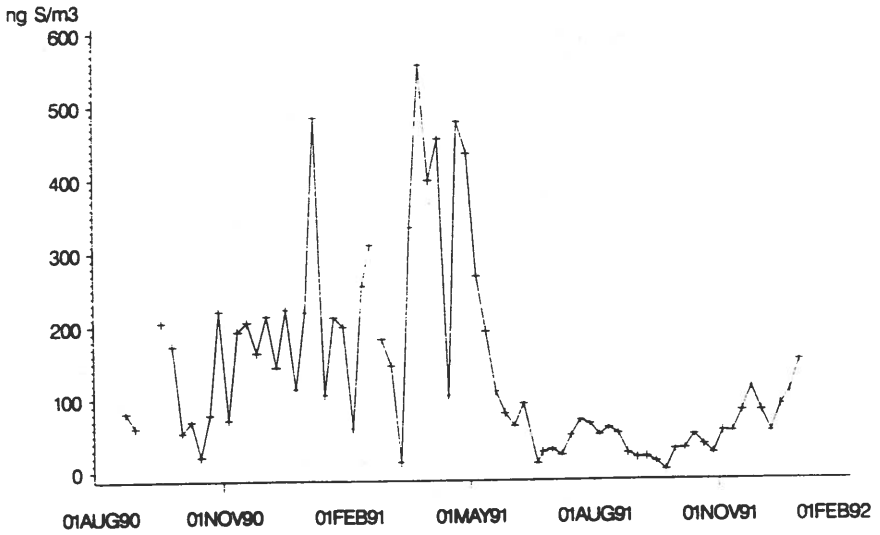

$NH_3 + NH_4^+$

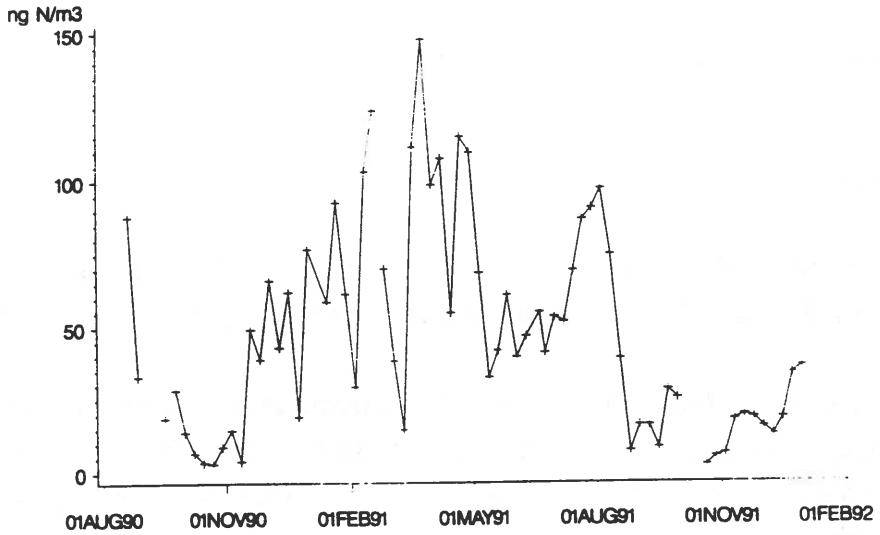

$HNO_3 + NO_3^-$

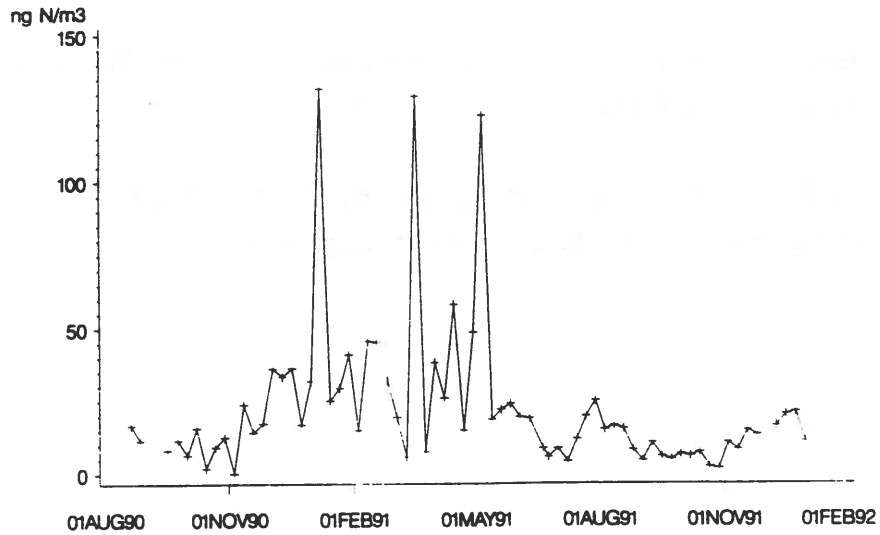

Figure 5b. Concentration af SO_4^{2-} in ng S/m^3, the sum of NH_3 and NH_4^+ and the sum of HNO_3 and NO_3^-, in ng N/m^3.

NO_2

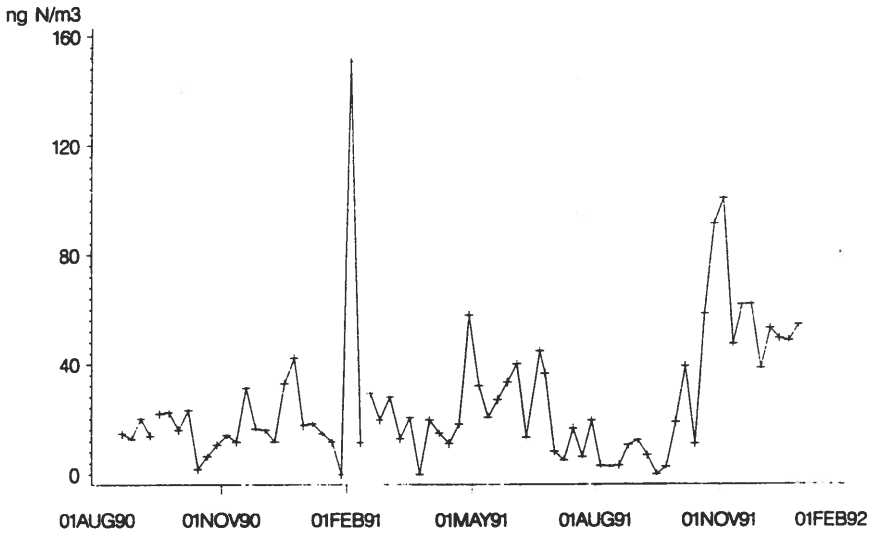

Figure 5c. Concentration of NO_2 in ng N/m^3.

References.

Ferm, M. (1992): A volumetric filter technique for determination of atmospheric NO_2 (In prep.). Swedish Environmental Research Institute, Gothenburg, Sweden.

Fuglsang, K. (1986): A filter pack for determination of total ammonia, total nitrate, sulfur dioxide and sulfate in the atmosphere. MST LUFT-A103, Air Pollution Laboratory, National Agency of Environmental Protection, Risø National Laboratory, DK-4000 Roskilde, Denmark.

Heidam, N.Z. (1992): The Danish Atmospheric Measuring Site, Station Nord in the Greenland Arctic. Present as a poster in these Proceedings.

Lewin, E. E. and Zachau - Christiansen, B. (1977): Efficiency of 0.5 N KOH-impregnated filters for SO_2 - collection. Atm. Environ. 11, 861-862.

Measurements

POLAR SUNRISE EXPERIMENT 1992.

L.A.Barrie and J.W. Bottenheim
Atmospheric Environment Service, 4905 Dufferin Street, Downsview, Ontario, M3H 5T4, Canada.

Between January 15 and April 20, 1992 a major study was conducted at Alert, Northwest Territories, Canada(82.5 N, 62.3 W). It involved approximately 15 scientists from four countries. The aim was to observe chemical changes in the Arctic troposphere at polar sunrise in order to better understand chemical mechanisms of lower tropospheric ozone destruction involving marine halogens and photochemical processing of lower tropospheric pollution at high latitudes.

In addition to aerosol physical measurements, aerosol chemical observations were conducted using a variety of techniques involving size segregation by low pressure impactor, dichotomous high volume samplers and high volume denuder followed by chemical analysis by ion chromatography, instrumental neutron activation analysis, proton-induced x-ray emission and FTIR-spectroscopy. A summary of the measurements performed and some preliminary results will be presented.

Abstract to the 5th International Symposium On Arctic Air Chemistry
8-10 September 1992 Copenhagen Denmark

Total ozone measurements over Ny-Ålesund, 1991-1992

B.A. Kåstad

G.O. Braathen (Norwegian Institute for Air Research, NILU, P.O.Box 64, N-2001 Lillestrøm, Norway)

R. Fabian (Institute for Remote Sensing FB1, Kufsteiner Strasse, University of Bremen, 2800 Bremen 33, Germany)

R. Neuber (Alfred Wegener Institute for Marine and Polar Research, Bremenhaven, Germany)

M. Rummukainen and J. Damski (Finnish Meteorological Institute, Air Quality Dept., Sahaajankatu 22 E, SF-00810, Helsinki, Finland)

ABSTRACT

The total ozone values from a visible diode array spectrometer (SAOZ) placed in Ny-Ålesund have been compared to data from the Total Ozone Mapping Spectrometer (TOMS) in the NIMBUS-7 satellite and ozonesondes launched at Ny-Ålesund and Bear Island. The agreement between SAOZ and other measurement methods is good in 1991 and in the beginning of 1992. After the vortex beaks up (around March 20, 1992), the zenith sky measurements by SAOZ give far too low total ozone values. The amount of aerosols increases over Ny-Ålesund as the vortex breaks up, and the altitude of the aerosols are lower inside the vortex than outside. SAOZ zenith sky measurements are found to be very sensitive to the stratospheric aerosol loading. SAOZ direct sun measurements agree well with TOMS but are lower than total ozone as calculated from ozonesondes.

INTRODUCTION

Several measurement methods are now in use to monitor the ozone layer in the Svalbard region. Ozonesondes are launched from Ny-Ålesund (79 ^{o}N,12^{o} E) and Bear Island (75^{o} N,19^{o} E). A UV-visible diode array spectrometer is located at Ny-Ålesund and a Dobson spectrophotometer is placed in Longyearbyen (78^{o}N, 15^{o} E). In addition TOMS data (version 6) is available from the National Space Science Data Center (NSSDC) in Greenbelt, Maryland.

The increased concentration of aerosols in the stratosphere due to the eruption of Mt. Pinatubo in June 1991 has increased the attenuation of the direct sunlight and increased the diffuse solar flux. This causes errors in the inferred total ozone from measurements by SAOZ and TOMS. The present work shows a comparison between SAOZ, TOMS and ozonesonde data for the time period February 1991 to May 1992.

1. THE VARIOUS MEASUREMENT METHODS

2.1 SAOZ

The SAOZ (System for Analysis of Observations at Zenith) is a diode array spectrometer which performs measurements of the total ozone column by looking at visible sunlight scattered at zenith.

Ozone is calculated in the Chappuis band around 510 nm, which is free of temperature dependence, after removing interfering absorption by NO_2, O_4 and H_2O, by least squares correlation with laboratory ozone absorption cross sections. Slant columns are then converted into vertical columns, knowing the ratio of the actual slant path of the light scattered through the atmosphere to the vertical path. This ratio is called the air mass factor.

While ultraviolet groundbased instruments like Dobson and Brewer spectrophotometers do not give reliable data at solar zenith angles larger than 80 - 82 ^{o}SZA, SAOZ can operate at solar zenith angles up to 92^{o} SZA. SAOZ makes observation of total ozone in polar regions possible almost throughout the year. In Ny-Ålesund the SAOZ instrument is taking zenith measurements from early February to the end of October.

SAOZ also measures total ozone by looking directly at the sun or at the moon. The moon measurements make it possible to do measurements also during the winter in Ny-Ålesund.

In this study only measurements taken when the solar zenith angles were between 87- 91^{o} are included in the mean values. The overall precision in total ozone measured with SAOZ at solar zenith angles between 87^{o} and 91^{o} is better than 8% (Pommereau et al., 1990).

2.2 Ozonsondes

The Koldewey station in Ny-Ålesund uses the Vaisala system with the ECC-5A (manufactured by Science Pump Corporation) electrochemical cell. A description of this instrument can be found in the Operations handbook (Komhyr, 1986). Ny-Ålesund is equipped with a Digicora receiving station.

The accuracy of the ECC-5A has been verified by comparisons with several different measurement methods (e.g. Aimedieu et al., 1987). It is estimated that the ECC sonde measurement accuracy is ± 5% at pressure altitudes of 1000 mbar to 10 mbar (Aimedieu et al., 1987).

2.3 TOMS

TOMS (Total Ozone Mapping Spectrometer) is an ozone mapping instrument mounted on the NIMBUS-7 satellite. TOMS gives a mapping of the total column ozone density on a latitude-longitude grid on the Earth's surface. To achieve this TOMS steps scans across the orbital track, sampling radiation backscattered from swaths that pass from side to side through nadir. TOMS is described in the NIMBUS-7 User's Guide (Heath, D.F., et.al., 1978).

The size of a grid-cell is dependent on the latitude but is approximately 110 km x 120 km. In this study direct overpass TOMS data have been used for 1991, whereas gridded data have been used for 1992. The comparison between SAOZ and TOMS data has been performed for the time period February 1991 to May 1992 (TOMS measures total ozone over Ny-Ålesund from late February to the middle of October, that is for SZA lower than 88^{o}).

3. RESULTS AND DISCUSSION

The total ozone values from the SAOZ zenith sky measurements and sondes launched at Ny-Ålesund for 1991 and 1992 are displayed in figure 1. For the time period day number 50 to day number 250 in 1991 the deviation 100•(sondes - SAOZ)/sonde is -3.4 ± 7.3% and hence shows that there is no systematic deviation between the SAOZ data and the sonde data at this time.

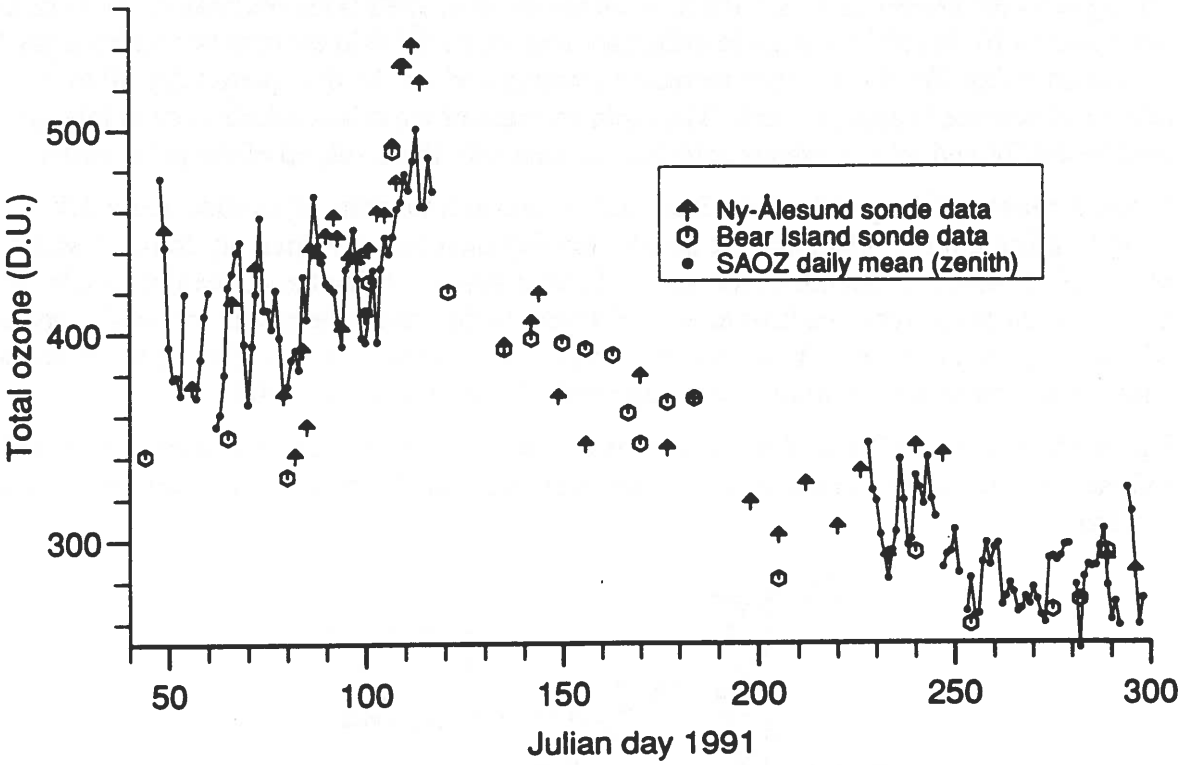

a)

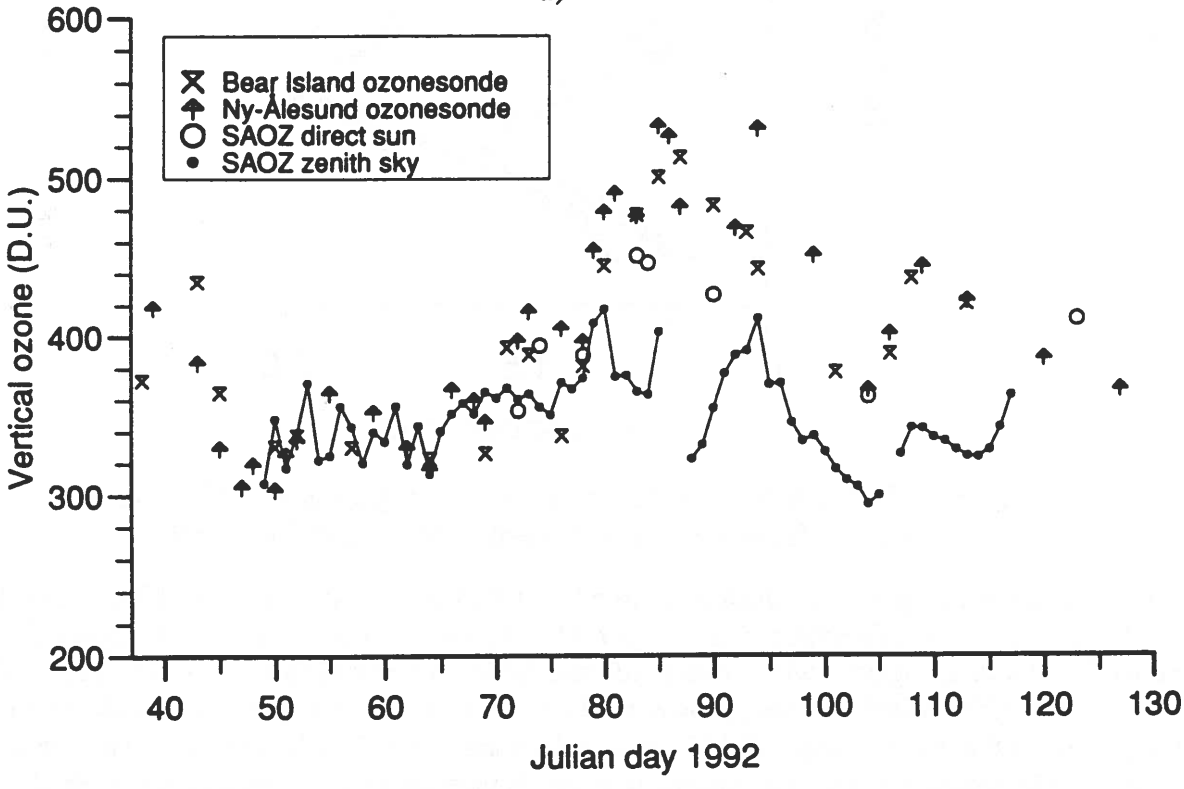

b)

Figure 1. Total ozone from SAOZ and ozone sondes in the period from a) February 1991 to October 1991. b) February 1992 to may 1992.

The agreement between sondes and SAOZ up to day 70 of 1992 is approximately the same as in 1991 (see Figure 1 b). In 1992 the relative difference was +2.3 ± 7.4% in the time period from day 50 to day 75, but after day 80 the difference increases abruptly and for the time period day 80 to day 120 the relative difference is approx. -35%. The rapid increase of the relative difference in total ozone measured by SAOZ and other methods coincides in time with the break-up of the polar vortex.

Figure 2 shows a lidar profile of the backscatter ratio as a function of altitude above Ny-Ålesund. From this figure it is evident that the aerosol loading increases considerably from 17 March to 23 March 1992. Also, the altitude of the aerosol layer is higher outside the vortex than inside. The SAOZ air mass factors are very sensitive to aerosol layers in the stratosphere, and the sensitivity increases with the altitude of the layer. Work is under way to calculate new air mass factors based on the aerosol lidar profiles by using a multiple scattering model (Dahlback, et. al., 1991)

Figure 1 b) also shows SAOZ direct sun measurements. The agreement with sondes is not satisfactory, and there is need to recalculate from the raw data. We also plan to use data from the UV part of the spectrum.

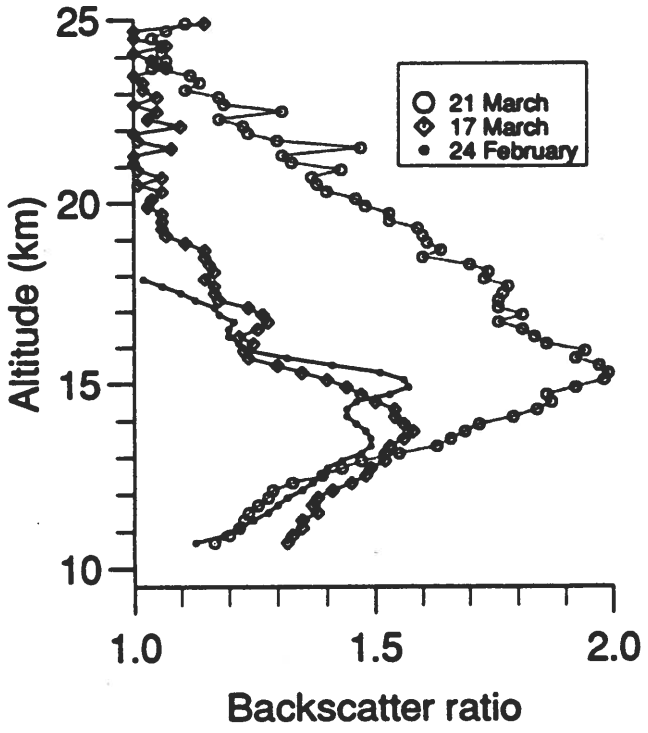

Figure 2. Backscatter ratio profiles as measured by the aerosol lidar at 353nm above Ny-Ålesund 24. February, 1. March and 23. March.

Figure 3a) shows total ozone values measured by TOMS and ozone sondes for 1991. The relative deviation 100 •(sondes -TOMS)/sondes is 3.4 ± 7.3 %. Figure 3 b) shows total ozone measured by TOMS above Ny-Ålesund together with ozonesonde and SAOZ direct sun data in the time period February 1992 to May 1992. TOMS measures lower total ozone values than the ozonesondes almost throughout the period. In the end of March TOMS ozone values are as much as 80 D.U. too low. The sensitivity of the TOMS measurements to stratospheric aerosols increases with increasing solar zenith angle and increasing altitude of the aerosol layer (A. Dahlback et. al., 1992). In late March both the aerosol optical thickness and the solar zenith angle (SZA) are large, and this causes a large deviation between TOMS and ozonesondes. In April the SZA is lower and the TOMS measurements are less influenced by the aerosols. It has not been possible to perform reliable corrections for TOMS due to lack of data on the solar zenith angle. When direct overpass data become available, the corrections can be made.

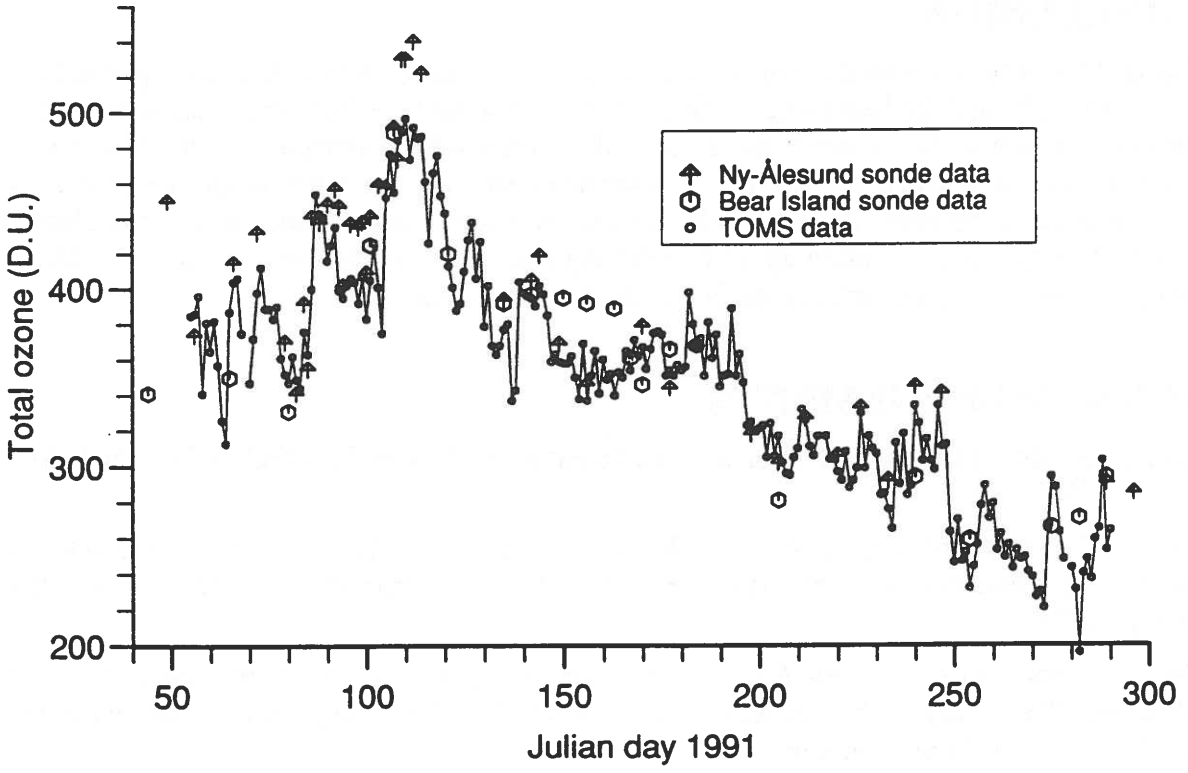

a)

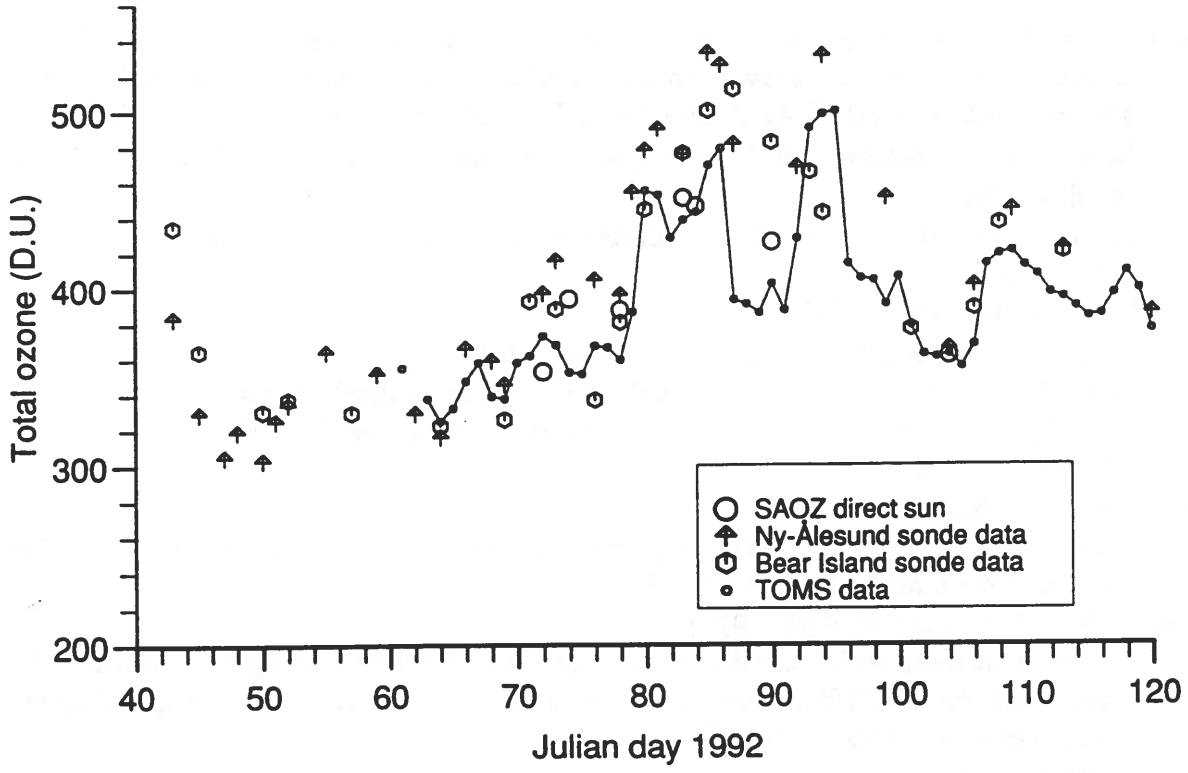

b)

Figure 3. Total ozone as obtained from a) ozonesonde and TOMS in the period February - October 1991 b) ozonesondes, TOMS and SAOZ direct sun data in the time period February - May 1992.

CONCLUSION

The agreement between total ozone measurements performed by SAOZ and other methods is satisfactory for 1991 and the beginning of 1992 when Ny-Ålesund is within the polar vortex. The agreement is very poor when the vortex breaks up and the stratospheric aerosol loading above Ny-Ålesund increases. The total ozone measurements performed near 90^{o} solar zenith angles become very unreliable when the stratosphere is loaded with volcanic aerosols. Work is under way to calculate new air-mass factors by use of radiative transfer modelling and aerosol profile data. Also the TOMS data are influenced by the stratospheric aerosols and must be corrected.

ACKNOWLEDGEMENTS

The authors are grateful to the National Space Science Data Center (NSSDC) in Greenbelt, Maryland. for the TOMS data.

The SAOZ instrument is founded by the Royal Norwegian Council for Scientific and Industrial Research. Ozonesondes from Bear Island are founded by grants from the State Pollution Control Authority (SFT).

The ozonesonde program at Ny-Ålesund is supported by grant from the Bundesministerium für Forschung und Technologie. The authors also like to thank the Alfred Wegener Institute for providing the ozonesonde ground equipment in Spitsbergen.

REFERENCES

Dahlback A., P. Rairuox, B. Stein, M. Del Guasta, E. Kyrö, L. Stefanutti, N. Larsen and G. Braathen, Effects of Stratospheric Aerosols from the Mt. Pinatubo on SAOZ, Brewer and TOMS Measurements at Sodankylä, Finland 1991/1992, To be published in Geophys. Res. Lett.

Aimedieu, P., W. A. Matthews, W. Attmannspacher, R. Hartmannsgruber, J. Cisneros, W. Komhyr, D.E. Robbins, (1987)
Comparison of in situ stratospheric ozone measurements obtained during the MAP/GLOBUS 1983 campaign,
Planet. Space Sci., **35**, 563 - 585

Pommereau, J.P., F. Goutail, M. Pinharanda, J. Piquard, A. Sarkissian,
Ground-based total ozone measurements in the visible Chappuis band,
Proc. First European Workshop on Polar Stratospheric Ozone Research,
Schliersee, October 1990

Dahlback, A., K. Stamnes, (1991)
A new spherical model for computing the radiation field available for photolysis and heating at twilight, *Planet. Space Sci*, **39**, 671-683

Heath,D.F., A.J. Krueger, H. Park (1978)
The Solar Backscatter Ultraviolet (SBUV) and Total Ozone Mapping Spectrometer (TOMS) experiment, *the NIMBUS-7 User's Guide*, edited by C.R. Madrid, NASA Goodard Space Flight Center, Greenbelt, MD., 175-211

Komhyr, W. D.,(1986)
NOAA Technical Memorandum ERL ARL-149:
Operations Handbook - Ozone measurement to 40 km Altitude with 4A Electromechanical Concentrations Cell (ECC) Ozonesondes (used with 1680 MH radiosondes)

Abstract for Fifth Symposium on Arctic Air Chemistry
Copenhagen Sept. 8-10, 1992

MEASUREMENTS OF AEROSOL ELEMENTAL CARBON IN THE RUSSIAN ARCTIC

A.V. Polissar

Institute of Atmospheric Physics
Russian Academy of Sciences, Moscow

From 1989 to 1992, aerosol samples have been collected on quartz fiber filters at Wrangel Island in the eastern Siberian sector of the Russian Arctic. The samples were analyzed by an optical transmission method to determine the concentrations of aerosol elemental (or 'black') carbon, with results ranging approximately from 1 to 500 nanograms per standard cubic meter. The results show that the highest concentrations are found in the winter and spring seasons, and the lowest concentrations in the summer.

These results are compared with the ongoing continuous measurements at the NOAA/CMDL monitoring station at Barrow, Alaska. Meteorological trajectories frequently connect directly from Barrow to Wrangel, giving us the possibility to estimate the loss of aerosol to the surface by deposition. This deposition of optically-absorbing material to the high-albedo ice surface may lead to a change in the solar radiation balance, premature thawing, and possible implications for climate change.

During the Springtime 'Arctic Haze' season of 1990, samples of the background aerosol were collected at Golomyannii Island, Severnaya Zemlya. The samples were analyzed by optical transmission to determine the concentration of aerosol elemental carbon, giving results ranging approximately from 10 to 500 nanograms per standard cubic meter. These results were compared with measurements of the particle size distribution. The highest correlation was found for particles of the smallest detectable diameter (approximately 0.45 micrometers). Five-day backward trajectories were obtained from synoptic maps of the 1000 and 500 hPa levels, and showed that the highest concentrations were found under conditions of transport from the Ural region. Differences in the particle size distribution spectrum were correlated with different trajectory categories.

This work shows that simultaneous measurements of aerosol elemental (or 'black') carbon concentration and particle size distribution can be used to estimate the carbonaceous particles' size, the contribution of anthropogenic aerosol at a remote location, and the influence of transport trajectory pathways.

15

Models

Fifth International Symposium on Arctic Air Chemistry
September 8-10, 1992

A MULTIVARIATE RECEPTOR MODEL WITH A PHYSICAL APPROACH

Peter Wåhlin
National Environmental Research Institute
Division of Emissions and Air Pollution
Frederiksborgvej 399, DK-4000 Roskilde, Denmark.

Introduction

The two main branches of receptor models are Chemical Mass Balance (CMB) models and multivariate factor analysis models (Henry *et al.*, 1984). CMB models need only one sample and assume knowledge of the sources and their composition, while factor analysis, by artful mathematics, attempts to apportion the sources and determine their composition on the basis of a series of observations at the receptor alone. That factor analysis without physical constraints attempts to get more information out of the data than is really there, has been emphasized by Henry (1987). In this paper is presented a simple hybrid model which unifies qualities from both branches of receptor models.

The fundamental hypothesis in mathematical receptor models is that the measured concentrations x_{ij} of n different chemical components in N samples can be satisfactorily expressed as a sum of contributions from a small number p ($p<n$) of sources with a constant composition,

$$x_{ij} \equiv \sum_k a_{ik} f_{kj} \quad . \tag{1}$$

In the equation (1) a_{ik} are constants representing the relative composition of the sources (the source profiles), and f_{kj} are the source strengths found in the different samples. Index i refers to the n chemical variables, index j refers to the N samples, and index k refers to the p sources. A simple, illustrative example is shown in fig. 1 with three chemical variables and two sources.

The physical receptor model

The physical receptor model is a hybrid model that is based on the CMB model, but which incorporates the ability of multivariate mathematics (e.g., factor analysis) to fit the components in the source profiles.

To solve (1) means to find any source profiles a_{ik} and source strengths f_{kj} that, by insertion in the right side of (1), give results close to the measured x_{ij}. From a physical point of view, the best solution will minimize χ^2, given by

$$\chi^2 = \sum_j \sum_i \frac{(x_{ij} - \sum_k a_{ik} f_{kj})^2}{\sigma_{ij}^2}, \qquad (2)$$

where σ_{ij} are the uncertainties of x_{ij}. In general an infinity of solutions are equally good in a purely mathematical sense, but the arbitrariness tends to disappear when physical restrictions are considered. To a simple linear model like (1), without mutual influence by chemical components from different sources, a fundamental physical demand is that both a_{ik} and f_{kj} must be non-negative. This demand can be complied with, if constraints are introduced in the minimizing process every time a_{ik} or f_{kj} hit the non-physical barrier. In addition, general constraints can be set up for the source profiles by the research worker using knowledge of real source composition. An iterative process is used, in which the minimizing of χ^2 is performed solving the systems of linear equations derived from

$$\frac{\partial \chi^2}{\partial f_{t'j}} = 0 \qquad (3a)$$

and

$$\frac{\partial \chi^2}{\partial a_{it'}} = 0 \qquad (4a)$$

alternately. Solving the equations derived from (3a) corresponds to the approach in the CMB model, which presupposes known source profiles, while (4a) leads to a multiple regression analysis searching for better fitting source profiles. The source index label indicates that some sources may be omitted in order to prevent violation of constraints. An initial profile matrix a_{ik} is set up, in which the column vectors are chosen freely. The idea in the iteration is illustrated in fig. 2. The research worker can use background knowledge to direct the iteration to a rational result by choosing, for example, vectors that are proportional to known source profiles, or vectors with a single non-zero component used as tracer, and by setting up constraints to prevent mixing of the source vectors. As more constraints are added to the hybrid model, it can be gradually changed from a pure multivariate model to a pure CMB model.

Each iteration loop thus involves two steps:

1. The source strengths are found for each sample j by solving the system of linear equations (3a), which after differentiation can be written:

$$\sum_{k'}\left(\sum_{i}\frac{a_{ik'}a_{i\ell'}}{\sigma_{ij}^2}\right)f_{k'j}=\sum_{i}\frac{x_{ij}a_{i\ell'}}{\sigma_{ij}^2}\ . \qquad (3b)$$

First all p sources are used, but if negative elements are found in the resulting source strength matrix f_{kj}, they are replaced by zeros and the affected columns are recalculated omitting the corresponding sources. The labels of the indices k' and ℓ' indicate that the number of sources in the individual samples may be reduced, $p_j \leq p$.

2. The finally achieved matrix f_{kj}, with non-negative elements, is used to calculate the residuals,

$$\Delta x_{ij}=x_{ij}-\sum_{k}a_{ik}f_{kj}\ , \qquad (5)$$

and a correction Δa_{ik} of the source profile matrix is calculated by solving the system of linear equations derived from (4a),

$$\sum_{k'}\left(\sum_{j}\frac{f_{k'j}f_{\ell'j}}{\sigma_{ij}^2}\right)\Delta a_{ik'}=\sum_{j}\frac{\Delta x_{ij}f_{\ell'j}}{\sigma_{ij}^2}\ . \qquad (4b)$$

The k' and ℓ' labels indicate that constraints may reduce the number of sources for the individual chemical component i: If an element a_{ik} is not allowed to change, the corresponding source is omitted, $p_i \leq p$.

The calculation of the matrix Δa_{ik} is completed by inserting zeros for the missing elements in the solution $\Delta a_{ik'}$ of (4b), and the resulting matrix is added to the original matrix a_{ik} to get a better overall fit. If negative elements are found in the new a_{ik} matrix, they are replaced by zeros, and the affected rows are recalculated without the corresponding sources taking the new constraints in account.

The iteration is continued until χ^2 reaches a stagnant minimum value. The degrees of freedom, given by

$$\nu=Nn-\sum_{j}p_j-\sum_{i}p_i\ , \qquad (8)$$

depends upon the number of negative values of a_{ik} and f_{kj} found in the last iteration loop, therefore both χ^2 and ν are determined by the iterative process.

A code implemented on IBM PC has been written to perform the iteration. As inputs are used three matrices: An $n \times p$ profile matrix containing the initial source vectors, an $n \times p$ form matrix containing information about the constraints on the profile matrix elements in 0 = fixed/1 = free format,

and a $2 \times n \times N$ data matrix containing the measured values and their absolute uncertainties. A negative uncertainty is interpreted by the code as an infinite value and can be used to exclude selected data from the fitting process. Output is a $p \times N$ non-negative source strength matrix, a $n \times p$ non-negative profile matrix, plus χ^2 and ν. The arithmetic mean strength values of the individual sources in the source strength matrix are normalized to unity, and, in consequence, the profile matrix elements are normalized to the arithmetic mean values of the source contributions. Furthermore, using multiple linear regression, a "one-factor" analysis can be performed on the residue to reveal a possibly ignored source, and the result is expressed as an extra row in the source strength matrix and an extra column in the source profile matrix.

A simple example

To illustrate the use of the physical receptor model in a simple way some aerosol data for Si, Mn and Pb have been analyzed. The data are weekly mean concentrations measured by PIXE analysis on fine fraction streaker samples from Station Nord in Northeastern Greenland. The inputs are summarized in table 1 and table 2. The output is summarized in table 3 and table 4. The fitted values were calculated by equation (1) and plotted together with the measured data in fig. 3. The large Si/Pb ratio in the initial urban profile was chosen to ensure minimum soil source strength values in the winter time when Northeastern Greenland is covered by snow. A mathematically equivalent solution could be obtained without any Si in the urban profile, but this would be very improbable from a physical point of view, also because the shapes of the midwinter Si and Pb signals are almost the same.

It is evident by inspection of fig. 3 that the two sources are sufficient to make a good fit. The reduced chi square, $\chi^2/\nu = 2.5$, is too large to be explained by the statistics alone, but this is probably due to source profile fluctuations in the sampling period.

References

Henry R.C., Lewis C.W., Hopke P.K. and Williamson H.J. (1984) Review of receptor model fundamentals. *Atmospheric Environment* **18**, 1507-1515.

Henry R.C. (1987) Current factor analysis receptor models are ill-posed. *Atmospheric Environment* **21**, 1815-1820.

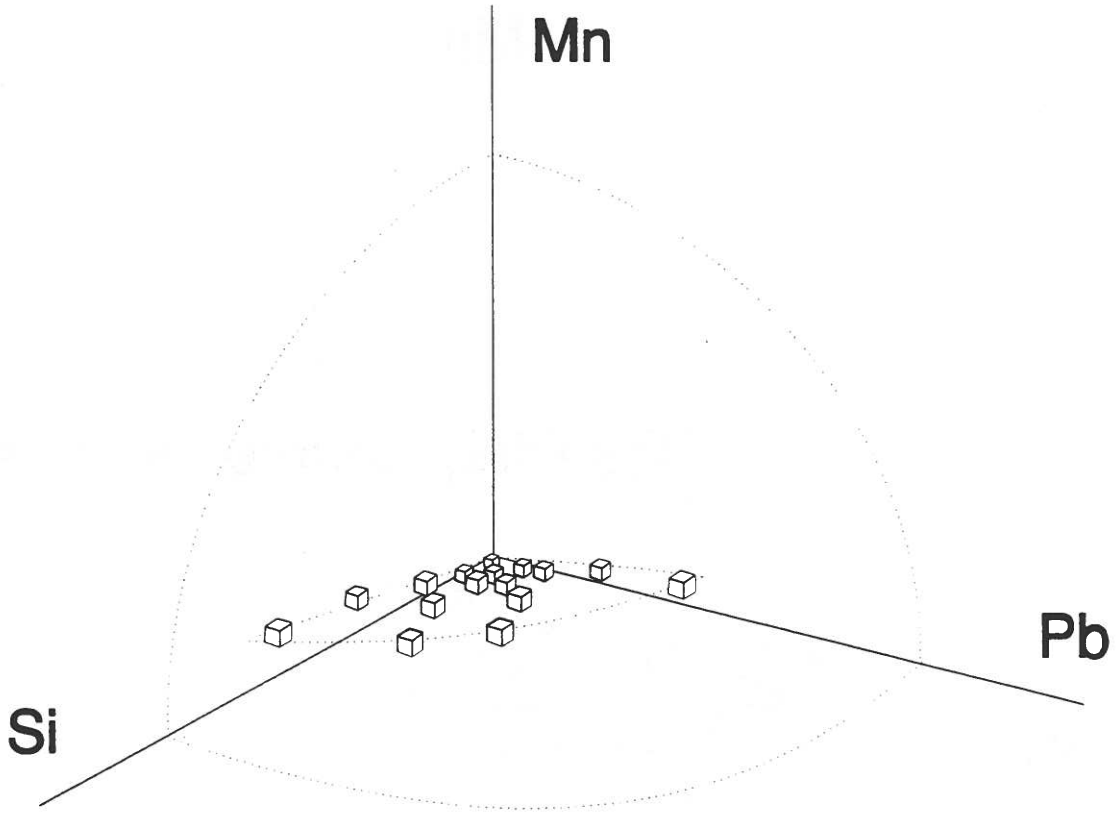

Fig. 1. Illustrative plot of measurements on an aerosol originating from a crustal source (soil) and an anthropogenic source (urban). Within uncertainties all measurements are positioned on a 2-dimensional subspace in the non-negative corner of the measurement space. The aim is to find two source vectors that not only lie in the subspace but also comply with physical restrictions, i.e., they must be non-negative and start in the origin, and the measurements must lie between the vectors.

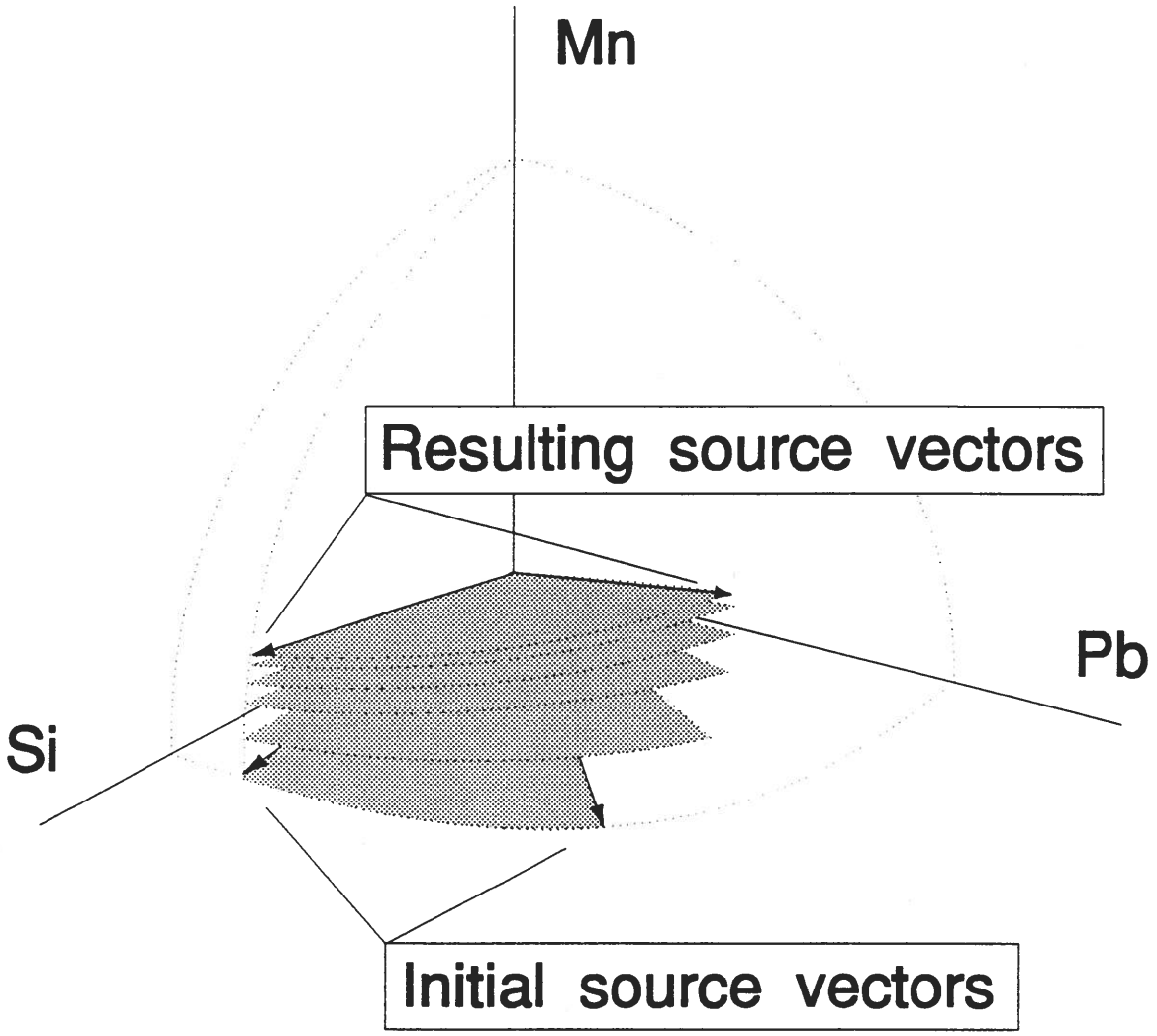

Fig. 2. Complying with the physical constraints the source vectors are found by a multivariate, iterative method that minimizes χ^2. The course of the iteration is guided by the choice of initial source vectors and additional constraints. In the illustrative example a surplus of Si in the initial urban vector is chosen to ensure maximum crustal content in the resulting urban vector, and a small, fixed Pb/Si ratio is chosen in the soil vector (e.g., the small ratio found in igneous rocks).

	Soil	Urban
Si	277200	20
Mn	1000	0
Pb	16	1

	Soil	Urban
Si	0	1
Mn	1	1
Pb	0	0

Table 1. The initial source profile matrix and the corresponding form matrix as set up in the illustrative example. The approximate composition of igneous rocks (in ppm) is used in the soil profile, in which the Si/Pb ratio is fixed by the zeros in the soil column of the form matrix.

Date	Si	σ(Si)	Mn	σ(Mn)	Pb	σ(Pb)
12-9-90	20.2	1.2	0.092	0.010	0.05	0.03
19-9-90	33.9	2.0	0.150	0.013	0.29	0.04
26-9-90	24.9	1.5	0.095	0.010	0.21	0.04
3-10-90	13.6	0.9	0.045	0.008	0.08	0.03
10-10-90	17.5	1.1	0.089	0.010	0.12	0.03
17-10-90	25.1	1.5	0.133	0.011	0.13	0.04
24-10-90	13.4	1.0	0.080	0.009	0.45	0.05
31-10-90	20.1	1.5	0.273	0.021	1.08	0.08
7-11-90	28.7	1.7	0.219	0.015	0.42	0.05
14-11-90	24.2	1.6	0.294	0.019	1.00	0.07
21-11-90	18.1	1.3	0.223	0.016	1.01	0.08
28-11-90	23.5	1.4	0.375	0.023	1.49	0.10
5-12-90	30.0	1.8	0.444	0.026	1.51	0.09
12-12-90	29.8	2.0	0.574	0.030	2.20	0.13
19-12-90	20.7	1.5	0.373	0.022	1.36	0.09
26-12-90	9.8	0.9	0.208	0.014	0.99	0.07
2-1-91	20.9	1.4	0.439	0.025	1.95	0.12
9-1-91	40.0	2.5	0.775	0.043	4.55	0.24
16-1-91	27.0	1.7	0.524	0.029	2.71	0.16
23-1-91	28.4	1.7	0.575	0.032	2.88	0.16
30-1-91	16.0	1.1	0.301	0.020	1.21	0.08
6-2-91	11.0	0.9	0.243	0.017	1.16	0.09
13-2-91	31.9	1.9	0.729	0.039	2.91	0.16
20-2-91	24.3	1.6	0.506	0.028	2.19	0.13
27-2-91	17.6	1.2	0.332	0.020	1.52	0.10
6-3-91	15.1	1.1	0.255	0.017	1.21	0.08
13-3-91	23.9	2.0	0.480	0.031	2.64	0.18
20-3-91	18.9	1.4	0.431	0.025	2.02	0.12
27-3-91	18.1	1.5	0.433	0.029	1.59	0.11
3-4-91	17.2	1.5	0.287	0.022	1.31	0.10

Table 2. Weekly mean concentrations of Si, Mn and Pb and corresponding analytical uncertainties (both in ng/m^3) measured by PIXE analysis on fine fraction streaker samples from Station Nord in Northeastern Greenland. The data is here used illustratively as input to the physical receptor model.

Date	Soil	Urban
12-9-90	2.31	0.04
19-9-90	3.49	0.19
26-9-90	2.51	0.13
3-10-90	1.46	0.04
10-10-90	1.90	0.09
17-10-90	2.82	0.11
24-10-90	1.07	0.25
31-10-90	1.14	0.81
7-11-90	2.93	0.35
14-11-90	1.70	0.78
21-11-90	1.02	0.70
28-11-90	1.06	1.14
5-12-90	1.79	1.19
12-12-90	0.95	1.74
19-12-90	0.84	1.09
26-12-90	0.06	0.72
2-1-91	0.27	1.47
9-1-91	0.14	2.97
16-1-91	0.32	1.88
23-1-91	0.26	2.05
30-1-91	0.50	0.93
6-2-91	0.02	0.85
13-2-91	0.39	2.29
20-2-91	0.39	1.66
27-2-91	0.39	1.11
6-3-91	0.46	0.87
13-3-91	0.09	1.78
20-3-91	0.00	1.49
27-3-91	0.26	1.29
3-4-91	0.57	0.95
10-4-91	0.61	0.68
17-4-91	0.26	0.36

Table 3. Source strengths calculated by means of the physical receptor model on basis of the data summarized in table 1 and table 2. The numbers have been normalized to unity arithmetic mean values.

	Soil	Urban	χ^2	ν
Si	8.7058	12.6887	4.52	
Mn	0.0304	0.2900	42.62	
Pb	0.0005	1.3486	27.66	
Total			74.80	30

Table 4. The resulting source profiles normalized to arithmetic mean values (in ng/m^3) together with the calculated values of χ^2 and the degrees of freedom, ν.

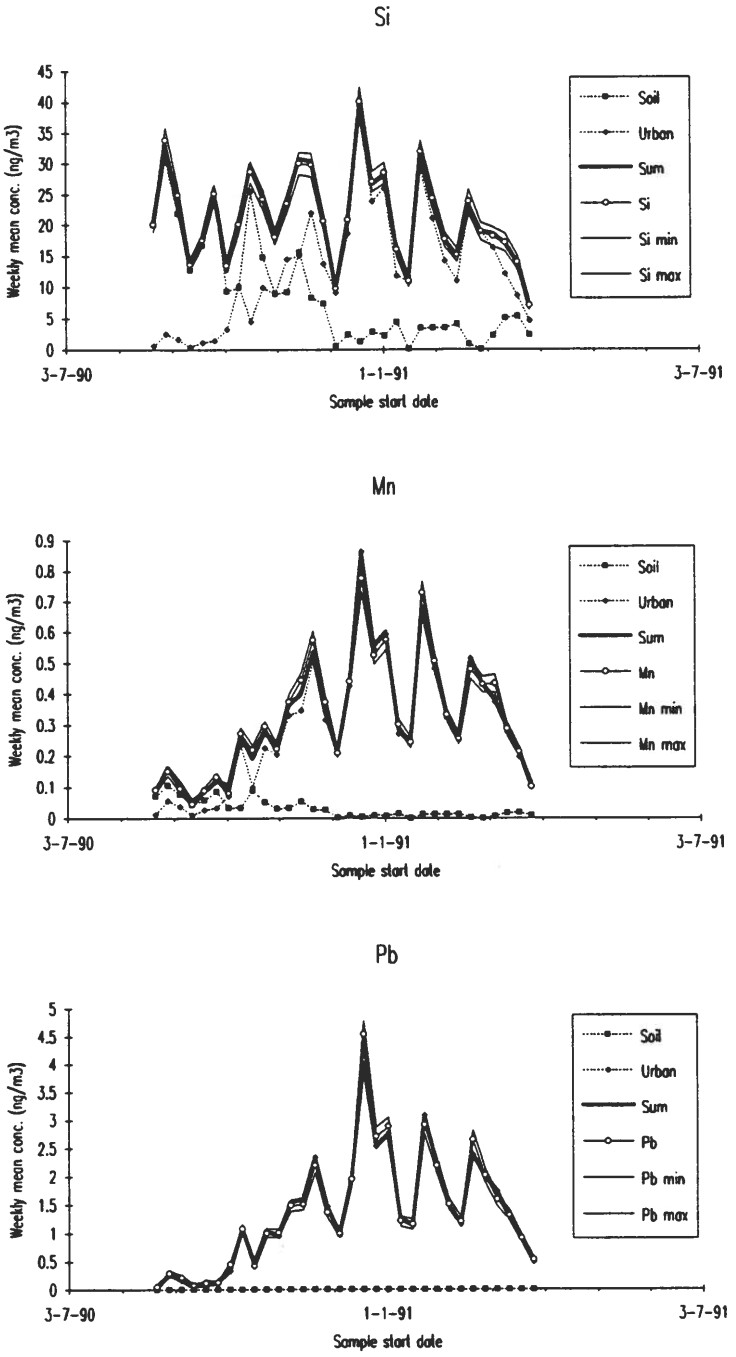

Fig. 3. Fits to the data in table 2. The physical receptor model was used together with the initial source profile matrix and the form matrix in table 1. The lines labeled min and max indicate the uncertainty of the measurements.

Participants of the 5th International Symposium on Arctic Air Chemistry

Dr. L.A. Barrie
Atmospheric Environment Service,
4905 Dufferin Street
Downsview, Ontario, Canada M3H 5T4

Dr. Jan W. Bottenheim
Atmospheric Environment Service,
4905 Dufferin Street
Downsview, Ontario, Canada M3H 5T4

Ph.D. stud. Jesper Christensen
National Environmental Research Institute
Frederiksborgvej 399
4000 Roskilde
Denmark

Henrik B. Clausen
Geofysisk Institut
Københavns Universitet
Haraldsgade 6
2200 København N

Dr. Arne Dahlback
Norwegian Institute for Air Research
P.O.Box 64
N-2001 Lillestrøm
Norge

Prof. Cliff I. Davidson
Carnegie Mellon University
Pittsburgh, PA 15213
USA

Dr. Jack Dibb
Institute for the Earch, Oceans and Space
University of New Hampshire
Durham, NH 03824-3525
USA

Dr. Hans Flyger
National Environmental Research Institute
Frederiksborgvej 399
4000 Roskilde
Denmark

Dr. Lone Grundahl
National Environmental Research Institute
Frederiksborgvej 399
4000 Roskilde
Denmark

Claus Hammer
Geofysisk Institut
Københavns Universitet
Haraldsgade 6
2200 København N

Dr. A.D.A. Hansen
Lawrence Berkeley Laboratory
University of California
1829 Fransisco Street
Berkeley, California 94703, USA

Dr. William Hart
Atmospheric Environment Service
Environment Canada
4905 Dufferin St.
Downsview Ontario
Canada M3H 5T4

D.Sc. Niels Zeuthen Heidam
National Environmental Research Institute
Frederiksborgvej 399
4000 Roskilde
Denmark

Prof. Philip K. Hopke
Clarkson University
Depatment of Chemistry
Potsdam, NY 13699-5810
USA

Lab.tek. Peter Iversen
Geofysisk Institut
Københavns Universitet
Haraldsgade 6
2200 København N

Ph.D. Kåre Kemp
National Environmental Research Institute
Frederiksborgvej 399
4000 Roskilde
Denmark

Ph.D. stud. Britt Ann Kåstad
Norwegian Institute for Air Research
P.O.Box 64
N-2001 Lillestrøm
Norge

Ph.D. Christian Lohse,
Director of Research Department
National Environmental Research Institute
Frederiksborgvej 399
4000 Roskilde
Denmark

Dr. W. Maenhaut
Institute for Nuclear Sciences
Rijksuniversity Gent
Proeftuinstraat 86
B-9000 Gent Belgium

Dr. H.C. Martin, Director Air Quality Research
Atmospheric Environment Service
Environment Canada
4905 Dufferin St.
Downsview Ontario
Canada M3H 5T4

Professor W. J. Megaw
Institute for Space and Terrestrial Science
York University
4700 Keele Street
North York
Ont L3Y7K1
Canada

A.V. Polissar
Institute of Atmospheric Physics
Russian Academy of Sciences
Pyzhevsky Per.3, Moscow 109017
Russia

Dr. Russell C. Schnell
Mauna Loa Observatory
154 Waianuenue Avenur, Rm. 202
P.O. Box 275
Hilo, Hawaii 96721-0275

Dr. Patrick J. Sheridan
CIRES, University of Colorado
Boulder, CO 80309 USA

Dr. Eric Silvente
Laboratoire de Glaciologie et Geophysique
de l'Environnement
54, Rue Moliére
Domaine Universitaire
P.B. 96
Saint-Martin-d'Héres CEDEX 38402
France

Dr. Irina Sokolik
CIRES, University of Colorado
Boulder, CO 80309 USA

Jørgen P. Steffensen
Geofysisk Institut
Københavns Universitet
Haraldsgade 6
2200 København N

Dr. Frode Stordal
Norwegian Institute for Air Research
P.O. Box 64
N-2001 Lillestrøm
Norge

Lene Thorsted, Secretary
National Environmental Research Institute
Frederiksborgvej 399
4000 Roskilde
Denmark

Dr. Frank Wania
University of Toronto
Dept. of Chemical Engineering and Applied Chemistry
200 College Street
Toronto, Ontario
Canada M55 1A4

Dr. Peter Wåhlin
National Environmental Research Institute
Frederiksborgvej 399
4000 Roskilde
Denmark

Dr. Zahari Zlatev
National Environmental Research Institute
Frederiksborgvej 399
4000 Roskilde, Denmark

National Environmental Research Institute

The National Environmental Research Institute - NERI - is a research institute of the Ministry of the Environment. Neri's tasks are primarily to do research, collect data and give advice on problems related to the environment and nature.

Addresses:

National Environmental
Research Institute
Frederiksborgvej 399
P.O. Box 358
DK-4000 Roskilde
Denmark

Tel: +45 46 30 12 00
Fax: +45 46 30 11 14

Management
Personnel and Economy Secretariat
Research and Development Secretariat
Department of Emissions and Air Pollution
Department of Environmental Chemistry
Department of Policy Analysis
Department of Marine Ecology and Microbiology

National Environmental
Research Institute
Vejlsøvej 25
P.O. Box 413
DK-8600 Silkeborg
Denmark

Tel: +45 89 20 14 00
Fax: +45 89 20 14 14

Department of Freshwater Ecology
Department of Terrestrial Ecology

National Environmental
Research Institute
Grenåvej 12, Kalø
DK-8410 Rønde
Denmark

Tel: +45 89 20 14 00
Fax: +45 89 20 15 14

Department of Wildlife Ecology

Publications:

NERI publishes professional reports, technical instructions, reprints of scientific and professional articles, a magazine of game biology and the Annual Report.

Included in the annual report is a review of the publications from the year in question. The annual reports and an up-to-date review of the year's publications are available on application to NERI.